JULIUS-MAXIMILIANS-UNIVERSITÄT WÜRZBURG

DEVELOPMENT OF NEW METHODS FOR TRIARYLBORANE SYNTHESIS

AND

INVESTIGATION OF TRIARYLBORANE CHROMOPHORES FOR DNA AND RNA SENSING AND SINGLET OXYGEN SENSITIZATION

Dissertation zur Erlangung des naturwissenschaftlichen Doktorgrades

der Julius-Maximilians-Universität Würzburg

Matthias Ferger

aus Oerlenbach

Würzburg, 2021

Eingereicht bei der Fakultät für Chemie und Pharmazie am

_____

Gutachter der schriftlichen Arbeit

1. Gutachter: Prof. Dr. Dr. h. c. Todd B. Marder

2. Gutachter: Prof. Dr. Holger Brauschweig

Prüfer des öffentlichen Promotionskolloquiums

1. Prüfer: Prof. Dr. Dr. h. c. Todd B. Marder

2. Prüfer: Prof. Dr. Holger Brauschweig

3. Prüfer: _____

Datum des öffentlichen Promotionskolloquiums

_____

Doktorurkunde ausgehändigt am

_____

Affidavit

I hereby confirm that my thesis entitled "Development of New Methods for Triarylborane Synthesis and Investigation of Triarylborane Chromophores for DNA and RNA Sensing and Singlet Oxygen Sensitization" is the result of my own work. I did not receive any help or support from commercial consultants. All sources and/or materials applied are listed and specified in the thesis.

Furthermore, I confirm that this thesis has not yet been submitted as part of another examination process neither in identical nor in similar form.

Würzburg, 19.01.2021   _____

Eidesstattliche Erklärung

Hiermit erkläre ich an Eides statt, die Dissertation „Development of New Methods for Triarylborane Synthesis and Investigation of Triarylborane Chromophores for DNA and RNA Sensing and Singlet Oxygen Sensitization" eigenständig, d.h. insbesondere selbstständig und ohne Hilfe eines kommerziellen Promotionspartners angefertigt und keine anderen als die von mir angegebenen Quellen und Hilfsmittel verwendet zu haben.

Ich erkläre außerdem, dass die Dissertation weder in gleicher noch in ähnlicher Form bereits in einem anderen Prüfungsverfahren vorgelegen hat.

Würzburg, 19.01.2021   _____

ACKNOWLEDGEMENTS

First of all, I want to thank you **Prof. Dr. Dr. h. c. Todd B. Marder**, for the opportunity to do my PhD in your group. Thanks for the great amount of freedom and trust, but also for your good advice and helpful discussions, whenever I was stuck. I learned a lot from you concerning chemistry and life! Thanks for the good times, many laughs, and many discussions outside of chemistry. I am grateful that I was able to attend several conferences and that you enabled my trips to Croatia, which resulted in a nice collaboration and a publication. Thanks to you and **Anne** for all the summer parties and Christmas celebrations at your house. You made us all feel at home!

Next, I want to thank **Dr. Ivo Piantanida**. Thanks for introducing me into the field of DNA and RNA sensing and for allowing me to work in your fantastic group. Thanks for taking the time to show us around Zagreb, explaining so much about the history of the city and your country, and for the delicious Croatian food that we tried! I also want to thank **Dr. Željka Ban**, **Ivona Krošl**, **Iva Orehovec**, **Dr. Marija Matković**, **Dr. Ivo Crnolatac**, **Dr. Dijana Saftić**, and **Dr. Marijana Stojković** for making me feel welcome in your group, being very helpful all the time and also for the nice times we spent outside of work. I especially enjoyed the day we went gathering and preparing chestnuts! Special thanks to **Željka** and **Ivona** for training me regarding DNA titrations, CD spectra, etc. and for the hike up the mountain north of Zagreb. Thanks to **Dr. Sanja Tomić** for molecular modelling and **Dr. Adriana Kenđel** and **Prof. Dr. Snežana Miljanić** for the Raman and SERS measurements.

Thans to **Dr. Ivo Krummenacher** from the working group of **Prof. Dr. Holger Braunschweig** for performing the CV measurements and help with the discussion of the results.

I want to thank **Chantal Roger** from the working group of **Prof. Dr. Christoph Lambert** for transient absorption measurements and opening the door to your floor at least a thousand times for me, whenever I needed your ultra-sensitive scales!

Most importantly I want to thank all former and current members of the Marder group. Thanks for all the help and support I received from everybody, during my time here! Thank you **Dr. Alexandra Friedrich**, **Dr. Daniel Sieh** and **Johannes Krebs** for measuring crystal structures for me. Thanks to **Dr. Jörn Nitsch** for the help with the spectrometer. I am really glad you were there when the thing had to be moved to the new building! Thank you, **Dr. Stephan Wagner** for technical support and general help with the GC-MS. Special thanks to **Christoph Mahler** (for what feels like millions of HRMS measurements. You helped me on so many occasions by squeezing in a measurement when it was (or at least felt) really important) and **Sabine Lorenzen** (for helping me with my synthesis, providing starting materials, proof reading, taking

imagine, how our kitchen would look like without you!), **Alfred Schertzer** for argon and dry ice supply, as well as lending out your tools, the glass blowers **Berthold Fertig** and **Bernhard Werner** and the workshop team **Alois Ruf**, **Wolfgang Obert**, **Frank Förtsch**, **Michael Ramold**, and **Manfred Reinhart**. I also want to thank **Bianca Putz**, **Stefanie Ziegler**, **Birgit Zepke** and especially **Maria Eckhardt** and **Cornelia Walter** for organizing so many things in our group and for the whole institute.

Außerdem möchte ich mich beim ganzen Anorganischen Institut bedanken. Vor allem im alten Gebäude war es eine unglaublich gute Arbeitsatmosphäre und die Abende in den Kaffeeräumen des AK Braunschweig, des AK Radius oder hinter der AC bleiben unvergesslich! Ich bin froh so viele tolle Leute kennengelernt zu haben! Speziell möchte ich hier noch **Lena**, **Raphael**, **Julia** und **Laura** nennen, da DWF auf jeden Fall einen besonderen Platz in meiner Danksagung verdient hat!

Ganz besonders möchte ich mich bei **Johanna**, **Mosi**, **Moby**, **Alex**, **Uwe**, **Domi**, **Paddy** und **Laura** bedanken! Ohne euch wäre das ganze Studium nicht vorstellbar gewesen! Es gibt so viele Momente die ich nie vergessen werde und ich bin froh über die Zeit die wir hier in Würzburg zusammen verbracht haben! Auch wenn es uns inzwischen schon ein bisschen verstreut hat, bin ich mir sicher, dass wir in Kontakt bleiben. Unser Weihnachtsessen ist ja zum Glück schon längst Tradition! **Domi**, danke dass ich immer auf dich zählen konnte und kann!

Natürlich gibt es auch noch ein paar Nicht-Chemiker bei denen ich mich hier bedanken möchte. **Sid**, **Nell**, **Thomas**, **Nile**, **Flo**, **Hubsn**, **Pete** und **Andi**. Ich bin froh, Freunde wie euch zu haben und dass es mit euch immer gleich „wie früher" ist, auch wenn ich leider nicht mehr so oft in Oerlenbach bin. **Tristan**, **Janik** und **Mützel**, zum Glück haben wir uns nie aus den Augen verloren, obwohl es ja aus irgendeinem Grund keiner solange in Würzburg ausgehalten hat wie ich. Würde sagen, die WE-Gruppe hat sich gelohnt!

Der größte Dank gilt meiner Familie! Ein Sohn, der 10 Jahre studiert ist bestimmt der Traum aller Eltern ;) Ohne euch, eure Unterstützung und die Sicherheit, mich immer auf euch verlassen zu können, wäre das alles auf jeden Fall nicht möglich gewesen. **Mama**, **Papa**, **Olf** und **Nicki**, ihr seid die Besten!!!

Laura, ich kenne dich inzwischen fast mein halbes Leben, du bist meine beste Freundin und ich liebe dich. Ich bin dir unendlich dankbar für deine Hilfe, dein Verständnis und dass du einfach immer für mich da bist! Während ich das schreibe ist unsere Wohnung schon halb in Kartons verpackt und es geht bald nach Aschaffenburg. Ich freue mich auf die Zukunft mit dir und unseren Mäusen **Hermine** und **Kasimir**.

LIST OF PUBLICATIONS

The publications listed below are partly reproduced and slightly modified in this dissertation with permission from Wiley-VCH. They are published under a creative common license and do not require a further permission statement from the publisher.

Publication	Position
Synthetic Approaches to Triarylboranes from 1885 to 2020, Sarina M. Berger, <u>Matthias Ferger</u>, Todd B. Marder*, *Chem. Eur. J.*, **2021**, DOI: 10.1002/chem.202005302.	Chapter 1
Bis(phenylethynyl)arene Linkers in Tetracationic bis-Triarylborane Chromophores Control Fluorimetric and Raman Sensing of Various DNA and RNA, <u>Matthias Ferger</u>, Željka Ban, Ivona Krošl, Sanja Tomić*, Lena Dietrich, Sabine Lorenzen, Florian Rauch, Daniel Sieh, Alexandra Friedrich, Stefanie Griesbeck, Adriana Kenđel, Snežana Miljanić, Ivo Piantanida*, Todd B. Marder*, *Chem. Eur. J.*, **2021**, DOI: 10.1002/chem.202005141.	Chapter 3

Further publications:

Optimization of Aqueous Stability versus π-Conjugation in Tetracationic Bis(triarylborane) Chromophores: Applications in Live-Cell Fluorescence Imaging, Stefanie Griesbeck, <u>Matthias Ferger</u>, Corinna Czernetzi, Chenguang Wang, Rüdiger Bertermann, Alexandra Friedrich, Martin Haehnel, Daniel Sieh, Masayasu Taki, Shigehiro Yamaguchi*, Todd B. Marder*, *Chem. Eur. J.* **2019**, *25*, 7679.

Tetracationic Bis-Triarylborane 1,3-Butadiyne as a Combined Fluorimetric and Raman Probe for Simultaneous and Selective Sensing of Various DNA, RNA, and Proteins, Hashem Amini, Željka Ban, <u>Matthias Ferger</u>, Sabine Lorenzen, Florian Rauch, Alexandra Friedrich, Ivo Crnolatac, Adriana Kenđel, Snežana Miljanić, Ivo Piantanida*, Todd B. Marder*, *Chem. Eur. J.* **2020**, *26*, 6017.

LIST OF ABBREVIATIONS

A	acceptor
Å	Ångström (1 Å = 10^{-10} m)
Abs	absorption
APCI	atmospheric-pressure chemical ionization
Ar	aryl
ASAP	atmospheric solids analysis probe
bpy	2,2′-bipyridine
br	broad
CD	circular dichroism
CI	configuration interaction
COD	1,5-cyclooctadiene
COE	cyclooctene
CT	charge transfer
CV	cyclic voltammetry
D	donor
d	doublet
dba	dibenzylidene acetone
DFT	densityfunctional theory
DMF	dimethylformamide
DMSO	dimethyl sulfoxide
DNA	deoxyribonucleic acid
dtbpy	4,4'-di-*tert*-butyl-2,2-dipyridyl
EDOT	3,4-ethylenedioxythiophene
Em	emission
eq	equivalents
FLP	frustrated Lewis pair
GP	general procedure
HCl	hydrochloric acid
HOMO	highest occupied molecular orbital
HPLC	high-pressure liquid chromatography
i	iso
ICD	induced circular dichroism
ICT	intramolecular charge

IRF	instrument response transfer
k_r	radiative decay rate
k_{nr}	non-radiative decay rate
LE	locally excited
LUMO	lowest unoccupied molecularorbital
m	multiplet
MeCN	acetonitrile
Mes	mesityl, 2,4,6-trimethylbenzene
MS	mass spectrometry
NIR	near-infrared
NMR	nuclear magnetic resonance
pin	pinacolato
q	quartet
RNA	ribonucleic acid
ROS	reactive oxygen species
r.t.	room temperature
S	singlet
s	singlet
SERS	Surface-Enhanced Raman Scattering
sPhos	2-dicyclohexylphosphino-2′,6′-dimethoxybiphenyl
T	triplet
t	triplet
t	*tert*
TD-DFT	time-dependent density functional theory
THF	tetrahydrofuran
TLC	thin-layer chromatography
UV	ultraviolet
Vis	visible
Xyl	xylene, 2,6-dimethylbenzene

TABLE OF CONTENTS

CHAPTER 1

-

SYNTHETIC APPROACHES TO TRIARYLBORANES

FROM 1885 TO 2020

1 Synthetic Approaches to Triarylboranes from 1885 to 2020

1.1 Introduction

Within the last few decades, compounds containing three-coordinate boron motifs have found increasing applicability in various fields including optoelectronics,[1-3] selective sensors for anions[4-6] or small molecules,[7, 8] and bioimaging agents[9-15] due to the empty p-orbital at the boron center. Whereas numerous compounds and their potential applications have been reviewed by several groups,[16-23] synthetic methodology for the preparation of triarylboranes has been reviewed only rarely. In 1956, a summary by Lappert, *et al.* gave a very general overview of the syntheses of many different types of organoboron compounds.[24] Very recently, Melen and co-workers summarized synthetic pathways to halogenated triarylboranes as well as their use in catalysis and frustrated Lewis pair (FLP) chemistry.[25] This review presents developments in the synthesis of triarylboranes since their first report in 1885.[26]

In theory, it is possible to synthesize 3-fold symmetric triarylboranes bearing one type of aromatic system (BAr_3) as well as those containing two or three different aromatic systems (BAr_2Ar' or $BArAr'Ar''$). Furthermore, their synthesis should be possible from all known boron trihalides. Recently, the synthesis of triarylboranes from potassium aryltrifluoroborates[27-31] and boronic esters[32] was reported. Dibenzoboroles[33] or boron containing poly-aromatic hydrocarbons (B-PAHs)[34-36] are not discussed in this review as both topics have been reviewed recently.

This review is divided into sections based on symmetrically- (BAr_3, BAr_2Ar') and unsymmetrically-substituted ($BArAr'Ar''$) triarylboranes depending on the starting material used as the boron source. In this context, the term unsymmetrically-substituted triarylboranes means that the boron center is bound to three different aromatic systems. Symmetrically-substituted triarylboranes bear one or two different types of aromatic groups as indicated in parentheses (*vide infra*) and, thus, have either (exact or approximate) 3-fold or 2-fold symmetry, respectively.

1.2 Synthesis of Symmetrically-Substituted Triarylboranes

1.2.1 Boron Trichloride, Tribromide and Boronic Esters as Boron Sources

In 1880, Michaelis and coworkers began to investigate arylboranes to determine the valency of boron which was, at the time, debated to be three or five.[37] They reacted gaseous BCl_3 with diphenylmercury at elevated temperatures in a sealed tube and observed the formation of

dichlorophenylborane **1** and $HgCl_2$ (**Scheme1**). Compound **1** was isolated *via* distillation and was characterized by elemental analysis and conclusive follow-up chemistry.

$$3 \; BCl_{3 \; (g)} \;+\; HgPh_2 \xrightarrow{180 - 200 \; °C} \underset{1}{\text{BCl}_2} \;+\; HgCl_2$$
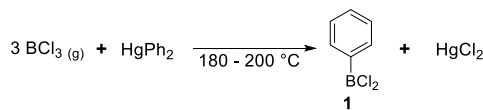
Scheme 1. Synthesis of dichlorophenylborane **1** from BCl_3.[37]

After addition of different aqueous solutions, they obtained phenylboronic acid, the respective ethyl ester and the sodium, calcium and silver salts of the acid, as well as their *p*-tolyl analogues.[38] On an interesting side note, phenylboronic acid, as well as its sodium salt, were also investigated for their antiseptic behavior, and were consumed by humans on a gram scale without causing any considerable complaints.[38] In 2015,[39] a series of boronic acids and esters were tested using the Ames assay,[40, 41] and most of them were found to be mutagenic. Thus, this class of compounds should be treated with appropriate care and due testing should be performed prior to use in humans, although several boronic acids or related compounds have been approved for use as drugs.[39]

In a different approach, Michaelis and coworkers developed a procedure to generate triphenyl derivatives of various main group elements (M), namely phosphorus, arsenic, antimony, and boron.[42, 43] The respective MCl_3 compound was reacted with a phenylhalide and elemental sodium at low temperature to generate the corresponding triphenyl compound according to **Scheme 2**.

$$MCl_3 \;+\; 3 \; PhX \;+\; Na \xrightarrow[\text{cooled with water bath}]{\text{Et}_2\text{O or benzene,}} \underset{M = B: \; \mathbf{2}}{M} \;+\; 6 \; NaX$$

M = P, As, Sb, B
X = Br, Cl
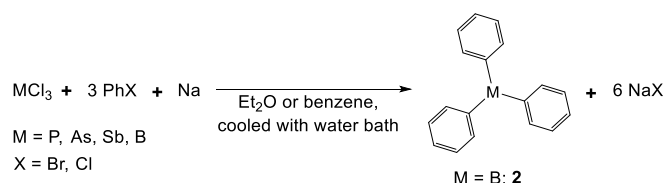
Scheme 2. Synthesis of triphenyl derivatives of main group elements.[26, 42, 43]

In 1885, Michaelis and coworkers mentioned that, *via* this general route, a small amount of triphenylborane **2** was obtained, but it was not discussed further.[26] Presumably, this was the first literature report of the synthesis of a triarylborane. Four years later, the synthesis of **2** was improved by reacting dichlorophenylborane **1** with chlorobenzene and sodium.[44] This time, compound **2** was characterized by elemental analysis and the appearance of a green flame characteristic of boron[45] when burning the compound.

In 1889, Gattermann and coworkers reported a convenient method for the synthesis of BCl_3.[46] Thus, access to the starting material was facilitated. Therefore, Michaelis *et al.* synthesized more dichloroarylboranes and their respective boronic acids, namely the *o*-tolyl, *α*-naphthyl, *β*-

naphthyl, p-methoxyphenyl, *o*-methoxyphenyl and *p*-ethoxyphenyl *derivatives.[47]* For the latter three compounds, the reaction proceeded smoothly at room temperature. Furthermore, chlorodiphenylborane **3** and its borinic acid derivative were reported and characterized. Compound **3** was formed by reacting dichlorophenylborane with diphenylmercury at ca. 300 °C in a sealed tube (**Scheme 3**). It was noted that triphenylborane **2** was not obtained this way.
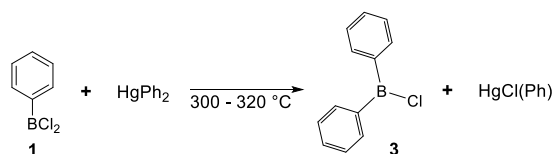
Scheme 3. Synthesis of chlorodiphenylborane **3** under harsh conditions.[47]

In 1901, Michaelis and coworkers reported an improved method for the synthesis of mono- and diarylboranes in which they replaced gaseous BCl_3 with liquid and, thus, easier to handle BBr_3 as the boron source.[48] For this purpose, they developed a convenient and large-scale synthesis of BBr_3 from elemental boron and bromine. BBr_3 was then reacted with diphenylmercury in dry benzene. The reaction was performed in a flask with a reflux condenser at 80 °C. Depending on the stoichiometry, dibromophenylborane **4** and bromodiphenylborane **5** were synthesized and isolated *via* distillation. Some derivatives, namely dibromo-*p*-tolylborane, dibromo-2,4-dimethylphenylborane, and dibromo-2,4,5-trimethylphenyl were synthesized and characterized, accordingly. The respective boronic and borinic acids were obtained and characterized after hydrolysis. Again, it was mentioned that, despite extensive studies in this direction, triphenylborane could not be isolated. They assumed that triphenylborane had been formed, but complete separation from diphenyl impurities could not be achieved.
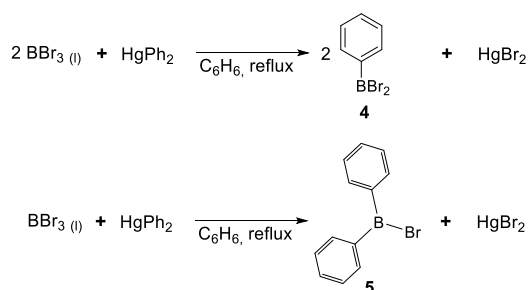
Scheme 4. Synthesis of mono- and diarylboranes, starting from BBr_3.[48]

Another difficulty of arylborane syntheses were the often laborious and multi-step syntheses of the required diarylmercury compounds. With the discovery of the Grignard reagent in 1900, a powerful tool for the transfer of aryl groups became available.[49] The first to utilize this in arylborane chemistry, were Khotinsky and Melamed.[50] They reacted various alkylborate esters with an aryl Grignard reagent in a cold Et_2O solution. The best results were obtained for

the *iso*butylborate ester. Furthermore, Khotinsky and Melamed characterized the phenylboronic *iso*-butyl ester and the *m*-tolylboronic *iso*-butyl ester, as well as the respective boronic acids after saponification. In an attempt to attach two arenes to the boron using Grignard reagents, Strecker reacted an excess of phenyl magnesiumbromide with BCl_3, but obtained only phenylboronic acid after aqueous work up.[51] A more extensive study of the reactions of aryl Grignard reagents with the *iso*-butylborate ester was carried out by König and Scharrnbeck in 1915. The results were reported in 1930.[52] They characterized several novel arylboronic acids and diarylborinic acids which were synthesized according to **Scheme 5** and isolated after aqueous work-up indicating that the organometallic reagent used was too unreactive to form the corresponding triarylborane. More than 70 years later, it was demonstrated by several groups that triarylboranes can also be synthesized using boronic esters as starting materials and more reactive organometallic reagents (*vide infra*).[39, 53-58]

$$B(OiBu)_3 \xrightarrow[\text{cold Et}_2\text{O}]{\text{ArMgX}} \begin{array}{c} ArB(OH)_2 \\ or \\ Ar_2BOH \end{array}$$
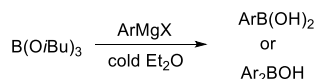
Scheme 5. Synthesis of boronic acids and borinic acids, starting from *iso*-butylborate ester.[52]

1.2.2 Boron Trifluoride as the Boron Source

Despite reports of the synthesis of triphenylborane,[26, 44] reproducible synthetic access was only available for mono- and diarylboranes in the beginning of the 20th century. This changed with the studies of Krause, who made use of the synthesis of gaseous borontrifluoride (BF_3) from boric anhydride (B_2O_3), sulfuric acid (H_2SO_4) and potassium tetrafluoroborate (KBF_4), reported by Schiff *et al.*[59] In 1921, Krause and coworkers used gaseous BF_3 in combination with Grignard reagents to yield trialkylboranes as well as alkylboronic acids.[60] Subsequently, Krause *et al.* applied this method for the synthesis of triphenylborane **2**.[61]

$$B_2O_3 + KBF_4 \xrightarrow{\text{1. H}_2\text{SO}_4} BF_{3\,(g)} \xrightarrow[\text{Et}_2\text{O, reflux}]{\text{2. PhMgBr}}$$
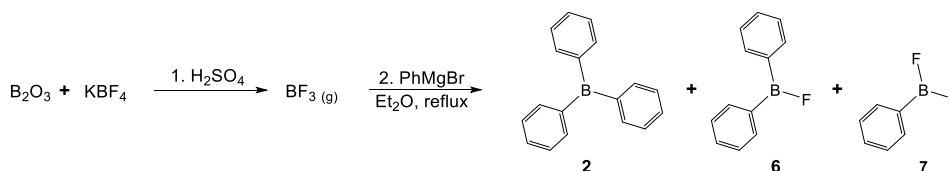
Scheme 6. Synthesis of the first reported triarylborane **2** according to Krause *et al.*[61]

They isolated BPh_3 **2** by distillation of the crude reaction mixture in ca. 50% yield. The product crystallized easily, but it was also mentioned that **2** decomposes in air. Furthermore, Krause and coworkers observed the formation of phenyldifluoroborane **6** as well as

diphenylfluoroborane **7**, but the isolation of these two compounds was not possible by distillation. This indicates that the reactivity of the Grignard reagent is insufficient to generate only BPh₃, as byproducts **6** and **7** were observed. However, with BPh₃ **2** in hand, the group investigated its reactivity with neat sodium[62] and the other alkali metals potassium, lithium, rubidium and cesium.[63] Krause and coworkers observed the formation of intensely colored solutions as well as the formation of, mostly, yellow crystals. Both solutions and solids were reported to be highly air sensitive, as the solutions turned colorless when exposed to air. The colorless solution was converted into the colored solution again if neat metal was still present in the solution. After Krause and coworkers had isolated the reaction product of BPh₃ **2** with neat sodium,[63] they titrated the reaction product under a nitrogen atmosphere with elemental iodine which regenerated BPh₃ and sodium iodide. In the same study, the synthesis of tri-*p*-tolylborane **8** was mentioned. Its final synthesis and full characterization were reported two years later.[64] Again, the reactivity of **8** with sodium and potassium was investigated as well as its reaction with nitrogenous based bases such as ammonia, pyridine, and piperidine. The reaction of **8** with neat sodium was described to be the same as for **2**. During the reactions of **8** with nitrogenous based bases, the group observed a temperature increase of the reaction mixture as well as the formation of crystalline and more air-stable products which were assigned to be addition products of the nitrogenous based base with **8**. This assumption was confirmed by elemental analysis of the reaction products. In 1930, Krause and coworkers also reported the synthesis of tri-*p*-xylylborane **9** and tri-*α*-napthylborane **10**, which were investigated similarly to the previous compounds **2** and **8**.[65] For the isolation of **9** and **10**, the work up was slightly modified. Thus, to quench the remaining Grignard reagent, water was added and the resulting crude mixture was distilled with exclusion of air, as none of the previously synthesized triarylboranes are stable to air.
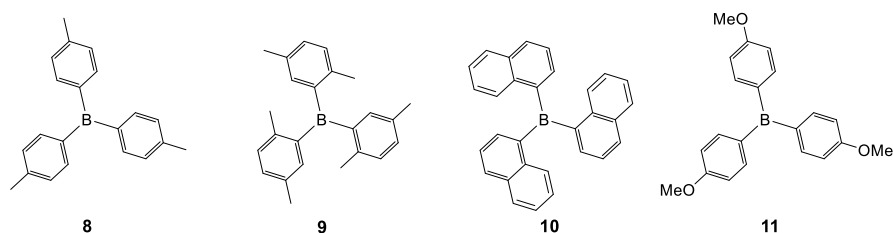
Scheme 7. Structures of compounds **8-11**.[64-66]

Nevertheless, what they refer to as an "oxidation process" of compound **10** starts only after two weeks in air. Furthermore, Krause *et al.* reported that solutions of **10** in benzene, chloroform, tetrachloromethane, carbon disulfide, and diethyl ether show a light blueish fluorescence that was more clearly visible with a quartz lamp. They did not provide any further information regarding what kind of lamp or which wavelength they used for excitation. Furthermore, the observed fluorescence was not investigated in detail. In 1931, the same

group reported another triarylborane, namely tri-*p*-anisylborane **11**, which was found to be as air-sensitive as triphenylborane **2**.[66] In addition, Krause *et al.* had to change their work up once again, as they could not isolate **11** in pure form from the crude reaction mixture. Therefore, they reacted a crude mixture of **11** with gaseous ammonia to form the corresponding tetra-coordinate Lewis acid-base adduct which was then purified and subsequently reacted with sulfuric acid with exclusion of air to yield compound **11**.

Based on this work, Brown *et al.* re-synthesized tri-*α*-naphthylborane **10** as a reference Lewis acid to estimate the Lewis base strength of primary, secondary, and tertiary amines,[67] having slightly modified the synthesis of the triarylborane. To make the synthesis safer, Brown and coworkers used boron trifluoride etherate (BF$_3$·OEt$_2$) instead of gaseous boron trifluoride. Furthermore, they found that the triarylborane they synthesized was stable to air for more than one year. As this finding was in contrast with the reports of Krause *et al.*,[65] Brown *et al.* had a closer look into the geometry of the compound. They assigned the discrepancy between their and the earlier results to the existence of two possible rotational conformers, i.e., steric hindrance resulted in restricted rotation around the B-C bonds.

In 1947, Wittig *et al.* investigated the possible application of triphenylborane **2** as a catalyst for the lithiation of hydrocarbons.[68] Instead of successful catalysis of the reaction, they found the formation of a stable complex which was later identified as lithium tetraphenylborate **12-Li**.[69] Further investigations of such compounds, especially the reaction of sodium tetraphenylborate **12-Na** with various mono-cationic elements in aqueous solution, led to the discovery of an almost insoluble complex **12-K** formed after addition of potassium salts. Later on, compound **12-Na** became commercially available as Kalignost® for the quantitative analysis of potassium in aqueous solution.[70]
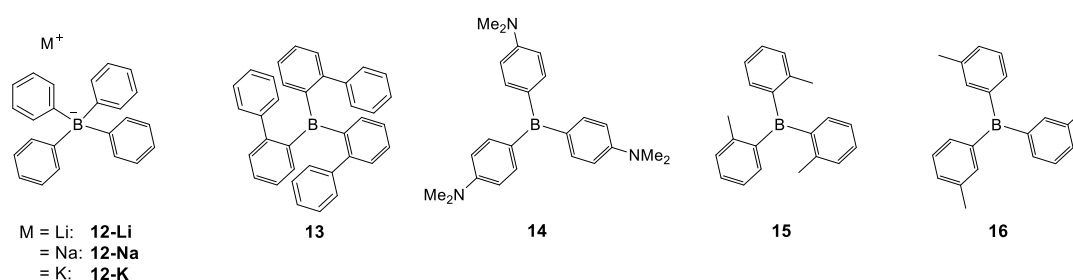
Scheme 8. Structures of compounds **12-16**.[69, 70]

Wittig and coworkers found that triarylboranes such as **2** can also be synthesized from the corresponding, more reactive lithiated species instead of the Grignard reagent.[69] As long as it was possible to synthesize the desired compounds from Grignard reagents and BF$_3$ etherate, they did so. But for tri(*o*-diphenylyl)- **13** and tri(4-(*N*,*N*-dimethylamino)phenyl)borane **14**, Wittig *et al.* used the corresponding aryllithium reagent.[70] Nevertheless, the synthesis of **14** was still

challenging, as the amine formed complexes with excess BF_3. Furthermore, this group reported a yellowish fluorescence from **14** in the solid state as well as a blue fluorescence in acetone upon irradiation with UV light. Compounds **15** and **16** were described as having a yellowish-white fluorescence upon UV-irradiation. None of these observations were further explained or investigated by Wittig *et al*. Very recently, Marder and co-workers reported that a sample of pure **16** showed only blue fluorescence, with no phosphorescence being observed at room temperature.[71]

In 1956, Lappert summarized the preparation, chemical and physical properties, reactivities, etc. of almost all organo-boranes that had been synthesized up to that date.[24] In this summary, several methods to synthesize monohaloboranes as well as unsymmetrically-substituted diaryl borinic esters were described. However, almost none of these syntheses were utilized for the formation of triarylboranes, especially not for the formation of boranes bearing three different aromatic systems.

One year later, Brown *et al*. reported the synthesis of the sterically-demanding trimesitylborane **17** from the corresponding Grignard reagent and BF_3 etherate.[72] The group heated the reagents in toluene under reflux for 4 h which they described as forcing conditions. If the reaction was stopped after 2 h, only fluorodimesitylborane **18** was isolated showing once again that the formation of triarylboranes from Grignard reagents is possible, but requires heat to achieve completion due to the lower reactivity of arylmagnesium reagents compared to, *e.g.,* aryllithium reagents. Furthermore, Brown and coworkers examined the reactivity of **17** with amines as well as its decomposition with water and oxygen. It was found that **17** was less reactive than tri-α-naphthyl- **10** or triphenylborane **2** due to its greater steric hindrance.
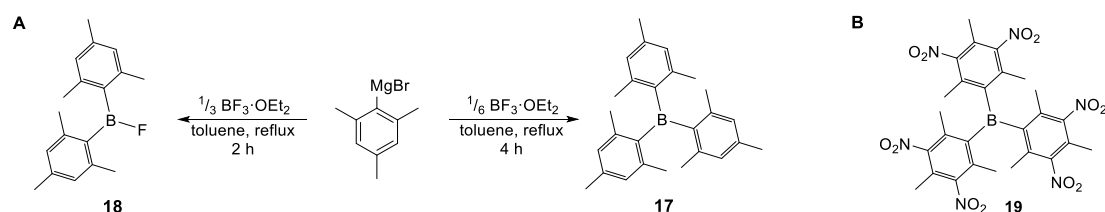
Scheme 9. A) Reaction sequences for the synthesis of compounds **17** and **18**.[72] B) Structure of compound **19**.[73]

Subsequently, the syntheses of compounds **17** and **18** were further improved by Hawkins *et al*.[73] who changed the solvent for the formation of the Grignard reagent from diethyl ether to THF according to a general procedure reported by Ramsden *et al*.[74] This change resulted in a shorter reaction time for the formation, as well as an increased yield, of the Grignard reagent. In addition, this led to the isolation of fluorodimesitylborane **18** in 96% yield. Due to its steric hinderance, the reaction of excess mesityl Grignard reagent with BF_3 etherate at 55 °C stops at the fluorodimesitylborane stage as long as the reaction time is shorter than 2 h. Furthermore, Hawkins and coworkers were able to nitrate **17** to yield compound **19**.

In 1967, at Eastman Kodak, Grisdale and coworkers began to investigate the photophysical reactions of tetraaryl borates and triarylboranes in solution.[75] They again found trimesitylborane **17** to be more stable than triphenylborane **2**. To investigate further the influence of different substituents on the stability of triarylboranes, Grisdale *et al.* had a closer look at the influence of the *para*-substituent in various dimesitylphenylboranes.[76] To synthesize a variety of these new triarylboranes **20**, this group was the first to combine the methods previously developed by different groups. First, Grisdale and coworkers isolated fluorodimesitylborane **18** as reported by Brown.[72] This fluoroborane was then added to a lithiated species prepared from the corresponding halogenated aromatics yielding **20a-e** in 40 - 90%, as Wittig *et al.* had found lithium reagents to be suitable to react with boronhalides.[69] This reaction sequence reflects the different reactivities of Grignard and organolithium reagents. Grisdale *et al.* also conducted one of the first systematic investigations of the photophysical properties of the new triarylboranes in various solvents, observing emission solvatochromism, suggesting the stabilization of charge transfer excited states in polar solvents.
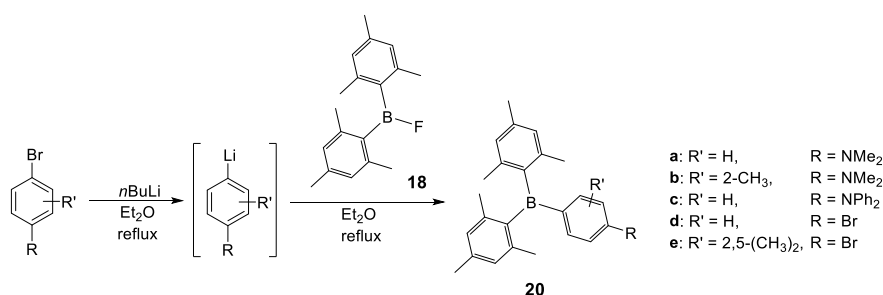
Scheme 10. Synthetic route to symmetrically-substituted triarylboranes **20a-e** reported by Grisdale *et al.*[76]

1.2.3 Metal-Boron Exchange Reactions for the Synthesis of Triarylboranes

To date, the most widely used method for the synthesis of triarylboranes is the procedure developed by Grisdale and coworkers (**Scheme 10**)[76] i.e., reaction of BF_3 with either Grignard reagents or lithium reagents as discovered by Krause *et al.*[61] and Wittig *et al.*,[69] respectively. However, mercury, zinc, copper, silicon, and tin reagents have also been employed in the synthesis of triarylboranes with different reactivities, solvent compatibilities, stabilities, and accessibilities of these organometallic reagents. Furthermore, while mercury and tin reagents are not widely used currently due to their toxicities, other safety aspects may dominate the choice of organometallic reagent, depending on the organic group to be transferred..

Arylmercury compounds were the first ArM reagents to be used for the synthesis of arylboranes (*vide supra*), but apart from a few reports on arylboronic acid syntheses,[77, 78] they have

generally been replaced by Grignard or organolithium reagents. However, in 2001, Piers and coworkers obtained the diborylated ferrocene compound **21** by reacting 1,1'-Fc(HgCl)$_2$ with ClB(C$_6$F$_5$)$_2$ (**Scheme 11A**).[79] The same group made use of Hg-B exchange to generate the diborylated compound **22**, which was then converted into a triarylborane *via* Zn-B exchange (**Scheme 11B**).[80] A year before, they reported Zn(C$_6$F$_5$)$_2$ as a potential C$_6$F$_5$ transfer agent, which reacted with BCl$_3$ to generate inseparable mixtures of mono-, di- and triarylboranes.[81]
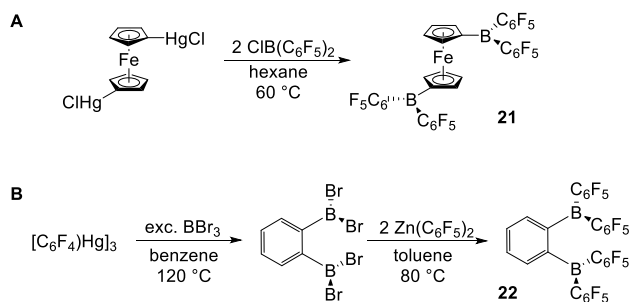
Scheme 11. A) Hg-B exchange reaction by Piers and coworkers.[79] **B**) Sequential Hg-B and Zn-B exchange reaction by Piers, Collins, Marder and coworkers.[80]

In 2003, Jäkle *et al.* demonstrated the applicability of arylcopper reagents in Cu-B exchange reactions.[82] Using mesitylcopper, a maximum of two arenes were attached even when the reaction with BX$_3$ (X = Cl, Br) was heated to 100 °C, or when dichlorophenylborane **1** was used as the starting material to decrease the steric demand around the boron. Reaction of C$_6$F$_5$Cu with BX$_3$ at room temperature gave B(C$_6$F$_5$)$_3$ **23** irrespective of stoichiometry (**Scheme 12A**). Pentafluorophenylcopper was also employed by Ashley, O'Hare and coworkers as an aryl transfer reagent for the synthesis of triarylboranes **24** and **25** (**Scheme 12B, C**) and, in one case, they made use of a Zn-B exchange to form the dibromoarylborane precursor (**Scheme 12B**).[83]
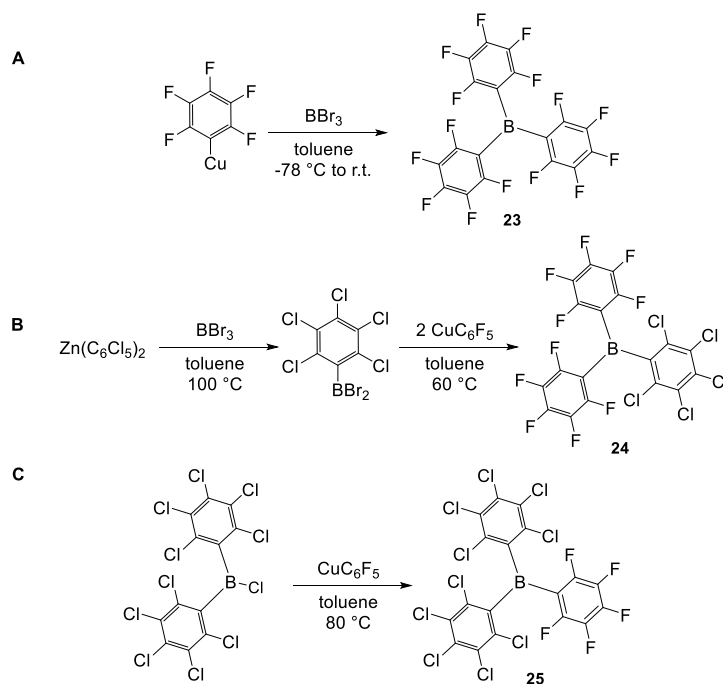
Scheme 12. Triarylborane formation using CuC$_6$F$_5$ as an aryl transfer reagent by Jäkle and coworkers and O'Hare and coworkers, respectively.[82, 83]

Later, Jäkle and coworkers demonstrated that 2,4,6-tri*iso*-propylphenylcopper (CuTip) could also be employed in Cu-B exchange reactions. Thus, CuTip was reacted with sterically unhindered bromodiarylboranes to add the third arene to the boron center,[84, 85] and these triarylborane precursors were used in the formation of organoborane macrocycles and borazine oligomers.

Apart from Grignard and lithium reagents, the most widely used substrates for exchange reactions with boron are organosilanes and organotin reagents. Aryltin reagents were used in Sn-B exchange reactions in the 1960s. In a first approach by Burch *et al.*, the phenyl groups of SnPh$_4$ were transferred to BCl$_3$ to give compound **1**.[86] Reaction of SnPh$_4$ with BCl$_3$ in CH$_2$Cl$_2$ transferred one of the four phenyl rings from tin to boron. Without the use of solvent, and under reflux conditions, all four rings were transferred (**Scheme 13A**). In 1970, a more selective method was reported by Chivers, who synthesized *ortho*-substituted monoarylboranes from the corresponding monoaryltrimethylsilanes according to **Scheme 13B**.[87] Halogen exchange between BCl$_3$ and the *ortho*-trifluoromethylgroup was observed.
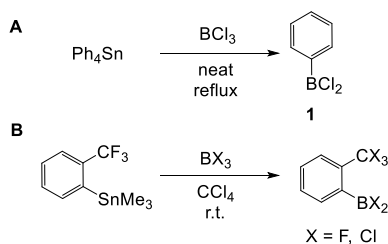
Scheme 13. Formation of monoarylboranes *via* Sn-B exchange by Burch *et al.* and Chivers, respectively.[86, 87]

In 2005, Jäkle and coworkers reported the synthesis of triarylborane-containing polymers *via* Sn-B exchange,[88] reacting a distannylated bithiophene precursor with different dibromoarylboranes to obtain the respective polymers (**Scheme 14**).
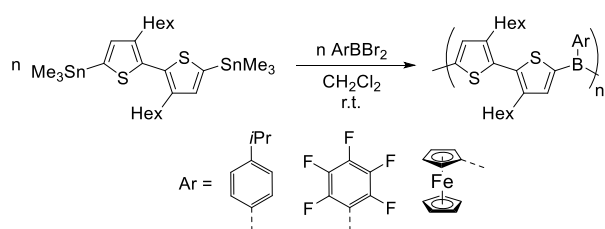
Scheme 14. Formation of triarylborane containing polymers *via* Sn-B exchange.[88]

Based on this procedure, many different triarylborane containing polymers and also triarylborane model compounds were synthesized.[89, 90]

In 1986, Haubold and coworkers reported the synthesis of several mono- and diarylboranes *via* Si-B exchange.[91] The exchange reaction was tolerant to some functional groups, and even an unsymmetrically-substituted ArAr'BBr compound was generated (**Scheme 15**). Starting from BBr$_3$, 35% of triphenylborane **2** was formed under harsh reaction conditions, whereas starting from BCl$_3$ gave the monoarylboranes exclusively.
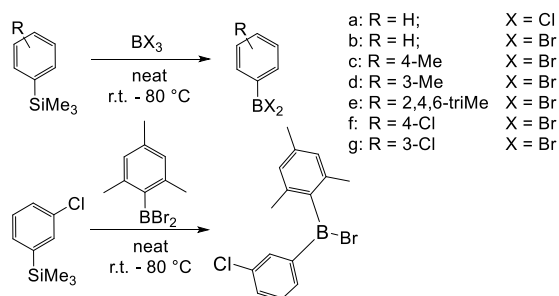
Scheme 15. Si-B exchange reactions reported by Haubold and coworkers.[91]

Further studies as well as potential applications were reported one year later by Kaufmann *et al.* [92, 93] and Snieckus *et al.*[94] Jäkle and co-workers reported an efficient method for the introduction of a triarylborane moiety into the side chain of polystyrene.[95, 96] The first step

involved Si-B exchange and, in the next step, the triarylborane was formed *via* Sn-B and Cu-B exchanges, respectively (**Scheme 16**).
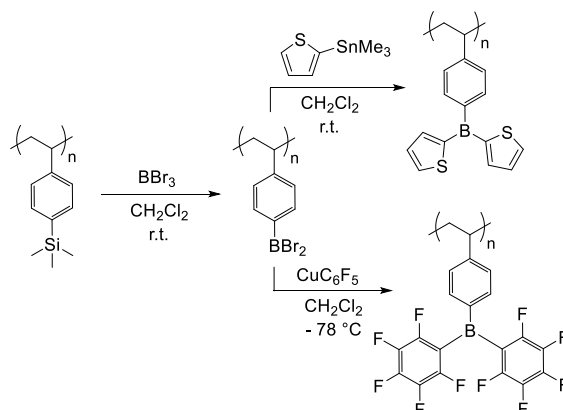
Scheme 16. Si-B exchange reaction followed by Sn-B or Cu-B exchange for triarylborane formation by Jäkle and coworkers.[95, 96]

More recently, Helten and coworkers improved the Si-B exchange reaction significantly by employing a catalytic amount of Me$_3$SiNTf,[97] synthesizing three triarylboranes *via* Si-B exchange and subsequent Li-B exchange reactions (**Scheme 17**). Helten and coworkers employed this method for the synthesis of triarylborane-containing macromolecules and polymers. In each case, the third arene was attached to the boron using an aryl lithium reagent.[98, 99]
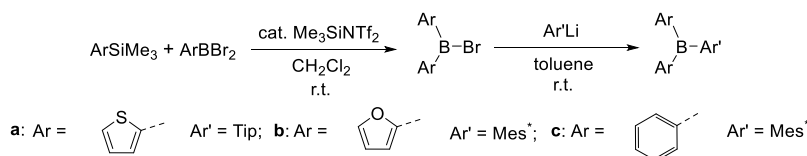
Scheme 17. Catalyzed Si-B exchange followed by Li-B exchange for triarylborane formation.[97]

1.2.4 Potassium Aryltrifluoroborates as Boron Sources

Potassium aryltrifluoroborates (ArBF$_3$K salts) have been known since 1960.[100] Chambers *et al.* reported the synthesis of potassium (trifluoromethyl)trifluoroborate from a boiling, aqueous solution of trimethyltin (trifluoromethyl)trifluoroborate and potassium fluoride (**Scheme 18A**). In 1963, Stafford reported the synthesis of a potassium vinyltrifluoroborate that was isolated in a similar way to that previously described by Chambers.[101] Two years later, Chambers reported the synthesis of an aromatic potassium trifluoroborate **26** which was obtained from reaction of (pentafluorophenyl)difluoroborane and potassium fluoride (**Scheme 18B**).[102] In 1967, Thierig and Umland reported the synthesis of potassium phenyltrifluoroborate **27** from Flavognost® and potassium bifluoride (**Scheme 18C**).[103]
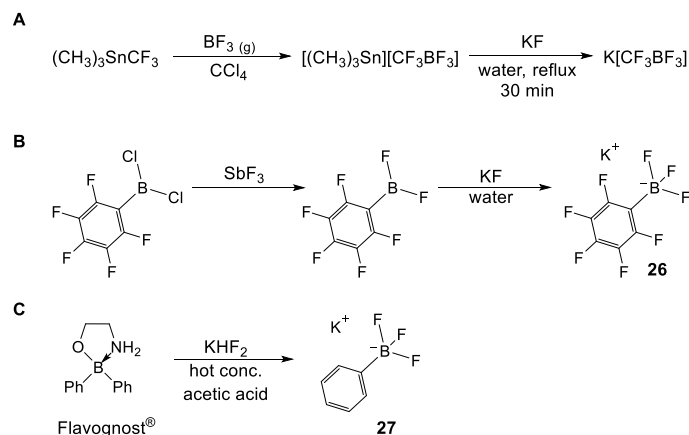
Scheme 18. Synthetic pathways to potassium trifluoroborates by Chambers, Stafford, and Thierig, respectively.[100, 102, 103]

About 20 years later, Kaufmann and coworkers made use of the solubility of potassium fluoride in acetonitrile to convert $RBBr_2$ compound into their RBF_2 analogues or the corresponding potassium trifluoroborates (**Scheme 19A**).[104] They also found $BF_3 \cdot OEt_2$ to be a suitable reagent to convert the latter salts *in situ* into RBF_2 compounds.
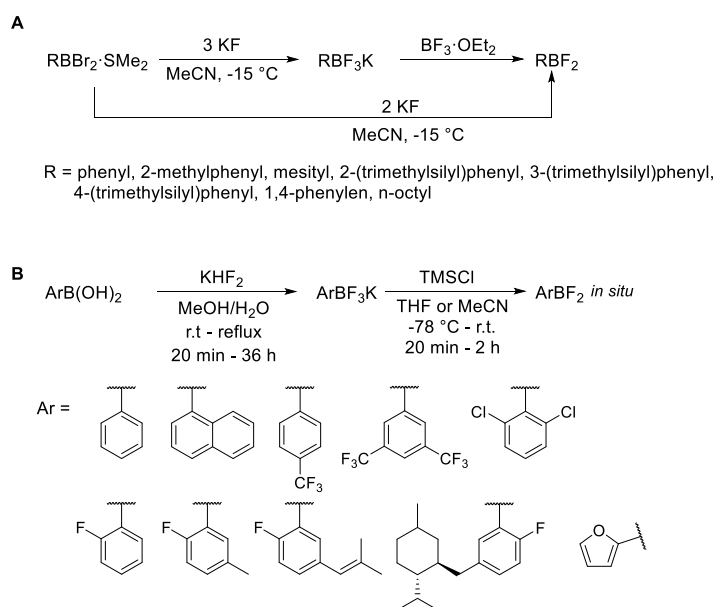
Scheme 19. A) Conversion of aryldibromoboranes to potassium aryltrifluoroborates or aryldifluoroboranes.[104] **B**) A convenient route to potassium aryltrifluoroborates and their activation reactions.[105]

Another way to activate potassium aryltrifluoroborates was reported by Vedejs in 1995,[105] who showed that potassium aryltrifluoroborates can be activated *in situ* to form aryldifluoroboranes by addition of trimethylsilyl chloride (TMSCl). Furthermore, they provided a convenient route to potassium aryltrifluoroborates from the corresponding boronic acids and potassium bifluoride, KHF_2 (**Scheme 19B**).

To date, BF$_3$K salts are mostly employed in reactions in which the boron motif is lost, *e.g.* in coupling reactions.[106] However, such compounds can also be used as the boron source for the syntheses of triarylboranes.

In 2004, Morrison *et al.* were the first to synthesize triarylboranes **28** from potassium aryltrifluoroborate reagents which were activated with BF$_3$ etherate and then reacted with the Grignard reagent C$_6$F$_5$MgBr (**Scheme 20**).[27]
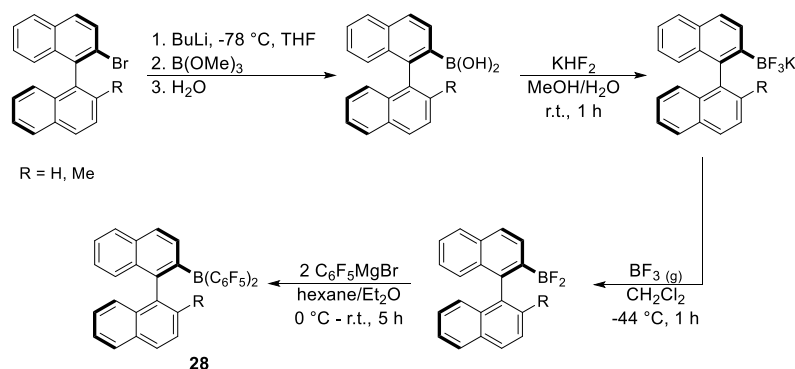
Scheme 20. First reported synthesis of triarylboranes from potassium aryltrifluoroborates.[27]

Since then, a few other groups reported the synthesis of triarylboranes from these bench-stable boron precursors. Especially for applications in frustrated Lewis pairs, this approach was used for the synthesis of triarylboranes bearing aromatic systems in which multiple fluoro- and chloro-substituents are desired. Soós and coworkers[28, 107, 108] and Hoshimoto *et al.*[109] synthesized triarylboranes **29**-**35** from potassium aryltrifluoroborates and Grignard reagents without prior activation of the BF$_3$K salt. The Grignard reagents in these cases were each prepared from the corresponding brominated precursor in combination with the so called 'Turbo-Grignard' *iso*-propyl magnesium chloride (*i*PrMgCl) as summarized in **Scheme 21A**. A very similar strategy, without the use of the Turbo-Grignard, was used by Marder and coworkers to synthesize a push-pull system with a pyrene core **36** (**Scheme 22A**).[30]
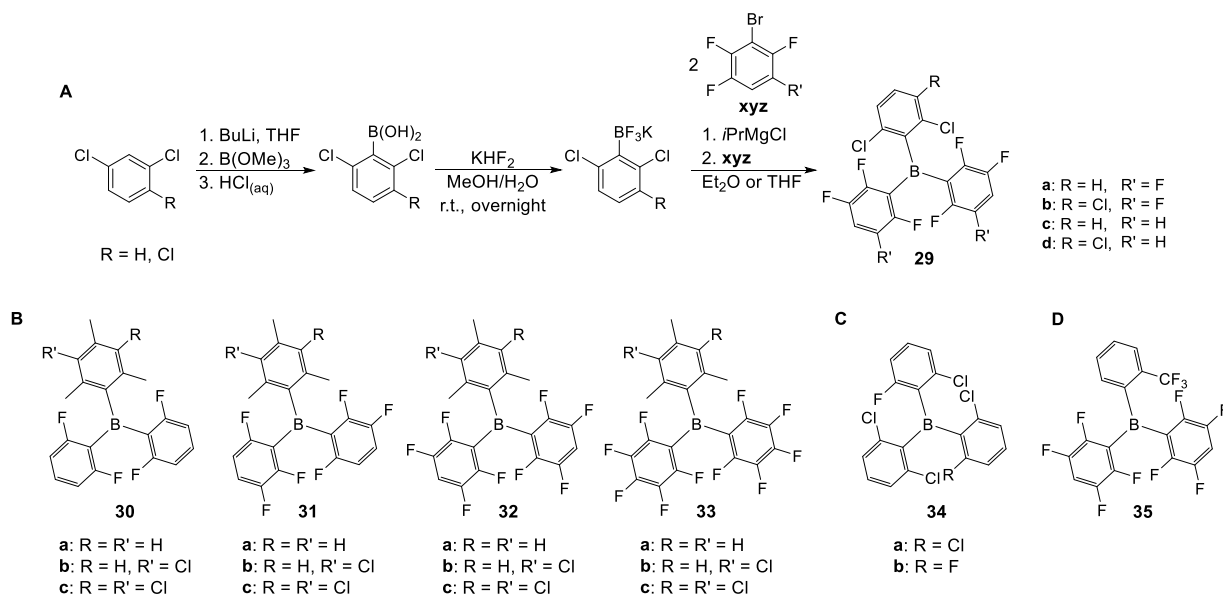
Scheme 21. A) General reaction sequence for the synthesis of multi-halogenated triarylboranes.[28] **B**,[107] **C**,[108] **D**)[109] Structures of compounds **29-35** synthesized according to Scheme **21A**.

In contrast, Wagner and coworkers synthesized triarylboranes as precursors to polycyclic aromatic hydrocarbons[29] or quadruply annulated borepins.[110] In both cases, the required triarylboranes were synthesized from potassium aryltrifluoroborates which were reacted with various aryl lithium reagents yielding compounds **37-40** (**Scheme 22B**, **C**).
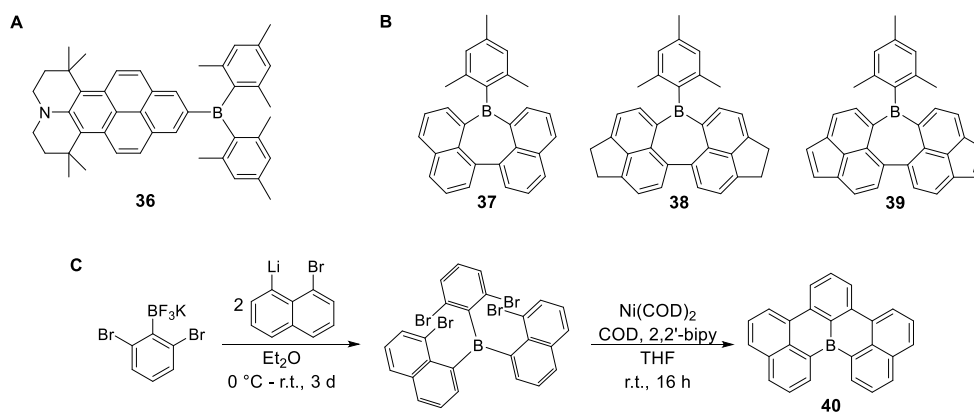
Scheme 22. A) Structure of compound **36**.[30] **B**) Structures of compounds **37-39**.[110] **C**) Synthetic route to planarized triarylboranes.[29]

1.2.5 Direct Dimesitylborylation

Ito and coworkers reported the direct dimesitylborylation of various aryl halides[111] by reaction of (diphenylmethylsilyl)dimesitylborane with aryl halides in the presence of a base (**Scheme 23A**). The halide was replaced by boron or silicon in a ratio of ca. 9 to 1. Furthermore, the reaction was tolerant to several functional groups, and the resulting triarylboranes were

isolated in moderate to good yields. In 2019, the same group reported an iridium-catalyzed C–H dimesitylborylation of benzofuran using a silyldimesitylborane reagent (**Scheme 23B**),[112] preparing several derivatives and isolating the triarylboranes in moderate to good yields. Under optimized conditions, they reported the formation of the silylated side product in ca. 29% yield.
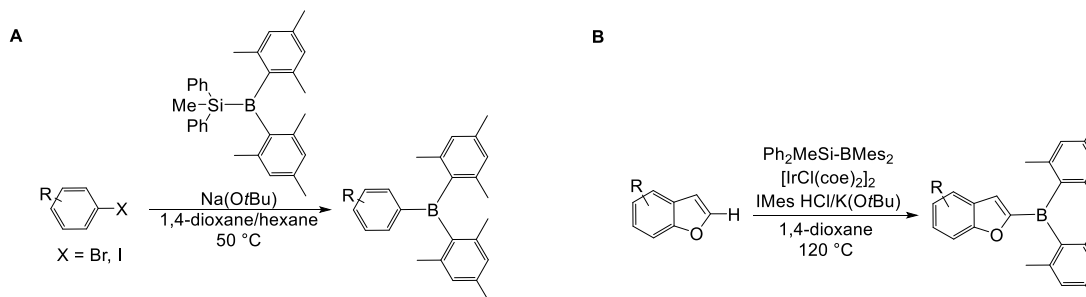
Scheme 23. A) Dimesitylborylation of aryl halides.[111] **B**) Dimesitylborylation of benzofuran derivatives.[112]

1.3 Synthesis of Unsymmetrically-Substituted Triarylboranes

Thus far, the syntheses of symmetrically-substituted BAr$_3$ and BAr$_2$Ar' triarylboranes were summarized. The synthesis of unsymmetrically-substituted BArAr'Ar'' triarylboranes bearing three different aromatic rings bound to the boron center can be achieved by different routes, most of which use the same approaches used for the syntheses of symmetrically-substituted triarylboranes. However, other routes employed symmetrically-substituted triarylboranes as precursors.

One of the first unsymmetrically-substituted triarylboranes was reported in 1971 by Grisdale *et al.* at Eastman Kodak.[113] As mentioned above, this group investigated the photolysis of triarylboranes and tetraarylborates. During these studies, they observed an organoboron compound, formed after irradiation of potassium dimesityldiphenylborate, which contained three different aromatic systems bound to the boron center.

1.3.1   Boronic Esters as Boron Sources

In 1955, Letsinger and coworkers reported the synthesis of the first unsymmetrically-substituted borinic acid starting from a boronic ester.[114] They reacted phenylboronic acid butyl ester with *α*-naphthylmagnesium bromide and isolated the borinic acid as its *β*-aminoethyl ester, which was readily hydrolyzed to the borinic acid (**Scheme 24**). They also demonstrated that the synthesis works when the aryl starting materials are switched to *α*-naphthylboronic acid butyl ester and phenylmagnesium bromide, respectively, but the product was not used for the synthesis of a BArAr'Ar'' triarylborane.
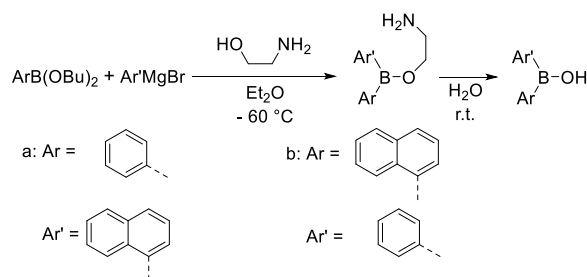
Scheme 24. Synthesis of an unsymmetrical borinic acid by Letsinger and coworkers.[114]

In 1958, Mikhailov *et al.* reported the sequential synthesis of unsymmetrically-substituted triarylboranes[115] (**Scheme 25**) starting from an *iso*-butyl borinic ester wherein the boron atom is additionally bound to one phenyl and one chlorine atom, respectively. In the first step, the chlorine atom was substituted by an *o*-tolyl group introduced from a Grignard reagent. In the second step, the *iso*-butyl substituent was converted to a chlorid *via* reaction with PCl_5. The chlorine atom was subsequently substituted by other arenes introduced from Grignard reagents yielding two different unsymmetrically-substituted triaryboranes (**41** and **42**). Mikhailov and coworkers reported the synthesis of two other borinic acids (**43** and **44**), but their conversion to unsymmetrically-substituted triarylboranes was not described.
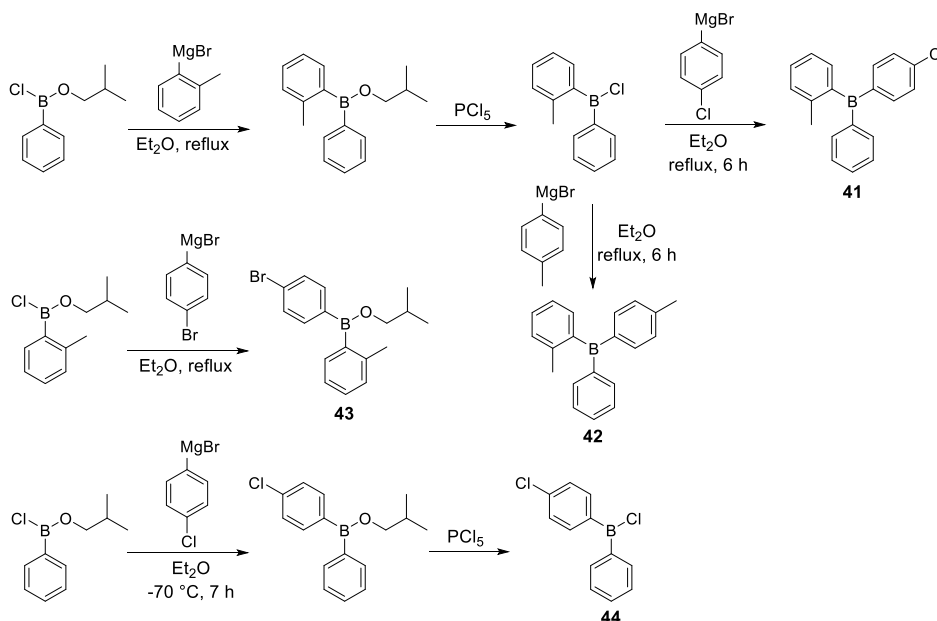
Scheme 25. Syntheses of unsymmetrically-substituted triarylboranes **41** and **42**.[115]

Recently, Liu *et al.*[7, 116] synthesized the unsymmetrically-substituted triarylboranes **46a, b** from BAr_2Ar' **45**. Compound **45** was synthesized from the boronic ester $TipB(OMe)_2$ (Tip = Tri-*iso*-propyl) which was obtained from reaction of trimethoxyborane ($B(OMe)_3$) with 2,4,6-tri-*iso*-propylphenyl magnesium bromide (TipMgBr).[117] This boronic ester was then converted to the symmetrically-substituted triarylborane **45** by reaction with a lithiated species (**Scheme 26A**).

Stepwise substitution of the bromides then yielded the unsymmetrically-substituted triarylboranes **46a, b** (**Scheme 26A**).
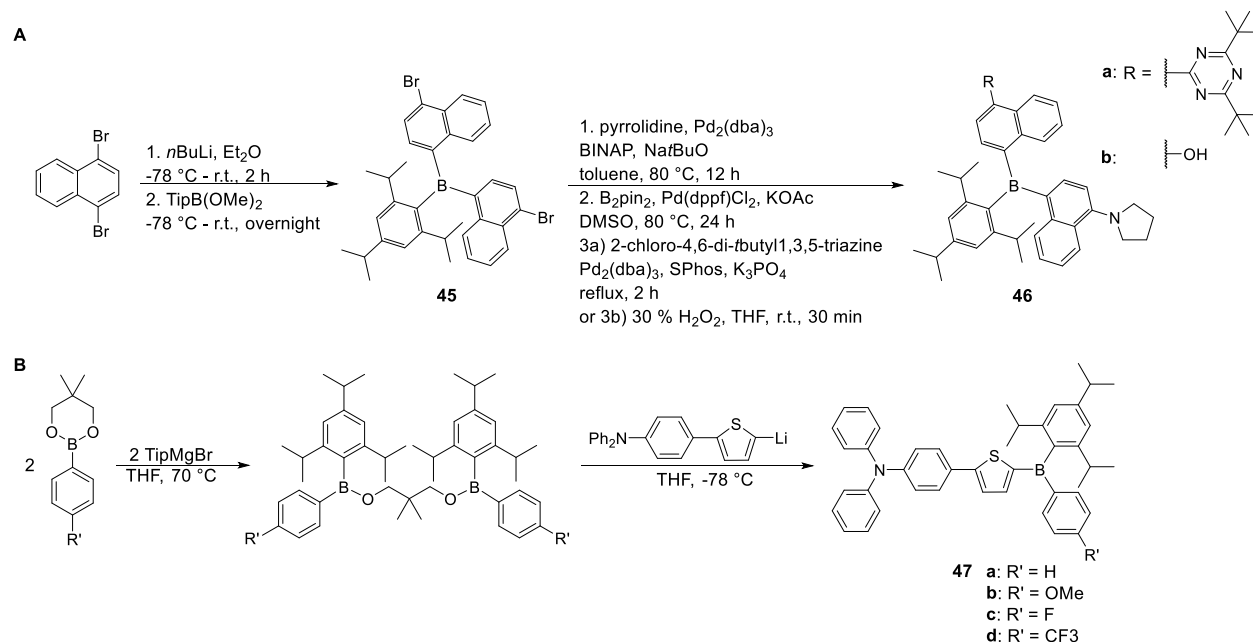
Scheme 26. A) Synthesis of unsymmetrically-substituted triarylborane **46** from a symmetrically-substituted precursor.[7, 116] **B**) Synthesis of unsymmetrically-substituted triarylboranes **47a-d** from a boronic ester.[32]

Yamaguchi and coworkers reported the synthesis of a series of unsymmetrically-substituted triarylboranes **47a-d** from a boronic ester precursor (**Scheme 26B**).[32] This was then converted with TipMgBr to a dimeric intermediate, which was cleaved by the addition of a lithiated species yielding compounds **47a-d** (**Scheme 26B**). In the same paper, Yamaguchi and coworkers reported the synthesis of a derivative of compound **47** bearing *tert*-butyl groups instead of the *iso*-propyl groups, but it was not possible to synthesize **47e** according to **Scheme 26B**. Therefore, they used a different approach starting from boron tribromide (*vide infra*, **Scheme 30B**).

1.3.2 Borane Dimethyl Sulfide as the Boron Source

In 2016, Blagg *et al.* reported the synthesis of the "first 1:1:1 hetero-tri(aryl)borane", by their own account.[118] In terms of investigating the Lewis acidity of such 'hetero-tri(aryl)boranes', they substituted the hydrogen atoms of a borane dimethyl sulfide complex stepwise with arenes (**Scheme 27**). The first aromatic groups were introduced using aryl lithium reagents. The resulting intermediate was converted to a borinic acid with methanol and was then activated with BBr$_3$ for reaction with an organozinc reagent yielding the unsymmetrically-substituted triarylborane **48**.
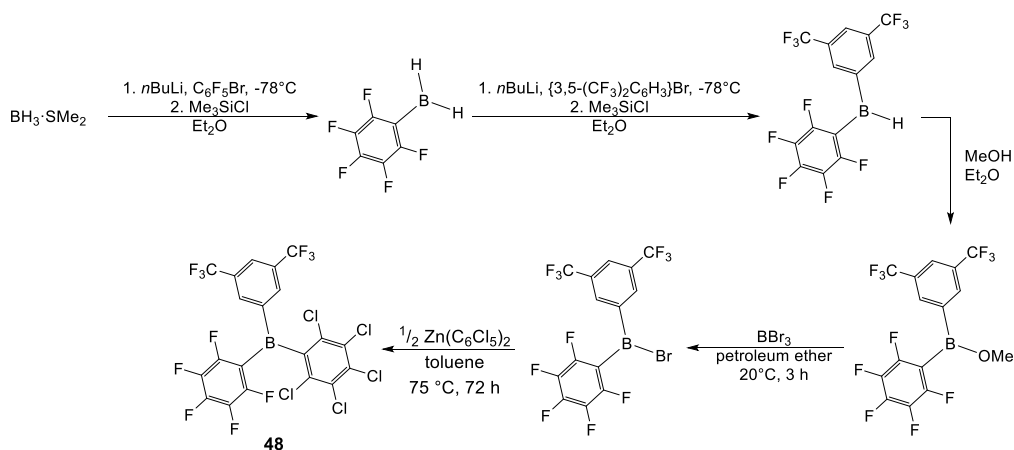
Scheme 27. Synthesis of unsymmetrically-substituted triarylborane 48 from borane dimethyl sulfide.[118]

1.3.3 Boron Trifluoride as the Boron Source

Liu *et al.* used the symmetrically-substituted compound **49**, which was prepared from BF$_3$·OEt$_2$ and the respective aryl lithium reagent, to prepare unsymmetrically-substituted triarylborane **50** *via* sequential cross-coupling reactions.[119]
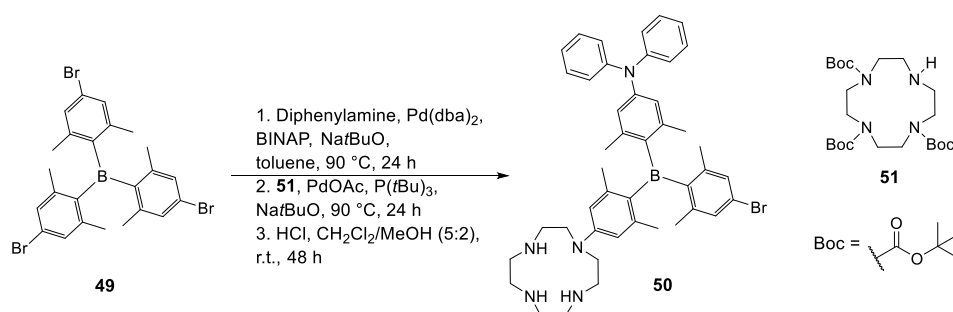
Scheme 28. Synthesis of unsymmetrically-substituted triarylborane **50** by stepwise modification of a symmetrically-substituted precursor.[119]

1.3.4 Boron Tribromide as the Boron Source

In 2005, Jäkle and coworkers reported the synthesis of different unsymmetrically-substituted triarylboranes as reference compounds for their polymers.[88] Both monomeric and polymeric boron-containing systems were synthesized from aryldibromoboranes and organotin reagents (*vide supra*, **Scheme 14**; *vide infra*, **Scheme 29**). They subsequently used this strategy for similar applications with slight modifications of the synthetic procedure, the third aryl group being added *via* a tin,[88] a copper[120-122] or a Grignard reagent[123] (**Scheme 29**).
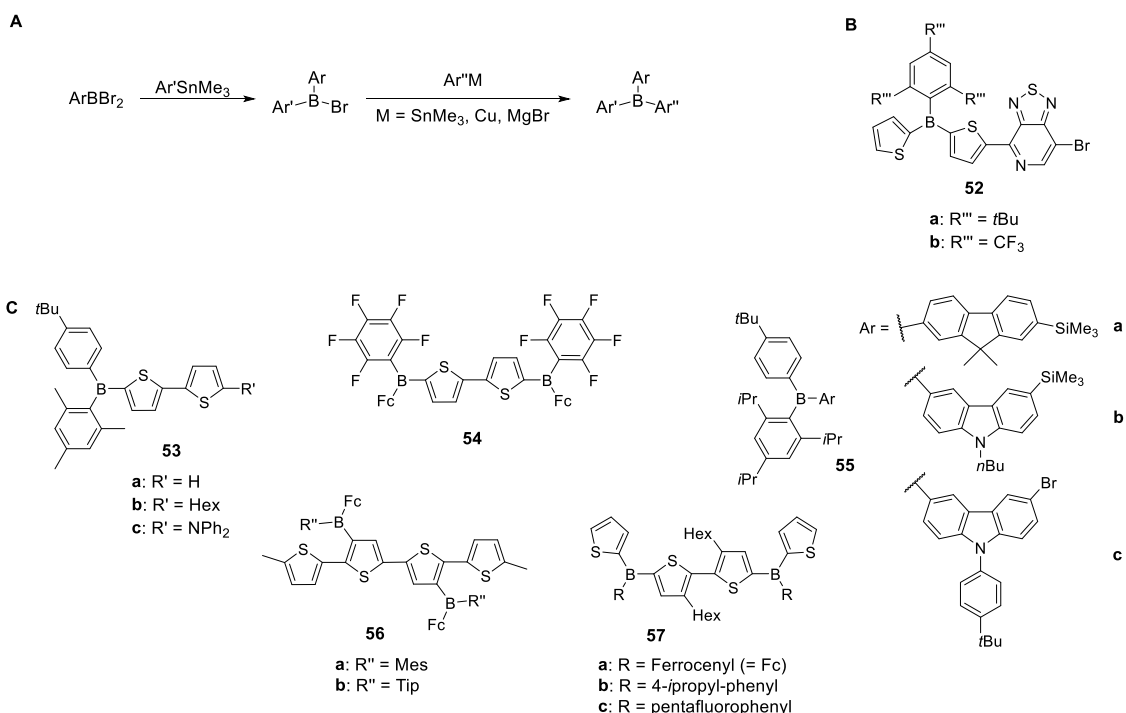
Scheme 29. A) Synthetic route to unsymmetrically-substituted triarylboranes developed by Jäkle and coworkers.[88] **B**) Structure of compound **52**.[124] **C**) Compounds **53-57** synthesized according to **Scheme 29A**.[88, 120-124]

The same group then reported the synthesis of an unsymmetrically-substituted triarylborane **52** (**Scheme 29B**) *via* stochiometric Stille coupling of a symmetric precursor[124] which had been obtained from boron tribromide and an excess of a tin reagent.[125]

In 2014, Kelly *et al.* reported the synthesis of a ferrocene-containing triarylborane bearing three different aromatic systems by stepwise reaction of dibromoferrocenylborane with two different aryl lithium reagents (**Scheme 30A**).[126]
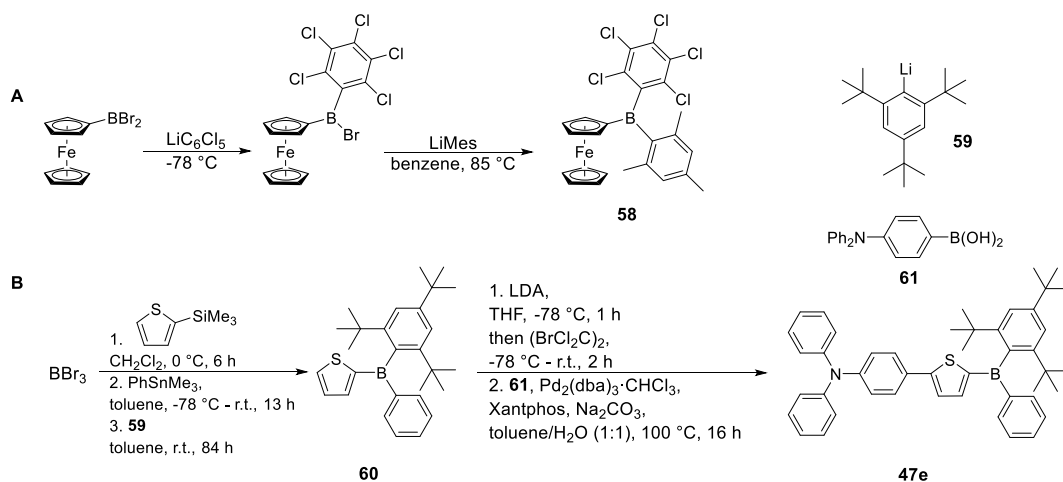
Scheme 30. A) Synthesis of unsymmetrically-substituted triarylborane **58** by Kelly *et al.*[126] **B**) Synthesis of sterically more demanding, unsymmetrically-substituted triarylborane **47e** by Yamaguchi and coworkers.[32]

As shown in **Scheme 26B**, Yamaguchi and coworkers reported a route to unsymmetrically-substituted triarylboranes from boronic esters,[32] but for **47e**, the route was not successful as the incorporated arene was sterically too demanding. Therefore, they used a route established by Jäkle and coworkers: after a boron-silicon exchange at the thiophene, the $ArBBr_2$ system was reacted with a tin reagent followed by 2,4,6-tri-*tert*-butylphenyllithium to give **47e** (**Scheme 30B**).

1.4 Summary and Outlook

Over the years, the synthetic approaches to triarylboranes presented herein has led to the generation of countless compounds containing triarylborane motifs. Inititially, examination of their properties was limited to their reactivity with other metals or as Lewis acids. Some of the early reaction sequences, such as those developed by Krause *et al.* and Grisdale *et al.*, are still used. Today, the applications of these compounds are no longer limited to their reactivity. The photophysical and electronic properties of triarylboranes and compounds containing this structural motif remain under increasingly active investigation as such properties lead to numerous applications, *e.g.* in OLEDS,[2] optoelectronics,[1, 3, 23] sensors for anions[4-6] or small molecules,[7, 8], catalysts for *e.g.* hydrogenation or amination of carbonyls[28, 107, 108] or bioimaging agents.[9, 10, 12, 14, 15] With the further exploration of more general routes to unsymmetrically-substituted triarylboranes, the applicability of these compounds can be expected to continue to increase as this structural motif provides the possibility for fine tuning of the photophysical and electronical properties of the resulting small molecules and, therefore, also of potential macromolecules and polymers.

CHAPTER 2

-

SYNTHESIS OF HIGHLY FUNCTIONALIZABLE
UNSYMMETRICALLY- AND SYMMETRICALLY-
SUBSTITUTED TRIARYLBORANES FROM BENCH-STABLE
BORON PRECURSORS

2 Synthesis of Highly Functionalizable Unsymmetrically- and Symmetrically-Substituted Triarylboranes from Bench-Stable Boron Precursors

2.1 Introduction

Triarylboranes or compounds containing this structural motif can potentially find applications in various fields as functional materials.[16-19] The interesting properties of these functional materials originate from the vacant p_z-orbital of the boron center that can efficiently conjugate with adjacent π-systems. The electronic and optical,[1-3, 76, 127-139] physical,[4, 140-142] biological,[9-12, 15, 143-145] and chemical[5, 7, 8, 27, 28, 107-109, 146-149] properties of such systems can be tuned by variation of the substituents on the three aryl rings attached to the boron atom. In general, there are three types of triarylboranes (**Figure 1**). The first type bears three identical substituents on the boron center (BAr_3) resulting in a high symmetry (D_3) and, due to its simplicity, this type of triarylborane was the first to be reported in 1885.[26] A reliable methodology for the synthesis of these compounds was reported by Krause and coworkers in 1922.[61] In this strategy, aryl Grignard reagents are reacted with gaseous boron trifluoride to form the corresponding triarylborane. Other reactive aryl metalates can be used and the boron source was changed to the more convenient boron trifluoride etherate,[129, 150, 151] making this strategy widely applicable. In the second type, two of the three aryl moieties are identical (BAr_2Ar') and, thus, such triarylboranes are of C_2 symmetry. Synthetic access to these systems was reported by Grisdale and co-workers in 1972.[76] In this procedure, sterically demanding aryl metalates are reacted with BX_3 species to form the corresponding $XBAr_2$ derivative. Due to the steric congestion, the reaction stops when two aryl moieties are attached to the boron center. Then, a second aryl metalate, with a higher reactivity, is used to attach the third aryl ring to the boron center. Grisdale and co-workers achieved this with the subsequent use of aryl Grignard and aryl lithium reagents, which is still the most common way to synthesize C_2 symmetrically-substituted triarylboranes.[152] The third type bears three different aryl substitutents ($BArAr'Ar''$) and will in the following be referred to as unsymmetrically-substituted triarylboranes. Only a few examples of unsymmetrically-substituted $BArAr'Ar''$ triarylboranes have been reported in the literature, and no general synthetic methodology is known. For a detailed review on the historical development of synthetic strategies for triarylboranes see the review article by Marder and co-workers (Chapter 1).[152]
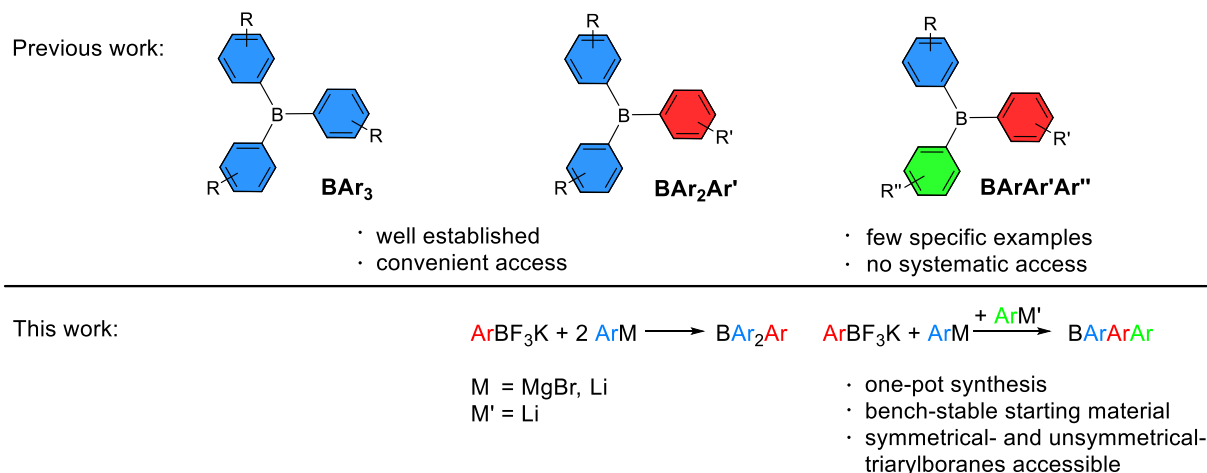
Figure 1. General types of triarylboranes[152] and schematic summary of this work.

The optional functional groups to incorporate, and the possibilities to do follow-up reactions on triarylboranes, have increased considerably over the past years. The applicability of triarylboranes in many fields is limited by their instability towards hydrolysis. One of the easiest and most common ways to stabilize triarylboranes kinetically is to introduce *ortho*-methyl groups around the boron center. It was demonstrated that compounds bearing six *ortho*-methyl groups around the boron are stable in pure water for several days.[9, 140] Due to the kinetic stabilization of the boron center, the $BXyl_3$ moiety exhibits a high tolerance to different reaction conditions employed in functionalization reactions. An overview of the numerous reported reaction conditions and selected functional groups attached to the $BXyl_3$ moiety is given in **Figure 2**.
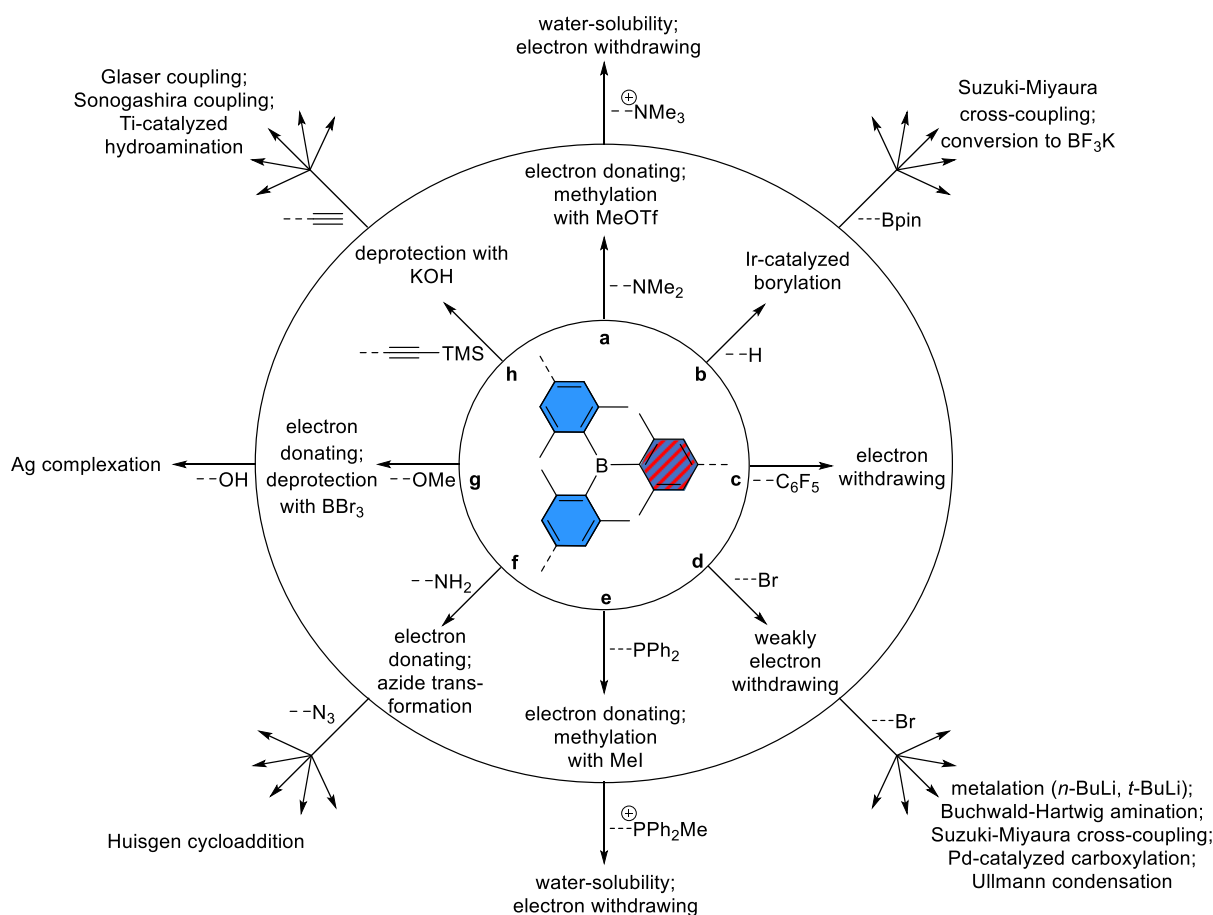
Figure 2. Overview of reported follow-up reactions, to which the BXyl₃ moiety (BAr₃ or BAr₂Ar') is tolerant, and selected functional groups that have been attached. Examples of each path are given in the following references: a,[9-12, 140, 141] b,[9, 11, 12, 153-155] c,[130, 156] d,[14, 144, 146, 148, 149, 157-167] e,[4, 138, 142, 168-170] f,[162, 171-175] g,[136, 176-180] h.[181-190]

The most notable effect on the properties of triarylboranes is obtained by functionalization of the *para*-position on the 2,6-dimethylphenyl substituents. This can be achieved, for example, via iridium-catalyzed C–H borylation which exhibits very high, sterically-driven regioselectivity.[191, 192] The resulting boronate ester moieties can be employed in various functional group transformations as well as Suzuki-Miyaura cross-coupling reactions (**Figure 2b**). This way, triarylboranes can also be attached to chromophores or stationary phases. Even deprotonation or lithium-halide exchange reactions can be employed to functionalize triarylboranes due to their high tolerance towards different reaction conditions (**Figure 2d**). By reaction with different electrophiles, various functional groups, *e.g.* CO_2H or COH, can be introduced. In general, introduction of electron donating or accepting groups has a strong effect on the optoelectronic properties of triarylboranes. By carefully choosing the specific substituents, the properties can be fine-tuned to meet different requirements. For example, water solubility of triarylboranes can be facilitated by the introduction of cationic ammonium or phosphonium substituents (**Figure 2e** and **f**).

Due to the limited synthetic access to unsymmetrically-substituted triarylboranes, structure-property relationship studies have been mostly limited to symmetrically-substituted

triarylboranes (BAr$_3$ or BAr$_2$Ar'). Consequently, even though a plethora of functional groups is available, a maximum of two can be realized at once. Thus, a systematic synthetic methodology to access unsymmetrically-substituted triarylboranes would greatly enhance the options available for designing functional materials.

The main boron sources for triarylborane syntheses are boron trihalides, mostly employed in the form of boron trifluoride etherate.[152] In recent years, the Marder group and others have employed aryltrifluoroborates as convenient, benchstable precursors for the synthesis of triarylboranes.[29, 30, 110, 193] Previously, aryltrifluoroborates were found to be efficient reagents for cross-coupling reactions.[194, 195] Aryltrifluroborate salts are easily accessible via fluorination of the corresponding boronate ester or boronic acid via reaction with KHF$_2$.[105]

Based on these results, a synthetic route to symmetrically- and unsymmetrically-substituted, sterically congested and, therefore, air-stable triarylboranes starting from bench-stable boron precursors, namely potassium aryltrifluoroborates is presented.

2.2 Synthesis of a Symmetrically-Substituted Triarylborane

In a first approach to obtain *para* substituted BXyl$_3$ from potassium aryltrifluoroborates, the synthesis of compound **HBr$_2$** (*the nomenclature used herein refers to the para substituents*) was attempted (**Scheme 31**, **Table 1**).
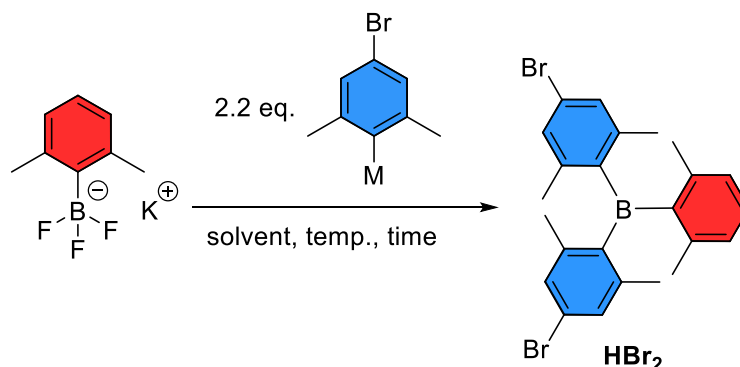
Scheme 31. Synthesis of the C$_2$ symmetric triarylborane **HBr$_2$**.

Therefore, 2.2 equivalents of (4-bromo-2,6-dimethylphenyl)metalate were reacted with potassium (2,6-dimethylphenyl)trifluoroborate **H-BF$_3$K**. Using a Grignard reagent in THF as the metalate, compound **HBr$_2$** was isolated in 19% yield after stirring for 2 d at 90 °C in a sealed vessel (**Table 1**). It was further demonstrated that the reaction time can be significantly reduced to 1 h when using microwave irradiation at 200 °C.

Table 1. Summary of conditions applied for the synthesis of the symmetrically-substituted triarylborane **HBr₂**.

Entry	BAr₂Ar'	M	R	Solvent	Temperature	Time	Yield[a]
1	**HBr₂**	MgBr	Br	THF	90 °C	2 d	19%
2		MgBr	Br	THF	200 °C[b]	1 h	19%

[a] Isolated yield; [b] Microwave irradiation in a sealed tube.

From these reactions, it can be concluded that sterically very congested triarylboranes can be synthesized from **H-BF₃K** and two equivalents of aryl Grignard reagent at elevated temperatures. In contrast, at room temperature, the reaction of **H-BF₃K** with two equivalents of an aryl Grignard reagent stops after the attachment of one additional aryl ring to the boron center, for reaction times of up to five days. This leads to a diarylfluoroborane (ArAr'BF) with four *ortho*-methyl groups. However, it was demonstrated previously[9] that the formation of *para* substituted BXyl₃ from a diarylfluoroborane and an aryl lithium reagent already proceeds at room temperature.

2.3 Synthesis of Unsymmetrically-Substituted Triarylboranes

As aryl Grignard and aryl lithium reagents differ significantly in their reactivities towards potassium aryltrifluoroborates, this approach was used for the synthesis of unsymmetrically-substituted triarylboranes according to **Scheme 32** and **Table 2**.
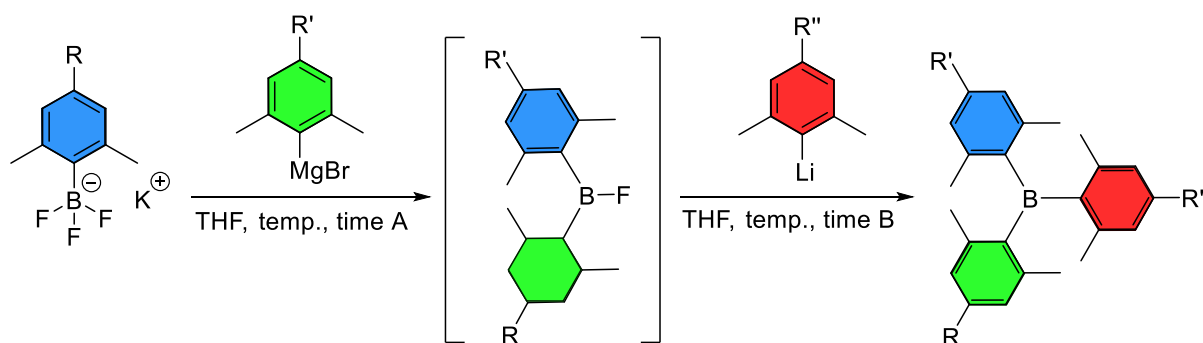
Scheme 32. Summary of synthesis of the unsymmetrically-substituted triarylboranes **HBrMe** and **HBrSi**.

H-BF₃K was reacted with one equivalent of (4-bromo-2,6-dimethylphenyl)magnesium bromide at room temperature, to form the corresponding fluoroborane (FBArAr'), as indicated by *in situ* ¹⁹F and ¹¹B NMR spectroscopy. Then, the more reactive 2,4,6-trimethylphenyllithium (MesLi) was added and the unsymmetrically-substituted triarylborane **HBrMe** was isolated in 18% yield. The formation of FBArAr' is rather fast, and the same yields were obtained for shorter

reaction times (**Table 2** Entry 1 vs. Entry 2). Thus, the synthesis of **HBrMe** is possible in a one pot process within 24 h.

Table 2. Summary of conditions applied for the synthesis of the unsymmetrically-substituted triarylboranes **HBrMe** and **HBrSi**.

Entry	BArAr'Ar''	R	R'	R''	Temperature	Time A	Time B	Yield[a]
1	**HBrMe**	H	Br	Me	r.t.	18 h	3 d	18%
2		H	Br	Me	r.t.	30 min	18 h	18%
3		Me	Br	H	r.t.	30 min	18 h	35%
4		Br	H	Me	r.t.	30 min	18 h	3%
5	**HBrSi**	H	Br	SiMe$_3$	r.t.	30 min	18 h	16%

[a] Intermediate diaryl fluoroborane was isolated.

To optimize the conditions further, the influence of the *para*-substituents on the potassium aryltrifluoroborate was examined. The synthesis of **HBrMe** was carried out starting from the respective aryltrifluoroborate **H-BF$_3$K**, potassium mesityltrifluoroborate **Me-BF$_3$K** and potassium 4-bromo-(2,6-dimethylphenyl)trifluoroborate **Br-BF$_3$K**. The reaction procedure was performed starting from each potassium aryltrifluoroborate according to **Scheme 33** and **Table 2**, Entries 2-4.
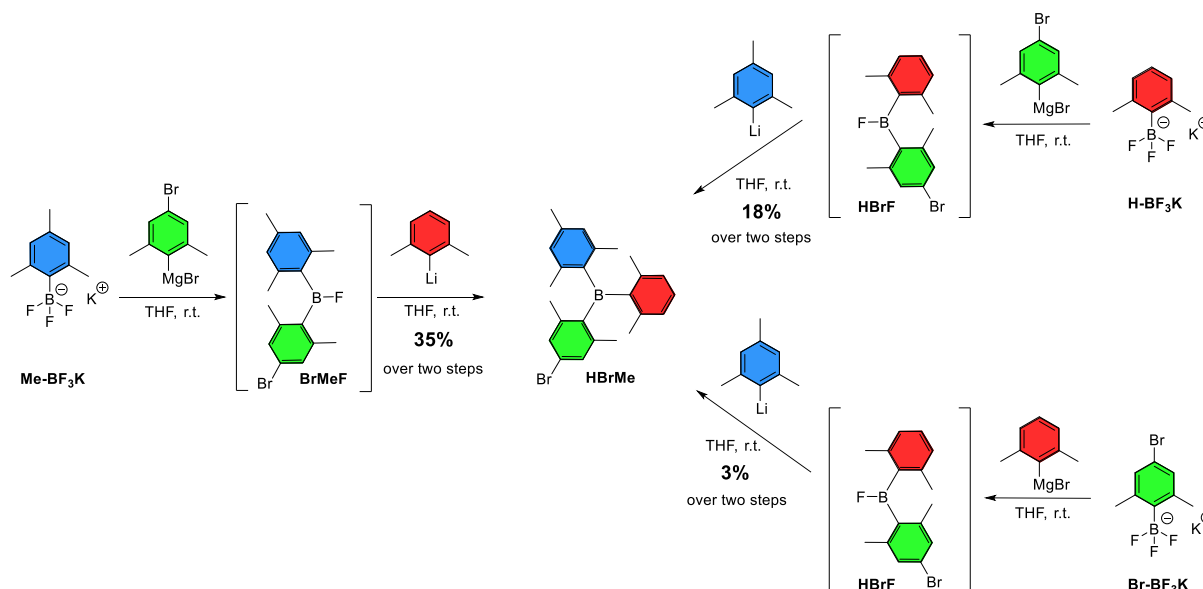
Scheme 33. Different reaction pathways to compound **HBrMe**.

For each reaction, the desired product **HBrMe** was isolated. Using **H-BF$_3$K** as the starting material, a yield of 18% over two steps (*vide supra*) was obtained. Starting from **Me-BF$_3$K**, the yield doubled to 35% over two steps. With **Br-BF$_3$K** as the starting material, the yield over two steps decreased to 3%. These drastic differences in yield were surprising, as the electronic differences of the potassium aryltrifluoroborates were considered minor in comparison to the

equal steric demand at the boron centers of all aryltrifluoroborates. The electronic differences for substituents at the *para* position can be assessed by the Hammett values and are σ_p = -0.17 for CH$_3$, 0 for H and 0.23 for bromide.[196] The trend found in the isolated yields of **HBrMe** are in good accordance with the trend given by the *para* Hammett values of the respective substituents in the potassium aryltrifluoroborates **Me-BF$_3$K**, **H-BF$_3$K** and **Br-BF$_3$K**. It is well documented that electron donating groups enhance solvolysis of aryltrifluoroborates, whereas electron withdrawing groups hinder solvolysis.[197, 198] In analogy to their benzotrifluoride analogues,[199, 200] this is explained by the proclivity of aryltrifluoroborate to lose a fluorine atom in the first step of the solvolysis. According to **Scheme 34**, the first step of the solvolysis is described as an equilibrium between aryltrifluoroborate and the short-lived aryldifluoroborane. This intermediate is stabilized by electron donating groups, whereas electron withdrawing groups stabilize the negative charge at the boron in the case of aryltrifluoroborates. Even though the mechanism of this triarylborane synthesis is unknown, both a dissociative as well as an associative mechanism would energetically benefit from electron donating groups at the *para* position of the aryltrifluoroborate salts. Thus, while this method provides considerable flexibility, to enhance the yield, electron-rich potassium aryltrifluoroborates should be chosen as the boron source, if possible.
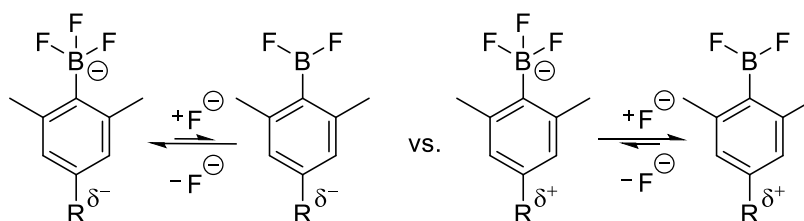
Scheme 34. Influence of the inductive effect of *para* substituent R on the first step of the solvolysis of aryltrifluoroborates.

The unsymmetrically-substituted triarylborane **HBrMe** allows further orthogonal functionalization at two positions, namely the *para* bromide and the *para* proton (**Figure 2**). The mesitylene unit does not possess a position that can be conveniently functionalized. To obtain a triarylborane that can be orthogonally functionalized at all three aromatic rings, the *para* methyl group of mesitylene was exchanged for a trimethylsilyl group. This moiety permits many different functionalization reactions[201-205] and should be robust enough to tolerate the reaction conditions required for the triarylborane formation. The compound **H-BF$_3$K** was chosen as the starting material and compound **HBrSi** synthesized in a yield of 16% over two steps in a one pot synthesis (**Scheme 32**, **Table 2** Entry 5).

All triarylboranes synthesized bear at least two positions that can be functionalized after the formation of the triarylborane, making these compounds versatile building blocks for the synthesis of larger, boron-containing compounds.

2.4 Selected Examples for Post-Functionalization

Iridium-catalyzed C–H borylation using [Ir(COD)OMe]$_2$ as the precatalyst, 4,4'-di-*tert*butylbipyridine as the ligand and B$_2$pin$_2$ as the boron source[191, 192] exhibits very high sterically-driven selectivity and has been applied by Marder and co-workers for the synthesis of many different functional materials,[30, 31, 206-209] including triarylboranes.[9-12] To demonstrate the utility of the novel compounds, a small library of AB, AAB, and ABC type, orthogonally functionalizable triarylboranes was created, where A, B, and C indicate orthogonally functionalizable groups. Therefore, iridium-catalyzed C–H borylation was applied to **HBrMe**, **HBr$_2$** and **HBrSi**, which takes place selectively at the *para* C–H bond of the dimethylphenyl ring. The products shown in **Scheme 35a** were synthesized in up to 68% yield.
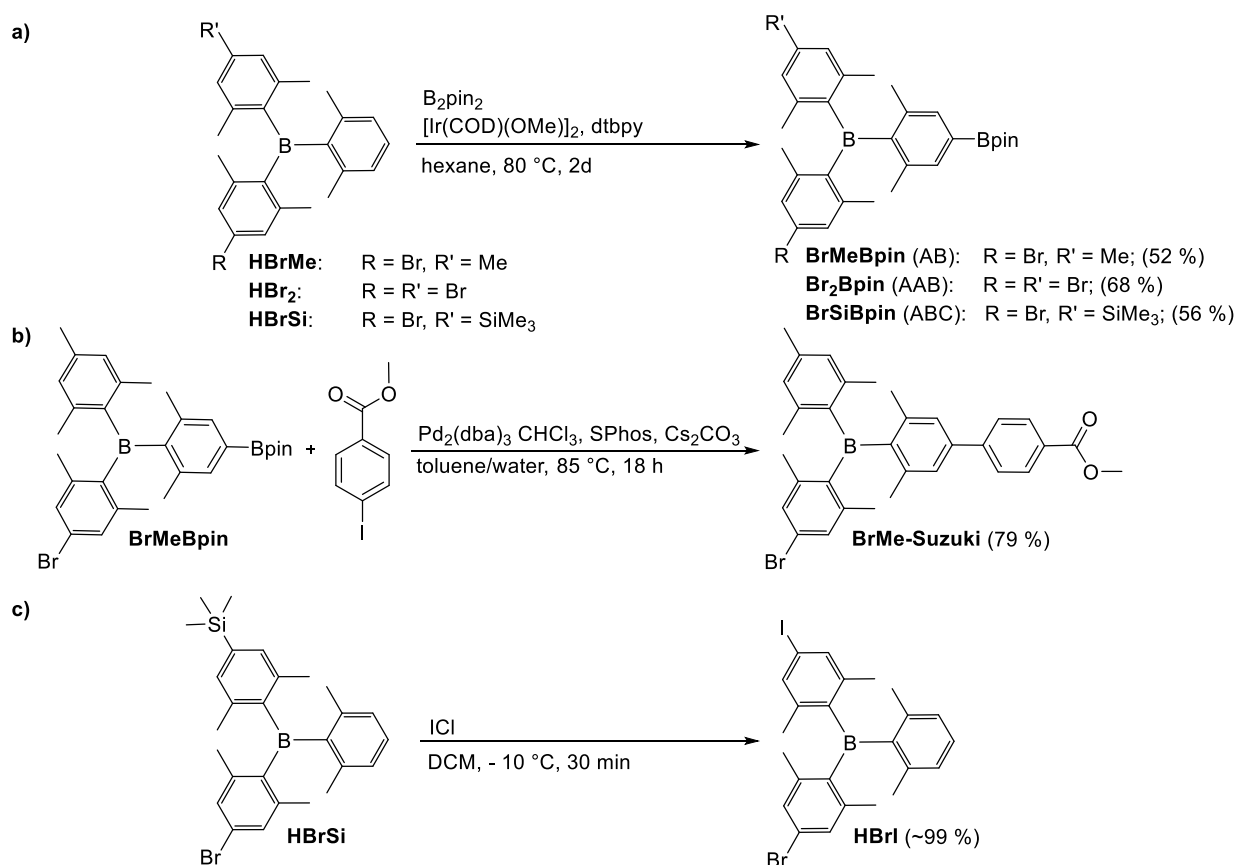
Scheme 35. a) Synthesis of highly functionalizable triarylboranes **BrMeBpin**, **Br$_2$Bpin** and **BrSiBpin** obtained *via* iridium-catalyzed C–H borylation. The letters A, B and C in brackets indicate possible orthogonal post-functionalization reactions. **b)** Selective Suzuki-Miyaura cross-coupling of **BrMeBpin** with iodo methylbenzoate. **c)** Conversion of trimethylsilyl of **HBrSi** to iodide with iodine monochloride.

As shown in **Figure 2**, borylated triarylboranes have already been employed successfully in Suzuki-Miyaura cross-coupling reactions with different aryl halides. However, the bromide, which is present the borylated triarylboranes, might lead to unwanted side reactions. To see if this can be circumvented by choice of an appropriate, more reactive aryl halide, compound

BrMeBpin was employed in a Suzuki-Miyaura cross-coupling reaction with methyl iodobenzoate (**Scheme 35b**). The coupling product **BrMe-Suzuki** was isolated in a good yield of 79% and the presence of the bromide in **BrMe-Suzuki** was confirmed.

As mentioned above, the trimethylsilyl group permits many functionalization reactions. However, this functional group has not been used for functionalizations, when attached to a BXyl$_3$ moiety. To demonstrate the applicability of this functional group in these system, the trimethylsilyl group of **HBrSi** was converted with iodine monochloride into iodide (**Scheme 35c**). The reaction was performed open to air and was complete within half an hour. Compound **HBrI** was isolated in quantitative yield.

2.5 Conclusion

In summary, a generally applicable synthetic route to highly functionalizable, kinetically stable, symmetrically- and unsymmetrically-substituted triarylboranes is provided. It is shown that it is possible to synthesize the same unsymmetrically-substituted triarylborane starting from the three possible aryl BF$_3$K salts in one pot syntheses, but the most electron-rich aryl BF$_3$K should be chosen, if possible. To illustrate the utility of this method, the triarylboranes synthesized were functionalized by iridium-catalyzed C–H borylation leading to versatile AB, AAB and ABC type systems that can be further functionalized orthogonally and, thus, be used as building blocks in the design of boron-containing functional materials. Further, the trimethylsilyl group was found to be a convenient halide protecting group in triarylborane chemistry.

CHAPTER 3

-

BIS(PHENYLETHYNYL)ARENE LINKERS IN TETRACATIONIC BIS-TRIARYLBORANE CHROMOPHORES CONTROL FLUORIMETRIC AND RAMAN SENSING OF VARIOUS DNA AND RNA

3 Bis(phenylethynyl)arene Linkers in Tetracationic bis-Triarylborane Chromophores Control Fluorimetric and Raman Sensing of Various DNA and RNA

3.1 Introduction

One of the most essential tasks of living organisms is the reproduction of their own genome.[210] This requires the production of proteins from information that is stored in their DNA. The central dogma of molecular biology,[211] which is under ongoing debate,[212-214] explains this protein production as a one-way information flow, where DNA is the source of genetic information, DNA sequences are transcribed into RNA and RNA is translated into proteins. Detailed investigation of these biomacromolecules and understanding of the interactions that influence their communication on a molecular level is a broad and interdisciplinary research field. One well established way to approach the subject is to study the interactions and binding behaviors of small molecules with DNA and RNA.[215-226]
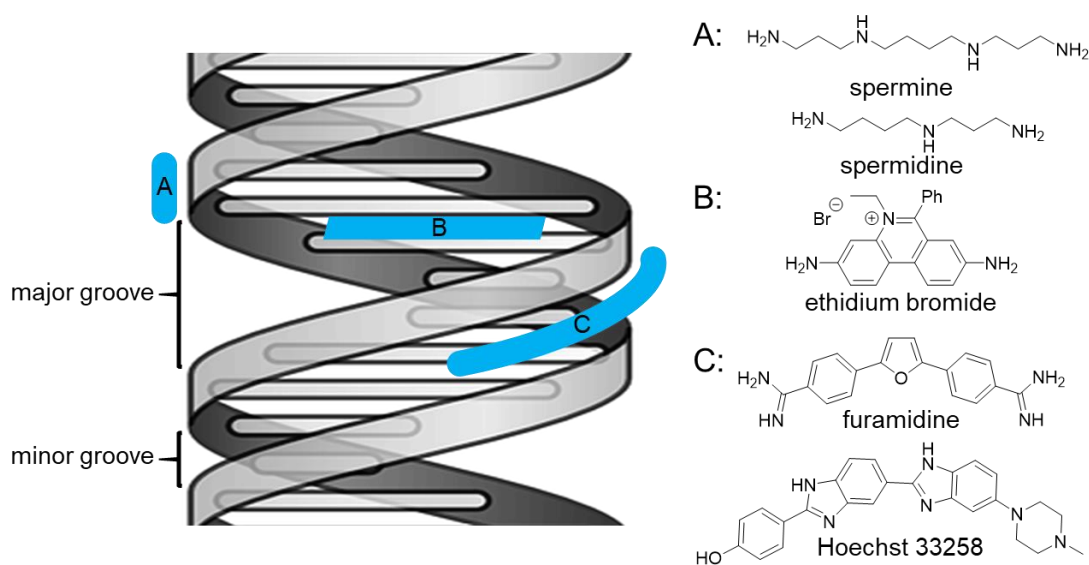
Figure 3. Simplified illustration of the three main binding modes of small molecules (blue shapes) to a helical biomacromolecule (grey helical ribbon represents phosphate backbone; grey horizontal sticks represent two interacting nucleobases) and selected examples for each binding mode. A: external binder (polyamines[227]); B: intercalator (ethidium bromide[228]); C: groove binder (furamidine,[229] Hoechst 33258[230]).

There are three main binding modes, namely intercalation, groove binding and external binding (**Figure 3**).[231, 232] For intercalation to occur, the helical structure of the biomacromolecule needs to unwind to allow for a small molecule to insert in between the coplanarly arranged nucleobases. Typical intercalators possess rigid and planar polycyclic aromatic moieties, which are required for efficient π-π-stacking with the nucleobases.[233] Groove binding can occur into the major or the minor groove. Larger molecules, such as natural and synthetic oligonucleotides and proteins, usually bind in the major groove, while synthetic small

molecules prefer the minor groove.[234] Such small molecules are curved and consist of several flexibly connected aromatic moieties.[235] Most groove binders possess functional groups which form hydrogen bonds with the nucleobases of the biomacromolecule. Other important driving forces are van der Waals interactions[236] and a significant energy gain when the hydrophobic part of the small molecule is transferred from the aqueous environment into the less polar groove of the biomacromolecule, accompanied by a transfer of the respective amount of water molecules from the groove into the aqueous environment.[237] External binding is mostly caused by attractive electrostatic interactions between the negatively charged phosphate backbone and a small molecule. Furthermore, the release of positively charged counterions (from the so-called ion atmosphere that surrounds charged biomacromolecules in solution) provides a positive entropic contribution.[238-240] Some dye aggregates bind to biomacromolecules *via* external binding, as they are too large to fit into any of the binding sites.[232, 233, 241] It should be noted that more than one binding mode may be relevant to explain the binding event of a small molecule with a biomacromolecule, and that relatively small changes in the design of a small molecule can significantly alter the predominant mode of binding.[242]

If the binding event significantly changes the structure of the biomacromolecule, which usually occurs upon intercalation, but is also possible when the groove has to adjust its size, *i.e.*, for the binding of a sterically demanding dye aggregate, it influences their behavior in biological processes.[243, 244] Thus, such small molecules have great potential as anti-cancer, anti-viral and anti-infective drugs, with DNA[244-248] as well as RNA[249-253] as possible targets. If the binding event significantly changes the properties of the small molecule, these property changes can be monitored to visualize DNA and RNA *in vitro* and *in vivo*. Thus, a further, widely studied application of small molecules binding to biomacromolecules is DNA and RNA staining in biological imaging.[254-257]

Within the past few years, several chromophores containing triarylboryl moieties have been shown to be applicable in biological imaging.[7, 9-12, 58, 116, 119, 143-145, 174, 258-262] Since their first report in the literature 135 years ago,[26, 152] triarylboranes have found applications in many different fields, such as metal-organic framework (MOF) chemistry, anion sensing and optoelectronics.[16, 17, 19] The three-coordinate boron in a triarylboryl moiety serves as a strong π-acceptor and as a strong Lewis-acid, due to its vacant p_z-orbital. When employing triarylboranes in functional materials, bulky substituents have to be employed to stabilize the three-coordinate boron against decomposition by air and moisture.[76, 125, 130, 131, 133, 134, 136, 137, 146, 190, 193, 263-267] Using Gabbaï's approach,[140] Marder and co-workers recently developed compound **Z'** (**Figure 4**) as a water-stable, water-soluble, and non-cytotoxic live cell imaging agent.[9]

In further studies, it was found that **Z'** serves as an efficient sensor for DNA, RNA and protein.[13] The fluorescence emission from **Z'** was found to increase upon addition of all biomacromolecules which were examined. However, emission maxima were strongly dependent on the type of biomacromolecule (DNA/RNA vs. protein), which allowed us to suggest a protein-like binding site for **Z'** in the cell. In contrast, the emission of 1,3-butadiyne analogue **II** (**Figure 4**) was strongly quenched by DNA, RNA and protein.[189] Thus, it was indicated that the linker connecting the two triarylborane moieties in tetracationic bis-triarylboranes has a profound impact on its fluorescence response when sensing biomacromolecules. In contrast to **Z'**, compound **II** can be applied as a combined fluorimetric and Raman probe for simultaneous and selective sensing of various DNA, RNA and proteins, due to its strong Raman signal. Dual Raman and fluorescence spectroscopy has attracted increasing interest in recent years, as a method that circumvents some of the intrinsic problems of Raman spectroscopy, *i.e.*, long acquisition times and low signal strengths.[268-270] This multimodal approach, has been successfully utilized in cell imaging,[271, 272] disease diagnostics[273-276] and monitoring of drug delivery.[277, 278] As fluorescence can adversely interfere with Raman measurements by causing significant background noise,[279] the design of suitable small molecules for the specific purpose of dual Raman and fluorescence imaging[280, 281] is a rather novel approach and remains challenging. Extended conjugated poly-ynes have been employed to shift the energy of the Raman active stretching of the $C\equiv C$ bonds systematically, thus allowing selective labelling and multiplex imaging.[282] The question remained whether these multiple triple bonds need to be directly conjugated to gain the selectivity, or if it is possible to insert various aromatics inbetween the triple bonds possibly gaining additional selectivity, while maintaining the high Raman signal intensity. This is an important question, as current research in bio-applicable Raman-based sensing[283, 284] requires a broad choice of dyes, preferably ones suitable for dual Raman and fluorescent operation modes. Therefore, several dual Raman and fluorescent chromophores were synthesized, following the basic design of compounds **Z'** and **II**, thus extending this novel class of biomacromolecule sensors (**Figure 4**).
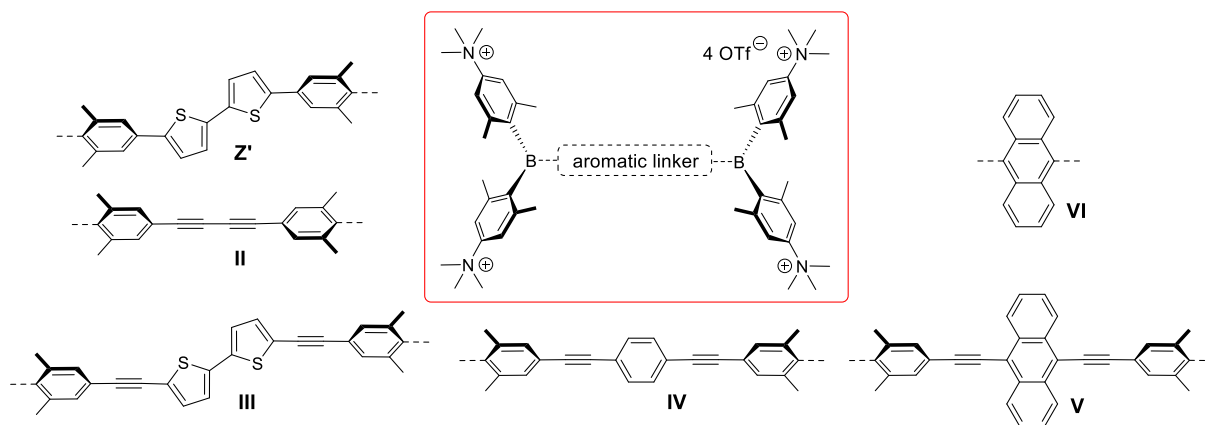
Figure 4. General structure of the novel class of DNA/RNA sensors with different aromatic linkers including the target molecules **III**-**VI** of this study.

In this design of the new compounds, the favorable fluorescence increase upon binding to DNA and RNA observed for the bithiophene **Z'** was combined with the two triple bonds, responsible for the strong Raman signal of compound **II**, which led to compound **III** (**Figure 4**), resembling 2,5-bis(phenylethynyl)thiophene (BPET) chromophores investigated by the Marder group and others.[285, 286] For comparison, a reference compound in the form of the 1,4-phenylene analogue **IV** was prepared, a bis(phenylethynyl)benzene (BPEB) derivative[287-293] in which the overall length of the linker is somewhat shorter than in compound **III**. The bis(phenylethynyl)anthracene (BPEA) derivative **V**, was chosen because BPEAs are strong fluorophores[294-301] and the long axis of anthracene in compound **V** is perpendicular to the bis-triarylborane longitudinal axis. Such an orientation of a large and rigid aromatic moiety is expected to have a significant effect on the nature of the binding interactions with DNA/RNA. The much shorter anthracene analogue **VI** prepared previously,[10] which showed intriguing live cell imaging properties was studied to test the importance of linker length and rigidity between the two triarylborane units.

3.2 Synthesis and Solid State Structures

Starting material **A** was synthesized according to the literature procedure previously reported by Marder and co-workers.[189] The bisethynyl arenes **IIIN**, **IVN** and **VN** were prepared *via* Sonogashira coupling reactions of **A** with the respective aryl halides using Pd(PPh$_3$)$_2$Cl$_2$ and CuI as the catalytic system and NEt$_3$ in THF as the base (**Scheme 36**). The neutral compounds **IIIN**, **IVN** and **VN** were methylated at the amine groups with MeOTf in dichloromethane, to afford the tetracationic species **III**, **IV** and **V**.
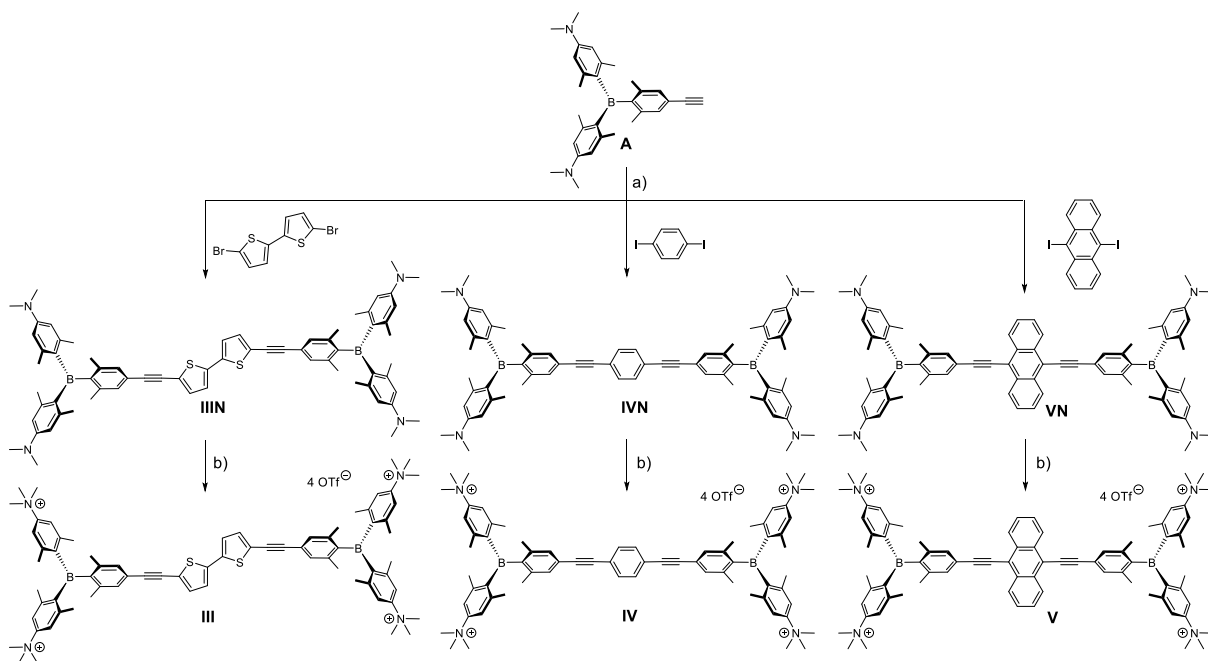
Scheme 36. Synthesis of the compounds **IIIN**, **IVN**, **VN** and **III**, **IV**, **V**. a) Pd(PPh₃)₂Cl₂, CuI, THF/NEt₃, r.t.. b) MeOTf, CH₂Cl₂ , r.t..

Single crystals of **IIIN** and **IVN** suitable for X-ray diffraction analysis were obtained. Even though the following investigations on interactions with DNA and RNA were performed with the tetracationic analogues, the solid state molecular structures of the neutral precursors are given in **Figure 5**, to provide an indication of the size and shape of this class of compounds. The B1−B1B distance is 22.471(12) Å for **IIIN** and 19.525(14) Å for **IVN**. The linkers in both structures are slightly curved, which reveals a degree of flexibility for both compounds as is often the case for alkynyl systems. This is in accordance with the respective C6-C11-C12, C6B-C11B-C12B, C11-C12-C13, C11B-C12B-C13B and C16-C11B-C12B angles, which differ slightly from 180° in all cases (**Figure 5**). The evident flexibility in the solid state suggests at least a similar flexibility in solution, which was further corroborated by the binding experiments with DNA and RNA (*vide infra*). Single crystals suitable for X-ray diffraction analysis for the trimethylsilyl-protected precursor to compound **A** were obtained. The solid state molecular structure of **C**[189] is reported in the Supporting Information (Table S2 and Figure S50) and the geometry of **C** does not exhibit a significant deviation from those of the triarylborane groups in **IIIN** and **IVN**.
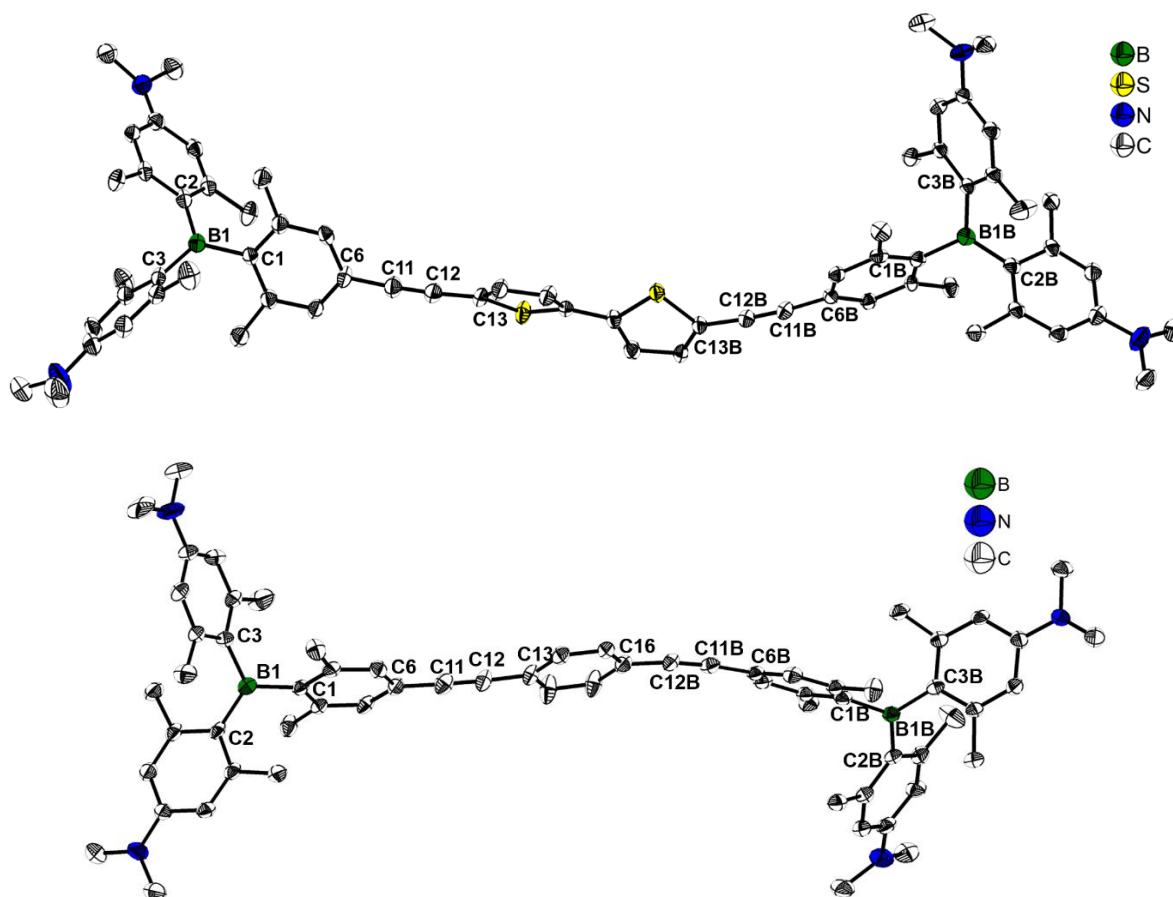
Figure 5. Molecular structures of **IIIN** (top) and **IVN** (bottom) in the solid state at 100 K. Atomic displacement ellipsoids are drawn at the 50% probability level, and H atoms and co-crystallized solvent molecules (EtOAc) are omitted for clarity. Selected distances and angles for 3N: B1-B1B 22.471(12) Å, B1–C1 1.600(5) Å, B1B–C1B 1.592(5) Å, B1–C2 1.569(6) Å, B1B–C2B 1.573(5) Å, B1–C3 1.567(6) Å, B1B–C3B 1.551(6) Å, C6–C11 1.449(5) Å, C6B–C11B 1.437(5) Å, C11–C12 1.191(5) Å, C11B–C12B 1.190(5) Å, C12–C13 1.429(5) Å, C12B–C13B 1.421(5) Å, C1-B1-C2 120.8(3)°, C1B-B1B-C2B 119.6(3)°, C1-B1-C3 118.4(3)°, C1B-B1B-C3B 119.5(3)°, C2-B1-C3 120.7(3)°, C2B-B1B-C3B 120.9(3)°, C6-C11-C12 175.7(5)°, C6B-C11B-C12B 174.7(4)°, C11-C12-C13 175.7(4)°, C11B-C12B-C13B 175.5(4)°, BC$_3$–Aryl (C1) 55.10(14)°, BC$_3$–Aryl (C2) 42.53(14)°, BC$_3$–Aryl (C3) 51.82(14)°, BC$_3$–Aryl (C1B) 48.54(13)°, BC$_3$–Aryl (C2B) 51.66(13)°, BC$_3$–Aryl (C3B) 43.71(13)°. Selected distances and angles for 4N: B1–B1B 19.525(14) Å, B1–C1 1.592(7) Å, B1B–C1B 1.593(6) Å, B1–C2 1.568(7) Å, B1B–C2B 1.570(6) Å, B1–C3 1.562(6) Å, B1B–C3B 1.561(7) Å, C6–C11 1.436(7) Å, C6B–C11B 1.432(6) Å, C11–C12 1.199(6) Å, C11B–C12B 1.203(6) Å, C12–C13 1.433(7) Å, C12B–C16 1.432(6) Å, C1-B1-C2 121.0(4)°, C1B-B1B-C2B 118.5(4)°, C1-B1-C3 118.0(4)°, C1B-B1B-C3B 120.4(3)°, C2-B1-C3 120.9(4)°, C2B-B1B-C3B 121.0(4)°, C6-C11-C12 178.2(5)°, C6B-C11B-C12B 173.9(4)°, C11-C12-C13 177.8(5)°, C11B-C12B-C16 173.2(4)°, BC$_3$–Aryl (C1) 55.25(13)°, BC$_3$–Aryl (C2) 43.82(13)°, BC$_3$–Aryl (C3) 49.94(14)°, BC$_3$–Aryl (C1B) 47.56(13)°, BC$_3$–Aryl (C2B) 42.21(13)°, BC$_3$–Aryl (C3B) 52.71(13)°.

3.3 Physico-Chemical Properties

All of the positively charged compounds (**III**-**VI**) were found to be moderately soluble in water (c = 1 ×10^{-4} M) and, when stored in the dark, their aqueous solutions were stable for months. Photophysical data for the novel compounds **III-V** in acetonitrile and water are summarized in **Table 3**, while the photophysical data for **VI** are reported in a previous publication.[10] Additionally, computational studies on the compounds **III-V** were carried out. Results of those studies and a short discussion can be found in the Supporting Information.

Table 3. Photophysical data for compounds **III**-**V** in acetonitrile and water.

	solvent	λ_{abs} / nm	ε / M^{-1} cm^{-1}	λ_{em} / nm	Stoke's shift / cm^{-1}	Φ_f	τ / ns	k_r / 10^8 s^{-1}	k_{nr} / 10^8 s^{-1}
III	MeCN	413	65 000	535	5 500	0.31	1.27	2.4	5.4
	H$_2$O	413	62 000	558	6 300	0.26	<1	-	-
IV	MeCN	373	60 000	452	4 700	0.58	3.27	1.8	1.3
	H$_2$O	371	62 000	452	4 800	0.73	3.63	2.0	0.7
V	MeCN	483	52 000	505	900	0.72	2.45	2.9	1.1
	H$_2$O[a]	485	47 000	501	700	0.72	2.33	3.1	1.2

[a] At concentrations >1 ×10^{-5} M compound **V** begins to aggregate. This results in a gradual shift of the emission maximum towards λ$_{em}$ = 578 nm (see **Figure S55**).

The UV/Vis spectra of the aqueous sodium cacodylate buffer solutions (**Figure 6**, pH 7) of the compounds studied were proportional to their concentration in the c = 5-15 ×10^{-6} M range, and the corresponding absorption maxima and molar extinction coefficients are listed in the Supporting Information (**Table S5**).
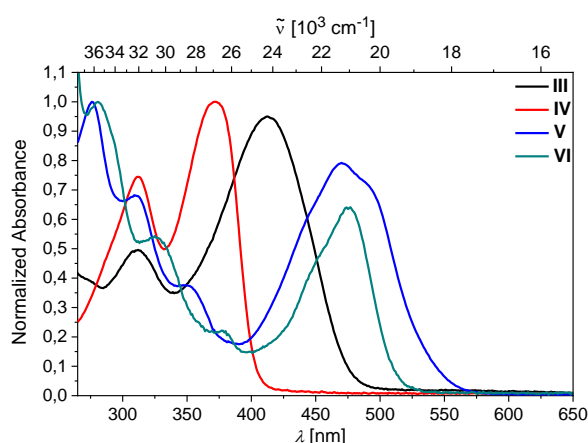
Figure 6. UV/Vis spectra of compounds **III-VI** at c = 1 ×10^{-6} M in sodium cacodylate buffer solution at pH 7, I = 0.05 M.

Upon heating the solutions, the UV/Vis spectra of **III-VI** exhibited quite different properties. While the UV/Vis spectra of **IV** and **VI** showed only a negligible decrease with temperature (**Figure 7** left, SI **Figure S60b**) the spectra of **III** and **V** changed significantly, showing a strong increase in absorbance and a pronounced hypsochromic shift (**Figure 7** right, SI **Figure S60c**). In all cases, the spectral changes were fully reversible upon cooling back to 25 °C, suggesting that no chemical changes took place.
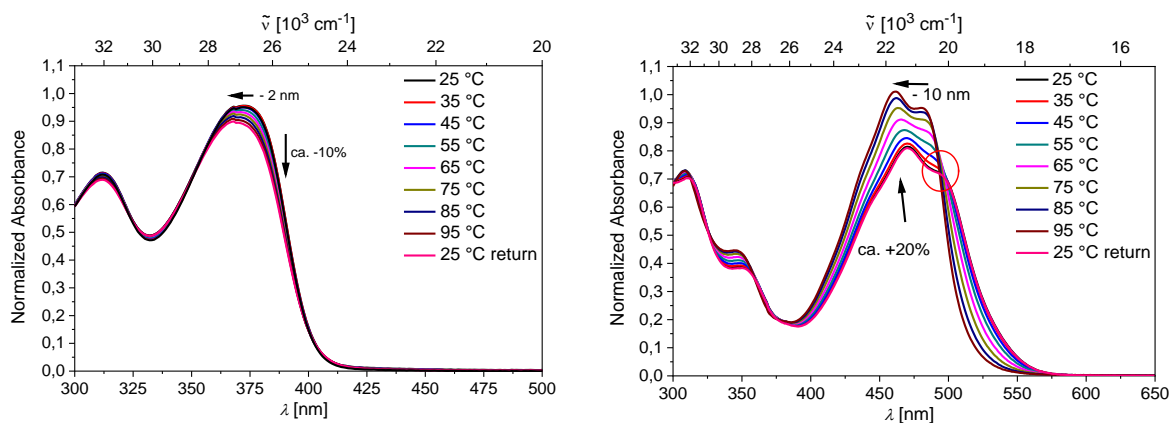
Figure 7. Temperature dependence at c = 1.3-1.7 ×10^{-5} M in buffered solution at pH 7, I = 0.05 M. Left: hypochromic effect in the absorption spectra of **III** (> 10%); right: hyperchromic effect (+ 20%) in the absorption spectra of **V**, suggesting that **V** is aromatically stacked; red circle indicates absence of isosbestic point.

Aqueous sodium cacodylate solutions of compounds **III**-**VI** were strongly fluorescent (SI **Figures S61-S63**); however, their emission properties differed remarkably. The 1,4-diethynylbenzene-derivative **IV** and the shortest 9,10-anthraceneylene compound **VI** were characterized by emission intensities proportional to compound concentrations up to 5 ×10^{-7} M (**IV**) and 8 ×10^{-6} M (**VI**), respectively, and their spectra (SI **Figures S62** and **S62**) revealed only minor changes upon heating to 95 °C, suggesting the absence of intermolecular interactions. In contrast, emission from the 9,10-diethynylanthracene analogue **V** was strongly non-proportional to concentration, even at c < 1 ×10^{-7} M (**Figure 8c**), and for both, **III** (SI **Figure S63**) and **V** (**Figure 8b**), the emission spectra at 5 ×10^{-7} M changed significantly with increasing temperature.

This temperature dependence of fluorescence and UV/Vis spectra of **III** and **V** strongly support intermolecular non-covalent aromatic stacking interactions between the chromophores. Particularly interesting is the emission spectrum of **V** (**Figure 8**), which is characterized by two distinct maxima: 503 and 578 nm. The ratio of the intensities of the maxima (r = I$_{503}$ / I$_{578}$) changes strongly and non-linearly with concentration and temperature. The maximum at 503 nm can be attributed[294, 302-304] to individual, non-stacked molecule **V**, whereas the maximum at 578 nm corresponds to aggregate emission. The emission changes plotted vs. the concentration of **V** fit well to a 1st exponential (**Figure 8c**), suggesting a well-defined, one-type aggregation process.

In pure water, the aggregation processes appear to be significantly less favorable. For compound **III**, a linear dependence of the absorbance on the concentration was found throughout the whole measurable range from 1 ×10^{-6} - 3.75 ×10^{-5} M (SI **Figure S53**). Only in the case of compound **V** was a non-linear dependence of the absorbance on the concentration found for concentrations > 1 ×10^{-5} M (**Figure 8d**). The emission of **V** in pure water changes accordingly (SI **Figures S55**). Between 1 ×10^{-6} - 1 ×10^{-5} M, only emission from the monomer is detectable. At concentrations > 1 ×10^{-5} M, the emission maximum gradually shifts

bathocromically and at 1 ×10⁻⁴ M, only aggregate emission with a maximum at 578 nm is detectable.

Thus, in sodium cacodylate buffer solution, aggregates are predominant for compounds **III** and **V** even at concentrations below 5 ×10⁻⁷ M (**Figure 6**, **Figure S58**), whereas in pure water, aggregates were only observed for compound **V** at concentrations higher than 1 ×10⁻⁵ M (**Figure 6d**, **Figure S55**). The tendency of these compounds to form aggregates is, therefore, strongly dependent on the ionic strength of the solution, a phenomenon previously observed[305] and is in the order **V** > **III** >> **IV**, **VI**.
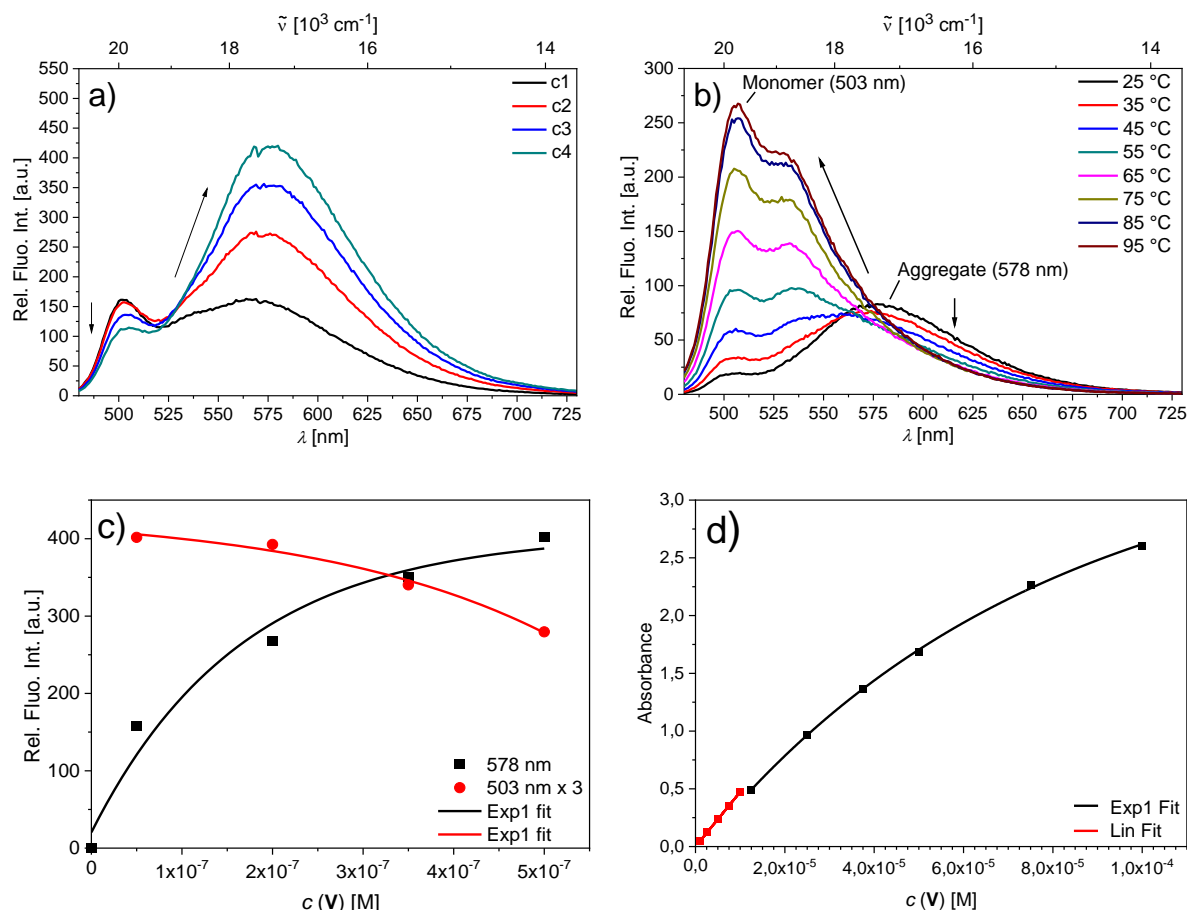
Figure 8. a) Fluorescence spectra of **V** (λ_{exc} = 470 nm) in sodium cacodylate buffer (pH 7.0, I = 0.05 M) at c(**V**) = 5; 20; 35; 50 ×10⁻⁸ M; b) temperature dependence of emission c(**V**) = 50 ×10⁻⁸ M in sodium cacodylate buffer (pH 7.0, I = 0.05 M); c) concentration dependence of the emission of **V** (λ_{exc} = 470 nm) in sodium cacodylate buffer (pH 7.0, I = 0.05 M) at 578 nm and 503 nm (multiplied by 3 for improved visibility); note the good fit of the experimental points to a 1st exponential; d) concentration dependence of the absorbance of 5 in pure water, with linear fit for c(**V**) < 1 ×10⁻⁵ M and 1st exponential fit for c(**V**) > 1 ×10⁻⁵ M.

3.4 Study of Interactions with DNA and RNA

Several typical types of DNA and RNA were chosen to investigate the interaction of the compounds **III**-**VI** with those macromolecules (SI, **Table S6**). *Calf thymus* (ct)-DNA, which is naturally occurring, represents a typical *B*-helix structure with a balanced ratio of GC-(48%) and AT-(52%) base pairs. The synthetic alternating polynucleotides poly (dGdC)₂ and poly (dAdT)₂, consist of only GC- or AT-base pairs, respectively. Thus, they represent two extreme situations with very different secondary structures and a very different level of minor groove

availability for binding of a small molecule. The sterically demanding guanine amino group, for example, hinders the deep penetration of small molecules. Double stranded poly rA - poly rU RNA was chosen as an *A*-helical structure with a major groove that is generally available[306] for binding of bulky small molecules, for comparison between double stranded (ds) DNA and ds-RNA.

To understand better the DNA/RNA binding of these novel chromophores, the single stranded synthetic (ss)-RNA polynucleotides poly rG, poly rA, poly rU and poly rC, which are each characterized by different properties, were also investigated. Poly rG is related to guanine-rich sequences in both DNA and RNA. Adenine ss-RNA (Poly rA) mimics 50 to 250 adenine nucleotides at the 3' end of mRNA. Poly rC and poly rU represent less organized secondary structures and are significantly more flexible than purine-RNAs. Also, ss-DNA poly dA and poly dT were studied, which are analogous to the aforementioned ss-RNA.

Thermal denaturation experiments

Thermal denaturation, which is the dissociation of ds-helices of polynucleotides into two single stranded polynucleotides, occurs at characteristic and well-defined temperatures (*Tm* value). The thermal stability of ds-helices is generally increased upon non-covalent binding of small molecules to ds-polynucleotides. This causes a significant increase of the *Tm* value (Δ*Tm*), which can be indicative of various binding modes.[307]

The three compounds with longer linkers (**III**-**V**) all strongly stabilized the ds-DNA/RNA even at rather low ratios of compound to polynucleotide (in the following, this ratio is generally given as: $r_{[compound] / [polynucleotide]}$) (SI **Figures S64-S72**), with anthracene analogue **V** causing the strongest stabilization (**Table 4**). The previously reported bithiophene compound **Z'**[13] and 1,3-butadiyne compound **II**[189] stabilized DNA and RNA to a similar extent (Δ*Tm* = 7-10 °C). Intriguingly, the short anthracene compound **VI** had a very weak effect on the thermal stability of DNA/RNA (SI **Figures S73** and **S74**). These findings suggest that once a certain length and level of flexibility is exceeded, the nature of the aromatic linker in these tetracationic bis-triarylboranes does not strongly influence the thermal stabilization effect of those compounds.

Table 4. The Δ*Tm* values[a] (°C) of the ds-polynucleotides studied upon addition of compounds **III-VI** at pH 7.0 (sodium cacodylate buffer, *I* = 0.05 M) at different ratios r[b].

	r[b]	ctDNA	poly rA - poly rU	poly (dAdT)$_2$
III	0.1	4	7	3
IV	0.1	2	9	2
V	0.1	10	8	6
VI	0.1	1	0	n.d.

[a] Error in Δ*Tm* : ±0.5°C; [b] r = $r_{[compound] / [polynucleotide]}$.

Fluorimetric titrations with DNA and RNA

As all compounds are highly emissive (**Table 3**), fluorimetric titration experiments were performed for a variety of double stranded (ds)-DNA/RNA, as well as single-stranded (ss)-DNA/RNA. Due to the aggregation properties of **III** and **V**, the titration experiments proved to be non-trivial and had to be performed at as low a concentration of the compound as possible. To obtain comparable data, compounds **IV** and **VI** were also studied at the lowest possible concentrations, although these compounds did not show aggregation-related effects. The calculation of binding constants was possible for most titrations by non-linear fitting of the data by means of the Scatchard equation[308, 309] (**Table 5**).

Table 5. Binding constants (log K_S) of **III**-**VI** with polynucleotides calculated by analyses of fluorimetric titrations[a]; at pH = 7.0 in sodium cacodylate buffer, I = 0.05 M.

		III	IV	V	VI
ds	ct-DNA	8.8	8.6	8.5	7.5
	poly (dAdT)$_2$	5.1[c]	7.8	7.7	7.4
	poly (dGdC)$_2$	6.6[c]	8.4	7.9	7.8
	poly rA - poly rU	6.0[c]	8.6	> 9	7.9
ss	poly rA	> 9[b]	8.4	7.8	7.1
	poly dA	7.6	> 9[b]	> 9[b]	n.d.
	poly rU	7.0	7.4	8.8	7.1
	poly dT	7.6	8.5	7.4	n.d.
	poly rG	7.1	8.7	8.7	7.3
	poly rC	7.4	7.1	> 9[b]	7.2

[a] Analyses of titration data by means of the Scatchard equation[308, 309] gave values of the ratio n [bound **compd.**] / [polynucleotide] = 0.2 - 0.5; for easier comparison, all log K_S values were re-calculated for fixed n = 0.25 (ds-polynucleotides) and n = 0.5 (ss-RNA/RNA). Correlation coefficients were > 0.99 for all calculated K_S values. [b] The first addition of DNA/RNA even at the lowest c(dye) yielded strong and maximum emission change, not allowing accurate calculation of the binding constant. [c] Due to competition of single molecule binding with aggregation, apparent binding constants are lower.

Detailed analysis of the binding constants (**Table 5**) revealed that all of these compounds bind to DNA/RNA with comparatively high affinities[308] for small molecules (LogK_S > 7). In many cases, the affinity is even in the nM range, which is considered exceptionally strong for small molecule / polynucleotide interactions. Intriguingly, **III**-**VI** show similar affinities for ds-DNA/RNA and ss-DNA/RNA, which is uncommon, as single stranded polynucleotides usually bind small molecules at least 2-3 orders of magnitude weaker than ds-polynucleotides.[231]

The somewhat weaker binding of **VI** compared to **III**, **IV**, **V** to ds-DNA/RNA agrees nicely with the thermal denaturation results (**Table 4**), again indicating that the short and very rigid linker of **VI** interferes to some extent with binding to the ds-polynucleotides. Below, selected

examples are discussed in greater detail, starting with the results for the non-aggregating compounds **IV** and **VI**.

Addition of any ds-DNA/RNA or ss-DNA/RNA resulted in very similar, strong quenching (ca. 90%) of the emission of compound **IV**, accompanied by a hypsochromic shift of the emission maximum of around 30 nm (2 000cm^{-1}) (**Figure 9**). The short anthracene compound **VI** showed similar, non-selective quenching for all ds-DNA/RNA. Very intriguingly, the fluorescence response of compound **VI** was highly sensitive to the base-composition of ss-RNA (**Figure 10**): poly rC (10% quenching); poly rG (40%); poly rU (60%) and poly rA (>95%). This selectivity concerning emission quenching was not observed for the binding affinity, as all ss-RNA show very similar binding constants (**Table 5**). In addition, it does not correlate with the redox potentials of the nucleobases and their impact on quenching efficiency.[310] Therefore, such a selective fluorimetric response could be correlated with the positioning of the very rigid fluorophore **VI** within a particular ss-RNA polynucleotide, whereby a combination of the nucleobase size, electronic properties and flexibility control interactions of the fluorophore with the target and the consequent emission of the complex formed.
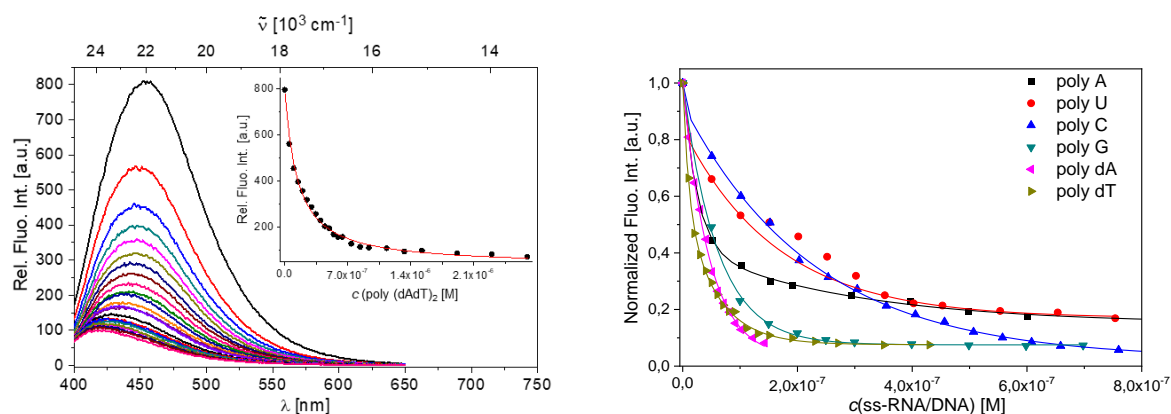
Figure 9. Left: Fluorimetric titration of **IV** (c = 5 ×10^{-9} M ; λ_{exc}= 372 nm) with poly (dAdT)$_2$ as representative of all ds-DNA/RNA titrations (SI **Figures S75-S78**), insert: dependence of relative fluorescence intensity at 448 nm on c (poly (dAdT)$_2$. Right: dependence of normalized fluorescence at λ_{max}= 448 nm on c (ss-DNA/RNA), the fitting to the Scatchard equation[308, 309] yielded parameters shown in **Table 5**. All measurements performed at pH 7, in sodium cacodylate buffer, I = 0.05 M.
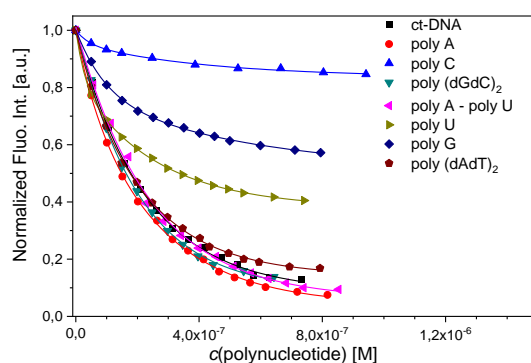
Figure 10. Fluorimetric titrations of compound **VI** (c = 5 ×10^{-8} M; λ_{exc}= 476 nm) with various ds-DNA/RNA and ss-RNA; dependence of fluorescence at λ_{max} = 527 nm on c(polynucleotide), the fitting to the Scatchard equation[308, 309] yielded parameters shown in **Table 5**. All measurements performed at pH 7, in sodium cacodylate buffer, I = 0.05 M.

However, aggregation-inclined analogues **III** and **V** showed more complex behavior in the fluorimetric titrations with DNA/RNA.

For example, titration with ct-DNA at two different concentrations of **III** (1 and 50 ×10^{-8} M), revealed significantly different profiles (**Figure 11**). Thus, at higher concentration (**Figure 11** top) and at an excess of **III** with respect to DNA (ratio r$_{[3] / [DNA]}$ > 0.25) the dye aggregated along the DNA helix and emission of **III** was quenched. At an excess of DNA (r$_{[3] / [DNA]}$ << 0.2) the dye molecules were re-distributed along the DNA helix, each to a separate binding site, and emission of **III** was partially restored; however, it did not reach the starting intensity of free **III**. At 50 times lower concentration (**Figure 11** bottom), DNA-induced aggregation of **III** was not observed, and the dominant process was quenching of emission, attributed to a single type of binding process.
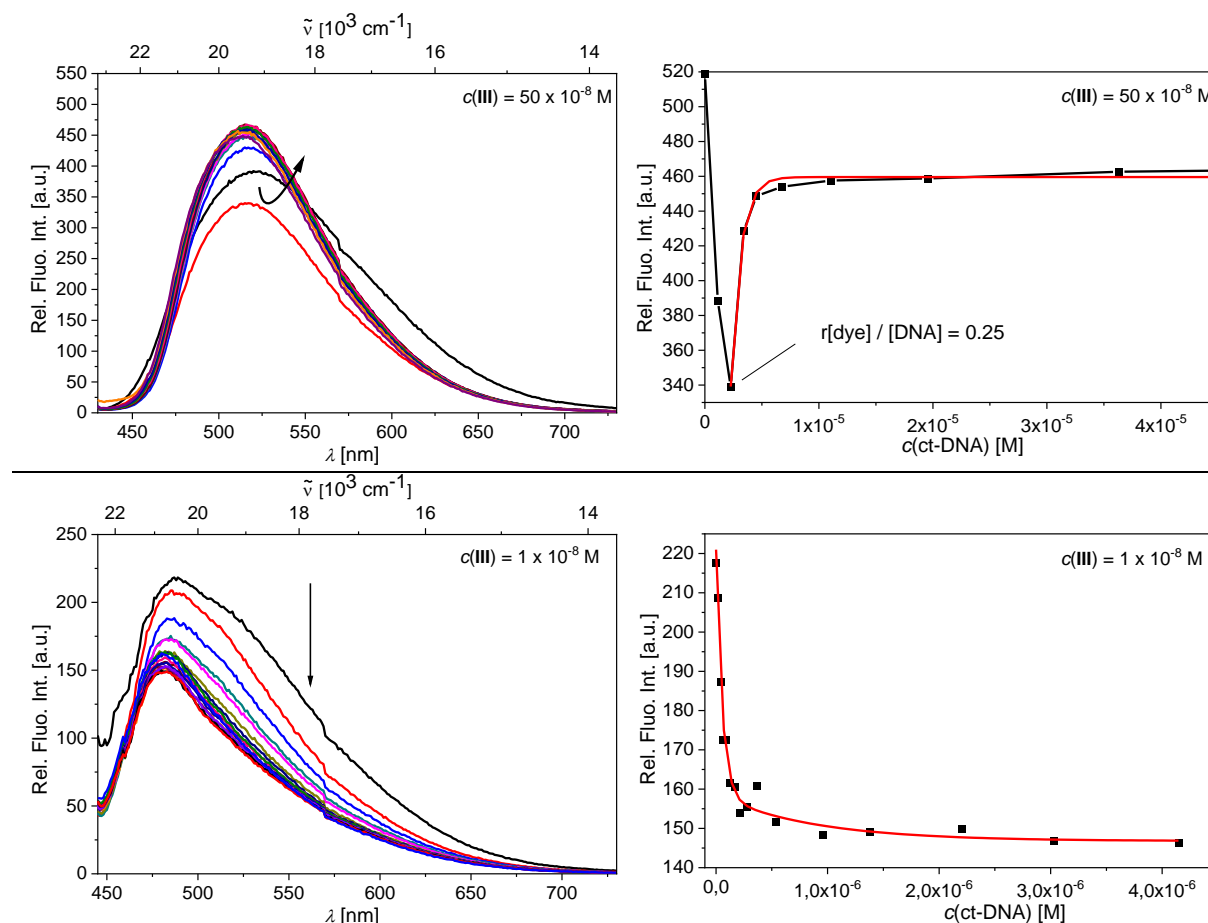
Figure 11. Top*:* fluorimetric titrations of **III** at *c* = 50 ×10^{-8} M and dependence of fluorescence at λ$_{max}$ = 519 nm on *c*(ct-DNA); bottom: fluorimetric titrations of **III** at *c* = 1 ×10^{-8} M with ct-DNA and dependence of fluorescence at λ$_{max}$ = 519 nm on *c*(ct-DNA), the fitting to the Scatchard equation[308, 309] yielded parameters shown in **Table 5**. All measurements performed at pH 7, in sodium cacodylate buffer, *I* = 0.05 M, λ$_{exc}$= 412 nm.

For the other ds- or ss-polynucleotides, all titrations were performed at the lowest possible concentration of **III**. The titration profiles are summarized in **Figure 12**. However, as the secondary structure and consequently the availability of binding sites of the various DNA/RNA differ strongly from each other (see SI **Table S5**), in some cases (poly rG, poly rC, all ds-

DNA/RNA except ct-DNA) the aggregation of **III** along the polynucleotide at ratios $r_{[compound] / [polynucleotide]} > 0.25$ could not be avoided. Nevertheless, considering changes at large excesses of DNA/RNA with respect to dye ($r_{[compound] / [polynucleotide]} << 0.2$) as representative for single molecule binding, analyses of this part of the titration data *via* the Scatchard equation[308, 309] can give a good estimate of the binding constants (**Table 5**).
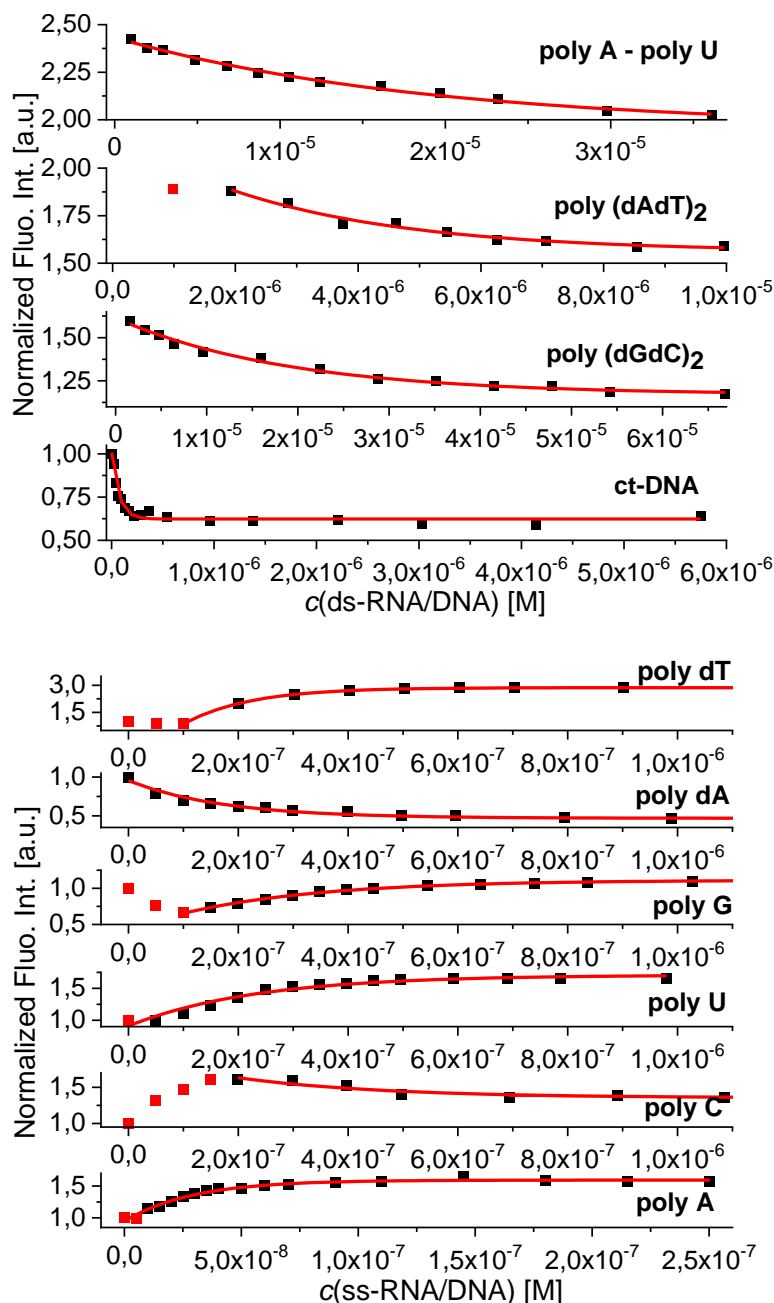
Figure 12. Fluorimetric titration of **III** ($c = 5 \times 10^{-8}$ M ; $\lambda_{exc} = 412$ nm) with DNA/RNA; dependence of normalized fluorescence at $\lambda_{max} = 500$ nm on c(DNA/RNA), the fitting to the Scatchard equation[308, 309] yielded parameters shown in **Table 5**. All measurements at pH 7, in sodium cacodylate buffer, $I = 0.05$ M.

Similarly, DNA/RNA-induced aggregation in the presence of an excess of dye was observed for anthracene analogue **V** (**Figure 13**). The titration of compound **V** with poly (dAdT)$_2$ (**Figure 13** top) showed a very well resolved aggregation - deaggregation process, as indicated by a

gradual red shift of the emission maximum toward 550 nm for ratios $r_{[5] / [poly(dAdT)_2]} > 0.25$, followed by a gradual blue shift of the emission maximum back to 520 nm for ratios $r_{[5] / [poly(dAdT)_2]} < 0.25$. This, again, suggests aggregation along the polynucleotide helix for comparatively high dye concentrations and re-distribution of the dye molecules into separate binding sites for an excess of polynucleotide. For the titration with poly rA - poly rU, such an aggregation-deaggregation process was not observed. Only one binding process was observed, as indicated by a systematic shift of the emission maximum toward 550 nm, even at a large excess of RNA ($r_{[5] / [poly A – poly U]} < 0.05$, SI **Figure S102**). Thus, it is suggested that the much deeper major groove of RNA (SI **Table S5**) can accommodate dimeric aggregates of **V** much more efficiently, than the smaller minor groove of poly (dAdT)$_2$.
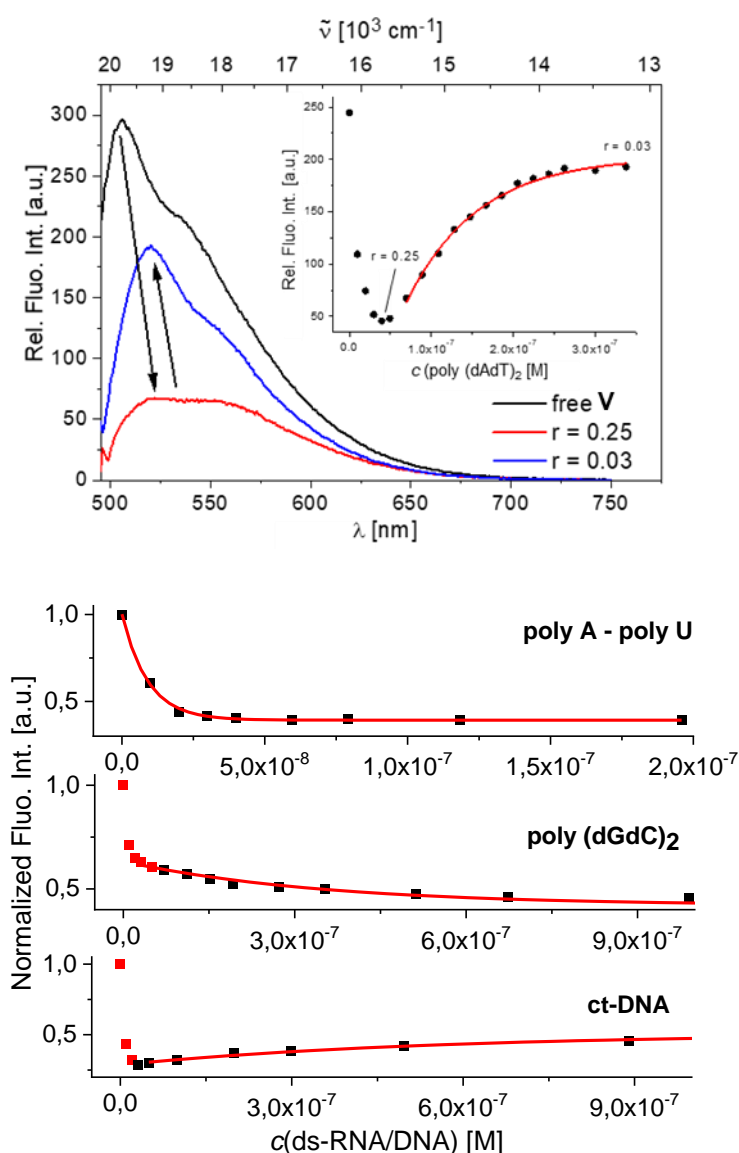
Figure 13. Top: Changes in the emission spectra of **V** upon titration with poly (dAdT)$_2$, insert: dependence of relative fluorescence intensity at 520 nm on c (poly (dAdT)$_2$). Bottom: Fluorimetric titrations of **V** (c = 1 ×10^{-8} M ; λ_{exc} = 470 nm) with ds-DNA/RNA; dependence of normalized fluorescence at λ_{max} = 550 nm on c(DNA/RNA), the fitting to the Scatchard equation[308, 309] yielded parameters shown in **Table 5**. All measurements performed at pH 7, in sodium cacodylate buffer, I = 0.05 M.

CD experiments

Having studied the changes of the spectroscopic properties of the compounds upon interaction with polynucleotides, circular dichroism (CD) spectroscopy was chosen as a highly sensitive method to gain insight into the conformational changes of the secondary structure of polynucleotides induced by small molecule binding.[311] In addition, achiral compounds **III**-**VI** might display induced circular dichroism (ICD) upon interaction with polynucleotides, which would provide information on the type of interaction present.[312, 313]

The short anthracene compound **VI** did not have any measurable influence on the CD spectra of ds-DNA/RNA (SI **Figure S104**), suggesting that its binding does not disturb the secondary structure of the respective polynucleotide. Also, for compound **VI**, no ICD bands > 300 nm were observed upon binding to any ds-DNA/RNA. Thus, molecules of **VI** were either not uniformly oriented with respect to the chiral axis of ds-DNA/RNA or the transition vectors of **VI** were oriented with respect to the chiral axis of ds-DNA/RNA to yield ICD bands of negligible intensity.[312, 313] Similarly, addition of **III** or **IV** caused only minor decreases in intensity in the CD spectra of ds-DNA/RNA and no measurable ICD bands for the compounds (SI **Figures S105** and **S106**), also suggesting only small changes in the secondary structure of the polynucleotides. These CD results along with the strong binding affinities of **III**, **IV** and **VI** to ds-DNA/RNA (**Table 5**) and the observed thermal stabilization effects (**Table 4**), support binding within the minor groove of ds-DNA and the major groove of ds-RNA, respectively. This is in accordance with earlier studies by Marder, Piantanida and co-workers on this novel class of DNA/RNA sensors.[13, 189]

In contrast, addition of the longer anthracene derivative **V** significantly decreased the intensity of the CD spectra of ds-DNA/RNA (**Figure 14**, Λ = 270-290 nm), suggesting unwinding of helical structures, which causes a partial loss of chirality. Complexes of compound **V** with polynucleotides containing A, T and U base pairs displayed ICD bands in the absorption range of the compound (**Figure 14**, Λ = 450 - 550 nm), which suggests a very uniform orientation of the transition vectors of the molecules (Λ = 450 - 550 nm) with respect to the chiral axis of DNA.[308, 309] Intriguingly, the complex of **V** with GC-DNA (poly (dGdC)$_2$) showed no measurable ICD bands and the CD spectrum of GC-DNA (Λ < 300 nm) changed only marginally upon addition of **V**. The main structural difference between GC-DNA and AT-DNA (poly (dAdT)$_2$) is a better availability of the minor groove of the latter for binding of small molecules (SI **Table S5**). Thus, the CD results suggest that only in the case of AT-DNA does compound **V** insert deeply enough into the minor groove to yield a uniform orientation of the molecules with respect to the chiral axis of DNA, while simultaneously disturbing the DNA helicity by this insertion process. The same is suggested, analogously, for the major groove of AU-RNA (poly A - poly U), which is the common binding site for small molecules with RNA.[306] In GC-DNA, amino groups of guanine in the minor groove sterically hinder small molecule insertion and, thus,

molecules of **V** occupy a more heterogeneous orientation along the DNA helix, consequently displaying negligible ICD bands.
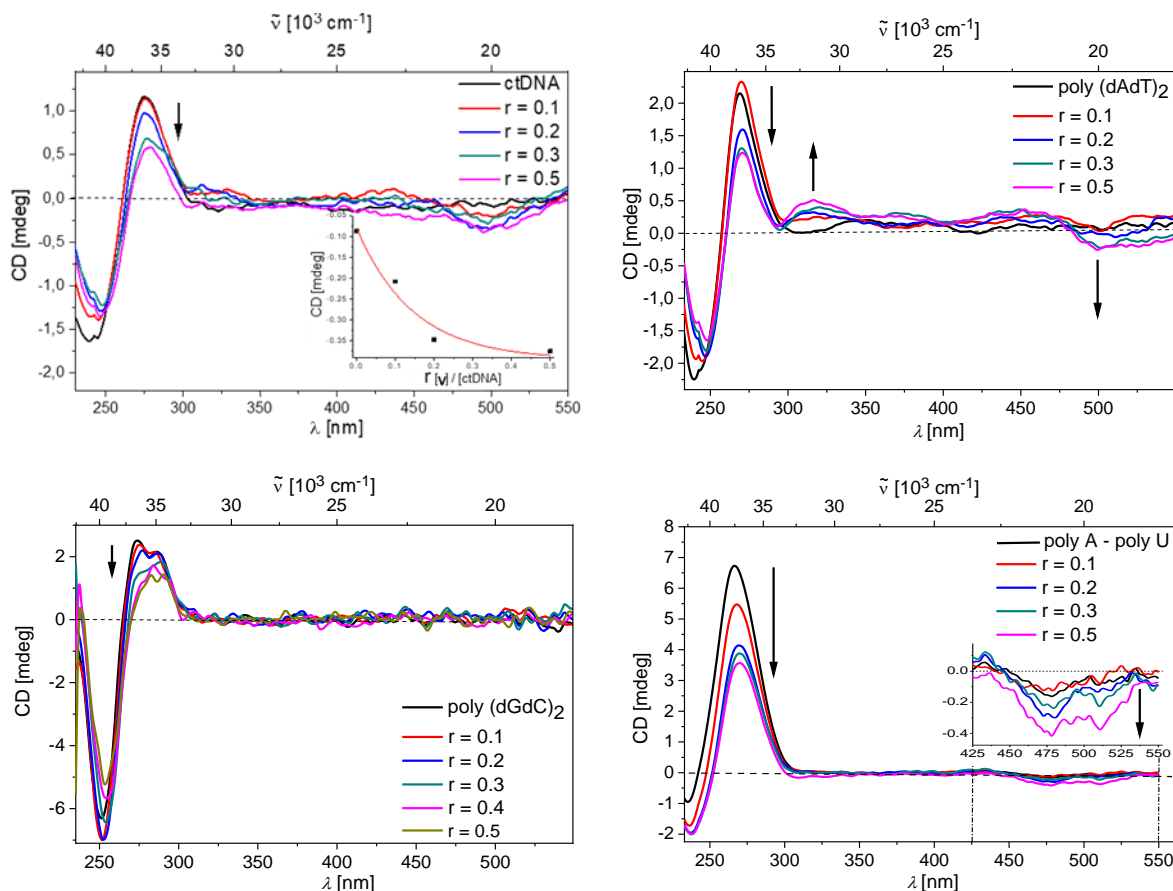
Figure 14. CD titration of ct-DNA (insert: dependence of CD at 500 nm on r [5]/[ctDNA]), poly A - poly U, poly (dAdT)$_2$, poly (dGdC)$_2$ (all DNA/RNA c = 2 ×10^{-5} M) with **V** at molar ratios r [5]/[polynucleotide] = 0.1-0.5. All measurements performed at pH 7.0, in sodium cacodylate buffer, I = 0.05 M.

3.5 Molecular Modelling

To corroborate and explain further the experimental findings, especially concerning compound **V**, a better structural understanding of the observed intramolecular interactions was required.

The observed aggregation of the compounds, particularly that of anthracene derivative **V**, is not trivial to explain due to the sterically demanding triarylboron dications attached to both sides of the linker. Those dications would additionally impose charge repulsion when two anthracenes moieties are stacked in a dimer.

Thus, molecular modelling was first performed of a dimer of compound **V** in water (for details see: SI General Information). The minimized structure obtained after 200 ns of molecular dynamics (MD) simulation in water is shown in **Figure 15**. It is characterized by the asymmetric off-set of two anthracenes, which are partly overlapping.
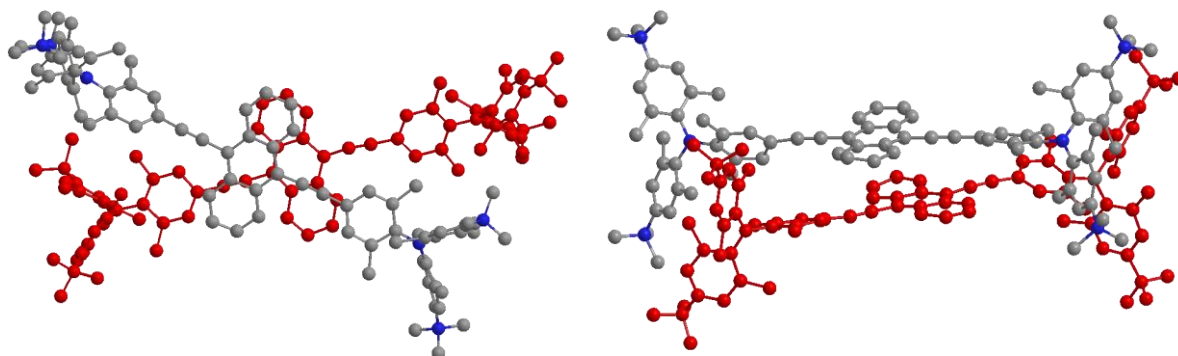
Figure 15. Structure of the dimer aggregate of **V**, displayed from two different views, obtained after 200 ns of MD simulation in water. Hydrogen atoms of **V** are omitted for clarity.

The fluorimetric results suggest two binding modes for complexes of **V** with AT-containing DNAs (poly (dAdT)$_2$). One (at ratios $r_{[5]/[DNA]} > 0.25$) is characterized by emission of aggregated **V**, and the other (at ratios $r_{[5]/[DNA]} << 0.25$) by monomer emission (cf. **Figure 13**). The binding mode of the monomer is supported by induced CD bands and suggests AT-DNA minor groove binding of **V**. To determine the structural arrangement of **V** within the minor groove of AT-DNA, docking was performed using PyMOL software and compound **V** was docked into the minor groove of AT-DNA using the optimized position previously determined for analogue **Z'**[13] as a template. Compound **V** slightly reoriented within the groove and remained inside the groove during the entire 300 ns of MD simulation (**Figure 16**). Multipoint measurements of the distances between opposite strand backbones (P atoms of paired nucleobases) revealed only a slight broadening (<10%) of the minor groove upon binding of **V**.
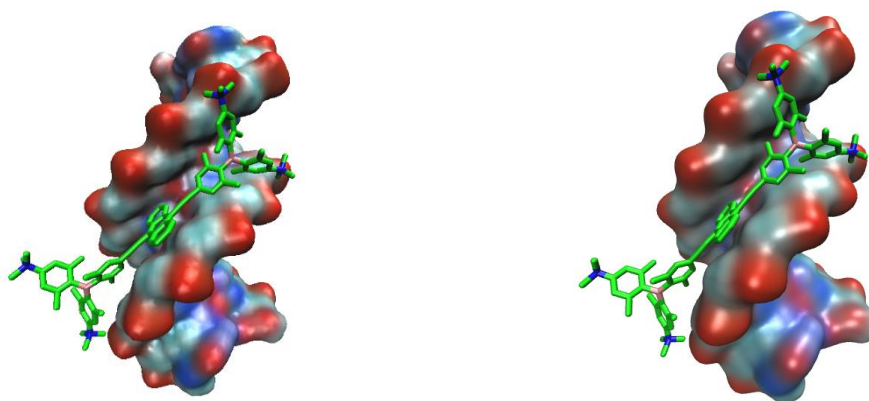
Figure 16. The result of 100 ns (left) and 300 ns (right) of molecular dynamics simulation of **V**/DNA complexes. Hydrogen atoms of **V** are omitted for clarity.

The aggregation process observed at ratios $r_{[5]/[DNA]} > 0.25$, can either be explained by insertion of dimers of **V** into the minor or major groove of DNA or by the stacking of molecules of **V** in long stacks parallel to the DNA helix (similar to a process observed for porphyrins[314]). To investigate this aggregation process, a dimer of **V** was first inserted into the minor groove of AT-DNA using the obtained monomer complex (**Figure 16**) as a template. During the first 150 ns of MD, the dimer remained bound into the minor groove (**Figure 17**), revealing a further slight broadening (<5%) of the minor groove with respect to the monomer complex. However,

at about 200 ns the dimer started to migrate through the minor groove towards the polynucleotide termini and, after 300 ns of MD simulation, it nested there, stabilized by stacking interactions with the terminal base pair (**Figure 17**). Such a "capping" effect is frequently observed when studying the binding of large aromatic moieties to short oligonucleotides due to the very stable stacking interactions with base pairs at the termini.[315] Thus, the results suggest that a dimer of **V** can efficiently bind into the minor groove of a long AT-polynucleotide.
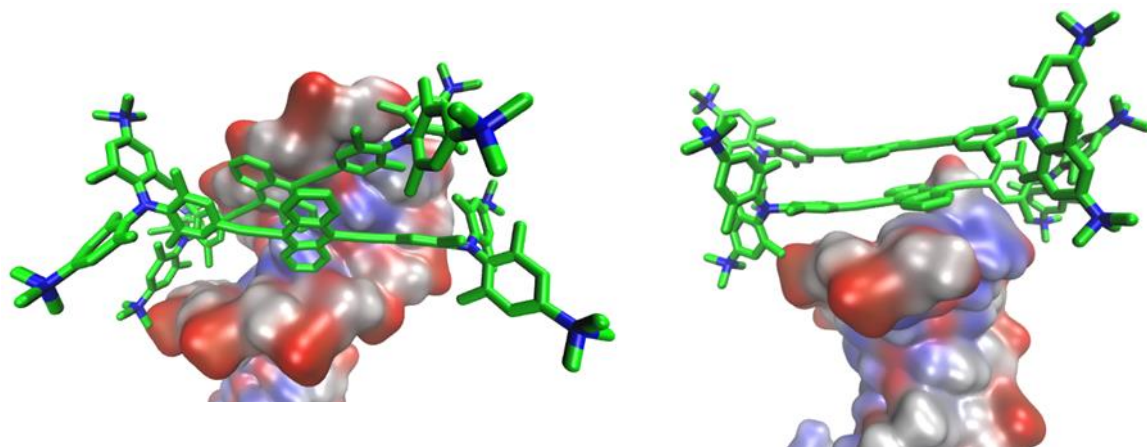
Figure 17. The MM results after 150 ns (left) and 300 ns (right) of molecular dynamics simulation of the **5**/DNA complex with **V** bound initially into the minor groove. Hydrogen atoms of **V** are omitted for clarity.

Second, a dimer of **V** was inserted into the major groove of AT-DNA (**Figure 18**), to see if a stable complex within the major groove of AT-DNA can be formed, as determined for other bulky molecules.[316] This time, the dimer started to migrate out of the groove after 90 ns. For the following 150 ns, it oscillated around the groove entrance, never staying deeply inserted within the groove. At the end of 300 ns of MD simulation, it adopted an almost identical position at the polynucleotide end to that observed for the dimer bound into the minor groove. The major groove of AT-DNA is, thus, considered a much less adequate binding site for dimers of **V**.
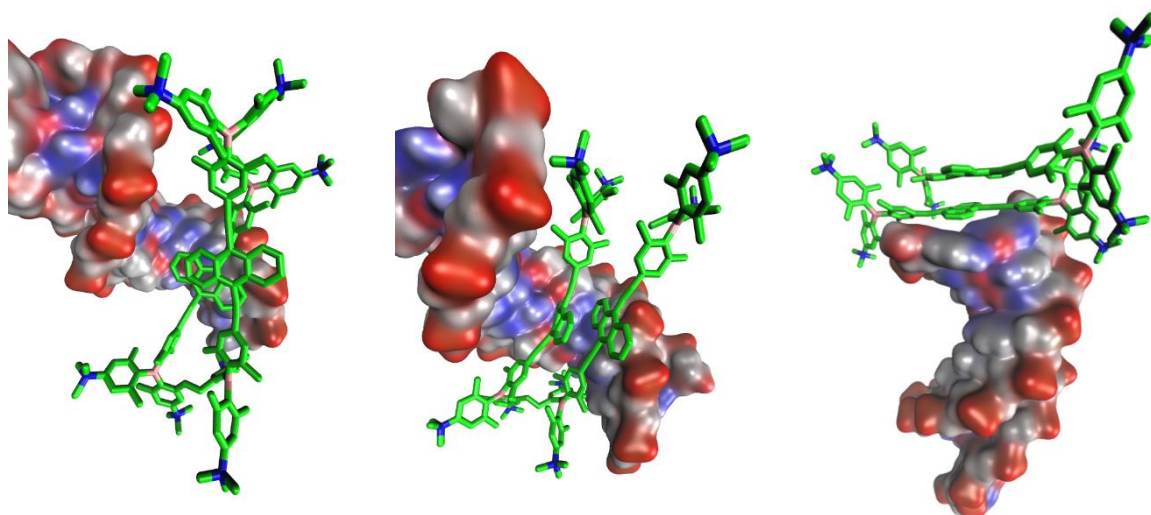
Figure 18. The results of 90 ns (left), 95 ns (middle) and 300 ns (right) of molecular dynamics simulation of the **5**/DNA complex with the dimer of **V** bound initially into the major groove. Hydrogen atoms of **V** are omitted for clarity.

Thus, the molecular modelling results strongly support binding of **V** into the minor groove of DNA as a dominant binding mode. However, at "crowding conditions", i.e. an excess of **V** over DNA binding sites, dimers of **V** can also form within the minor groove, without significantly disturbing the DNA helix. Binding of dimers of **V** within the major groove of DNA is less probable due to the much larger size of this binding site, not allowing all positive charges of the dimer of **V** to reach the negatively charged backbones efficiently at the same time. In addition, insertion of a dimer of **V** would not displace all water molecules inside the major groove and, thus, the hydrophobic driving force is diminished.

Due to the structural similarity and the fact that, for compounds **Z'** and **V**, the minor groove was determined to be the most likely binding site *via* molecular modelling, it is suggested that compounds **III**, **IV** and **VI** form similar complexes with DNA.

3.6 Raman and Surface-Enhanced Raman Scattering (SERS) Spectroscopy

As strong Raman responses were observed for previously reported compound **II**,[189] analogues **III-V**, as well as the short anthracene derivative **VI** were studied under the same conditions.

The Raman spectra of **III**-**V** in aqueous solutions (c = 1 ×10^{-4} M) were of low intensity, dominated by the broad water stretching and bending bands around 3220 cm^{-1} and 1640 cm^{-1}, respectively (SI **Figure S108**). Nevertheless, some bands originating from the compounds were observed and could be assigned (SI **Table S6**). Calculated Raman spectra for compounds **III-V** are in good agreement with the experimental data (SI **Table S11**). The characteristic band in the C≡C stretching region (around 2200 cm^{-1}) was observed in the spectra of **IV** and **V** and the exact band position was affected by the aromatic substituent

between the triple bonds. The C≡C stretching bands occur at 2209 and 2182 cm^{-1} for the compounds containing benzene (**IV**) and anthracene (**V**) cores, respectively, in agreement with the fact that lower energy C≡C stretching band frequencies characterize larger π-conjugated systems.[317] A characteristic band at around 1590 cm^{-1} was observed in the spectra of all three compounds, which can be attributed to aromatic stretching, distributed over the respective aromatic linker between the two boron atoms. In the Raman spectrum of **III**, possessing a bithiophene moiety between the triple bonds, the C≡C bond was hardly observable, while bands attributed to thiophene ring stretching modes (1472 and 1453 cm^{-1}) were observed. According to calculations, the energy of the C≡C stretching mode of **III** should be between the values obtained for **IV** and **V**. This is consistent with the data obtained by SERS spectroscopy (*vide infra*). In contrast to compounds **III**-**V**, the Raman scattering of anthracene derivative **VI**, not containing triple bonds, was overlapped by fluorescence and thus not observed at all, even at higher concentration ($c = 2 \times 10^{-3}$ M). This clearly pointed out the significance of the triple bonds in the structure, which provide strong Raman bands, allowing Raman detection of the molecule in the sub-millimolar concentration range.

Unlike the Raman spectra, the SERS spectra of all compounds, **III**, **IV**, **V** and **VI**, were obtained and preliminarily assigned (**Figure 19**, SI **Table S7**). The observed surface-enhanced Raman scattering pointed to adsorption of the molecules onto the enhancing silver nanoparticles, mostly driven by attractive electrostatic interactions between the negatively charged citrate ions on the silver surface and positively charged trimethylamino groups of the compounds. For compounds **III**-**V**, the characteristic SERS bands were observable at a concentration as low as 5×10^{-7} M, which is an order of magnitude higher than the lowest detectable concentration for **II**.[189] In contrast, the SERS response of the short anthracene analogue **VI** was very weak, with weak bands characteristic of anthracene (1549, 1329 and 1263 cm^{-1}) and phenyl (1588 and 1421 cm^{-1}) moieties, and observed only at the highest measured concentration of 5×10^{-6} M (**Figure 19d**). This confirms the essential role of the triple bonds in the molecular structure for the Raman scattering ability of these molecules. It also demonstrates that, even though directly connected triple bonds increase the Raman intensity, the insertion of different aromatic moieties between them still gives satisfying Raman responses and is thus an alternative approach for the design of dual Raman and fluorescent chromophores.
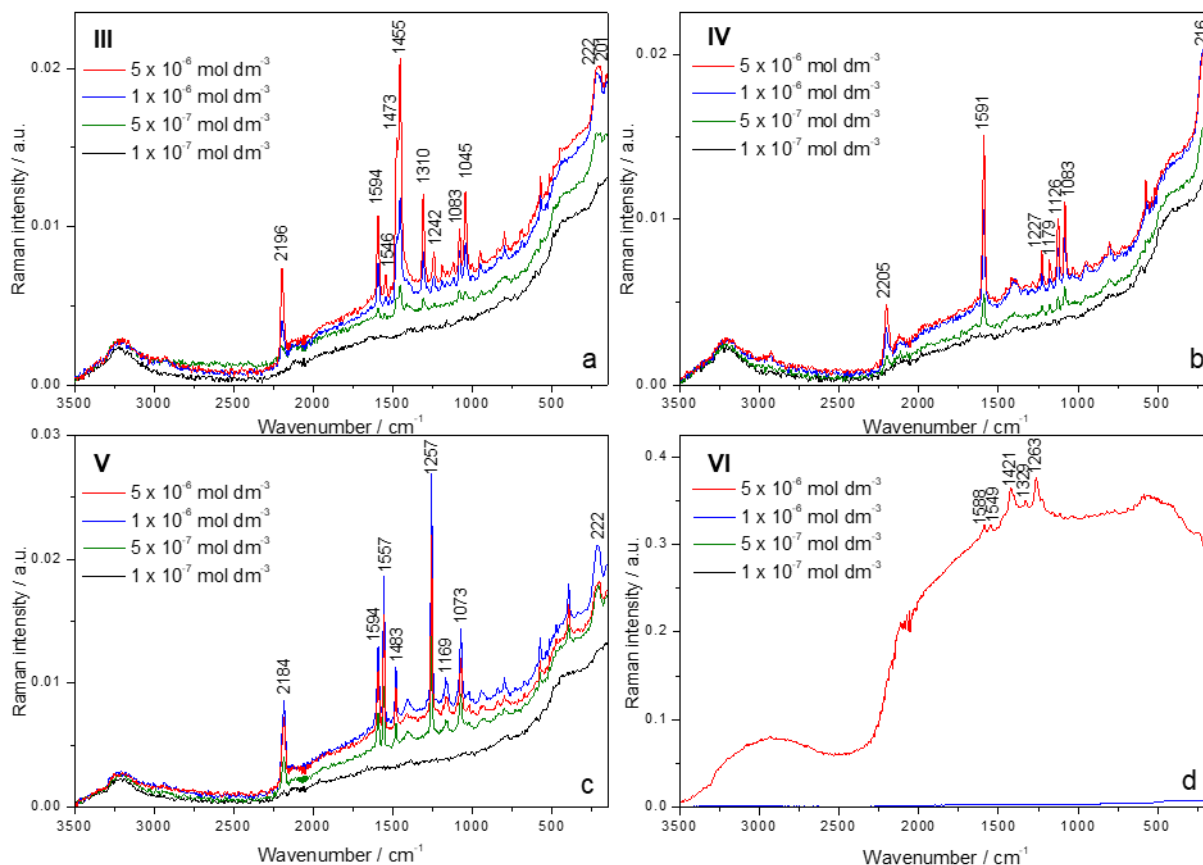
Figure 19. Concentration dependent SERS spectra of **III**-**VI** in the silver colloid, $c = 1 \times 10^{-7}$, 5×10^{-7}, 1×10^{-6}, 5×10^{-6} M; $\lambda_{ex} = 1064$ nm.

In the SERS spectra of **III**, **IV** and **V** the following common bands were observed, respectively: a band at ca. 2200 cm^{-1}, assigned to the stretching of the C≡C bonds, a band at ca. 1595 cm^{-1}, attributed to the aryl stretching distributed over the respective aromatic linker between the two boron atoms, and a band at ca. 1080 cm^{-1}, associated with the stretching of the bonds between the boron atom and the aryl rings. The position of the C≡C bond stretching bands at 2184 cm^{-1} (**V**), 2196 cm^{-1} (**III**) and 2205 cm^{-1} (**IV**) are significantly dependent on the respective aromatic moiety, namely, anthracene, thiophene and benzene. In addition, moderate to strong bands associated with thiophene were observed at 1473, 1455, 1310, 1242 and 1045 cm^{-1} in the spectrum of **III**, while medium to intense bands distinctive of anthracene were observed at 1557, 1483, 1257 and 1169 cm^{-1} in the spectrum of **V**.

By decreasing concentration from 5×10^{-6} M to 1×10^{-7} M, the SERS intensity diminished for all compounds except for **V**, for which the most intense SERS spectrum was observed at a concentration of 1×10^{-6} M (**Figure 19c**). In accordance with UV/Vis absorbance and fluorescence measurements which indicated stacking of **V** in aqueous solution, by lowering concentration the equilibrium was shifted to monomeric molecules, which upon adsorption onto the enhancing metal surface adopted a position different from that of the aggregated molecules. Thus, it was very likely that at 1×10^{-6} M the bis-triarylborane longitudinal axes of

the monomeric molecules were oriented perpendicular to the silver surface, giving rise to the most enhanced scattering.

Furthermore, the SERS spectra of **III**, **IV** and **V** were studied upon addition of ct-DNA. When compared to the spectrum of the neat compound ($c = 1 \times 10^{-6}$ M) measured in the buffered silver colloid, the SERS spectra of the complexes of **III-V** with ct-DNA were very weak at the molar ratio $r_{[compound]/[ct-DNA]} = 0.2$, and not observed at all at the molar ratio $r_{[compound]/[ct-DNA]} = 0.1$ (**Figure 20**). Presumably, bis-triarylborane molecules are efficiently bound to the nucleic acid when there is an excess of ct-DNA, resulting in a loss of the SERS intensity as the highly negatively charged phosphate backbone of ct-DNA prevented efficient adsorption of the complexes onto the silver nanoparticles. Nevertheless, for the complexes of **IV** and **V** in equimolar ratio with ct-DNA, $r_{[compound]/[ct-DNA]} = 1$, the bands at 1557 and 1258 cm^{-1} (**IV** / ct-DNA) and at 1557 and 1257 cm^{-1} (**V** / ct-DNA) were selectively enhanced (**Figures 20b** and **20c**). The former band (1557 cm^{-1}) was attributed to stretching of the aromatic moieties, and the latter (1258/1257 cm^{-1}) to in-plane deformation of the aromatic CH groups. Both bands, in essence, originate from arene ring vibrations and can be easily associated with three phenyl substituents as well. Thus, it can be assumed that, upon binding with the nucleic acid, either the central part of the molecule (benzene, anthracene) or the phenyl moieties linked to boron were placed closer and/or more perpendicular towards the enhancing silver surface. New bands originating from the nucleic acid were not observed in the SERS spectra of the complexes.
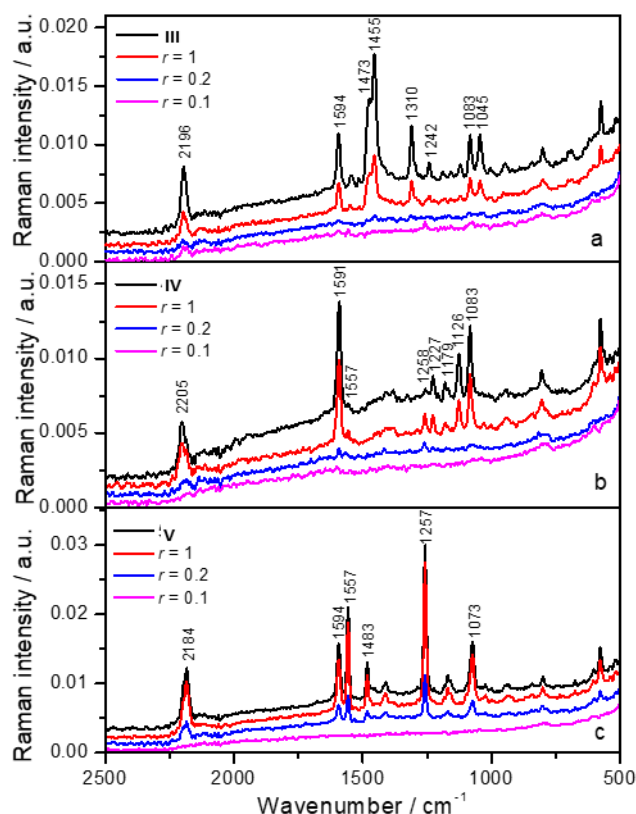
Figure 20. SERS spectra of **III-V** and their complexes with ct-DNA in molar ratios $r_{[compound]/[ct-DNA]}$ = 1, 0.2 and 0.1; c(**III-V**) = 1 ×10^{-6} M; λ_{ex} = 1064 nm. The spectra are displaced for visual clarity.

3.7 Conclusion

The novel class of tetracationic bis-triarylborane DNA and RNA sensors was successfully extended by four molecules **III-VI**. Three of them contain long bis(phenylethynyl)aryl (**III**: aryl = 5,5'-2,2'-bithiophene; **IV**: aryl = 1,4-benzene; **V**: 9,10-anthracene) linkers between the two boryl moieties and can be considered as dual Raman and fluorescence chromophores, while the short analogue **VI** possesses only an anthracene moiety as the linker and can be considered a fluorophore probe. Analysis of the solid state structures of the neutral precursors to **III** and **IV** reveal a high level of flexibility for ethynyl-containing aryl linkers. Concentration and temperature dependent UV/Vis and fluorescence experiments suggest a tendency for aggregation for compounds **III** and **V**, increasing with the ionic strength of the solution. Thermal denaturation experiments revealed strong stabilization of ds-DNA/RNA for complexes formed with compounds **III-V**, similar to that observed for the previously studied compounds **Z'** and **III**. The very weak stabilization observed for compound **VI** demonstrates that a certain length and flexibility of the aromatic linker needs to be exceeded for efficient thermal stabilization to occur. All four compounds bind to ds-DNA/RNA and ss-DNA/RNA with similar affinities, which contrasts with the fact that binding affinities for ss-polynucleotides are typically 2-3 orders of magnitude lower than for ds-polynucleotides. This is consistent with previous studies by

Marder, Piantanida and co-workers[13, 189] and it is suggested that ss-RNA is chain-wrapping around the tetracationic bis-triarylborane motif like a thread around a spindle.

In general, binding of compound **VI** is somewhat weaker to the tested polynucleotides than that of the other compounds, which agrees nicely with the thermal denaturation experiments and, again, demonstrates the importance of the linker length and flexibility. For compounds **III** and **V**, aggregation - deaggregation processes were observed in fluorimetric titration experiments with DNA and RNA. Thus, at an excess of dye, an aggregation of the dye along the helical axis of the polynucleotide or in dimeric form inside a groove is suggested while, at an excess of polynucleotide, the molecules are separated and are each transferred to separate binding sites. Based on all of the experimental data, including CD results, the minor groove is suggested as the dominant binding site for ds-DNA and the major groove for ds-RNA for compounds **III**, **IV** and **VI**. This is in accordance with previous findings for compounds **Z'** and **II**.[13, 189] For compound **V**, the CD results suggest an unwinding of the helical structure of the polynucleotide upon binding and very uniform orientation with respect to the helical axis for all ds-polynucleotides tested containing A, T and U base pairs. A molecular modelling study on complexes of compound **V** with AT-DNA also suggests the minor groove as the dominant binding site and that even dimers of **V** can be accommodated by the minor groove, while their binding into the major groove is much less efficient. Strong SERS responses were obtained for **III**-**V** at low concentrations. For compound **VI**, weak SERS signals were observed only at the highest concentration measured. This confirms the important role of the triple bonds for strong Raman scattering and demonstrates that the insertion of aromatic moieties between two triple bonds, by which the absorption and emission properties of a molecule can be conveniently tuned, is a feasible alternative for the design of dual Raman and fluorescence chromophores. In addition, the energy of the stretching vibration of the characteristic $C{\equiv}C$ bonds was found to be significantly dependent on the aromatic moiety between the triple bonds. In analogy to a variation of the length of the poly-yne chain,[282] this might be applied as a useful tool in the design of new chromophores suitable for multiplex Raman imaging purposes.

CHAPTER 4

-

SYNTHESIS AND INVESTIGATION OF WATER-STABILITY,
PHOTOPHYSICAL- AND SINGLET OXYGEN
SENSITIZATION PROPERTIES

OF

THIOPHENE AND RED-TO-NIR EMITTING EDOT-LINKED
WATER-SOLUBLE TETRACATIONIC BIS-
TRIARYLBORANE CHROMOPHORES

4 Synthesis and Investigation of Water-Stability, Photophysical- and Singlet Oxygen Sensitization Properties of Thiophene and Red-to-NIR Emitting EDOT-linked Water-Soluble Tetracationic bis-Triarylborane Chromophores

4.1 Introduction

Increasing research interest has been focused on triarylboranes over the last three decades and the structural motif has been incorporated in numerous functional materials.[16, 17, 19] More recently, several triarylboryl-containing chromophores have been successfully employed in different biological applications.[7, 9-13, 58, 116, 119, 143-145, 174, 189, 190, 258-260, 262] The empty p_z-orbital at boron makes it a strong π-acceptor and strong Lewis-acid and needs to be protected sufficiently to obtain robust materials. A common way to achieve this is *via* kinetic stabilization by use of sterically demanding substituents, a concept first investigated by Krause and co-workers.[62, 63, 65] In 1957, Brown and Dodson reported $BMes_3$ (Mes = mesityl = 2,4,6-trimethylphenyl) as the first air-stable triarylborane[72] and, later, it was found that, in many cases, two mesityl groups provide enough steric protection to obtain compounds that are stable under ambient conditions in the solid state and in typical organic solvents.[76, 133, 134, 137, 146, 263-267] Electronic effects also play an important role in the stability of triarylboranes. In 1955, Wittig and co-workers reported tri-4-(*N*,*N*-dimethylamino)phenylborane, lacking any steric protection from the 2- and 6- positions of the phenyl substituents, and found that it was air-stable as a solid for ca. one week.[70] The stability was explained by the electronic +M-effect of the amine substituents. In reverse, when enhancing the Lewis-acidity of boranes by introducing electron-withdrawing groups, stability issues have to be carefully considered. The 2,4,6-tris-(trifluoromethyl)phenyl (FMes) group was shown to be a convenient and very efficient aryl moiety that is both very strongly electron-withdrawing and sufficiently bulky giving highly electron deficient and stable boranes.[125, 131, 193, 318] A systematic study by Marder and co-workers on donor-acceptor thienyl-BAr_2 compounds demonstrates the influence of electron-withdrawing groups on the reduction potential of the systems.[130] For the thienyl-$BMes_2$ compound, sterically protected by four *ortho*-methyl groups, a reduction potential of -2.23 V (*unless otherwise noted, all reduction potentials discussed are referenced vs. ferrocene/ferrocenium (Fc/Fc⁺)*) was reported, that is increased to -2.04 V by replacing the *para*-methyl groups with either C_6F_5 or 3,5-$(CF_3)_2$-C_6H_3.[130] In the analogous thienyl-B^FMes_2 compound, the reduction potential was further increased to -1.61 V. Song and co-workers used *para*-cyano substituents in triarylboranes in which the boron was sterically protected by six *ortho*-methyl groups, and reported reduction potentials of ca. -1.8 V.[159, 160] Gabbaï and co-workers obtained water-soluble and strongly Lewis-acidic triarylboranes by stepwise

substitution of the *para*-methyl groups of BMes$_3$ with trimethylammonium cations.[140] The reduction peak potential was increased by 0.26 V for each substitution. Two substitutions were found to be sufficient to obtain a water-soluble triarylborane with a reduction potential of - 2.09 V. Despite its strong Lewis acidity, this compound was water-stable, even in the low concentration range required for photophysical measurements. This approach was combined with the experience of the Marder group with acceptor-π-acceptor (A-π-A) chromophores[319-321] to design compounds with a (4-(*N,N,N*-trimethylammonio)-2,6-dimethylphenyl)$_2$B-(linker)-B(4-(*N,N,N*-trimethylammonio)-2,6-dimethylphenyl)$_2$ structural motif (**Figure 21**), and several chromophores of this type were reported with applications in live-cell imaging[9, 10, 12] and biomacromolecule sensing.[13, 189, 190] The boron atoms in these chromophores are strongly Lewis acidic, due to the electron-withdrawing effect of the trimethylammonium cations, and thus need to be protected by six *ortho*-methyl groups (e.g. compound **Z'**, **Figure 21**) in order to be stable in pure water. In further studies, it was found that employing 9,10-anthracenylene as the linker also provides a water-stable compound, while the 1,4-phenylene analog decomposes within three hours in deuterated methanol under ambient conditions.[10] When a thienyl group is directly adjacent to boron as part of the aromatic linker, the resulting compounds **X'** and **Y'** were generally found to be air- and moisture-stable in organic solvents.[9, 10] Stability was even sufficient for photophysical measurements in acetonitrile under ambient conditions over the course of one day. However, both compounds decompose too quickly at low concentrations in pure water to be applied in aqueous biological environments.
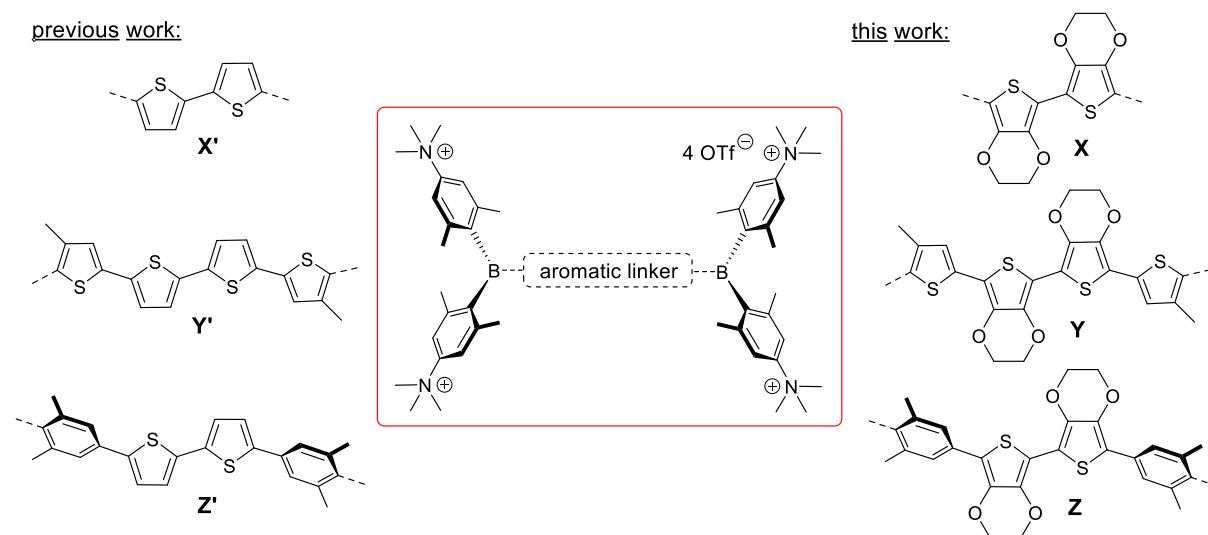
Figure 21. General structure of water-soluble A-π-A chromophores with different aromatic linkers including the target molecules **X**, **Y**, and **Z** of this study.

In this study the two thiophenes in compounds **X'**, **Y'**, and **Z'** are substituted with similar, but more electron-rich, 3,4-ethylenedioxythiophene (EDOT) groups. As a monomeric building block of the widely used and commercially applied conductive polymer poly(3,4-ethylenedioxythiophene):poly(styrenesulfonic acid) PEDOT:PSS,[322-324] EDOT itself, and

oligomers thereof, are well investigated compounds with application in several functional π-conjugated systems.[325-337] Compounds **X**, **Y**, and **Z** should be less Lewis-acidic and, thus, possibly more stable than their respective analogs **X'**, **Y'**, and **Z'**, due to greater electron density at boron. As previously observed by Marder and co-workers,[321] a more electron-rich π-bridge in A-π-A chromophores is expected to result in significant bathochromic shifts in absorption and emission. The red and near infrared (NIR) region (600-1100 nm) is considered to be the "optically transparent window" of tissue and cells, as endogenous molecules do not absorb efficiently in this region.[338] Thus, a more red-shifted emission is generally a desirable feature for applications of chromophores in biological imaging. In addition, red-emitting imaging agents are still rather rare, but are desirable for multiplex imaging.[339, 340]

4.2 Synthesis

Compounds **X'**, **Y'**, and **Z'**, and the building blocks **A**, **B**, and **C** were previously reported.[9, 10] The compound 2,2´-*bis*(3,4-ethylenedioxythiophene) was synthesized by Ullman coupling of 2 equivalents of 3,4-ethylenedioxythiophene according to the literature.[325] Compound **XN** was synthesized by twofold lithiation of *bis*(3,4-ethylenedioxythiophene) and subsequent reaction with **A** (**Scheme 37**). The bromination of *bis*(3,4-ethylenedioxythiophene) with *N*-bromosuccinimide to obtain 5,5´-dibromo-2,2´-*bis*(3,4-ethylenedioxythiophene) was attempted according to several literature procedures,[327, 329, 341] often affording an insoluble blue solid instead of the desired product. Based on these literature procedures, optimized reaction conditions are reported, yielding the product reproducibly in 91 % yield on a 2 mmol scale in the Supporting Information (SI).
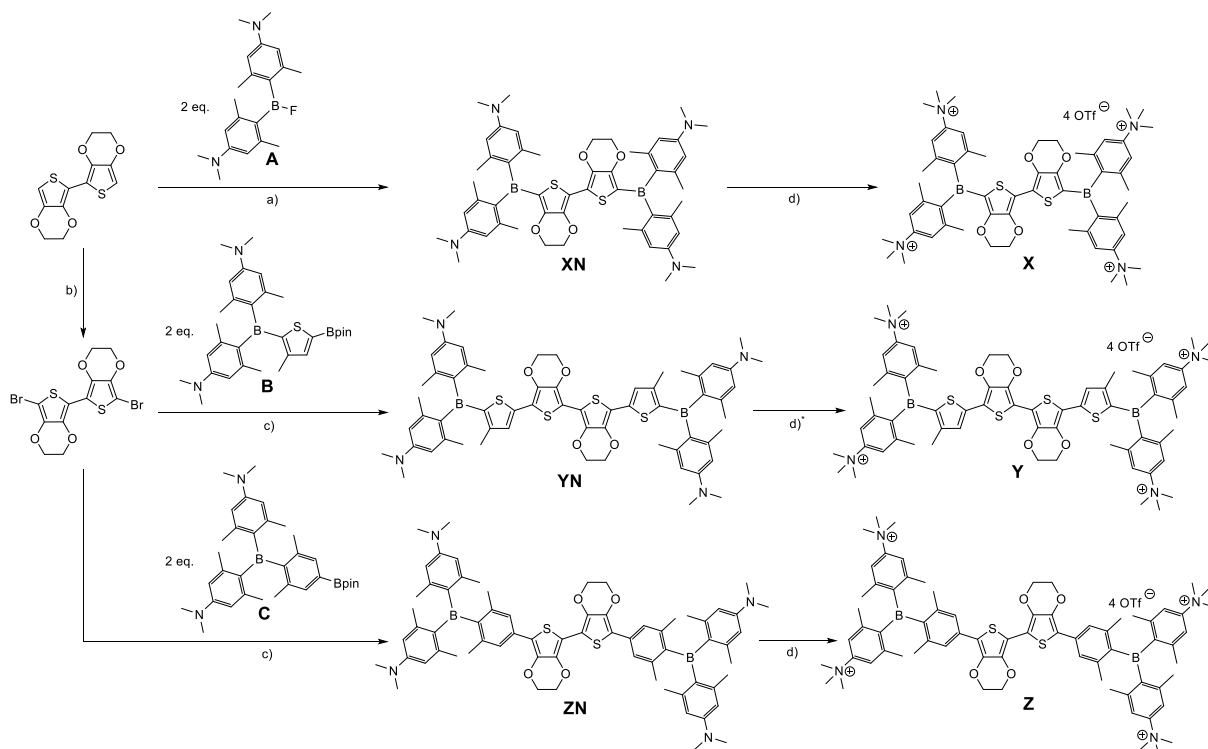
Scheme 37. Synthesis of compounds **XN**, **YN**, **ZN**, **X**, **Y** and **Z**. a) *n*-BuLi, THF, -78 °C to r.t.; b) NBS, CH$_2$Cl$_2$, -15 °C; c) Pd$_2$(dba)$_3$·CHCl$_3$, SPhos, CsCO$_3$, toluene/H$_2$O (2/1), 85 °C; d) MeOTf, CH$_2$Cl$_2$, r.t.; d)* excess MeOTf, unidentified impurity in the compound, see Discussion for further information.

Compounds **YN** and **ZN** were prepared *via* Suzuki-Miyaura cross-coupling reactions of 5,5´-dibromo-2,2´-*bis*(3,4-ethylenedioxythiophene) with the respective borylated triarylboranes **B** or **C**. Methylation of the neutral compounds **XN** and **ZN** at the amine groups was performed according to the standard methylation protocol reported by Marder and co-workers[9-12] with 4.5 equivalents of MeOTf in CH$_2$Cl$_2$, with the tetracationic compounds **X** and **Z** precipitating from the reaction mixture. Methylation of compound **YN** under the same conditions yielded a mixture of the twofold and threefold methylated compounds according to high resolution mass spectrometry (HRMS) studies of the precipitate. Performing the reaction in pure MeOTf or with nitromethane as the solvent led to decomposition of the starting material. Using 32 equivalents of MeOTf and a tenfold increase in the amount of solvent led to compound **Y**, characterized by ^{1}H NMR spectroscopy and HRMS, without any residual twofold or threefold methylated side product. However, an unidentified impurity (^{1}H NMR (300 MHz, CD$_3$OD): δ = 4.6 ppm, presumably from decomposition due to excess MeOTf) could not be separated from the product. Therefore, the discussion of the properties of compound **Y** will be kept to a minimum and should be treated with caution.

4.3 Linear Optical Properties of and TD-DFT Calculations on the Neutral Precursor Compounds

Photophysical data for compounds **XN**, **YN**, and **ZN** were obtained in different solvents of increasing polarity (**Figure 22**). No significant dependence of the lowest energy absorption maxima on solvent polarity was observed for any of these compounds (**Table 6**), which indicates a weakly polarized ground state in all cases.

Figure 22. Absorption (solid line) and emission (dashed line) spectra of **XN** (top, left), **YN** (top, right) and **ZN** (bottom, left) in various solvents.

TD-DFT calculations were carried out for all molecules at the CAM-B3LYP/6-31G+(d,p) level of theory (SI). In **XN** the $S_1 \leftarrow S_0$ transition (calculated in toluene at 422 nm and observed in toluene at 478 nm), can be attributed to a HOMO to LUMO transition with a minor contribution from HOMO-4 to LUMO (**Table S20** and **Table S21**). Both HOMO and HOMO-4 are delocalized over the whole π-system of the molecule, including the *N,N*-dimethylamino-2,6-dimethylphenyl substituents (**Figure 23**). The LUMO is mainly located at the π-bridge and the boron atoms. A moderate charge transfer (CT) character can thus be attributed to this transition (orbital overlap parameter (Λ) = 0.63, with $\Lambda = \dfrac{\Sigma_{i,a} c_{i,a}^2 \langle | \varphi_a | || \varphi_i | \rangle}{\Sigma_{i,a} c_{i,a}^2}$ resulting in $0 \leq \Lambda \leq 1$, with 0 corresponding to no overlap and 1 to complete overlap).[342] For most neutral precursors to the

tetracationic A-π-A chromophores, the occupied molecular orbitals relevant to the $S_1 \leftarrow S_0$ transitions are localized only at the *N,N*-dimethylamino-2,6-dimethylphenyl substituents and the lowest energy absorption corresponds to strong CT from the *N,N*-dimethylamino-2,6-dimethylphenyl donor to the π-bridge and the boron acceptor.[12, 189, 190] The $S_1 \leftarrow S_0$ transitions in compounds **YN** and **ZN** (calculated in toluene at 482 nm and 424 nm and observed in toluene at 524 nm and 463 nm, respectively) can be attributed to HOMO to LUMO transitions in both cases (**Table S22**-**S25**). Both HOMO and LUMO are delocalized over the π-bridges of the respective molecule (**Figure 23**) and the lowest energy transitions can therefore be classified as locally excited (LE) transitions (Λ = 0.76 and 0.71, respectively). Similar behavior in neutral precursors to tetracationic A-π-A chromophores has previously only been observed when the much larger (and in case of the former strongly electron-donating) bis(phenylthienyl)diketopyrrolopyrrol-[12] or bis(phenylethynyl)anthracene-based[190] π-systems were employed as linkers.
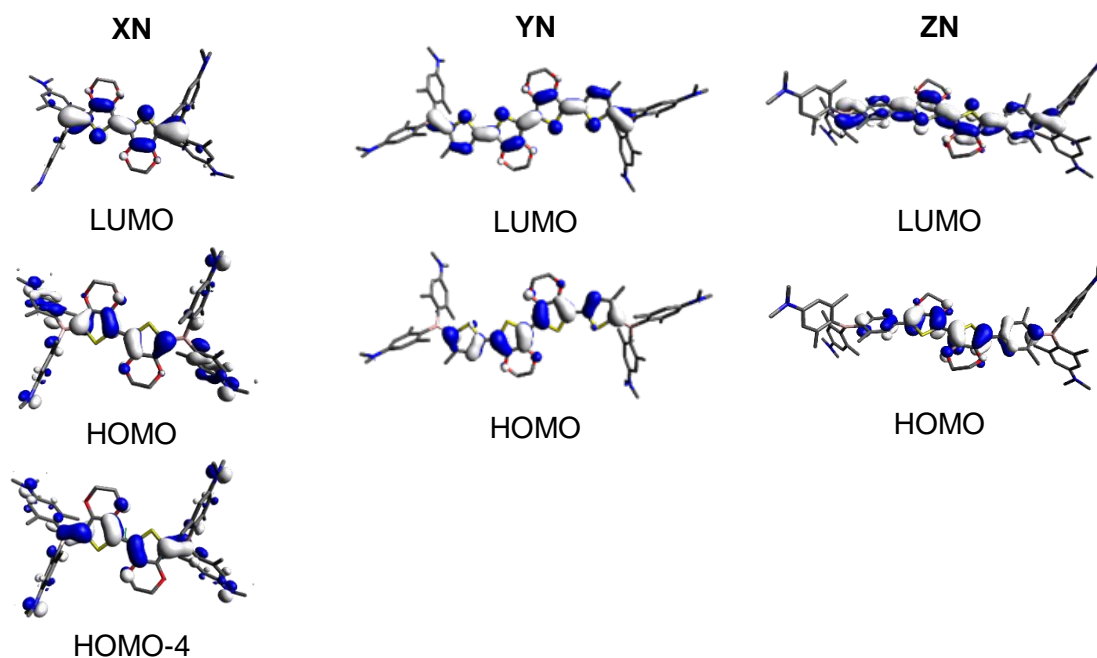
Figure 23. Orbitals relevant to the $S_1 \leftarrow S_0$ transition in toluene for compounds **XN**, **YN**, and **ZN** calculated by TD-DFT at the CAM-B3LYP/6-31G+(d,p) level of theory.

The emission maximum of compound **XN** shifts bathochromically with increasing solvent polarity, which results in an increase of the apparent Stokes shift from 2300 cm^{-1} in toluene to 3900 cm^{-1} in Et$_2$O, and 5700 cm^{-1} in CH$_2$Cl$_2$. This positive solvatochromism with increasing solvent polarity suggests large (local) dipole moments in the excited state and is in accordance with the moderate CT character of the lowest energy absorption band determined for this compound. In accordance with a stronger CT character of the $S_1 \leftarrow S_0$ transitions of most analogous, neutral A-π-A chromophores, the Stokes shifts in these analogs are ca. 1500 to 2000 cm^{-1} larger in each solvent than those of **XN**.[12, 189, 190] The fluorescence quantum yields of **XN** decrease with increasing solvent polarity from 0.16 in toluene to 0.07 in Et$_2$O, to 0.02 in

CH$_2$Cl$_2$. Together with increased nonradiative decay rate constants (**Table 6**), this trend is consistent with the energy gap law,[343] which dictates more efficient internal conversion processes as the energy gap between excited and ground state becomes smaller. Thus, in accordance with the LE character of the lowest energy transitions for **YN** and **ZN**, no significant dependence of emission maxima on solvent polarity was observed and the fluorescence quantum yields in all solvents are in the range between 0.2 and 0.3 (**Table 6**).

Table 6. Photophysical data for compounds **XN**, **YN**, and **ZN** in various solvents.

	solvent	λ_{abs} / nm	ε / M^{-1} cm^{-1}	λ_{em} / nm	Stokes shift^a / cm^{-1}	Φ_f	τ / ns	k_r / 10^8 s^{-1}	k_{nr} / 10^8 s^{-1}
XN	toluene	478	65 000	538	2 300	0.16	2.0	0.8	4.3
	Et$_2$O	471		578	3 900	0.07	1.6	0.4	5.8
	CH$_2$Cl$_2$	475		650	5 700	0.02	0.6	0.4	17.8
YN	toluene	524	81 000	545	700	0.26	0.5	5.3	15.1
	Et$_2$O	517		539	800	0.32	0.7	4.9	10.5
	CH$_2$Cl$_2$	522		550	1 000	0.22	0.5	4.8	17.0
ZN	toluene	463	61 000	494	1 400	0.17	0.3	6.8	33.2
	Et$_2$O	457		490	1 500	0.21	0.3	6.2	23.2
	CH$_2$Cl$_2$	456		501	2 000	0.21	0.5	4.7	17.6

^{a} apparent Stokes shift.

4.4 Linear Optical Properties of and TD-DFT Calculations on the Tetracationic Target Molecules

Upon methylation of the neutral compounds at the four dimethylamino groups, electron donation from amine to boron is no longer possible and, thus, the acceptor strength of boron is increased and the resulting salts become water-soluble. Photophysical data for compounds **X**, **Y**, and **Z** were obtained in MeCN and water (**Figure 24**). TD-DFT calculated sata suggests, in all cases, that the S$_1$ ← S$_0$ transitions are attributed to HOMO to LUMO excitations. HOMO and LUMO of compounds **X** and **Y** are delocalized over the respective π-bridges and the boron atoms (**Figure 25**) and the transitions can thus be classified as LE π-π* transitions (Λ = 0.71 and 0.67, respectively). The situation is similar for **Z**; however, due to the twist introduced by the sterically bulky dimethylphenly group, the orbital distribution is uneven over the bridge. As the HOMO is mostly located at the EDOT and the LUMO at boron, the S$_1$ ← S$_0$ HOMO to LUMO transition of **Z** has slight CT character (Λ = 0.47). The observed trend that the lowest energy absorption energy decreases in the order **X** > **Z** > **Y** (e.g. observed in MeCN: 462 nm, 482 nm, 536 nm (**Table 7**)) is well reproduced by the TD-DFT calculated data, when solvent effects are included (e.g. calculated in MeCN: 418 nm, 459 nm, 509 nm (**Tables S27**, **S29**, **S31**)). As **Z** exhibits a higher CT character than **X** and **Y**, the influence of the solvent on the

transition is more pronounced for **Z**, and calculations including solvent correction reproduce the experimental data more accurately.
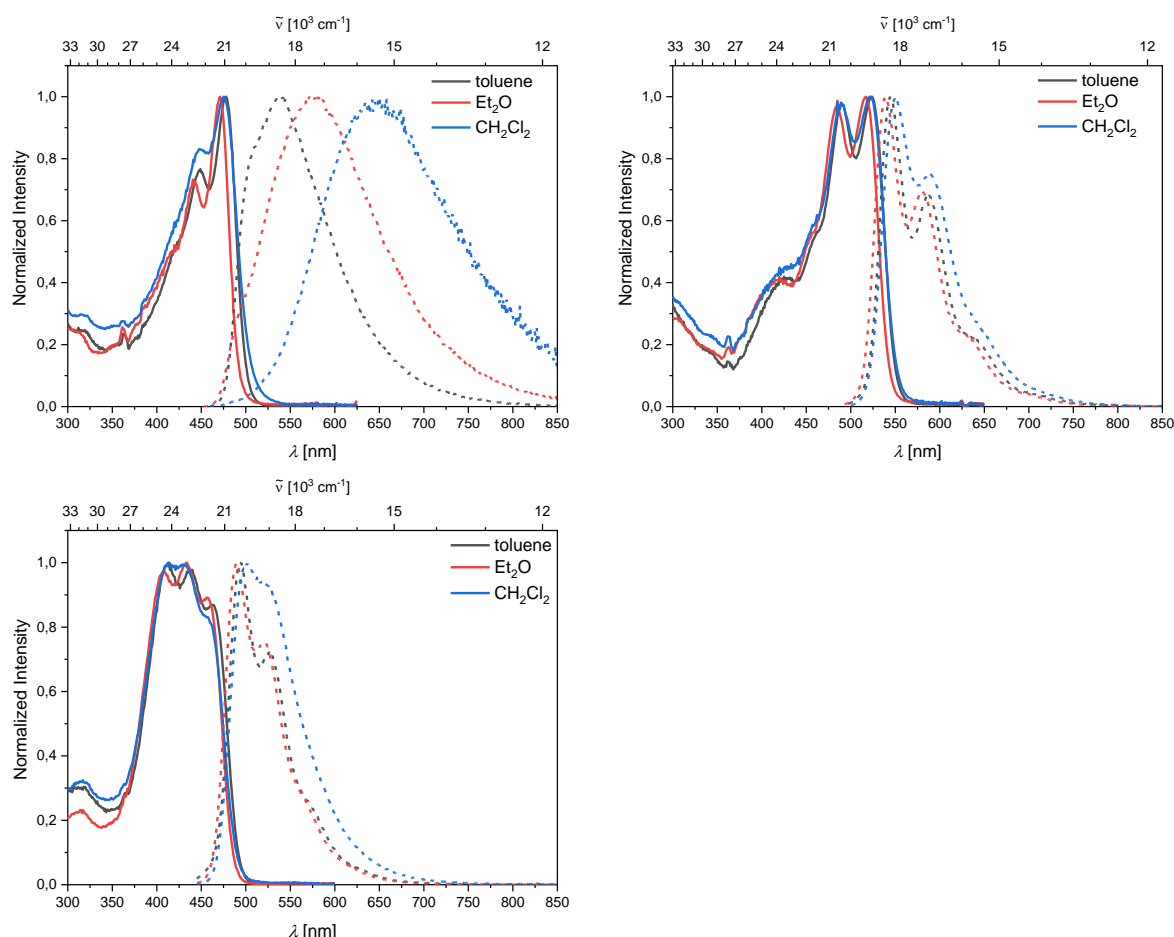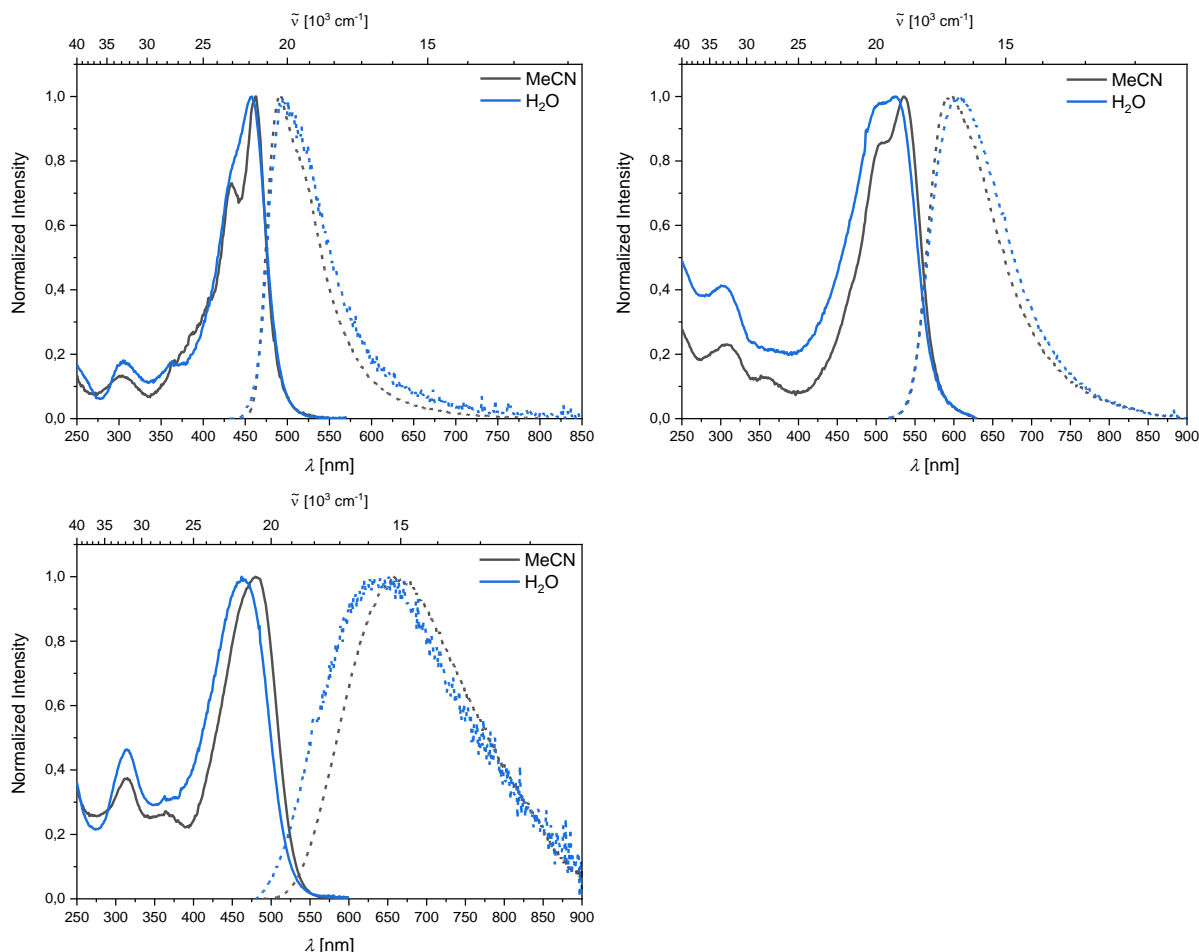

Figure 24. Absorption (solid line) and emission (dashed line) spectra of **X** (top, left), **Y** (top, right) and **Z** (bottom, left) in various solvents.

The emission maxima of **X**, **Y**, and **Z** do not shift significantly upon changing the solvent from MeCN to water. The most notable solvent effect is a broadening of the emission spectra in the more polar solvent water for all three compounds as was previously observed for similar systems.[12] In accordance with the slight CT character of the lowest energy transition and suggested (locally) polarized excited state for **Z**, large Stokes shifts of ca. 6000 cm^{-1} are observed for this compound in MeCN and water (**Table 7**), whereas for **X** and **Y** they are ca. 1500 and 2500, respectively.
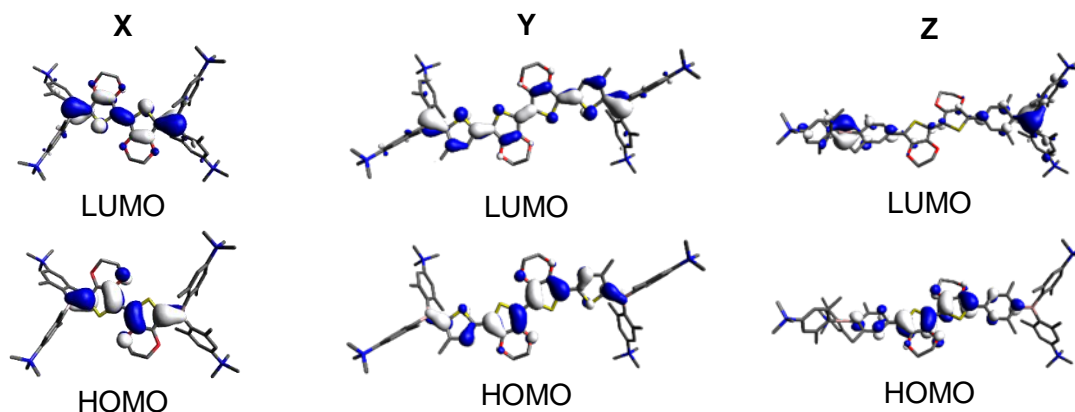
Figure 25. Orbitals relevant to the $S_1 \leftarrow S_0$ transition in MeCN for compounds **X**, **Y** and **Z** calculated by TD-DFT at the CAM-B3LYP/6-31G+(d,p) level of theory.

Due to the large Stokes shift, the emission of **Z** (λ_{em} (MeCN) = 662 nm; λ_{em} (H$_2$O) = 651 nm) is even more bathochromically shifted than that of its bis(phenylthienyl)diketopyrrolopyrrol analog (λ_{em} (MeCN) = 617 nm; λ_{em} (H$_2$O) = 620 nm)[12] and is the most redshifted of all tetracationic water-soluble bis-triarylborane chromophores reported to date. However, the redshift comes at the expense of the fluorescence quantum yield,[343] which was determined to be 0.07 in MeCN and 0.01 in water.

In **Table 7**, the photophysical data for EDOT-containing compounds **X**, **Y**, and **Z** are compared with their thiophene-containing analogs **X'**, **Y'**, and **Z'**. As expected for A-*π*-A chromophores,[321] the introduction of a more electron rich *π*-bridge leads to a bathochromic shift in absorption and emission in all cases. However, as dictated by the energy gap law[343] (*vide supra*), a significant decrease of fluorescence quantum yield is also observed in all cases in which fluorescence quantum yield could be measured.

Table 7. Comparison of photophysical data for compounds **X**, **Y**, **Z** and compounds **X'**, **Y'**, **Z'**[9, 10] in MeCN and water.

	solvent	λ_{abs} / nm	λ_{em} / nm	Stokes shift[a] / cm^{-1}	Φ_f
X	MeCN	462	492	1 300	0.03
	H_2O	458	495	1 600	-[b]
X'	MeCN	426	448	1 200	0.41
	H_2O	426	451	1 300	-[b]
Y[c]	MeCN	536	601	2 000	-[c]
	H_2O	526	614	2 700	-[c, b]
Y'	MeCN	464	558	3 600	0.27
	H_2O	463	570	4 100	0.21
Z	MeCN	482	662	5 600	0.07
	H_2O[a]	465	651	6 100	0.01
Z'	MeCN	428	554	5 300	0.41
	H_2O[a]	425	563	5 800	0.10

[a] apparent Stokes shift; [b] not measurable due to rapid decomposition; [c] for **Y** only the spectra are given and they should be interpreted with care due to an unidentified impurity. For the same reason, measurements of Φ_f were not performed.

4.5 Cyclic Voltammetry and Stability

The red-shifted lowest energy absorption and emission maxima of compounds **X**, **Y**, and **Z**, compared to **X'**, **Y'**, and **Z'**, respectively, are consistent with the stronger electron-donating effect of EDOT compared to thiophene in these systems. As a greater electron density at the boron should results in increased stability against nucleophilic attack, it was investigated to what extent the substitution of thiophene by EDOT increases the electron density at the boron centers. A common way to quantify this is by measuring the reduction potential *via* cyclic voltammetry.[140, 344, 345] All cyclic voltammograms were obtained in MeCN and are referenced to the Fc/Fc$^+$ ion couple. Half-wave reduction potentials were determined for all six compounds even though their reduction events are not always fully chemically reversible. In particular, reductions of the sterically less protected compounds **X**, **X'**, **Y**, and **Y'** are accompanied by irreversible processes (**Figures S122-S127**). In the cyclic voltammograms of **X** vs. **X'**, with comparatively shorter π-bridges, two half-wave reduction potentials were observed at -1.59 V and -1.93 V vs. -1.46 V and -1.79 V, respectively (**Table 8**), indicating a pronounced electronic communication between the two boron atoms. For the larger analogs **Y** vs. **Y'** (-1.78 V vs. -1.71 V) and **Z** vs. **Z'** (-1.97 V vs. 1.92 V) only one half-wave reduction potential was observed for each compound, suggesting inefficient communication between the two boron atoms. Taking each pair (i.e. **X** vs. **X'**, **Y** vs. **Y'**, **Z** vs. **Z'**) into account, a consistent but rather small shift to more negative reduction potentials is observed for the respective EDOT-containing compounds when compared with their thiophene analogs.

Table 8. Half-wave potentials of partially reversible reduction processes of compounds **X**, **X'**, **Y**, **Y'**, **Z** and **Z'**. All measurements were performed in acetonitrile with [nBu$_4$N][PF$_6$] as the electrolyte with a scan rate of 250 mV s^{-1} and are referenced to the Fc/Fc$^+$ ion couple.

	X	X'	Y	Y'	Z	Z'
1st reduction: E$_{1/2}$ [V] vs. Fc/Fc$^+$	-1.59	-1.46	-1.78	-1.71	-1.97	-1.92
2nd reduction: E$_{1/2}$ [V] vs. Fc/Fc$^+$	-1.93	-1.79	-	-	-	-

The three EDOT-containing compounds **X**, **Y**, and **Z** are air and moisture stable in the solid state for several months and are also stable during photophysical measurements at low concentrations in MeCN solutions under ambient conditions, as are their thiophene analogs **X'**, **Y'**, and **Z'**. However, compounds **X'** and **Y'** decomposed quickly in pure water at low concentrations, while **Z'** shows no sign of decomposition over a period of 48 h.[9, 10] Thus, water-stability was also examined for **X**, **Y**, and **Z** *via* UV/Vis spectroscopy at low concentrations (**Figure 26**). As the sterically less protected compounds **X** and **Y** start to decompose within minutes, it is concluded that the slight increase in electron density at the boron does not significantly affect their water-stability. Only the sterically most protected compound **Z** is stable over a period of 48 h.
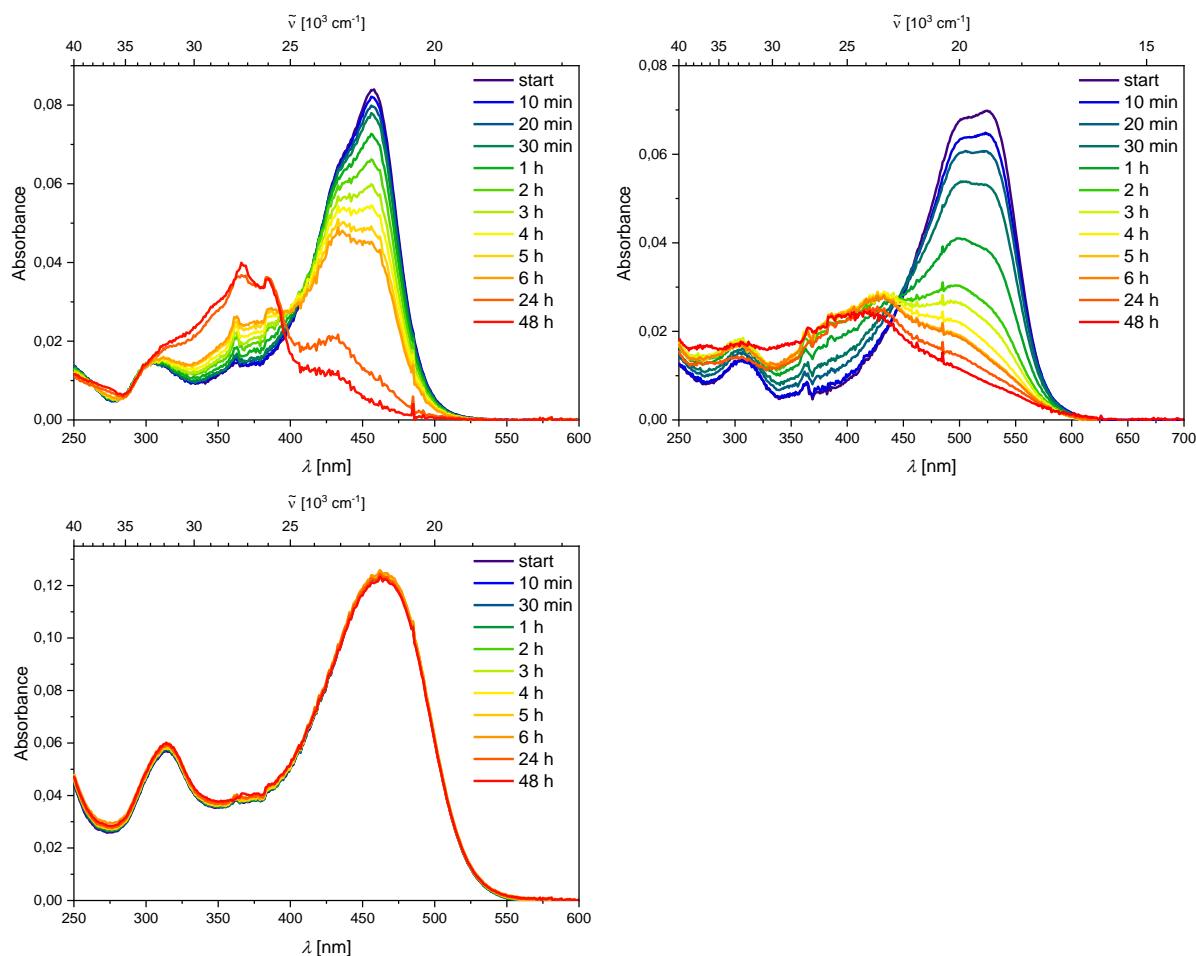
Figure 26. UV/Vis spectra of solutions of **X** (top, left), **Y** (top, right) and **Z** (bottom, left) over a period of 48 h in water. Preparation of stock solutions with the same concentrations of **X**, **Y** and **Z** was not possible, as the dilution takes time and a measurement of absorption spectra at t = 0 min would, thus, not be possible.

4.6 Reactivity with Oxygen

After α-terthienyl had been identified as the nematicidally-active species in Tagetes (African marigold) roots,[346] it was demonstrated that its nematicidal activity increases under UV-light irradiation.[347] Later, it was found that the nematicidal activity of α-terthienyl is due to singlet oxygen generated upon UV-light irradiation.[348] Since then, it has been well established that thiophene- and EDOT-containing compounds are able to generate singlet oxygen *via* efficiently populated triplet states.[332, 335, 349-352] In addition, the Marder group recently reported persistent room temperature phosphorescence from simple triarylboranes, sensitive to oxygen quenching in the solid state.[71]

The photosensitized production of singlet oxygen *via* organic molecules has been a very pertinent research field for many decades.[31, 353-365] Singlet oxygen has found many applications,[366] e.g., as a synthetic reagent,[367] an insecticide[368] and, perhaps most prominently, as a reactive oxygen species (ROS) leading to cell-death in unwanted tissue *via* photodynamic therapy.[369-371] Still, the design of water-soluble and biocompatible singlet

oxygen-generating molecules remains a challenge.[372-375] As **Z'** was shown to be water-soluble, water-stable and, to some extent, biocompatible,[9] this compound and its water-soluble and water-stable analog **Z** were examined for the sensitization of singlet oxygen.

The presence of singlet oxygen in solution can be observed and quantified by its luminescence at 1272 nm.[364, 376] Upon excitation of an O_2-saturated solution of compound **Z'** in MeCN, emission at 1272 nm was detected (**Figure 27**).
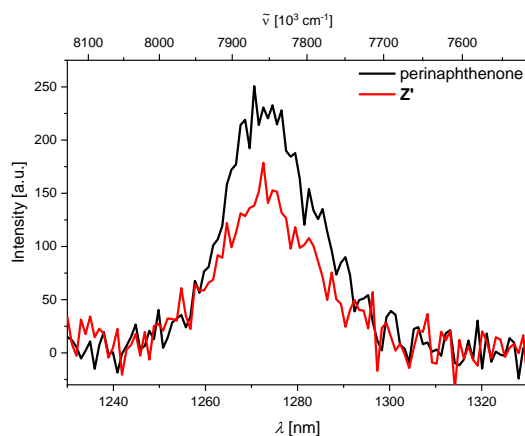
Figure 27. Emission spectrum of singlet oxygen generated from sensitization of a perinaphthenone standard (black) vs. that generated by sensitization by compound **Z'** (red) excited at 404 nm in MeCN.

The quantum yield for singlet oxygen formation (Φ_Δ) (**Table 9**) was determined to be 0.6 by comparison to the standard perinaphthenone which is known to sensitize singlet oxygen with an efficiency close to unity in MeCN.[360] A comparatively small radiative rate constant of 0.45 s^{-1}[377] for the luminescence of singlet oxygen at 1272 nm in MeCN explains the very low signal to noise ratio obtained. A measurement of singlet oxygen generation in water was not possible, as an even lower radiative rate constant of 0.16 s^{-1}[377] in water precluded detection of singlet oxygen luminescence with the experimental setup at hand, even after sensitization by perinaphthenone.

Table 9. Fluorescence quantum yield (Φ_f)[9] and quantum yield for singlet oxygen formation (Φ_Δ) of compound **Z'** in MeCN.

	Φ_f	Φ_Δ[a]
Z'	0.41	0.6

[a] due to the very low signal to noise ratio an error of $\pm$ 0.1 is assumed.

For compound **Z**, the detection of singlet oxygen luminescence was not possible. The emission of the compound is bathochromically shifted compared to **Z'** with a maximum at 662 nm in MeCN. However, due to its extremely broad emission band, it is still detectable well into the NIR range, possibly overlapping with the weak phosphorescence of singlet oxygen (**Figure 28**). An attempt to time-gate the detection, to exclude the short-lived fluorescence, using a

µF920 pulsed 60 W Xenon microsecond flashlamp for excitation, gave no significant signal at 1272 nm even with sensitization by perinaphthenone, presumably due to an even lower signal to noise ratio.
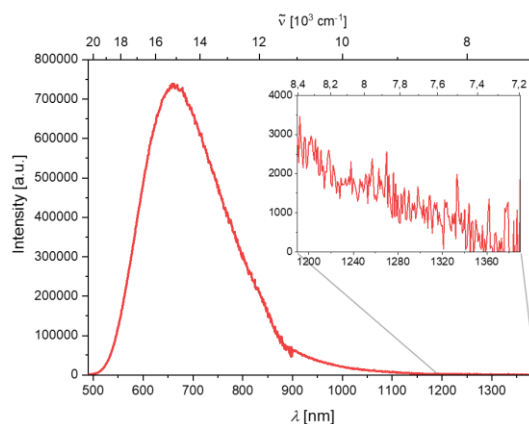
Figure 28. Emission spectrum of compound **Z** in MeCN; insert: enlarged section from the spectrum, showing detectable emission until circa 1360 nm.

To confirm the population of possible triplet states, transient absorption measurements were performed on both **Z** and **Z'**. In both cases, excited state absorption was observed (**Figure 29**). In case of **Z'** the long-lived excited state absorbs in the range of 480 nm to 800 nm and has a lifetime of 94.6 µs (**Figure S128**). The absorbance of the long-lived state of **Z**, with a lifetime of 105 µs (**Figure S129**), is much weaker. The absorbance is observable in the range of 520 nm to 620 nm, but is difficult to distinguish from noise at wavelengths higher than that. Both long-lived states are completely quenched when oxygen is introduced to the solutions.
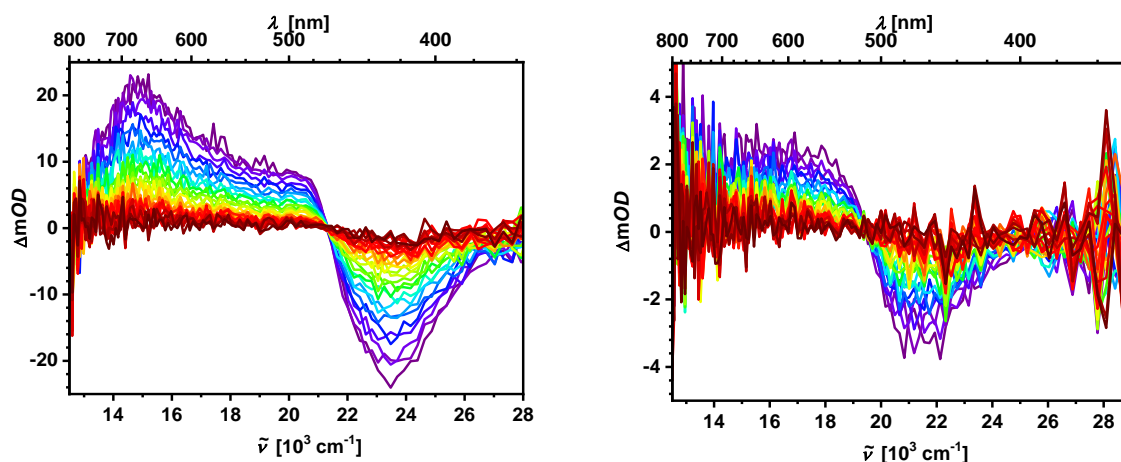
Figure 29. Nanosecond transient absorption spectra of **Z'** (left) and **Z** (right) in degassed MeCN solutions.

4.7 Conclusions

Three novel EDOT-linked, water-soluble tetracationic bis-triarylborane chromophores **X**, **Y**, and **Z** and their neutral precursors **XN**, **YN**, and **ZN** are reported. A significant red shift of

absorption and emission is observed for these compounds, compared to their thiophene-containing analogs. Compound **Z** exhibits the most bathochromically shifted emission of all of the water-soluble A-π-A chromophores prepared to date which is still observable well into the NIR region. Even though a small increase in electron density at the boron atoms was found for the three EDOT-containing compounds, compared to their thiophene-containing analogs, increased water-stability was not achieved, and only compound **Z** was found to be water-stable.

The two water-stable compounds **Z** and **Z'** were investigated *via* transient absorption spectroscopy and long-lived (ca. 100 μs) excited states, completely quenched by oxygen, were observed in both cases. For compound **Z'**, the characteristic luminescence of singlet oxygen was observed and a quantum yield for singlet oxygen formation of 0.6 was determined. This was not possible for compound **Z**, as the NIR emission of the compound prevented a detection of singlet oxygen luminescence. Studies concerning a possible phototoxicity, a property applicable in photodynamic therapy, will be performed for both compounds in the near future.

5 Summary

5.1 Chapter 1

The first chapter provides a detailed review of the development of synthetic approaches to triarylboranes from their first report nearly 135 years ago to the present.

5.2 Chapter 2

Air- and moisture-stable triarylboranes have applications in many different areas over the past few decades. Compounds in which the boron is protected by six *ortho*-methyl groups are stable even in pure water and, thus, one of the most common ways to employ triarylboranes in these materials is in the form of appropriately functionalized $BXyl_3$ moieties. Structure-property relationship studies have been mostly limited to symmetrically-substituted triarylboranes (BAr_3 or BAr_2Ar'), which contain a maximum of two functional groups.
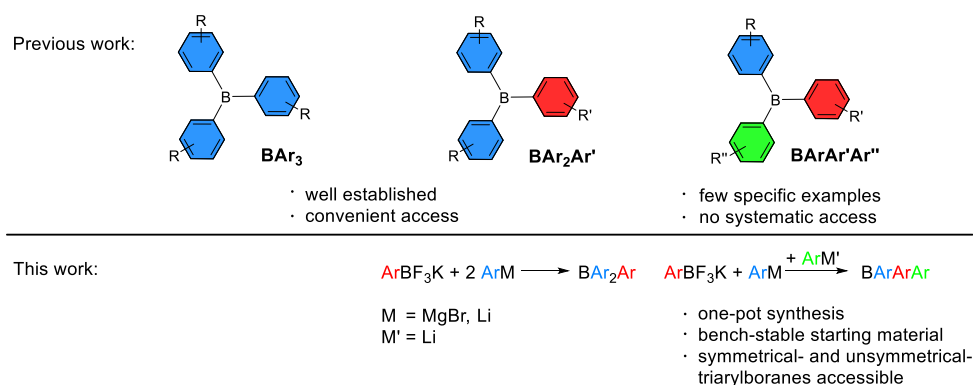
Figure 30. Schematic summary of the synthetic methodology developed in chapter 2.

In the second chapter of this thesis, a novel and convenient methodology is reported for the one-pot synthesis of sterically-congested triarylboranes, using bench-stable aryltrifluoroborates as the boron source. The new procedure gives access to symmetrically- and unsymmetrically-substituted triarylboranes of the types BAr_2Ar' and $BArAr'Ar''$. Three novel triarylboranes, as well as their iridium-catalyzed C–H borylation products, are reported. Furthermore, the trimethylsilyl group was shown to be a new and very convenient halide protecting group in triarylborane chemistry, being quantitatively convertible into an iodide moiety under ambient conditions.
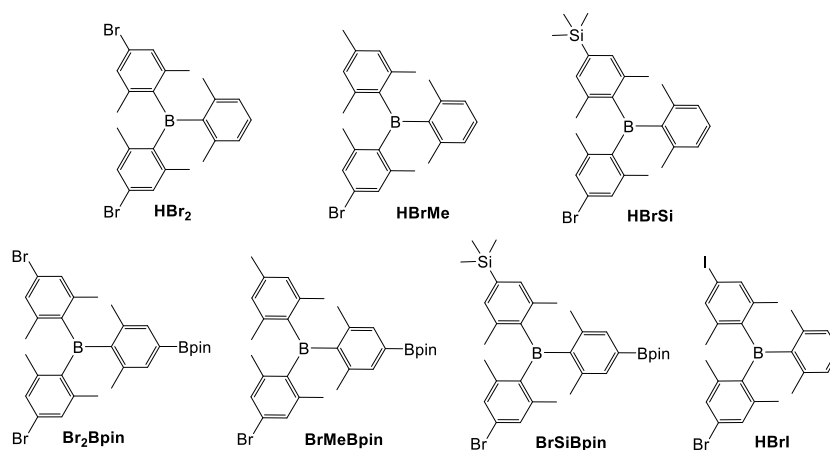
Figure 31. Novel triarylboranes synthesized in this study.

It was demonstrated that the same unsymmetrically-substituted triarylborane can be synthesized from the three possible aryl BF_3K salts, and that choosing the most electron-rich aryl BF_3K salt gives the highest yield. The borylated triarylboranes contain up to three positions that can subsequently be orthogonally functionalized, and can thus be considered as AB, AAB, and ABC-type precursors, applicable as building blocks for the design of boron-containing functional materials.

5.3 Chapter 3

In a collaboration with the research group of Dr. Ivo Piantanida at the Ruđer Bošković Institute, Croatia, four luminescent tetracationic bis-triarylborane DNA and RNA sensors that show high binding affinities, in several cases even in the nM range, are investigated in this chapter. Three of them are novel compounds that contain substituted bis(2,6-dimethylphenyl-4-ethynyl)arene linkers (**III**: arene = 5,5'-2,2'-bithiophene; **IV**: arene = 1,4-benzene; **V**: arene = 9,10-anthracene) between the two boryl moieties and serve as efficient dual Raman and fluorescence chromophores. The molecular structures of two of the neutral precursors were obtained *via* X-ray diffraction analysis and reveal some structural flexibility for these compounds in the solid state.
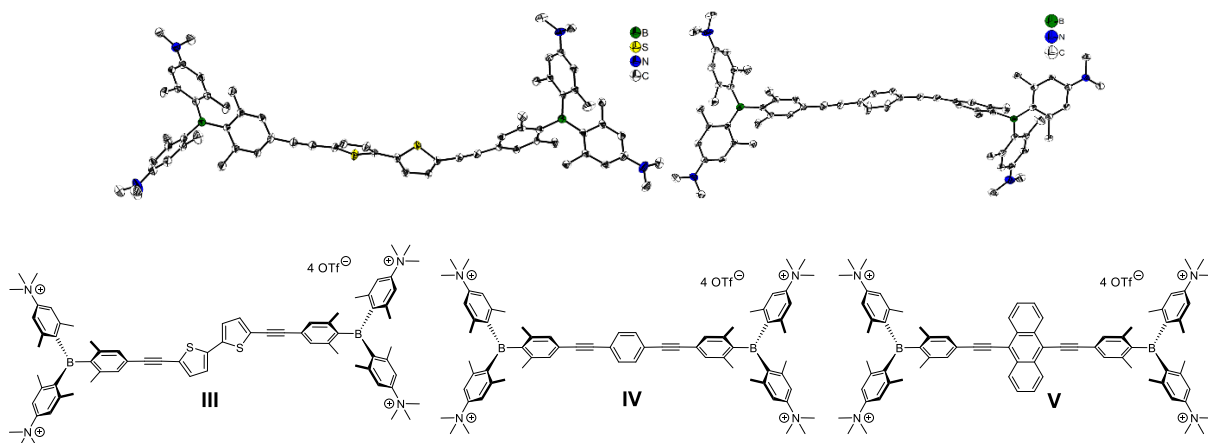
Figure 32. Top: molecular structures of neutral precursors **IIIN** (left) and **IVN** (right) in the solid state at 100 K; bottom: target molecules of this study.

As derivatives of the well investigated 2,5-bis(phenylethynyl)thiophene (BPET), bis(phenylethynyl)benzene (BPEB), and bis(phenylethynyl)anthracene (BPEA) chromophores, compounds **III-V** were found to be highly emissive even in water. The previously reported shorter analogue **VI** employs bis(2,6-dimethylphenyl-4-)-9,10-anthracene as the linker and demonstrates the importance of an adequate linker length with a certain level of flexibility by exhibiting generally lower binding affinities than **III-V**. Pronounced aggregation-deaggregation processes are observed in fluorimetric titration experiments with DNA for compounds **III** and **V**. Molecular modelling of complexes of **V** with AT-DNA, suggest the minor groove as the dominant binding site for monomeric **V**, but demonstrate that dimers of **V** can also be accommodated.
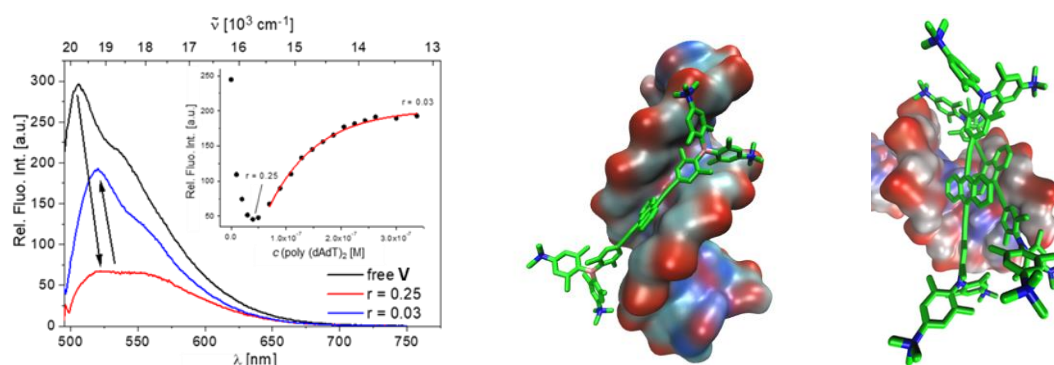
Figure 33. Left: changes in the emission spectra of **V** upon titration with poly $(dAdT)_2$, insert: dependence of relative fluorescence intensity at 520 nm on c (poly $(dAdT)_2$; right: monomer and dimer of compound **V** in the minor groove of poly $(dAdT)_2$, as obtained by molecular modelling.

Strong SERS responses for **III-V** vs. a very weak response for **VI**, particularly the strong signals from anthracene itself observed for **V** but not for **VI**, demonstrate the importance of triple bonds for strong Raman activity in molecules of this compound class. The energy of the characteristic stretching vibration of the C≡C bonds is significantly dependent on the aromatic moiety between the triple bonds. The insertion of aromatic moieties between two C≡C bonds thus

offers an alternative design for dual Raman and fluorescence chromophores, applicable in multiplex biological Raman imaging.

5.4 Chapter 4

In chapter 4 of this thesis, the compound class of water-soluble tetracationic bis-triarylborane chromophores is extended by EDOT-linked **X**, **Y**, and **Z** and the compounds are compared to their thiophene-containing analogs **X'**, **Y'**, and **Z'**. A discussion of the interesting photophysical properties of the neutral precursors **XN**, **YN**, and **ZN** is also presented.
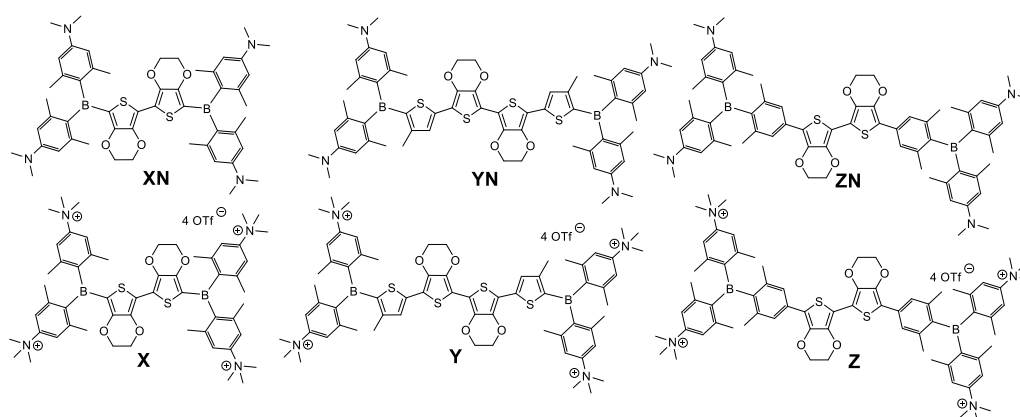
Figure 34. EDOT-containing target molecules of this study.

Absorption and emission are significantly red-shifted in these compounds, compared to their thiophene-containing analogs. Photophysical studies on the neutral precursors reveal positive solvatochromism of the emission maxima, a phenomenon typically observed for neutral precursors of this compound class, only in the case of **XN**. This is in accordance with a higher calculated charge transfer character of the lowest energy absorption of **XN**, compared to **YN** and **ZN**. The theoretical studies suggest that the HOMOs of **YN** and **ZN** are located at the respective π-bridges, while the HOMO of **XN** is delocalized over the whole π-system of the molecule, including the *N,N*-dimethylamino-2,6-dimethylphenyl substituents.
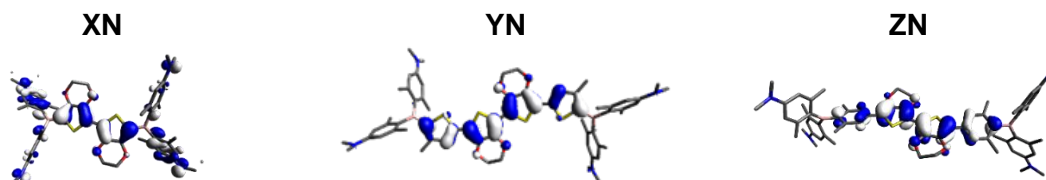
Figure 35. HOMOs of compounds **XN**, **YN**, and **ZN** calculated by TD-DFT at the CAM-B3LYP/6-31G+(d,p) level of theory.

While the lowest energy absorptions in tetracationic **X** and **Y** were classified as locally excited π-π* transitions, the $S_1 \leftarrow S_0$ transition of **Z** is characterized by a slight EDOT to boron charge transfer. Due to a large Stokes shift, compound **Z** exhibits the most bathochromically shifted

emission (λ_{em} (MeCN) = 662 nm; λ_{em} (H_2O) = 651 nm), observable well into the near infrared region, of all tetracationic water-soluble bis-triarylborane chromophores reported to date.
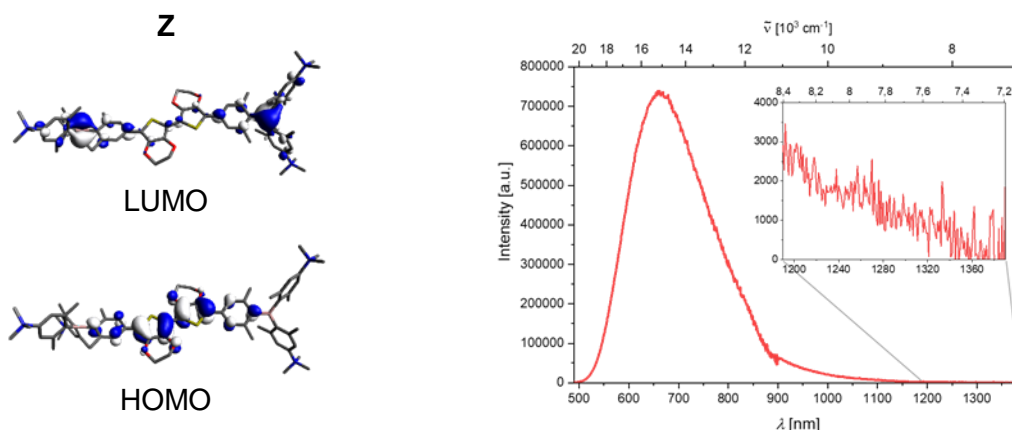
Figure 36. Left: orbitals relevant to the $S_1 \leftarrow S_0$ transition in MeCN for compound **Z** calculated by TD-DFT at the CAM-B3LYP/6-31G+(d,p) level of theory; right: emission spectrum of compound **Z** in MeCN; insert: enlarged section from the spectrum, showing detectable emission until circa 1360 nm.

Increased electron density at the boron atoms was indicated by more negative reduction potentials found for the three EDOT-containing compounds, compared to their thiophene-containing analogs. However, no increased water-stability was achieved and only compound **Z** was found to be water-stable.
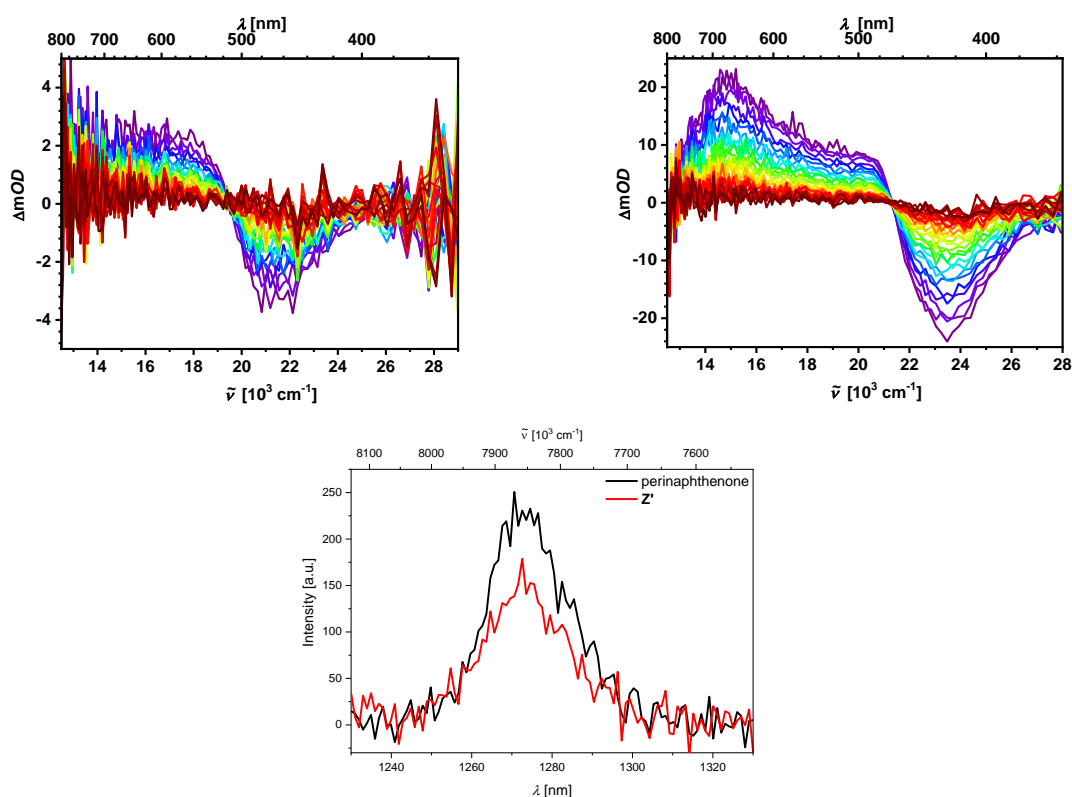
Figure 37. Top: transient absorption spectra of **Z** (left) and **Z'** (right) in a degassed MeCN solution; bottom: luminescence of singlet oxygen generated by sensitization by **Z'** and by the standard perinaphthenone.

Long-lived excited states, completely quenched by oxygen, were observed for the water-stable compounds **Z** and its thiophene analog **Z'** *via* transient absorption spectroscopy. A quantum

yield for singlet oxygen formation of 0.6 was determined for **Z'**, by comparison of the intensity of the characteristic luminescence at 1272 nm of the singlet oxygen generated to a known standard. The NIR emission of compound **Z** prevented the detection of singlet oxygen luminescence, and thus a determination of its quantum yield for singlet oxygen formation.

6 Zusammenfassung

6.1 Kapitel 1

Das erste Kapitel gibt einen detaillierten Überblick über die Entwicklung verschiedener Synthesemöglichkeiten von Triarylboranen seit ihrer erstmaligen Erwähnung vor rund 135 Jahren bis heute.

6.2 Kapitel 2

Luft- und feuchtigkeitsstabile Triarylborane fanden in den letzten Jahrzehnten in vielen verschiedenen Materialien Anwendung. Verbindungen, in denen das Borzentrum von sechs *ortho*-Methylgruppen sterische Abschirmung erfährt, sind sogar in reinem Wasser stabil. Daher besteht eine der häufigsten Möglichkeiten, Triarylborane in diesen Materialien einzusetzen, darin, entsprechend funktionalisierte $BXyl_3$-Einheiten zu verwenden. Struktur-Eigenschafts-Beziehungsstudien beschränken sich hauptsächlich auf symmetrisch substituierte Triarylborane (BAr_3 oder BAr_2Ar'), in denen maximal zwei unterschiedliche funktionelle Gruppen gleichzeitig realisiert werden können.
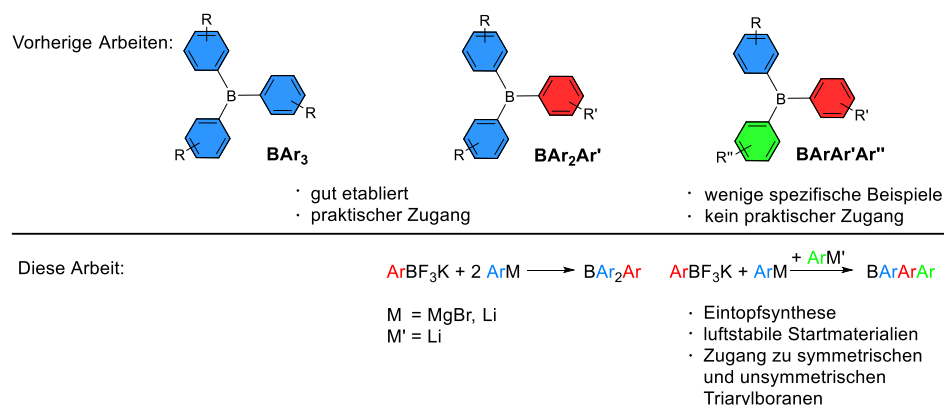
Abbildung 1. Schematische Zusammenfassung der synthetischen Methodik, die in diesem Kapitel entwickelt wurde.

In Kapitel 2 dieser Arbeit wurde eine neuartige und praktische Methode für die Eintopfsynthese von sterisch stabilisierten Triarylboranen unter Verwendung von luftstabilen Aryltrifluorboraten als Borquelle beschrieben. Das neue Verfahren ermöglicht den Zugang zu symmetrisch und unsymmetrisch substituierten Triarylboranen der Typen BAr_2Ar' und $BArAr'Ar''$. Drei neue Triarylborane sowie deren Iridium-katalysierten CH-Borylierungsprodukte wurden beschrieben. Ferner wurde gezeigt, dass die Trimethylsilylgruppe eine neue, sehr praktische Halogenidschutzgruppe in der Triarylboranchemie darstellt, da sie unter Umgebungsbedingungen quantitativ in Iodid umwandelbar ist.
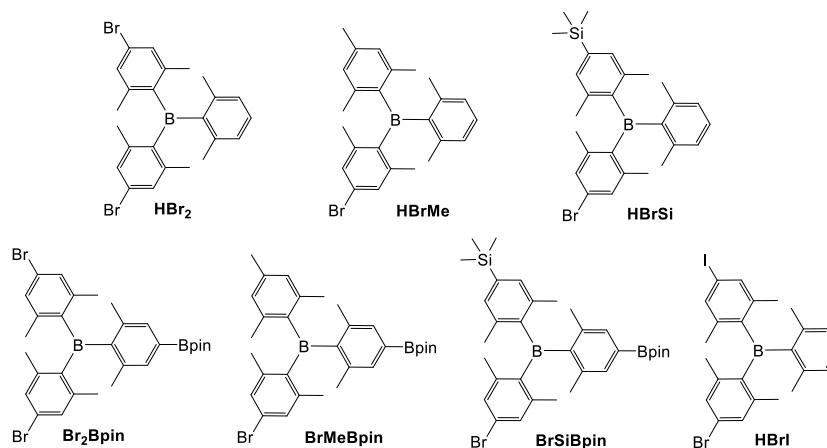
Abbildung 2. Neuartige Triarylborane, die im Zuge dieser Studie dargestellt wurden.

Es wurde gezeigt, dass das gleiche unsymmetrisch substituierte Triarylboran aus allen drei möglichen Aryl-BF$_3$K-Salzen synthetisiert werden kann und dass die Wahl des elektronenreichsten Aryl-BF$_3$K-Salzes dabei die höchste Ausbeute liefert. Alle borylierten Triarylborane enthalten bis zu drei Positionen, die orthogonal funktionalisiert werden können, und können daher als AB, AAB und ABC Vorstufen betrachtet werden, die als Bausteine bei der Konstruktion borhaltiger Funktionsmaterialien verwendet werden können.

6.3 Kapitel 3

In Zusammenarbeit mit der Arbeitsgruppe um Dr. Ivo Piantanida vom Ruđer Bošković-Institut, Kroatien, wurden in diesem Kapitel vier lumineszierende, tetrakationische Bis-Triarylborane bezüglich ihrer Fähigkeit zur DNA- und RNA-Sensorik untersucht, wobei hohe Bindungsaffinitäten, in mehreren Fällen sogar im nM-Bereich, festgestellt wurden. Drei davon sind neuartige Verbindungen, die substituierte Bis(2,6-dimethylphenyl-4-ethinyl)aren-Linker (**III**: Aren = 5,5'-2,2'-Bithiophen; **IV**: Aren = 1,4-Benzol; **V**: Aren = 9,10-Anthracen) zwischen den beiden Boryl-Einheiten enthalten und als effiziente duale Raman- und Fluoreszenz-Chromophore dienen. Die Molekülstrukturen von zwei neutralen Vorstufenverbindungen wurden durch Röntgenbeugungsanalyse erhalten und deuten auf eine gewisse strukturelle Flexibilität für diese Verbindungen im Festkörper hin.
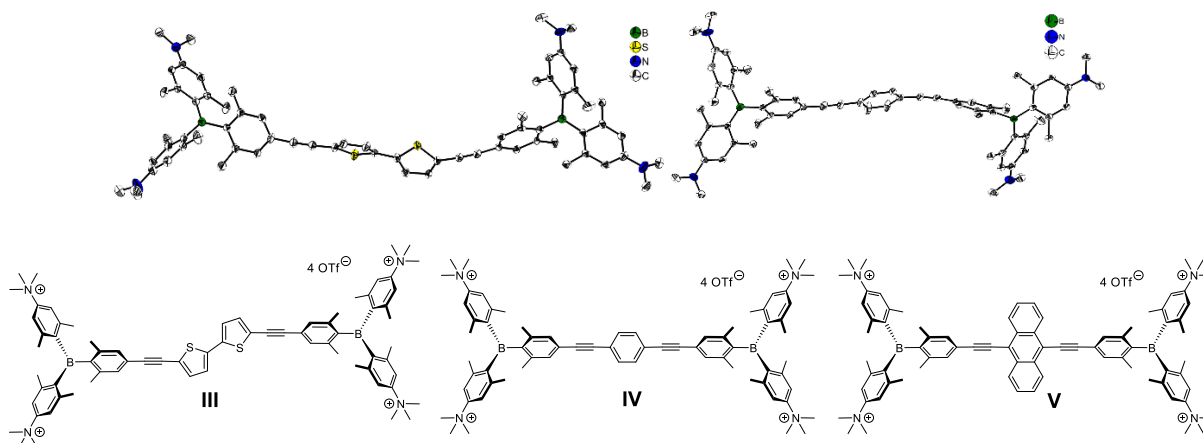
Abbildung 3. Oben: Molekülstrukturen der neutralen Vorstufen **IIIN** (links) und **IVN** (rechts) im Festkörper bei 100 K; unten: Zielverbindungen dieser Studie.

Als Derivate der gut untersuchten Chromophore 2,5-Bis(phenylethinyl)thiophen (BPET), Bis(phenylethinyl)benzol (BPEB) und Bis(phenylethinyl)anthracen (BPEA) erwiesen sich **III**-**V** selbst in Wasser als stark emittierend. Das literaturbekannte, kürzere Analogon **VI** enthält Bis(2,6-dimethylphenyl)-9,10-anthracen als Linker und zeigt die Bedeutung einer angemessenen Länge des Linkers mit einem gewissen Maß an Flexibilität, indem es im Allgemeinen geringere Bindungsaffinitäten als **III**-**V** aufweist. Ausgeprägte Aggregations - Deaggregationsprozesse wurden in fluorimetrischen Titrationsexperimenten mit DNA für die Verbindungen **III** und **V** beobachtet. „Molecular Modelling" von Komplexen von **V** mit AT-DNA legt die kleine Furche der DANN Helix als dominante Bindungsstelle für **V** als Monomer nahe und zeigt zudem, dass Dimere von **V** ebenfalls in die kleine Furche binden können.
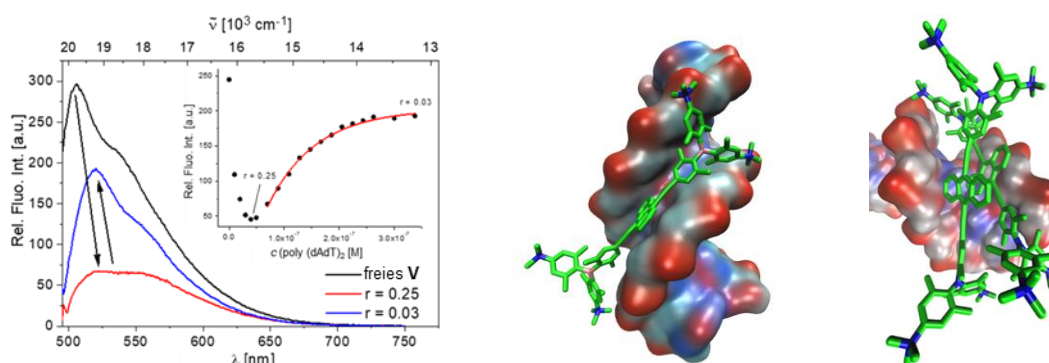
Abbildung 4. Links: Änderungen des Emissionsspektrums von **V** bei Titration mit Poly(dAdT)$_2$, Einschub: Abhängigkeit der relativen Fluoreszenzintensität bei 520 nm von c (Poly(dAdT)$_2$; rechts: Monomer und Dimer der Verbindung **V** in der kleinen Furche von Poly(dAdT)$_2$, erhalten durch „Molecular Modelling".

Starke SERS-Signale für **III**-**V** gegenüber sehr schwachen Signalen für **VI**, insbesondere die starken Signale von Anthracen selbst, die für **V**, aber nicht für **VI** beobachtet wurden, zeigen die Bedeutung von Dreifachbindungen für eine starke Raman-Aktivität in Molekülen dieser Verbindungsklasse. Die Energie der charakteristischen Streckschwingung der C≡C-Bindungen hängt signifikant von der aromatischen Einheit zwischen den

Dreifachbindungen ab. Die Insertion aromatischer Einheiten zwischen zwei C≡C-Bindungen bietet somit ein alternatives Design für duale Raman- und Fluoreszenzchromophore, welche in der multiplexen biologischen Raman-Bildgebung anwendbar sind.

6.4 Kapitel 4

In Kapitel 4 dieser Arbeit wurde die Verbindungsklasse wasserlöslicher tetrakationischer Bis-Triarylboran-Chromophore um die EDOT-verbrückten Verbindungen **X**, **Y** und **Z** erweitert und diese mit ihren literaturbekannten Thiophenanaloga **X'**, **Y'** und **Z'** verglichen. Eine Diskussion der interessanten photophysikalischen Eigenschaften der neutralen Vorstufen **XN**, **YN** und **ZN** ist ebenfalls Teil dieser Studie.
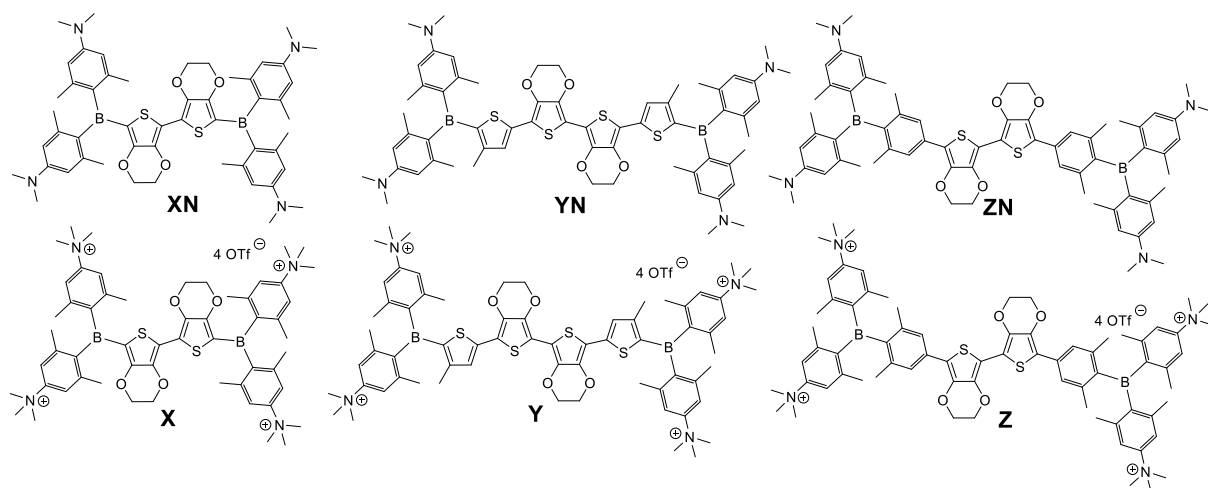
Abbildung 5. EDOT-verbrückte Zielverbindungen dieser Studie.

Absorption und Emission sind in diesen Verbindungen im Vergleich zu ihren Thiophen-haltigen Analoga signifikant rotverschoben. Photophysikalische Untersuchungen der neutralen Vorstufen zeigen eine positive Solvatochromie der Emissionsmaxima – ein Phänomen, das typischerweise für neutrale Vorstufen dieser Verbindungsklasse zu beobachten ist – lediglich im Fall von **XN**. Diese Beobachtung entspricht dem höheren berechneten Ladungstransfercharakter der niederenergetischsten Absorption von **XN** im Vergleich zu **YN** und **ZN**. Die theoretischen Studien zeigen, dass sich die HOMOs von **YN** und **ZN** an den jeweiligen π-Brücken befinden, während das HOMO von **XN** über das gesamte π-System des Moleküls, einschließlich des *N,N*-Dimethylamino-2,6-dimethylphenylsubstituenten, delokalisiert ist.

XN **YN** **ZN**
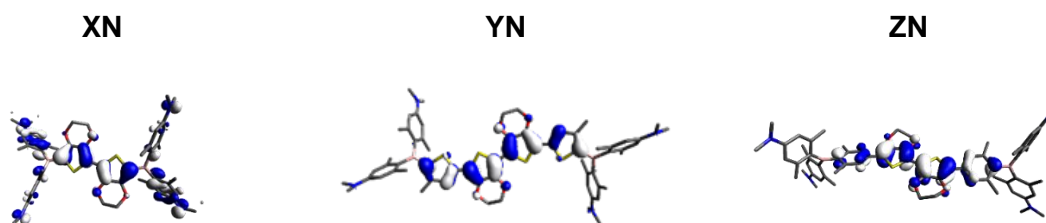
Abbildung 6. HOMOs der Verbindungen **XN**, **YN** und **ZN**, erhalten durch TD-DFT Berechnungen auf dem CAM-B3LYP/6-31G+(d,p) Theorielevel.

Während die niederenergetischsten Absorptionen in den tetrakationischen Verbindungen **X** und **Y** als lokal angeregte π-π^*-Übergänge klassifiziert wurden, ist der $S_1 \leftarrow S_0$-Übergang von **Z** durch einen schwachen Ladungstransfer von EDOT zu Bor gekennzeichnet. Aufgrund einer großen Stokes-Verschiebung zeigt Verbindung **Z** die am weitesten rotverschobene, noch weit im nahen Infrarotbereich detektierbare, Emission (λ_{em} (MeCN) = 662 nm; λ_{em} (H_2O) = 651 nm), aller bisher bekannten, tetrakationischen, wasserlöslichen Bis-Triarylboranchromophore.

Z

LUMO

HOMO
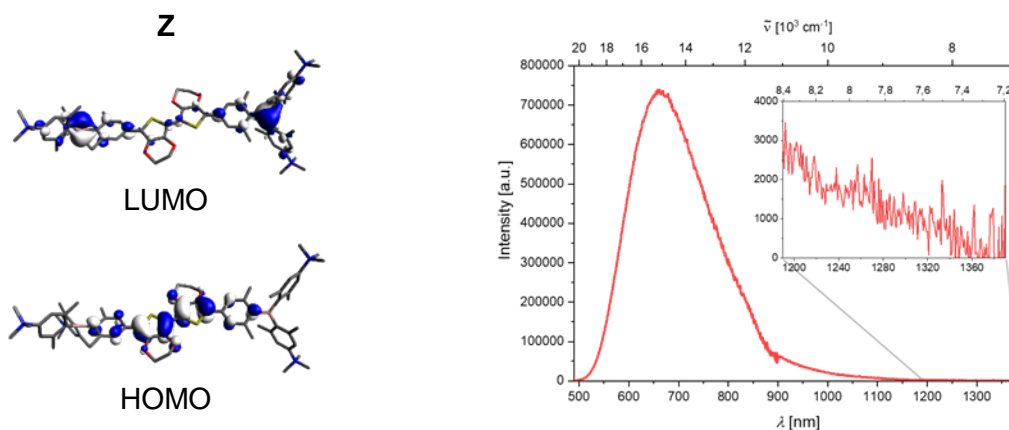
Abbildung 7. Links: relevante Orbitale für den $S_1 \leftarrow S_0$-Übergang von **Z** in MeCN, erhalten durch TD-DFT Berechnungen auf dem CAM-B3LYP/6-31G+(d,p) Theorielevel; rechts: Emissionsspektrum von **Z** in MeCN, Einschub: vergrößerter Ausschnitt, des Spektrums, in dem nachweisbare Emission bis ca. 1360 nm gezeigt wird.

Eine erhöhte Elektronendichte an den Boratomen wurde durch negativere Reduktionspotentiale für die drei EDOT-haltigen Verbindungen (**X**, **Y**, **Z**) im Vergleich zu ihren Thiophen-haltigen Analoga (**X'**, **Y'**, **Z'**) nachgewiesen. Es wurde dadurch jedoch keine erhöhte Wasserstabilität erreicht und nur Verbindung **Z** wurde als wasserstabil befunden.

Für die wasserstabilen Verbindungen **Z** und ihr Thiophenanalogon **Z'** wurden mittels transienter Absorptionsspektroskopie langlebige Zustände beobachtet, die vollständig durch Sauerstoff gequencht werden. Eine Quantenausbeute für die Singulett-Sauerstoffbildung von 0.6 wurde für **Z'** durch Vergleich der Intensität der charakteristischen Lumineszenz des erzeugten Singulett-Sauerstoffs bei 1272 nm mit einem bekannten Standard bestimmt. Die NIR-Emission der Verbindung **Z** verhinderte den Nachweis der Singulett-Sauerstofflumineszenz und damit die Bestimmung einer Quantenausbeute für die Singulett-Sauerstoffbildung.
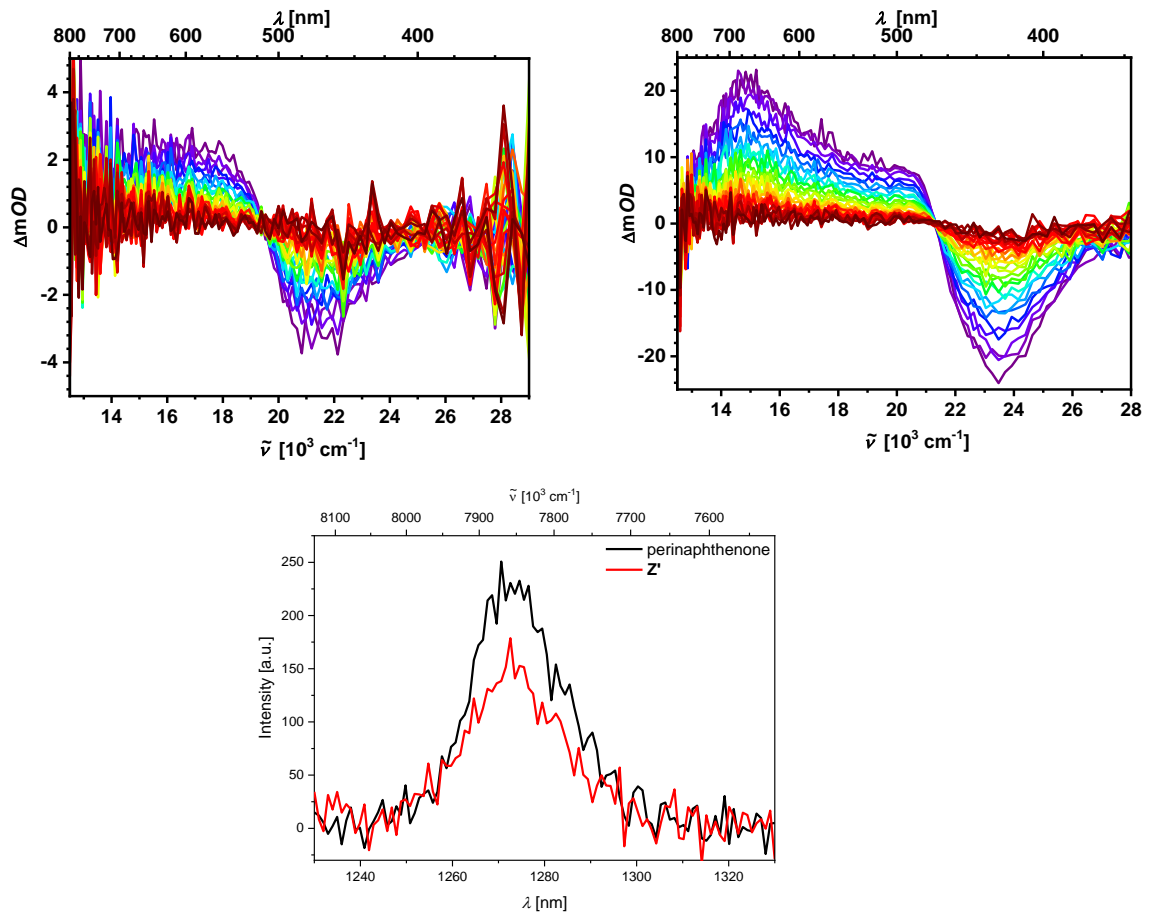
Abbildung 8. Oben: Transiente Absorptionsspektren von **Z** (links) und **Z'** (rechts) in entgaster MeCN Lösung; unten: Lumineszenz des Singulett-Sauerstoffs erzeugt durch Sensibilisierung mit **Z'** und dem Standard Perinaphtenon.

7 Experimental Details and Supporting Information

7.1 Chapter 2

7.1.1 General Information

Unless otherwise noted, the following conditions apply: each reaction was performed using standard Schlenk or glovebox (Innovative Technology Inc.) techniques under argon. Only oven-dried and additionally flame-dried glassware was used. The work up procedure was performed open to the air. Solvents used for reactions (THF, CH_2Cl_2, hexane, and Et_2O) were dried, deoxygenated and argon saturated using an Innovative Technology Inc. Pure Solvent Purification System. Deuterated solvents (CD_2Cl_2, acetone-d_6) used for nuclear magnetic resonance spectroscopy were purchased from Sigma Aldrich. Trimethylsilyl chloride was distilled and stored under argon prior to use. *n*-Butyllithium (2.5 M solution in hexane), *t*-butyllithium (1.7 M solution in pentane) and KHF_2 were purchased from Sigma Aldrich and used as received, and 2-iodo-5-bromo-1,3-dimethylbenzene was purchased from Apollo Scientific Limited and passed through a silica plug with hexane prior to use. B_2pin_2 was kindly provided by AllylChem Co. Ltd. (Dalian, China). [Ir(COD)(μ-OMe)]$_2$,[378] $Pd_2(dba)_3 \cdot CHCl_3$,[379] Potassium (2,6-dimethylphenyl) trifluoroborate (**H-BF$_3$K**),[380] and Potassium (2,4,6-trimethylphenyl) trifluoroborate (**Me-BF$_3$K**)[381] were synthesized according to literature procedures.

Reaction progress was monitored using a GC-MS system (Agilent 7890A gas chromatograph (column: HP-5MS 5% phenyl methyl siloxane, 10 m, 0.25 mm, film 0.25 µm; injector: 250 °C; oven: 40 °C to 180 °C (20 °C / min), 180 °C to 280 °C (50 °C / min); carrier gas: He (1.2 mL / min) equipped with an Agilent 5975C inert MSD detector operating in EI mode and an Agilent 7693A series liquid handling system functioning as auto sampler) or by thin layer chromatography (TLC) using plates pre-coated with a layer of either silica (Polygram® Sil G/UV254) with fluorescent indicator UV254 or aluminum oxide, purchased from Marchery-Nagel. Automated flash chromatography was performed using a Biotage® Isolera Four system on silica gel (Biotage SNAP cartridges HP-Sil and KP-Sil with the cartridge size depending on substance mass according to the Biotage handbook), obtained from Biotage. Solvents were generally removed using a rotary evaporator *in vacuo* at a maximum temperature of 50 °C. Column chromatography was performed using silica gel 60 (0.040 – 0.063 mm) or aluminum oxide 90 (basic, activity I) purchased from Macherey-Nagel as the stationary phase.

^{1}H, ^{13}C{^{1}H}, ^{11}B{^{1}H} NMR spectra were obtained, unless otherwise stated, at ambient temperature using a Bruker Avance 300 III (operating at 300 MHz for ^{1}H, 75 MHz for ^{13}C{^{1}H} and 96 MHz for ^{11}B{^{1}H}), or a Bruker Avance 500 NMR spectrometer (operating at 500 MHz for ^{1}H, 125 MHz for ^{13}C{^{1}H}, 160 MHz for ^{11}B{^{1}H}, and 470.6 MHz for ^{19}F). Chemical shifts (δ)

were referenced to solvent peaks as follows. ^{1}H NMR spectra were referenced via residual proton resonances of CD_2Cl_2 (5.32 ppm)and acetone-d_6 (2.05 ppm). ^{13}C NMR spectra were referenced to CD_2Cl_2 (53.84 ppm) and acetone-d_6 (206.06 ppm and 29.84 ppm). ^{11}B NMR signals are quoted relative to external $BF_3 \cdot OEt_2$.

Elemental analyses were performed on an Elementar vario MICRO cube elemental analyzer. High-resolution mass spectrometry was performed with a High-resolution Thermo Fisher Scientific Exactive Plus Orbitrap MS System. ESI measurements were performed with a HESI source at 50 °C. APCI and ASAP measurements were performed with an ACPI source and Corona needle at 400 °C, unless otherwise noted. LIFDI measurements were performed with a Linden CMS *LIFDI 700* unit.

The X-ray crystallographic data for **HBrSi** were collected on a BRUKER X8-APEX II diffractometer with a CCD area detector and graphite monochromated Mo-K$_\alpha$ radiation. The data for **HBr$_2$** were collected on a BRUKER X8-APEX II diffractometer with a CCD area detector and multi-layer mirror monochromated Mo-K$_\alpha$ radiation. The structures were solved using the intrinsic phasing method (SHELXT),[382] refined with the SHELXL program[383] and expanded using Fourier techniques. All non-hydrogen atoms were refined anisotropically. Hydrogen atoms were included in structure factors calculations. All hydrogen atoms were assigned to idealized geometric positions.

Crystallographic data have been deposited with the Cambridge Crystallographic Data Center as supplementary publication no. (see **Table S1**). These data can be obtained free of charge from The Cambridge Crystallographic Data Centre *via* www.ccdc.cam.ac.uk/data_request/cif.

Crystal structures were depicted using Diamond 4.5 software by *Crystal Impact*.

7.1.2 Synthesis

General procedure (GP) 1: synthesis of potassium aryl trifluoroborates

B(OMe)$_3$ (2.0 equiv.) was dissolved in THF (0.50 mL/mmol) and cooled to 0 °C. At this temperature, an aryl Grignard reagent (1.0 equiv.) was added dropwise. The reaction was allowed to warm to r.t. overnight. After addition of Et$_2$O (3 mL/mmol), the resulting solid was collected by filtration in air and washed with Et$_2$O (9 mL/mmol). The solvent of the filtrate was removed *in vacuo*. The resulting oil was redisolved in THF (1 mL/mmol) and a solution of KHF$_2$ (3 equiv.) in water (0.5 mL/mmol) was added slowly. The reaction mixture was stirred at r.t. for 30 – 60 min. The solvent was evaporated to dryness *in vacuo*. The resulting solid was extracted with acetone and the solid removed by filtration. The solvent was removed *in vacuo*.

GP 2: synthesis of symmetrically substituted triarylboranes with six *ortho*-methyl groups

Reaction with aryl **Grignard** reagent: A potassium aryl trifluoroborate (1.0 equiv.) was added to an aryl Grignard (2.2 equiv.) in THF (1.7 mL/mmol). The reaction mixture was stirred in a sealed vessel at 90 °C for 2 d. After the addition of water, the aqueous phase was extracted with Et_2O. The combined organic phases were washed with brine and dried over $MgSO_4$.The solvent was removed *in vacuo*. The resulting crude product was purified *via* column chromatography and recrystallization using the conditions described below.

GP 3: one-pot synthesis of unsymmetrically substituted triarylboranes

A potassium aryl trifluoroborate (1.0 equiv.) was added to a solution of an aryl Grignard solution (1.0 equiv.) in THF (1.5 mL/mmol). After stirring at r.t. for 30 minutes, the solution was cooled to -78 °C and a solution of an aryl lithium reagent (1.2 equiv.) was added. The dark coloured reaction mixture was allowed to warm to r.t. and stirred overnight. Water was added, and the aqueous phase was extracted with Et_2O. The combined organic phases were washed with brine and dried over $MgSO_4$. The solvent was removed *in vacuo* and the crude product was purified by automated flash column chromatography and recrystallization using the conditions described below.

GP 4: Ir-catalyzed CH borylation of triarylboranes

In a Young's-tube, a triarylborane (1.0 equiv.), B_2pin_2 (1.2 equiv.), [Ir(COD)(μ-OMe)]$_2$ (2 mol%) and dtbpy (4 mol%) were dissolved in hexane (10 mL/mmol). The reaction mixture was stirred at 80 °C for 2 d, until TLC showed consumption of the starting material. After cooling to r.t., work up was performed as described below.

Potassium (4-bromo-2,6-dimethylphenyl) trifluoroborate (Br-BF₃K)
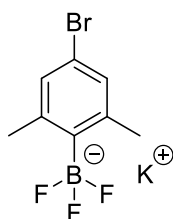
Compound **Br-BF₃K** was synthesized according to **GP 1** using B(OMe)₃ (3.6 mL, 32.2 mmol), 4-bromo-2,6-trimethylphenyl magnesium iodide freshly prepared from 4-bromo-1-iodo-2,6-dimethylbenzene (5.00 g, 16.1 mmol) and i-PrMgCl·LiCl (21.1 mL, 0.8 M, 16.9 mmol) and KHF₂ (3.77 g, 48.2 mmol). For further purification, the resulting solid was dissolved in acetone and precipitated with hexane, yielding **Br-BF₃K** as a colorless solid (1.59 g, 5.46 mmol, 34%).

¹H NMR (500 MHz, acetone-d₆) δ = 6.89 (m, 2H), 2.38 (m, 6H) ppm.

¹¹B{¹H} NMR (160 MHz, acetone-d₆) δ = 4 (q, J = 57 Hz) ppm.

¹³C{¹H} NMR (125 MHz, acetone-d₆) δ = 145.4, 129.7, 119.0, 23.4 (m) ppm.

¹⁹F NMR (470 MHz, acetone-d₆) δ = -132.70 (m, 3F) ppm.

HRMS (ESI-) m/z: [M-K]⁻ found: 252.9834; calc. for [C₈H₈BBrF₃]⁻: 252.9829 (|Δ| = 1.98 ppm).

Bis[4-bromo-2,6-dimethylphenyl]-2,6-dimethylphenylborane (HBr₂)
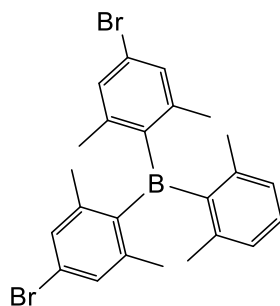
Compound **HBr₂** was synthesized according to **GP 2** using **H-BF₃K** (313 mg, 1.47 mmol) and 4-bromo-2,6-trimethylphenyl magnesium iodide freshly prepared from 4-bromo-1-iodo-2,6-dimethylbenzene (1.01 g, 3.24 mmol) and i-PrMgCl·LiCl (4.2 mL, 0.8 M, 3.40 mmol). Automated flash column chromatography was performed using hexane as the eluent. The crude product was recrystallized from hot hexane yielding **HBr₂** as a colorless solid (138 mg, 0.29 mmol, 19%).

¹H NMR (300 MHz, CD₂Cl₂) δ = 7.16 (m, 1H), 7.12 (br s, 4H), 6.94 (m, 2H), 2.00 (s, 6H), 1.99 (s, 6H), 1.97 (s, 6H) ppm.

^{11}B{^{1}H} NMR (96 MHz, CD$_2$Cl$_2$) δ = 78 (br) ppm.

^{13}C{^{1}H} NMR (75 MHz, CD$_2$Cl$_2$) δ = 146.3, 145.6, 143.2, 143.0, 140.8, 131.0, 131.0, 130.5, 128.3, 124.3, 23.1, 22.9, 22.8 ppm.

HRMS (EI$^+$) m/z: [M-C$_8$H$_9$]$^+$ found: 378.9684; calc. for [C$_{16}$H$_{16}$BBr$_2$]: 378.9686 (|Δ| = 0.53 ppm).

Elemental analysis Calc. (%) for C$_{24}$H$_{25}$BBr$_2$: C 59.55, H 5.21; found: C 59.51, H 5.35.

(4-Bromo-2,6-dimethylphenyl)-(mesityl)-2,6-dimethylphenylborane (HBrMe)
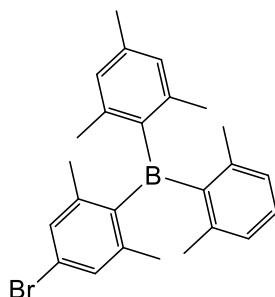
Compound **HBrMe** was synthesized according to **GP 3** using **Me-BF$_3$K** (2.04 g, 9.02 mmol), 4-bromo-2,6-trimethylphenyl magnesium iodide freshly prepared from 4-bromo-1-iodo-2,6-dimethylbenzene (2.81 g, 9.02 mmol) and *i*-PrMgCl·LiCl (11.8 mL, 0.8 M, 9.47 mmol) and 2,6-dimethylphenyllithium freshly prepared from 2-bromo-1,3-dimethylbenzene (1.5 mL, 10.8 mmol) and *t*-butyllithium (12.7 mL, 1.7 M, 21.7 mmol). Automated flash column chromatography was performed using hexane as the eluent. The crude product was recrystallized from hot hexane yielding **HBrMe** as a colorless solid (1.32 g, 3.16 mmol, 35%).

^{1}H NMR (300 MHz, CD$_2$Cl$_2$) δ = 7.14 (m, 1H), 7.11 (m, 2H), 6.93 (m, 2H), 6.77 (s, 2H), 2.27 (s, 3H), 2.00 (s, 6H), 1.99 (s, 3H), 1.97 (s, 6H) 1.96 (s, 3H) ppm.

^{11}B{^{1}H} NMR (96 MHz, CD$_2$Cl$_2$) δ = 78 (br) ppm.

^{13}C{^{1}H} NMR (75 MHz, CD$_2$Cl$_2$) δ = 147.1, 146.4, 143.7, 143.1, 143.0, 141.2, 141.0, 140.8, 140.6, 140.4, 130.8, 130.7, 130.0, 129.2, 129.2, 128.1, 128.1, 123.8, 23.0, 23.0, 22.9, 22.8, 22.7, 21.4 ppm.

HRMS (EI$^+$) m/z: [M-C$_8$H$_9$]$^+$ found: 315.0736; calc. for [C$_{17}$H$_{19}$BBr]: 315.0737 (|Δ| = 0.32 ppm).

Elemental analysis Calc. (%) for C$_{25}$H$_{28}$BBr: C 71.63, H 6.73; found: C 72.03, H 7.01.

(4-Bromo-2,6-dimethylphenyl)-[(4-trimethylsilyl)-2,6-dimethylphenyl]-2,6-dimethylphenylborane (HBrSi)
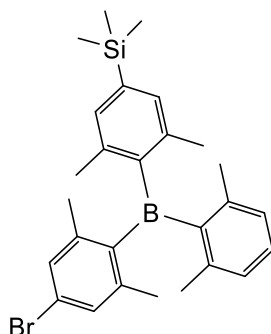
Compound **HBrSi** was synthesized according to **GP 3** using **H-BF₃K** (2.97 g, 14.0 mmol), 4-bromo-2,6-trimethylphenyl magnesium iodide freshly prepared from 4-bromo-1-iodo-2,6-dimethylbenzene (4.35 g, 14.0 mmol) and *i*-PrMgCl·LiCl (11.3 mL, 1.3 M, 14.7 mmol) and 4-trimethylsilyl-2,6-dimethylphenyllithium freshly prepared from 2-bromo-1,3-dimethyl-4-trimethylsilylbenzene (4.3 mL, 16.8 mmol) and *t*-butyllithium (19.8 mL, 1.7 M, 33.6 mmol). Automated flash column chromatography was performed using EtOAc in hexane (0% to 10%) as the eluent. The crude product was recrystallized from hot hexane yielding **HBrSi** as a colorless solid (1.07 g, 2.24 mmol, 16%).

¹H NMR (500 MHz, CD₂Cl₂) δ = 7.15 (m, 1H), 7.12 (m, 2H), 7.07 (m, 2H), 6.93 (m, 2H), 2.02 (s, 3H), 2.02 (s, 3H), 2.00 (s, 6H), 1.99 (s, 3H), 1.98 (s, 3H), 0.25 (s, 9H) ppm.

¹¹B{¹H} NMR (160 MHz, CD₂Cl₂) δ = 78 (br) ppm.

¹³C{¹H} NMR (125 MHz, CD₂Cl₂) 147.1, 146.8, 146.1, 143.1, 143.1, 142.8, 140.9, 140.7, 139.6, 139.4, 133.2, 133.1, 130.8, 130.8, 130.2, 128.2, 123.9, 23.1, 23.1, 23.0, 23.0, 22.8, 22.7, -1,11 ppm.

HRMS (EI⁺) m/z: [M+H]⁺ found: 479.1756; calc. for [C₂₇H₃₄BBrSi₄]: 479.1759 (|Δ| = 0.62 ppm).

Elemental analysis Calc. (%) for C₂₇H₃₄BBrSi: C 67.93, H 7.18; found: C 68.52, H 7.17.

Bis[4-bromo-2,6-dimethylphenyl]-[4-(pinacolboryl)-2,6-dimethylphenyl]borane (Br$_2$Bpin)
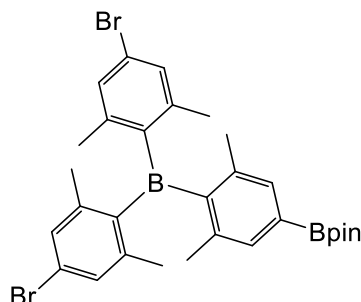
Compound **Br$_2$Bpin** was synthesized according to **GP 4** using **HBr$_2$** (115 mg, 238 μmol), B$_2$pin$_2$ (72 mg, 285 μmol), dtbpy (3 mg, 4.75 μmol), and [Ir(COD)(μ-OMe)]$_2$ (3 mg, 9.50 μmol).

Work up was performed by removing the solvent *in vacuo*. The crude product was purified by automated flash column chromatography using hexane/EtOAc (10:1 to 9:1) as the eluent. The resulting compound was recrystallized from hexane yielding **Br$_2$Bpin** as a colorless solid (98 mg, 0.16 mmol, 68%).

^{1}H NMR (300 MHz, CD$_2$Cl$_2$) δ = 7.32 (s, 2H), 7.11 (m, 4H), 2.01 (s, 6H), 1.99 (s, 6H), 1.96 (s, 6H), 1.32 (s, 12H) ppm.

^{11}B{^{1}H} NMR (96 MHz, CD$_2$Cl$_2$) δ = 78 (br), 31 (br) ppm.

^{13}C{^{1}H} NMR (75 MHz, CD$_2$Cl$_2$) δ = 149.4, 145.3, 143.2, 143.1, 139.8, 134.4, 131.0, 131.0, 124.4, 84.2, 25.1, 23.0, 22.9, 22.8 ppm.

HRMS (EI$^-$) m/z: [M]$^-$ found: 610.1262; calc. for [C$_{30}$H$_{36}$B$_2$Br$_2$O$_2$]: 610.1253 (|Δ| = 1.48 ppm).

Elemental analysis Calc. (%) for C$_{30}$H$_{36}$B$_2$Br$_2$O$_2$: C 59.07, H 5.95; found: C 59.65, H 6.15.

(4-Bromo-2,6-dimethylphenyl)-(mesityl)-[4-(pinacolboryl)-2,6-dimethylphenyl]borane (BrMeBpin)
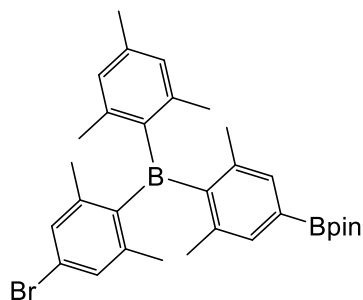
Compound **BrMeBpin** was synthesized according to **GP 4** using **HBrMe** (800 mg, 1.91 mmol), B_2pin_2 (582 mg, 2.29 mmol), dtbpy (20 mg, 76.3 μmol), and [Ir(COD)(μ-OMe)]$_2$ (25 mg, 38.2 μmol).

The work up was performed by removing the solvent *in vacuo*. The crude product was purified by automated flash column chromatography using hexane/EtOAc (10:1 to 9:1) as the eluent yielding **BrMeBpin** as a colorless solid (542 mg, 0.99 mmol, 52%).

^{1}H NMR (300 MHz, CD_2Cl_2) δ = 7.30 (s, 2H), 7.10 (s, 2H), 6.77 (m, 2H), 2.27 (s, 3H), 2.01 (s, 6H), 1.99 (s, 3H), 1.97 (s, 3H) 1.95 (s, 3H), 1.94 (s, 3H), 1.32 (s, 12H) ppm.

^{11}B{^{1}H} NMR (96 MHz, CD_2Cl_2) δ = 78 (br), 31 (br) ppm.

^{13}C{^{1}H} NMR (75 MHz, CD_2Cl_2) δ = 150.2, 146.1, 143.4, 143.1, 143.0, 141.2, 141.1, 140.5, 139.8, 139.6, 134.2, 134.2, 130.8, 130.8, 129.2, 123.9, 84.1, 25.1, 23.1, 23.0, 22.9, 22.8, 22.7, 21.37 ppm.

HRMS (EI$^+$) m/z: [M-C_8H_8Br]$^+$ found: 361.2503; calc. for [$C_{23}H_{31}B_2BrO_2$]: 361.2505 (|Δ| = 0.55 ppm).

Elemental analysis Calc. (%) for $C_{31}H_{39}B_2BrO_2$: C 68.30, H 7.21; found: C 68.34, H 7.43.

(4-Bromo-2,6-dimethylphenyl)-[4-(trimethylsilyl)-2,6-dimethylphenyl]-[4-(pinacolboryl)-2,6-dimethylphenyl]borane (BrSiBpin)
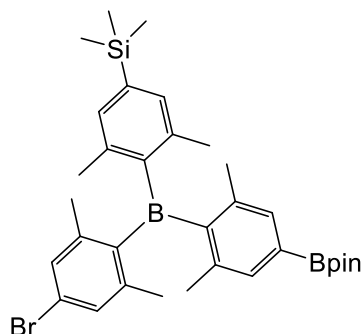
Compound **BrSiBpin** was synthesized according to **GP 4** using **HBrSi** (546 mg, 1.14 mmol), B_2pin_2 (349 mg, 1.37 mmol), dtbpy (12 mg, 45.8 μmol), and [Ir(COD)(μ-OMe)]$_2$ (15 mg, 22.9 μmol).

The work up was performed by passing the reaction mixture through a silica pad using EtOAc as the eluent. The crude product was recrystallized from EtOAc yielding **BrSiBpin** as a colorless solid (388 mg, 0.64 mmol, 56%).

^{1}H NMR (300 MHz, CD_2Cl_2) δ = 7.31 (m, 2H), 7.11 (s, 2H), 7.06 (m, 2H), 2.03 (s, 3H), 2.01 (s, 6H), 1.98 (s, 3H), 1.97 (s, 6H), 1.32 (s, 12H), 0.24 (s, 9H) ppm.

^{11}B{^{1}H} NMR (96 MHz, CD_2Cl_2) δ = 78 (br), 31 (br) ppm.

^{13}C{^{1}H} NMR (75 MHz, CD_2Cl_2) δ = 150.0, 146.9, 145.9, 143.2, 143.1, 142.9, 139.9, 139.7, 139.6, 139.5, 134.2, 133.2, 133.2, 130.8, 130.8, 124.0, 84.1, 25.1, 23.1, 23.0, 22.9, 22.9, 22.8, 22.7, -1.1 ppm.

HRMS (EI$^+$) m/z: [M+H]$^+$ found: 603.2622; calc. for [$C_{33}H_{47}B_2BrO_2Si$]: 603.2631 (|Δ| = 1.49 ppm).

Elemental analysis: Calc. (%) for $C_{33}H_{45}B_2BrO_2Si$: C 65.70, H 7.52; found: C 65.31, H 7.58.

4-Bromo-2,6-dimethylphenyl-4-iodo-2,6-dimethylphenyl-2,6-dimethylphenylborane (HBrI)
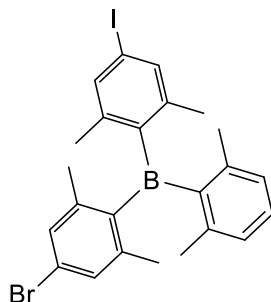
Compound **HBrSi** (50.0 mg, 105 μmol, 1.0 eq) was dissolved in CH_2Cl_2 (2 mL) and cooled to -10 °C. A solution of ICl (18.7 mg, 115 μmol, 1.1 eq) in CH_2Cl_2 (2 mL) was added dropwise. The reaction mixture was stirred for 30 min. The volatiles were removed giving **HBrI** as a colorless solid (56 mg, ~99%).

^{1}H NMR (300 MHz, CD_2Cl_2, r.t., ppm): δ = 7.35 (s, 2H), 7.17 (m, 1H), 6.95 (s, 2H), 6.94 (m, 2H), 2.00 (s, 6H), 2.00 (s, 3H), 1.97 (s, 3H), 1.96 (s, 3H), 1.95 (s, 3H).

^{11}B{^{1}H} NMR (96 MHz, CD_2Cl_2, r.t., ppm): δ = 78.

^{13}C{^{1}H} NMR (75 MHz, CD_2Cl_2, r.t., ppm): δ = 146.3, 146.1, 145.6, 143.2, 143.0, 142.9, 142.8, 140.8, 137.0, 137.0, 131.0, 131.0, 130.5, 128.3, 124.3, 97.0, 23.1, 23.1, 22.9, 22.7, 22.7, 22.5.

HRMS (EI$^+$) m/z: [M-C_8H_9]$^+$ found: 424.9562; calc. for [$C_{16}H_{16}BBrI$]: 424.9568 ($|\Delta|$ = 1.41 ppm).

Elem. Anal. Calc. (%) for $C_{24}H_{25}BBrI$: C 54.28, H 4.75; found: C 53.96, H 4.89.

4-Bromo-2,6-dimethylphenyl-4-[4-(methoxycarbonyl)phenyl]-2,6-dimethylphenyl-2,4,6-trimethylphenylborane (BrMe-Suzuki)
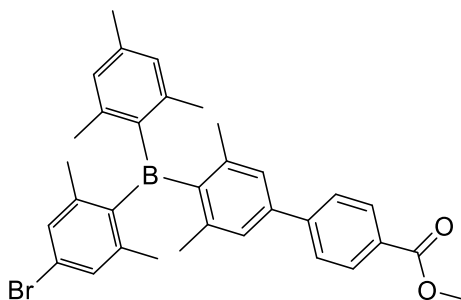
BrMeBpin (50.0 mg, 91.7 μmol, 1.0 eq), methyl 4-iodobenzoate (36.1 mg, 138 μmol, 1.5 eq), SPhos (5 mg, 12.8 μmol, 14 mol%), Pd$_2$(dba)$_3$·CHCl$_3$ (7 mg, 6.4 μmol, 7 mol%) and CsCO$_3$ (179 mg, 550 mmol, 6.0 eq) were dissolved in a mixture of toluene (2 mL) and water (1 mL). The mixture was stirred for 18 h at 85 °C, until the starting material was consumed according to TLC (EtOAc/hexane 1:9). The organic phase was separated and the aqueous phase was extracted with CH$_2$Cl$_2$ (2 x 5 mL). The organic phases were combined and, after removing the solvent *in vacuo*, the solid was purified by automated flash column chromatography (stepwise gradient from 0% to 4% EtOAc in hexane) to afford compound **BrMe-Suzuki** as a colorless solid (40 mg, 79%).

¹H NMR (300 MHz, CD$_2$Cl$_2$, r.t., ppm): δ = 8.05 (m, 2H), 7.72 (m, 2H), 7.25 (s, 2H), 7.13 (s, 2H), 6.79 (s, 2H), 3.91 (s, 3H), 2.28 (s, 3H), 2.09 (s, 6H), 2.02 (s, 6H), 2.01 (s, 3H), 2.00 (s, 3H).

¹¹B{¹H} NMR (96 MHz, CD$_2$Cl$_2$, r.t., ppm): δ = 77.

¹³C{¹H} NMR (75 MHz, CD$_2$Cl$_2$, r.t., ppm): δ = 167.2, 147.0, 146.2, 145.5, 143.6, 143.1, 143.0, 141.7, 141.5, 141.2, 141.1, 140.9, 140.6, 130.8, 130.3, 129.5, 129.2, 129.2, 127.1, 126.8, 123.9, 52.4, 23.2, 23.1, 22.8, 21.4.

HRMS (EI⁺) m/z: [M+H]⁺ found: 553.1899; calc. for [C$_{33}$H$_{35}$BBrO$_2$]: 553.1908 (|Δ| = 1.63 ppm).

Elem. Anal. Calc. (%) for C$_{33}$H$_{34}$BBrO$_2$: C 71.63, H 6.19; found: C 71.25, H 6.33.

7.1.3 NMR Spectra
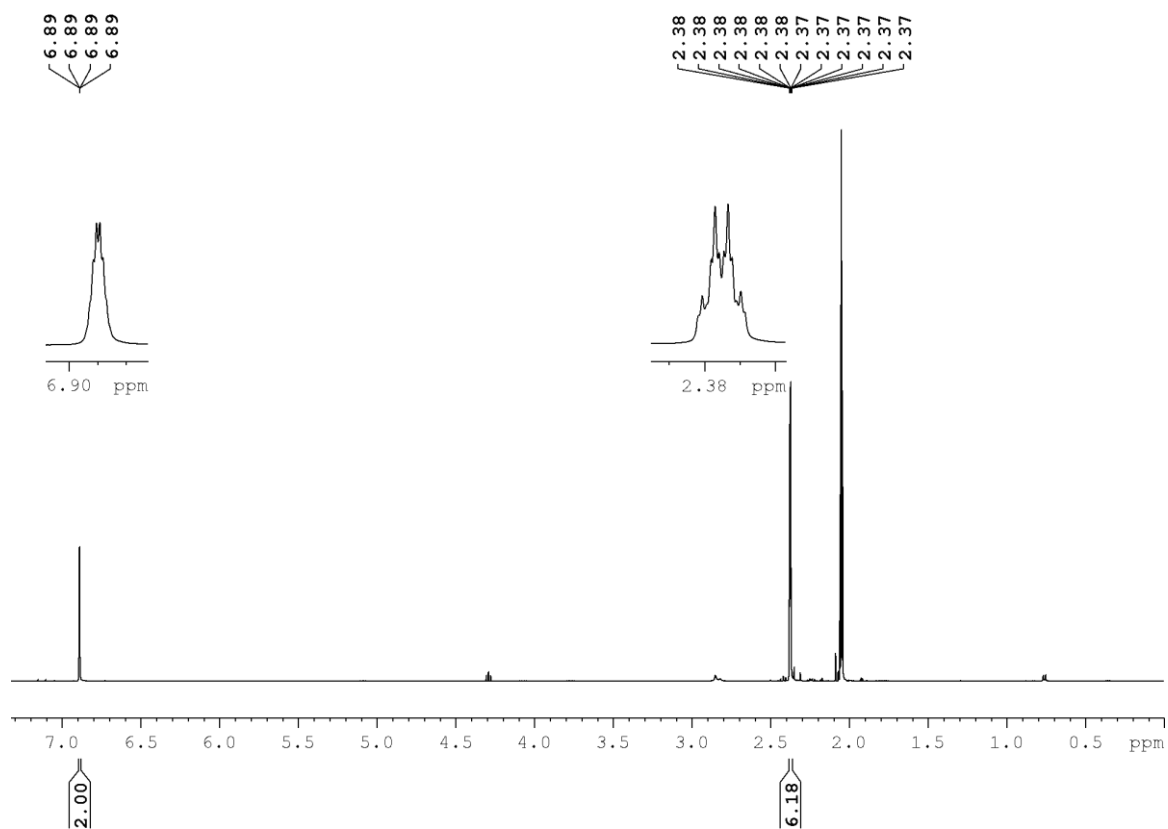
Figure S1. ^{1}H NMR spectrum of **Br-BF$_3$K** in acetone-d$_6$ at 500 MHz.
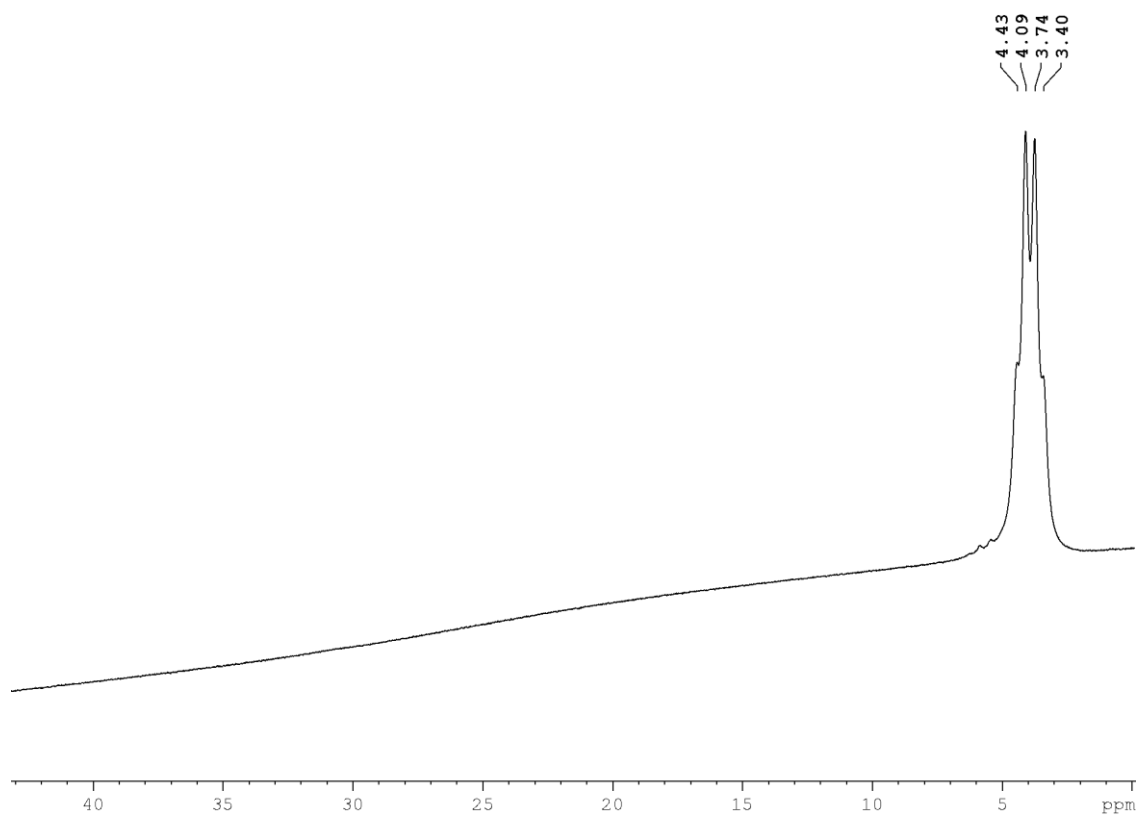
Figure S2. ^{11}B{^{1}H} NMR spectrum of **Br-BF$_3$K** in acetone-d$_6$ at 160 MHz.
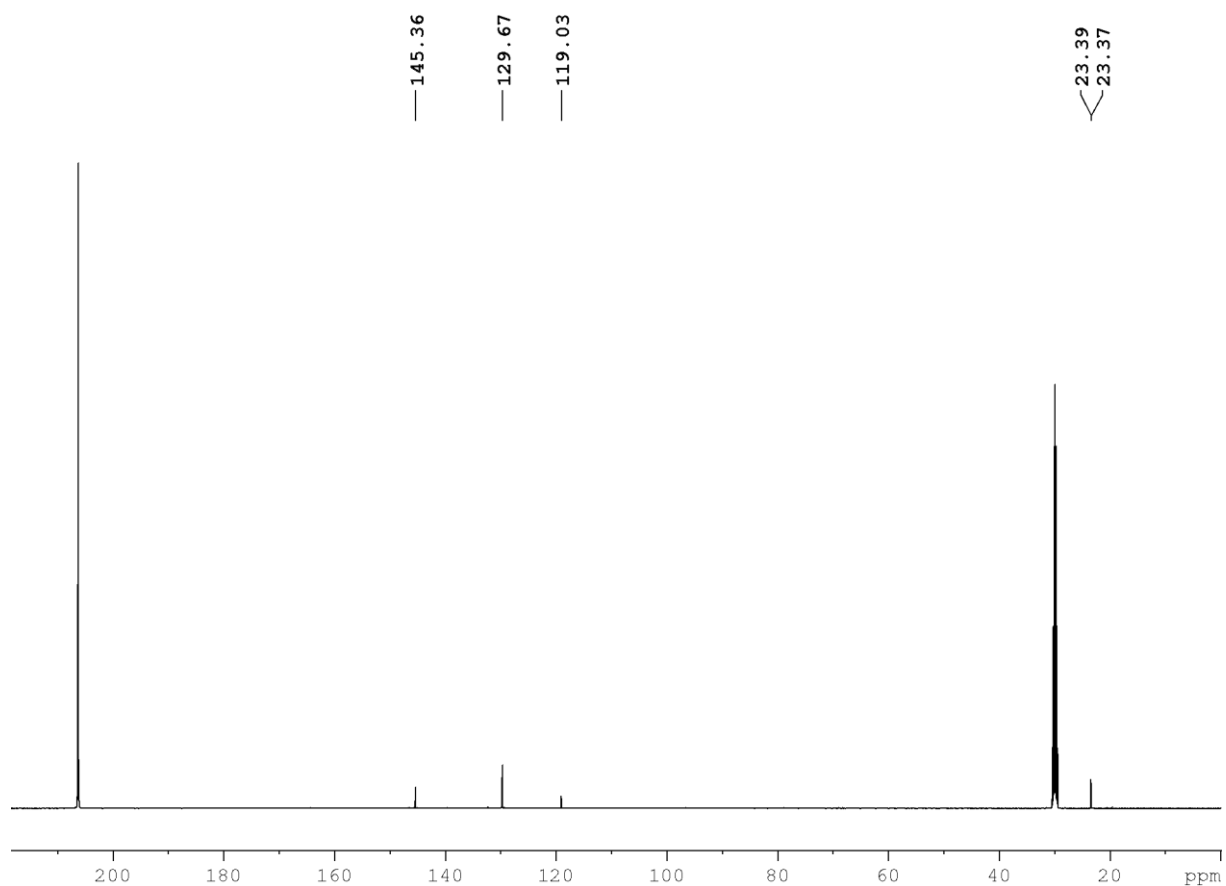
Figure S3. $^{13}C\{^1H\}$ NMR spectrum of **Br-BF$_3$K** in acetone-d$_6$ at 125 MHz.
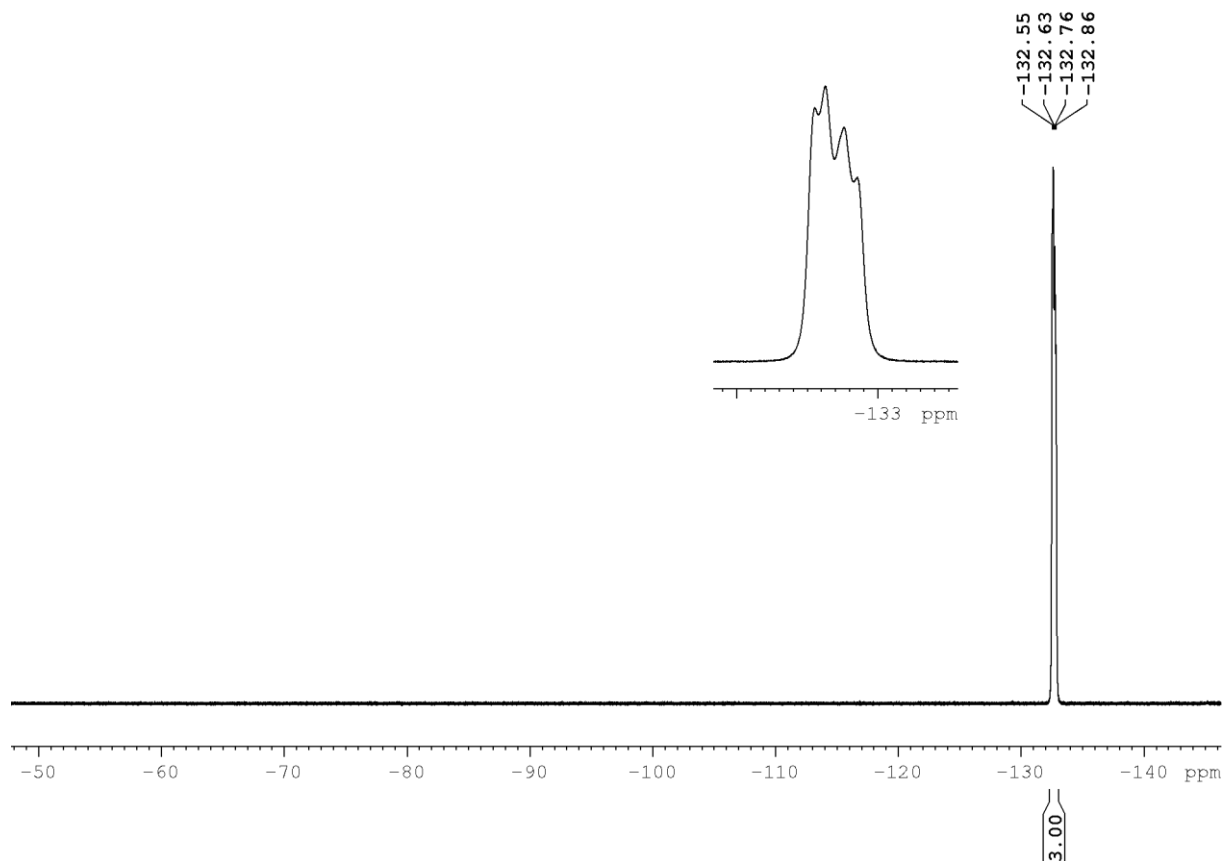
Figure S4. ^{19}F NMR spectrum of **Br-BF$_3$K** in acetone-d$_6$ at 470 MHz.
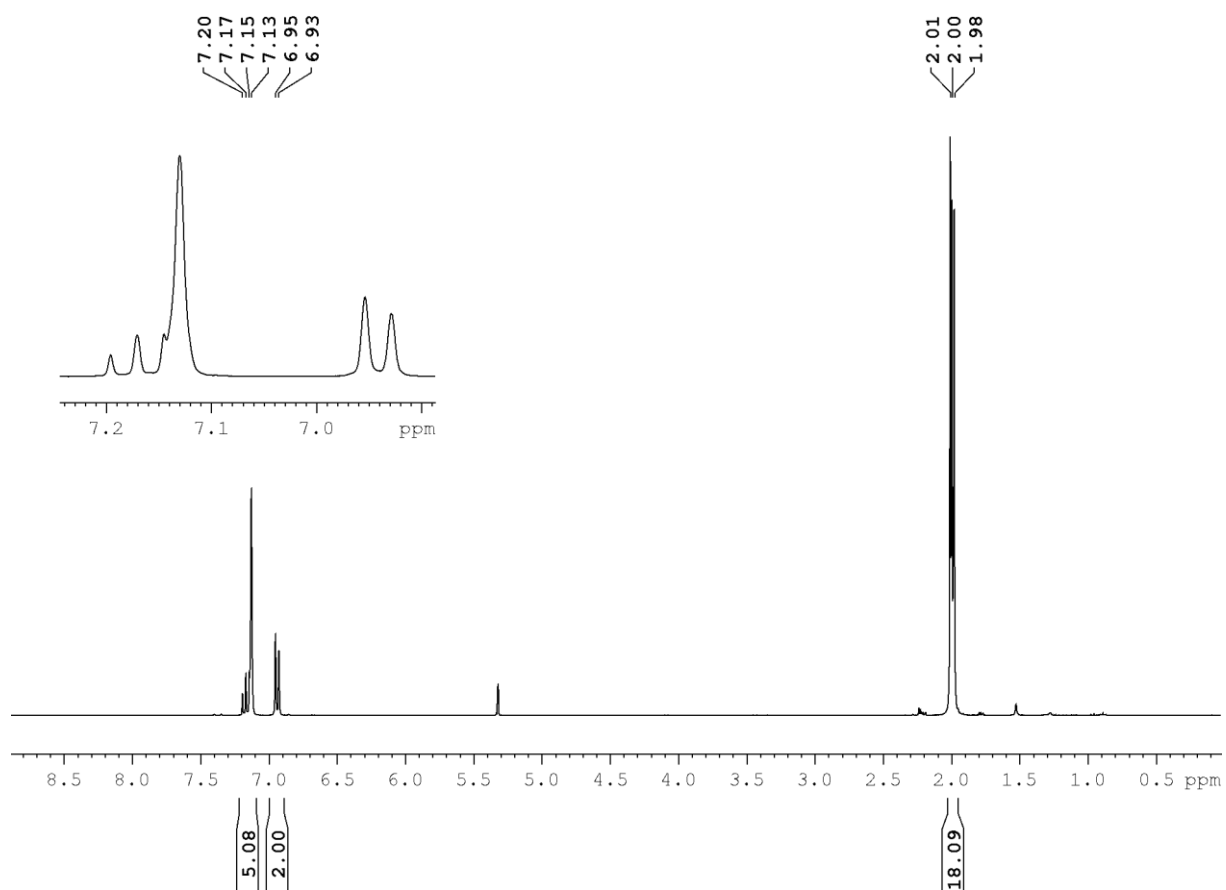
Figure S5. ^{1}H NMR spectrum of **HBr$_2$** in CD$_2$Cl$_2$ at 300 MHz.
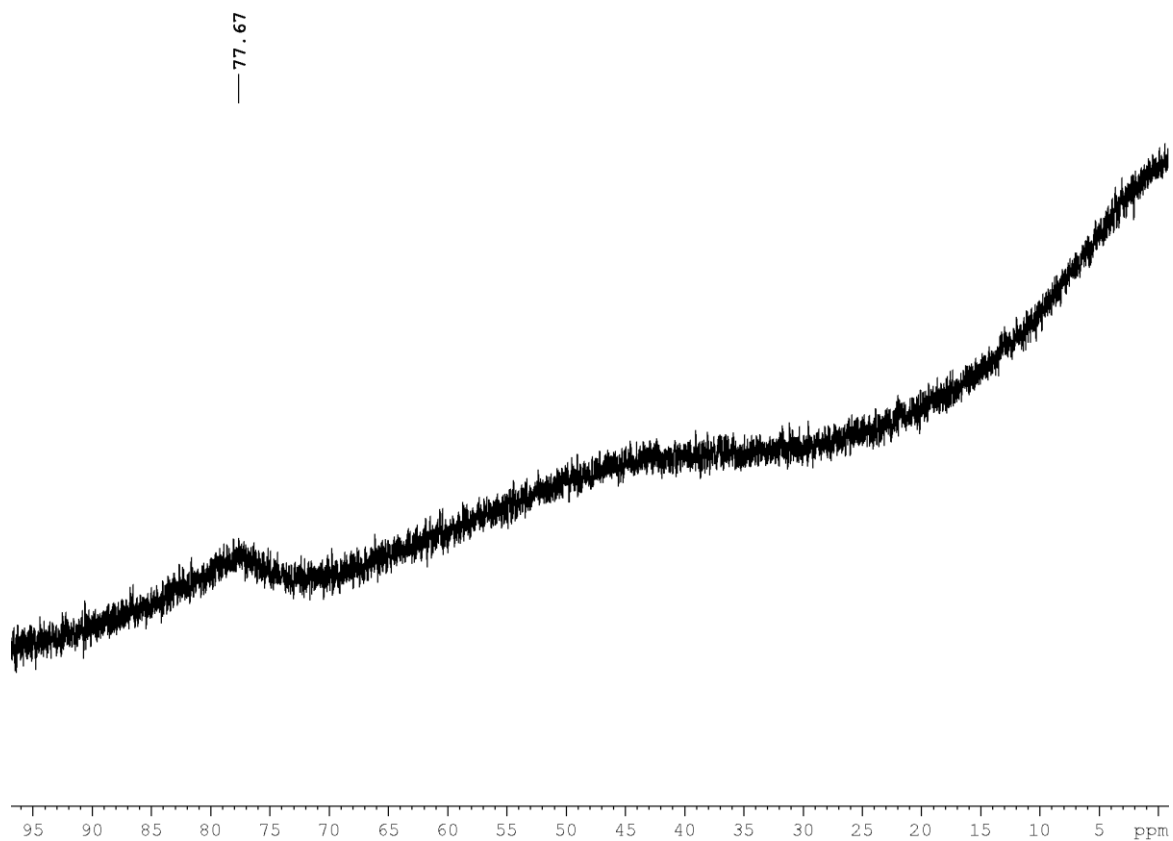
Figure S6. ^{11}B{^{1}H} NMR spectrum of **HBr$_2$** in CD$_2$Cl$_2$ at 96 MHz.
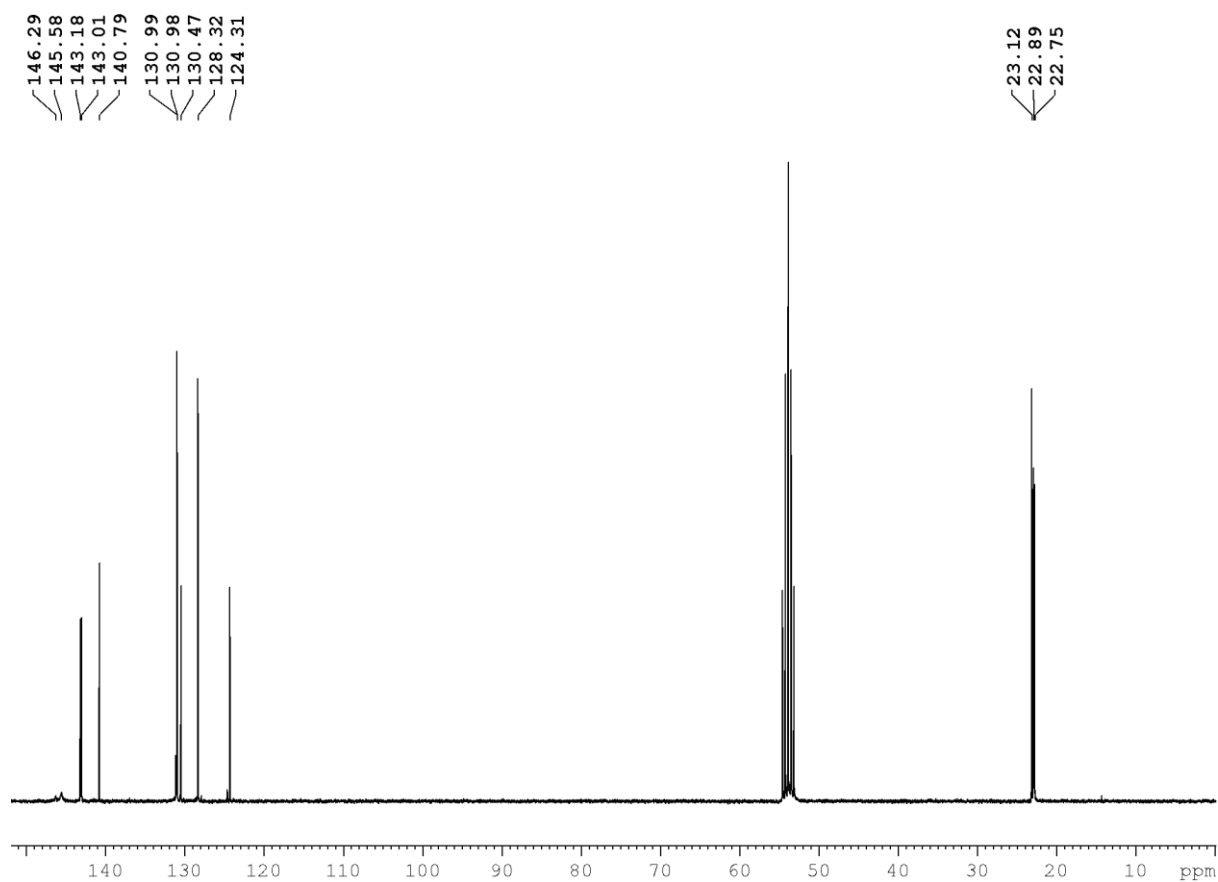
Figure S7. $^{13}C\{^1H\}$ NMR spectrum of **HBr₂** in CD_2Cl_2 at 75 MHz.
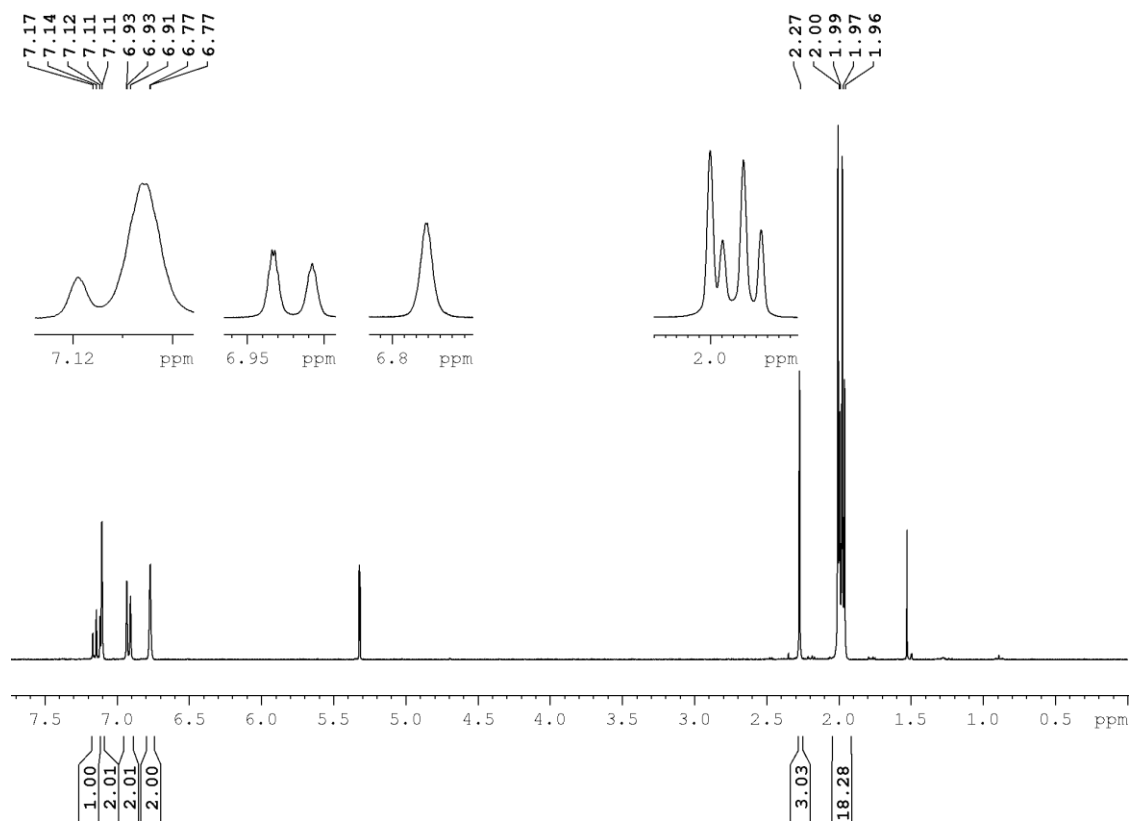
Figure S8. ^1H NMR spectrum of **HBrMe** in CD_2Cl_2 at 300 MHz.
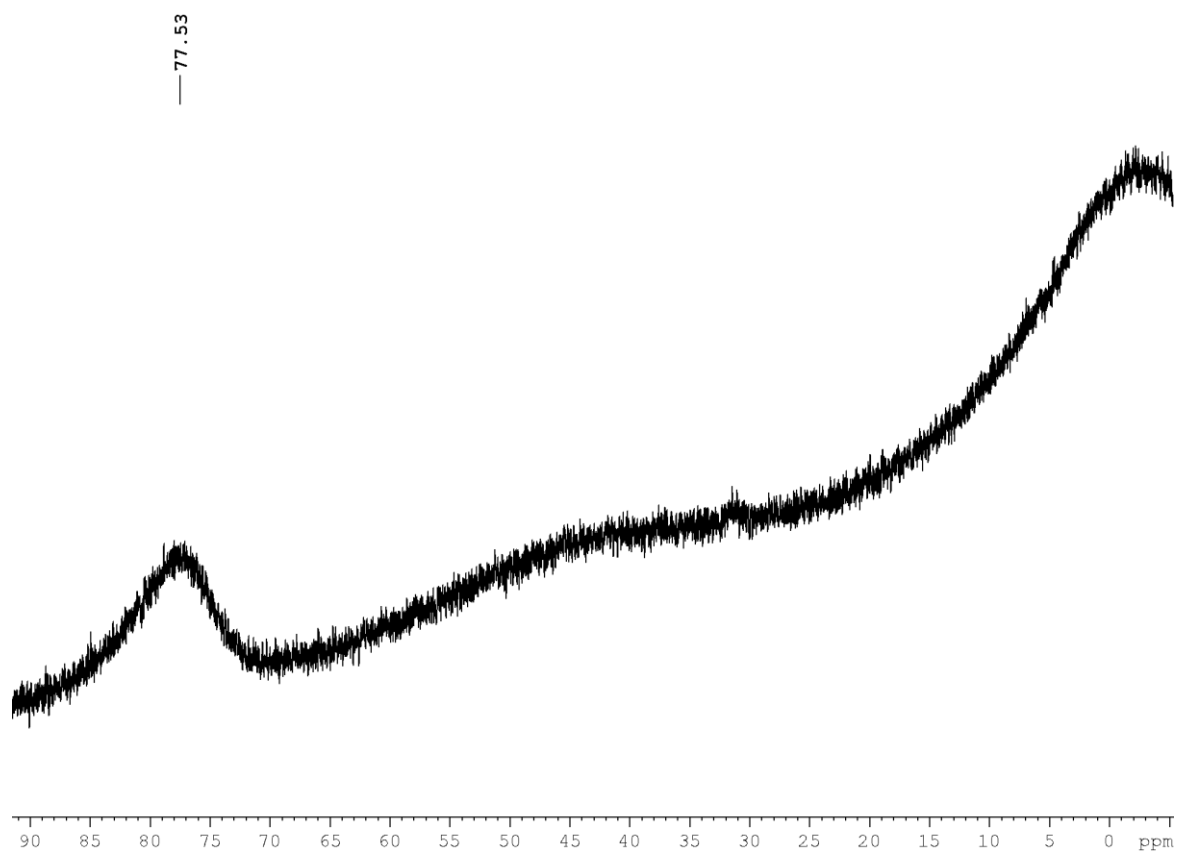
Figure S9. $^{11}B\{^1H\}$ NMR spectrum of **HBrMe** in CD_2Cl_2 at 96 MHz.
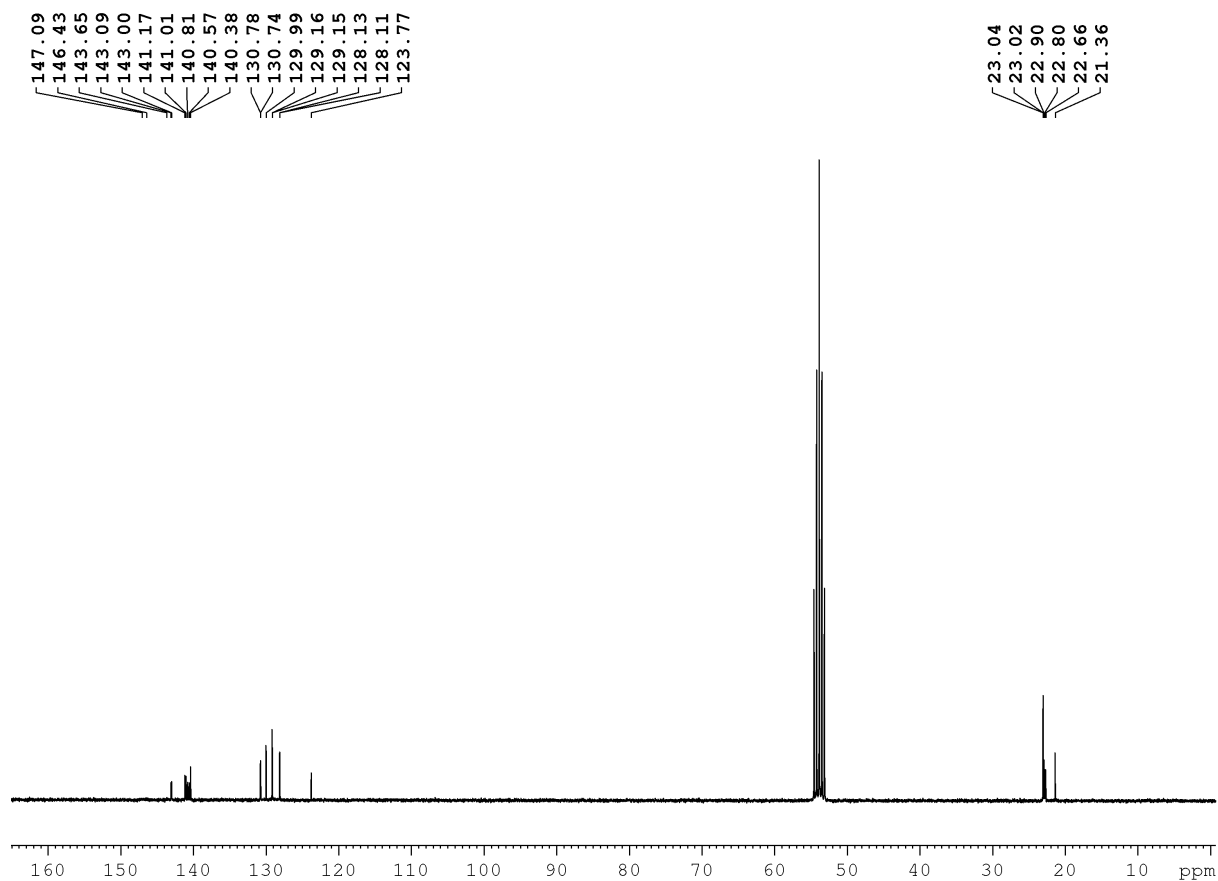
Figure S10. $^{13}C\{^1H\}$ NMR spectrum of **HBrMe** in CD_2Cl_2 at 75 MHz.
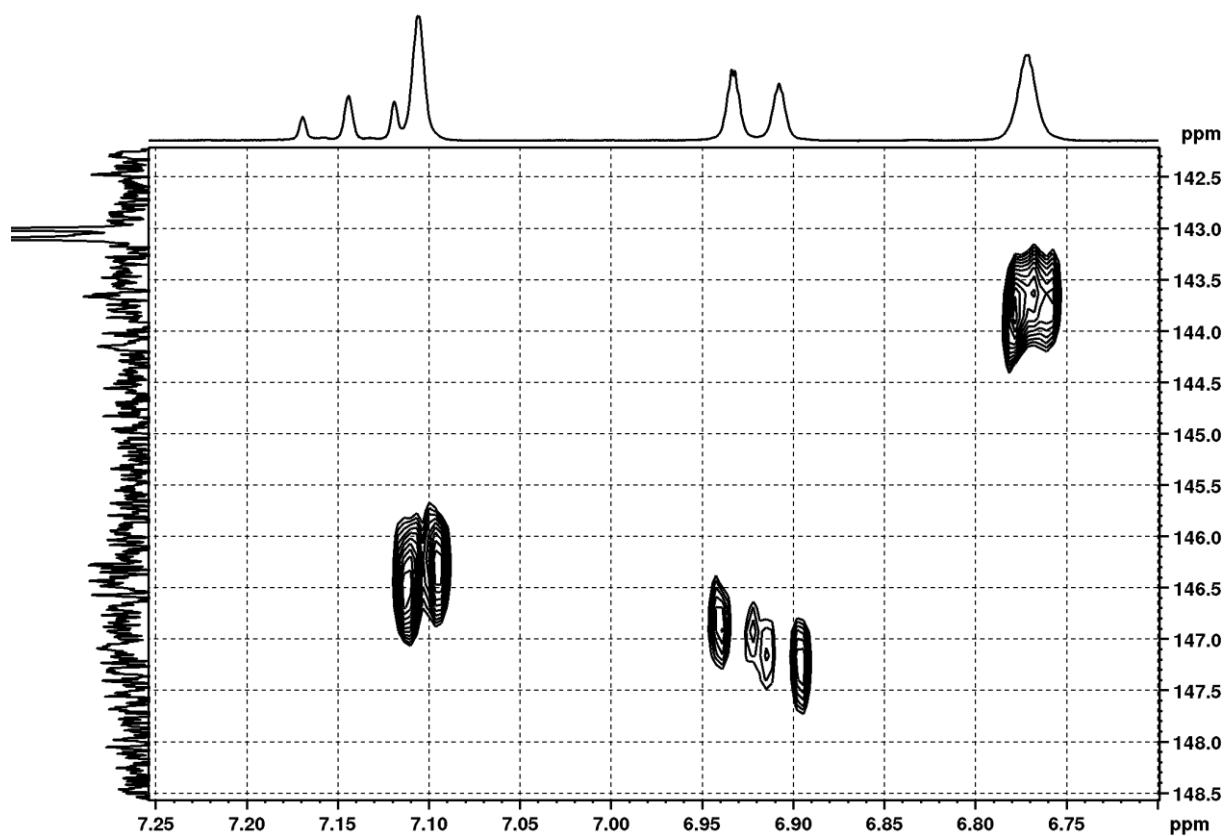
Figure S11. ^{1}H, ^{13}C HMBC NMR spectrum of **HBrMe** in CD_2Cl_2 at 300 MHz.
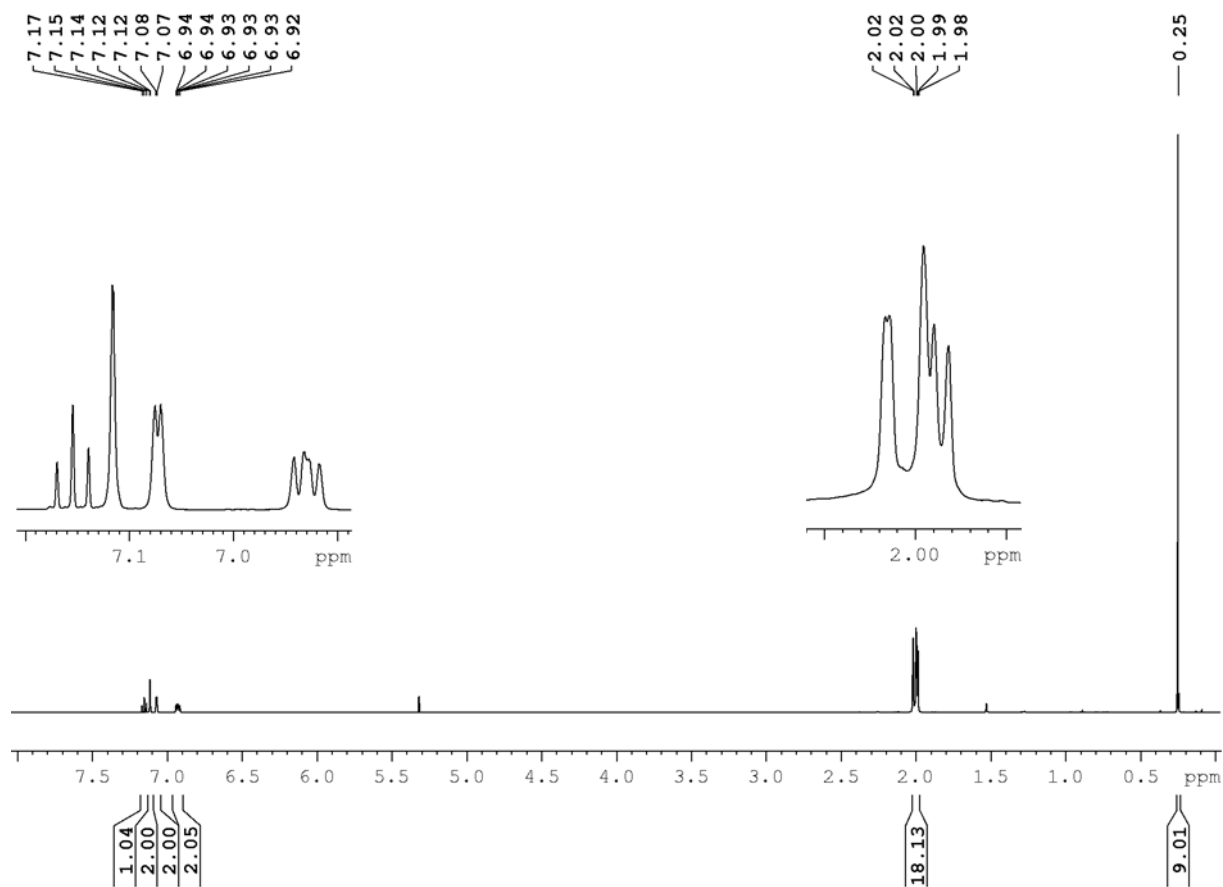
Figure S12. ^{1}H NMR spectrum of **HBrSi** in CD_2Cl_2 at 500 MHz.

—76.73
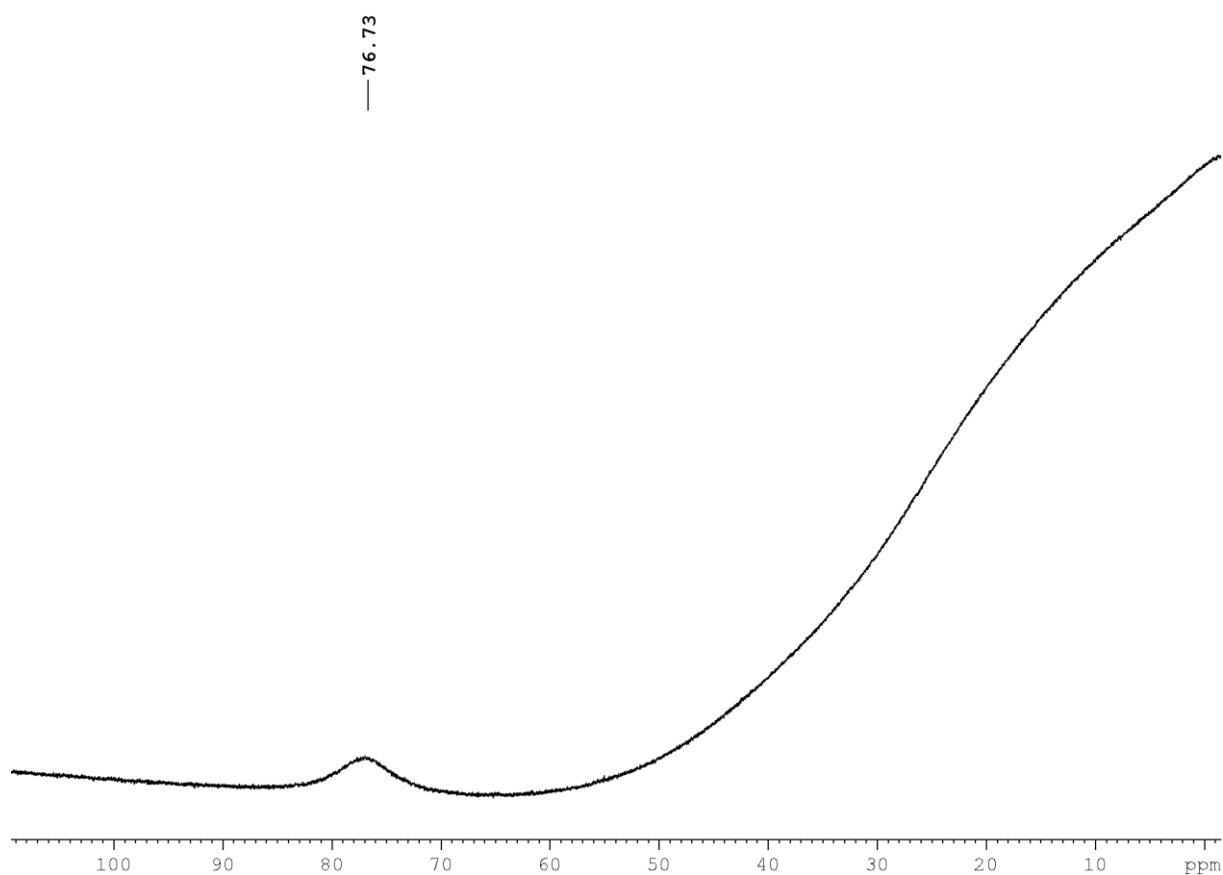
Figure S13. $^{11}B\{^1H\}$ NMR spectrum of **HBrSi** in CD_2Cl_2 at 160 MHz.

147.12
146.78
146.07
143.14
143.09
142.79
140.87
140.68
139.55
139.41
133.15
133.13
130.81
130.80
130.15
128.16
123.94

23.10
23.06
23.00
22.95
22.78
22.70

−1.11
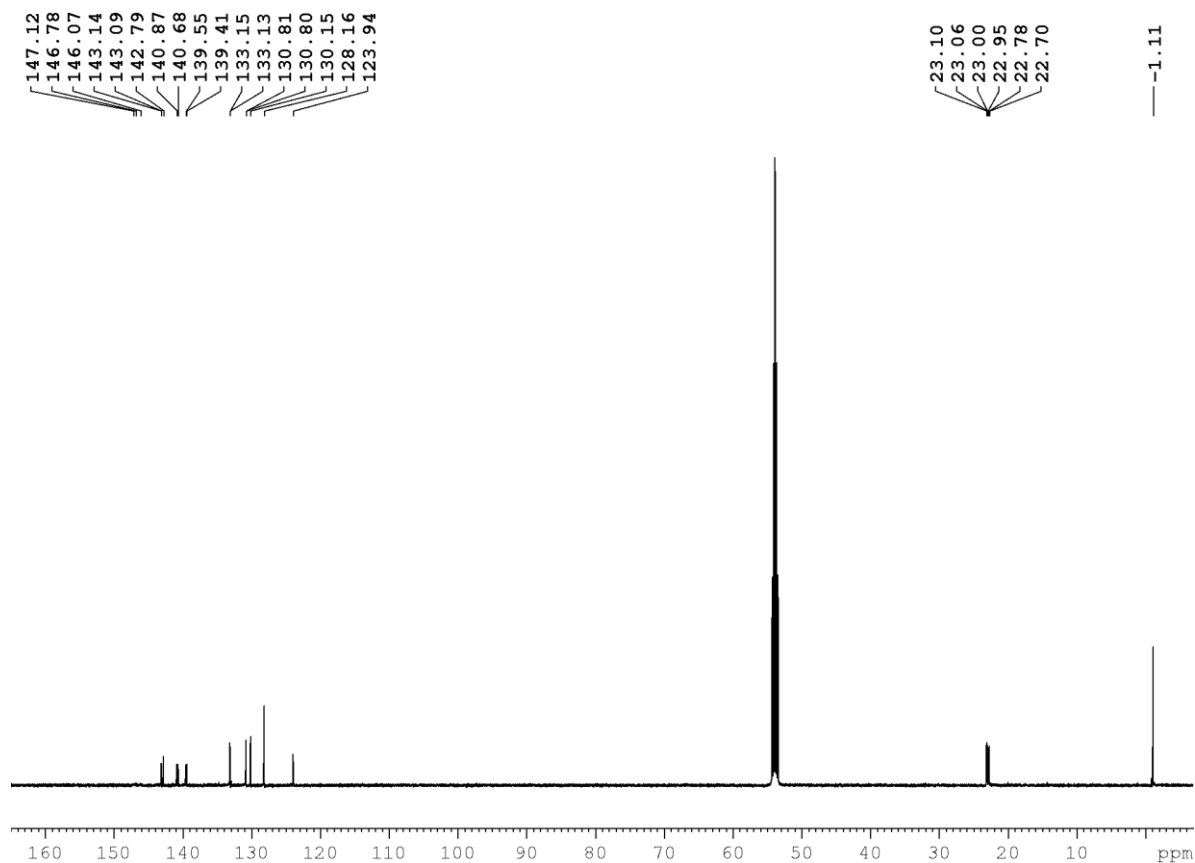
Figure S14. $^{13}C\{^1H\}$ NMR spectrum of **HBrSi** in CD_2Cl_2 at 125 MHz.
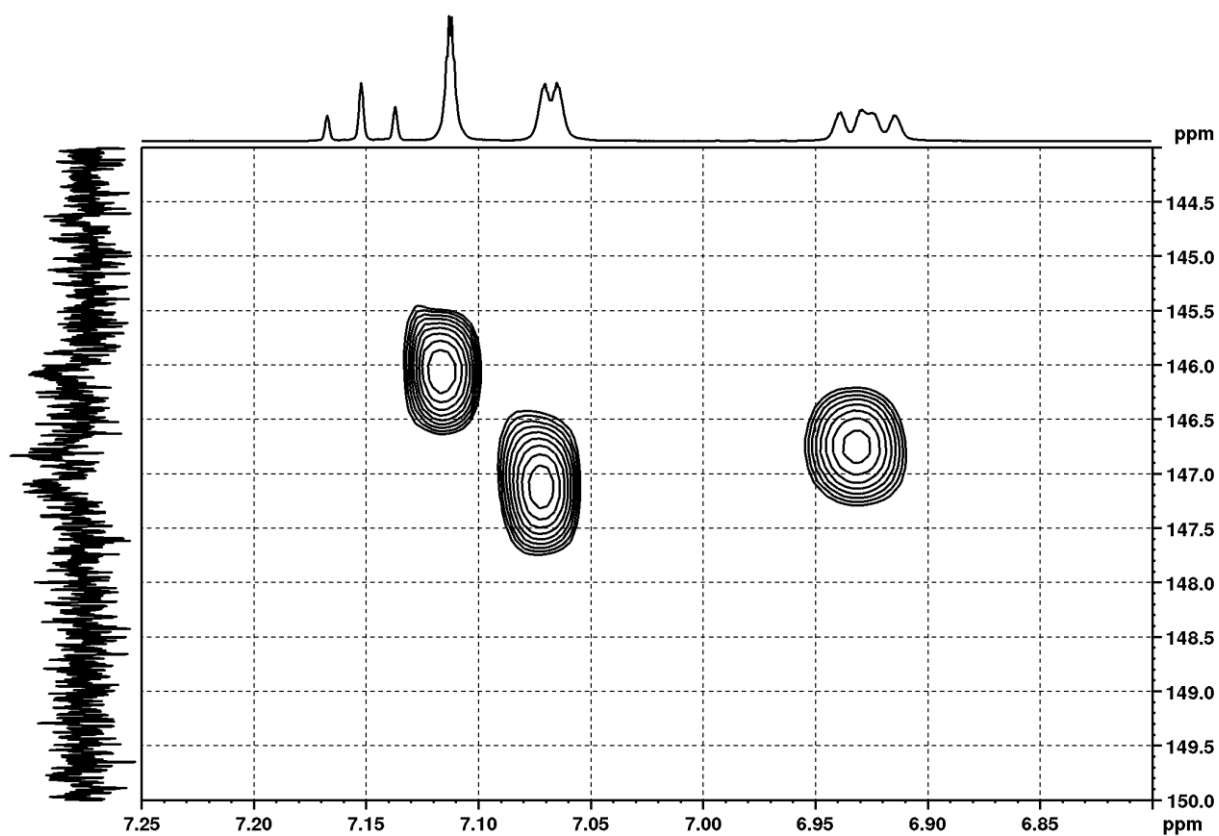
Figure S15. ^{1}H, ^{13}C HMBC NMR spectrum of **HBrSi** in CD$_2$Cl$_2$ at 500 MHz.
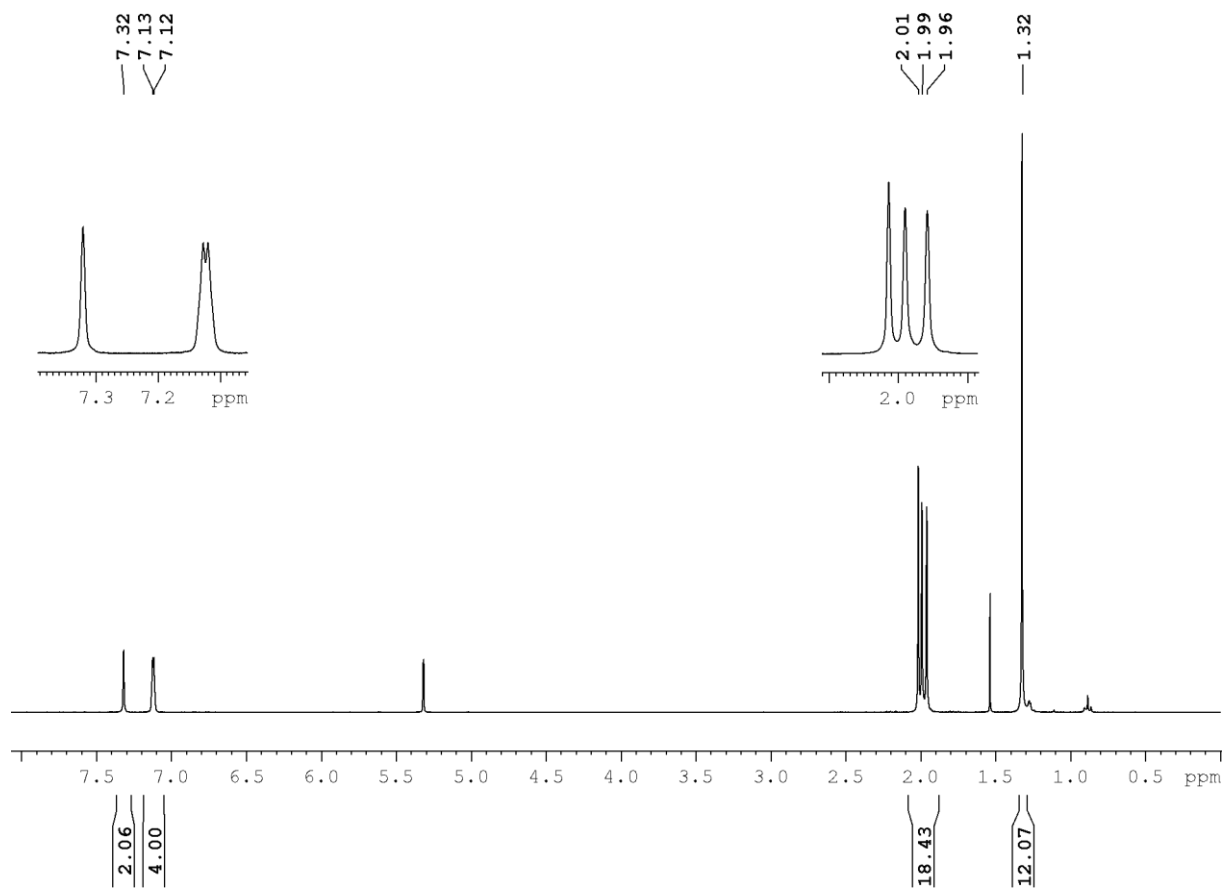
Figure S16. ^{1}H NMR spectrum of **Br$_2$Bpin** in CD$_2$Cl$_2$ at 300 MHz.
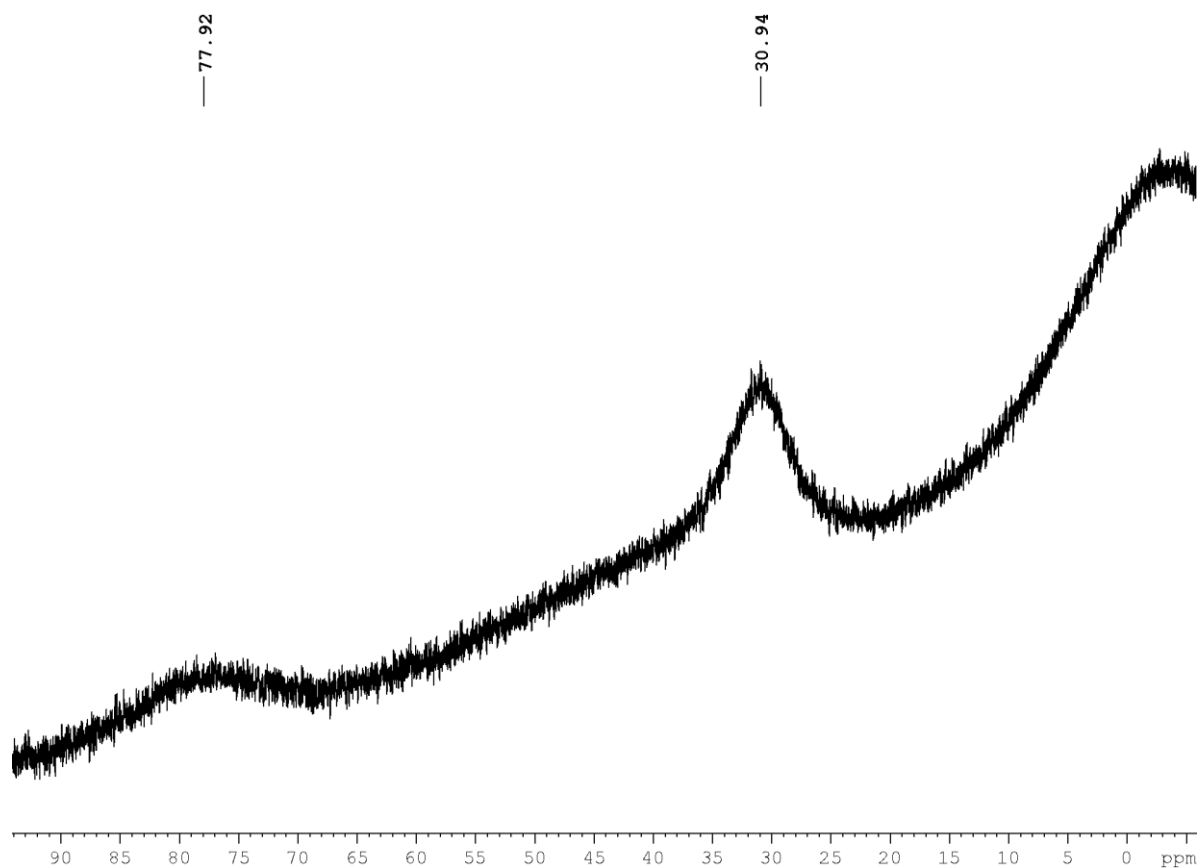
Figure S17. $^{11}B\{^{1}H\}$ NMR spectrum of **Br₂Bpin** in CD_2Cl_2 at 96 MHz.
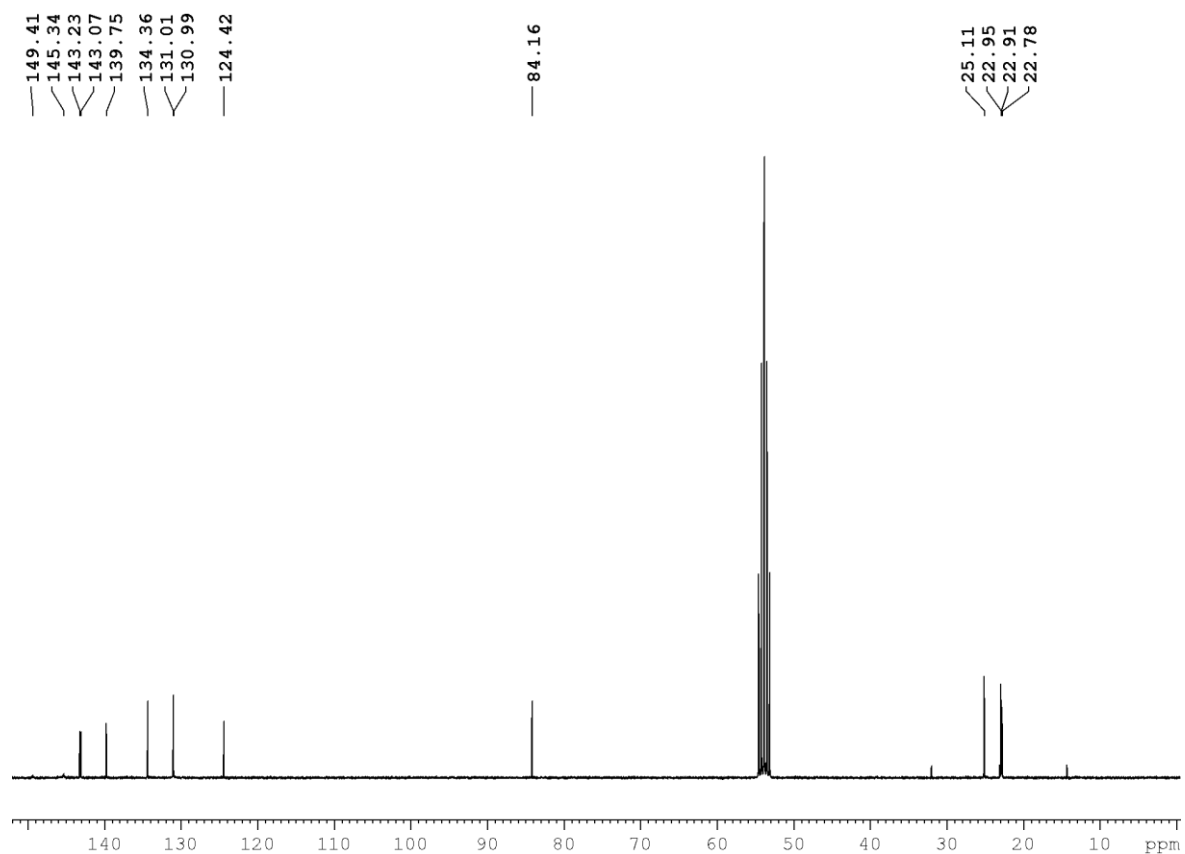
Figure S18. $^{13}C\{^{1}H\}$ NMR spectrum of **Br₂Bpin** in CD_2Cl_2 at 75 MHz.

Figure S19. ^{1}H, ^{13}C HMBC NMR spectrum of **Br$_2$Bpin** in CD$_2$Cl$_2$ at 300 MHz.
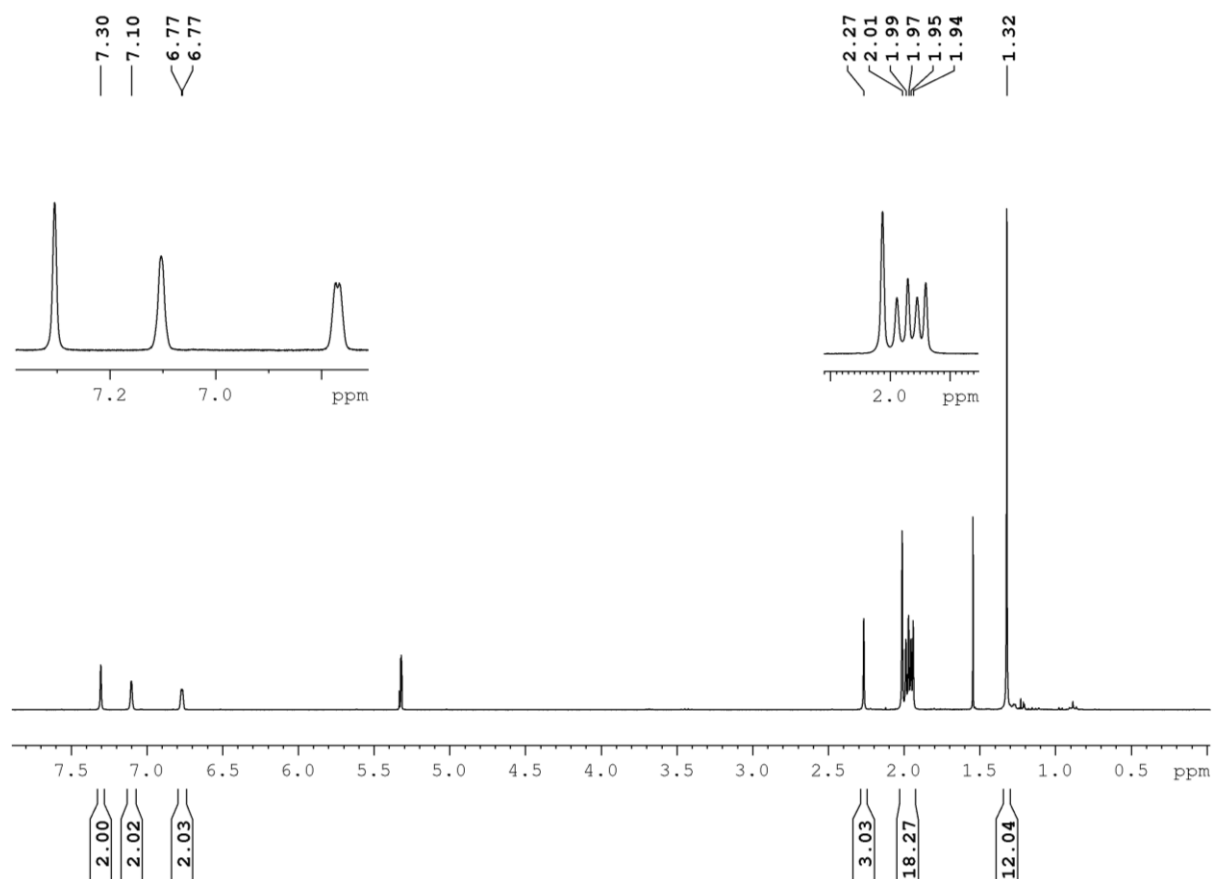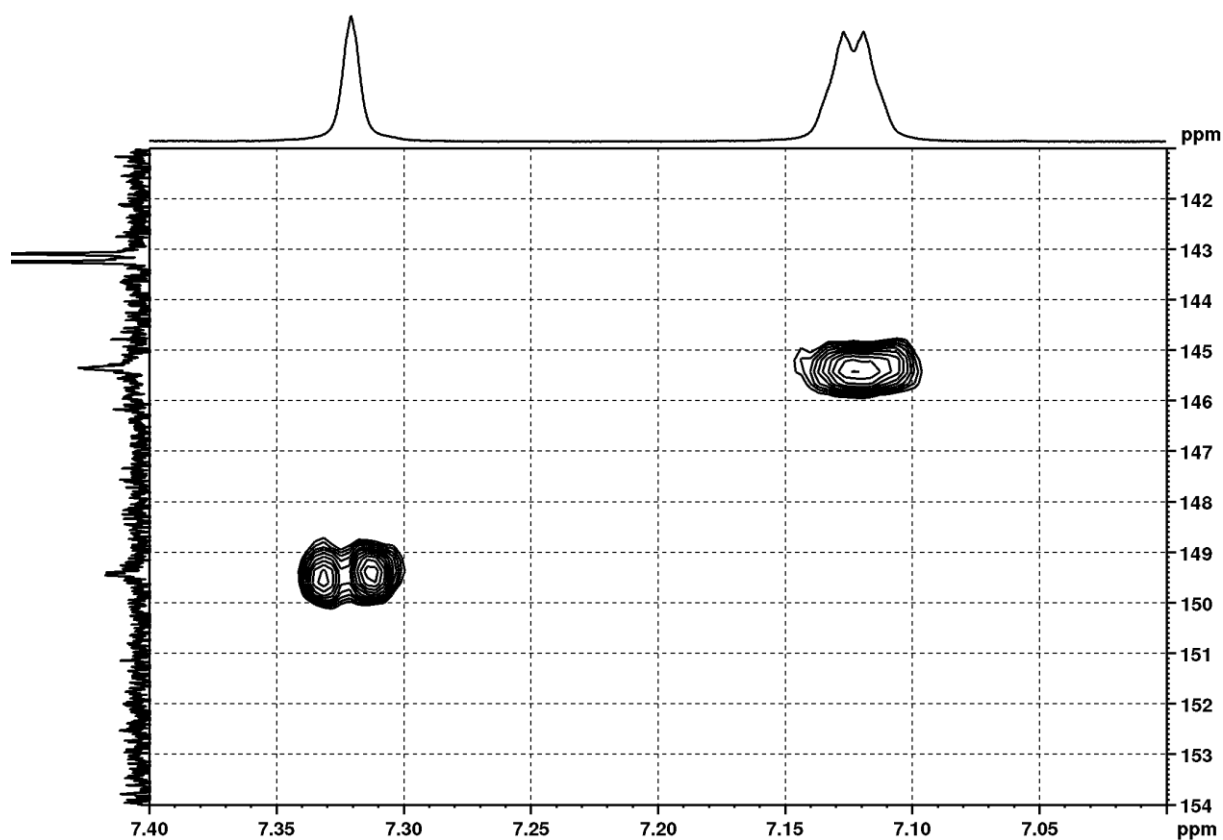
Figure S20. ^{1}H NMR spectrum of **BrMeBpin** in CD$_2$Cl$_2$ at 300 MHz.
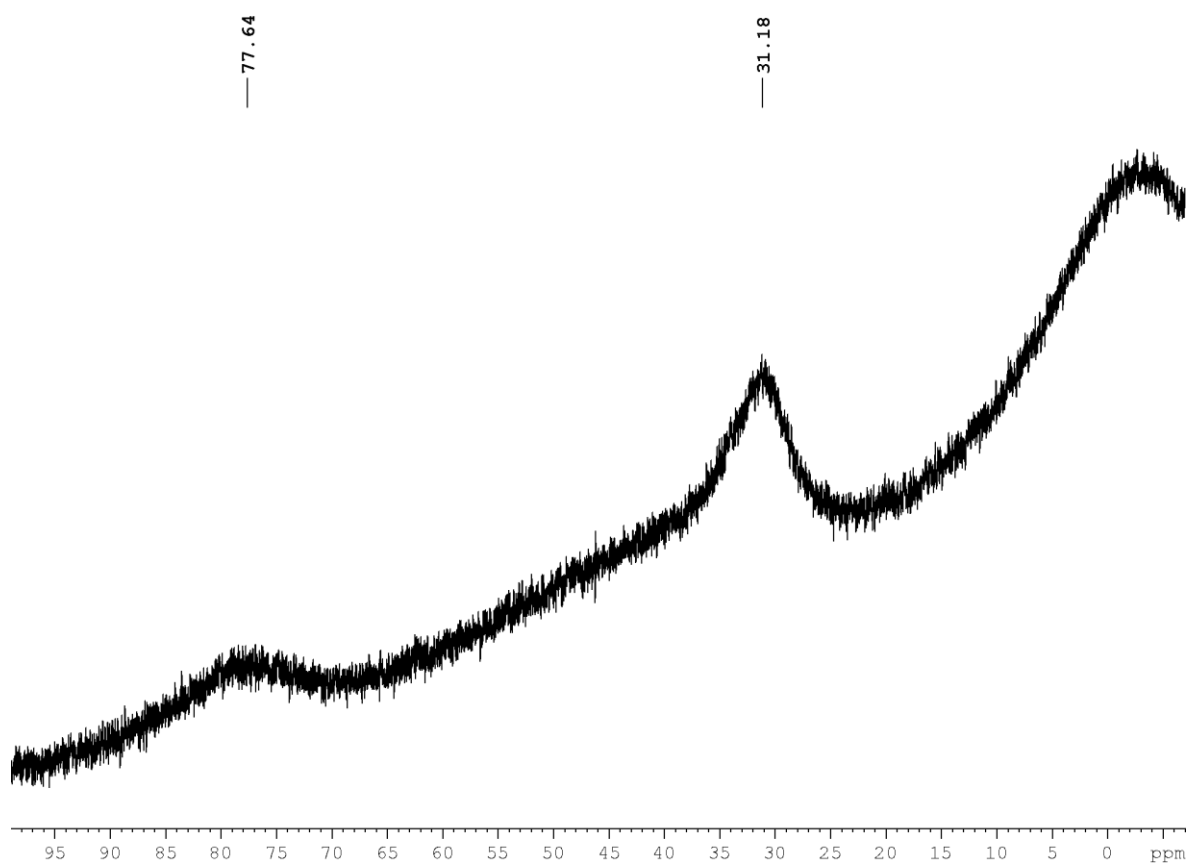
Figure S21. $^{11}B\{^1H\}$ NMR spectrum of **BrMeBpin** in CD_2Cl_2 at 96 MHz.
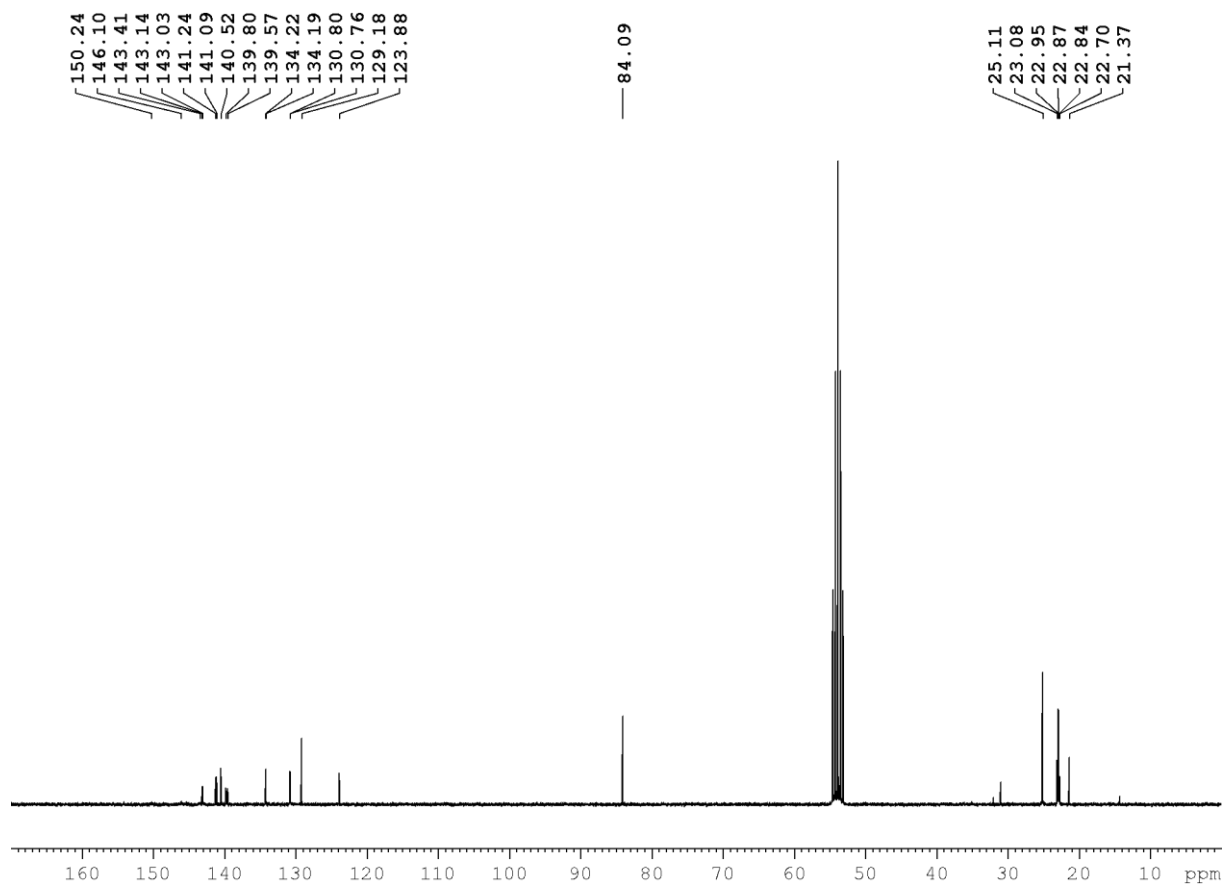
Figure S22. $^{13}C\{^1H\}$ NMR spectrum of **BrMeBpin** in CD_2Cl_2 at 75 MHz.
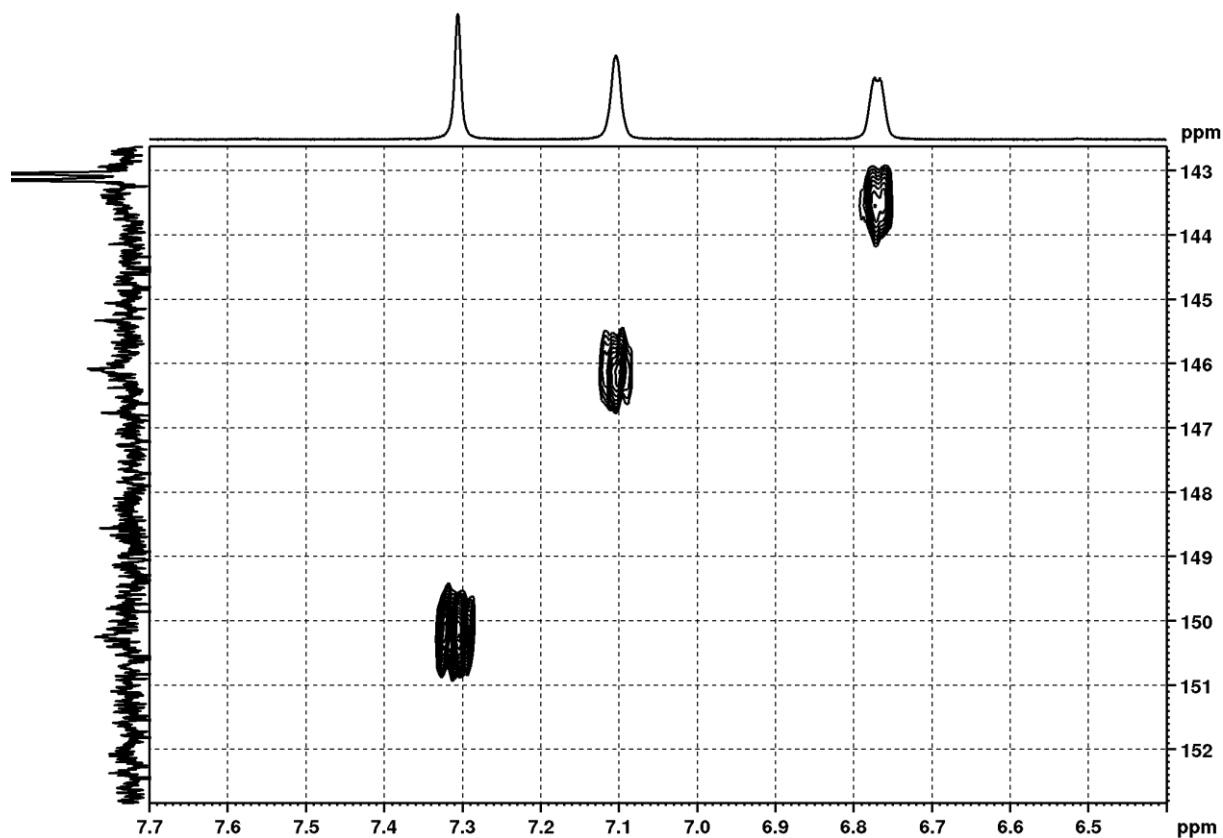
Figure S23. ^{1}H, ^{13}C HMBC NMR spectrum of **BrMeBpin** in CD_2Cl_2 at 300 MHz.
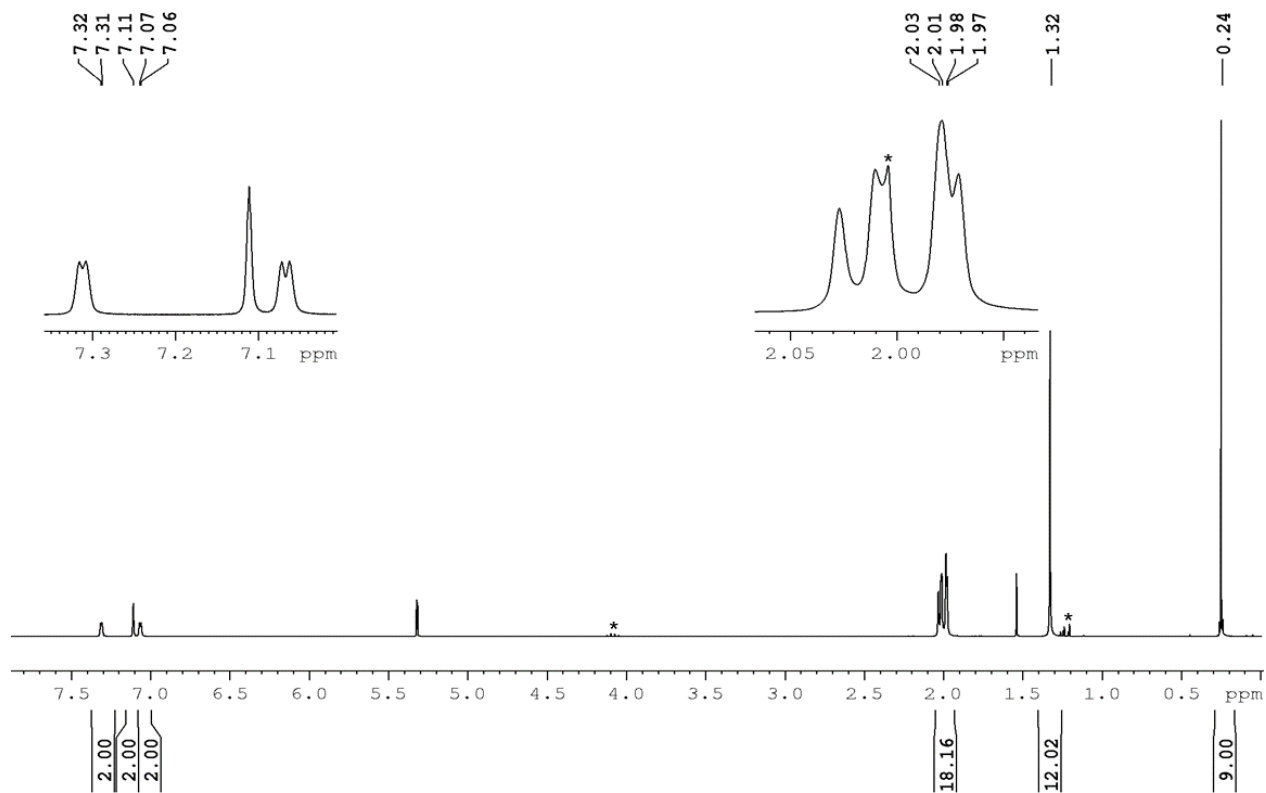
Figure S24. ^{1}H NMR spectrum of **BrSiBpin** in CD_2Cl_2 at 300 MHz. Residual solvent peaks (EtOAc) are marked with *.
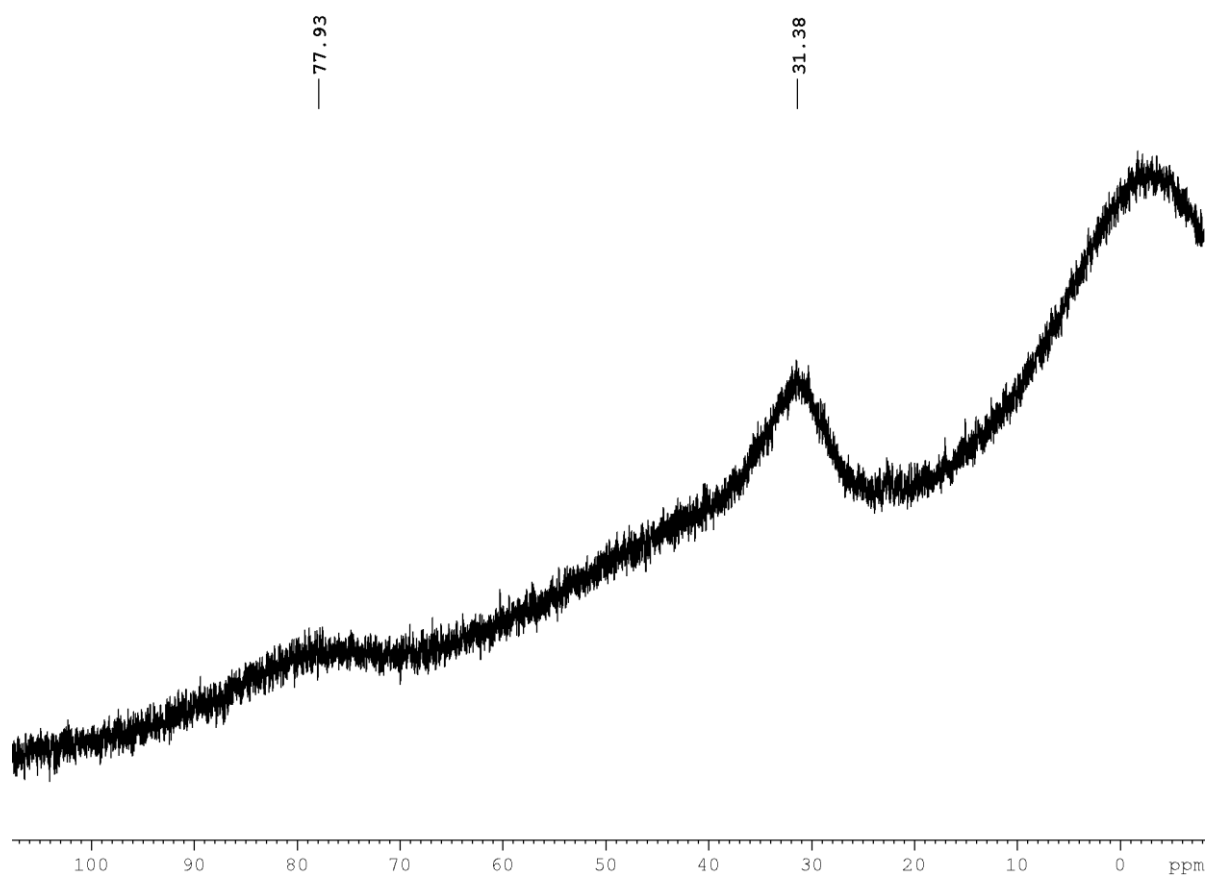
Figure S25. $^{11}B\{^1H\}$ NMR spectrum of **BrSiBpin** in CD_2Cl_2 at 96 MHz.
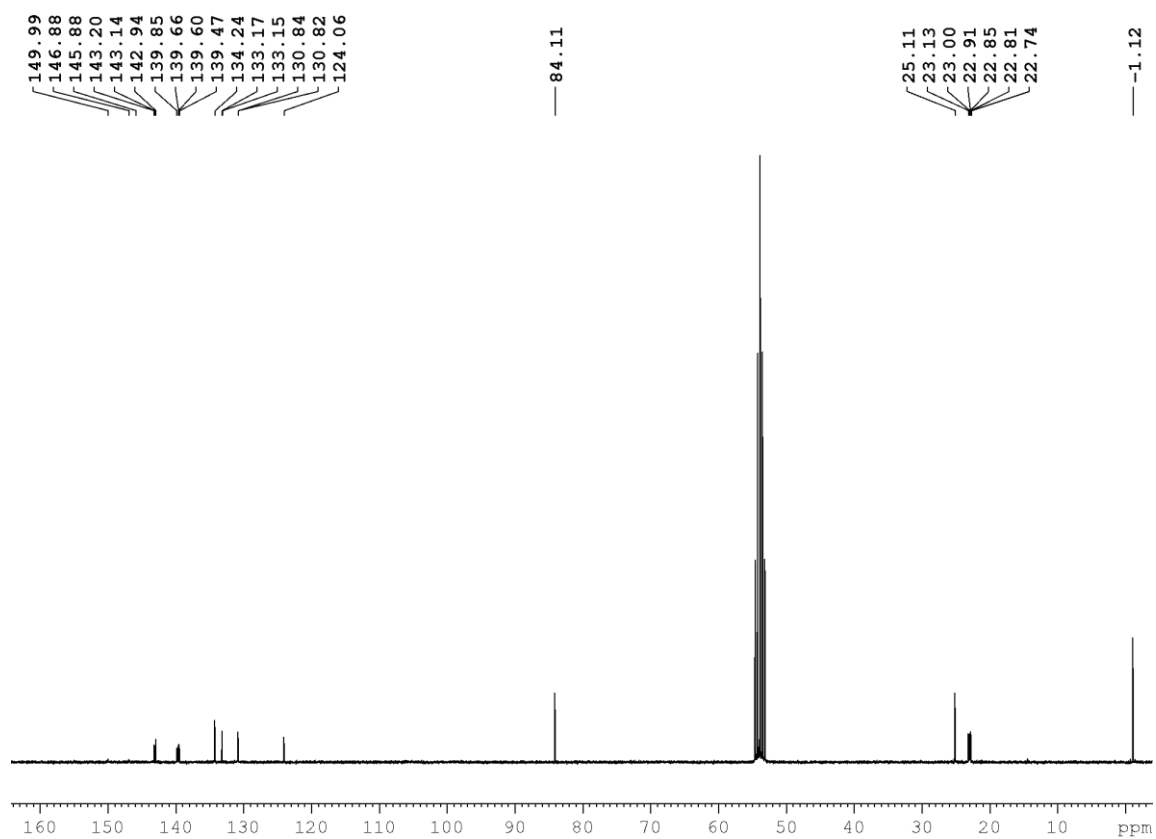
Figure S26. $^{13}C\{^1H\}$ NMR spectrum of **BrSiBpin** in CD_2Cl_2 at 75 MHz.
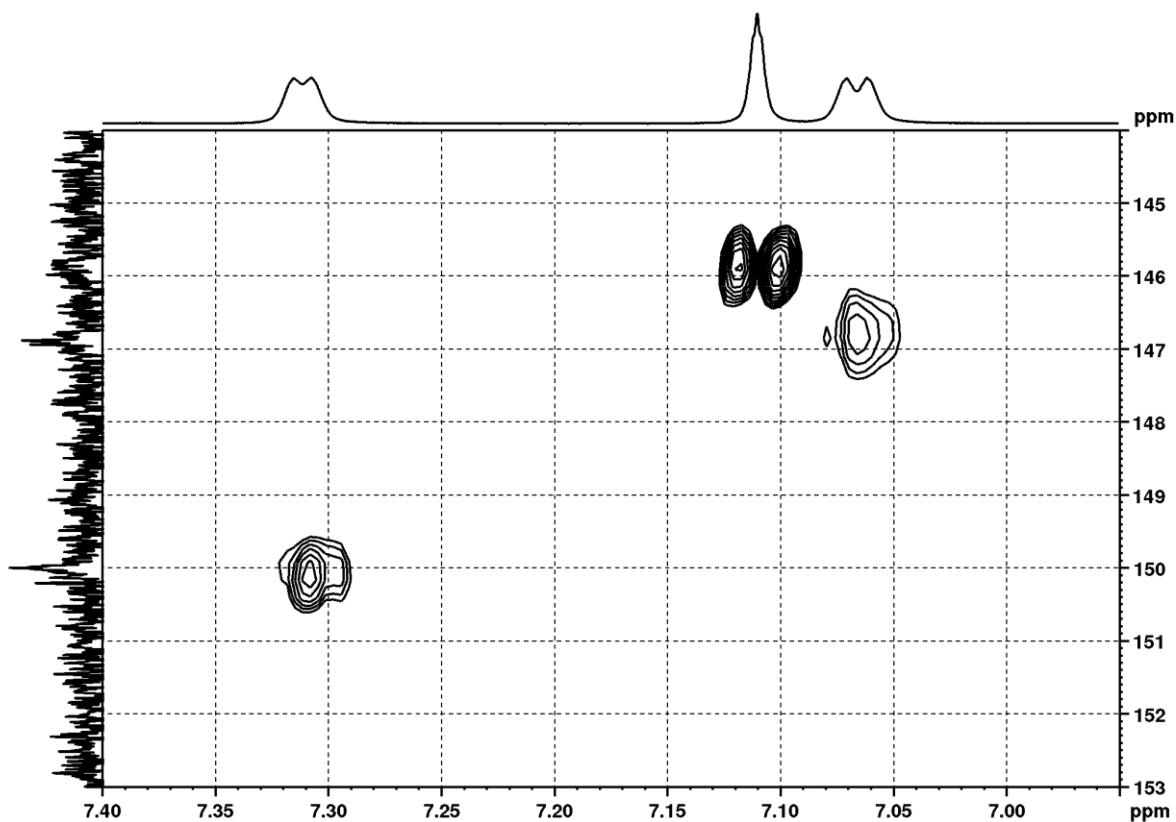
Figure S27. ^{1}H, ^{13}C HMBC NMR spectrum of **BrSiBpin** in CD_2Cl_2 at 500 MHz.
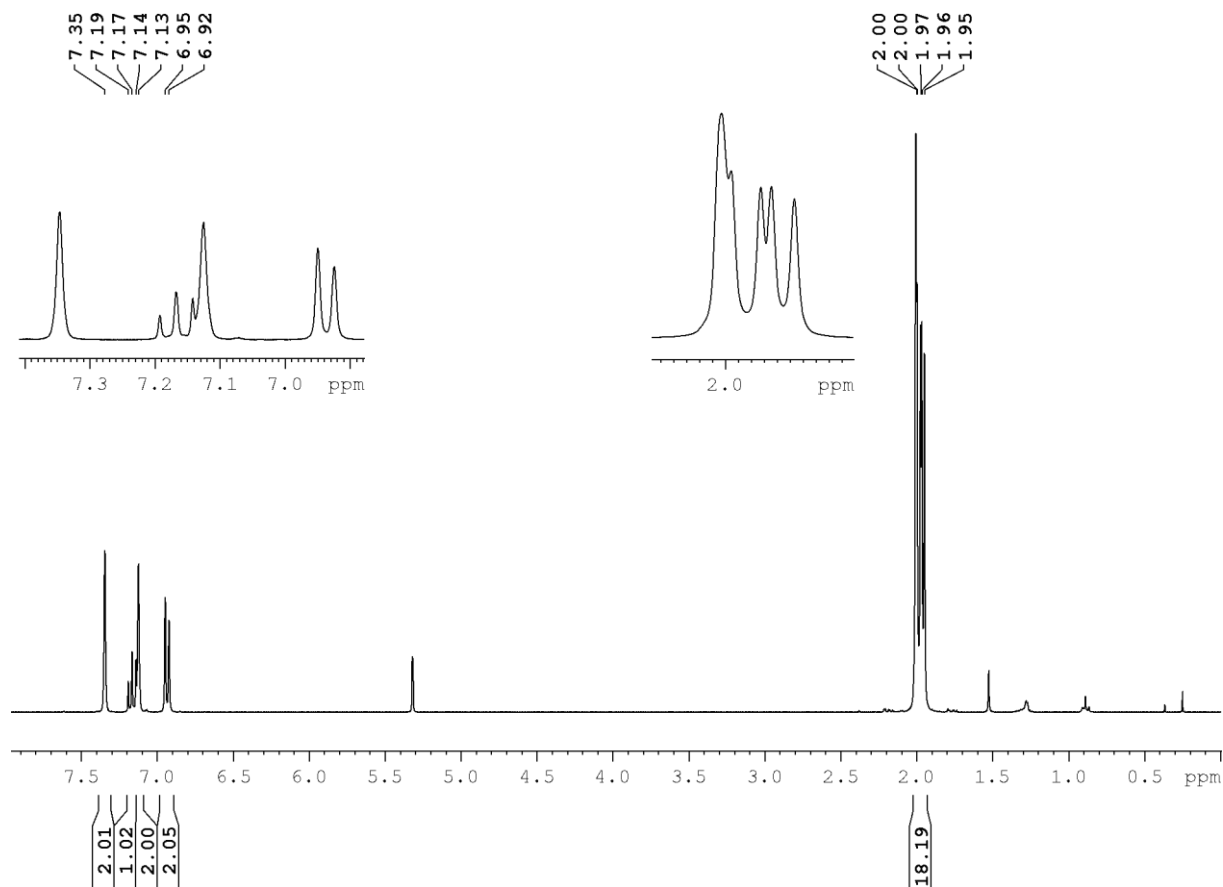
Figure S 28: ^{1}H NMR spectrum of **HBrI** in CD_2Cl_2 at 300 MHz.
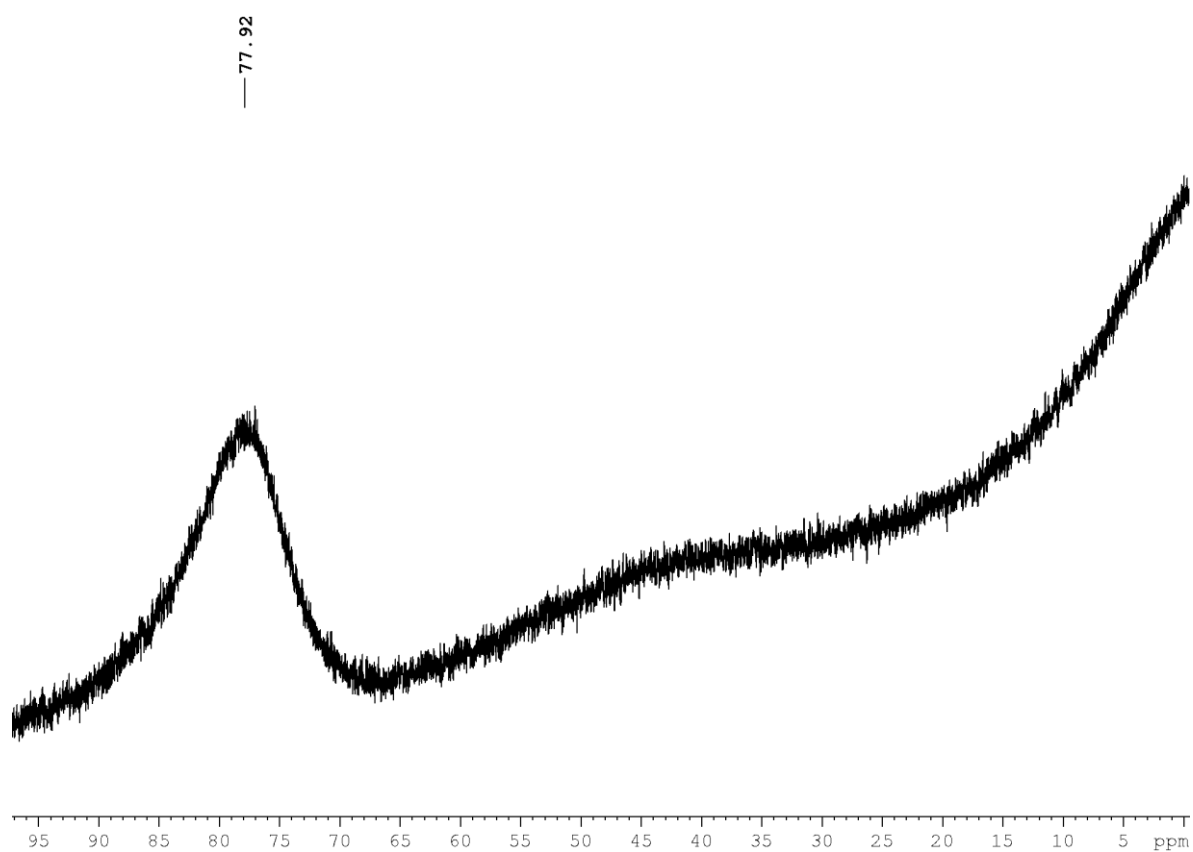
Figure S 29: $^{11}B\{^1H\}$ NMR spectrum of **HBrI** in CD_2Cl_2 at 96 MHz.
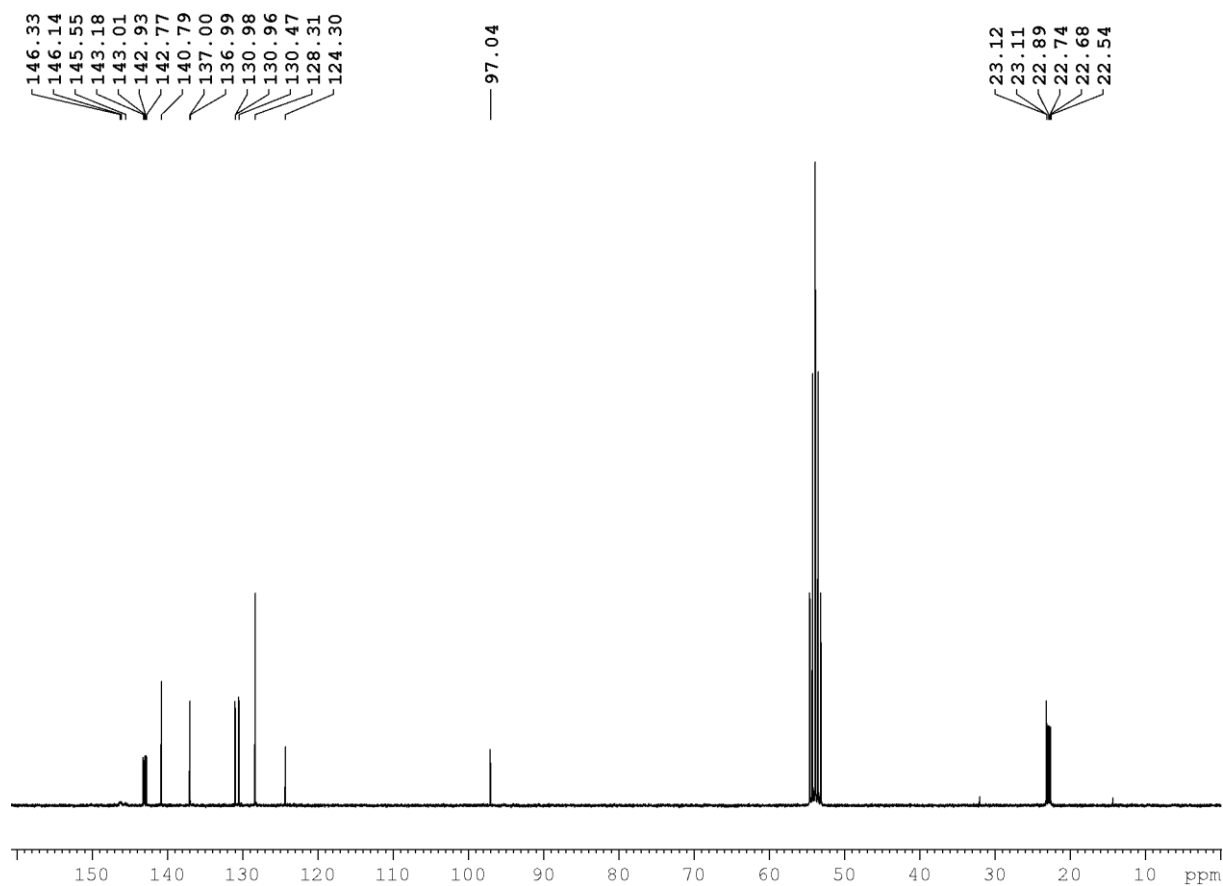
Figure S 30: $^{13}C\{^1H\}$ NMR spectrum of **HBrI** in CD_2Cl_2 at 75 MHz.
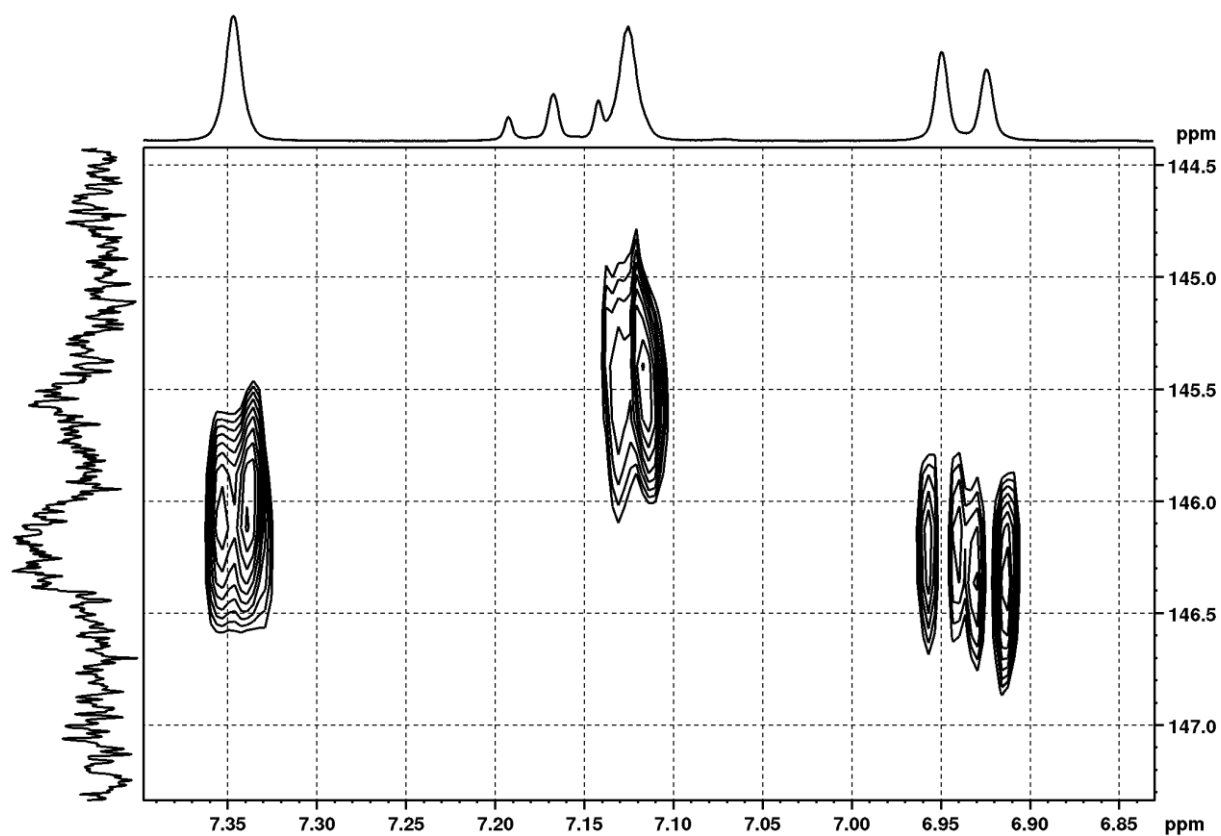
Figure S 31: ^{1}H, ^{13}C HMBC NMR spectrum of **HBrI** in CD$_2$Cl$_2$ at 300 MHz.
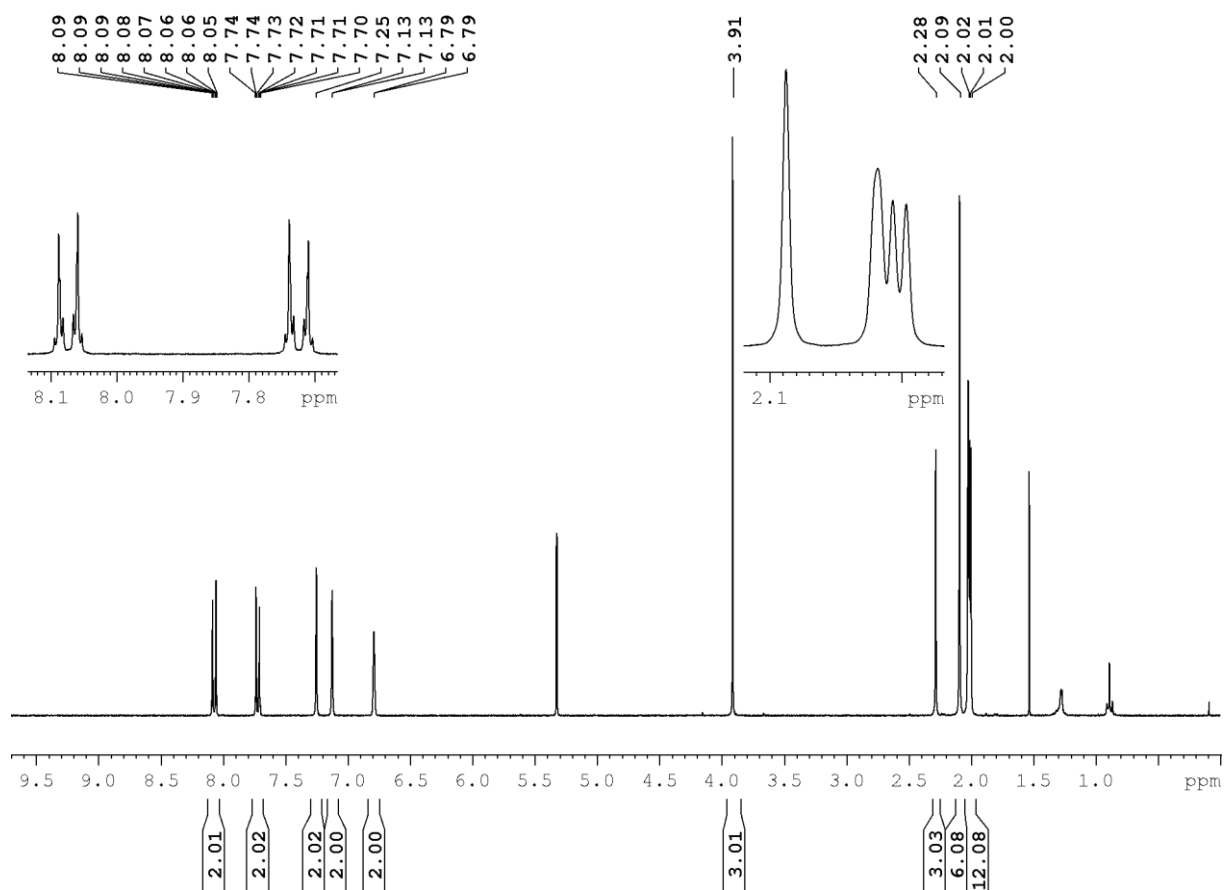
Figure S 32: ^{1}H NMR spectrum of **BrMe-Suzuki** in CD$_2$Cl$_2$ at 300 MHz.

—76.78

95 90 85 80 75 70 65 60 55 50 45 40 35 30 25 20 15 10 5 ppm
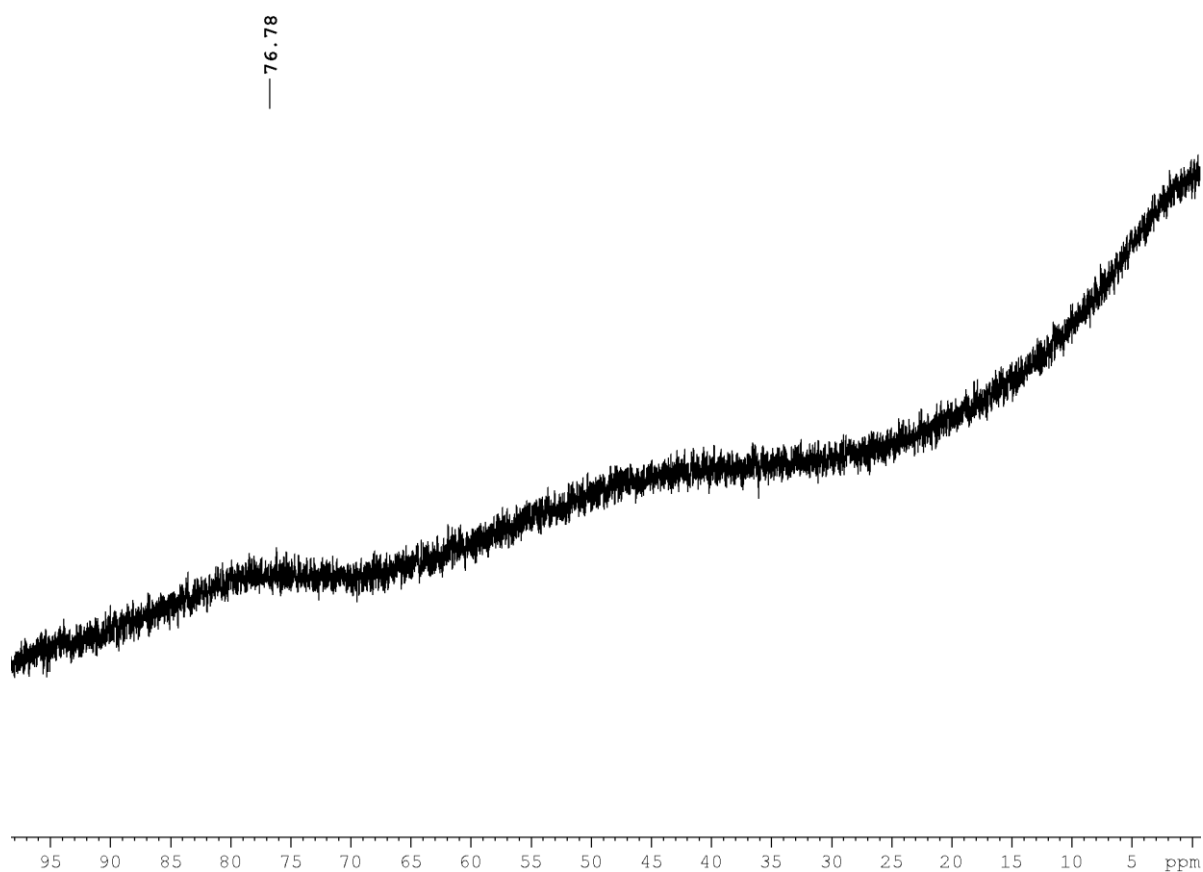
Figure S 33: $^{11}B\{^1H\}$ NMR spectrum of **BrMe-Suzuki** in CD_2Cl_2 at 96 MHz.

167.16
146.99
146.18
145.50
143.56
143.13
142.99
141.74
141.49
141.18
141.08
140.94
140.55
130.82
130.30
129.49
129.23
129.20
127.12
126.84
123.91

52.36

23.20
23.06
22.83
21.38

160 150 140 130 120 110 100 90 80 70 60 50 40 30 20 10 ppm
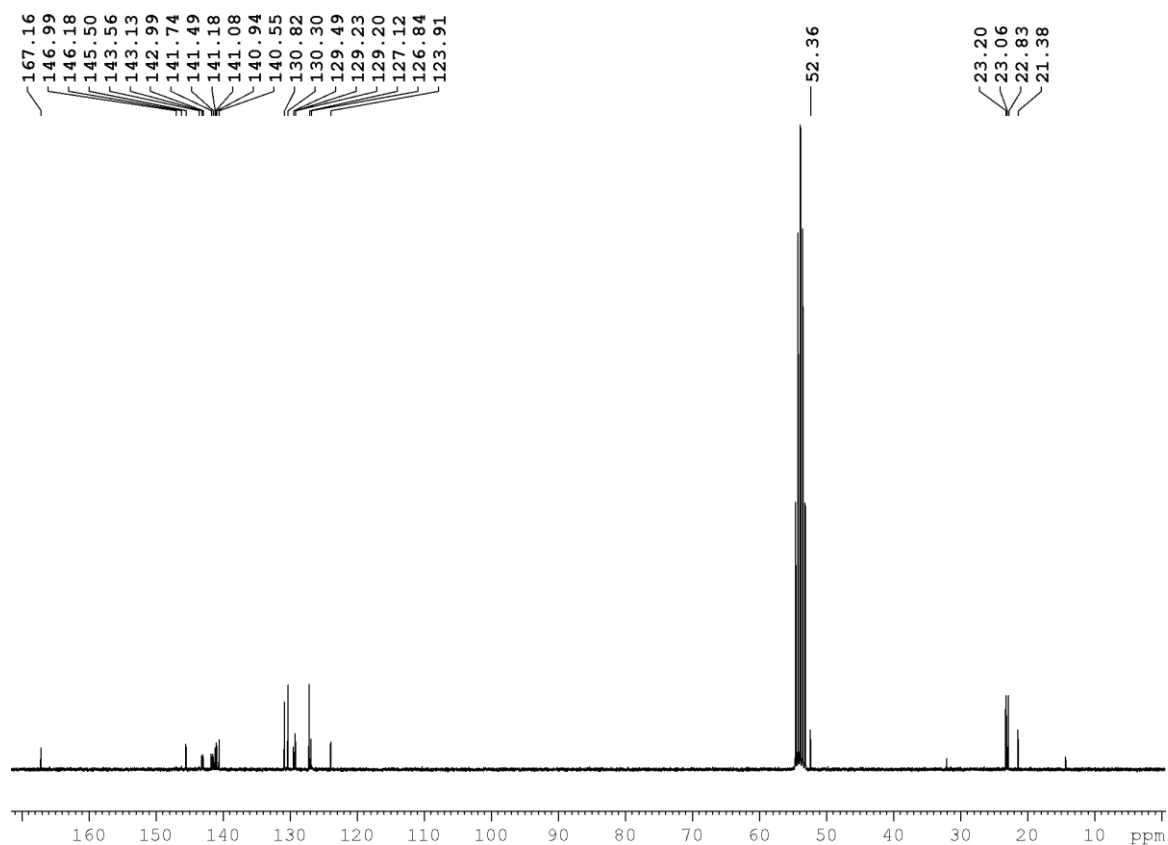
Figure S 34: $^{13}C\{^1H\}$ NMR spectrum of **BrMe-Suzuki** in CD_2Cl_2 at 75 MHz.
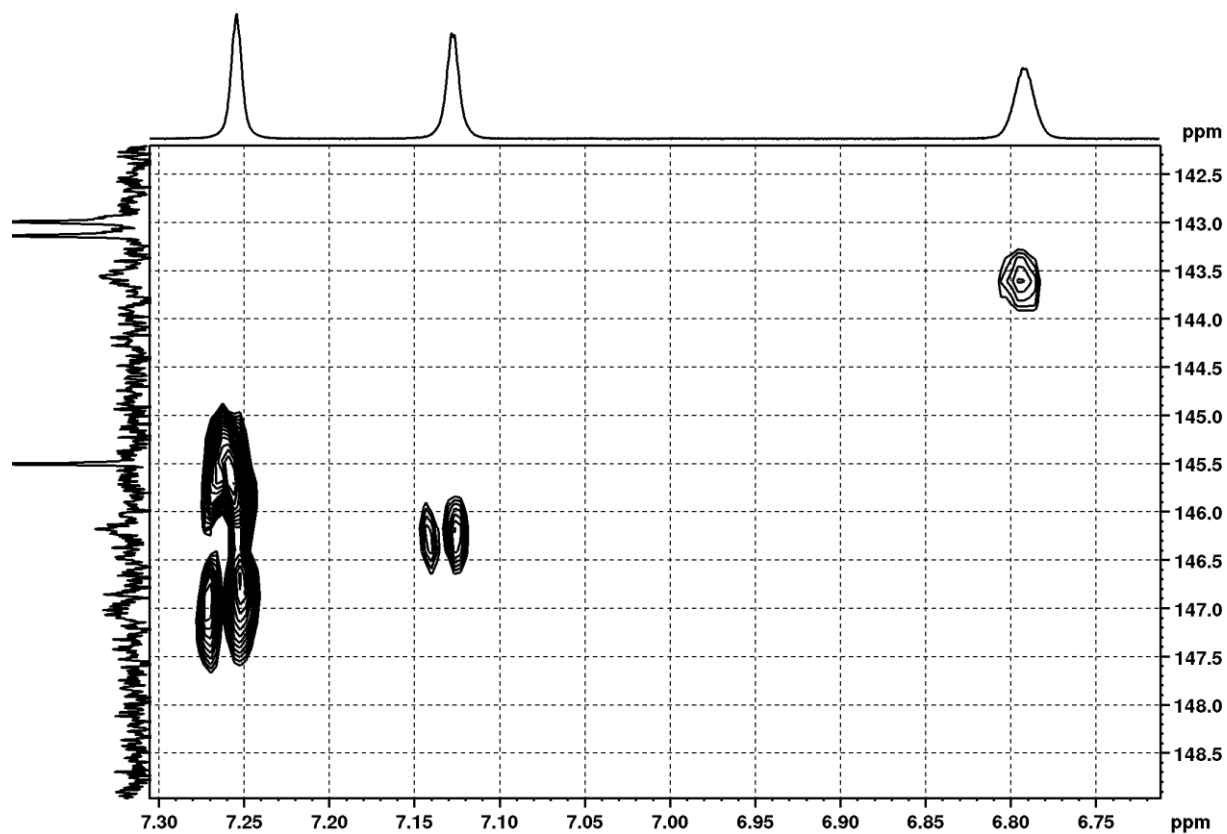
Figure S 35: ^{1}H, ^{13}C HMBC NMR spectrum of **BrMe-Suzuki** in CD_2Cl_2 at 300 MHz.

7.1.4   Single-Crystal X-Ray Diffraction

Table S1. Single-crystal X-ray diffraction data and structure refinements of **HBr$_2$** and **HBrSi**.

Data	HBr$_2$	HBrSi
CCDC number	2045568	2045569
Empirical formula	C$_{24}$H$_{25}$BBr$_2$	C$_{27}$H$_{34}$BBrSi
Formula weight (g·mol^{-1})	484.07	477.35
Temperature (K)	100(2)	100(2)
Radiation, λ (Å)	Mo-K$_\alpha$ 0.71073	Mo-K$_\alpha$ 0.71073
Crystal system	Monoclinic	Triclinic
Space group	*Cc*	*P* $\bar{1}$
Unit cell dimensions		
a (Å)	11.538(7)	8.307(5)
b (Å)	12.002(7)	12.676(6)
c (Å)	16.047(10)	13.537(7)
α (°)	90	106.688(15)
β (°)	107.553(17)	98.395(15)
γ (°)	90	107.363(14)
Volume (Å^3)	2119(2)	1260.7(12)
Z	4	2
Calculated density (Mg·m^{-3})	1.518	1.258
Abs. coefficient (mm^{-1})	3.832	1.689
F(000)	976	500
Theta range for collection	2.511 to 26.298°	2.618 to 28.386°
Reflections collected	31909	52032
Independent reflections	4298	6242
Minimum/maximum transmission	0.3396/0.4778	0.6240/ 0.7457
Refinement method	Full-matrix least-squares on F^2	Full-matrix least-squares on F^2
Data / parameters / restrains	4298 / 251 / 2	6242 / 280 / 0
Goodness-of-fit on F^2	1.023	1.057
Final R indices [I>2σ(I)]	R$_1$ = 0.0277, wR^2 = 0.0686	R$_1$ = 0.0319, wR^2 = 0.0818
R indices (all data)	R$_1$ = 0.0286, wR^2 = 0.0689	R$_1$ = 0.0401, wR^2 = 0.0854
Max./min. residual electron density (e·Å^{-3})	0.874 / –0.284	0.491 / –0.567
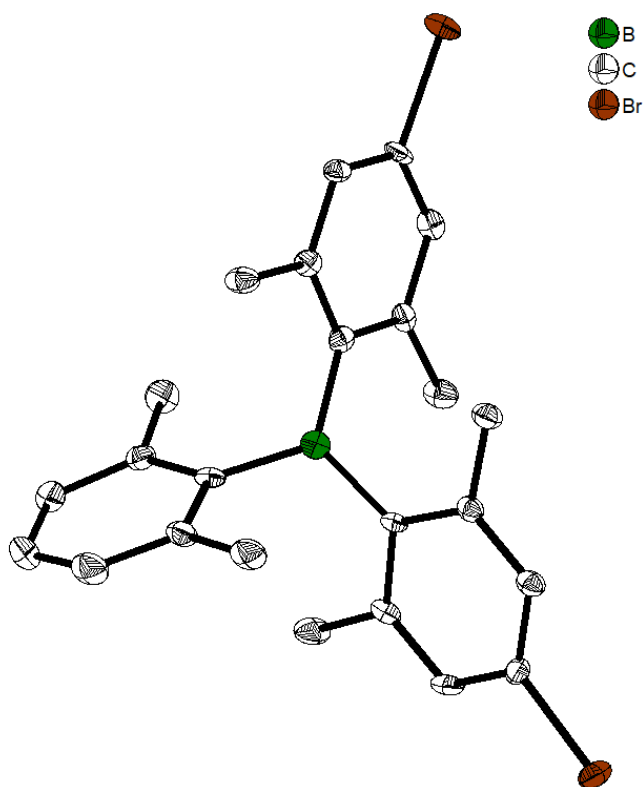
Figure S36. Molecular structure of **HBr₂** in the solid state at 100 K. Atomic displacement ellipsoids are drawn at the 50% probability level, and H atoms are omitted for clarity.
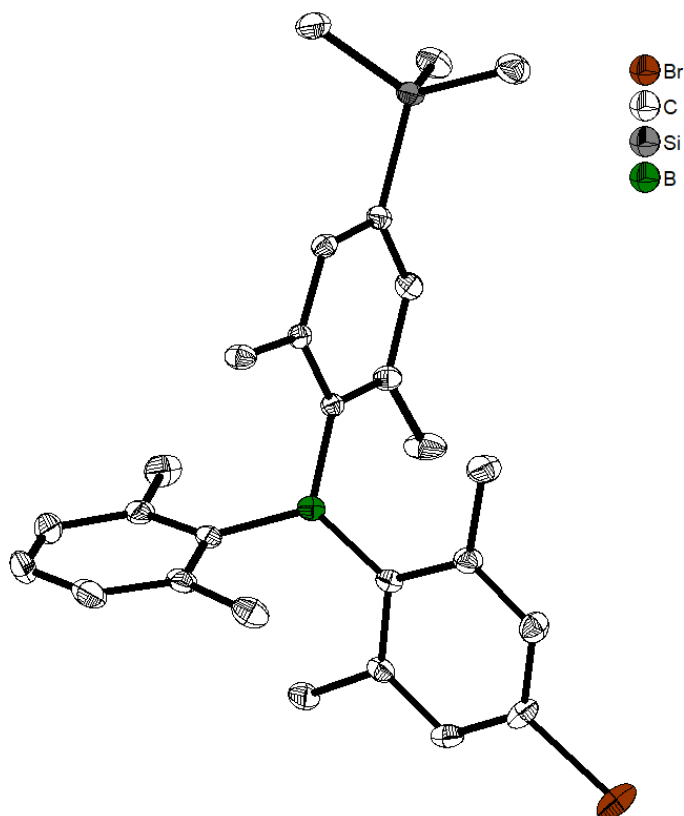
Figure S37. Molecular structure of **HBrSi** in the solid state at 100 K. Atomic displacement ellipsoids are drawn at the 50% probability level, and H atoms are omitted for clarity.

7.2 Chapter 3

7.2.1 General Information

Synthesis and Routine Characterization. Unless otherwise noted, the following conditions apply. Reactions were performed using standard Schlenk or glovebox (Innovative Technology Inc.) techniques under an atmosphere of argon. Only oven-dried glassware was used. Solvents used for reactions were HPLC grade, dried using an Innovative Technology Inc. Solvent Purification System, and further deoxygenated.

Compounds **Z'**,[9] **II**,[189] **VI**,[10] Bis[4-(*N*,*N*-dimethylamino)-2,6-dimethylphenyl]-(4-ethynyl-2,6-dimethylphenyl)borane,[189] 9,10-diiodoanthracene[384] and $Pd(PPh_3)_2Cl_2$[385] were synthesized according to literature procedures. All other starting materials were purchased from commercial sources and were used without further purification.

Reaction progress was monitored using thin layer chromatography (TLC) plates pre-coated with a layer of silica (Polygram® Sil G/UV254) with fluorescent indicator UV254 from Marchery-Nagel. Automated flash column chromatography was performed using a Biotage® Isolera Four system with silica gel (Biotage SNAP cartridge KP-Sil 50g or KP-Sil 100g obtained from Biotage) as the stationary phase and the solvent system indicated. Solvents were generally removed *in vacuo* using a rotary evaporator at a maximum temperature of 50 °C.

^1H and $^{13}C\{^1H\}$ solution NMR spectroscopic data were obtained at ambient temperature using a Bruker Avance 300 III (operating at 300 MHz for ^1H and 75 MHz for $^{13}C\{^1H\}$), or a Bruker Avance 500 NMR spectrometer (operating at 500 MHz for ^1H, 125 MHz for $^{13}C\{^1H\}$). Chemical shifts (δ) were referenced to solvent peaks as follows. ^1H NMR spectra were referenced via residual proton resonances of CD_2Cl_2 (5.32 ppm) and CD_3OD (3.31 ppm). ^{13}C spectra were referenced to CD_2Cl_2 (53.84 ppm) and CD_3OD (49.00 ppm).

Elemental analyses were performed on an Elementar vario MICRO cube elemental analyser. As is common for related organo-B(Aryl)$_2$ compounds, carbon analyses of **III**, **IV** and **V** were up to 2.3% below the calculated value, while hydrogen, nitrogen and sulphur analyses were satisfactory. This has been ascribed previously to the formation of boron carbide.[386] High resolution mass spectrometry (HRMS) was performed with a Thermo Fisher Scientific Exactive Plus Orbitrap MS System. ESI measurements were performed with a HESI source at 50 °C. APCI measurements were performed with an ACPI source and Corona needle at 400 °C, unless otherwise noted.

Single-Crystal X-Ray Diffraction. Crystals suitable for single-crystal X-ray diffraction were selected, coated in perfluoropolyether oil, and mounted on MiTeGen sample holders. Diffraction data of **IIIN** and **IVN** were collected on a Bruker X8-APEX II diffractometer with a

CCD area detector and multi-layer mirror monochromated Mo-K$_\alpha$ radiation. Diffraction data of **C** were collected on a RIGAKU OXFORD DIFFRACTION XtaLAB Synergy diffractometer with a semiconductor HPA-detector (HyPix-6000) and multi-layer mirror monochromated Cu-K$_\alpha$ radiation. The crystals were cooled using an Oxford Cryostream or Bruker Kryoflex low-temperature device. Data were collected at 100 K (**IIIN**, **IVN**) or 120 K (**C**). The images were processed and corrected for Lorentz-polarization effects and absorption as implemented in the Bruker software packages (**IIIN**, **IVN**) or in the CrysAlis[Pro] software (**C**), respectively. The structures were solved using the intrinsic phasing method (SHELXT)[382] and Fourier expansion technique. All non-hydrogen atoms were refined in anisotropic approximation, with hydrogen atoms 'riding' in idealized positions, by full-matrix least squares against F^2 of all data, using SHELXL[383] software and the SHELXLE graphical user interface.[387] For both, **IIIN** and **IVN**, each asymmetric unit contains one ethylacetate molecule disordered over three positions, while for **C** it contains two hexane molecules disordered over two positions each in addition to the main molecules. Diamond[388] software was used for graphical representation. Crystal data and experimental details are listed in **Table S2**; full structural information has been deposited with Cambridge Crystallographic Data Centre. CCDC-1997113 (**IIIN**), 1997114 (**IVN**), and 1997115 (**C**).

Linear Optical Properties. All measurements were performed in standard quartz cuvettes (1 cm x 1 cm cross-section) under ambient conditions. UV-visible absorption spectra were recorded using an Agilent 8453 diode array UV-visible spectrophotometer. The molar extinction coefficients were calculated from three independently prepared samples in hexane (**IIIN**-**VN**) and MeCN and H_2O (**III**-**V**) solution. The emission spectra were recorded using an Edinburgh Instruments FLSP920 spectrometer equipped with a double monochromator for both excitation and emission, operating in right-angle geometry mode, and all spectra were fully corrected for the spectral response of the instrument. All solutions used in photophysical measurements had a concentration lower than 5×10^{-6} M to minimize inner filter effects during fluorescence measurements. The **fluorescence quantum yields** were measured using a calibrated integrating sphere (inner diameter: 150 mm) from Edinburgh Instruments combined with the FLSP920 spectrometer described above. For solution-state measurements, the longest-wavelength absorption maximum of the compound in the respective solvent was chosen as the excitation wavelength, unless stated otherwise. **Fluorescence lifetimes** were recorded using the time-correlated single-photon counting (TCSPC) method using an Edinburgh Instruments FLS980 spectrometer equipped with a high speed photomultiplier tube positioned after a single emission monochromator. Measurements were made in right-angle geometry mode, and the emission was collected through a polarizer set to the magic angle. Solutions were excited with a pulsed diode laser at a wavelength of 376.6 nm (**IIIN**, **IVN**, **III**, **IV**) and 472.6 nm (**VN**, **V**) at repetition rates of 10 or 20 MHz, as appropriate. The full-width-at-

half-maximum (FWHM) of the pulse from the diode laser was ca. 80 ps with an instrument response function (IRF) of ca. 230 ps FWHM and ca. 200 ps with an instrument response function (IRF) of ca. 1120 ps FWHM, respectively. The IRFs were measured from the scatter of an aqueous suspension of Ludox at the excitation wavelength. Decays were recorded to 10 000 counts in the peak channel with a record length of 8 192 channels. The band pass of the emission monochromator and a variable neutral density filter on the excitation side were adjusted to give a signal count rate of <60 kHz. Iterative reconvolution of the IRF with one decay function and non-linear least-squares analysis were used to analyse the data. The quality of all decay fits was judged to be satisfactory, based on the calculated values of the reduced χ^2 and Durbin-Watson parameters and visual inspection of the weighted residuals.

Optical Properties in Sodium Cacodylate. UV-visible absorption spectra were recorded on a Varian Cary 100 Bio spectrometer; excitation and emission spectra were recorded on a Varian Cary Eclipse fluorimeter

Study of Interactions with DNA and RNA. Polynucleotides were purchased as noted: poly dGdC – poly dGdC, poly dAdT – poly dAdT, poly A – poly U, poly A, poly G, poly C, poly U (Sigma), *calf thymus* (ct)-DNA (Aldrich) and dissolved in sodium cacodylate buffer, I = 0.05 M, pH=7.0. The ct-DNA was additionally sonicated and filtered through a 0.45 mm filter to obtain mostly short (ca. 100 base pairs) rod-like B-helical DNA fragments.[389] The polynucleotide concentration was determined spectroscopically[390] as the concentration of phosphates (corresponds to c(nucleobase)). **Thermal melting experiments** were performed on a Varian Cary 100 Bio spectrometer in quartz cuvettes (1 cm). The measurements were carried out in aqueous buffer solution at pH 7.0 (sodium cacodylate buffer I = 0.05 M). Thermal melting curves for ds-DNA, ds-RNA and their complexes with **III**-**VI** were determined by following the absorption change at 260 nm as a function of temperature.[307] *Tm* values are the midpoints of the transition curves determined from the maximum of the first derivative and checked graphically by the tangent method. The Δ*Tm* values were calculated subtracting *Tm* of the free nucleic acid from *Tm* of the complex. Every Δ*Tm* value reported here was the average of at least two measurements. The error in Δ*Tm* is ± 0.5 °C. **Fluorimetric titrations** were performed by adding portions of polynucleotide solution into the solution of the compound studied and excitation wavelengths of λ_{exc} > 300 nm were used to avoid absorption of excitation light by added polynucleotides. After mixing polynucleotides with the compound, equilibrium was reached in less than 120 s. Fluorescence spectra were analyzed at an excess of DNA/RNA ($r_{[compd]/[DNA]}$ <0.2) to assure one dominant binding mode. To obtain binding constants (*Ks*), titration data were processed by means of non-linear fitting to the Scatchard equation (McGhee, von Hippel formalism),[308, 309] which gave values of the ratio of [bound com-pound] / [polynucleotide] in the range 0.1–0.3, but for easier comparison, all *Ks* values were re-calculated for the fixed n = 0.25 (for ds-DNA/RNA) or 0.5 (for ss-RNA). Calculated values for

Ks have satisfactory correlation coefficients (>0.99). For fluorimetric titrations fluorescence spectra were recorded on Varian Cary Eclipse fluorimeter in quartz cuvettes (1 cm) by adding portions of polynucleotide solution into the solution of the studied compound. **Circular dichroism (CD)** spectra were recorded on a JASCO J-815 spectropolarimeter at room temperature using appropriate 1 cm path quartz cuvettes with scanning speed of 200 nm/min. A background spectrum of the buffer was subtracted from each spectrum and each spectrum was the result of three accumulations. CD experiments were performed by adding portions of a stock solution of the compound into the solution of polynucleotide ($c = 2\times10^{-5}$ M).

Molecular Modelling. Compound **V** was optimized using Gaussian, version g09-D0.1 software, at the B3LYP/6-31G(d) level of theory, and the parametrization procedure was performed using the Antechamber module within the AMBER16 program suite wherein the Mullikan charges were used as the partial atomic charges. Parametrization, energy minimization, and molecular dynamics (MD) simulations of the complexes between compound **V** and DNA were performed using the AMBER16 suite of programs.[391] The solutes were prepared using the AMBER16 utility program tLeap wherein ligand and DNA were parametrized within general AMBER force field gaff[392] and ff99bsc0[393] force fields, respectively. For details of the parametrization procedure see previous work by Marder, Piantanida and co-workers.[13] Initial conformations were prepared in PyMOL (The PyMOL Molecular Graphics System, Version 1.7 SchroÈdinger, LLC), wherein compound **V** was docked into the DNA minor groove using DNA-**Z'** complex[13] as a template. The systems were solvated in the truncated octahedron box filled with TIP3P water molecules[394, 395] whereas the sodium ions were added to achieve electroneutrality. The complexes were minimized, equilibrated and simulated for 300 ns by the programs sander.MPI and pmemd.MPI. The simulations were performed using periodic boundary conditions (PBC). The particle mesh Ewald (PME) method was used for calculation of the long-range electrostatic interactions, and in the direct space the pairwise interactions were calculated within the cut-off distance of 8 Å. The solvated complexes were geometry optimized by using steepest descent and conjugate gradient methods (altogether 7000 steps), and equilibrated for 100 ps with time step of 1 fs. During the first stage of equilibration (30 ps), the temperature was linearly increased from 0 to 300 K and the volume was held constant. In the second stage (NPT ensemble with T and P about 300 K and 1 atm, respectively) the solution density was optimized. The equilibrated complexes were subjected to productive molecular dynamics simulation using NPT conditions and a time step of 2 fs. The temperature was held constant using a Langevin thermostat[396] with a collision frequency of 0.2 ps, and the pressure was regulated by a Berendsen barostat.[397]

Raman and SERS measurements. Raman and SERS spectra were measured on a Bruker Equinox 55 interferometer equipped with a FRA 106/S Raman module using Nd-YAG laser

excitation at 1064 nm of 500 mW laser power. The spectra were acquired in the 3500–100 cm^{-1} spectral range at 4 cm^{-1} resolution. A total of 512 and 128 scans were averaged for a Raman and SERS spectrum, respectively. Quartz cuvettes were used for handling samples. Solutions of the bis-triarylborane compounds were prepared by dissolution of the solid substance in water, the concentration of which was determined spectroscopically using the respective molar absorption coefficient. The stock solutions were further on diluted in water to obtain solutions of 1×10^{-4} M (**III**, **IV** and **V**) and 2×10^{-3} M (**VI**), used for Raman measurements. For the SERS measurement a silver colloidal suspension was used as the SERS active substrate, prepared by reduction of silver nitrate with trisodium citrate according to the procedure described in previous work by Marder, Piantanida and co-workers.[189] The resulting colloidal suspension was gray colored, characterized by a maximum at 416 nm in the UV/Vis spectrum, pointing to the typical silver plasmon resonance frequency. The pH value of the silver colloid was 7.5. Working samples for the SERS measurements were prepared by dissolution of bis-triarylborane compound solution in an appropriate volume of water, followed by addition of 400 μL of the silver colloid. The total sample volume was 500 μL. For the concentration dependent measurements the final concentrations of **III**-**VI** in the Ag colloid were 1×10^{-7}, 5×10^{-7}, 1×10^{-6} and 5×10^{-6} M. To measure the SERS spectra of the complexes of **III**-**V** with ct-DNA, samples were prepared in the buffered solution by mixing the appropriate volume of the bis-triarylborane compound with ct-DNA in molar ratios $r_{[compound]/[ct-DNA]}$ = 1, 0.2 and 0.1, followed by addition of the of 400 μL silver colloid. The total volume of the working sample was 500 μL and the final concentration of the bis-triarylborane compound was 1×10^{-6} M.

Theoretical Studies. All calculations (DFT and TD-DFT) were carried out with the Gaussian 16 (16.A.03)[398] program package and were performed on a parallel cluster system. GaussView (6.0.16), Avogadro (1.2.0)[399] and multiwfn[400] were used to visualize the results, to measure calculated structural parameters, and to plot orbital surfaces (isovalue: $\pm$ 0.030 [e $a_0^{-3}]^{1/2}$). The ground-state geometries were optimized using the B3LYP functional[401] in combination with the 6-31G(d) basis set.[402, 403] The ultrafine integration grid and no symmetry constraints were used for all molecules. Frequency calculations were performed on the optimized structures to confirm them to be local minima showing no negative (imaginary) frequencies. Based on these optimized structures, the lowest-energy vertical transitions (gas-phase) were calculated (singlets, 25 states) by TD-DFT, using the CAM-B3LYP functional in combination with the 6-31G(d) basis set.[402, 403] For calculations of the Raman spectra the ground state geometries were optimized at the B3LYP/6-31+G(d, p) level of theory. The resulting frequencies were multiplied by a scaling factor of 0.964 (as suggested by the Computational Chemistry Comparison and Benchmark database (https://cccbdb.nist.gov/vibscalejustx.asp)).

7.2.2 Synthesis

5,5'-Bis[4-(bis(4-(*N*,*N*-dimethylamino)-2,6-dimethylphenyl)boryl)-3,5-dimethyl-phenylethynyl]-2,2' bithiophene (IIIN)
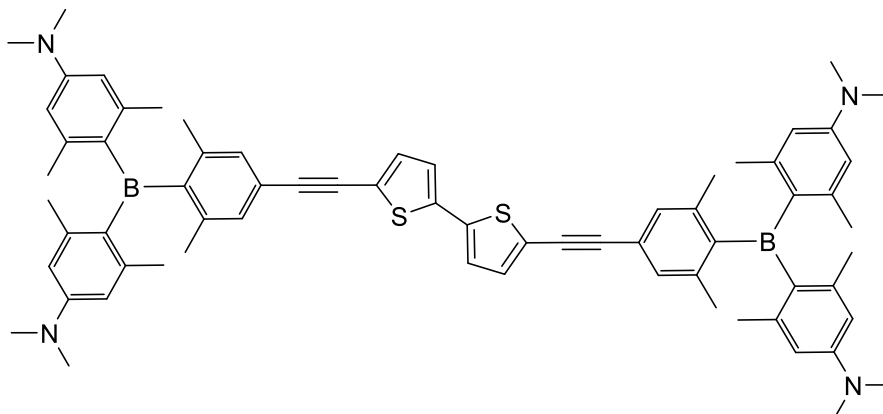
Bis[4-(*N*,*N*-dimethylamino)-2,6-dimethylphenyl]-(4-ethynyl-2,6-dimethylphenyl)borane (500 mg, 1.15 mmol, 2.1 eq), 5,5'-dibromo-2,2'-bithiophene (178 mg, 0.55 mmol, 1 eq), Pd(PPh$_3$)$_2$Cl$_2$ (8 mg, 11 μmol, 2 mol%) and CuI (2 mg, 11 μmol, 2 mol%) were dissolved in THF (10 mL) and NEt$_3$ (5 mL) was added. The reaction mixture was stirred at r.t. for 19 h, until the starting materials were consumed according to TLC (1% NEt$_3$ in hexane : EtOAc 4:1). After removing the solvent, the solid was purified by automated flash column chromatography (Biotage SNAP cartridge KP-Sil 50 g; 1% NEt$_3$ additive to 5% EtOAc in hexane). The solid was dissolved in CH$_2$Cl$_2$ and precipitated with MeOH to yield compound **IIIN** as a yellow solid (165 mg, 29%).

^{1}H NMR (300 MHz, CD$_2$Cl$_2$): δ = 7.17 (d, J = 4 Hz, 2H), 7.11 (d, J = 4 Hz, 2H), 7.07 (m, 4H), 6.31 (s, 8H), 2.95 (s, 24H), 2.03 (s, 12H), 2.00 (s, 12H), 1.93 (s, 12H) ppm.

^{13}C{^{1}H} NMR (75 MHz, CD$_2$Cl$_2$): δ = 151.8, 151.4, 143.4, 142.9, 140.8, 138.2, 135.8, 133.1, 130.2, 124.5, 123.3, 122.2, 111.9, 111.9, 95.9, 82.3, 40.1, 24.1, 23.8, 22.8 ppm.

HRMS (APCI) m/z: [M+H]$^+$ found: 1035.5758; calc. for [C$_{68}$H$_{77}$B$_2$N$_4$S$_2$]$^+$: 1035.5770 (|Δ| = 1.16 ppm).

Elemental analysis Calc. (%) for C$_{68}$H$_{76}$B$_2$N$_4$S$_2$: C 78.90, H 7.40, N 5.41, S 6.19; found: C 78.57, H 7.51, N 5.34, S 6.05.

5,5'-Bis[4-(*bis*(4-(*N,N,N*-trimethylammonium)-2,6-dimethylphenyl)boryl)-3,5-dimethyl-phenylethynyl]-2,2'-bithiophene tetratriflate (III)
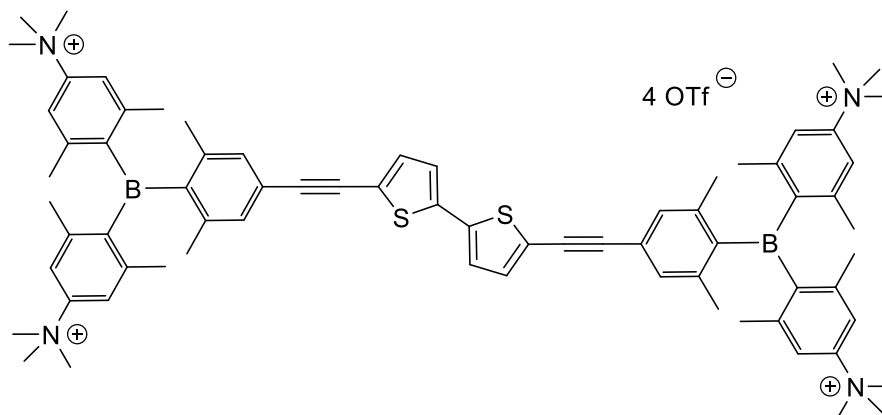
Compound **IIIN** (15.5 mg, 15.0 *µ*mol, 1 eq) was dissolved in CH$_2$Cl$_2$ (2 mL). Methyl triflate (7.63 *µ*L, 67.4 *µ*mol, 4.5 eq) was added and the reaction was stirred at r.t. for 42 h. The precipitate was collected by filtration and washed with CH$_2$Cl$_2$ (3 x 5 mL) to afford compound **III** as a yellow solid (22 mg, 88%).

¹H NMR (500 MHz, CD$_3$OD): δ = 7.58 (m, 8H), 7.27 (d, J = 4 Hz, 2H), 7.25 (d, J = 4 Hz, 2H), 7.19 (m, 4H), 3.66 (s, 36H), 2.22 (s, 12H), 2.16 (s, 12H), 2.04 (s, 12H) ppm.

¹³C{¹H} NMR (125 MHz, CD$_3$OD): δ = 149.8, 149.0, 145.0, 144.6,142.4, 139.5, 134.7, 131.8, 126.6, 125.8, 123.6, 121.8 (q, J = 318 Hz), 121.4, 120.3, 120.2, 95.4, 84.5, 57.5, 23.5, 23.5, 23.2 ppm.

HRMS (ESI pos) m/z: [M-2OTf]$^{2+}$ found: 696.2839; calc. for [C$_{74}$H$_{88}$B$_4$N$_4$S$_2$F$_6$O$_6$]$^{2+}$: 696.2833 (|Δ| = 0.86 ppm).

Elemental analysis Calc. (%) for C$_{76}$H$_{88}$B$_2$F$_{12}$N$_4$O$_{12}$S$_6$: C 53.97, H 5.24, N 3.31, S 11.37; found: C 51.70, H 5.47, N 3.08, S 10.62.

1,4-Bis[4-(*bis*(4-(*N,N*-dimethylamino)-2,6-dimethylphenyl)boryl)-3,5-dimethyl-phenylethynyl]-benzene (IVN)
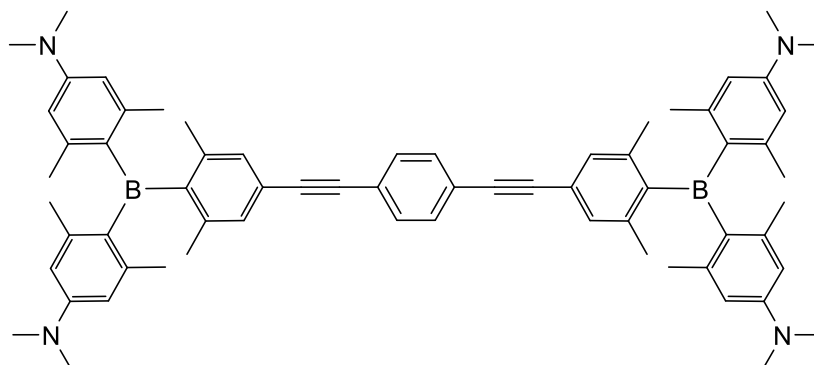
Bis[4-(*N,N*-dimethylamino)-2,6-dimethylphenyl]-(4-ethynyl-2,6-dimethylphenyl)borane (500 mg, 1.15 mmol, 2.2 eq), 1,4-diiodobenzene (172 mg, 0.52 mmol, 1 eq), Pd(PPh$_3$)$_2$Cl$_2$ (7.2 mg, 11 μmol, 2 mol%) and CuI (2 mg, 11 μmol, 2 mol%) were dissolved in THF (10 mL) and NEt$_3$ (5 mL) was added. The reaction mixture was stirred at r.t. for 20 h, until the starting materials were consumed according to TLC (10% EtOAc in hexane). After removing the solvent, the solid was purified by automated flash column chromatography (Biotage SNAP cartridge KP-Sil 50 g; 5% EtOAc in hexane). The solid was dissolved in EtOAc and precipitated with MeOH and then recrystallized from EtOAc to yield compound **IVN** as a yellow solid (234 mg, 48%).

^{1}H NMR (300 MHz, CD$_2$Cl$_2$): δ = 7.49 (s, 4H), 7.09 (s, 4H), 6.31 (s, 8H), 2.95 (s, 24H), 2.03 (s, 12 H), 2.00 (s, 12H),1.93 (s, 12H) ppm.

^{13}C{^{1}H} NMR (75 MHz, CD$_2$Cl$_2$): δ = 151.8, 151.2, 143.4, 142.9, 140.7, 135.8, 131.9, 130.5, 123.6, 122.6, 111.9, 111.9, 92.5, 89.0, 40.1, 24.1, 23.8, 22.8 ppm.

HRMS (APCI) m/z: found [M+H]$^+$: 947.6336; calc. for [C$_{66}$H$_{77}$B$_2$N$_4$]$^+$: 947.6329 (|Δ| = 0.74 ppm).

Elemental analysis Calc. for C$_{66}$H$_{76}$B$_2$N$_4$: C 83.71, H 8.09, N 5.92; found: C 83.52, H 8.24, N 5.91.

1,4-Bis[4-(*bis*(4-(*N,N,N*-trimethylammonium*)*-2,6-dimethylphenyl)boryl)-3,5-dimethyl-phenylethynyl]-benzene tetratriflate (IV)
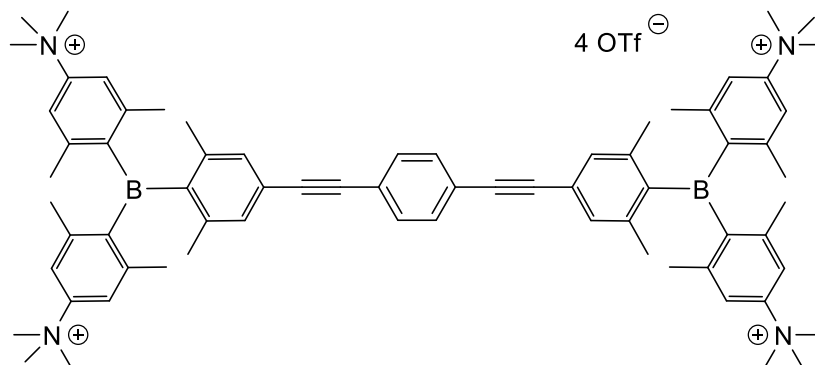
Compound **IVN** (15.0 mg, 15.8 μmol, 1 eq) was dissolved in CH_2Cl_2 (2 mL). Methyl triflate (8.96 μL, 79.2 μmol, 5.0 eq) was added and the reaction was stirred at r.t. for 48 h. The precipitate was collected by filtration and washed with CH_2Cl_2 (3 x 5 mL) to afford compound **IV** as a colorless solid (21 mg, 84%).

^{1}H NMR (500 MHz, CD_3OD): δ = 7.58 (m, 8H), 7.54 (s, 4H), 7.22 (m, 4H), 3.66 (s, 36H), 2.22 (s, 12H) 2.16 (s, 12H), 2.05 (s, 12H) ppm.

^{13}C{^{1}H} NMR (75 MHz, CD_3OD): δ = 149.8, 149.1, 146.9, 144.9, 144.6, 142.3, 132.8, 132.1, 126.9, 124.5, 121.8 (q, J = 318 Hz), 120.2, 92.1, 91.1, 57.5, 23.5, 23.5, 23.2 ppm.

HRMS (ESI pos) m/z: [M-2OTf]$^{2+}$ found: 652.3112; calc. for [$C_{74}H_{88}B_4N_4S_2F_6O_6$]$^{2+}$: 652.3112 (|$\Delta$| = 0 ppm).

Elemental analysis Calc. (%) for $C_{74}H_{88}B_2F_{12}N_4O_{12}S_4$: C 55.43, H 5.53, N 3.49, S 8.00; found: C 54.09, H 5.68, N 3.61, S 7.65.

9,10-Bis[4-(*bis*(4-(*N*,*N*-dimethylamino)-2,6-dimethylphenyl)boryl)-3,5-dimethyl-phenylethynyl]-anthracene (VN)
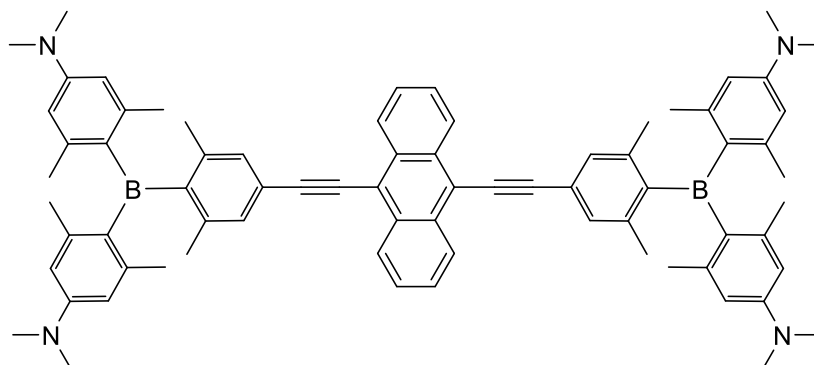
Bis[4-(*N*,*N*-dimethylamino)-2,6-dimethylphenyl]-(4-ethynyl-2,6-dimethylphenyl)borane (500 mg, 1.15 mmol, 2.2 eq), 9,10-diiodoanthracene (225 mg, 0.52 mmol, 1 eq), Pd(PPh$_3$)$_2$Cl$_2$ (18.2 mg, 22 μmol, 5 mol%) and CuI (5 mg, 22 μmol, 5 mol%) were dissolved in NEt$_3$ (50 mL). The reaction mixture was stirred at r.t. for 3d, until the starting materials were consumed according to TLC (10% EtOAc in hexane). After removing the solvent, the solid was purified by automated flash column chromatography (Biotage SNAP cartridge KP-Sil 10 g; 10% EtOAc in hexane). The solid was recrystallized from EtOAc to yield compound **VN** as a red-orange solid (193mg, 35%).

¹H NMR (300 MHz, CD$_2$Cl$_2$): δ = 8.73 (m, 4H), 7.67 (m, 4H), 7.37 (m, 4H), 6.34 (s, 8H), 2.97 (s, 24H), 2.13 (s, 12H), 2.05 (s, 12H), 2.00 (s, 12H) ppm.

¹³C{¹H} NMR (75 MHz, CD$_2$Cl$_2$): δ = 151.8, 151.6, 143.5, 143.0, 140.9, 135.8, 132.4, 130.6, 127.7, 127.3, 122.9, 118.9, 111.9, 111.9, 104.2, 86.4, 40.2, 24.1, 23.9, 22.9 ppm.

HRMS (APCI) m/z: [M+H]$^+$ found: 1047.6634; calc. for [C$_{74}$H$_{81}$B$_2$N$_4$]$^+$: 1047.6642 (|Δ| = 0.76 ppm).

Elemental analysis Calc. (%) for C$_{74}$H$_{80}$B$_2$N$_4$: C 84.88, H 7.70, N 5.35; found: C 84.58, H 7.84, N 5.24.

9,10-Bis[4-(*bis*(4-(*N,N,N*-trimethylammonium)-2,6-dimethylphenyl)boryl)-3,5-dimethyl-phenylethynyl]-anthracene tetratriflate (V)
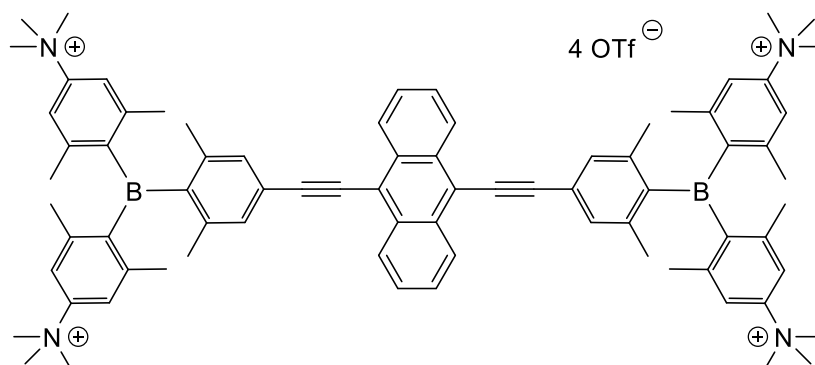
Compound **VN** (15.2 mg, 14.5 μmol, 1 eq) was dissolved in CH_2Cl_2 (2 mL). Methyl triflate (7.39 μL, 65.3 μmol, 4.5 eq) was added and the reaction was stirred at r.t. for 48 h. The precipitate was collected by filtration and washed with CH_2Cl_2 (3 x 5 mL) to afford compound **V** as a red solid (16 mg, 64%).

¹H NMR (500 MHz, CD_3OD): δ = 8.70 (m, 4H), 7.73 (m, 4H), 7.60 (m, 8H), 7.49 (s, 4H), 3.68 (s, 36H), 2.28 (s, 12H), 2.19 (s, 12H), 2.14 (s, 12H) ppm.

¹³C{¹H} NMR (125 MHz, CD_3OD): δ = 149.8, 149.1, 147.3, 145.0, 144.7, 142.6, 133.3, 132.1, 128.4, 128.1, 127.0, 121.8 (q, J = 318 Hz), 120.3, 119.5, 103.9, 88.4, 57.5, 23.6, 23.5, 23.3 ppm.

HRMS (ESI pos) m/z: [M-2OTf]²⁺ found: 702.3266; calc. for $[C_{74}H_{88}B_4N_4S_2F_6O_6]^{2+}$: 702.3269 (|$\Delta$| = 0.43 ppm).

Elemental analysis Calc. (%) for $C_{82}H_{92}B_2F_{12}N_4O_{12}S_4$: C 57.82, H 5.44, N 3.29, S 7.53; found: C 56.74, H 5.32, N 3.29, S 7.16.

7.2.3 NMR Spectra
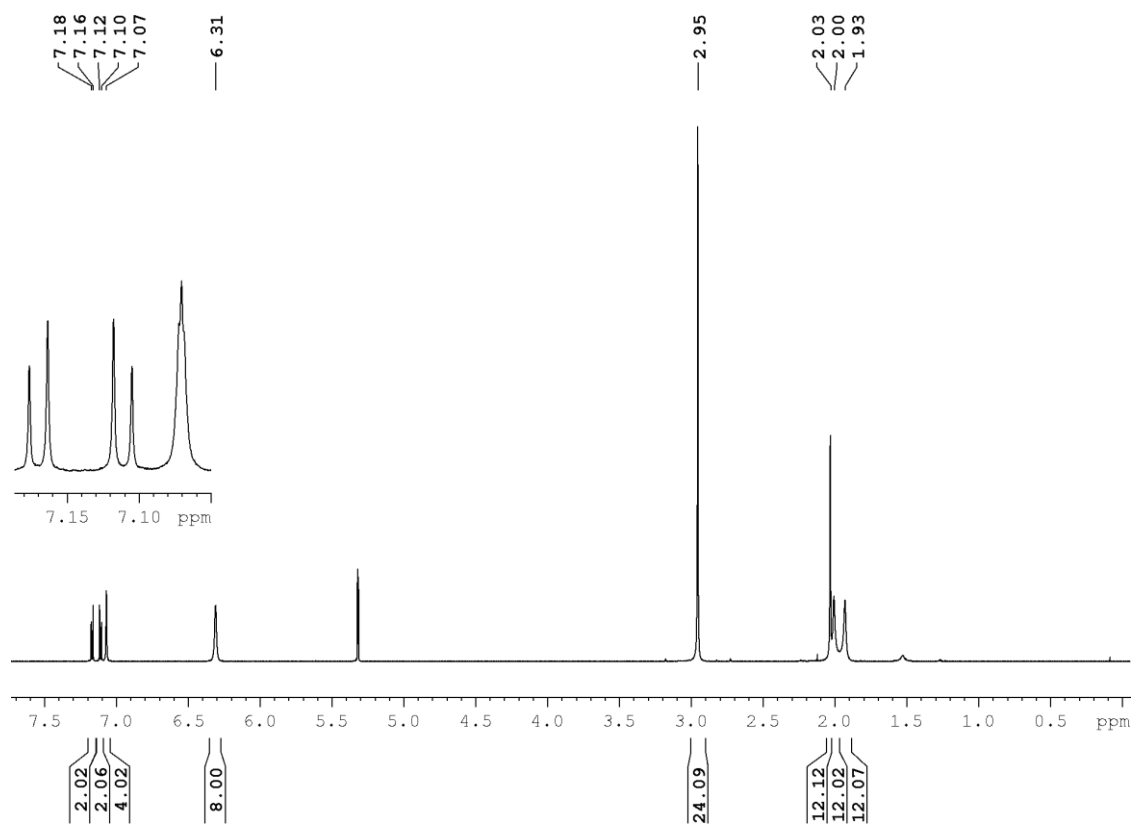
Figure S38. ^{1}H NMR spectrum of **IIIN** in CD$_2$Cl$_2$ at 300 MHz.
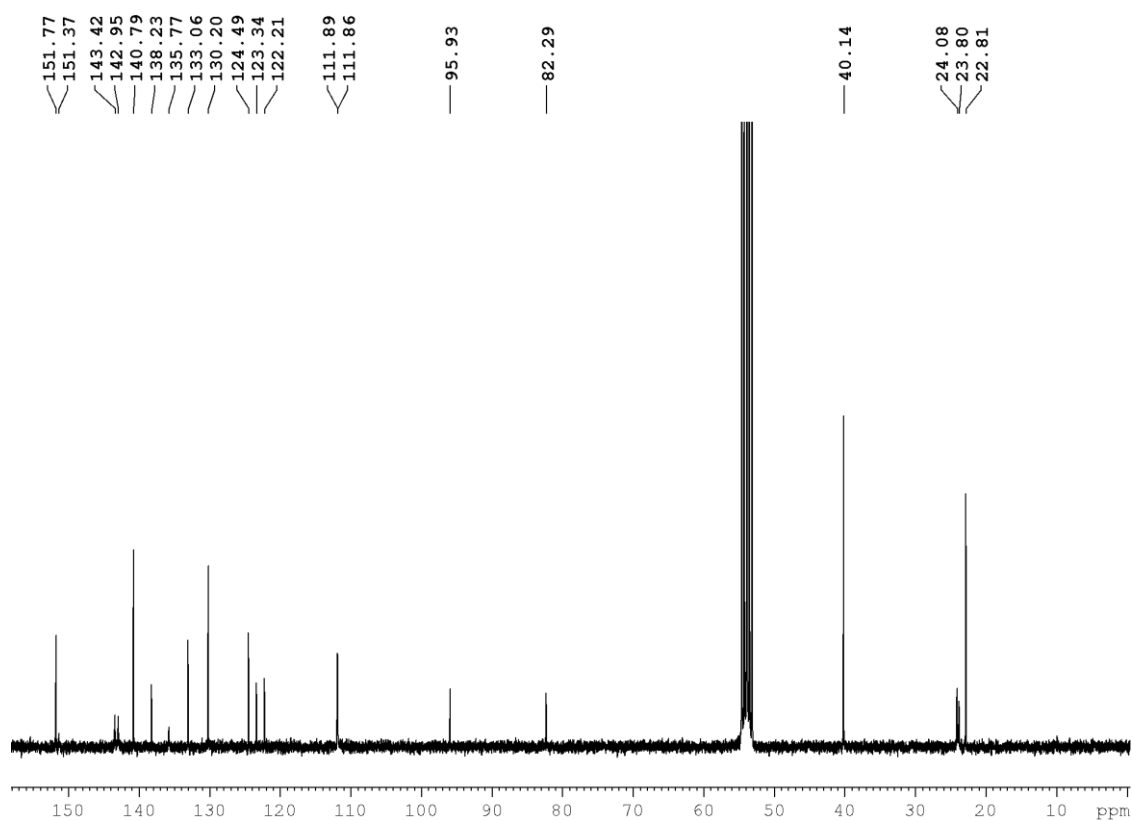
Figure S39. ^{13}C{^{1}H} NMR spectrum of **IIIN** in CD$_2$Cl$_2$ at 75 MHz.
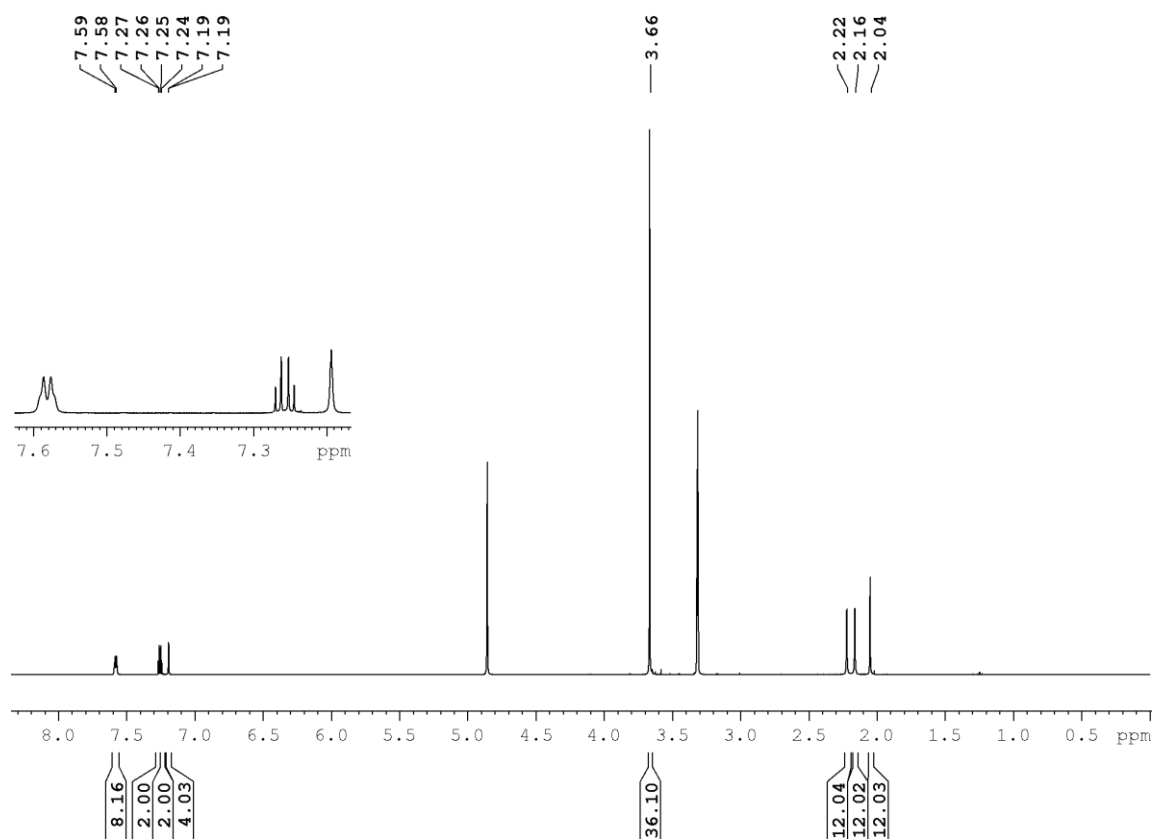
Figure S40. ^{1}H NMR spectrum of **III** in CD$_3$OD at 500 MHz.
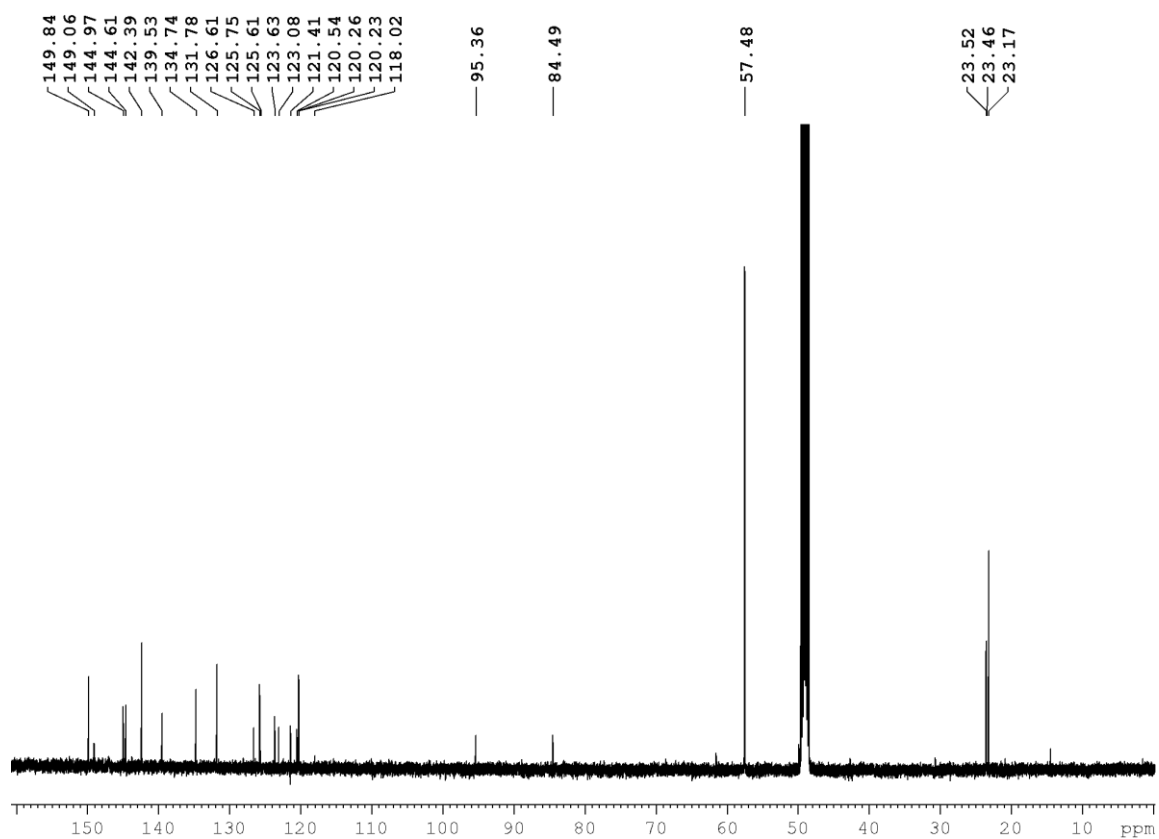
Figure S41. ^{13}C{^{1}H} NMR spectrum of **III** in CD$_3$OD at 125 MHz.
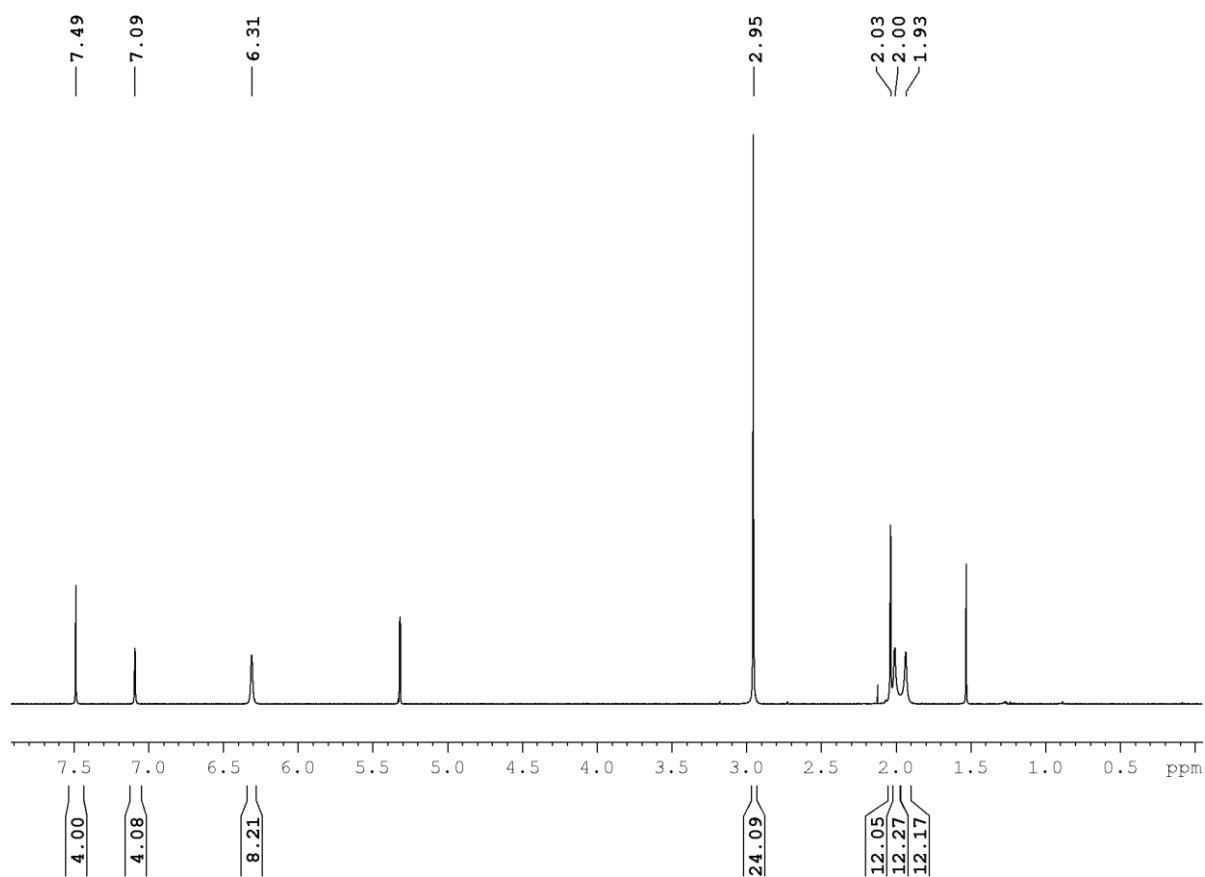
Figure S42. ^{1}H NMR spectrum of **IVN** in CD_2Cl_2 at 300 MHz.
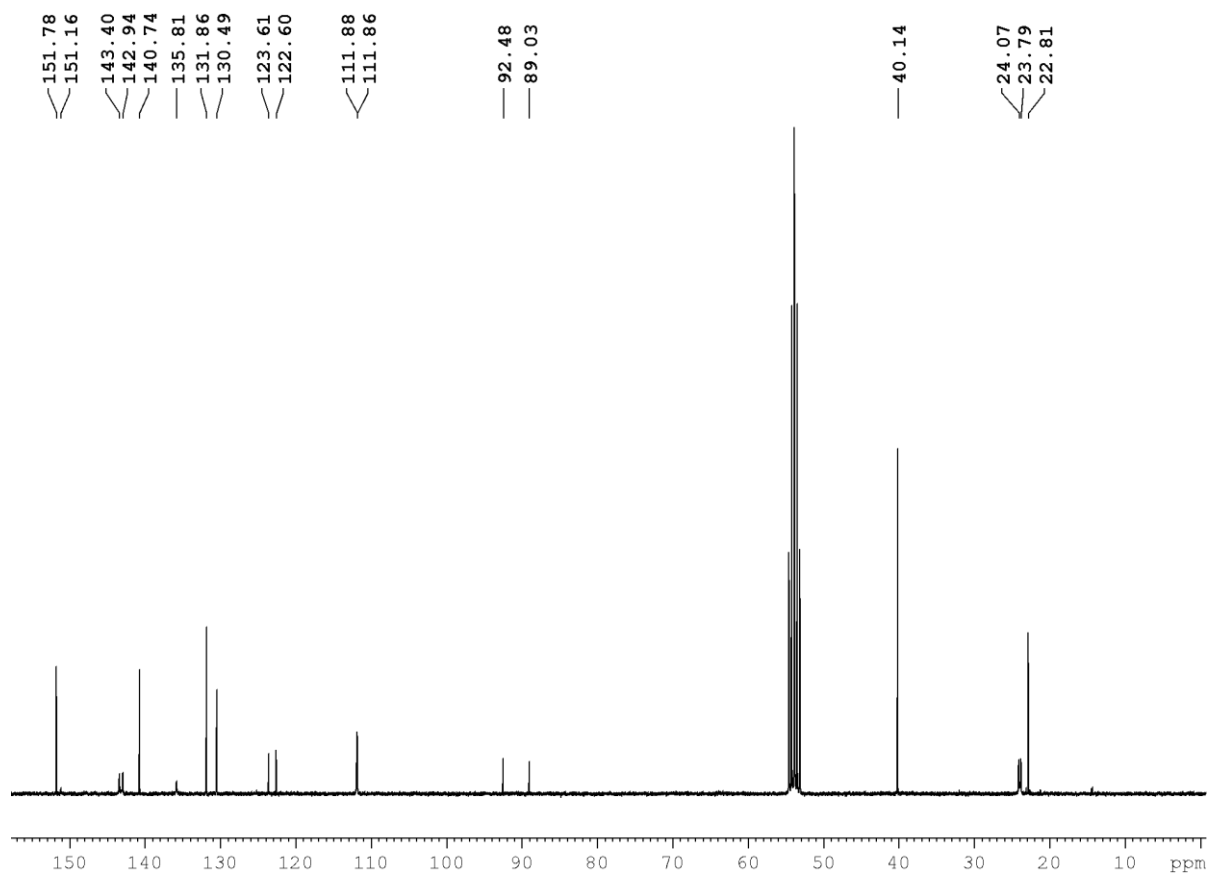
Figure S43. $^{13}C\{^1H\}$ NMR spectrum of **IVN** in CD_2Cl_2 at 75 MHz.
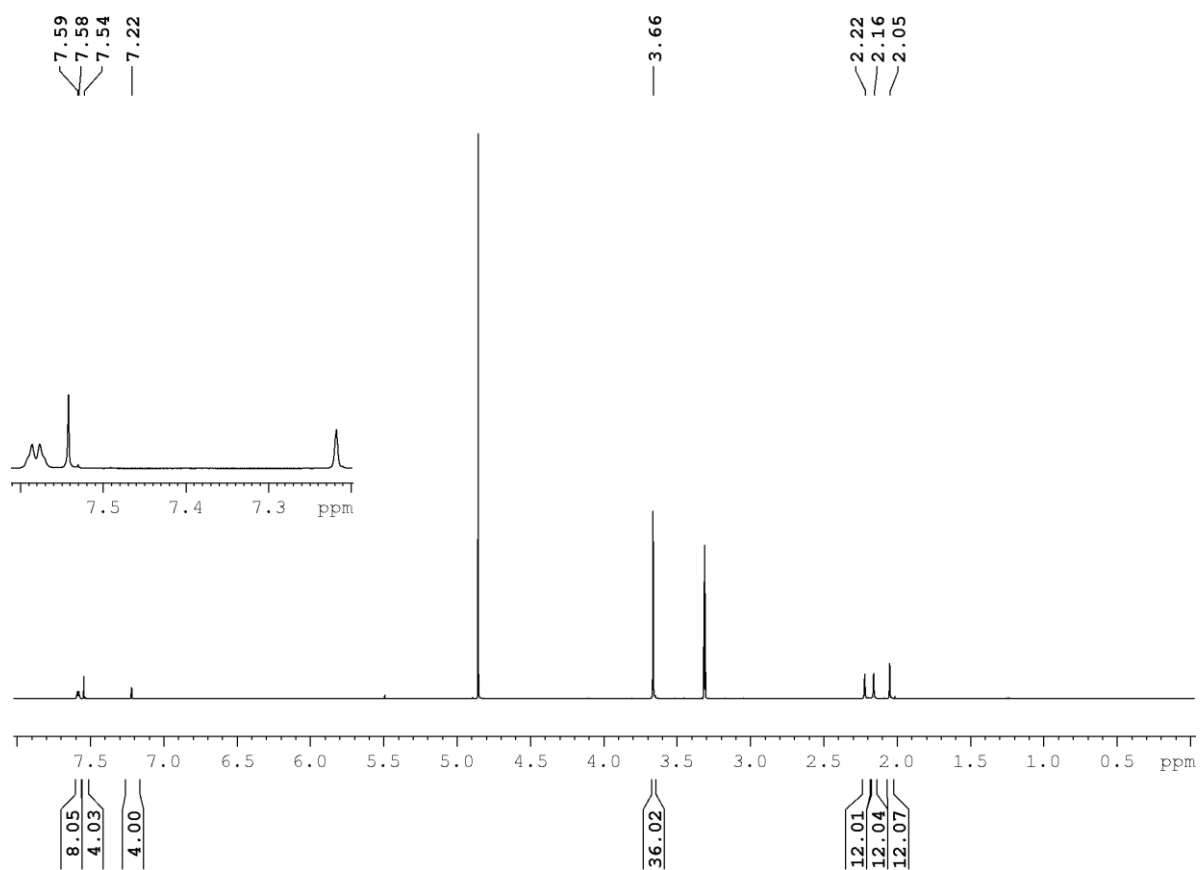
Figure S44. ^{1}H NMR spectrum of **IV** in CD$_3$OD at 500 MHz.
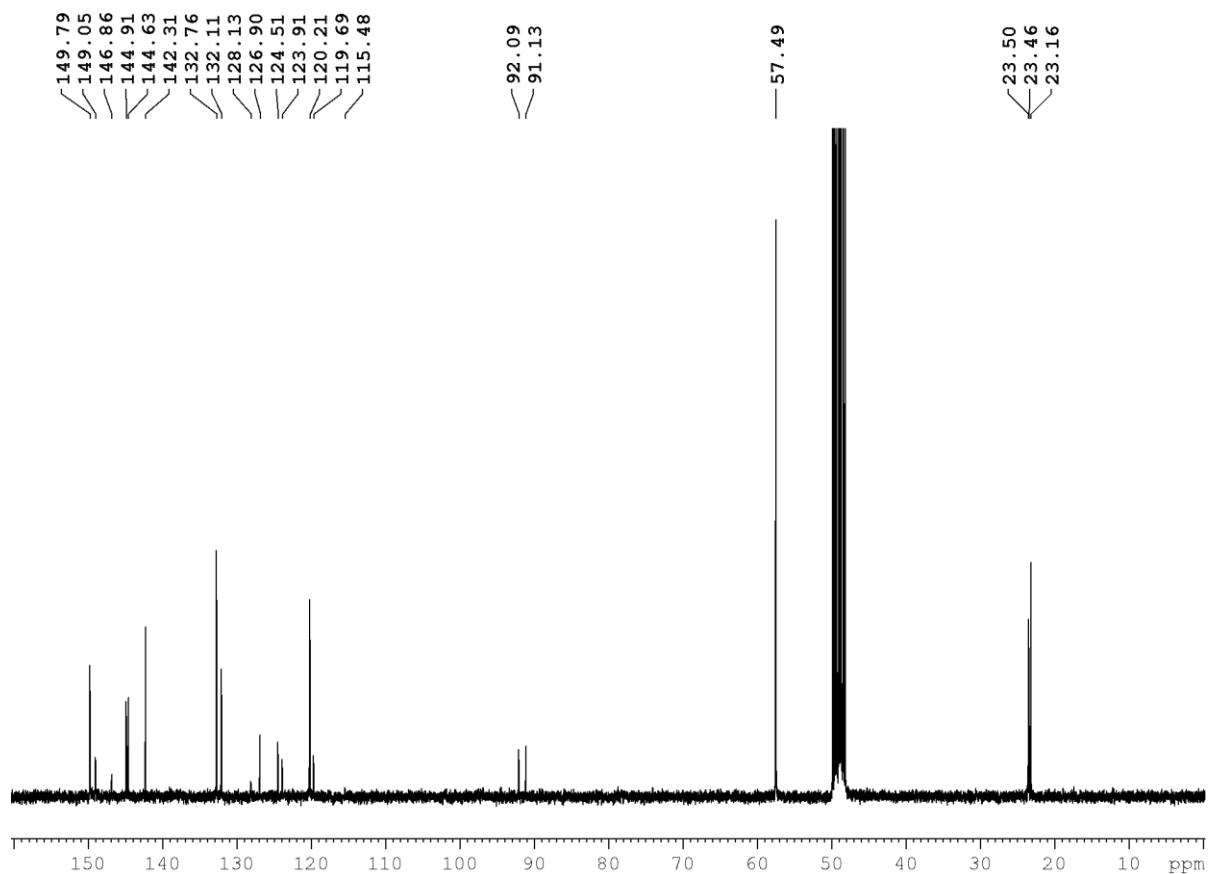
Figure S45. ^{13}C{^{1}H} NMR spectrum of **IV** in CD$_3$OD at 75 MHz.
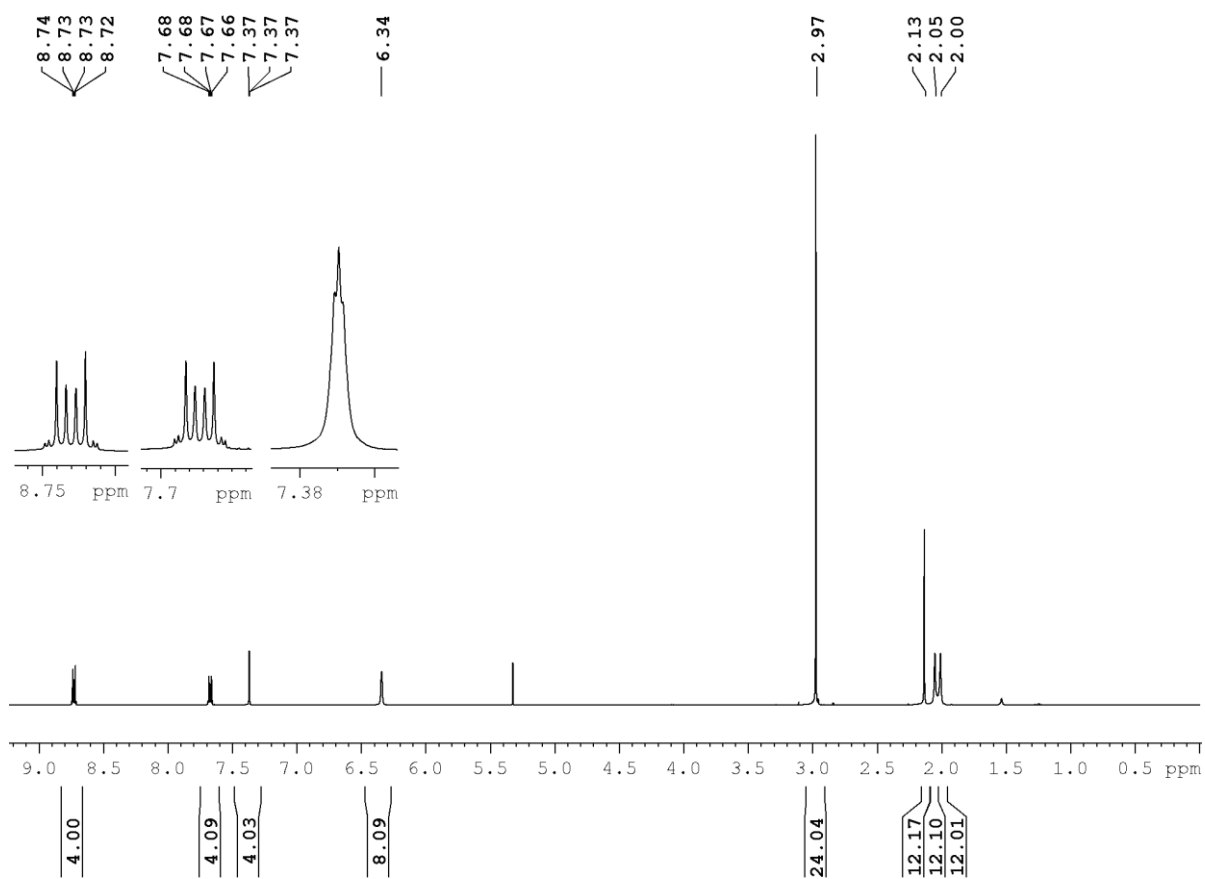
Figure S46. ^{1}H NMR spectrum of **VN** in CD$_2$Cl$_2$ at 300 MHz.
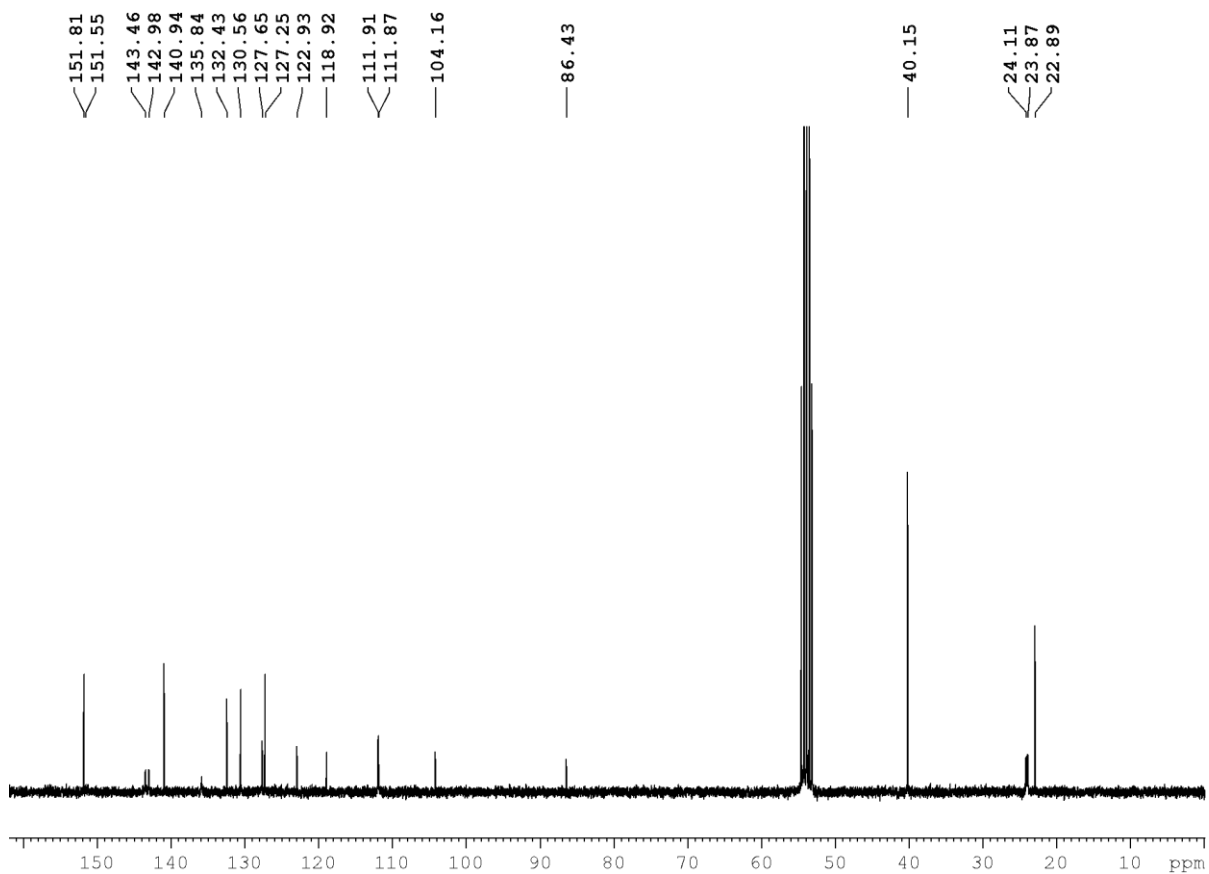
Figure S47. ^{13}C{^{1}H} NMR spectrum of **VN** in CD$_2$Cl$_2$ at 75 MHz.
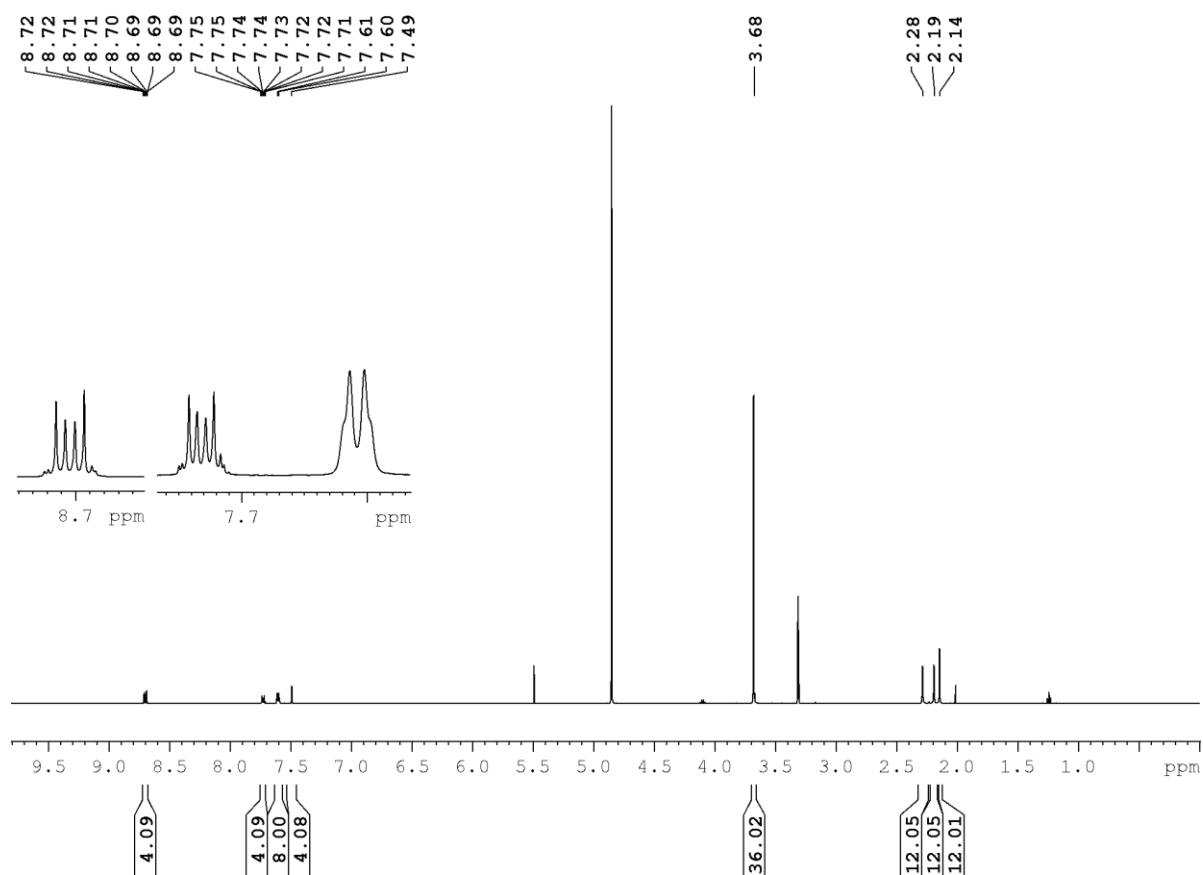
Figure S48. ^{1}H NMR spectrum of **V** in CD$_3$OD at 500 MHz.
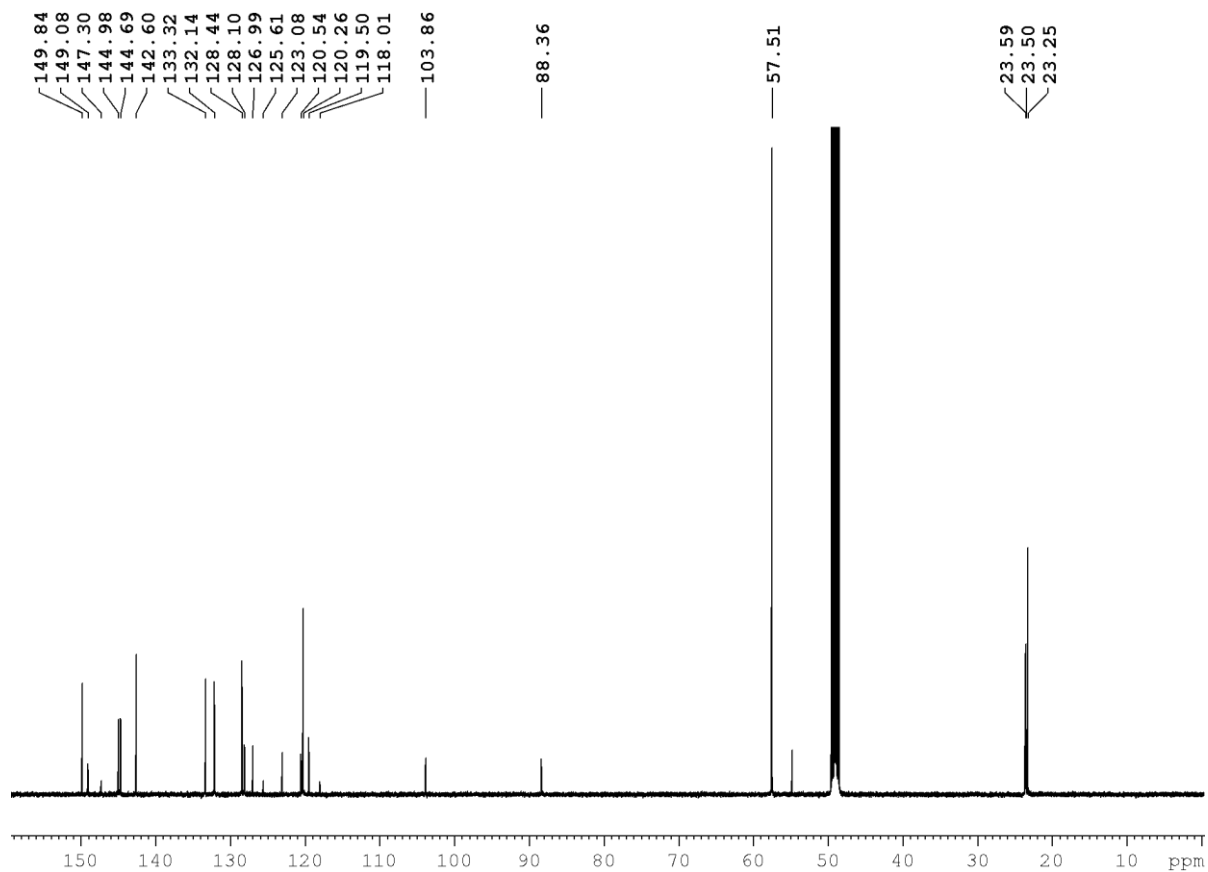
Figure S49. ^{13}C{^{1}H} NMR spectrum of **V** in CD$_3$OD at 125 MHz.

7.2.4 Single-Crystal X-Ray Diffraction

Table S2. Single-crystal X-ray diffraction data and structure refinements of compounds **IIIN** and **IVN** of this study and of compound **C** of an earlier study.[189]

Data	IIIN	IVN	C
CCDC number	1997113	1997114	1997115
Empirical formula	$C_{68}H_{76}B_2N_4S_2 \cdot$ $C_4H_8O_2$	$C_{66}H_{76}B_2N_4O_2 \cdot$ $C_4H_8O_2$	$C_{33}H_{45}BN_2Si \cdot$ C_6H_{14}
w (g·mol^{-1})	1123.17	1035.03	594.78
Temperature (K)	100(2)	100(2)	120(2)
Radiation, λ (Å)	Mo-K$_\alpha$ 0.71073	Mo-K$_\alpha$ 0.71073	Cu-K$_\alpha$ 1.54184
Crystal size (mm³)	0.12×0.27×0.32	0.09×0.14×0.48	0.13×0.19×0.33
Crystal color, habit	Yellow plate	Yellow plate	Yellow block
Crystal system	Monoclinic	Monoclinic	Monoclinic
Space group	$P2_1/n$	$P2_1/n$	$P2_1/c$
a (Å)	8.237(5)	8.237(7)	18.0602(3)
b (Å)	42.45(3)	38.52(3)	31.5746(5)
c (Å)	19.006(11)	19.425(15)	13.3605(2)
α (°)	90	90	90
β (°)	93.972(14)	93.31(2)	94.4160(10)
γ (°)	90	90	90
Volume (Å³)	6630(7)	6153(9)	7596.1(2)
Z	4	4	8
ρ_{calc} (g·cm^{-3})	1.125	1.117	1.040
μ (mm^{-1})	0.127	0.066	0.727
F(000)	2408	2232	2608
θ range (°)	1.440 – 27.134	1.490 – 25.532	2.454 – 74.503
Reflections collected	61704	40724	79492
Unique reflections	14135	11380	15459
Parameters / restraints	876 / 114	849 / 418	906 / 102
GooF on F^2	1.023	1.013	1.081
R_1 [I>2σ(I)]	0.0765	0.0732	0.0564
wR^2 (all data)	0.2232	0.2068	0.1601
Max./min. residual electron density (e·Å^{-3})	0.700 / –0.375	0.624 / –0.401	0.468 / –0.269
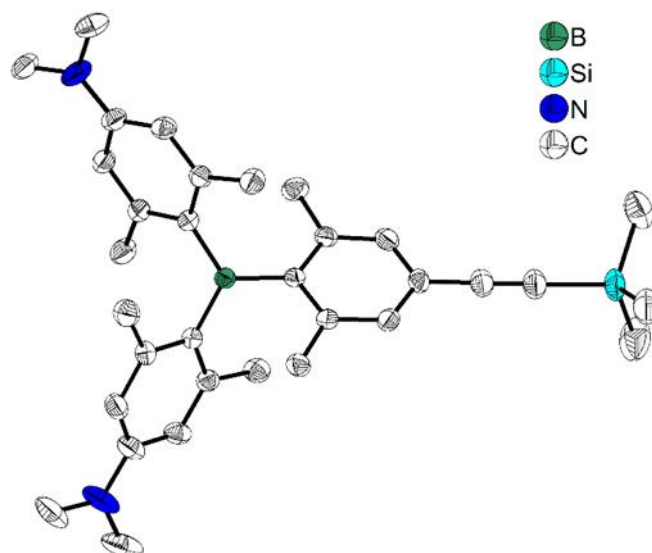
Figure S50. Molecular structure of compound **C** in the solid state at 120 K. Atomic displacement ellipsoids are drawn at the 50% probability level, and H atoms and co-crystallized solvent molecules (hexane) are omitted for clarity. Compound **C** contains two symmetry-independent molecules in the asymmetric unit. Only one of the two molecules is shown here. Selected angles for molecule 1: Sum (C–B1–C) 359.99(12)°, BC_3–Aryl (C1) 44.95(6)°, BC_3–Aryl (C2) 46.26(6)°, BC_3–Aryl (C3) 47.76(6)°. Selected angles for molecule 2: Sum (C–B1–C) 359.99(13)°, BC_3–Aryl (C1) 44.80(6)°, BC_3–Aryl (C2) 48.47(6)°, BC_3–Aryl (C3) 46.28(6)°.

7.2.5 Linear Optical Properties
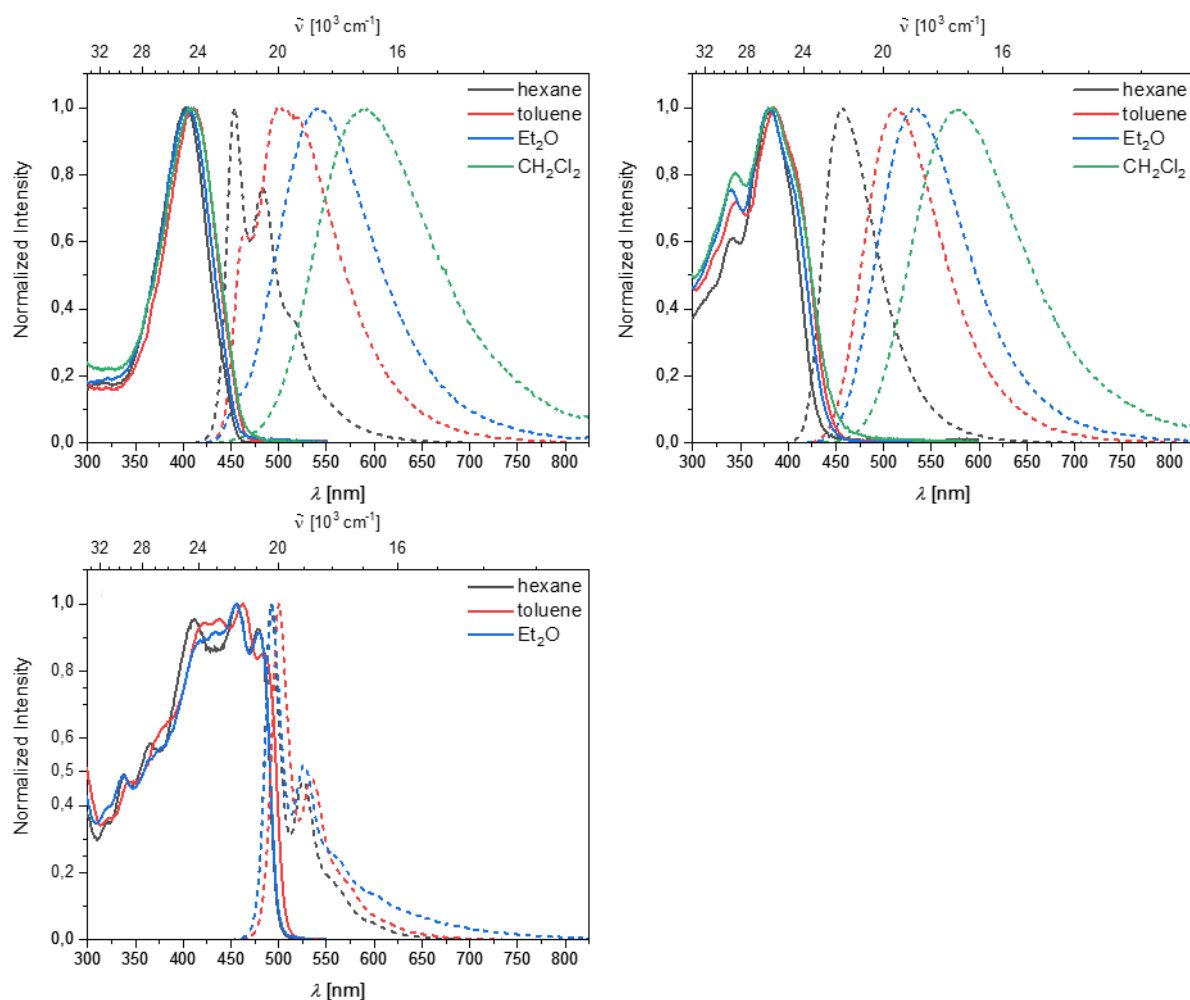
Figure S51. Absorption and emission spectra of **IIIN** (top, left), **IVN** (top, right) and **VN** (bottom, left) in various solvents.

Table S3. Photophysical data for compounds **IIIN**-**VN** in various solvents.

	solvent	λ_{abs} / nm	ε / M^{-1} cm^{-1}	λ_{em} / nm	Stoke's shift / cm^{-1}	Φ_f	τ / ns	k_r / 10^8 s^{-1}	k_{nr} / 10^8 s^{-1}
IIIN	hexane	404	111 000	454	2 700	0.28	<1	-	-
	toluene	411		503	4 500	0.29	3.59	0.8	2.0
	Et$_2$O	405		542	6 200	0.26	6.00	0.4	1.2
	CH$_2$Cl$_2$	408		589	7 500	0.11	3.69	0.3	2.4
IVN	hexane	383	82 000	458	4 300	0.12	1.79	0.7	4.9
	toluene	386		513	6 400	0.20	4.07	0.5	2.0
	Et$_2$O	379		533	7 600	0.18	5.82	0.3	1.4
	CH$_2$Cl$_2$	384		579	8 800	0.13	5.47	0.2	1.6
VN	hexane	479	58 000	493	600	0.78	1.95	4.0	1.1
	toluene	483		501	700	0.90	2.05	4.4	0.5
	Et$_2$O	479		493	600	0.28	3.68	0.8	2.0
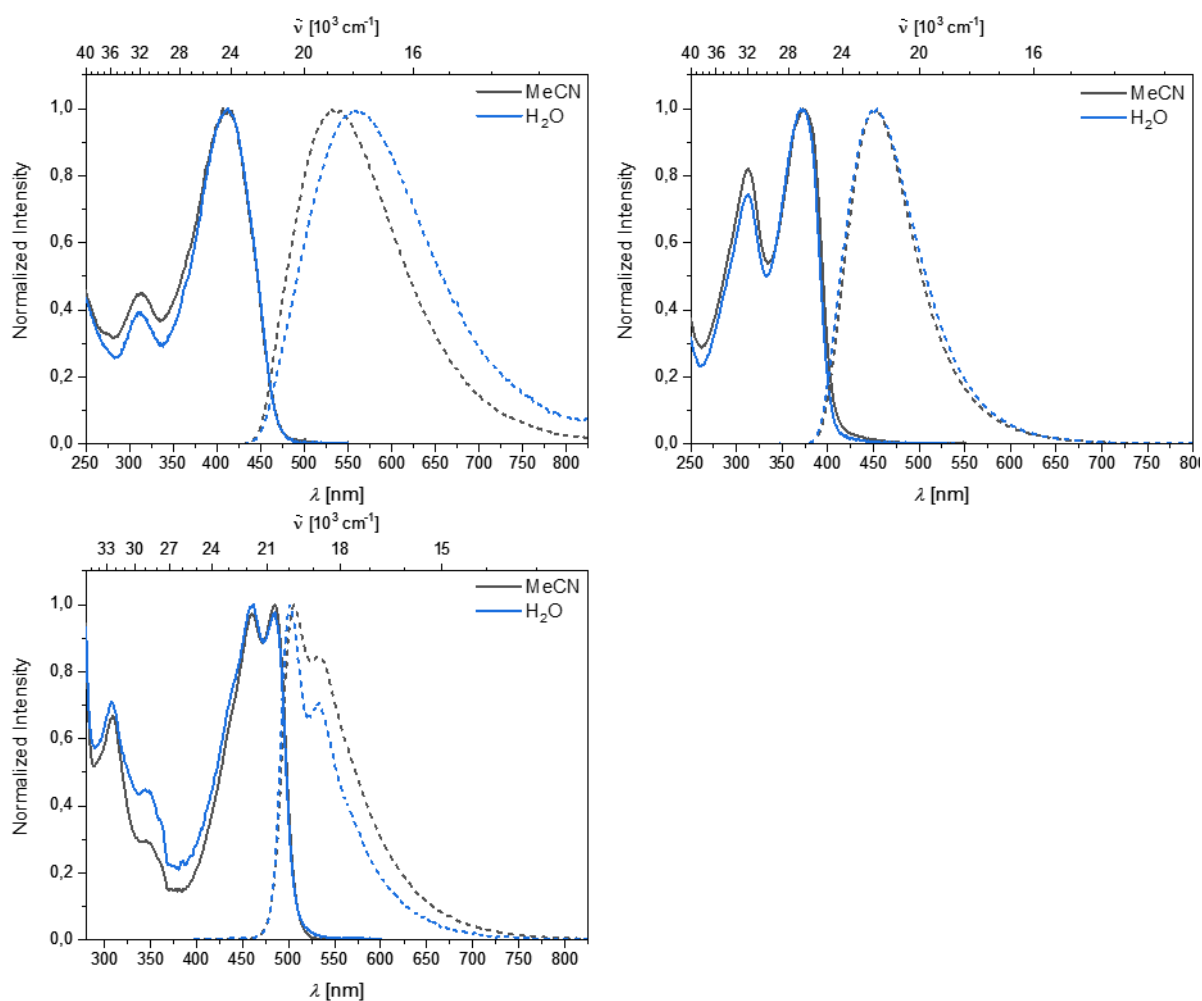
Figure S52. Absorption and emission spectra of **III** (top, left), **IV** (top, right) and **V** (bottom, left) in various solvents.
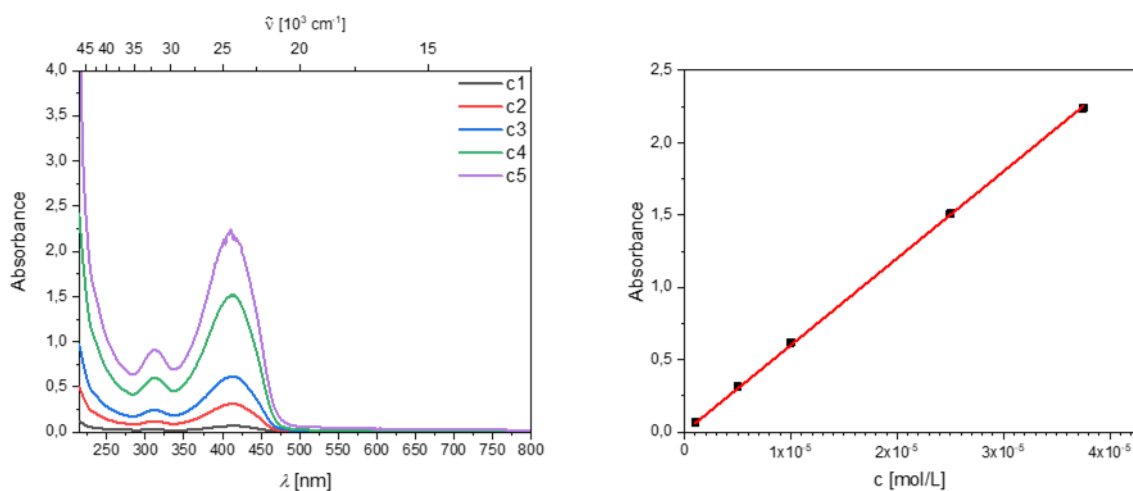
Figure S53. Linear dependence (—) of the absorbance at 413 nm in H_2O on the concentration of compound **III** in the range from $1 \times 10^{-6} – 3.75 \times 10^{-5}$ M (■).
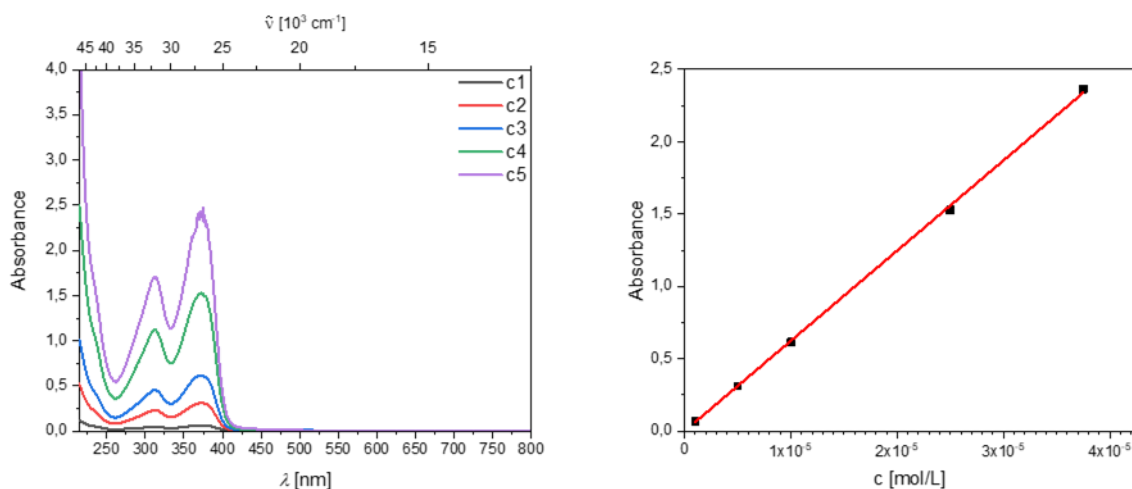
Figure S54. Linear dependence (—) of the absorbance at 371 nm in H_2O on the concentration of compound **IV** in the range from $1 \times 10^{-6} – 3.75 \times 10^{-5}$ M (■).
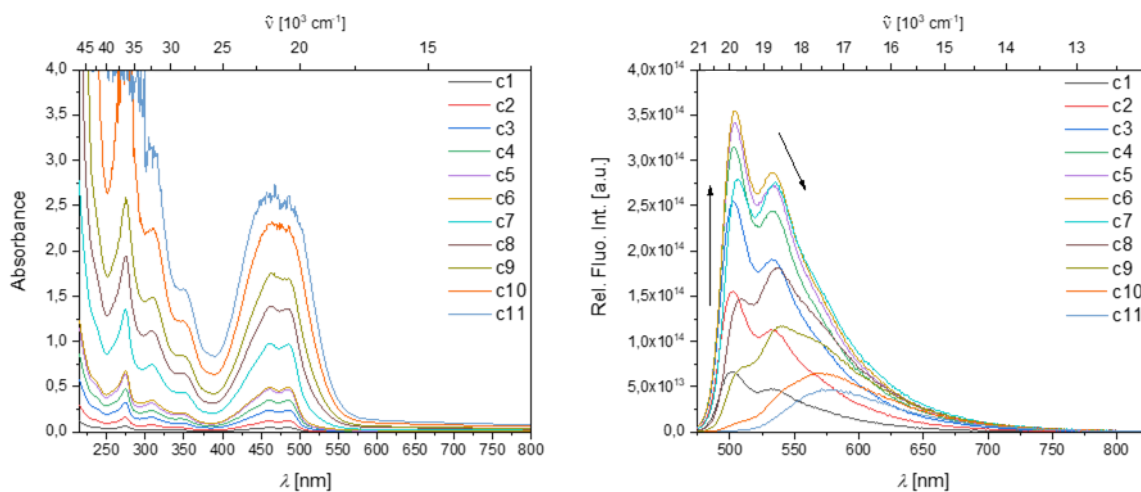
Figure S55. Left: Dependence of the absorbance of compound **V** on the concentration in the range from $1 \times 10^{-6} – 1 \times 10^{-4}$ M. Right: Dependence of the emission of compound **V** on the concentration in the range from $1 \times 10^{-6} – 1 \times 10^{-4}$ M.

7.2.6 Optical Properties in Sodium Cacodylate
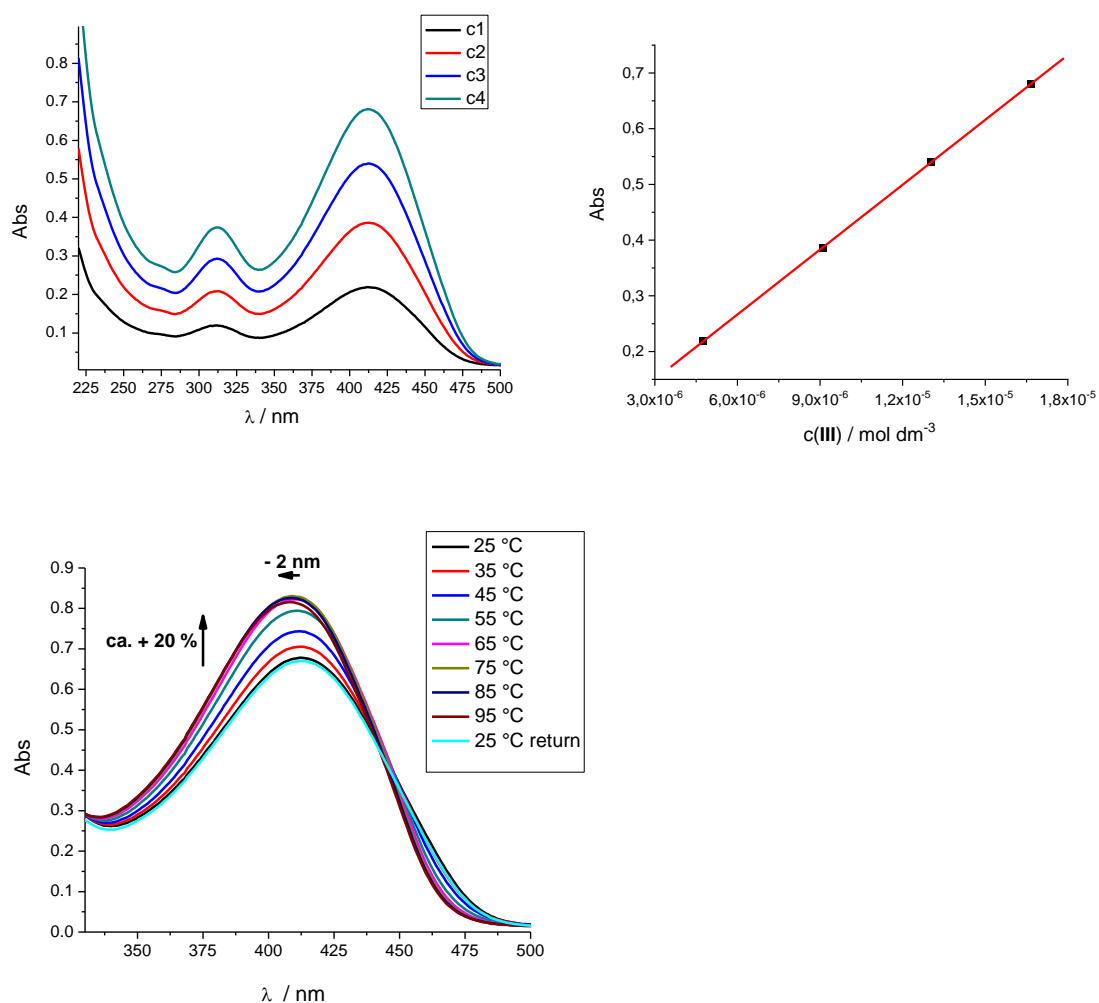
Figure S56. Top: UV/Vis spectra of **III**, c = 5 ×10^{-6} – 1.7 ×10^{-5} M (left); linear dependence (—) of the absorbance at 412 nm (■) on the **3** concentration (right); bottom: influence of temperature increase (T = 25 – 95 °C) on UV/Vis spectra of **III**, c = 1.7 ×10^{-5} M. Measured in sodium cacodylate buffer, pH = 7.0, I = 0.05 M.
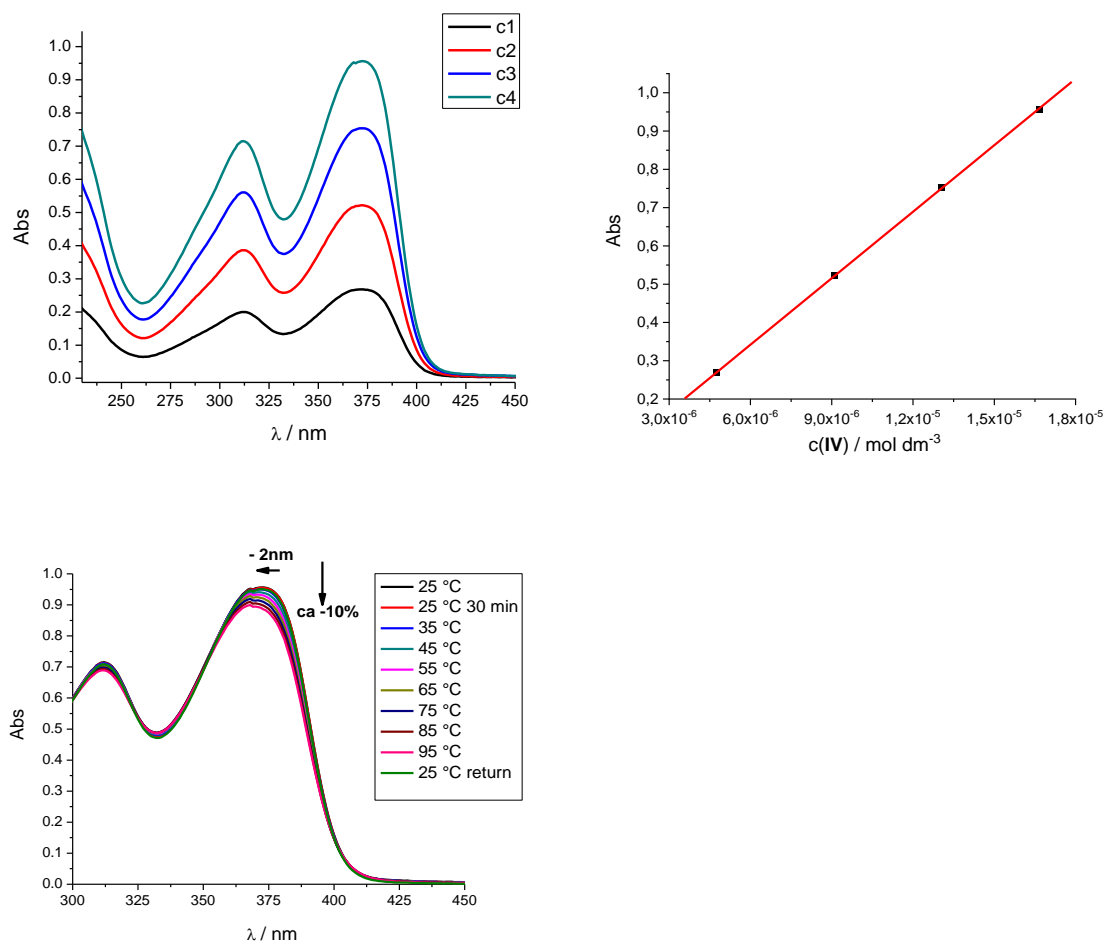
Figure S57. Top: UV/Vis spectra of **IV**, c = 5 ×10^{-6} – 1.7 ×10^{-5} M (left); linear dependence (—) of the absorbance at 372 nm (■) on the **IV** concentration (right); bottom: influence of temperature increase (T = 25 – 95 °C) on UV/Vis spectra of **4**, *c* = 1.7 ×10^{-5} M. Measured in sodium cacodylate buffer, pH = 7.0, *I* = 0.05 M.
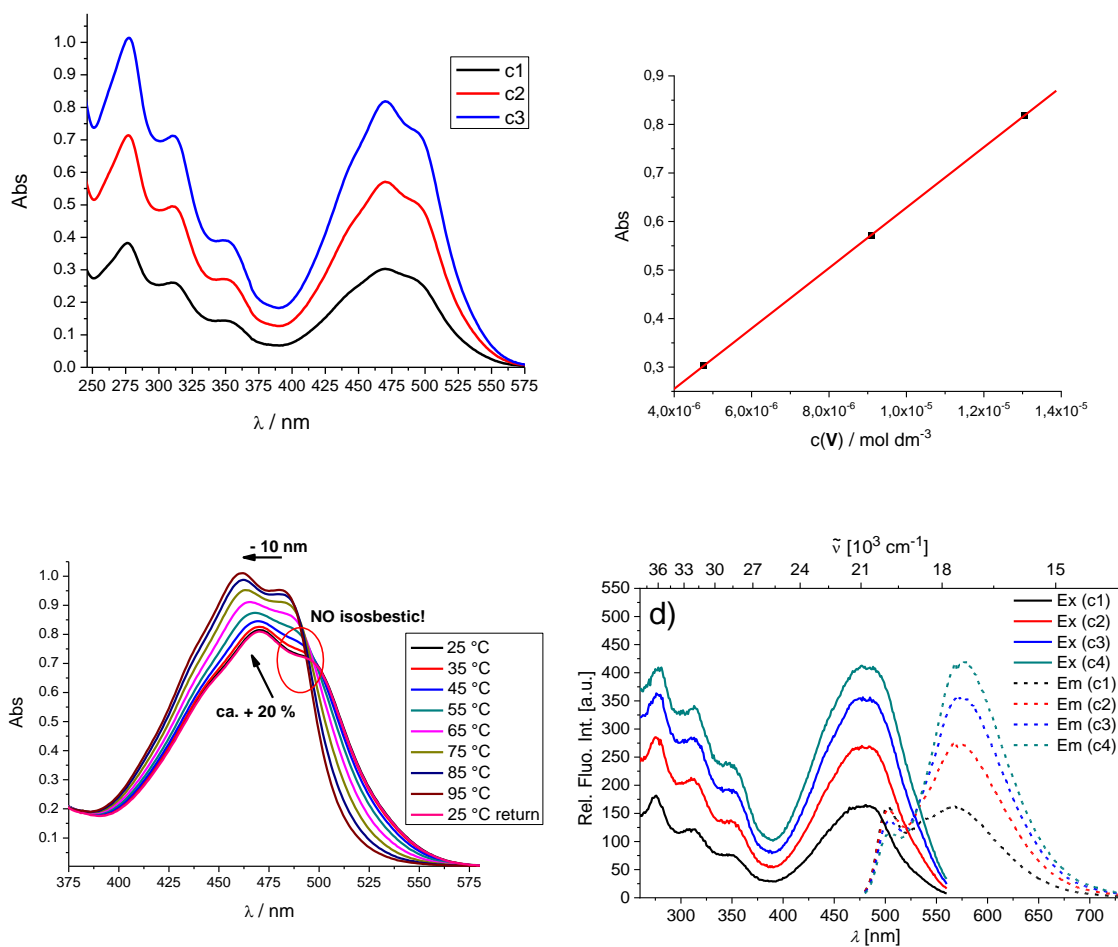
Figure S58. Top right: UV/Vis spectra of **V**, c = 5 ×10⁻⁶ – 1.3 ×10⁻⁵ M (left); top left: linear dependence (—) of the absorbance at 470 nm (■) on the **V** concentration (right); bottom left: influence of temperature increase (T = 25 – 95 °C) on UV/Vis spectra of **V**, *c* = 1.3 ×10⁻⁵ M (left).; bottom right: excitation / emission spectra overlap at *c*(**V**) = 5; 20; 35; 50 ×10⁻⁸ M. All measured in sodium cacodylate buffer, pH = 7.0, *I* = 0.05 M.
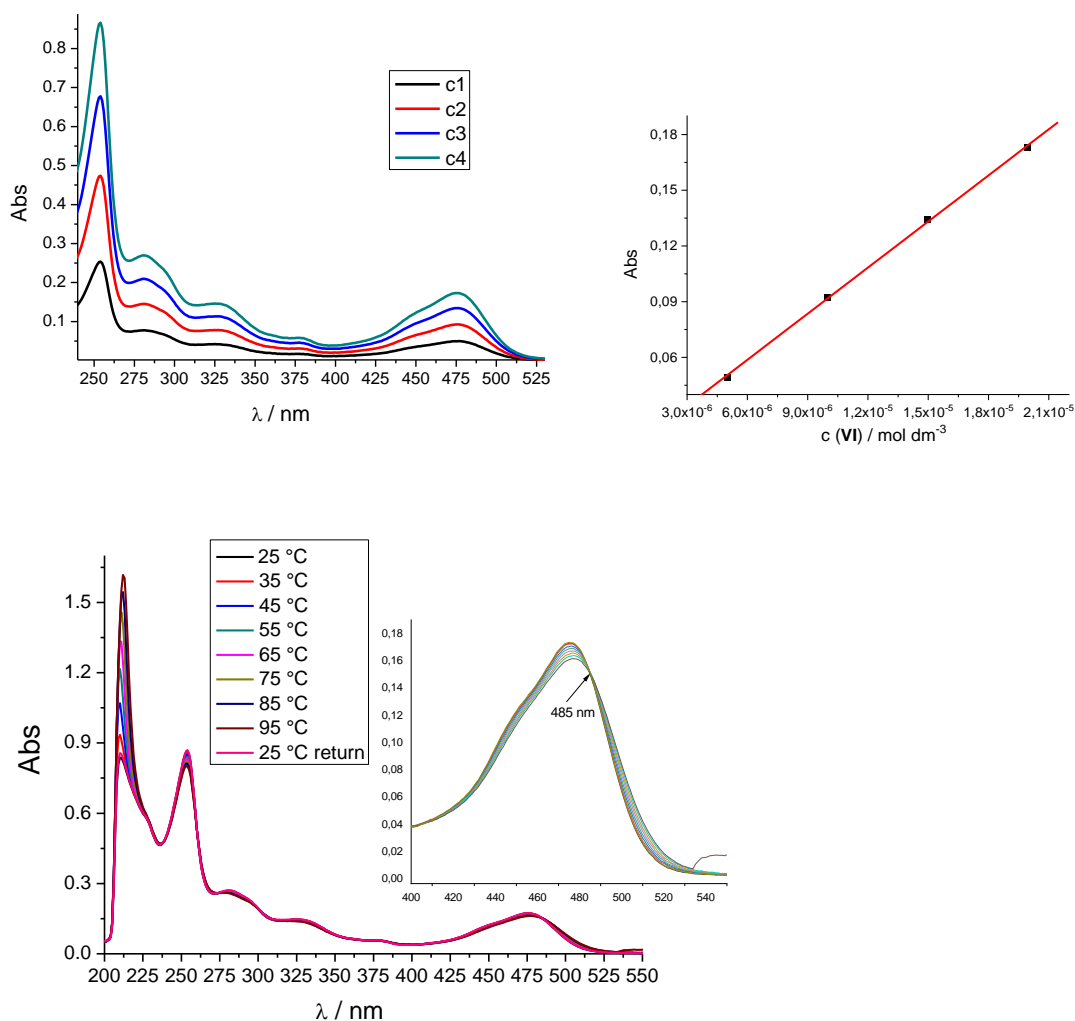
Figure S59. Top: UV/Vis spectra of **VI**, c = 5 ×10⁻⁶ – 2 ×10⁻⁵ M (left); linear dependence (—) of the absorbance at 476 nm (■) on the **VI** concentration (right); bottom: influence of temperature increase (T = 25 – 95 °C) on UV/Vis spectra of **VI**, c = 2 ×10⁻⁵ M. Measured in sodium cacodylate buffer, pH = 7.0, I = 0.05 M.

Table S4. Electronic absorption data of compounds **III**-**VI.**

Compound	λ_{max}/nm	$\varepsilon \times 10^3$/mmol^{-1} cm^2
III	412	38.8±0.1
IV	372	57.9±0.4
V	470	62.2±0.2
VI	476	8.3±0.1

(a)

(b)

(c)

(d)
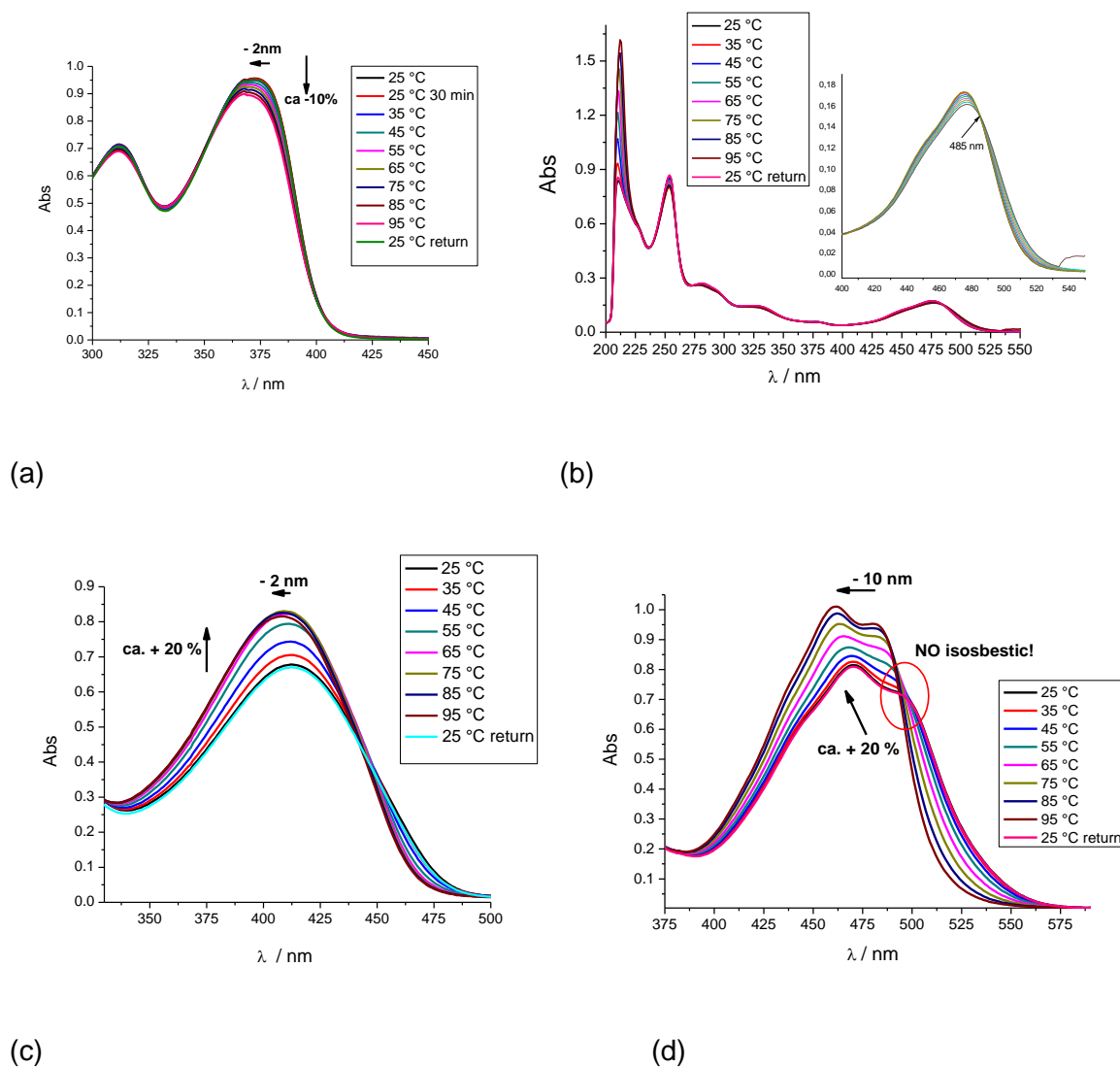
Figure S60. Temperature dependence of UV/Vis absorption spectra of compounds **III-VI**: (c = 1.7 ×10^{-5} M) Note: ref. compound **IV** (a) and **VI** (b) hypochromic effect (> 10%) at variance to **III** (c) and **V** (d) hyperchromic effect (>+ 20%), suggesting that **III** and **V** display π-stacking interactions.
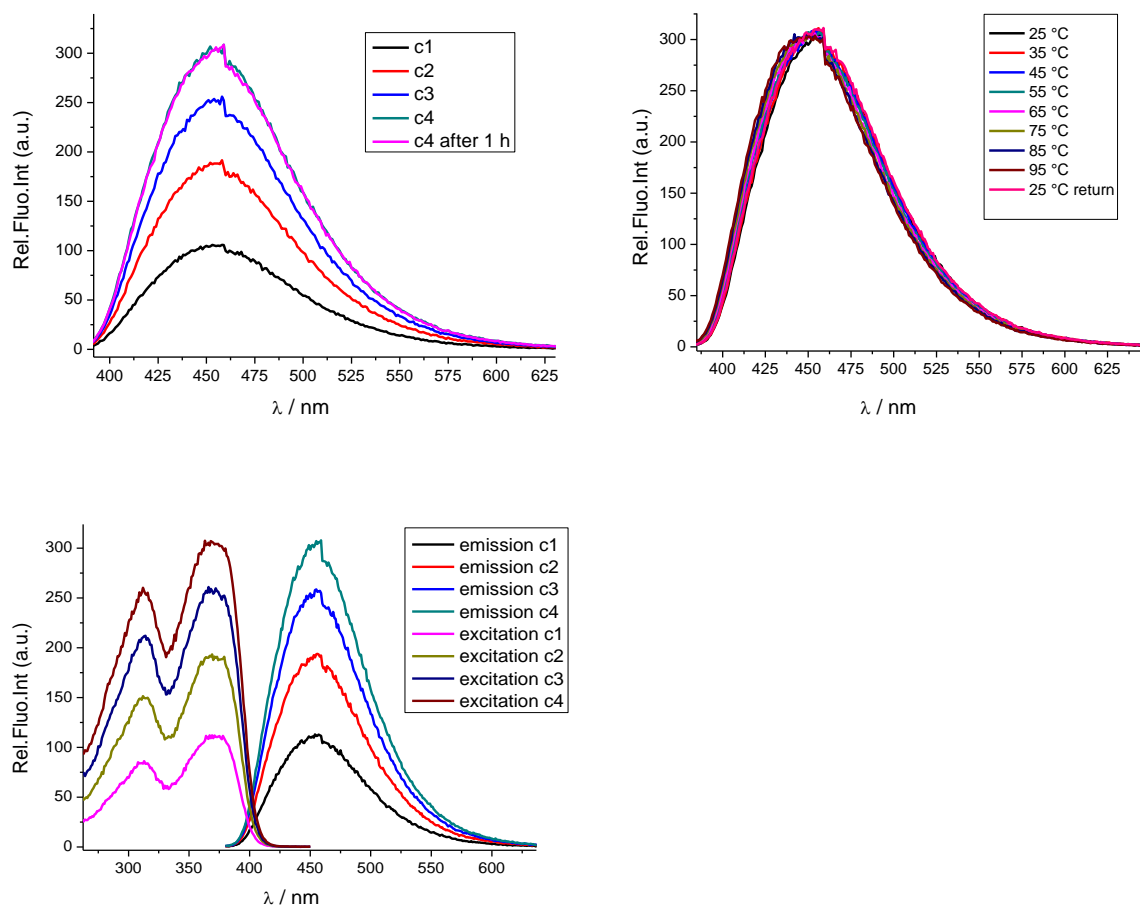
Figure S61. Top: fluorescence spectra of **IV** (λ_{exc} = 372 nm) in the concentration range c = 5 ×10^{-8}– 5 ×10^{-7} M (left); influence of temperature increase (T = 25 – 95 °C) on fluorescence spectra of **IV**, c = 5 ×10^{-7} M (right); bottom: comparison of emission and excitation spectra of **IV**. Measured in sodium cacodylate buffer (pH = 7.0, I = 0.05 M).
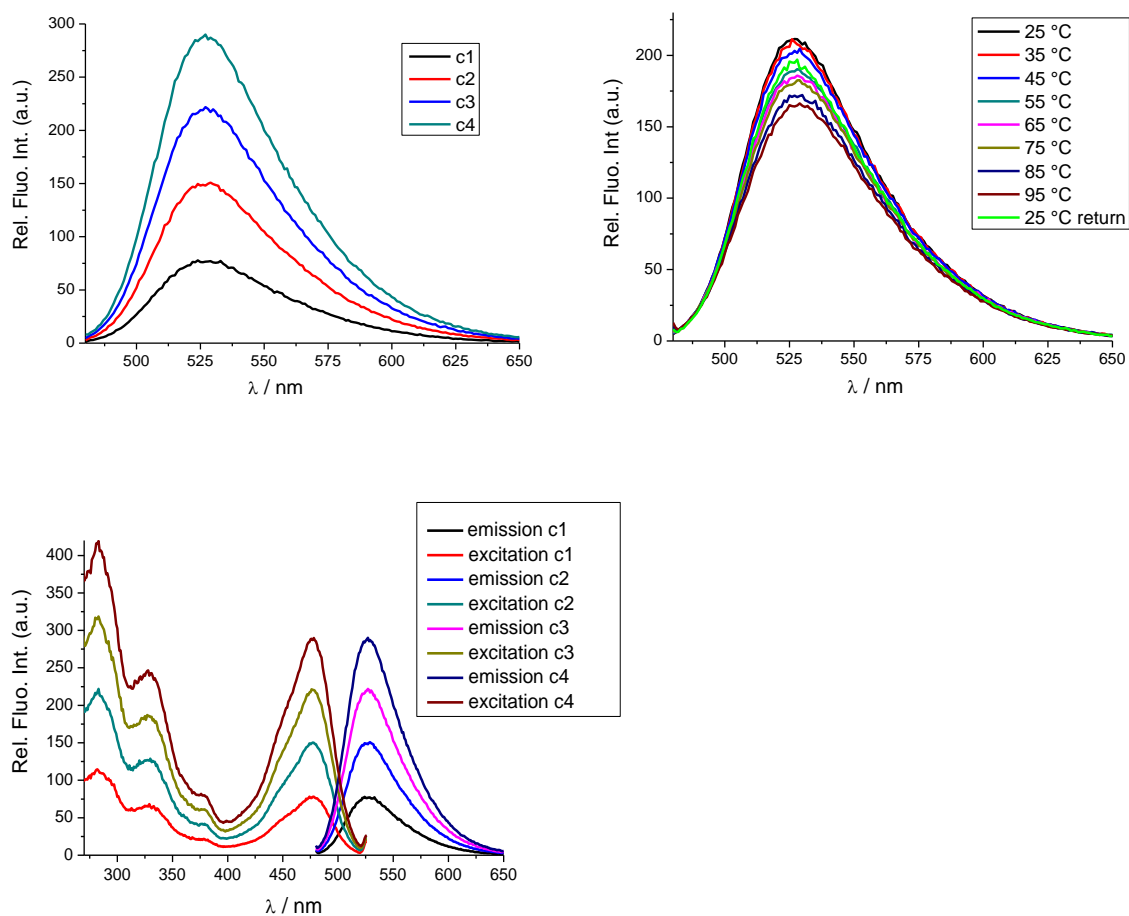
Figure S62. Top: fluorescence spectra of **VI** (λ_{exc} = 476 nm) in the concentration range c = 2 ×10^{-6}– 8 ×10^{-6} M (left); influence of temperature increase (T = 25 – 95 °C) on fluorescence spectra of **VI**, c = 8 ×10^{-6} M (right); bottom: comparison of emission and excitation spectra of **VI**. Measured in sodium cacodylate buffer (pH = 7.0, I = 0.05 M).
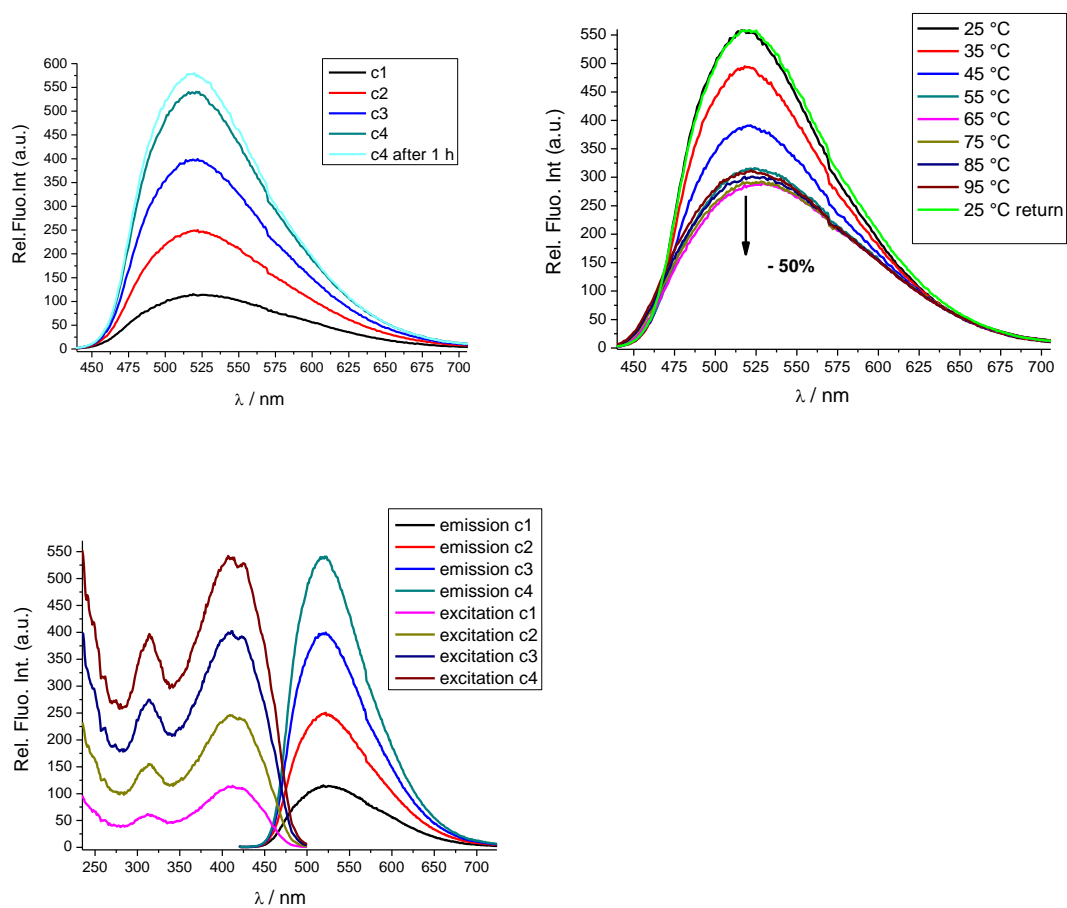
Figure S63. Top: fluorescence spectra of **III** (λ_{exc} = 412 nm) in the concentration range c = 5 ×10^{-8}– 5 ×10^{-7} M (left); influence of temperature increase (T = 25 – 95 °C) on fluorescence spectra of **III**, c = 5 ×10^{-7} M (right); bottom: comparison of emission and excitation spectra of **III**. Measured in sodium cacodylate buffer (pH = 7.0, I = 0.05 M).

7.2.7 Studies of Interactions with DNA and RNA

Table S5. Groove widths and depths for selected nucleic acid conformations.[404, 405]

Structure type	Groove width [Å]		Groove depth [Å]	
	major	minor	major	minor
poly rA – poly rU[a]	3.8	10.9	13.5	2.8
poly dA – poly dT[b]	11.4	3.3	7.5	7.9
poly dGdC – poly dGdC[c]	13.5	9.5	10.0	7.2
poly dAdT – poly dAdT[c]	11.2	6.3	8.5	7.5

[a] A-helical structure (e.g. A-DNA); [b] C-helical structure (e.g. C-DNA); [c] B- helical structure (i.e. B-DNA)

Thermal Melting Experiments
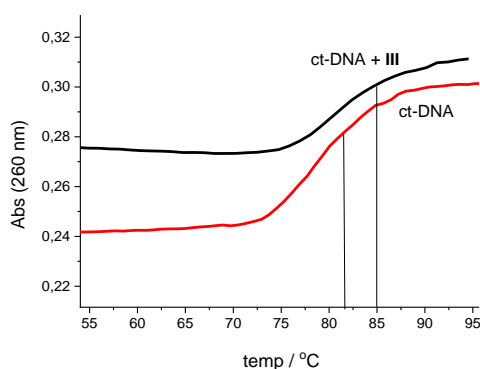
Figure S64. Thermal denaturation curves of ct-DNA (c(ct-DNA) = 2.5 × 10^{-5} M, $r_{[3]/[ct-DNA]}$ = 0.1) at pH 7.0 (sodium cacodylate buffer, I = 0.05 M) upon addition of **III**. Error in ΔTm values: ±0.5 °C.

Figure S65. Thermal denaturation curves of poly A – poly U (c(poly A – poly U) = 2.5 × 10^{-5} M, $r_{[3]/[poly A – poly U]}$ = 0.1) at pH 7.0 (sodium cacodylate buffer, I = 0.05 M) upon addition of **III**. Error in ΔTm values: ±0.5 °C.

Figure S66. Thermal denaturation curves of poly (dAdT)$_2$ (c(poly (dAdT)$_2$) = 2.5 × 10^{-5} M, r$_{[3]/[poly(dAdT)2]}$ = 0.1) at pH 7.0 (sodium cacodylate buffer, I = 0.05 M) upon addition of **III**. Error in ∆Tm values: ±0.5 °C.
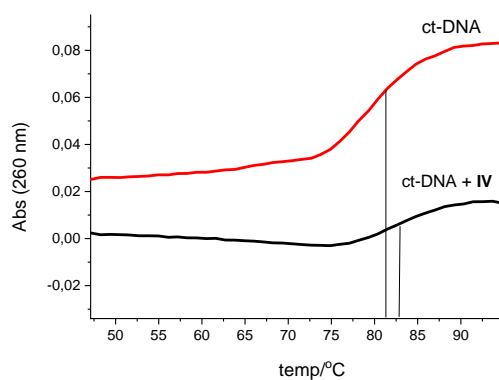
Figure S67. Thermal denaturation curves of ct-DNA (c(ct-DNA) = 2.5 × 10^{-5} M, r$_{[4]/[ct-DNA]}$ = 0.1) at pH 7.0 (sodium cacodylate buffer, I = 0.05 M) upon addition of **IV**. Error in ∆Tm values: ±0.5 °C.
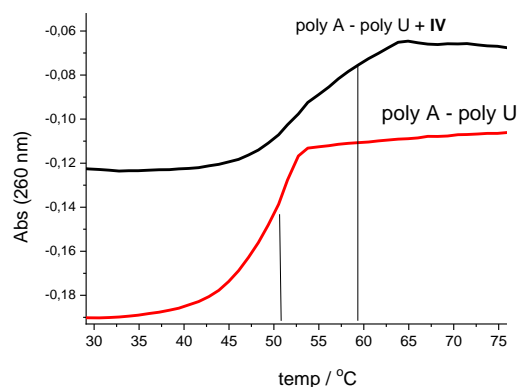
Figure S68. Thermal denaturation curves of poly A – poly U (c(poly A – poly U) = 2.5 × 10^{-5} M, r$_{[4]/[poly A – poly U]}$ = 0.1) at pH 7.0 (sodium cacodylate buffer, I = 0.05 M) upon addition of **IV**. Error in ∆Tm values: ±0.5 °C.
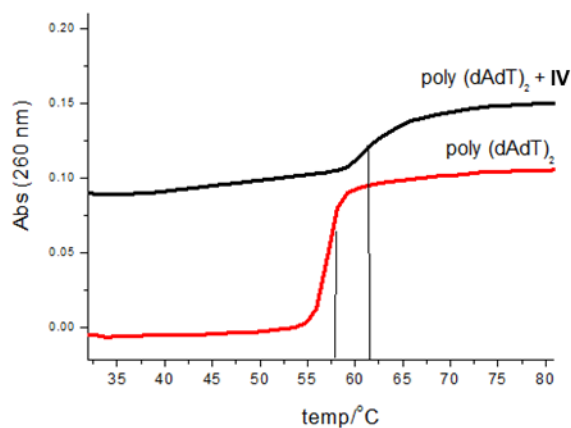
Figure S69. Thermal denaturation curves of poly (dAdT)$_2$ (c(poly (dAdT)$_2$) = 2.5 × 10^{-5} M, r$_{[4]/[\text{ poly(dAdT)2}]}$ = 0.1) at pH 7.0 (sodium cacodylate buffer, I = 0.05 M) upon addition of **IV**. Error in ΔTm values: ±0.5 °C.
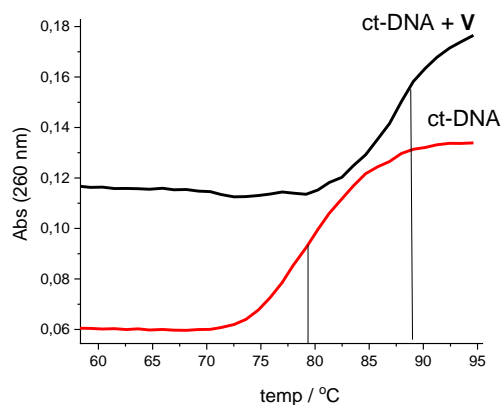
Figure S70. Thermal denaturation curves of ct-DNA (c(ct-DNA) = 2.5 × 10^{-5} M, r$_{[5]/[\text{ct-DNA}]}$ = 0.1) at pH 7.0 (sodium cacodylate buffer, I = 0.05 M) upon addition of **V**. Error in ΔTm values: ±0.5 °C.

Figure S71. Thermal denaturation curves of poly A – poly U (c(poly A – poly U) = 2.5 × 10^{-5} M, r$_{[5]/[\text{poly A – poly U}]}$ = 0.1) at pH 7.0 (sodium cacodylate buffer, I = 0.05 M) upon addition of **V**. Error in ΔTm values: ±0.5 °C.

Figure S72. Thermal denaturation curves of poly (dAdT)$_2$ (c(poly (dAdT)$_2$) = 2.5 × 10^{-5} M, r$_{[5]/[poly(dAdT)2]}$ = 0.1) at pH 7.0 (sodium cacodylate buffer, I = 0.05 M) upon addition of **V**. Error in ∆Tm values: ±0.5 °C.
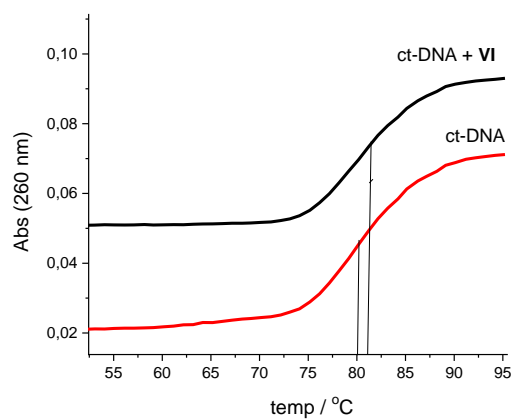
Figure S73. Thermal denaturation curves of ct-DNA (c(ct-DNA) = 2.5 × 10^{-5} M, r$_{[6]/[ct-DNA]}$ = 0.1) at pH 7.0 (sodium cacodylate buffer, I = 0.05 M) upon addition of **VI**. Error in ∆Tm values: ±0.5 °C.
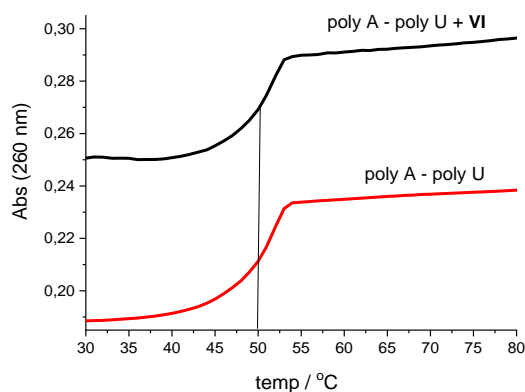
Figure S74. Thermal denaturation curves of poly A – poly U (c(poly A – poly U) = 2.5 × 10^{-5} M, r$_{[6]/[poly A – poly U]}$ = 0.3) at pH 7.0 (sodium cacodylate buffer, I = 0.05 M) upon addition of **VI**. Error in ∆Tm values: ±0.5 °C.

Fluorimetric Titrations
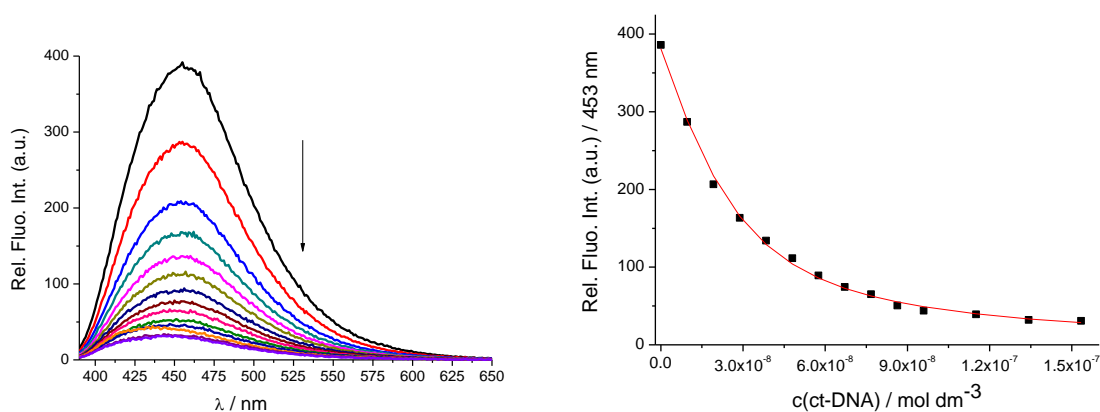
Figure S75. LEFT: Fluorimetric titration of **IV** (c = 5 ×10^{-9} M; λ_{exc}= 372 nm) with **ct-DNA**. RIGHT: Dependence of fluorescence at λ_{max} = 453 nm on c(DNA), red line is non-linear least square fitting of Scatchard eq. (McGhee, von Hippel formalism) to the experimental data. Measured at pH 7, sodium cacodylate buffer, I = 0.05 M
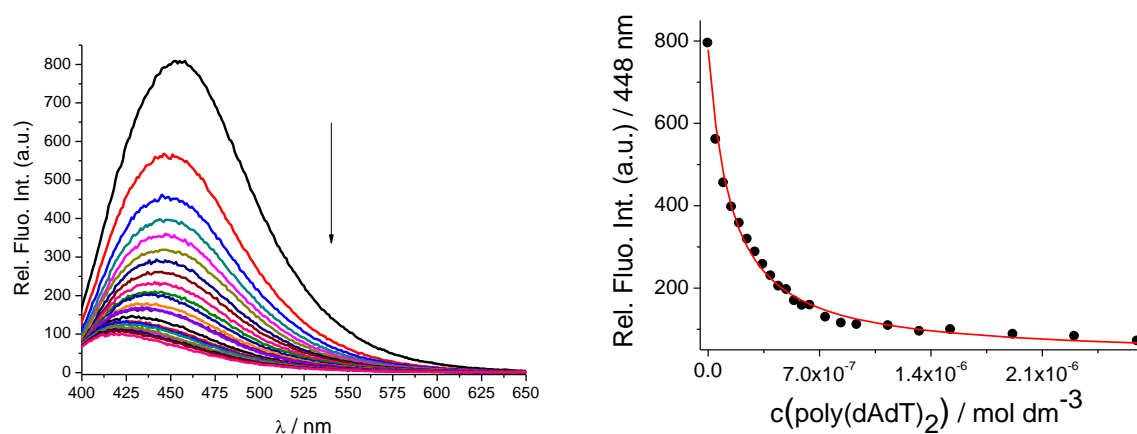
Figure S76. Left: Fluorimetric titration of **IV** (c = 5 ×10^{-9} M; λ_{exc}= 372 nm) with **poly (dAdT)$_2$**. Right: Dependence of fluorescence at λ_{max} = 448 nm on c(DNA), red line is non-linear least square fitting of Scatchard eq. (McGhee, von Hippel formalism) to the experimental data. Measured at pH 7, sodium cacodylate buffer, I = 0.05 M.
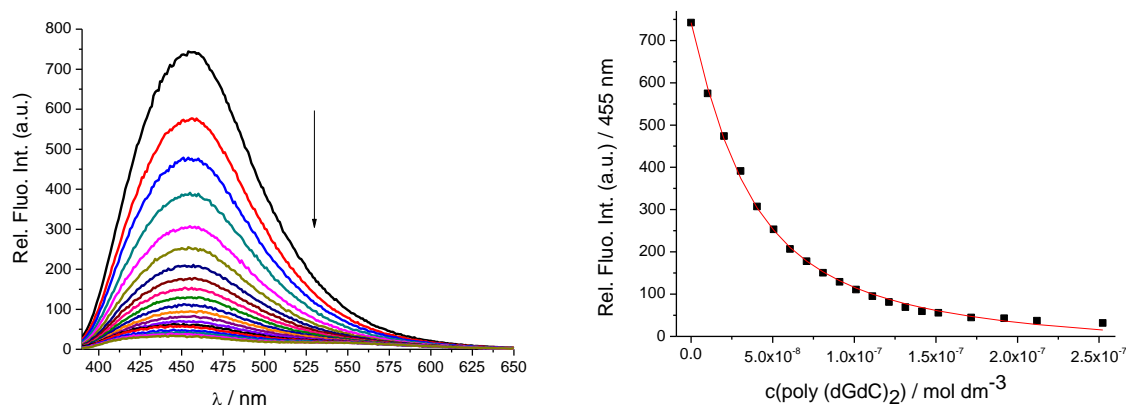
Figure S77. Left: Fluorimetric titration of **IV** (c = 5 ×10^{-9} M; λ_{exc}= 372 nm) with **poly (dGdC)$_2$**. Right: Dependence of fluorescence at λ_{max} = 455 nm on c(DNA), red line is non-linear least square fitting of Scatchard eq. (McGhee, von Hippel formalism) to the experimental data. Measured at pH 7, sodium cacodylate buffer, I = 0.05 M.
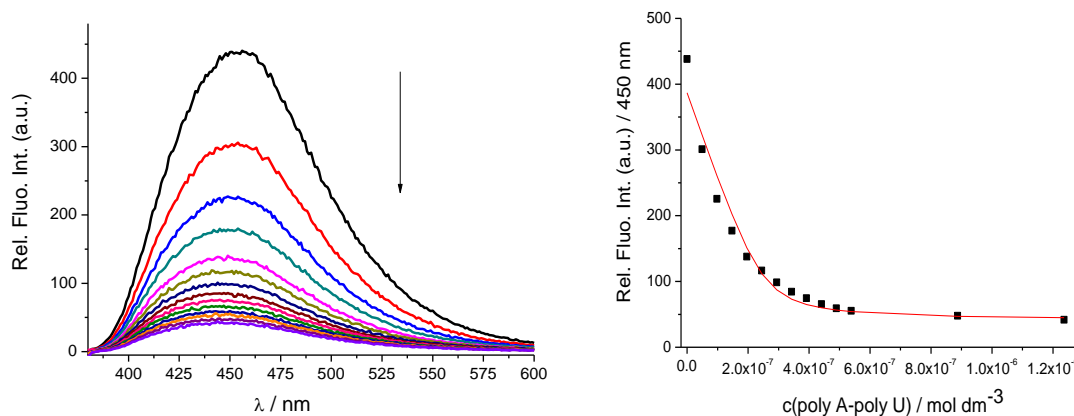
Figure S78. Left: Fluorimetric titration of **IV** (c = 5 ×10^{-8} M; λ_{exc}= 372 nm) with **poly A - poly U**. Right: Dependence of fluorescence at λ_{max} = 450 nm on c(RNA), red line is non-linear least square fitting of Scatchard eq. (McGhee, von Hippel formalism) to the experimental data. Measured at pH 7, sodium cacodylate buffer, I = 0.05 M.
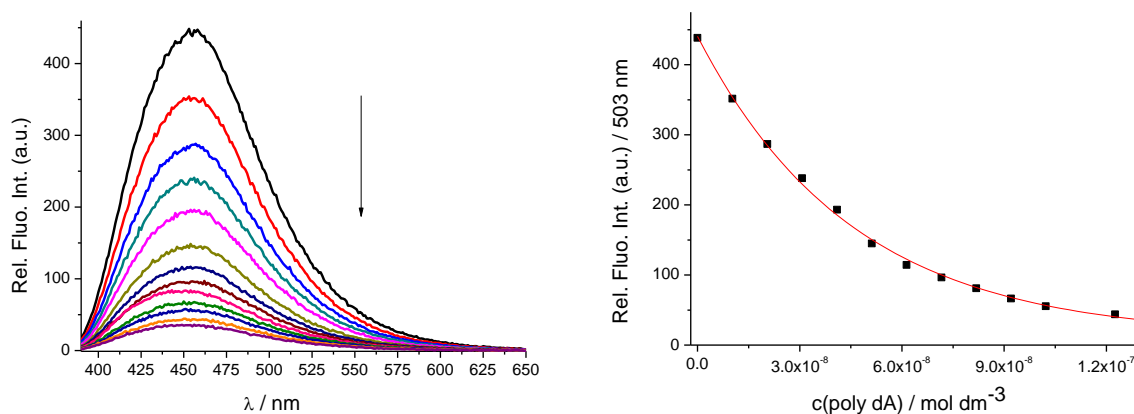
Figure S79. Left: Fluorimetric titration of **IV** (c = 5 ×10^{-8} M; λ_{exc}= 372 nm) with **poly dA**. Right: Dependence of fluorescence at λ_{max} = 503 nm on c(DNA), red line is non-linear least square fitting of Scatchard eq. (McGhee, von Hippel formalism) to the experimental data. Measured at pH 7, sodium cacodylate buffer, I = 0.05 M.
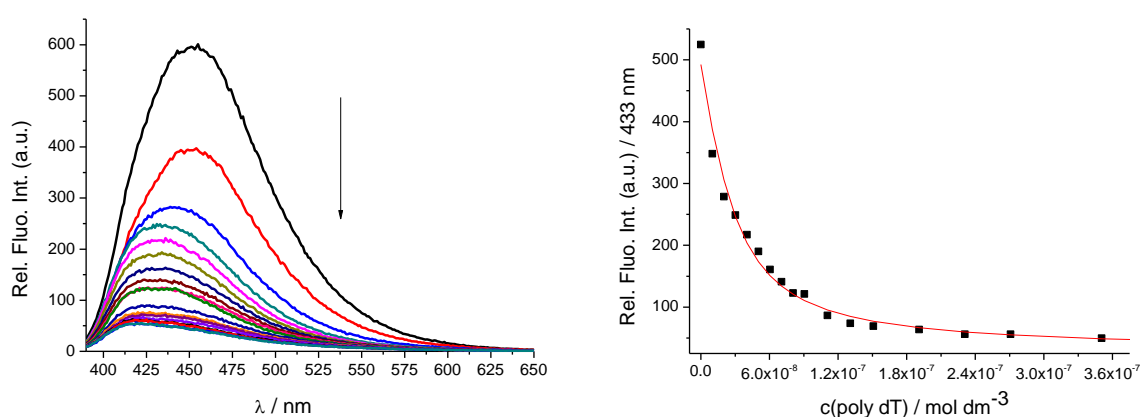
Figure S80. Left: Fluorimetric titration of **IV** (c = 5 ×10^{-9} M; λ_{exc}= 372 nm) with **poly dT**. Right: Dependence of fluorescence at λ_{max} = 433 nm on c(DNA), red line is non-linear least square fitting of Scatchard eq. (McGhee, von Hippel formalism) to the experimental data. Measured at pH 7, sodium cacodylate buffer, I = 0.05 M.
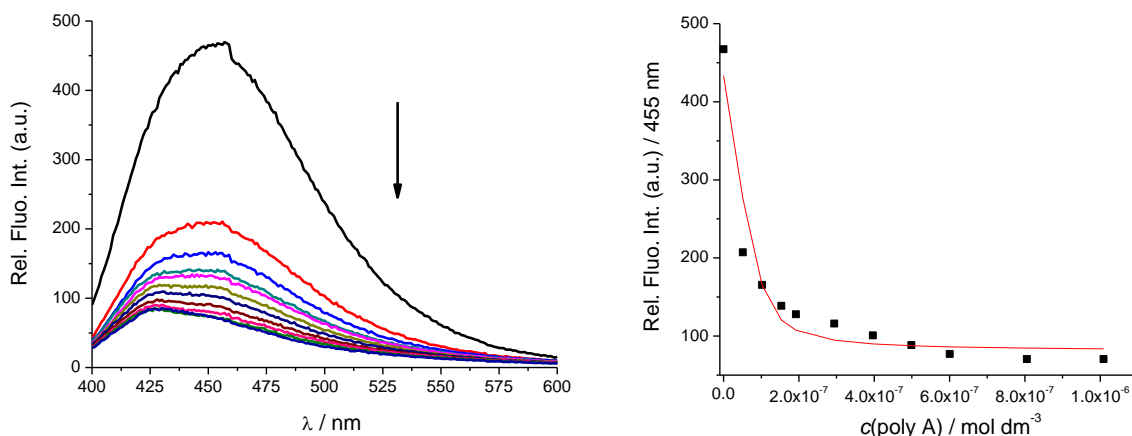
Figure S81. Left: Fluorimetric titration of **IV** (c = 5 ×10^{-8} M; λ_{exc}= 372 nm) with **poly A**. Right: Dependence of fluorescence at λ_{max} = 455 nm on c(RNA), red line is non-linear least square fitting of Scatchard eq. (McGhee, von Hippel formalism) to the experimental data. Measured at pH 7, sodium cacodylate buffer, I = 0.05 M.
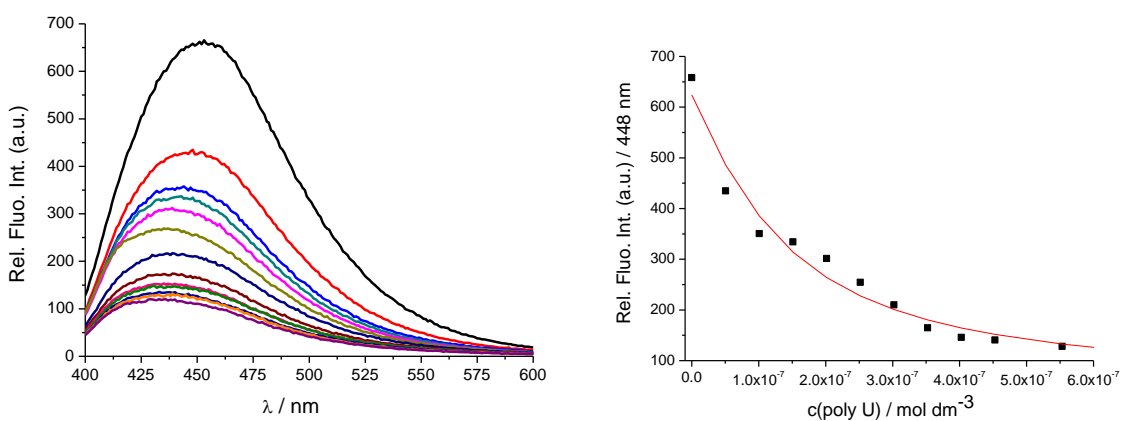
Figure S82. Left: Fluorimetric titration of **IV** (c = 5 ×10^{-8} M; λ_{exc}= 372 nm) with **poly U**. Right: Dependence of fluorescence at λ_{max} = 448 nm on c(RNA), red line is non-linear least square fitting of Scatchard eq. (McGhee, von Hippel formalism) to the experimental data. Measured at pH 7, sodium cacodylate buffer, I = 0.05 M.
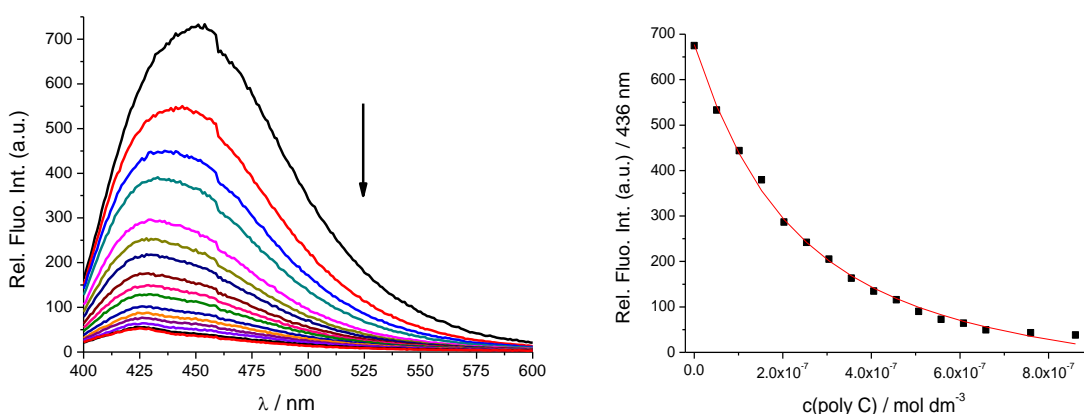
Figure S83. Left: Fluorimetric titration of **IV** (c = 5 ×10^{-8} M; λ_{exc}= 372 nm) with **poly C**. Right: Dependence of fluorescence at λ_{max} = 436 nm on c(RNA), red line is non-linear least square fitting of Scatchard eq. (McGhee, von Hippel formalism) to the experimental data. Measured at pH 7, sodium cacodylate buffer, I = 0.05 M.
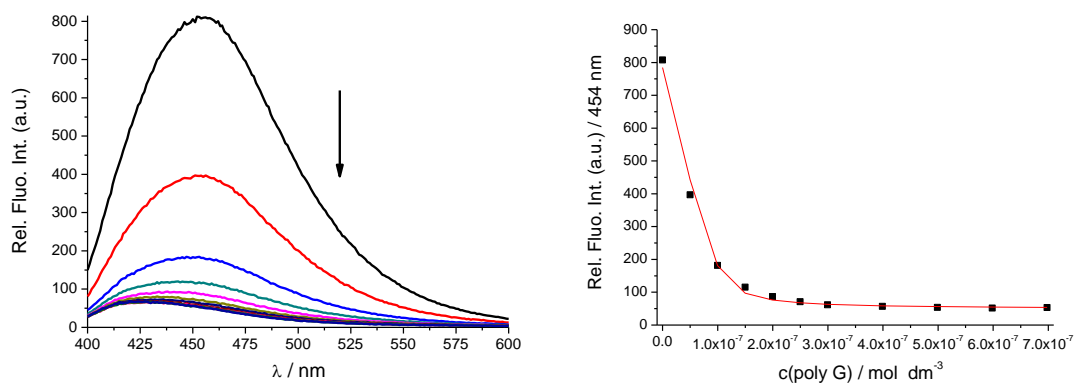
Figure S84. Left: Fluorimetric titration of **IV** ($c = 5 \times 10^{-8}$ M; $\lambda_{exc}= 372$ nm) with **poly G**. Right: Dependence of fluorescence at $\lambda_{max} = 454$ nm on c(RNA), red line is non-linear least square fitting of Scatchard eq. (McGhee, von Hippel formalism) to the experimental data. Measured at pH 7, sodium cacodylate buffer, $I = 0.05$ M.
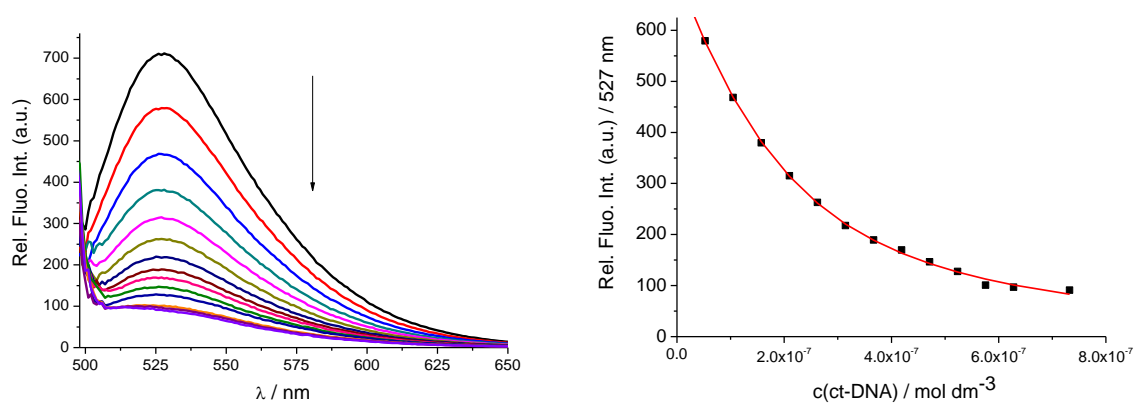
Figure S85. Left: Fluorimetric titration of **VI** ($c = 5 \times 10^{-8}$ M; $\lambda_{exc}= 476$ nm) with **ct-DNA**. Right: dependence of fluorescence at $\lambda_{max} = 527$ nm on c(DNA), red line is non-linear least square fitting of Scatchard eq. (McGhee, von Hippel formalism) to the experimental data. Measured at pH 7, sodium cacodylate buffer, $I = 0.05$ M.
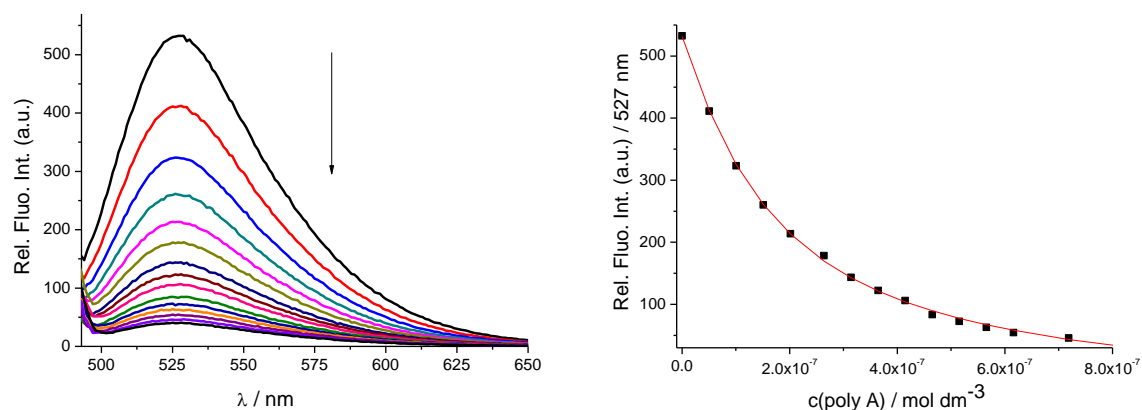
Figure S86. Left: Fluorimetric titration of **VI** ($c = 5 \times 10^{-8}$ M; $\lambda_{exc}= 476$ nm) with **poly A**. Right: dependence of fluorescence at $\lambda_{max} = 527$ nm on c(RNA), red line is non-linear least square fitting of Scatchard eq. (McGhee, von Hippel formalism) to the experimental data. Measured at pH 7, sodium cacodylate buffer, $I = 0.05$ M.
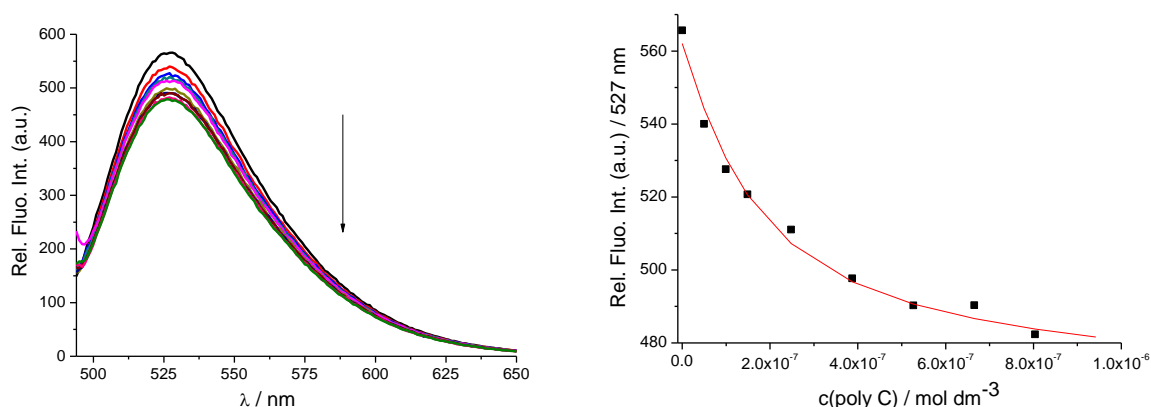
Figure S87. Left: Fluorimetric titration of **VI** (c = 5 ×10^{-8} M; λ_{exc}= 476 nm) with **poly C** Right: dependence of fluorescence at λ_{max} = 527 nm on c(RNA), red line is non-linear least square fitting of Scatchard eq. (McGhee, von Hippel formalism) to the experimental data. Measured at pH 7, sodium cacodylate buffer, I = 0.05 M.
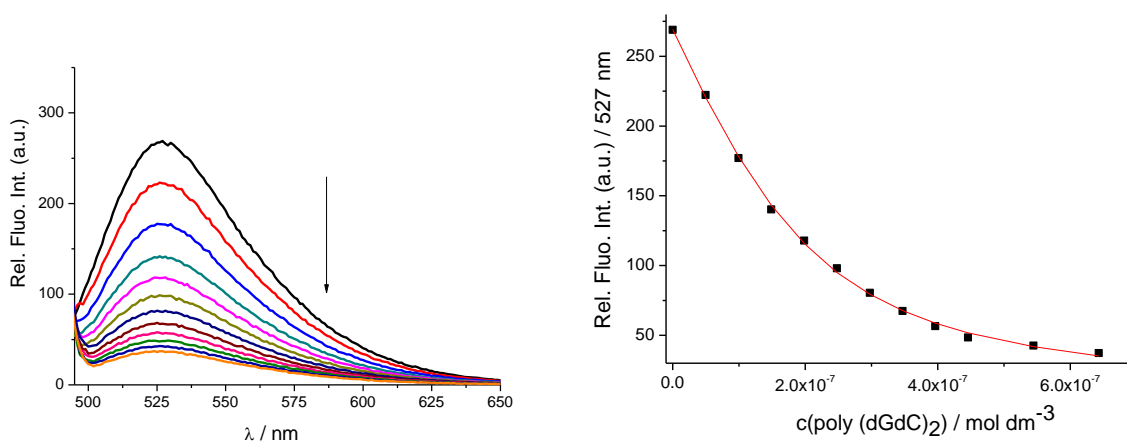
Figure S88. Left: Fluorimetric titration of **VI** (c = 5 ×10^{-8} M; λ_{exc}= 476 nm) with **poly (dGdC)$_2$** Right: dependence of fluorescence at λ_{max} = 527 nm on c(DNA), red line is non-linear least square fitting of Scatchard eq. (McGhee, von Hippel formalism) to the experimental data. Measured at pH 7, sodium cacodylate buffer, I = 0.05 M.
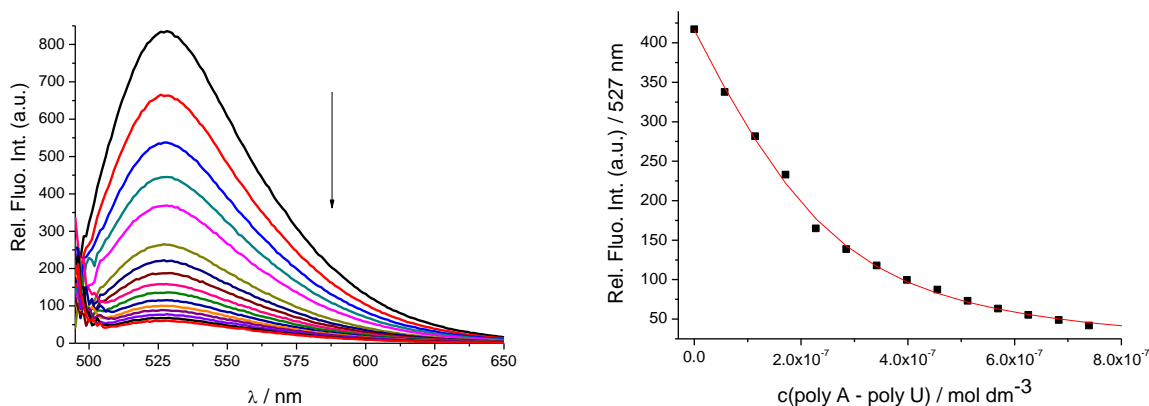
Figure S89. Left: Fluorimetric titration of **VI** (c = 5 ×10-8 M; λ_{exc}= 476 nm) with **poly A – poly U**. Right: dependence of fluorescence at λ_{max} = 527 nm on c(RNA), red line is non-linear least square fitting of Scatchard eq. (McGhee, von Hippel formalism) to the experimental data. Measured at pH 7, sodium cacodylate buffer, I = 0.05 M.

Figure S90. Left: Fluorimetric titration of **VI** (c = 5 ×10⁻⁸ M; λ_{exc}= 476 nm) with **poly U**. Right: dependence of fluorescence at λ_{max} = 527 nm on c(RNA), red line is non-linear least square fitting of Scatchard eq. (McGhee, von Hippel formalism) to the experimental data. Measured at pH 7, sodium cacodylate buffer, I = 0.05 M.

Figure S91. Left: Fluorimetric titration of **VI** (c = 5 ×10⁻⁸ M; λ_{exc}= 476 nm) with **poly G**. Right: dependence of fluorescence at λ_{max} = 527 nm on c(RNA), red line is non-linear least square fitting of Scatchard eq. (McGhee, von Hippel formalism) to the experimental data. Measured at pH 7, sodium cacodylate buffer, I = 0.05 M.

Figure S92. Left: Fluorimetric titration of **VI** (c = 5 ×10⁻⁸ M; λ_{exc}= 476 nm) with **poly (dAdT)₂**. Right: dependence of fluorescence at λ_{max} = 527 nm on c(DNA), red line is non-linear least square fitting of Scatchard eq. (McGhee, von Hippel formalism) to the experimental data. Measured at pH 7, sodium cacodylate buffer, I = 0.05 M.
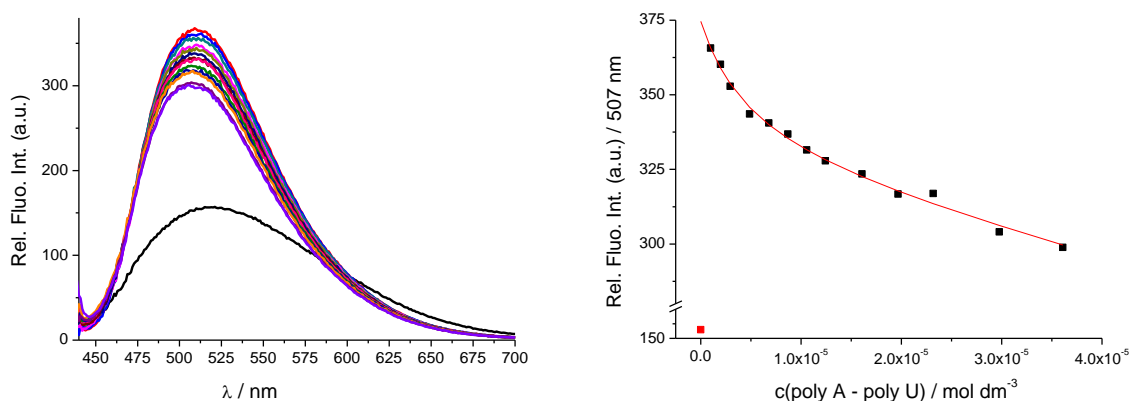
Figure S93. Left: Fluorimetric titration of **III** ($c = 5 \times 10^{-8}$ M; $\lambda_{exc}= 412$ nm) with **poly A-poly U**. Right: dependence of fluorescence at $\lambda_{max} = 507$ nm on c(RNA), red line is non-linear least square fitting of Scatchard eq. (McGhee, von Hippel formalism) to the experimental data. Measured at pH 7, sodium cacodylate buffer, $I = 0.05$ M.
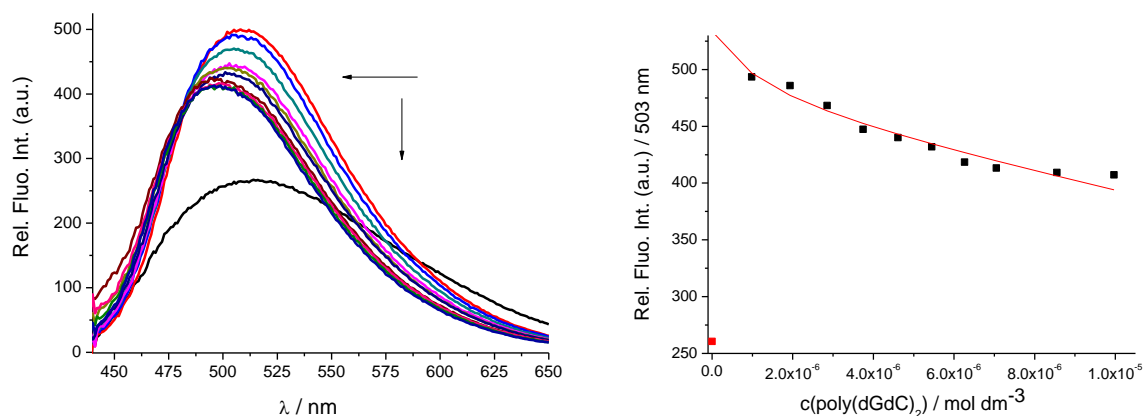
Figure S94. Left: Fluorimetric titration of **III** ($c = 5 \times 10^{-8}$ M; $\lambda_{exc}= 412$ nm) with **poly (dGdC)₂**. Right: dependence of fluorescence at $\lambda_{max} = 503$ nm on c(DNA), red line is non-linear least square fitting of Scatchard eq. (McGhee, von Hippel formalism) to the experimental data. Measured at pH 7, sodium cacodylate buffer, $I = 0.05$ M.
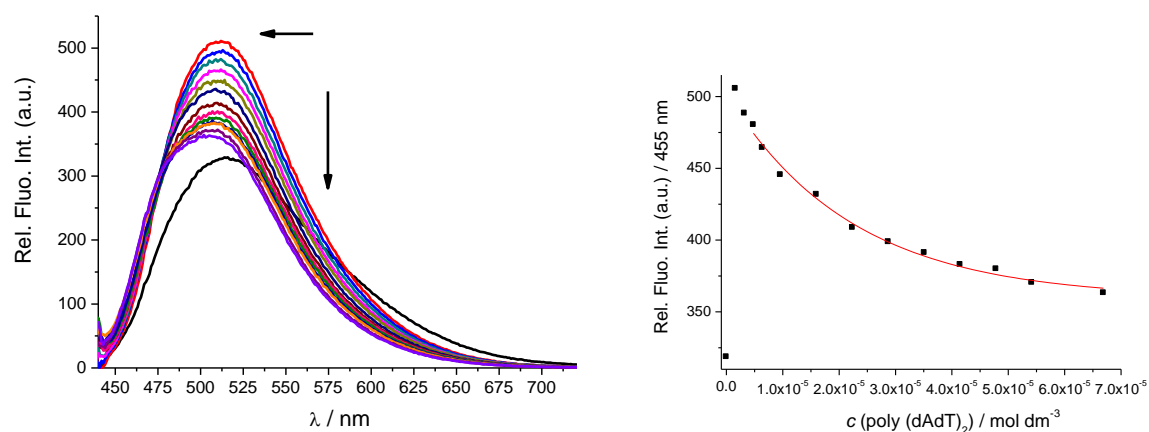
Figure S95. Left: Fluorimetric titration of **III** ($c = 5 \times 10^{-8}$ M; $\lambda_{exc}= 412$ nm) with **poly (dAdT)₂**. Right: dependence of fluorescence at $\lambda_{max} = 455$ nm on c(DNA), red line is non-linear least square fitting of Scatchard eq. (McGhee, von Hippel formalism) to the experimental data. Measured at pH 7, sodium cacodylate buffer, $I = 0.05$ M.
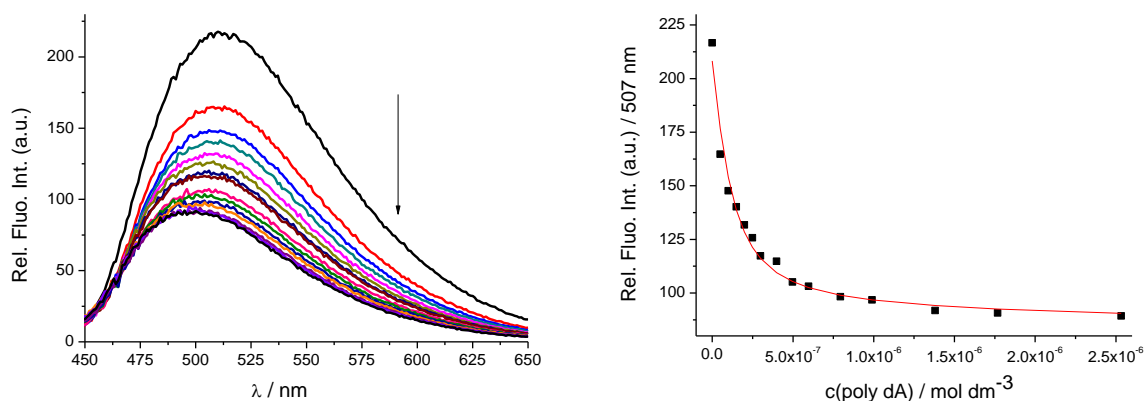
Figure S96. Left: Fluorimetric titration of **III** (c = 5 ×10^{-8} M; λ_{exc}= 412 nm) with **poly dA**. Right: dependence of fluorescence at λ_{max} = 507 nm on c(DNA), red line is non-linear least square fitting of Scatchard eq. (McGhee, von Hippel formalism) to the experimental data. Measured at pH 7, sodium cacodylate buffer, I = 0.05 M.
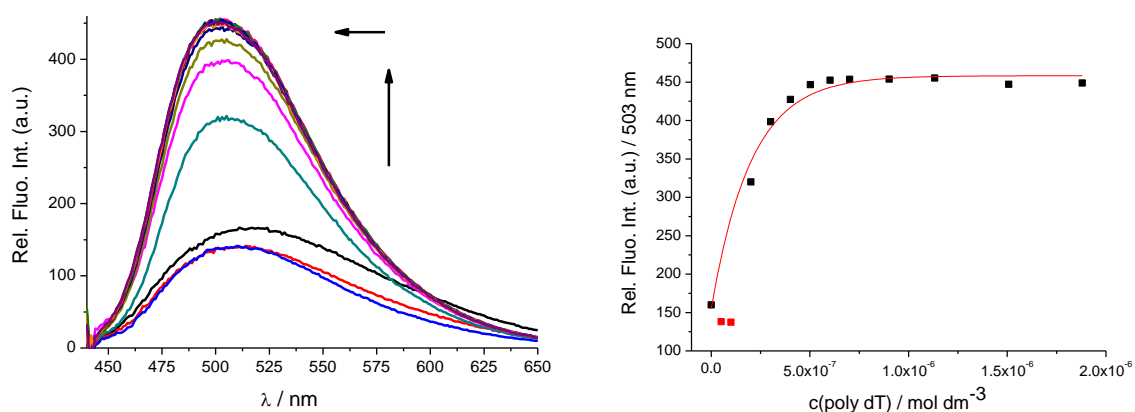
Figure S97. Left: Fluorimetric titration of **III** (c = 5 ×10^{-8} M; λ_{exc}= 412 nm) with **poly dT**. Right: dependence of fluorescence at λ_{max} = 503 nm on c(DNA), red line is non-linear least square fitting of Scatchard eq. (McGhee, von Hippel formalism) to the experimental data. Measured at pH 7, sodium cacodylate buffer, I = 0.05 M.

Figure S98. Left: Fluorimetric titration of **III** (c = 5 ×10^{-8} M; λ_{exc}= 412 nm) with **poly A**. Right: dependence of fluorescence at λ_{max} = 484 nm on c(RNA), red line is non-linear least square fitting of Scatchard eq. (McGhee, von Hippel formalism) to the experimental data. Measured at pH 7, sodium cacodylate buffer, I = 0.05 M.
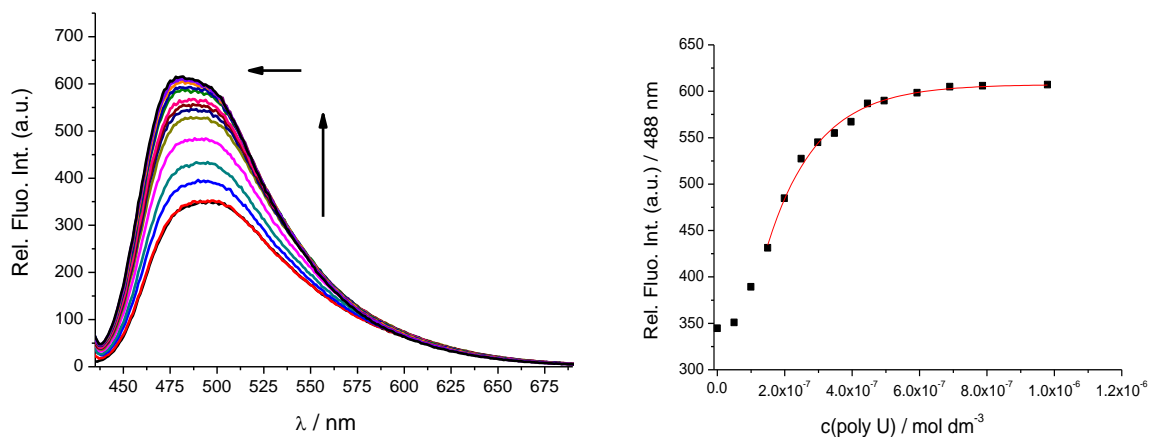
Figure S99. Left: Fluorimetric titration of **III** (c = 5 ×10^{-8} M; λ_{exc}= 412 nm) with **poly U**. Right: dependence of fluorescence at λ_{max} = 488 nm on c(RNA), red line is non-linear least square fitting of Scatchard eq. (McGhee, von Hippel formalism) to the experimental data. Measured at pH 7, sodium cacodylate buffer, I = 0.05 M.
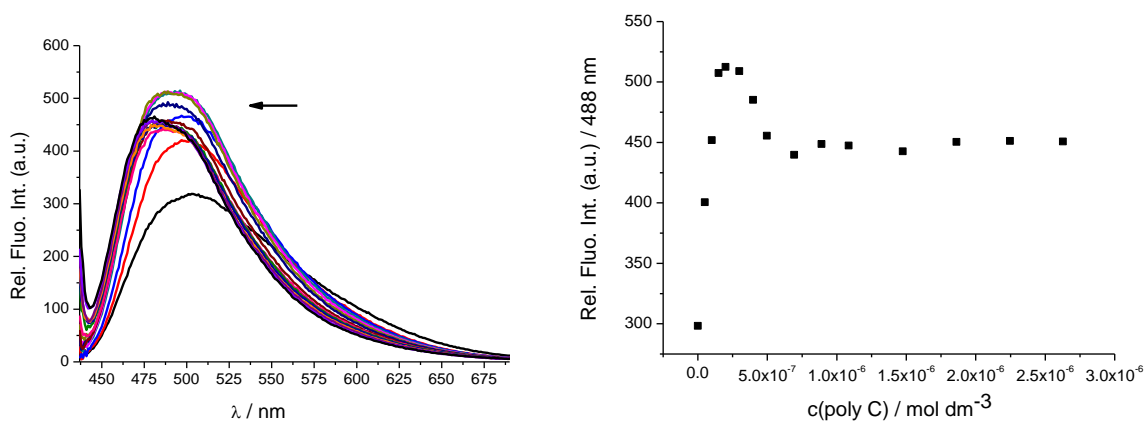
Figure S100. Left**:** Fluorimetric titration of **III** (c = 5 ×10^{-8} M; λ_{exc}= 412 nm) with **poly C**. Right: dependence of fluorescence at λ_{max} = 488 nm. Measured at pH 7, sodium cacodylate buffer, I = 0.05 M.
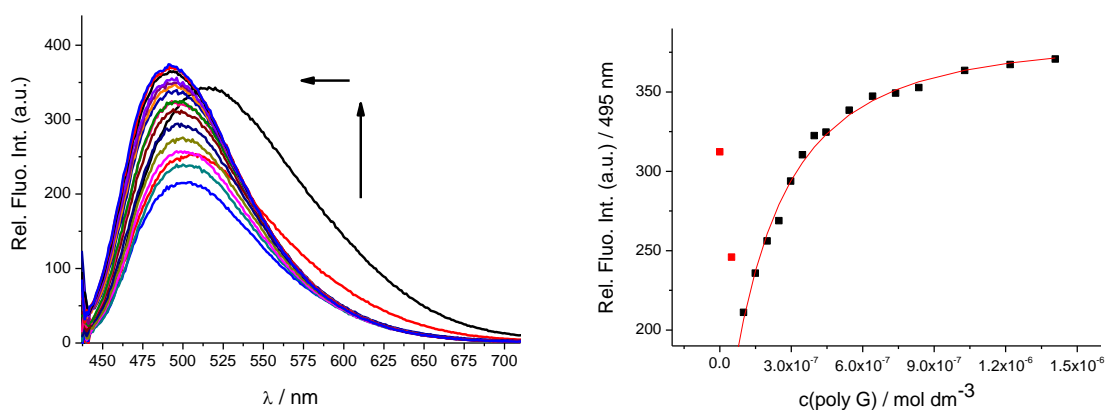
Figure S101. Left: Fluorimetric titration of **III** (c = 5 ×10^{-8} M; λ_{exc}= 412 nm) with **poly G**. Right: dependence of fluorescence at λ_{max} = 495 nm on c(RNA), red line is non-linear least square fitting of Scatchard eq. (McGhee, von Hippel formalism) to the experimental data. Measured at pH 7, sodium cacodylate buffer, I = 0.05 M.
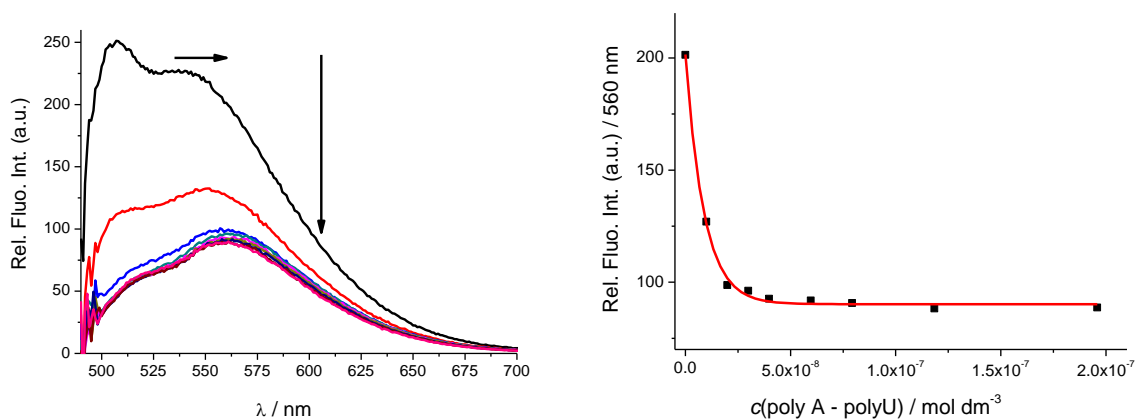
Figure S102. Left: Fluorimetric titration of **V** (c = 1 ×10^{-8} M; λ$_{exc}$= 470 nm) with **poly A- poly U**. Right: Dependence of fluorescence at λ$_{max}$ = 560 nm on c(RNA). Measured at pH 7, sodium cacodylate buffer, I = 0.05 M.
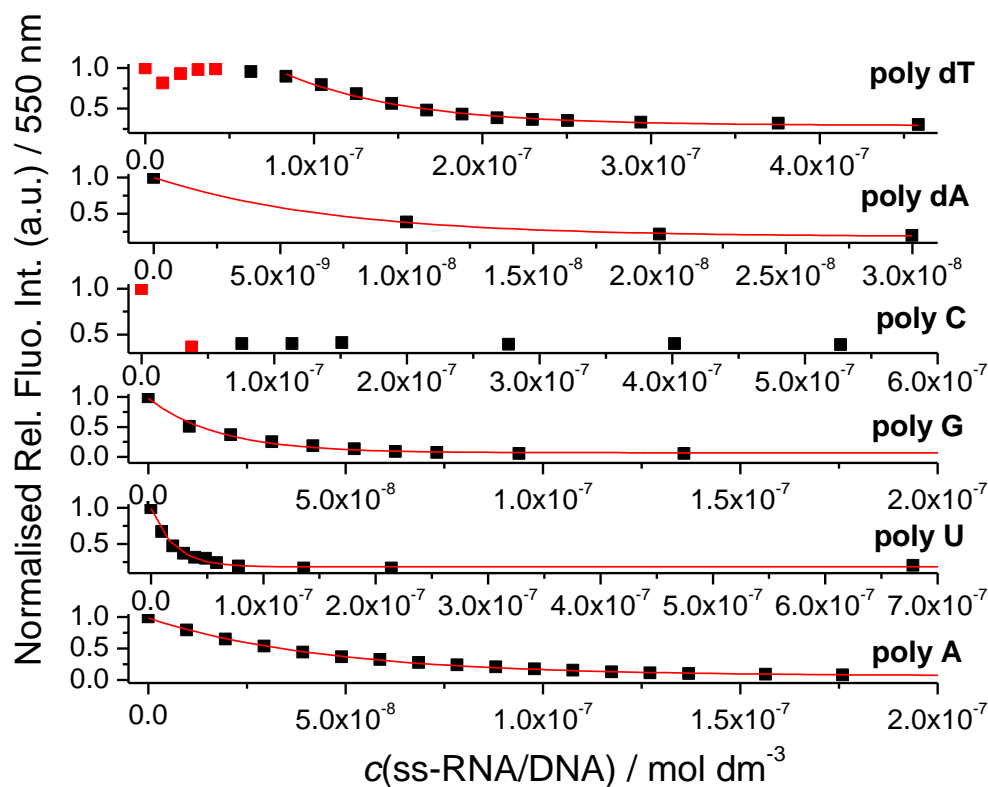
Figure S103. Fluorimetric titrations of **V** (c = 1 ×10^{-8} M; λ$_{exc}$= 470 nm) with **ss-DNA/RNA**; dependence of normalized fluorescence at λ$_{max}$ = 550 nm on c(DNA/RNA). Measured at pH 7, sodium cacodylate buffer, I = 0.05 M.

Circular Dichroism
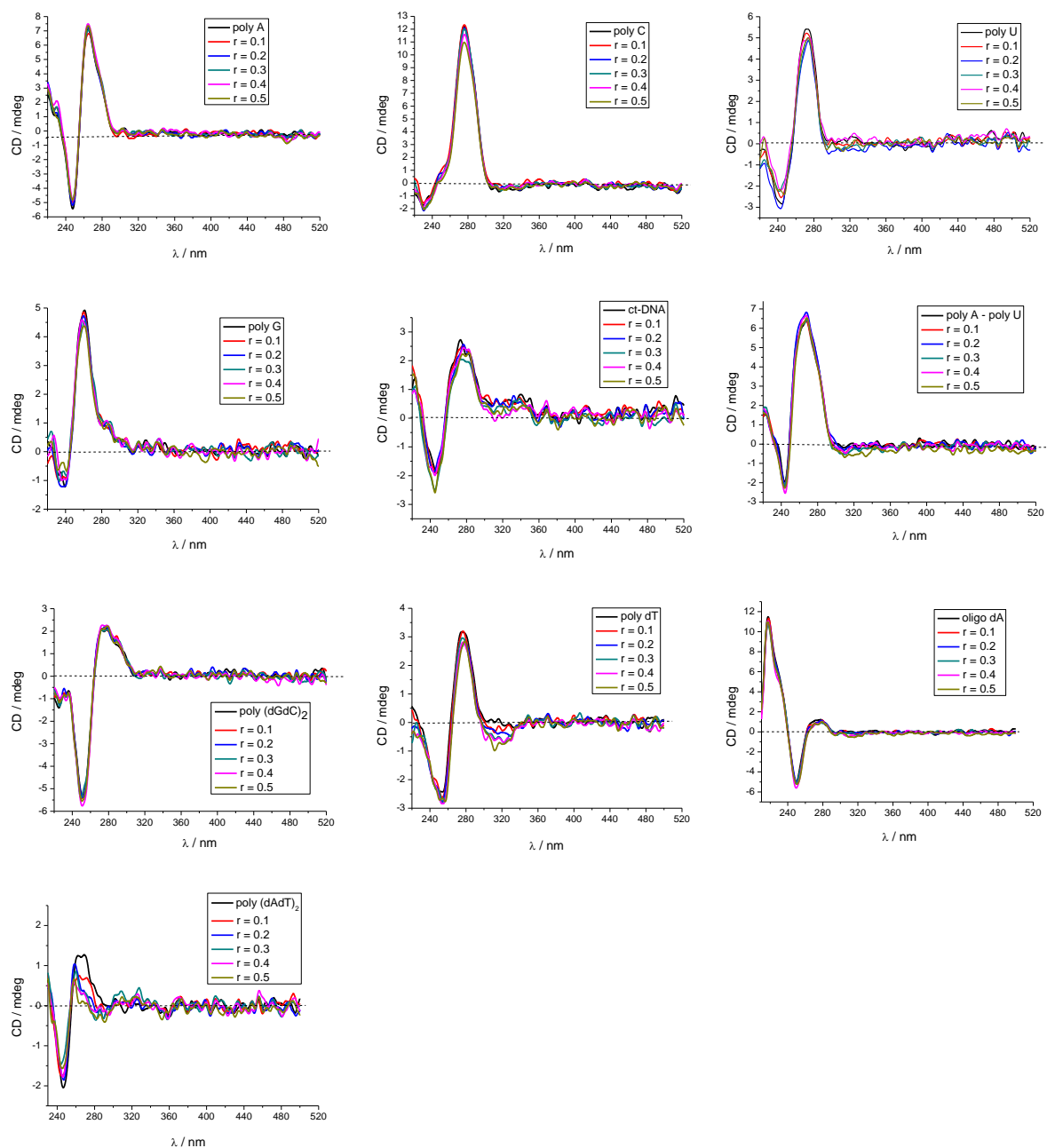
Figure S104. CD titration of **poly A**, **poly C**, **poly U**, **poly G**, **ct-DNA**, **poly A - poly U**, **poly (dGdC)$_2$**, **poly dT**, **oligo dA** and **poly (dAdT)$_2$** (all ss-DNA, DNA/RNA c = 2×10^{-5} M) with **VI** at molar ratios r = [compound] / [polynucleotide] (pH 7.0, sodium cacodylate buffer, I = 0.05 M).
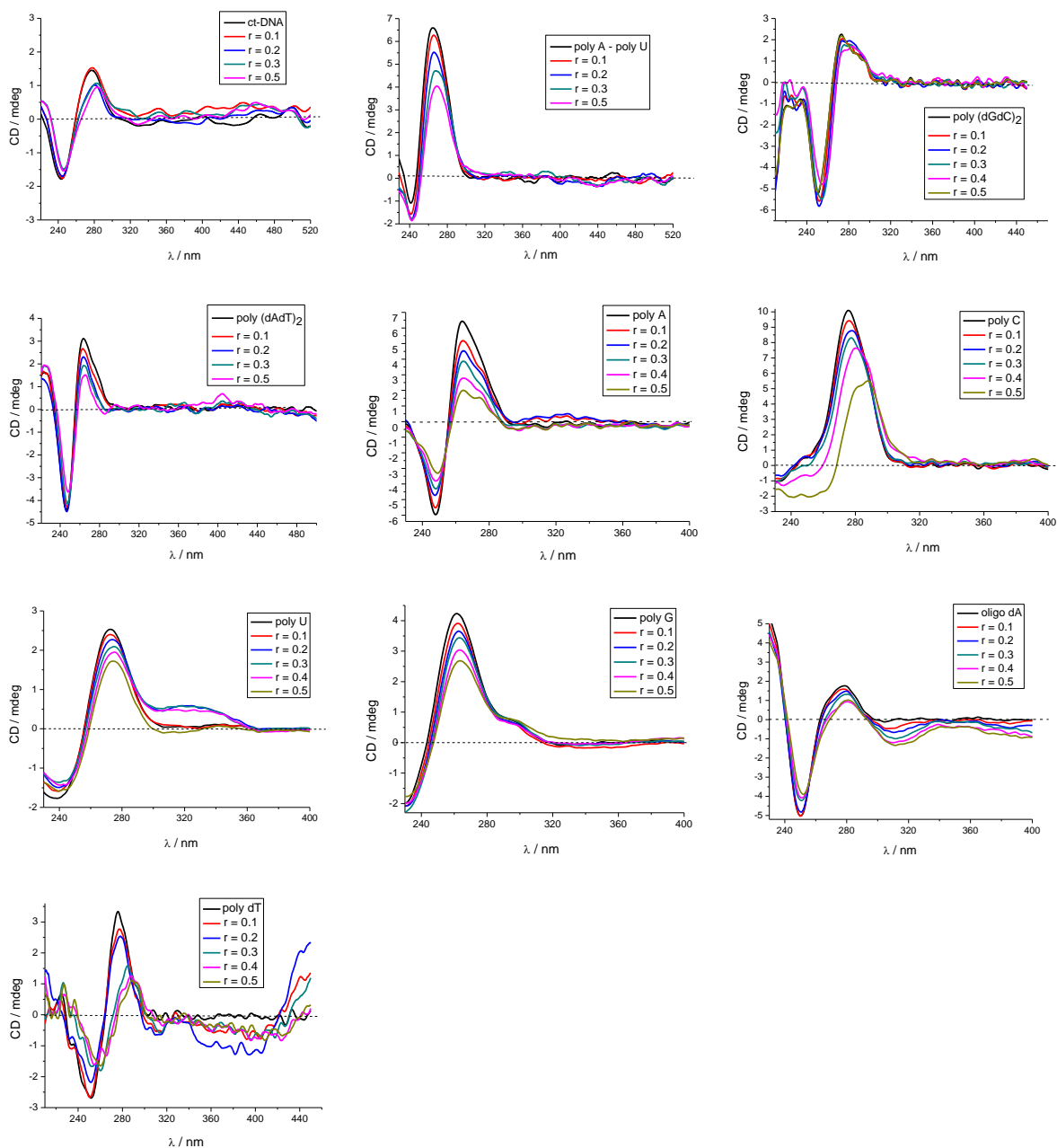
Figure S105. CD titration of **ctDNA**, **poly A - poly U**, **poly (dAdT)₂**, **poly (dGdC)₂**, **poly A** ($c = 1{\times}10^{-5}$ M), **poly C**, **poly U**, **poly G**, **oligo dA**, **poly dT** (all ss-DNA, DNA/RNA $c = 2{\times}10^{-5}$ M) with **III** at molar ratios $r =$ [compound] / [polynucleotide] (pH 7.0, sodium cacodylate buffer, $I = 0.05$ M).
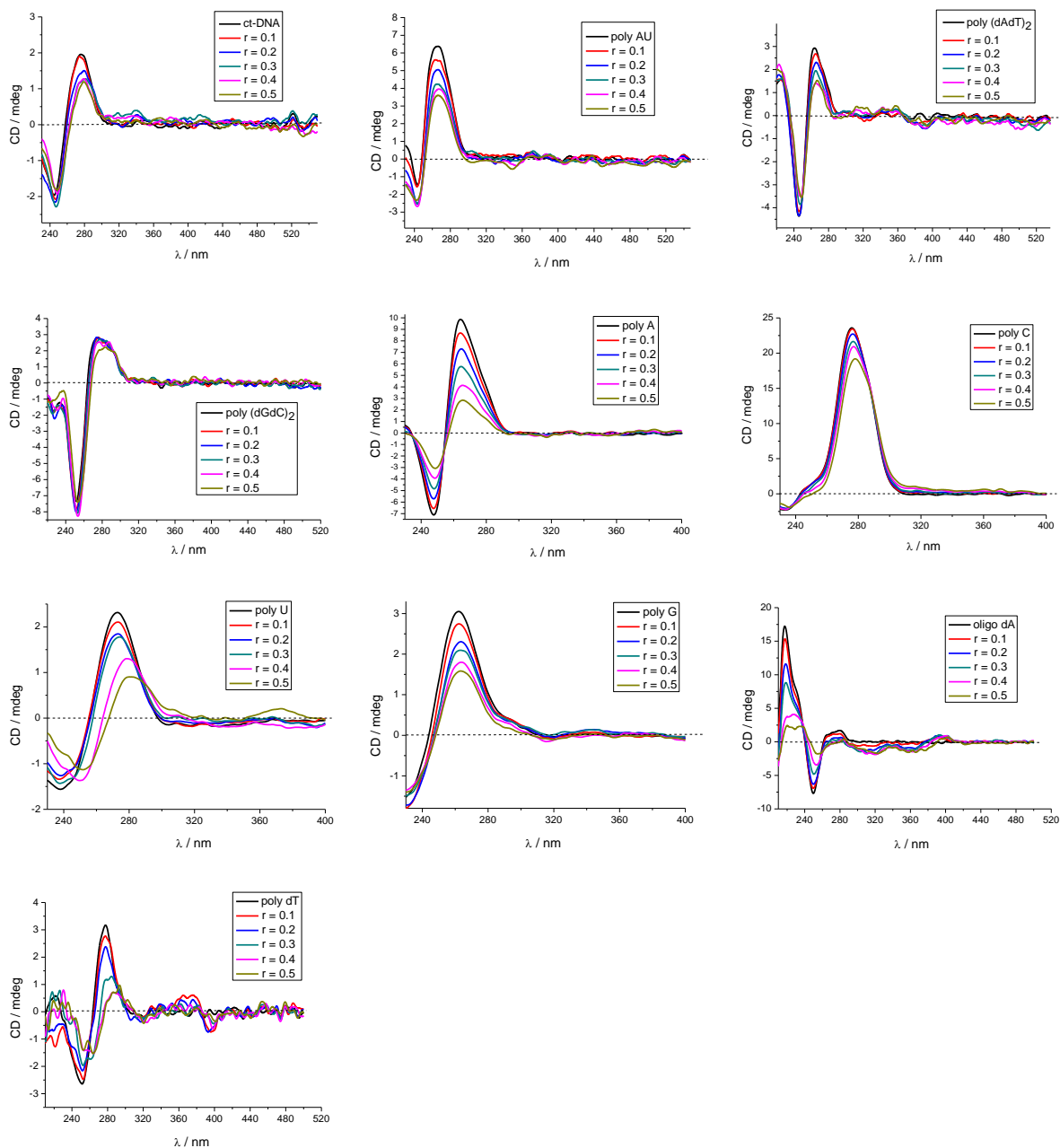
Figure S106. CD titration of **ctDNA**, **poly A - poly U**, **poly (dAdT)₂**, **poly (dGdC)₂**, **poly A** ($c = 1\times10^{-5}$ M**), poly C**, **poly U**, **poly G**, **oligo dA**, **poly dT** (all ss-DNA, DNA/RNA $c = 2\times10^{-5}$ M) with **IV** at molar ratios r = [compound] / [polynucleotide] (pH 7.0, sodium cacodylate buffer, $I = 0.05$ M).
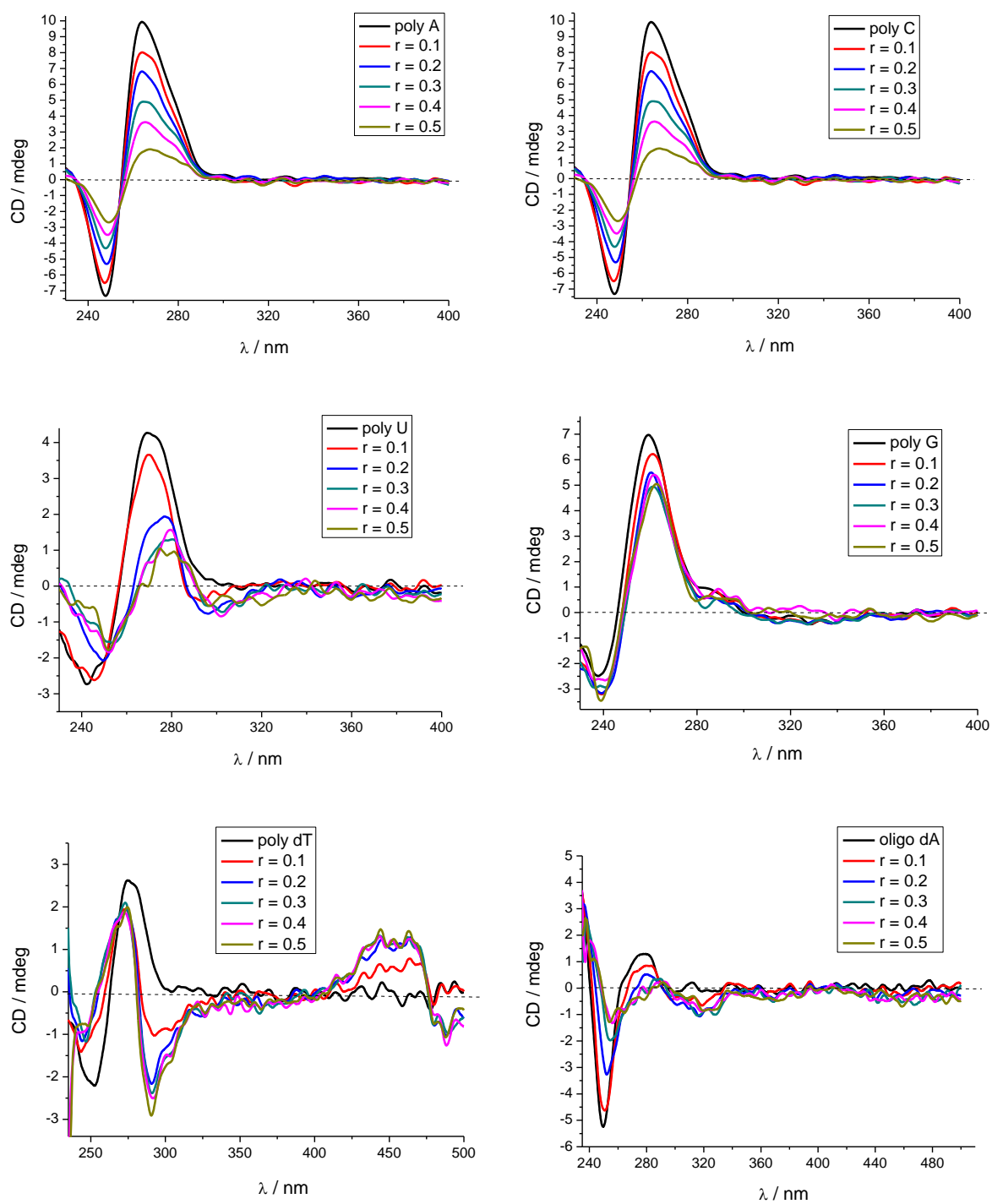
Figure S107. CD titrations of **poly A** ($c = 1 \times 10^{-5}$ M), **poly C**, **poly U**, **poly G**, **poly dT**, **oligo dA** (all ss-DNA/RNA $c = 2 \times 10^{-5}$ M), with compound **V** at molar ratios $r = $ [compound] / [polynucleotide] (pH 7.0, sodium cacodylate buffer, $I = 0.05$ M).

7.2.8 Raman and SERS Measurements

Table S6. A preliminary assignment of the Raman bands observed in the spectra of aqueous solution of **III-V** ($c = 1 \times 10^{-4}$ M).

Wavenumber / cm^{-1}			Assignment
III	**IV**	**V**	
	2209	2182	ν C≡C
1595	1591	1594	ν CC (aromatic linker)
		1556	ν CC (anthracene)
		1481	ν CC (anthracene)
1472			ν CC (thiophene)
1453			ν CS (thiophene)
		1257	δ_{ip} CH (anthracene)
		1158	δ_{ip} CH (anthracene)

Figure S108. Raman spectra of aqueous solution of **III-V** ($c = 1 \times 10^{-4}$ M) and **VI** ($c = 2 \times 10^{-3}$ M); λ_{ex} = 1064 nm. Spectra are displaced for visual clarity.

Table S7. A preliminary assignment of the SERS bands observed in the spectra of **III-V** (c = 1 ×10^{-6} M) and **VI** (c = 5 ×10^{-6} M).

Wavenumber / cm^{-1}				Assignment
III	IV	V	VI	
2196	2205	2184		ν C≡C
1594	1591	1594	1588	ν CC (aromatic linker)
		1557	1549	ν CC (anthracene)
1546				ν ring (thiophene)
		1483		ν CC (anthracene)
			1463	ν CC (phenyl)
1473				ν CC (thiophene)
1455				ν CS (thiophene)
			1421	ν CC (phenyl)
1403	1395	1407	1405	citrates
			1329	δ_{ip} CH (anthracene)
1310				ν ring (thiophene)
		1257	1263	δ_{ip} CH (anthracene)
1242				δ_{ip} CH (thiophene)
	1227			δ_{ip} CH (phenyl)
			1224	δ_{ip} CH (anthracene)
1192				δ_{ip} CH (thiophene)
	1179			δ_{ip} CH (phenyl)
		1169	1160	δ_{ip} CH (anthracene)
	1126			δ_{ip} CH (phenyl)
1083	1083	1073	1081	ν B–(C$_{ar}$)$_3$
1045				δ_{ip} CH (thiophene)
		1022	1040	δ_{ip} CH (anthracene)
951	953	946		δ_{ip} CH (phenyl)
843				ν ring (thiophene)
799	803	800	769	δ_{oop} CH (phenyl)
574	576	577		δ CC (phenyl)

7.2.9 Theoretical Studies

TD-DFT Calculations

For compounds **III**-**V,** DFT and TD-DFT studies were carried out at the B3LYP/6-31G(d) (optimization) and CAM-B3LYP/6-31G(d) level of theory, respectively. The calculated lowest energy transitions for compounds **III**-**V** in the gas phase underestimate the transition energies as compared to the data obtained in MeCN solution (**III**: $\lambda_{max,\,abs}$ (MeCN) = 413 nm, calc. $S_1 \leftarrow S_0$ = 483 nm; **IV**: $\lambda_{max,\,abs}$ (MeCN) = 373 nm, calc. $S_1 \leftarrow S_0$ = 415 nm; **V**: $\lambda_{max,\,abs}$ (MeCN) = 483 nm, calc. $S_1 \leftarrow S_0$ = 538 nm). The trend in absorption energies between the three compounds is well reproduced (**IV** > **III** > **V**). In all cases, the $S_1 \leftarrow S_0$ transitions can be predominantly attributed (contribution > 60%) to HOMO to LUMO transitions. In all three cases, the HOMO is localized at the bridge moiety (e.g. bithiophene, phenyl, or anthracene and alkynes, as well as minor contributions from the boron bound xylene moiety), and the LUMO is mainly localized at the two boron moieties (with minor contributions from the bridge bound xylene and terminal *N,N,N*,3,5-pentamethylbenzenaminium moieties).

Compound **III**:

Calculated absorption spectra	Orbital	Energy [eV]	Symmetry
	L+4	-5.64	A_u
	L+3	-5.64	A_g
	L+2	-5.81	A_u
	L+1	-6.79	A_g
	LUMO	-6.87	A_u
	HOMO	-10.95	A_g
	H-1	-12.14	A_u
	H-2	-12.99	A_u
	H-3	-13.15	A_g
	H-4	-13.19	A_g

TD-DFT CAM-B3LYP/6-31G(d), gas phase

Orbitals relevant to the $S_1 \leftarrow S_o$ transition	other relevant orbitals	
LUMO	HOMO-1	LUMO+1
HOMO	HOMO-2	LUMO+2
	HOMO-3	LUMO+3

Table S8. Lowest energy singlet electronic transition of **III** (TD-DFT CAM-B3LYP/6-31G(d), gas phase).

State	E [eV]	λ [nm]	f	Symmetry	Major contributions
1	2.56	483.41	2.616	A$_U$	H-1->L+1 (10%), HOMO->LUMO (66%), HOMO->L+2 (16%)
2	2.92	425.33	0.0	A$_G$	H-1->LUMO (16%), HOMO->L+1 (73%)
3	3.44	360.22	0.3595	A$_U$	HOMO->L+2 (65%)
4	3.80	325.99	0.0	A$_G$	H-1->LUMO (45%), HOMO->L+1 (23%)
5	3.89	318.76	0.0	A$_G$	H-6->L+1 (43%), H-5->LUMO (48%)
6	3.89	318.75	0.0278	A$_U$	H-6->LUMO (47%), H-5->L+1 (43%)
7	3.91	317.18	0.1435	A$_U$	H-3->LUMO (12%), H-1->L+1 (35%), HOMO->LUMO (23%)
8	4.09	303.17	0.0	A$_G$	H-1->L+2 (18%), HOMO->L+5 (49%)
9	4.35	285.33	0.0	A$_G$	HOMO->L+3 (83%)
10	4.35	285.33	0.0221	A$_U$	HOMO->L+4 (83%)
11	4.40	281.56	0.0	A$_G$	H-11->LUMO (42%), H-10->L+1 (42%)
12	4.40	281.54	0.211	A$_U$	H-11->L+1 (42%), H-10->LUMO (42%)
13	4.54	272.89	0.0	A$_G$	H-9->LUMO (12%), H-1->L+2 (21%), HOMO->L+5 (20%)
14	4.57	271.54	0.0005	A$_U$	H-8->L+1 (17%), H-8->L+5 (10%), H-7->LUMO (35%), H-7->L+2 (23%)
15	4.58	270.96	0.0	A$_G$	H-8->LUMO (32%), H-8->L+2 (22%), H-7->L+1 (18%), H-7->L+5 (11%)
16	4.61	269.21	0.0846	A$_U$	H-1->L+5 (10%), HOMO->L+8 (18%), HOMO->L+10 (24%)
17	4.66	266.00	0.0	A$_G$	H-2->LUMO (44%), H-2->L+2 (36%)
18	4.72	262.49	0.0124	A$_U$	H-9->L+1 (11%), H-1->L+1 (28%)
19	4.81	257.84	0.0	A$_G$	H-13->LUMO (22%), H-12->L+1 (26%), H-1->L+2 (11%)
20	4.81	257.67	0.0506	A$_U$	H-4->LUMO (11%), H-3->LUMO (10%), HOMO->L+8 (18%)
21	4.81	257.56	0.0	A$_G$	HOMO->L+7 (71%)
22	4.81	257.56	0.0053	A$_U$	HOMO->L+6 (70%)
23	4.85	255.43	0.0291	A$_U$	H-13->L+1 (22%), H-12->LUMO (15%), H-3->LUMO (10%)
24	4.87	254.37	0.0	A$_G$	H-15->LUMO (21%), H-14->L+1 (22%), HOMO->L+7 (15%)
25	4.87	254.34	0.0538	A$_U$	H-15->L+1 (27%), H-14->LUMO (26%), HOMO->L+6 (17%)

Compound **IV**:

Calculated absorption spectra	Orbital	Energy [eV]	Symmetry
TD-DFT CAM-B3LYP/6-31+G(d, p), gas phase	L+4	-5.81	Ag
	L+3	-5.81	Au
	L+2	-5.90	Au
	L+1	-6.97	Ag
	LUMO	-7.08	Au
	HOMO	-11.82	Ag
	H-1	-12.92	Au
	H-2	-13.42	Ag
	H-3	-13.46	Au
	H-4	-13.46	Ag
Orbitals relevant to the S$_1$←S$_o$ transition	**other relevant orbitals**		
LUMO **HOMO**	**HOMO-1** **HOMO-2** **HOMO-3**	**LUMO+1** **LUMO+2** **LUMO+3**	
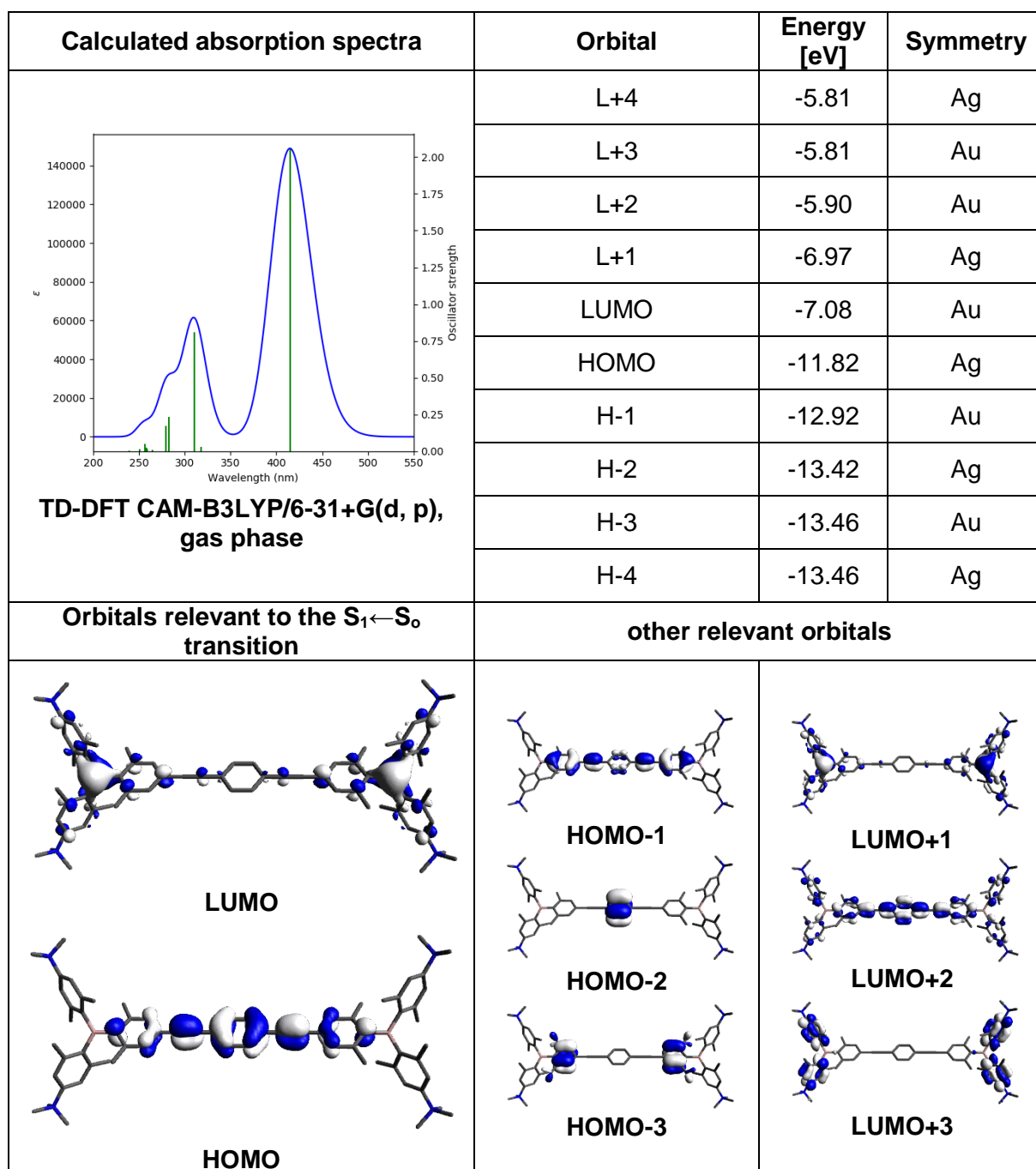
Table S 9. Lowest energy singlet electronic transition of **IV** (TD-DFT CAM-B3LYP/6-31+G(d), gas phase).

State	E [eV]	λ [nm]	f	Symmetry	Major contributions
1	2.99	414.88	2.0547	AU	H-1->L+1 (15%), HOMO->LUMO (69%)
2	3.27	379.47	0	AG	H-1->LUMO (24%), HOMO->L+1 (63%)
3	3.90	318.05	0	AG	H-4->L+1 (41%), H-3->LUMO (49%)
4	3.90	318.02	0.0274	AU	H-4->LUMO (49%), H-3->L+1 (42%)
5	4.00	310.10	0.8103	AU	H-1->L+1 (15%), HOMO->L+2 (57%)
6	4.30	288.19	0	AG	H-6->L+1 (12%), H-1->LUMO (35%), HOMO->L+1 (33%)
7	4.38	283.04	0	AG	H-9->LUMO (44%), H-8->L+1 (43%)
8	4.38	283.01	0.2341	AU	H-9->L+1 (43%), H-8->LUMO (44%)
9	4.43	279.79	0.174	AU	H-6->LUMO (14%), H-1->L+1 (19%), HOMO->LUMO (28%), HOMO->L+2 (18%)
10	4.55	272.61	0	AG	H-5->LUMO (40%), H-5->L+2 (29%)
11	4.57	271.22	0	AU	H-7->LUMO (29%), H-7->L+2 (19%), H-5->L+1 (14%)
12	4.68	264.78	0.0094	AU	H-2->LUMO (37%), H-2->L+2 (29%), HOMO->L+18 (19%)
13	4.69	264.61	0	AG	H-1->L+2 (27%), HOMO->L+5 (32%), HOMO->L+9 (10%)
14	4.79	258.76	0	AG	H-1->L+3 (15%), HOMO->L+4 (73%)
15	4.79	258.76	0.0134	AU	H-1->L+4 (15%), HOMO->L+3 (73%)
16	4.81	257.78	0.0249	AU	H-11->LUMO (35%), H-10->L+1 (31%)
17	4.81	257.60	0	AG	H-11->L+1 (33%), H-10->LUMO (28%)
18	4.84	256.23	0	AG	H-13->LUMO (32%), H-12->L+1 (33%)
19	4.84	256.22	0.0521	AU	H-13->L+1 (33%), H-12->LUMO (33%)
20	4.91	252.37	0	AG	H-15->L+1 (33%), H-14->LUMO (32%), H-1->LUMO (11%)
21	4.94	250.82	0.013	AU	H-15->LUMO (37%), H-14->L+1 (28%), H-1->L+1 (15%)
22	5.18	239.23	0.002	AU	H-4->L+2 (31%), H-3->L+5 (10%), H-1->L+12 (11%), HOMO->L+11 (18%)
23	5.18	239.23	0	AG	H-4->L+5 (10%), H-3->L+2 (32%), H-1->L+11 (11%), HOMO->L+12 (18%)
24	5.27	235.05	0	AG	H-16->LUMO (12%), H-1->L+2 (10%), HOMO->L+5 (39%)
25	5.31	233.58	0	AG	H-1->L+6 (14%), HOMO->L+7 (81%)

Compound **V**:

Calculated absorption spectra	Orbital	Energy [eV]	Symmetry
	L+4	-5.82	A_g
	L+3	-5.82	A_u
	L+2	-6.21	A_u
	L+1	-6.95	A_g
	LUMO	-7.12	A_u
	HOMO	-10.92	A_g
	H-1	-12.62	A_g
	H-2	-12.81	A_g
TD-DFT CAM-B3LYP/6-31+G(d, p), gas phase	H-3	-12.84	A_u
	H-4	-13.14	A_u

Orbitals relevant to the $S_1 \leftarrow S_o$ transition	other relevant orbitals	
LUMO	HOMO-1	LUMO+1
	HOMO-2	LUMO+2
HOMO	HOMO-3	LUMO+3
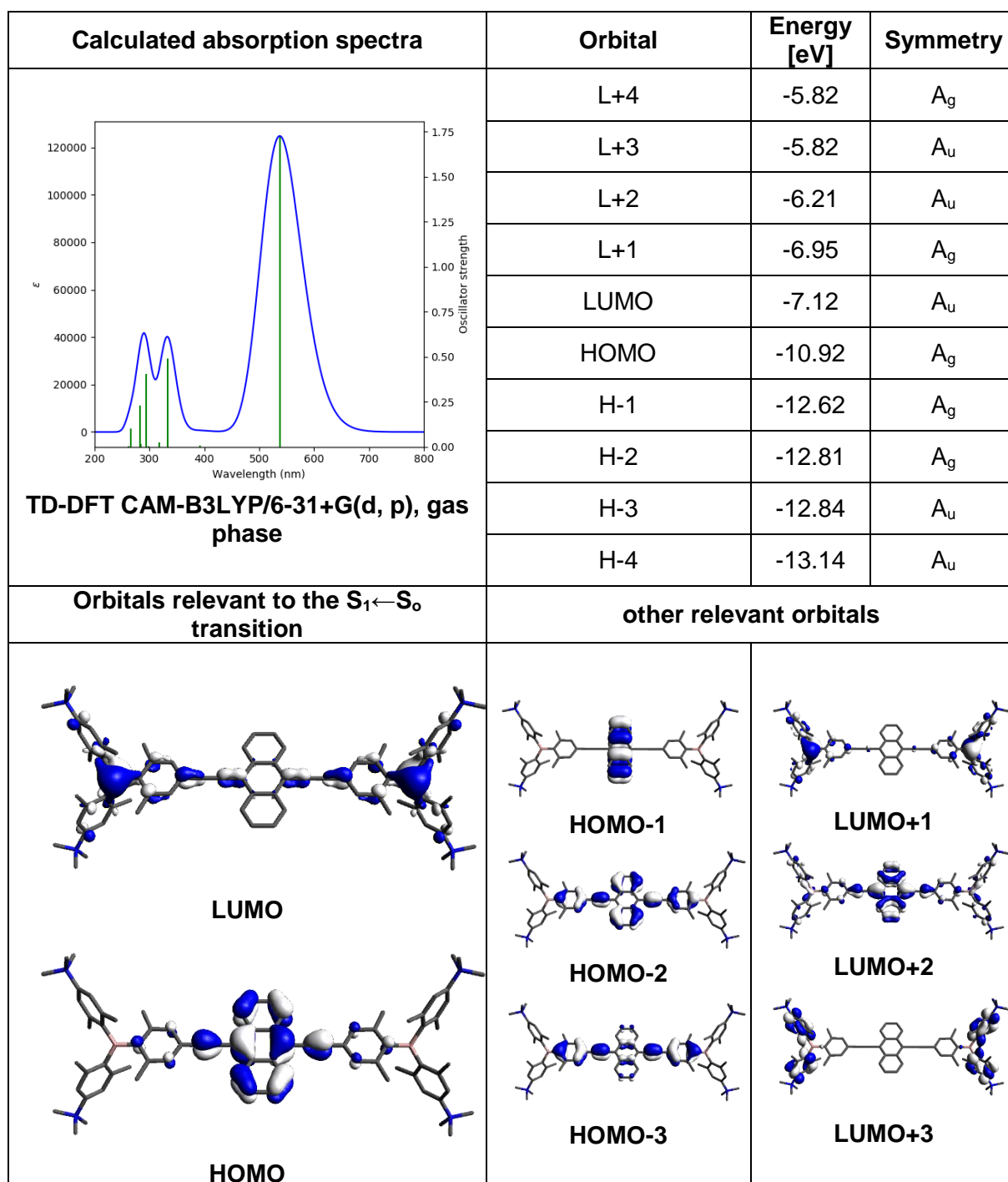
Table S10. Lowest energy singlet electronic transition of **V** (TD-DFT CAM-B3LYP/6-31G(d), gas phase).

State	E [eV]	λ [nm]	f	Symmetry	Major contributions
1	2.31	537.61	1.7224	A_U	HOMO->LUMO (76%), HOMO->L+2 (17%)
2	2.80	443.50	0.0	A_G	HOMO->L+1 (87%)
3	3.16	392.72	0.0082	A_U	HOMO->LUMO (13%), HOMO->L+2 (72%)
4	3.72	333.26	0.0487	A_U	H-1->LUMO (35%), H-1->L+2 (36%), HOMO->L+13 (22%)
5	3.72	333.20	0.4889	A_U	H-3->L+1 (24%), H-2->LUMO (47%)
6	3.73	332.23	0.0	A_G	H-3->LUMO (48%), H-2->L+1 (24%)
7	3.89	318.40	0.0	A_G	H-6->LUMO (50%), H-5->L+1 (40%)
8	3.89	318.38	0.0243	A_U	H-6->L+1 (40%), H-5->LUMO (50%)
9	4.16	298.29	0.0	A_G	HOMO->L+4 (94%)
10	4.16	298.29	0.0051	A_U	HOMO->L+3 (94%)
11	4.17	297.10	0.0	A_G	HOMO->L+5 (57%), HOMO->L+9 (21%)
12	4.22	294.14	0.4029	A_U	H-2->L+2 (22%), HOMO->L+10 (35%)
13	4.27	290.40	0.0	A_G	H-4->LUMO (51%), H-4->L+2 (44%)
14	4.37	283.57	0.0158	A_U	H-2->L+2 (26%), HOMO->L+10 (23%)
15	4.39	282.38	0.0	A_G	H-12->LUMO (43%), H-11->L+1 (43%)
16	4.39	282.35	0.2297	A_U	H-12->L+1 (43%), H-11->LUMO (43%)
17	4.39	282.27	0.0004	A_U	H-7->LUMO (46%), H-7->L+2 (30%)
18	4.46	277.92	0.0	A_G	H-8->LUMO (45%), H-8->L+2 (27%)
19	4.53	273.90	0.0	A_G	H-3->LUMO (12%), H-3->L+2 (43%)
20	4.65	266.53	0.0994	A_U	H-1->LUMO (60%), HOMO->L+13 (26%)
21	4.66	265.84	0.0	A_G	H-1->L+1 (96%)
22	4.68	265.17	0.0002	A_U	HOMO->L+6 (95%)
23	4.68	265.16	0.0	A_G	HOMO->L+7 (95%)
24	4.74	261.61	0.0025	A_U	HOMO->L+8 (67%), HOMO->L+10 (14%)
25	4.74	261.43	0.0	A_G	HOMO->L+5 (22%), HOMO->L+9 (54%)

Calculated Raman Data

Compound **III**

Compound **IV**
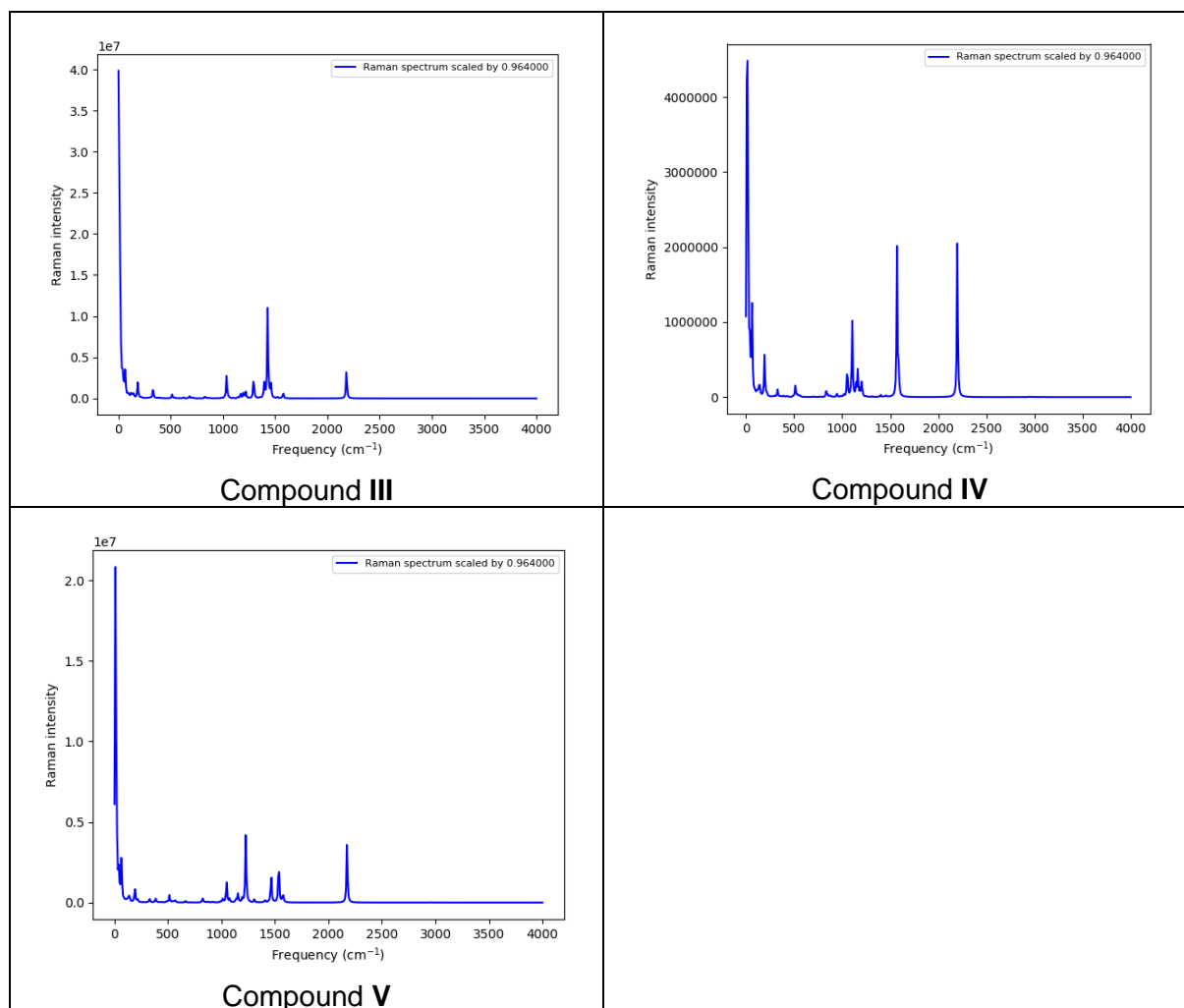
Compound **V**

Table S11. Comparison of experimentally observed (exp.) and calculated (calc.) Raman bands of compounds **III**-**V**.

Wavenumber / cm^{-1}						Assignment
III		**IV**		**V**		
exp.	calc.	exp.	calc.	exp.	calc.	
-	2183	2209	2198	2182	2174	ν C≡C
1595	1578	1591	1570	1594	1576	ν CC (aromatic linker)
				1556	1535	ν CC (anthracene)
				1481	1465	ν CC (anthracene)
1472						ν CC (thiophene)
1453	1428					ν CS (thiophene)
				1257	1227	δ_{ip} CH (anthracene)
				1158	1154	δ_{ip} CH (anthracene)

Cartesian Coordinates

Compound **III**

DFT B3LYP/6-31G(d), gas phase, S_0
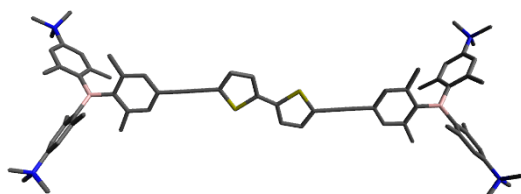
Point group: C_i

Total energy: – 2,422,550.60

kcal mol^{-1}

Dipole moment: 0 D

Immaginary frequencies: 0

C	-0.66075900	0.20042800	0.21038100
C	0.66075900	-0.20042800	-0.21038100
C	1.01265800	-1.13430300	-1.17411100
C	2.40240900	-1.28684100	-1.33847200
C	3.15113900	-0.47075900	-0.50226600
S	2.09401400	0.50672000	0.50968900
C	-1.01265800	1.13430300	1.17411100
C	-2.40240900	1.28684100	1.33847200
C	-3.15113900	0.47075900	0.50226600
S	-2.09401400	-0.50672000	-0.50968900
H	0.28148100	-1.69412900	-1.74726000
H	2.85989400	-1.96961400	-2.04470900
H	-0.28148100	1.69412900	1.74726000
H	-2.85989400	1.96961400	2.04470900
C	-4.54456100	0.37520500	0.41104100
C	4.54456100	-0.37520500	-0.41104100
C	5.76011400	-0.29161800	-0.33059000
C	-5.76011400	0.29161800	0.33059000
C	7.17165200	-0.21699300	-0.25858700
C	7.97970700	-1.04234800	-1.06393800
C	7.81200600	0.68073800	0.61648000
C	9.36910400	-1.00128200	-0.99378800
H	7.49740000	-1.72669300	-1.75505800
C	9.19941600	0.77644400	0.68141600
H	7.20037100	1.31193100	1.25379200
C	10.02680900	-0.07634500	-0.11922000
C	-7.17165200	0.21699300	0.25858700
C	-7.81200600	-0.68073800	-0.61648000
C	-7.97970700	1.04234800	1.06393800
C	-9.19941600	-0.77644400	-0.68141600
H	-7.20037100	-1.31193100	-1.25379200
C	-9.36910400	1.00128200	0.99378800
H	-7.49740000	1.72669300	1.75505800
C	-10.02680900	0.07634500	0.11922000
C	-10.11535100	1.94362100	1.92143700
H	-9.43160400	2.36281900	2.66472400
H	-10.56118900	2.78447400	1.37900000
H	-10.92270900	1.44810900	2.47005900
C	-9.75679900	-1.78464900	-1.67044700
H	-8.96559800	-2.13764600	-2.33760400
H	-10.17436100	-2.66364500	-1.16738500
H	-10.54784900	-1.36717800	-2.30165800

C	9.75679900	1.78464900	1.67044700
H	10.17436100	2.66364500	1.16738500
H	8.96559800	2.13764600	2.33760400
H	10.54784900	1.36717800	2.30165800
C	10.11535100	-1.94362100	-1.92143700
H	10.56118900	-2.78447400	-1.37900000
H	9.43160400	-2.36281900	-2.66472400
H	10.92270900	-1.44810900	-2.47005900
B	11.58676400	-0.00234400	-0.04106100
B	-11.58676400	0.00234400	0.04106100
C	12.47091800	-1.34058600	-0.00380900
C	13.53279800	-1.57115100	-0.91334400
C	12.20213400	-2.34032800	0.97207400
C	14.27916600	-2.75986200	-0.86259900
C	12.97529900	-3.50649400	1.02050300
C	13.99999800	-3.71879400	0.10215700
H	15.06635700	-2.89452300	-1.59286200
H	12.74294800	-4.23986800	1.78586300
C	-12.47091800	1.34058600	0.00380900
C	-12.20213400	2.34032800	-0.97207400
C	-13.53279800	1.57115100	0.91334400
C	-12.97529900	3.50649400	-1.02050300
C	-14.27916600	2.75986200	0.86259900
C	-13.99999800	3.71879400	-0.10215700
H	-12.74294800	4.23986800	-1.78586300
H	-15.06635700	2.89452300	1.59286200
C	-12.34221000	-1.41224500	-0.00215200
C	-12.08231700	-2.38475500	1.00318500
C	-13.28260100	-1.73711100	-1.01110700
C	-12.74890300	-3.61574500	0.98440000
C	-13.92110300	-2.98803700	-1.02461200
C	-13.65494500	-3.91828800	-0.02853600
H	-12.52872400	-4.32581800	1.77492600
H	-14.61677800	-3.19238700	-1.82800000
C	12.34221000	1.41224500	0.00215200
C	13.28260100	1.73711100	1.01110700
C	12.08231700	2.38475500	-1.00318500
C	13.92110300	2.98803700	1.02461200
C	12.74890300	3.61574500	-0.98440000
C	13.65494500	3.91828800	0.02853600
H	14.61677800	3.19238700	1.82800000
H	12.52872400	4.32581800	-1.77492600
C	-13.90248900	0.57953400	1.99770700
H	-14.32598300	-0.33680800	1.57456300
H	-13.03527200	0.28806400	2.59919600
H	-14.64264000	1.00158100	2.68332900
C	13.90248900	-0.57953400	-1.99770700
H	13.03527200	-0.28806400	-2.59919600
H	14.32598300	0.33680800	-1.57456300
H	14.64264000	-1.00158100	-2.68332900
C	-11.08813600	2.21598500	-1.99259500
H	-10.10825900	2.37159200	-1.52981400
H	-11.05948100	1.22977300	-2.46413600
H	-11.20349100	2.95752000	-2.78857200
C	11.08813600	-2.21598500	1.99259500
H	11.05948100	-1.22977300	2.46413600
H	10.10825900	-2.37159200	1.52981400
H	11.20349100	-2.95752000	2.78857200
C	13.62893100	0.78190000	2.13511200
H	12.73530200	0.41538500	2.65089800
H	14.17062800	-0.09368200	1.76364800
H	14.25802800	1.26732100	2.88654400
C	-13.62893100	-0.78190000	-2.13511200
H	-14.17062800	0.09368200	-1.76364800
H	-12.73530200	-0.41538500	-2.65089800
H	-14.25802800	-1.26732100	-2.88654400
C	11.09063500	2.16114700	-2.12765000
H	11.20211900	1.17927400	-2.59612000
H	10.05979700	2.22040500	-1.76392000
H	11.21263600	2.91465000	-2.91128100
C	-11.09063500	-2.16114700	2.12765000
H	-10.05979700	-2.22040500	1.76392000
H	-11.20211900	-1.17927400	2.59612000
H	-11.21263600	-2.91465000	2.91128100
N	14.32728800	5.27600300	0.01229100
N	-14.32728800	-5.27600300	-0.01229100
N	14.78536500	-5.01188700	0.18450800

N	-14.78536500	5.01188700	-0.18450800
C	13.84897800	-6.19070300	-0.00701400
H	14.43379600	-7.11064100	0.04374700
H	13.09543400	-6.18497100	0.77806500
H	13.37184200	-6.09427200	-0.98250300
C	-13.84897800	6.19070300	0.00701400
H	-13.09543400	6.18497100	-0.77806500
H	-14.43379600	7.11064100	-0.04374700
H	-13.37184200	6.09427200	0.98250300
C	13.27635300	6.36701100	0.10255600
H	13.77972200	7.33525900	0.10044800
H	12.60570700	6.29429700	-0.75134800
H	12.71751200	6.22858200	1.02834700
C	-13.27635300	-6.36701100	-0.10255600
H	-12.60570700	-6.29429700	0.75134800
H	-13.77972200	-7.33525900	-0.10044800
H	-12.71751200	-6.22858200	-1.02834700
C	15.28421100	5.47191200	1.16450300
H	14.73879400	5.39424300	2.10436700
H	16.07172200	4.72098500	1.11149500
H	15.71828000	6.46767400	1.07203600
C	-15.28421100	-5.47191200	-1.16450300
H	-16.07172200	-4.72098500	-1.11149500
H	-14.73879400	-5.39424300	-2.10436700
H	-15.71828000	-6.46767400	-1.07203600
C	15.11940500	5.44178900	-1.27106000
H	15.86655800	4.64924700	-1.31764500
H	14.44677800	5.37001900	-2.12344200
H	15.60136100	6.42076100	-1.25809200
C	-15.11940500	-5.44178900	1.27106000
H	-14.44677800	-5.37001900	2.12344200
H	-15.86655800	-4.64924700	1.31764500
H	-15.60136100	-6.42076100	1.25809200
C	15.46077100	-5.11747600	1.53896400
H	14.70489500	-5.11157500	2.32177200
H	16.02603400	-6.05027000	1.57378900
H	16.12719400	-4.26284500	1.65739700
C	-15.46077100	5.11747600	-1.53896400
H	-16.02603400	6.05027000	-1.57378900
H	-14.70489500	5.11157500	-2.32177200
H	-16.12719400	4.26284500	-1.65739700
C	15.86304100	-5.11347000	-0.86909700
H	15.40660500	-5.07635100	-1.85761200
H	16.57246100	-4.29679800	-0.74007200
H	16.37222000	-6.06799200	-0.73443400
C	-15.86304100	5.11347000	0.86909700
H	-16.57246100	4.29679800	0.74007200
H	-15.40660500	5.07635100	1.85761200
H	-16.37222000	6.06799200	0.73443400

DFT B3LYP/6-31+G(d, p), gas phase, S_0

Point group: C_1

Total energy: –2,422,664.70

kcal mol^{-1}

Dipole moment: 0.13 D

Immaginary frequencies: 0

C	0.59369800	0.29359300	-0.28246200
C	1.42704100	-0.26962300	-1.23979100
C	2.58860800	0.48529600	-1.49743300
C	2.67128400	1.64712900	-0.74091900
S	1.27222900	1.79428600	0.31506000
C	-2.73418500	-1.57131600	0.69078800
C	5.60719300	4.42197500	-0.81598600
C	5.58936000	5.55311700	0.02323800
C	6.61394000	6.49779600	0.00122700
C	7.70535400	6.36806300	-0.91759900
C	7.70799100	5.22555200	-1.78183000
C	6.69072200	4.27652100	-1.70466600
B	8.84974400	7.43507100	-0.97858200
C	9.39414300	7.97184600	-2.38913400
C	9.50395400	8.01571600	0.36620000
C	10.77090500	7.95043400	-2.72522600
C	11.21441000	8.41559200	-3.97565700
C	10.30625700	8.92991000	-4.89261000
C	8.95054500	8.98028900	-4.57721300
C	8.48291300	8.49790900	-3.34779700
C	9.59490000	9.40666800	0.62250100
C	10.16444000	9.88331800	1.81624800
C	10.67224400	8.99212400	2.75328900
C	10.61163000	7.62112400	2.51530000
C	10.02436000	7.12280000	1.34497100
C	6.98751700	8.56676100	-3.11023100
C	11.82790000	7.40677600	-1.78540500
C	9.06595200	10.44665800	-0.34430400
C	9.97634800	5.61561200	1.19182000
C	8.81508300	4.94441900	-2.78234500
C	6.46913200	7.66957600	0.95598900
C	4.56952100	3.45780700	-0.77259800
C	3.68436000	2.61522100	-0.75555900
N	10.75115400	9.44128100	-6.24758400
N	11.29505400	9.47288900	4.04805000
C	11.29626500	10.97865700	4.17761000
C	10.51853200	8.91550700	5.22810200
C	12.24338400	9.32816800	-6.45905600
C	10.07414000	8.63943400	-7.34533400
C	-5.62558400	-4.39060300	0.81942000
C	-5.52430900	-5.59544800	0.09675600
C	-6.51545800	-6.57317300	0.16023100
C	-7.70101400	-6.36032600	0.93588000
C	-7.80804200	-5.12363300	1.65120700
C	-6.77936200	-4.18503700	1.60132800
B	-8.83524700	-7.43791400	1.00111200
C	-10.37768300	-7.01187000	0.88352900
C	-8.48082100	-8.99102000	1.19038600
C	-11.34220200	-7.39222900	1.84990200
C	-12.68294300	-6.98707500	1.72729700
C	-13.08699700	-6.22712800	0.63676500
C	-12.16170300	-5.85898500	-0.33707300
C	-10.81535000	-6.22884500	-0.22166400
C	-7.66025700	-9.40307000	2.27226300
C	-7.35394600	-10.76297000	2.46021300
C	-7.82959800	-11.71986500	1.57325800
C	-8.63236600	-11.33784000	0.50034100
C	-8.97171000	-9.99268800	0.30903800
C	-9.87879600	-5.75360000	-1.31446400
C	-10.98806500	-8.21870700	3.06958600
C	-7.06713900	-8.43170500	3.27391200
C	-9.84747800	-9.66490600	-0.88267000
C	-8.99315200	-4.77495800	2.53418600
C	-6.28065300	-7.82333800	-0.66902700
C	-4.60128900	-3.41287400	0.76430800
C	-3.73057800	-2.55590700	0.72920500
N	-14.52387300	-5.77489400	0.47469200
N	-7.49322400	-13.18804500	1.73705300
C	-6.61787800	-13.46106800	2.93876300
C	-8.76842800	-13.99303300	1.91090400
C	-15.41899300	-6.24288700	1.59896200
C	-14.58351200	-4.25760900	0.44746300
C	-6.74797600	-13.68281800	0.50991000
C	10.38077800	10.90654800	-6.39231700
C	12.73809400	9.00787900	4.12958200
C	-15.09435300	-6.32484700	-0.82038300
C	-2.70243400	-0.35972900	1.36905200
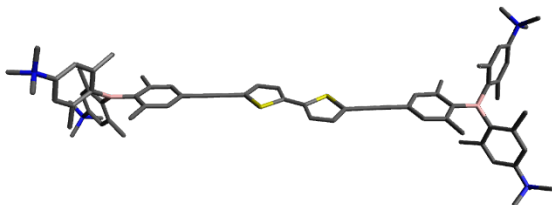
C	-1.54792200	0.40241200	1.10093900
C	-0.66944600	-0.20469700	0.21332900
S	-1.29073200	-1.76151900	-0.29633500
H	1.19909200	-1.20037000	-1.74667400
H	3.35078900	0.20383300	-2.21379800
H	4.75310400	5.68521800	0.70243100
H	6.72551400	3.40030400	-2.34425800
H	12.27331500	8.35761700	-4.18933800
H	8.22352500	9.38179100	-5.27501600
H	10.19079200	10.95368800	1.97087000
H	11.00537300	6.90647300	3.23009100
H	6.52952900	7.57581900	-3.18505500
H	6.73869200	8.95301300	-2.11892000
H	6.50532200	9.21526000	-3.84620800
H	11.57112400	6.41136500	-1.41194700
H	12.79558700	7.32368800	-2.28610900
H	11.95836500	8.05617700	-0.91461900
H	8.03324100	10.24209500	-0.64099200
H	9.08171500	11.44399500	0.10189300
H	9.66528900	10.48167200	-1.25892500
H	8.96228000	5.23493700	1.34708400
H	10.28596900	5.28580500	0.19722700
H	10.63194600	5.12873900	1.91835900
H	9.81399300	5.06164800	-2.35231000
H	8.74159000	3.91795000	-3.14935800
H	8.75615700	5.60677400	-3.65198100
H	5.46573600	7.68405700	1.38804900
H	7.18096300	7.60972800	1.78543800
H	6.62254100	8.63562800	0.46610900
H	11.75974800	11.22978000	5.13124400
H	11.87534200	11.41249500	3.36377900
H	10.27099000	11.34523900	4.16128400
H	10.97365700	9.28478400	6.14790800
H	10.55670400	7.82880800	5.20532300
H	9.48574100	9.25401600	5.15006500
H	12.46867500	9.71676300	-7.45179900
H	12.76244100	9.92117500	-5.70752800
H	12.54030300	8.28215400	-6.39951400
H	10.41904700	9.01298200	-8.31024100
H	8.99575200	8.75633600	-7.26593000
H	10.34558700	7.59136300	-7.22207700
H	-4.64806500	-5.75989900	-0.52231100
H	-6.86230400	-3.26797800	2.17591000
H	-13.37392000	-7.28672000	2.50388200
H	-12.45455700	-5.27019000	-1.19975300
H	-6.73321700	-11.02542900	3.30644800
H	-9.01239600	-12.06601100	-0.20818400
H	-9.23749500	-4.94124100	-0.95940500
H	-9.21449600	-6.54525500	-1.66929900
H	-10.44053600	-5.38495200	-2.17659000
H	-10.13237000	-7.80496500	3.61065900
H	-11.82369800	-8.26244900	3.77230900
H	-10.73115700	-9.24583100	2.79381400
H	-7.79011900	-7.68759500	3.61589100
H	-6.69655700	-8.95954800	4.15638900
H	-6.22936700	-7.87838100	2.83836600
H	-9.99900500	-10.54352200	-1.51445500
H	-10.83191200	-9.30692900	-0.56752400
H	-9.40595000	-8.88661300	-1.51204100
H	-9.27566600	-5.59105000	3.20546700
H	-8.75722500	-3.91103400	3.16002700
H	-9.87898500	-4.51837600	1.94442200
H	-5.44273200	-7.67154500	-1.35355300
H	-6.03822600	-8.68787700	-0.04283900
H	-7.14778300	-8.09628300	-1.27751500
H	-6.42973400	-14.53370800	2.97544800
H	-5.67501200	-12.92730200	2.82971300
H	-7.13639100	-13.14912900	3.84413000
H	-8.50147500	-15.04271900	2.03914800
H	-9.39377800	-13.87495400	1.02893700
H	-9.29134500	-13.62212500	2.79200700
H	-16.42444200	-5.87368700	1.39884700
H	-15.42766500	-7.33147000	1.62684500
H	-15.06029000	-5.83441800	2.54252900
H	-15.62593600	-3.95361700	0.34499200
H	-14.00440300	-3.88801700	-0.39571200
H	-14.16557700	-3.88083300	1.38057500

H	-5.84071100	-13.09000300	0.39698300
H	-6.50169100	-14.73535100	0.65498400
H	-7.37943800	-13.56721800	-0.36802100
H	10.87133600	11.46523100	-5.59572100
H	10.72041400	11.25526400	-7.36831100
H	9.30161300	11.01670800	-6.31428800
H	13.27840800	9.41277100	3.27433400
H	13.16862500	9.37524400	5.06189300
H	12.76994600	7.92095000	4.10953200
H	-15.03921000	-7.41254200	-0.78557800
H	-16.13100200	-5.99775600	-0.90911500
H	-14.51409500	-5.94923500	-1.66006500
H	-3.49816000	-0.04560700	2.03348400
H	-1.36416200	1.37646000	1.53985800

Compound **IV**

DFT B3LYP/6-31G(d), gas phase, S_0
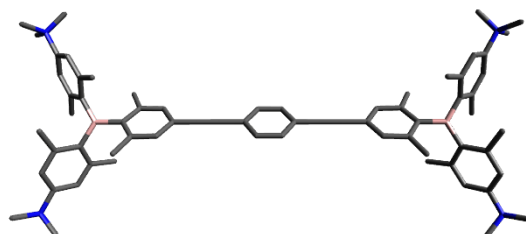
Point group: C_i
Total energy: –1,874,995.57
kcal mol^{-1}
Dipole moment: 0 D
Immaginary frequencies: 0

C	-0.89702814	-0.81899906	-0.69335247
C	-0.89702028	-0.81901498	0.69328653
C	0.00022722	0.00002189	-1.41254795
C	-0.00022722	-0.00002189	1.41254795
C	0.89702814	0.81899906	0.69335247
C	0.89702028	0.81901498	-0.69328653
C	0.00020851	0.00005284	-2.83492095
C	0.00019490	0.00009166	-4.05329195
C	0.00014518	0.00007460	-5.47365495
C	0.86595091	0.83864249	-6.19830656
C	-0.86576614	-0.83852731	-6.19818934
C	0.86484014	0.86603538	-7.59134455
H	1.54920771	1.47998032	-5.65008012
C	-0.86481305	-0.86597935	-7.59120536
H	-1.54897379	-1.47981088	-5.64983879
C	0.00000082	0.00000051	-8.33297995
C	1.84952974	1.81731426	-8.24745056
C	-1.84965485	-1.81715835	-8.24721335
B	-0.00008125	-0.00001344	-9.90036395
H	2.56780293	2.18689716	-7.51043014
H	2.42618230	1.34566038	-9.04968533
H	1.34824300	2.69038353	-8.67942619
H	-1.34847730	-2.69003005	-8.67969271
H	-2.56760255	-2.18704323	-7.51002777
H	-2.42668333	-1.34526341	-9.04904958
C	0.01463460	1.37776860	-10.72057597
C	-0.01479784	-1.37780140	-10.72057794
C	0.97355004	1.64343984	-11.72954655
C	-0.96225350	2.37628125	-10.45104962
C	-0.97357735	-1.64343228	-11.72970636
C	0.96205388	-2.37633341	-10.45098229
C	0.96618870	2.86307906	-12.42613677
C	2.06362517	0.65645210	-12.09557639

Atom	X	Y	Z
C	-0.96625197	3.57414260	-11.17574184
C	-2.03273872	2.21507019	-9.38990746
C	-0.96611386	-2.86303256	-12.42635614
C	-2.06362625	-0.65646005	-12.09584952
C	0.96614676	-3.57416378	-11.17573807
C	2.03243872	-2.21522777	-9.38971245
C	-0.00254398	3.81896798	-12.15043641
H	1.73183758	3.02306256	-13.17397228
H	2.60544449	0.29680591	-11.21503624
H	1.65325923	-0.22154250	-12.60470079
H	2.80041965	1.11209556	-12.76305583
H	-1.73462681	4.30523936	-10.94643975
H	-2.52508439	1.23944751	-9.43569529
H	-1.61069332	2.30789085	-8.38413053
H	-2.80847417	2.97857293	-9.49885038
C	0.00258238	-3.81893985	-12.15057650
H	-1.73164812	-3.02297206	-13.17431563
H	-2.60604633	-0.29743605	-11.21542368
H	-1.65314883	0.22191023	-12.60422912
H	-2.79992183	-1.11189060	-12.76402308
H	1.73449357	-4.30526785	-10.94636716
H	2.52476579	-1.23959702	-9.43530362
H	1.61029243	-2.30818478	-8.38398638
H	2.80819212	-2.97870536	-9.49869353
C	-0.00020851	-0.00005284	2.83492095
C	-0.00019490	-0.00009166	4.05329195
C	-0.00014518	-0.00007460	5.47365495
C	0.86576614	0.83852731	6.19818934
C	-0.86595091	-0.83864249	6.19830656
C	0.86481305	0.86597935	7.59120536
H	1.54897379	1.47981088	5.64983879
C	-0.86484014	-0.86603538	7.59134455
H	-1.54920771	-1.47998032	5.65008012
C	-0.00000082	-0.00000051	8.33297995
C	1.84965485	1.81715835	8.24721335
C	-1.84952974	-1.81731426	8.24745056
B	0.00008125	0.00001344	9.90036395
H	2.56760255	2.18704323	7.51002777
H	1.34847730	2.69003005	8.67969271
H	2.42668333	1.34526341	9.04904958
H	-2.42618230	-1.34566038	9.04968533
H	-2.56780293	-2.18689716	7.51043014
H	-1.34824300	-2.69038353	8.67942619
C	-0.01463460	-1.37776860	10.72057597
C	0.01479784	1.37780140	10.72057794
C	0.96225350	-2.37628125	10.45104962
C	-0.97355004	-1.64343984	11.72954655
C	-0.96205388	2.37633341	10.45098229
C	0.97357735	1.64343228	11.72970636
C	0.96625197	-3.57414260	11.17574184
C	2.03273872	-2.21507019	9.38990746
C	-0.96618870	-2.86307906	12.42613677
C	-2.06362517	-0.65645210	12.09557639
C	-0.96614676	3.57416378	11.17573807
C	-2.03243872	2.21522777	9.38971245
C	0.96611386	2.86303256	12.42635614
C	2.06362625	0.65646005	12.09584952
C	0.00254398	-3.81896798	12.15043641
H	1.73462681	-4.30523936	10.94643975
H	1.61069332	-2.30789085	8.38413053
H	2.52508439	-1.23944751	9.43569529
H	2.80847417	-2.97857293	9.49885038
H	-1.73183758	-3.02306256	13.17397228
H	-1.65325923	0.22154250	12.60470079
H	-2.60544449	-0.29680591	11.21503624
H	-2.80041965	-1.11209556	12.76305583
C	-0.00258238	3.81893985	12.15057650
H	-1.73449357	4.30526785	10.94636716
H	-1.61029243	2.30818478	8.38398638
H	-2.52476579	1.23959702	9.43530362
H	-2.80819212	2.97870536	9.49869353
H	1.73164812	3.02297206	13.17431563
H	1.65314883	-0.22191023	12.60422912
H	2.60604633	0.29743605	11.21542368
H	2.79992183	1.11189060	12.76402308
H	1.59158615	1.45179781	-1.23681295
H	1.59160022	1.45176916	1.23677005
H	-1.59160022	-1.45176916	-1.23677005
H	-1.59158615	-1.45179781	1.23681295
N	0.04103859	-5.14287906	-12.88617721
N	-0.04103859	5.14287906	12.88617721
N	0.04150064	-5.14283027	12.88614479
C	-0.12021931	-6.28192010	11.89638831
H	-0.10046673	-7.22459579	12.44575677
H	-1.07461325	-6.15799816	11.38419918
H	0.69532692	-6.25372892	11.17644294
C	0.12030307	6.28187808	11.89655278
H	-0.69487679	6.25378988	11.17618815
H	0.10039363	7.22455304	12.44591732
H	1.07494255	6.15783584	11.38485092
C	-0.12030307	-6.28187808	-11.89655278
H	-1.07494255	-6.15783584	-11.38485092
H	-0.10039363	-7.22455304	-12.44591732
H	0.69487679	-6.25378988	-11.17618815
N	-0.04150064	5.14283027	-12.88614479
C	0.12021931	6.28192010	-11.89638831
H	1.07461325	6.15799816	-11.38419918
H	0.10046673	7.22459579	-12.44575677
H	-0.69532692	6.25372892	-11.17644294
C	-1.36505042	5.28871269	-13.61273345
H	-1.36759548	6.24299296	-14.14201283
H	-1.46290823	4.46195684	-14.31660244
H	-2.17909971	5.26205557	-12.89106807
C	1.05784432	5.27669617	-13.91430775
H	2.02612132	5.21234071	-13.41913951
H	0.95207933	4.49004707	-14.66058174
H	0.95217132	6.25178390	-14.39025756
C	-1.05735233	-5.27646867	-13.91489916
H	-0.95156711	-6.25151476	-14.39090834
H	-2.02580770	-5.21211588	-13.42008240
H	-0.95127274	-4.48974456	-14.66105016
C	1.36541676	-5.28882560	-13.61244545
H	1.46365879	-4.46204879	-14.31623647
H	2.17921467	-5.26234345	-12.89049184
H	1.36799850	-6.24307816	-14.14177208
C	-1.05784432	-5.27669617	13.91430775
H	-2.02612132	-5.21234071	13.41913951
H	-0.95217132	-6.25178390	14.39025756
H	-0.95207933	-4.49004707	14.66058174
C	1.36505042	-5.28871269	13.61273345
H	2.17909971	-5.26205557	12.89106807
H	1.46290823	-4.46195684	14.31660244
H	1.36759548	-6.24299296	14.14201283
C	1.05735233	5.27646867	13.91489916
H	0.95127274	4.48974456	14.66105016
H	2.02580770	5.21211588	13.42008240
H	0.95156711	6.25151476	14.39090834
C	-1.36541676	5.28882560	13.61244545
H	-2.17921467	5.26234345	12.89049184
H	-1.46365879	4.46204879	14.31623647
H	-1.36799850	6.24307816	14.14177208

DFT B3LYP/6-31G(d), gas phase, S_0

Point group: C_1

Total energy: −1,875,107.16

kcal mol⁻¹

Dipole moment: 0 D

Immaginary frequencies: 0

C	-0.69412900	-0.80247600	0.91221000
C	0.69410400	-0.80247600	0.91221400
C	-1.41418200	0.00001900	-0.00030500
C	1.41416200	0.00002000	-0.00029600
C	0.69410800	0.80251400	-0.91281300
C	-0.69412400	0.80251400	-0.91281700
C	-2.83811300	0.00002100	-0.00030300
C	-4.05764500	0.00001800	-0.00029400
C	-5.47987200	-0.00000100	-0.00024100
C	-6.20476600	0.82437200	-0.88066500
C	-6.20467900	-0.82438700	0.88024300
C	-7.59934400	0.85193300	-0.87880200
H	-5.65761600	1.45423000	-1.57494300
C	-7.59925500	-0.85197700	0.87849600
H	-5.65745900	-1.45422800	1.57448200
C	-8.34072300	-0.00003100	-0.00012500
C	-8.25814400	1.78593000	-1.87821500
C	-8.25795100	-1.78597600	1.87797500
B	-9.91040200	-0.00001700	-0.00005000
H	-7.51971000	2.15985700	-2.59136200
H	-9.04625300	1.29717500	-2.45862300
H	-8.70784600	2.65507900	-1.38762200
H	-8.70765900	-2.65515100	1.38743300
H	-7.51945200	-2.15986300	2.59107600
H	-9.04603400	-1.29723600	2.45843100
C	-10.72901700	1.37878100	-0.01366300
C	-10.72905500	-1.37879300	0.01368900
C	-11.73812300	1.64513900	-0.97270600
C	-10.45726600	2.37817900	0.96277200
C	-11.73804000	-1.64510400	0.97286600
C	-10.45748300	-2.37820700	-0.96278200
C	-12.43270600	2.86753300	-0.96601100
C	-12.10651600	0.65800100	-2.06193900
C	-11.18097200	3.57781300	0.96641100
C	-9.39707400	2.21494200	2.03365900
C	-12.43267300	-2.86747400	0.96627900
C	-12.10627600	-0.65793400	2.06212600
C	-11.18123400	-3.57781300	-0.96631100
C	-9.39744900	-2.21501700	-2.03383400
C	-12.15593400	3.82416500	0.00257900
H	-13.17931400	3.02804800	-1.73220400
H	-11.22682000	0.28667800	-2.59484300
H	-12.62795500	-0.21174400	-1.65088000
H	-12.76299100	1.11795800	-2.80454700
H	-10.95042200	4.30789200	1.73479000
H	-9.44471200	1.23959600	2.52430400
H	-8.39164700	2.30620400	1.61188000
H	-9.50556600	2.97725300	2.80931600
C	-12.15606600	-3.82412600	-0.00233700
H	-13.17918700	-3.02794800	1.73257100
H	-11.22650500	-0.28662500	2.59491500
H	-12.62774100	0.21181700	1.65111300
H	-12.76267300	-1.11785800	2.80482300
H	-10.95082600	-4.30790300	-1.73472300
H	-9.44512600	-1.23967200	-2.52447600
H	-8.39195900	-2.30631500	-1.61221100
H	-9.50609100	-2.97732800	-2.80946900
C	2.83809200	0.00002200	-0.00028900
C	4.05762500	0.00002100	-0.00026700
C	5.47985200	0.00001700	-0.00019300
C	6.20475100	0.82440100	-0.88060200
C	6.20465200	-0.82437400	0.88029100
C	7.59932800	0.85197400	-0.87872100
H	5.65760500	1.45425800	-1.57488600
C	7.59922900	-0.85195500	0.87856000
H	5.65742700	-1.45423000	1.57451200
C	8.34070300	0.00001000	-0.00003700
C	8.25813300	1.78597200	-1.87813000
C	8.25791800	-1.78596800	1.87803100
B	9.91038000	-0.00000100	0.00004700
H	7.51970700	2.15987800	-2.59129600
H	8.70780900	2.65513500	-1.38753700
H	9.04626300	1.29722500	-2.45851700
H	9.04597000	-1.29722500	2.45852700
H	7.51940700	-2.15989500	2.59109800
H	8.70766400	-2.65511600	1.38747700
C	10.72901000	-1.37879100	0.01365700
C	10.72903100	1.37877500	-0.01353400
C	10.45739700	-2.37811900	-0.96288900
C	11.73800800	-1.64520200	0.97279800
C	10.45737700	2.37812300	0.96298100
C	11.73810000	1.64514700	-0.97261000
C	11.18112600	-3.57773800	-0.96653300
C	9.39733700	-2.21481700	-2.03389800
C	12.43261700	-2.86758100	0.96609300
C	12.10625500	-0.65813500	2.06214500
C	11.18113900	3.57772400	0.96665700
C	9.39724800	2.21486300	2.03392600
C	12.43273400	2.86751300	-0.96588100
C	12.10640600	0.65805200	-2.06191200
C	12.15597600	-3.82414500	-0.00260200
H	10.95068500	-4.30776100	-1.73499800
H	8.39185900	-2.30612600	-1.61225200
H	9.44502300	-1.23943200	-2.52446300
H	9.50593900	-2.97706700	-2.80959900
H	13.17913700	-3.02813600	1.73236200
H	12.62775600	0.21163300	1.65121200
H	11.22648800	-0.28684000	2.59495000
H	12.76262500	-1.11814100	2.80481400
C	12.15605600	3.82409600	0.00278400
H	10.95066500	4.30776300	1.73509600
H	8.39179900	2.30619300	1.61221500
H	9.44487500	1.23948300	2.52450500
H	9.50582200	2.97712100	2.80962300
H	13.17931000	3.02803800	-1.73210200
H	12.62785100	-0.21172300	-1.65092500
H	11.22666900	0.28677300	-2.59477900
H	12.76284500	1.11803100	-2.80453900
H	-1.23601400	1.42263300	-1.61898200
H	1.23600200	1.42263300	-1.61897500
H	-1.23602200	-1.42259400	1.61837400
H	1.23599300	-1.42259400	1.61838000
N	-12.89014900	-5.14885300	-0.04001900
N	12.89013800	5.14881900	0.04061300
N	12.89003400	-5.14888300	-0.04040600
C	11.89951300	-6.28864300	0.12192900
H	12.44952300	-7.23031600	0.10614200
H	11.38450000	-6.16300100	1.07394100
H	11.18253500	-6.26390800	-0.69553300
C	11.89962900	6.28859900	-0.12166000
H	11.18265900	6.26383300	0.69581000
H	12.44965000	7.23026500	-0.10584000
H	11.38460400	6.16300700	-1.07367200
C	-11.89965000	-6.28861800	0.12241900
H	-11.38462800	-6.16289600	1.07441500
H	-12.44968100	-7.23028100	0.10673200
H	-11.18267800	-6.26397700	-0.69505100
N	-12.88995700	5.14892200	0.04036700
C	-11.89942100	6.28864800	-0.12211600
H	-11.38449300	6.16294100	-1.07416500
H	-12.44940500	7.23033600	-0.10633600
H	-11.18237300	6.26393600	0.69528600
C	-13.61657900	5.29787300	1.36544400
H	-14.14694800	6.25085300	1.36452900
H	-14.31877300	4.47090300	1.46728500
H	-12.89492700	5.27625000	2.17883200
C	-13.91941500	5.28386100	-1.05826600
H	-13.42678700	5.22025000	-2.02735200
H	-14.66833500	4.50040400	-0.95235600
H	-14.39289000	6.25944700	-0.95179900
C	-13.91952100	-5.28371200	1.05870400
H	-14.39302100	-6.25929600	0.95233000
H	-13.42681300	-5.22005400	2.02774700
H	-14.66843600	-4.50024900	0.95281000
C	-13.61688700	-5.29781400	-1.36503100
H	-14.31906100	-4.47082400	-1.46683400
H	-12.89529900	-5.27623200	-2.17847900
H	-14.14728400	-6.25077800	-1.36405100
C	13.91940600	-5.28386200	1.05830200

H	13.42669900	-5.22030100	2.02735200
H	14.39289900	-6.25943800	0.95182700
H	14.66832600	-4.50039300	0.95248900
C	13.61676600	-5.29773800	-1.36543300
H	12.89517900	-5.27607600	-2.17887800
H	14.31895300	-4.47074900	-1.46716600
H	14.14715200	-6.25070900	-1.36453700
C	13.91948300	5.28381700	-1.05811800
H	14.66835100	4.50028600	-0.95239300
H	13.42674000	5.22037100	-2.02715700
H	14.39304800	6.25935200	-0.95157800
C	13.61690800	5.29762300	1.36562500
H	12.89534300	5.27596800	2.17908900
H	14.31907100	4.47060800	1.46732100
H	14.14732600	6.25057700	1.36473300

Compound **V**

DFT B3LYP/6-31G(d), gas phase, S_0
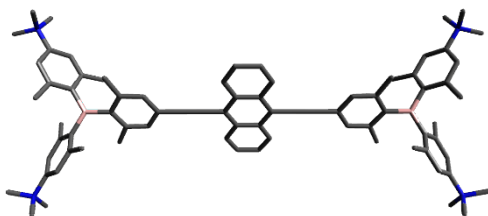
Point group: C_i

Total energy: –2067818.29

kcal mol^{-1}

Dipole moment: 0 D

Immaginary frequencies: 0

C	2.54661103	-0.70979169	2.64895344
C	1.72577458	-1.40014405	1.79413486
C	0.85870694	-0.71917273	0.89081595
C	0.85873649	0.71909539	0.89085403
C	1.72583153	1.39998218	1.79421074
C	2.54663955	0.70955043	2.64899137
C	-0.00002950	-1.42705512	-0.00003466
C	0.00002950	1.42705512	0.00003466
C	-0.85870694	0.71917273	-0.89081595
C	-0.85873649	-0.71909539	-0.89085403
C	-1.72583153	-1.39998218	-1.79421074
H	-1.72247102	-2.48444155	-1.79328899
C	-2.54663955	-0.70955043	-2.64899137
C	-2.54661103	0.70979169	-2.64895344
C	-1.72577458	1.40014405	-1.79413486
H	3.19906501	-1.24777889	3.33040749
H	1.72237030	-2.48460386	1.79315335
H	1.72247102	2.48444155	1.79328899
H	3.19911506	1.24747431	3.33047503
H	-3.19911506	-1.24747431	-3.33047503
H	-3.19906501	1.24777889	-3.33040749
H	-1.72237030	2.48460386	-1.79315335
C	-0.00005534	-2.84413324	-0.00006202
C	-0.00001335	-4.06529836	-0.00009307
C	-0.00000481	-5.48331150	-0.00010139
C	-0.90300772	-6.21046555	-0.79850033

C	0.90300355	-6.21046559	0.79827241
C	-0.93080983	-7.60268606	-0.79468443
H	-1.59601661	-5.66380743	-1.43074487
C	0.93082898	-7.60269635	0.79442638
H	1.59601091	-5.66382060	1.43053069
C	0.00001444	-8.34615978	-0.00012913
C	-1.95569129	-8.25749606	-1.70350370
C	1.95573487	-8.25748247	1.70323623
B	0.00000388	-9.91197294	-0.00010128
H	-2.37784342	-7.52012508	-2.39187095
H	-1.53031155	-9.06057691	-2.31391314
H	-2.78861714	-8.68816142	-1.13710789
H	2.78862778	-8.68820319	1.13683913
H	2.37792948	-7.52008030	2.39154307
H	1.53036940	-9.06052081	2.31371670
C	-1.37587144	-10.73259901	0.07904981
C	1.37586332	-10.73264905	-0.07915741
C	-1.71000057	-11.74237736	-0.86341783
C	-2.29974058	-10.46739369	1.12253862
C	1.70990935	-11.74236690	0.86339865
C	2.29978748	-10.46758033	-1.12263905
C	-2.92308203	-12.43312499	-0.76590283
C	-0.80305702	-12.10303799	-2.02190857
C	-3.50075053	-11.19113528	1.21569118
C	-2.06523435	-9.40805445	2.18179024
C	2.92296533	-12.43318144	0.76598368
C	0.80290186	-12.10295531	2.02186440
C	3.50076374	-11.19137891	-1.21568748
C	2.06533173	-9.40834534	-2.18200243
C	-3.81173896	-12.15979849	0.27108941
H	-3.14633266	-13.18297530	-1.51780947
H	-0.50534749	-11.22157553	-2.59915080
H	0.11494101	-12.58798159	-1.67534173
H	-1.30010662	-12.78877862	-2.71382088
H	-4.16658328	-10.95755606	2.03621466
H	-1.04836864	-9.43238157	2.58283607
H	-2.21971532	-8.40258640	1.77663634
H	-2.75280288	-9.53804195	3.02265069
C	3.81166935	-12.15998589	-0.27099737
H	3.14615206	-13.18297528	1.51796675
H	0.50466784	-11.22141531	2.59869824
H	-0.11480683	-12.58846490	1.67530353
H	1.30012709	-12.78821198	2.71413129
H	4.16664687	-10.95788911	-2.03619524
H	1.04857698	-9.43295317	-2.58331438
H	2.21946537	-8.40282109	-1.77686633
H	2.75314536	-9.53822700	-3.02267786
C	0.00005534	2.84413324	0.00006202
C	0.00001335	4.06529836	0.00009307
C	0.00000481	5.48331150	0.00010139
C	-0.90300355	6.21046559	-0.79827241
C	0.90300772	6.21046555	0.79850033
C	-0.93082898	7.60269635	-0.79442638
H	-1.59601091	5.66382060	-1.43053069
C	0.93080983	7.60268606	0.79468443
H	1.59601661	5.66380743	1.43074487
C	-0.00001444	8.34615978	0.00012913
C	-1.95573487	8.25748247	-1.70323623
C	1.95569129	8.25749606	1.70350370
B	-0.00000388	9.91197294	0.00010128
H	-2.37792948	7.52008030	-2.39154307
H	-2.78862778	8.68820319	-1.13683913
H	-1.53036940	9.06052081	-2.31371670
H	1.53031155	9.06057691	2.31391314
H	2.37784342	7.52012508	2.39187095
H	2.78861714	8.68816142	1.13710789
C	1.37587144	10.73259901	-0.07904981
C	-1.37586332	10.73264905	0.07915741
C	2.29974058	10.46739369	-1.12253862
C	1.71000057	11.74237736	0.86341783
C	-2.29978748	10.46758033	1.12263905
C	-1.70990935	11.74236690	-0.86339865
C	3.50075053	11.19113528	-1.21569118
C	2.06523435	9.40805445	-2.18179024
C	2.92308203	12.43312499	0.76590283
C	0.80305702	12.10303799	2.02190857
C	-3.50076374	11.19137891	1.21568748

C	-2.06533173	9.40834534	2.18200243
C	-2.92296533	12.43318144	-0.76598368
C	-0.80290186	12.10295531	-2.02186440
C	3.81173896	12.15979849	-0.27108941
H	4.16658328	10.95755606	-2.03621466
H	2.21971532	8.40258640	-1.77663634
H	1.04836864	9.43238157	-2.58283607
H	2.75280288	9.53804195	-3.02265069
H	3.14633266	13.18297530	1.51780947
H	-0.11494101	12.58798159	1.67534173
H	0.50534749	11.22157553	2.59915080
H	1.30010662	12.78877862	2.71382088
C	-3.81166935	12.15998589	0.27099737
H	-4.16664687	10.95788911	2.03619524
H	-2.21946537	8.40282109	1.77686633
H	-1.04857698	9.43295317	2.58331438
H	-2.75314536	9.53822700	3.02267786
H	-3.14615206	13.18297528	-1.51796675
H	0.11480683	12.58846490	-1.67530353
H	-0.50466784	11.22141531	-2.59869824
H	-1.30012709	12.78821198	-2.71413129
N	5.11030821	12.93784668	-0.33278125
N	-5.11030821	-12.93784668	0.33278125
N	-5.11020789	12.93809389	0.33259616
N	5.11020789	-12.93809389	-0.33259616
C	5.91468569	-12.68975081	0.93015368
H	5.34419055	-13.02467651	1.79420885
H	6.84987394	-13.24794599	0.86165004
H	6.11243894	-11.62031757	1.00575797
C	-5.91468569	12.68975081	-0.93015368
H	-6.84987394	13.24794599	-0.86165004
H	-5.34419055	13.02467651	-1.79420885
H	-6.11243894	11.62031757	-1.00575797
C	5.91478576	12.68958270	0.92998385
H	6.11248389	11.62014671	1.00568871
H	6.85000256	13.24772364	0.86141821
H	5.34431659	13.02462307	1.79401272
C	-5.91478576	-12.68958270	-0.92998385
H	-5.34431659	-13.02462307	-1.79401272
H	-6.85000256	-13.24772364	-0.86141821
H	-6.11248389	-11.62014671	-1.00568871
C	5.97616832	-12.54478454	-1.50656480
H	6.23623104	-11.48992365	-1.42622615
H	6.88153735	-13.15100757	-1.47054857
H	5.43886586	-12.74077910	-2.43382202
C	-5.97616832	12.54478454	1.50656480
H	-6.88153735	13.15100757	1.47054857
H	-6.23623104	11.48992365	1.42622615
H	-5.43886586	12.74077910	2.43382202
C	-4.81569747	-14.42054914	0.46125381
H	-5.76283257	-14.96009587	0.51261942
H	-4.24601219	-14.75252371	-0.40447403
H	-4.23745290	-14.57759571	1.37204898
C	4.81569747	14.42054914	-0.46125381
H	5.76283257	14.96009587	-0.51261942
H	4.23745290	14.57759571	-1.37204898
H	4.24601219	14.75252371	0.40447403
C	-5.97624932	-12.54440594	1.50672335
H	-5.43895325	-12.74034842	2.43399578
H	-6.23626896	-11.48954161	1.42630058
H	-6.88164193	-13.15059604	1.47075954
C	5.97624932	12.54440594	-1.50672335
H	6.23626896	11.48954161	-1.42630058
H	5.43895325	12.74034842	-2.43399578
H	6.88164193	13.15059604	-1.47075954
C	-4.81554242	14.42079674	0.46094822
H	-4.23729320	14.57789620	1.37173135
H	-4.24584467	14.75268123	-0.40480555
H	-5.76265759	14.96038212	0.51226847
C	4.81554242	-14.42079674	-0.46094822
H	4.24584467	-14.75268123	0.40480555
H	4.23729320	-14.57789620	-1.37173135
H	5.76265759	-14.96038212	-0.51226847

DFT B3LYP/6-31+G(d, p), gas phase, S_0
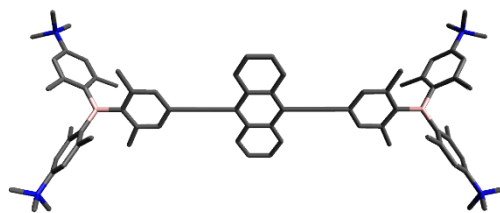
Point group: C_i

Total energy: –2,067,937.82

kcal mol^{-1}

Dipole moment: 0 D

Immaginary frequencies: 0

C	1.90216600	-0.70838600	3.14808900
C	1.28939900	-1.39953600	2.13227800
C	0.64174100	-0.71899500	1.05834200
C	0.64140400	0.72020300	1.05772500
C	1.28874100	1.40196700	2.13107700
C	1.90183200	0.71197600	3.14748100
C	0.00033400	-1.42844200	0.00061200
C	-0.00033400	1.42844200	-0.00061200
C	-0.64174100	0.71899500	-1.05834200
C	-0.64140400	-0.72020300	-1.05772500
C	-1.28874100	-1.40196700	-2.13107700
H	-1.28631700	-2.48590100	-2.13139500
C	-1.90183200	-0.71197600	-3.14748100
C	-1.90216600	0.70838600	-3.14808900
C	-1.28939900	1.39953600	-2.13227800
H	2.38788700	-1.24604900	3.95653100
H	1.28748400	-2.48347000	2.13352400
H	1.28631700	2.48590100	2.13139500
H	2.38730000	1.25056000	3.95546100
H	-2.38730000	-1.25056000	-3.95546100
H	-2.38788700	1.24604900	-3.95653100
H	-1.28748400	2.48347000	-2.13352400
C	0.00066500	-2.84678600	0.00122200
C	0.00094000	-4.06861600	0.00173000
C	0.00122000	-5.48861400	0.00223700
C	-0.70666000	-6.21637500	-0.97388600
C	0.70939800	-6.21539200	0.97887700
C	-0.73485800	-7.61019000	-0.97440400
H	-1.24578800	-5.67126100	-1.74214700
C	0.73814800	-7.60919400	0.98040200
H	1.24832500	-5.66951000	1.74673300
C	0.00178200	-8.35274600	0.00327500
C	-1.53728800	-8.26841600	-2.08259900
C	1.54086200	-8.26631300	2.08904700
B	0.00206800	-9.92096000	0.00386000
H	-1.81682100	-7.53022100	-2.83803600
H	-0.98092100	-9.05828100	-2.59576800
H	-2.46224600	-8.71581100	-1.70504900
H	2.46594700	-8.71369100	1.71179600
H	1.82018700	-7.52745300	2.84391100
H	0.98477800	-9.05597200	2.60284600
C	-1.36283300	-10.74012800	-0.19296500
C	1.36726800	-10.73947600	0.20131200
C	-1.50168300	-11.75019800	-1.18399400
C	-2.47771200	-10.47306300	0.64325100
C	1.50647200	-11.74877600	1.19307300
C	2.48208100	-10.47255600	-0.63503400
C	-2.71187300	-12.43898100	-1.33352000
C	-0.38027200	-12.11294500	-2.13572200

- 190 -

C	-3.67470400	-11.19621000	0.49230300
C	-2.45893100	-9.41495300	1.72892700
C	2.71692600	-12.43697400	1.34314800
C	0.38515500	-12.11129400	2.14500100
C	3.67935400	-11.19511900	-0.48351400
C	2.46292500	-9.41521100	-1.72144700
C	-3.79119400	-12.16505900	-0.49592100
H	-2.77983600	-13.18735200	-2.11576900
H	0.03853900	-11.23177800	-2.63012700
H	0.44091000	-12.61126000	-1.61210100
H	-0.73198500	-12.78699600	-2.92057600
H	-4.49083000	-10.96177600	1.16257600
H	-1.54393000	-9.44188000	2.32514200
H	-2.52657200	-8.40966800	1.30166700
H	-3.30073100	-9.54424100	2.41397700
C	3.79617700	-12.16322300	0.50540100
H	2.78515200	-13.18475200	2.12594200
H	-0.03421500	-11.22992900	2.63857000
H	-0.43568100	-12.61054200	1.62172000
H	0.73715400	-12.78445300	2.93049300
H	4.49542200	-10.96083300	-1.15390900
H	1.54795800	-9.44292400	-2.31767600
H	2.53014100	-8.40960000	-1.29488300
H	3.30480600	-9.54463600	-2.40637200
C	-0.00066500	2.84678600	-0.00122200
C	-0.00094000	4.06861600	-0.00173000
C	-0.00122000	5.48861400	-0.00223700
C	-0.70939800	6.21539200	-0.97887700
C	0.70666000	6.21637500	0.97388600
C	-0.73814800	7.60919400	-0.98040200
H	-1.24832500	5.66951000	-1.74673300
C	0.73485800	7.61019000	0.97440400
H	1.24578800	5.67126100	1.74214700
C	-0.00178200	8.35274600	-0.00327500
C	-1.54086200	8.26631300	-2.08904700
C	1.53728800	8.26841600	2.08259900
B	-0.00206800	9.92096000	-0.00386000
H	-1.82018700	7.52745300	-2.84391100
H	-2.46594700	8.71369100	-1.71179600
H	-0.98477800	9.05597200	-2.60284600
H	0.98092100	9.05828100	2.59576800
H	1.81682100	7.53022100	2.83803600
H	2.46224600	8.71581100	1.70504900
C	1.36283300	10.74012800	0.19296500
C	-1.36726800	10.73947600	-0.20131200
C	2.47771200	10.47306300	-0.64325100
C	1.50168300	11.75019800	1.18399400
C	-2.48208100	10.47255600	0.63503400
C	-1.50647200	11.74877600	-1.19307300
C	3.67470400	11.19621000	-0.49230300
C	2.45893100	9.41495300	-1.72892700
C	2.71187300	12.43898100	1.33352000
C	0.38027200	12.11294500	2.13572200
C	-3.67935400	11.19511900	0.48351400
C	-2.46292500	9.41521100	1.72144700
C	-2.71692600	12.43697400	-1.34314800
C	-0.38515500	12.11129400	-2.14500100
C	3.79119400	12.16505900	0.49592100
H	4.49083000	10.96177600	-1.16257600
H	2.52657200	8.40966800	-1.30166700
H	1.54393000	9.44188000	-2.32514200
H	3.30073100	9.54424100	-2.41397700
H	2.77983600	13.18735200	2.11576900
H	-0.44091000	12.61126000	1.61210100
H	-0.03853900	11.23177800	2.63012700
H	0.73198500	12.78699600	2.92057600
C	-3.79617700	12.16322300	-0.50540100
H	-4.49542200	10.96083300	1.15390900
H	-2.53014100	8.40960000	1.29488300
H	-1.54795800	9.44292400	2.31767600
H	-3.30480600	9.54463600	2.40637200
H	-2.78515200	13.18475200	-2.12594200
H	0.43568100	12.61054200	-1.62172000
H	0.03421500	11.22992900	-2.63857000
H	-0.73715400	12.78445300	-2.93049300
N	5.07686300	12.94093900	0.69670700
N	-5.07686300	-12.94093900	-0.69670700
N	-5.08214700	12.93844300	-0.70680300
N	5.08214700	-12.93844300	0.70680300
C	5.61766400	-12.68810200	2.10577100
H	4.88911900	-13.02790300	2.83834400
H	6.54995100	-13.24159300	2.22409700
H	5.79110300	-11.61853200	2.22086700
C	-5.61766400	12.68810200	-2.10577100
H	-6.54995100	13.24159300	-2.22409700
H	-4.88911900	13.02790300	-2.83834400
H	-5.79110300	11.61853200	-2.22086700
C	5.61253500	12.69182900	2.09583400
H	5.78638900	11.62241000	2.21170600
H	6.54461600	13.24576300	2.21371500
H	4.88389300	13.03188800	2.82819000
C	-5.61253500	-12.69182900	-2.09583400
H	-4.88389300	-13.03188800	-2.82819000
H	-6.54461600	-13.24576300	-2.21371500
H	-5.78638900	-11.62241000	-2.21170600
C	6.16632900	-12.54464100	-0.27028400
H	6.40590600	-11.49026600	-0.14110300
H	7.04581900	-13.14958500	-0.05162900
H	5.82894200	-12.74309800	-1.28649000
C	-6.16632900	12.54464100	0.27028400
H	-7.04581900	13.14958500	0.05162900
H	-6.40590600	11.49026600	0.14110300
H	-5.82894200	12.74309800	1.28649000
C	-4.81750100	-14.42557800	-0.51342500
H	-5.75769500	-14.96129900	-0.64953600
H	-4.09098100	-14.75983400	-1.25054100
H	-4.43001700	-14.58502400	0.49245500
C	4.81750100	14.42557800	0.51342500
H	5.75769500	14.96129900	0.64953600
H	4.43001700	14.58502400	-0.49245500
H	4.09098100	14.75983400	1.25054100
C	-6.16116400	-12.54686300	0.28013800
H	-5.82365700	-12.74444500	1.29647500
H	-6.40117100	-11.49267900	0.15019900
H	-7.04041900	-13.15232000	0.06195900
C	6.16116400	12.54686300	-0.28013800
H	6.40117100	11.49267900	-0.15019900
H	5.82365700	12.74444500	-1.29647500
H	7.04041900	13.15232000	-0.06195900
C	-4.82338800	14.42331800	-0.52458900
H	-4.43600500	14.58364900	0.48119000
H	-4.09697400	14.75733100	-1.26191900
H	-5.76379200	14.95856200	-0.66112300
C	4.82338800	-14.42331800	0.52458900
H	4.09697400	-14.75733100	1.26191900
H	4.43600500	-14.58364900	-0.48119000
H	5.76379200	-14.95856200	0.66112300

7.3 Chapter 4

7.3.1 General Information

Synthesis and Routine Characterization. Unless otherwise noted, the following conditions apply. Reactions were performed using standard Schlenk or glovebox (Innovative Technology Inc.) techniques under an atmosphere of argon. Only oven-dried glassware was used. Solvents used for reactions were HPLC grade, dried using an Innovative Technology Inc. Solvent Purification System, and further deoxygenated by saturation of the solvent with argon.

Bis[4-(*N*,*N*-dimethylamino)-2,6-dimethylphenyl]fluoroborane,[406] 2,2´-*bis*(3,4-ethylenedioxythiophene),[325] *bis*[4-(*N*,*N*-dimethylamino)-2,6-dimethylphenyl]-3-methyl-5-pinacolborylthiophene-2-ylborane,[10] *bis*[4-(*N*,*N*-dimethylamino)-2,6-dimethylphenyl]-2,6-dimethyl-4-pinacolboryl-phenylborane,[9] $Pd_2(dba)_3 \cdot CHCl_3$ (dba = dibenzylideneacetone)[379] and [Ir(COD)(*μ*-OMe)]$_2$ (COD = 1,5-cyclooctadiene)[378] were synthesized according to literature procedures. All other starting materials were purchased from commercial sources and were used without further purification.

Reaction progress was monitored using thin layer chromatography (TLC) plates pre-coated with a layer of silica (Polygram® Sil G/UV254) with fluorescent indicator UV254 from Marchery-Nagel. Automated flash column chromatography was performed using a Biotage® Isolera Four system with silica gel (Biotage SNAP cartridge KP-Sil 50g or KP-Sil 100g obtained from Biotage) as the stationary phase and the solvent system indicated. Solvents were generally removed *in vacuo* using a rotary evaporator at a maximum temperature of 50 °C.

^{1}H, ^{13}C{^{1}H} and ^{11}B{^{1}H} solution NMR spectroscopic data were obtained at ambient temperature using a Bruker Avance 300 III (operating at 300 MHz for ^{1}H, 75 MHz for ^{13}C{^{1}H} and 96 MHz for ^{11}B{^{1}H}), or a Bruker Avance 500 NMR spectrometer (operating at 500 MHz for ^{1}H, 125 MHz for ^{13}C{^{1}H} and 160 MHz for ^{11}B{^{1}H}). Chemical shifts (δ) were referenced to solvent peaks as follows. ^{1}H NMR spectra were referenced via residual proton resonances of CD_2Cl_2 (5.32 ppm), $CDCl_3$ (7.26 ppm) and CD_3OD (3.31 ppm). ^{13}C{^{1}H} spectra were referenced to CD_2Cl_2 (53.84 ppm) and CD_3OD (49.00 ppm).

Elemental analyses were performed on an Elementar vario MICRO cube elemental analyzer. As is common for related organo-B(Aryl)$_2$ compounds, carbon analyses of the compounds were up to 2.3% below the calculated value, while hydrogen, nitrogen and sulfur analyses were satisfactory. This has been ascribed previously to the formation of boron carbide.[386] High resolution mass spectrometry (HRMS) was performed with a Thermo Fisher Scientific Exactive Plus Orbitrap MS System. ESI measurements were performed with a HESI source at 50 °C.

APCI measurements were performed with an ACPI source and Corona needle at 400 °C, unless otherwise noted.

Single-Crystal X-Ray Diffraction. Crystals suitable for single-crystal X-ray diffraction were selected, coated in perfluoropolyether oil, and mounted on MiTeGen sample holders. Diffraction data of **YN** were collected on a Rigaku Oxford Diffraction XtaLAB Synergy diffractometer with a semiconductor HPA-detector (HyPix-6000) and multi-layer mirror monochromated Cu-K$_\alpha$ radiation. The crystal was cooled using an Oxford Cryostream or Bruker Kryoflex low-temperature device. Data were collected at 100 K. The images were processed and corrected for Lorentz-polarization effects and absorption as implemented in the CrysAlis[Pro] software. The structure was solved using the intrinsic phasing method (SHELXT)[382] and Fourier expansion technique. All non-hydrogen atoms were refined in anisotropic approximation, with hydrogen atoms 'riding' in idealized positions, by full-matrix least squares against F^2 of all data, using SHELXL[383] software and the SHELXLE graphical user interface.[387]

Reflections were slightly smeared along the c* direction, which correspond to the longest c axis (ca. 46 Å) in direct space. Hence, the reflections were not always well resolved along this axis and reflection overlap may lead to wrong intensities on integration. As a result, a few reflections with too high intensities had to be omitted from the refinement.

One disordered hexane solvent molecule was found. The remaining residual density was fitted by an ethyl acetate molecule of low occupancy disordered via inversion symmetry as the best model. Several restraints were applied to the anisotropic displacement parameters (SIMU and ISOR) and 1,2- and 1,3-distances (DFIX and SADI) of the disordered solvent molecules.

Diamond[388] software was used for graphical representation. Crystal data and experimental details are listed in Table S12.

Linear Optical Properties. All measurements were performed in standard quartz cuvettes (1 cm x 1 cm cross-section) under ambient conditions, unless stated otherwise. UV-visible absorption spectra were recorded using an Agilent 8453 diode array UV-visible spectrophotometer. The molar extinction coefficients were calculated from three independently prepared samples in toluene (**XN**-**ZN**) and MeCN (**X**, **Z**) solutions. Emission spectra were recorded using an Edinburgh Instruments FLSP920 spectrometer equipped with a 450 W Xenon arc lamp, double monochromator for both excitation and emission, and a red-sensitive photomultiplier (PMT-R928P) and a near-IR PMT as detectors, operating in right-angle geometry mode, and all spectra were fully corrected for the spectral response of the instrument. All solutions used in photophysical measurements had concentrations lower than 5×10^{-6} M to minimize inner filter effects during fluorescence measurements. The

fluorescence quantum yields were measured using a calibrated integrating sphere (inner diameter: 150 mm) from Edinburgh Instruments combined with the FLSP920 spectrometer described above. For solution-state measurements, the longest-wavelength absorption maximum of the compound in the respective solvent was chosen as the excitation wavelength, unless stated otherwise. **Fluorescence lifetimes** were recorded using the time-correlated single-photon counting (TCSPC) method using an Edinburgh Instruments FLS980 spectrometer equipped with a high speed photomultiplier tube positioned after a single emission monochromator. Measurements were made in right-angle geometry mode, and the emission was collected through a polarizer set to the magic angle. Solutions were excited with a pulsed diode laser at a wavelength of 472.6 nm at repetition rates of 10 or 20 MHz, as appropriate. The full-width-at-half-maximum (FWHM) of the pulse from the diode laser was ca. 80 ps with an instrument response function (IRF) of ca. 230 ps FWHM and ca. 200 ps with an instrument response function (IRF) of ca. 1120 ps FWHM, respectively. The IRFs were measured from the scatter of an aqueous suspension of Ludox at the excitation wavelength. Decays were recorded to 10 000 counts in the peak channel with a record length of 8 192 channels. The band pass of the emission monochromator and a variable neutral density filter on the excitation side were adjusted to give a signal count rate of <60 kHz. Iterative reconvolution of the IRF with one decay function and non-linear least-squares analysis were used to analyze the data. The quality of all decay fits was judged to be satisfactory, based on the calculated values of the reduced χ^2 and Durbin-Watson parameters and visual inspection of the weighted residuals.

Electrochemical Measurements. All cyclic voltammetry experiments were conducted in an argon-filled glovebox using a Gamry Instruments Reference 600 potentiostat. A standard three-electrode cell-configuration was employed using a platinum disk working electrode, a platinum wire counter electrode, and a silver wire reference electrode separated by a Vycor frit, serving as the reference electrode. The redox potentials are referenced to the ferrocene/ferrocenium ([Fc/Fc$^+$]) redox couple by using decamethylferrocene as an internal standard. Tetra-*n*-butylammonium hexafluorophosphate ([*n*Bu$_4$N][PF$_6$]) was employed as the supporting electrolyte. Compensation for resistive losses (*iR* drop) was employed for all measurements.

Transient Absorption Measurements. Transient absorption spectra were measured with an Edinburgh LP920 laser flash spectrometer equipped with a EKSPLA NT340 Nd:YAG laser with integrated optical parametric oscillator, a 450 W Xe arc flash lamp, a Hamamatsu R955 photomultiplier and a Tektronix TD3012B oscilloscope for detection of the spectra. The pump and white light beams were perpendicular to each other. The transient maps were obtained by measuring temporal decay profiles in 4 nm steps between *ca.* 33 333 cm^{-1} (300 nm) and 12500 cm^{-1} (800 nm) and corrected for fluorescence. The instrument response (*ca.* 8 ns) of

the set-up was determined by measuring the scattered light using a LUDOX AS-30 colloidal silica suspension in water. Decay curves were fitted with the tailfit function of the spectrometer software. The quality of all decay fits was judged to be satisfactory, based on the calculated values of the reduced χ^2 and Durbin-Watson parameters and visual inspection of the weighted and autocorrelated residuals. All solvents were spectroscopic grade and were used without further purification. The samples were dissolved in MeCN, degassed by at least 5 freeze-pump-thaw cycles, and placed in 10 x 10 mm quartz-cuvettes equipped with a *Young´s* valve. The samples were excited with *ca.*~5 ns laser pulses at 10 Hz repetition rate. Measurements were performed at pulse energies of 1.2 mJ (excitation at 460 and 550 nm). The stability of the samples was verified by recording the steady-state absorption spectra before and after the time-resolved measurements.

Theoretical studies. All calculations (DFT and TD-DFT) were carried out with the Gaussian 16 (16.A.03)[398] program package and were performed on a parallel cluster system. GaussView (6.0.16), Avogadro (1.2.0)[399] and multiwfn[400] were used to visualize the results, to measure calculated structural parameters, and to plot orbital surfaces (isovalue: ± 0.030 [e a_0^{-3}]$^{1/2}$). The ground-state geometries were optimized using the B3LYP functional[401] in combination with the 6-31G+(d,p) basis set.[402, 403] The ultrafine integration grid and no symmetry constraints were used for all molecules. Frequency calculations were performed on the optimized structures to confirm them to be local minima showing no negative (imaginary) frequencies. Based on these optimized structures, the lowest-energy vertical transitions (gas-phase) were calculated (singlets, 25 states) by TD-DFT, using the CAM-B3LYP functional in combination with the 6-31G+(d,p) basis set.[402, 403] Solvent effects were included using the PCM model as implemented in Gaussian.

7.3.2 Synthesis

5,5´-Dibromo-2,2´-*bis*(3,4-ethylenedioxythiophene)
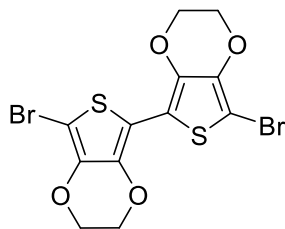
With the exclusion of light, 2,2´-*bis*(3,4-ethylenedioxythiophene) (555 mg, 1.97 mmol, 1.0 eq) was dissolved in CH_2Cl_2 (150 mL) and cooled to -15 °C. *N*-bromosuccinimide (770 mg, 4.32 mmol, 2.20 eq) was added in small portions within 45 min and the reaction was stirred for another 1 h at -15 °C. The reaction mixture was poured into a mixture of ice water / 25% aqueous NH_3 (500 mL / 12 mL) and extracted with CH_2Cl_2 (4 x 100 mL). Residual solid was removed from the organic phases by filtration and the combined organic phase was washed with water (2 x 100 mL) and brine (100 mL). The solvent was removed *in vacuo* at a maximum temperature of 30 °C. The product 5,5´-dibromo-2,2´-*bis*(3,4-ethylenedioxythiophene) was obtained as an off-white solid (788 mg, 91%) and stored at 8 °C. The spectroscopic data matched those reported previously.[329]

¹H NMR (300 MHz, $CDCl_3$): $δ$ = 4.31 (m, 8H) ppm.

5,5'-Bis[*bis*(4-(*N,N*-dimethylamino)-2,6-dimethylphenyl)boryl]-2,2'-bis(3,4-ethylenedioxythiophene) (XN)
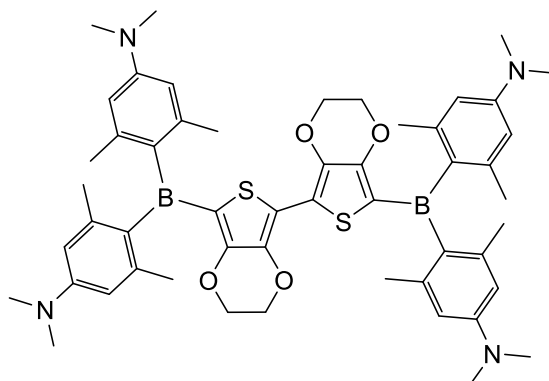
The compound 2,2´-*bis*(3,4-ethylenedioxythiophene) (200 mg, 703 μmol, 1 eq) was dissolved in THF (6 mL), cooled to -78 °C and treated dropwise with *n*-butyllithium (2.5 mol in hexane, 620 μL, 2.2 eq). The solution was stirred for 45 min at -78 °C. *Bis*[4-(*N,N*-dimethylamino)-2,6-dimethylphenyl]fluoroborane (460 mg, 1.41 mmol, 2.0 eq) was dissolved in THF (10 mL) and added to the reaction mixture. The mixture was warmed to r.t. and stirred for 3 d, until the starting material was consumed according to TLC (EtOAc /hexane 1:4). Water (5 mL) was added and the product was extracted with CH_2Cl_2. After removing the solvent *in vacuo*, the solid was purified by automated flash column chromatography (hex/EtOAc 4:1), giving compound **XN** as an orange solid (173 mg, 27%).

^{1}H NMR (500 MHz, CD_2Cl_2): δ = 6.35 (s, 8H), 4.21 (m, 8H), 2.95 (s, 24H), 2.09 (s, 24H) ppm.

^{13}C{^{1}H} NMR (125 MHz, CD_2Cl_2): δ = 151.3, 147.8, 142.9, 139.8, 133.5, 125.4, 121.9, 111.6, 65.2, 65.2, 40.3, 23.8 ppm.

HRMS (APCI) m/z: [M+H]$^+$ found: 895.4624; calc. for [$C_{52}H_{65}B_2N_4O_4S_2$]$^+$: 895.4589 (|Δ| = 3.91 ppm).

Elemental analysis Calc. (%) for $C_{52}H_{64}B_2N_4O_4S_2$: C 69.80, H 7.21, N 6.26, S 7.17; found: C 69.69, H 7.41, N 6.26, S 6.85.

5,5'-Bis[4-(*bis*(*N,N*-dimethylamino)-2,6-dimethylphenyl)boryl)-4-methylthiophen-2-yl]-2,2'-bis(3,4-ethylenedioxythiophene) (YN)
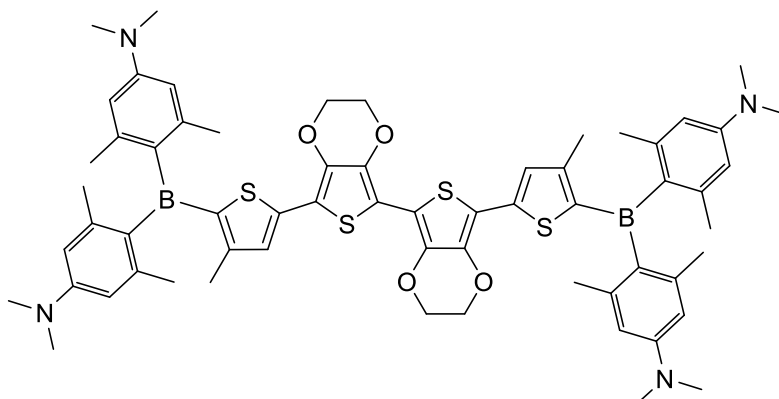
Bis[4-(*N,N*-dimethylamino)-2,6-dimethylphenyl]-3-methyl-5-pinacolborylthiophene-2-ylborane (133 mg, 251 μmol, 2.0 eq), 5,5´-dibromo-2,2´-*bis*(3,4-ethylenedioxythiophene) (55.3 mg, 125 μmol, 1.0 eq), SPhos (7.2 mg, 17.6 μmol, 14 mol%), Pd$_2$(dba)$_3$·CHCl$_3$ (9.1 mg, 8.8 μmol, 7 mol%) and Cs$_2$CO$_3$ (246 mg, 754 mmol, 6.0 eq) were dissolved in a mixture of toluene (3 mL) and water (1.5 mL). The mixture was stirred for 2 d at 85 °C, until the starting material was consumed according to TLC (EtOAc /hexane 1:2). The organic phase was separated and the aqueous phase was extracted with CH$_2$Cl$_2$ (4 x 10 mL). After removing the solvent *in vacuo* from the combined organic phase, the solid was purified by automated flash column chromatography (hex/EtOAc 4:1). For further purification, the solid was recrystallized from CH$_2$Cl$_2$/MeOH, giving **YN** as a red solid (20 mg, 15%).

^{1}H NMR (300 MHz, CD$_2$Cl$_2$): δ = 7.22 (m, 2H), 6.37 (s, 8H), 4.37 (s, 8H), 2.96 (s, 24H), 2.08 (s, 24H), 2.00 (s, 6H) ppm.

^{13}C{^{1}H} NMR (125 MHz, CD$_2$Cl$_2$): δ = 151.4, 148.4, 145.6, 143.6, 142.6, 138.4, 137.9, 134.3, 128.6, 111.7, 111.2, 108.8, 65.6, 65.5, 40.3, 23.7, 16.2 ppm.

HRMS (APCI) m/z: [M+H]$^+$ found: 1087.4684; calc. for [C$_{62}$H$_{73}$B$_2$N$_4$O$_4$S$_4$]$^+$: 1087.4695 (|Δ| = 1.01 ppm).

Elemental analysis Calc. (%) for C$_{62}$H$_{72}$B$_2$N$_4$O$_4$S$_4$: C 68.50, H 6.68, N 5.15, S 11.80; found: C 66.36, H 7.11, N 5.01, S 11.40.

5,5'-Bis[4-(*bis*(4-(*N,N*-dimethylamino)-2,6-dimethylphenyl)boryl)-3,5-dimethylphenyl]-2,2'-*bis*(3,4-ethylenedioxythiophene) (ZN)
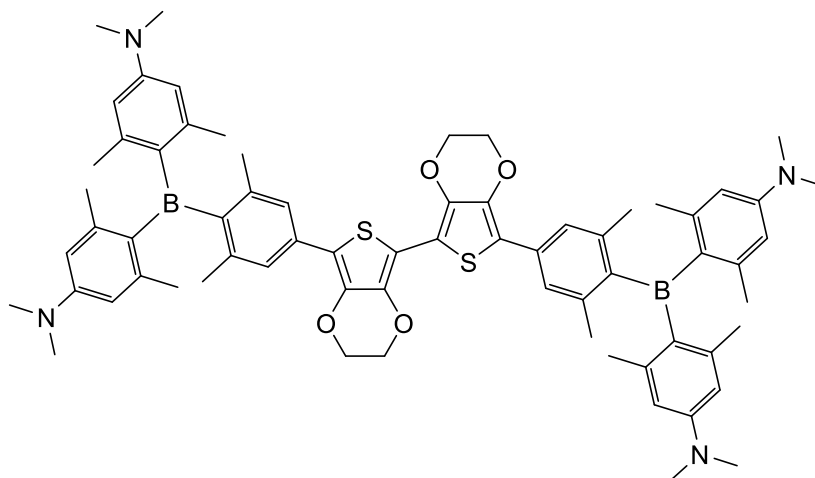
Bis[4-(*N,N*-dimethylamino)-2,6-dimethylphenyl]-2,6-dimethyl-4-pinacolboryl-phenylborane (375 mg, 697 μmol, 2.0 eq), 5,5′-dibromo-2,2′-*bis*(3,4-ethylenedioxythiophene) (153 mg, 349 μmol, 1.0 eq), SPhos (20 mg, 48.9 μmol, 14 mol%), Pd$_2$(dba)$_3$·CHCl$_3$ (25 mg, 24.4 μmol, 7 mol%) and Cs$_2$CO$_3$ (682 mg, 2.09 mmol, 6.0 eq) were dissolved in a mixture of toluene (8 mL) and water (4 mL). The mixture was stirred for 2 d at 85 °C, until the starting material was consumed according to TLC (EtOAc /hexane 1:2). Water (15 mL) was added and the product was extracted with CH$_2$Cl$_2$. After removing the solvent *in vacuo* from the combined organic phase, the solid was purified by automated flash column chromatography (hex/EtOAc 4:1). For further purification, the solid was recrystallized from CH$_2$Cl$_2$/MeOH, giving compound **ZN** as a yellow solid (74 mg, 19%).

^{1}H NMR (500 MHz, CD$_2$Cl$_2$): δ = 7.31 (s, 4H), 6.31 (m, 8H), 4.39 (m, 8H), 2.95 (s, 24H), 2.05 (s, 12H), 2.01 (s, 12H), 1.97 (s, 12H) ppm.

^{13}C{^{1}H} NMR (125 MHz, CD$_2$Cl$_2$): δ = 151.7, 148.5, 143.2, 142.9, 141.0, 138.5, 138.1, 136.3, 133.3, 124.7, 115.9, 111.9, 111. 8, 108.4, 65.4, 65.2, 40.2, 24.0, 23.8, 23.1 ppm.

HRMS (APCI) m/z: [M+H]$^+$ found: 1103.5890; calc. for: [C$_{68}$H$_{81}$B$_2$N$_4$O$_4$S$_2$]$^+$: 1103.5841 (|Δ| = 4.44 ppm).

Elemental analysis Calc. (%) for C$_{68}$H$_{80}$B$_2$N$_4$O$_4$S$_2$: C 74.04, H 7.31, N 5.08, S 5.81; found: C 73.51, H 7.49, N 5.06, S 5.44.

5,5'-Bis[*bis*(4-(*N,N,N*-trimethylammonium)-2,6-dimethylphenyl)boryl]-2,2'-bis(3,4-ethylenedioxythiophene) tetratriflate (X)
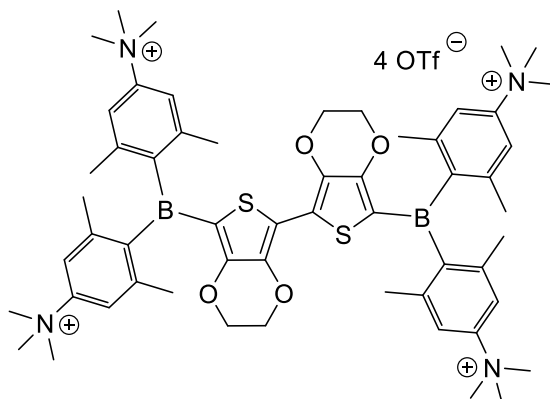
Compound **XN** (14.7 mg, 16.4 μmol, 1.0 eq) was dissolved in CH_2Cl_2 (2 mL). Methyl triflate (9.3 μL, 82.1 μmol, 5 eq) was added and the reaction was stirred at r.t. for 1 d. The precipitate was collected by filtration and washed with CH_2Cl_2 (3 x 5 mL), giving compound **X** as a green-yellow solid (12.3 mg, 48%).

¹H NMR (500 MHz, CD_3OD): δ = 7.54 (s, 8H), 4.21 (m, 8H), 3.66 (s, 36H), 2.33 (s, 24H) ppm.

¹³C{¹H} NMR (125 MHz, CD_3OD): 152.3, 148.8, 146.6, 144.9, 141.9, 126.4, 123.5, 121.8 (q, J = 318 Hz), 119.2, 66.3, 66.0, 57.5, 23.7 ppm.

HRMS (ESI pos) m/z: [M-2OTf]²⁺ found: 626.2263; calc. for $[C_{58}H_{76}B_2N_4S_4F_6O_{10}]^{2+}$: 626.2262 ($|\Delta|$ = 0.16 ppm).

Elemental analysis Calc. (%) for $C_{60}H_{76}B_2F_{12}N_4O_{16}S_6$: C 46.46, H 4.94, N 3.61, S 12.40; found: C 44.19, H 5.13, N 3.43, S 11.73.

5,5'-Bis[4-(*bis*(4-(*N,N,N*-trimethylammonium)-2,6-dimethylphenyl)boryl)-4-methylthiophen-2-yl]-2,2'-bis(3,4-ethylenedioxythiophene) tetratriflate (Y)
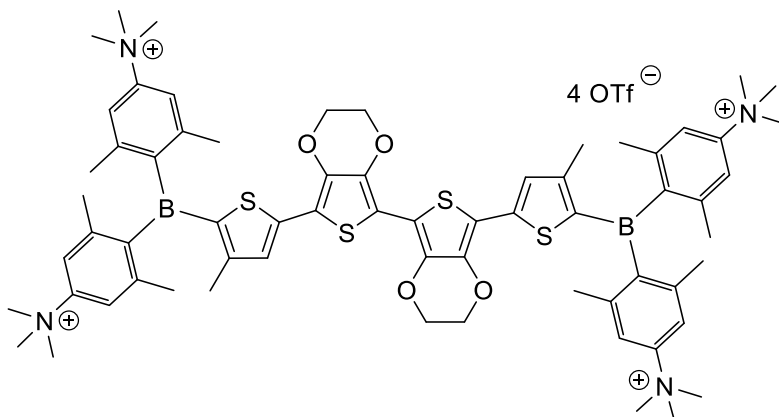
Compound **YN** (8.2 mg, 7.54 μmol, 1.0 eq) was dissolved in CH_2Cl_2 (20 mL). Methyl triflate (27.3 μL, 241 μmol, 32 eq) was added and the reaction was stirred at r.t. for 1 d. The precipitate was collected by filtration and washed with CH_2Cl_2 (3 x 5 mL), giving 9.7 mg of compound **Y**, contaminated with an unidentified impurity, as a violet solid.

Despite a prominent signal of an unidentified impurity at δ = 4.59 ppm in the ^{1}H NMR spectrum, a reasonable assignment of the remaining signals to the respective protons of compound **Y** was possible. Together with an unambiguous identification of **Y** *via* HRMS, **Y** is proposed as the main product of the described reaction. A broader discussion of this is given in the main text.

^{1}H NMR (300 MHz, CD_3OD): δ = 7.59 (m, 8H), 7.35 (s, 2H), 3.67 (m, 36H), 2.33 (m, 24H), 2.02 (s, 6H) ppm.

HRMS (ESI pos) m/z: [M-2OTf]$^{2+}$ found: 722.2300; calc. for $[C_{68}H_{84}B_2N_4S_6F_6O_{10}]^{2+}$: 722.2296 (|$\Delta$| = 0.55 ppm).

5,5'-*Bis*[4-(*bis*(4-(*N,N,N*-trimethylammonium)-2,6-dimethylphenyl)boryl)-3,5-dimethylphenyl]-2,2'-*bis*(3,4-ethylenedioxythiophene) tetratriflate (Z)
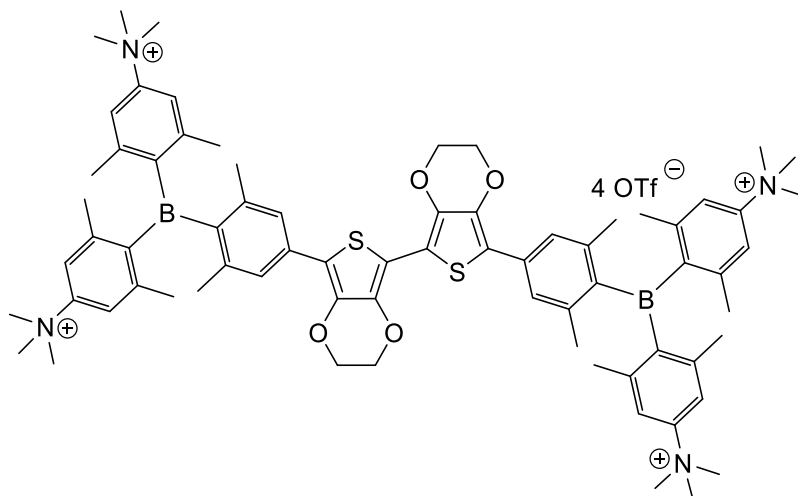
Compound **ZN** (15.0 mg, 13.6 μmol, 1.0 eq) was dissolved in CH$_2$Cl$_2$ (2 mL). Methyl triflate (6.9 μL, 61.2 μmol, 4.5 eq) was added and the reaction was stirred at r.t. for 1 d. The precipitate was collected by filtration and washed with CH$_2$Cl$_2$ (3 x 5 mL), giving compound **Z** as a dark red solid (16 mg, 67%).

^{1}H NMR (500 MHz, CD$_3$OD,): δ = 7.57 (m, 8H), 7.42 (m, 4H), 4.42 (m, 8H), 3.66 (s, 36H), 2.25 (s, 12H), 2.15 (s, 12H), 2.04 (s, 12H) ppm.

^{13}C{^{1}H} NMR (125 MHz, CD$_3$OD): 149.7, 149.6, 145.0, 144.4, 142.7, 140.7, 139.4, 137.5, 126.2, 121.8 (q, J = 318 Hz), 120.1, 115.8, 110.5, 66.3, 66.2, 57.5, 23.6, 23.4 ppm.

HRMS (ESI pos) m/z: [M-2OTf]$^{2+}$ found: 730.2910; calc. for [C$_{74}$H$_{92}$B$_2$N$_4$S$_4$F$_6$O$_{10}$]$^{2+}$ 730.2888 (|Δ| = 3.01 ppm).

Elemental analysis Calc. (%) for C$_{76}$H$_{92}$B$_2$F$_{12}$N$_4$O$_{16}$S$_6$: C 51.88, H 5.27, N 3.18, S 10.93; found: C 50.31, H 5.58, N 2.94, S 10.33.

7.3.3 NMR Spectra
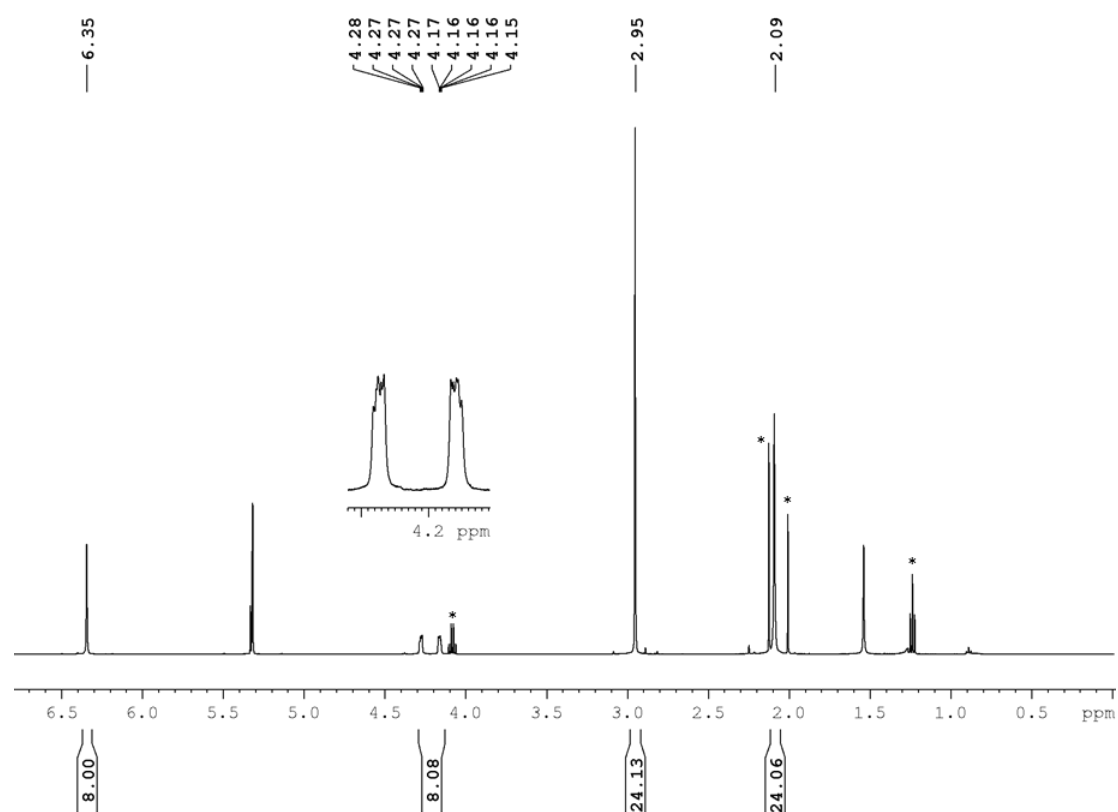
Figure S109. ^{1}H NMR spectrum of **XN** in CD_2Cl_2 at 500 MHz. Residual solvent peaks (EtOAc, acetone) are marked with *.
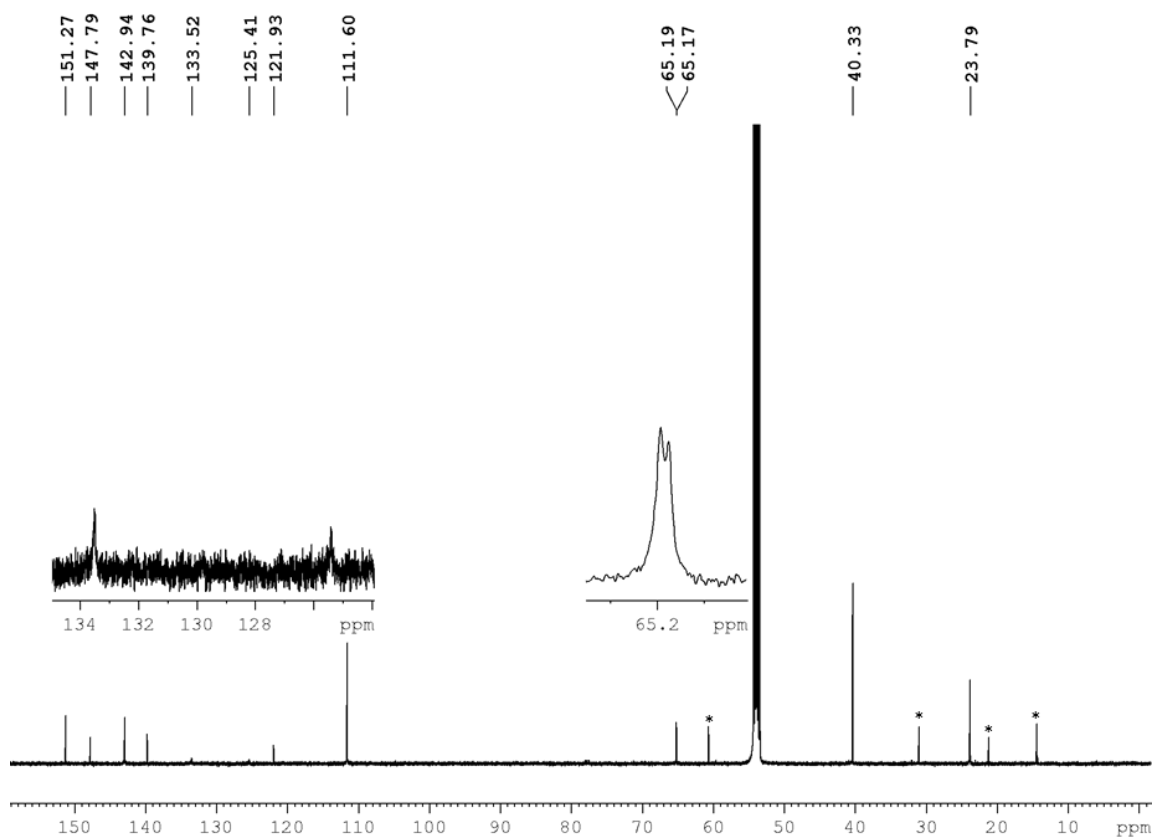
Figure S110. ^{13}C{^{1}H} NMR spectrum of **XN** in CD_2Cl_2 at 75 MHz. Residual solvent peaks (EtOAc, acetone) are marked with *.
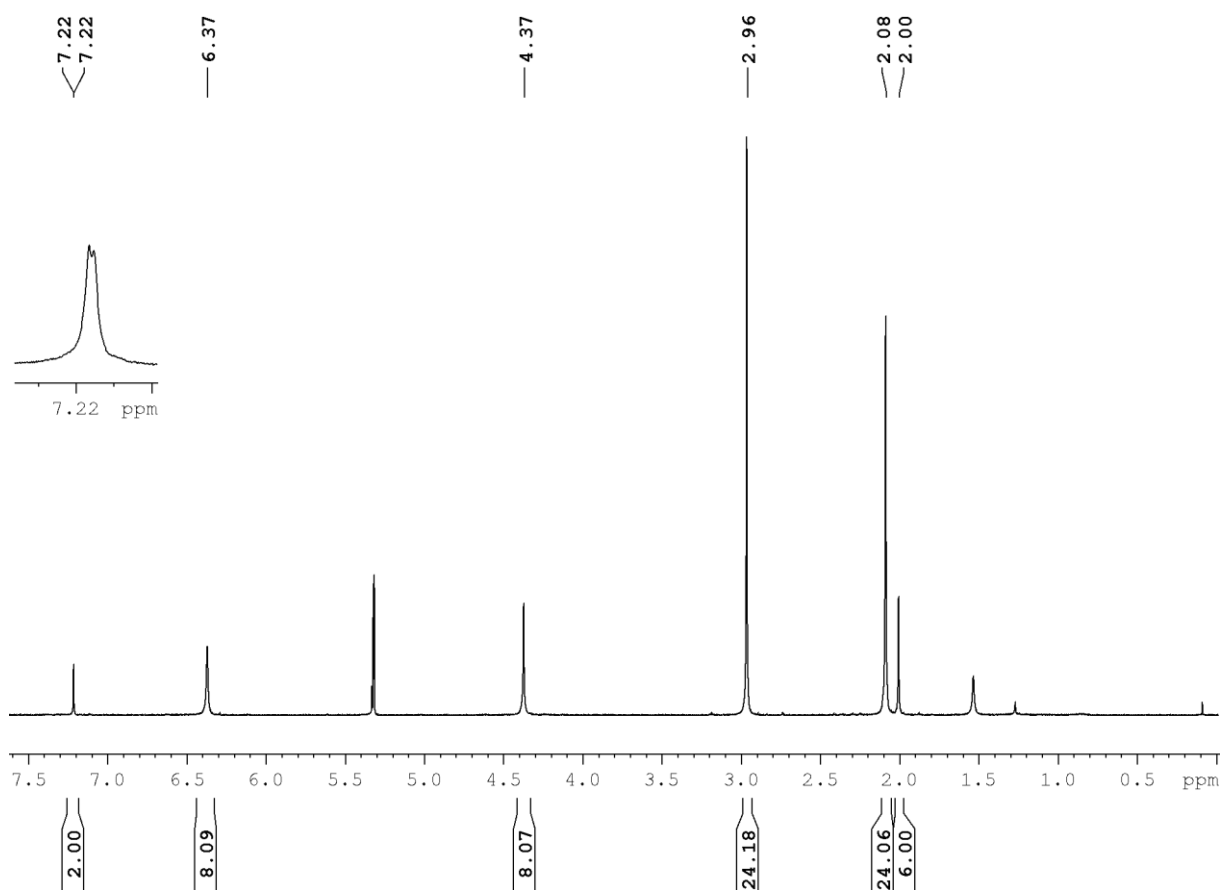
Figure S111. ^{1}H NMR spectrum of **YN** in CD_2Cl_2 at 300 MHz.
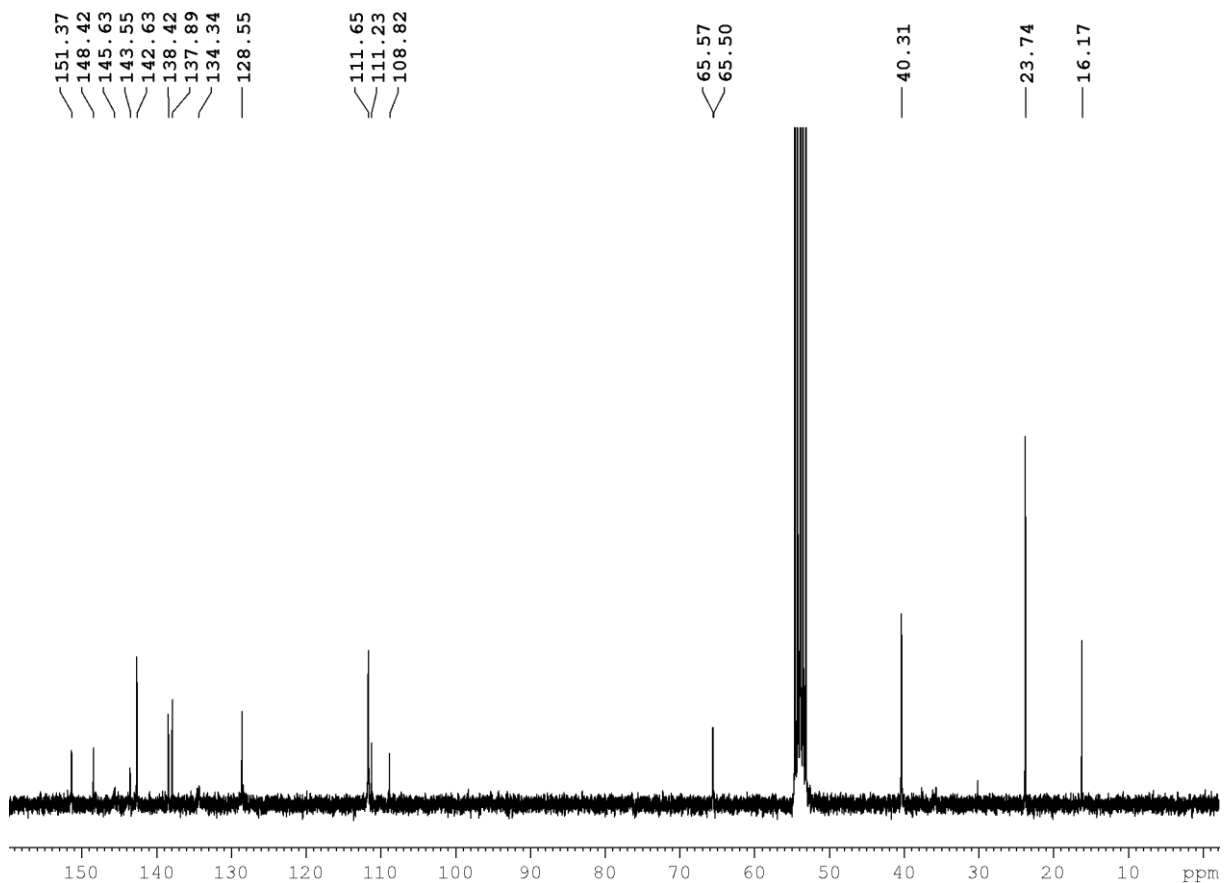
Figure S112. $^{13}C\{^1H\}$ NMR spectrum of **YN** in CD_2Cl_2 at 75 MHz.
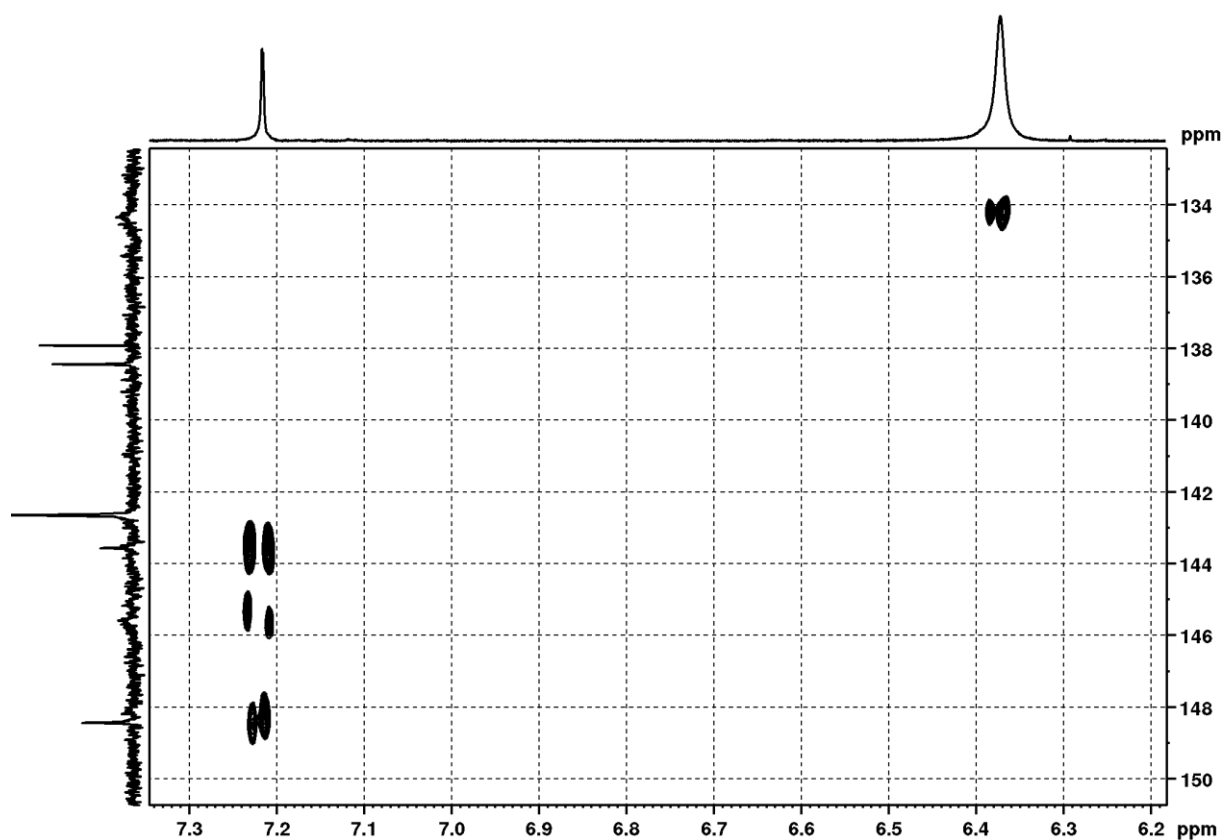
Figure S113. ^{13}C, ^{1}H HMBC NMR spectrum of **YN** in CD_2Cl_2 at 300 MHz.
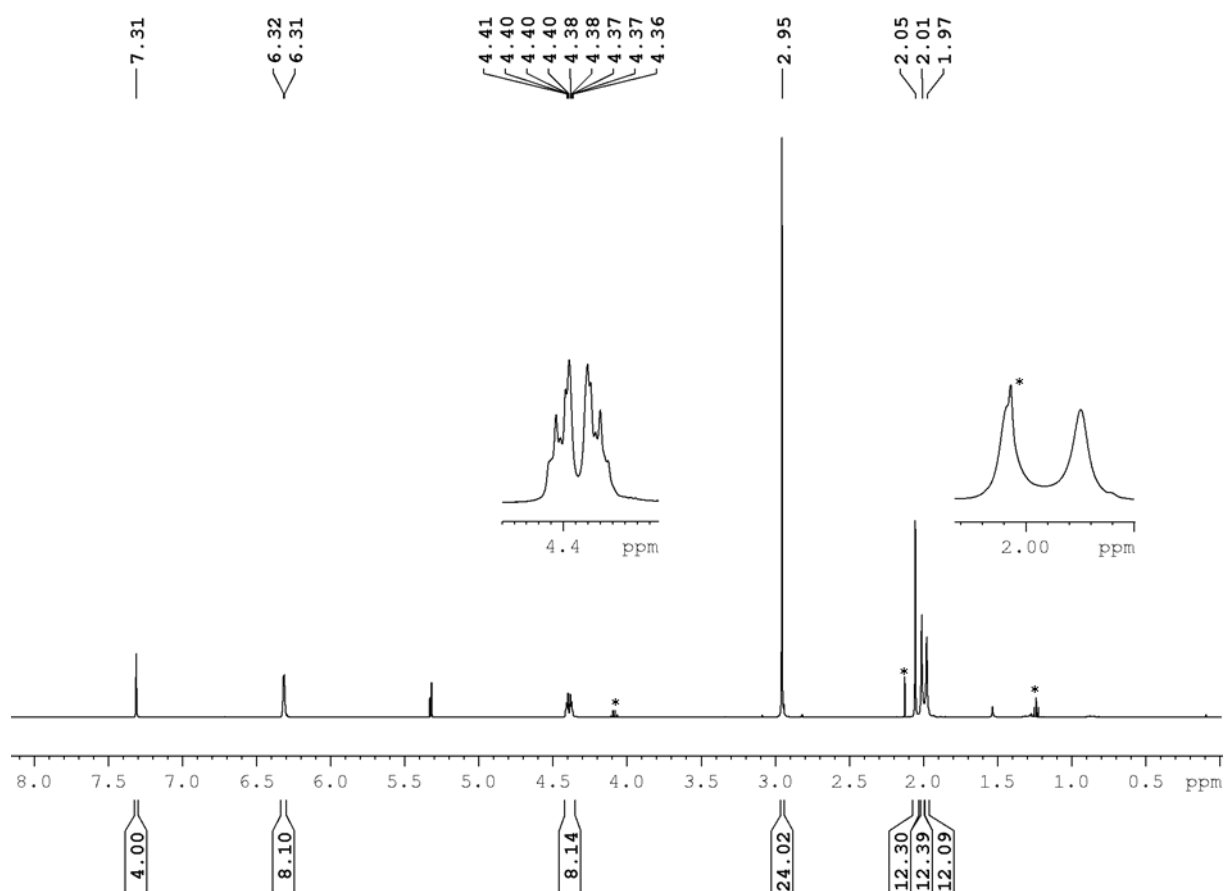
Figure S114. ^{1}H NMR spectrum of **ZN** in CD_2Cl_2 at 500 MHz. Residual solvent peaks (EtOAc, acetone) are marked with *.
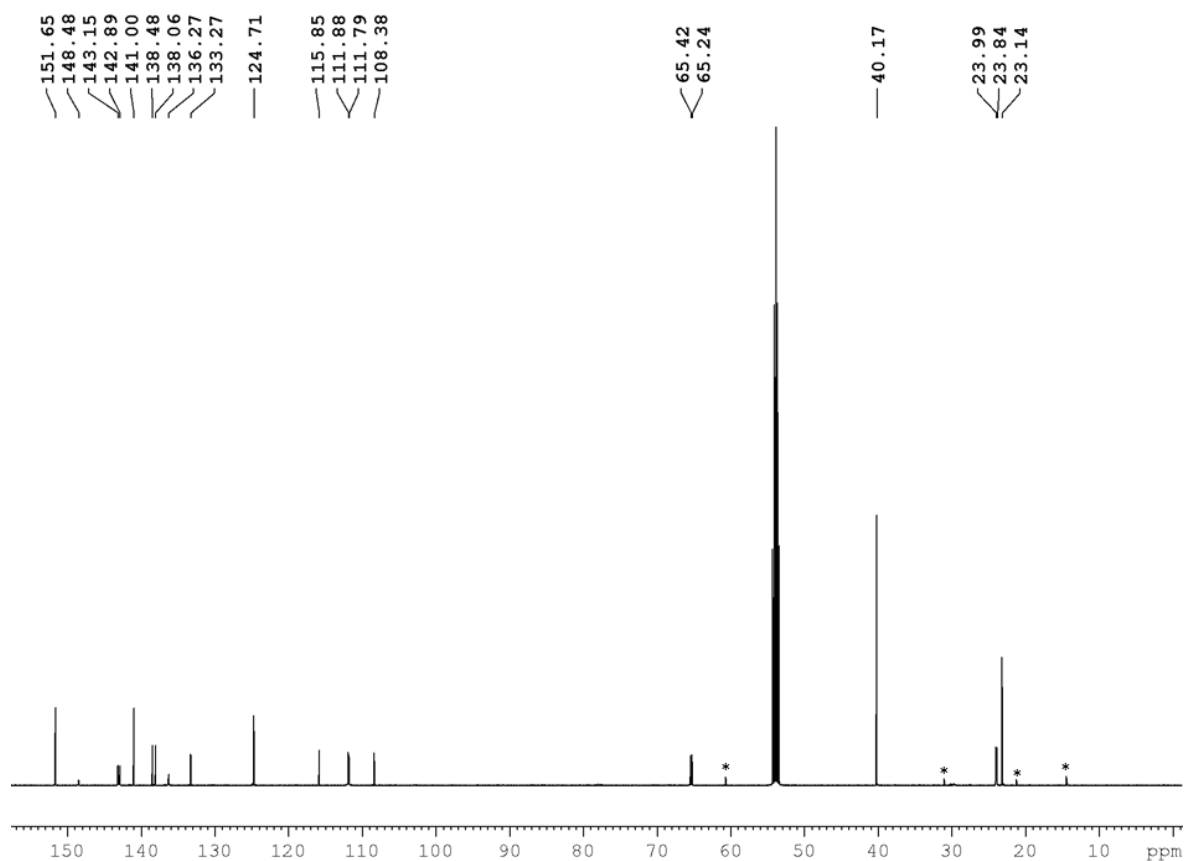
Figure S115. $^{13}C\{^1H\}$ NMR spectrum of **ZN** in CD_2Cl_2 at 125 MHz. Residual solvent peaks (EtOAc, acetone) are marked with *.
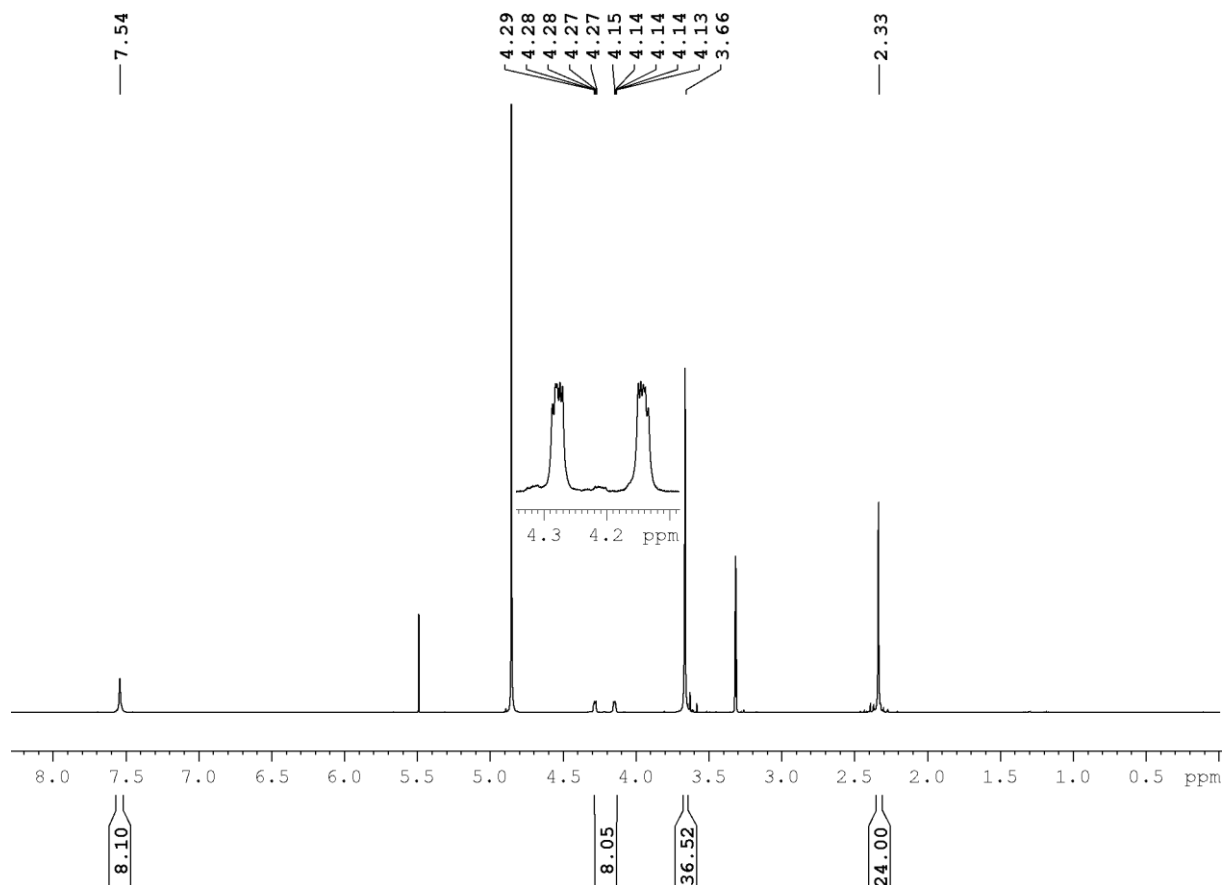
Figure S116. ^1H NMR spectrum of **X** in CD_3OD at 500 MHz.
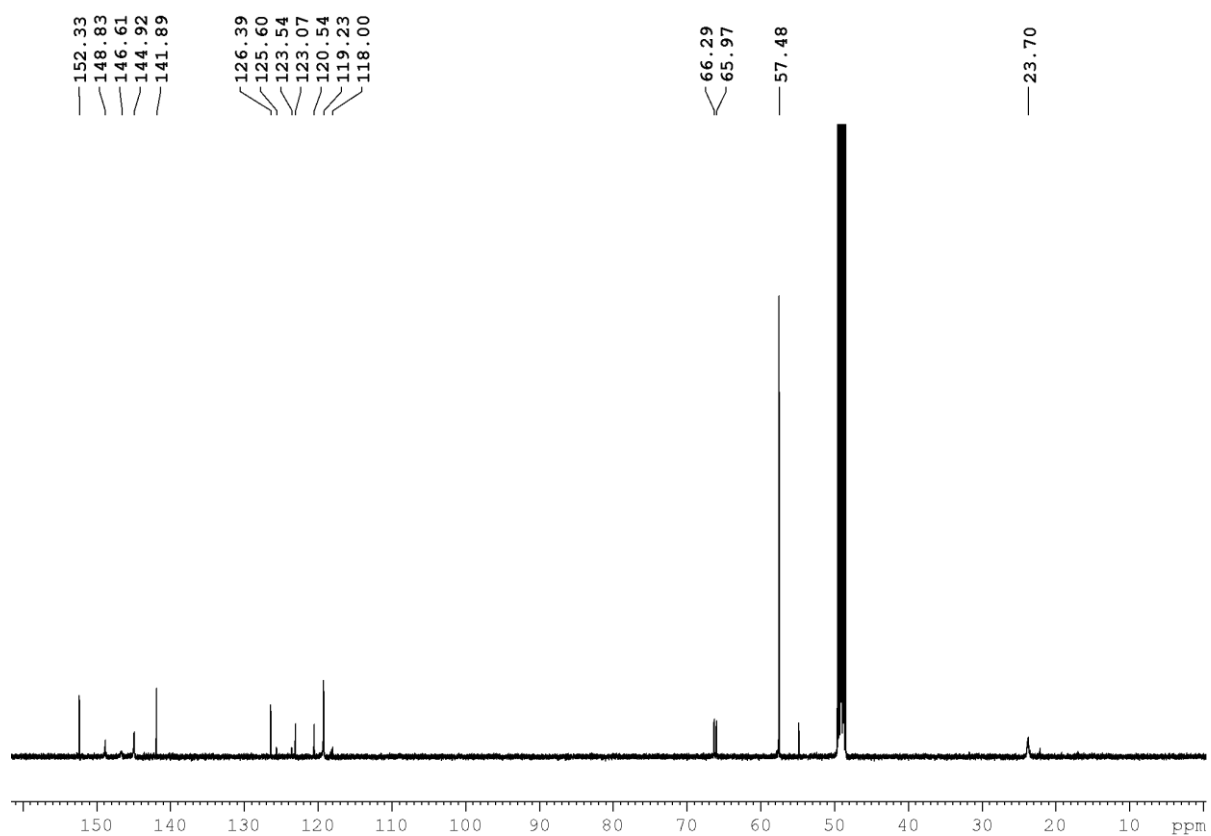
Figure S117. $^{13}C\{^{1}H\}$ NMR spectrum of **X** in CD$_3$OD at 125 MHz.
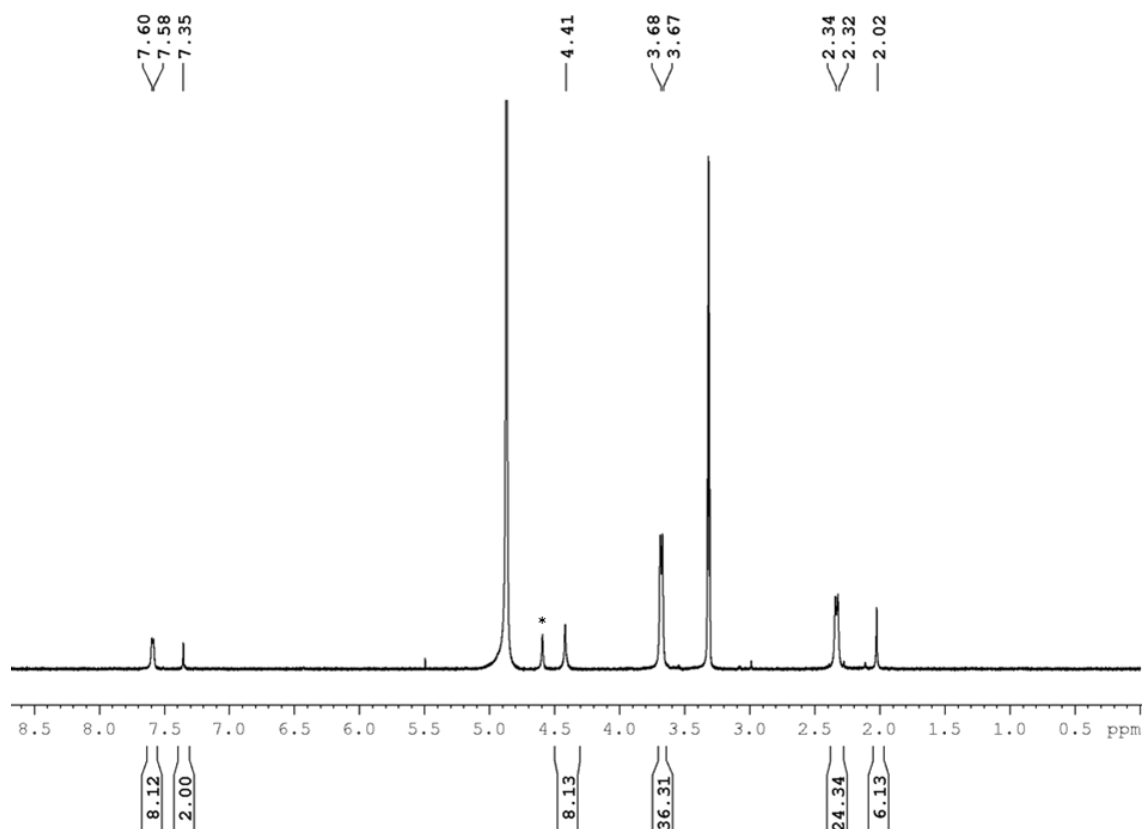
Figure S118. ^{1}H NMR spectrum of **Y** in CD$_3$OD at 300 MHz. Unidentified impurity is marked with *.
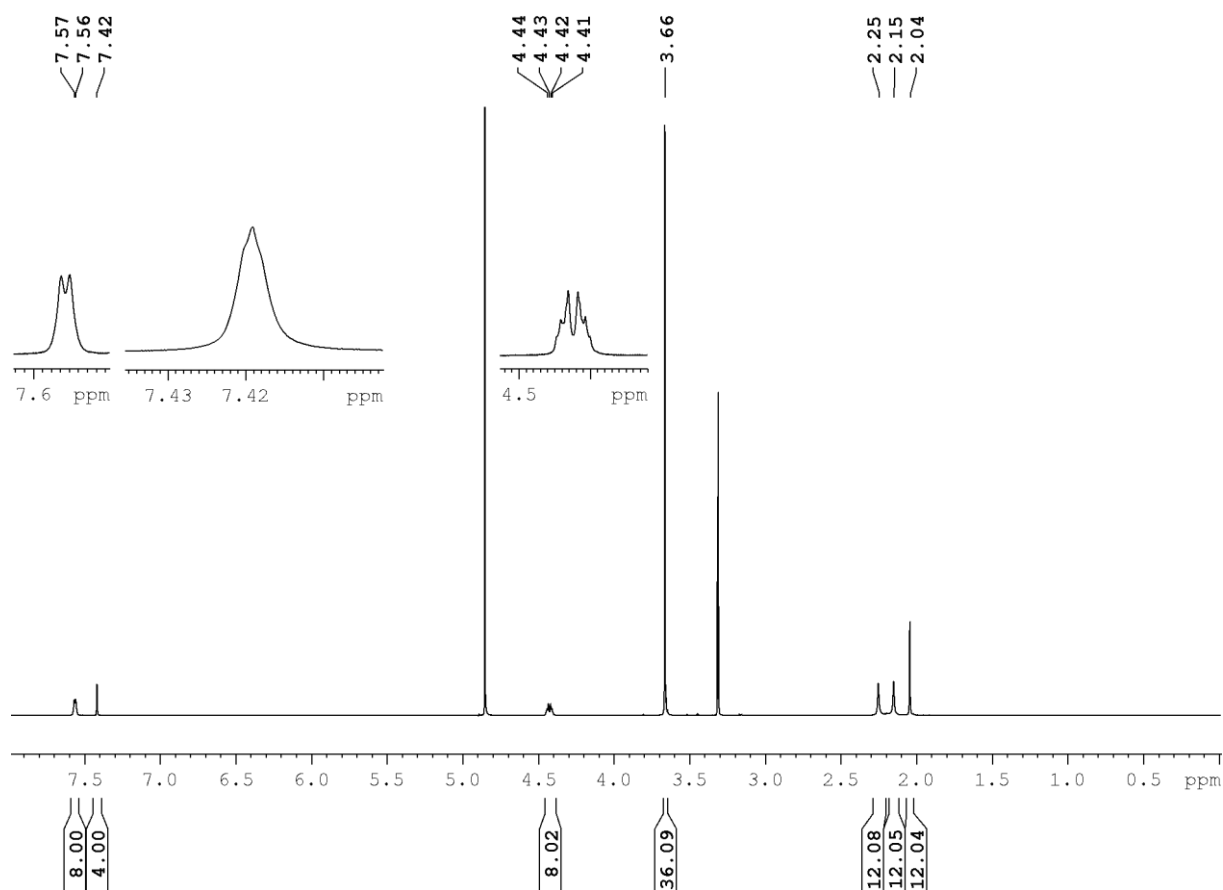
Figure S119. ^{1}H NMR spectrum of **Z** in CD$_3$OD at 500 MHz.
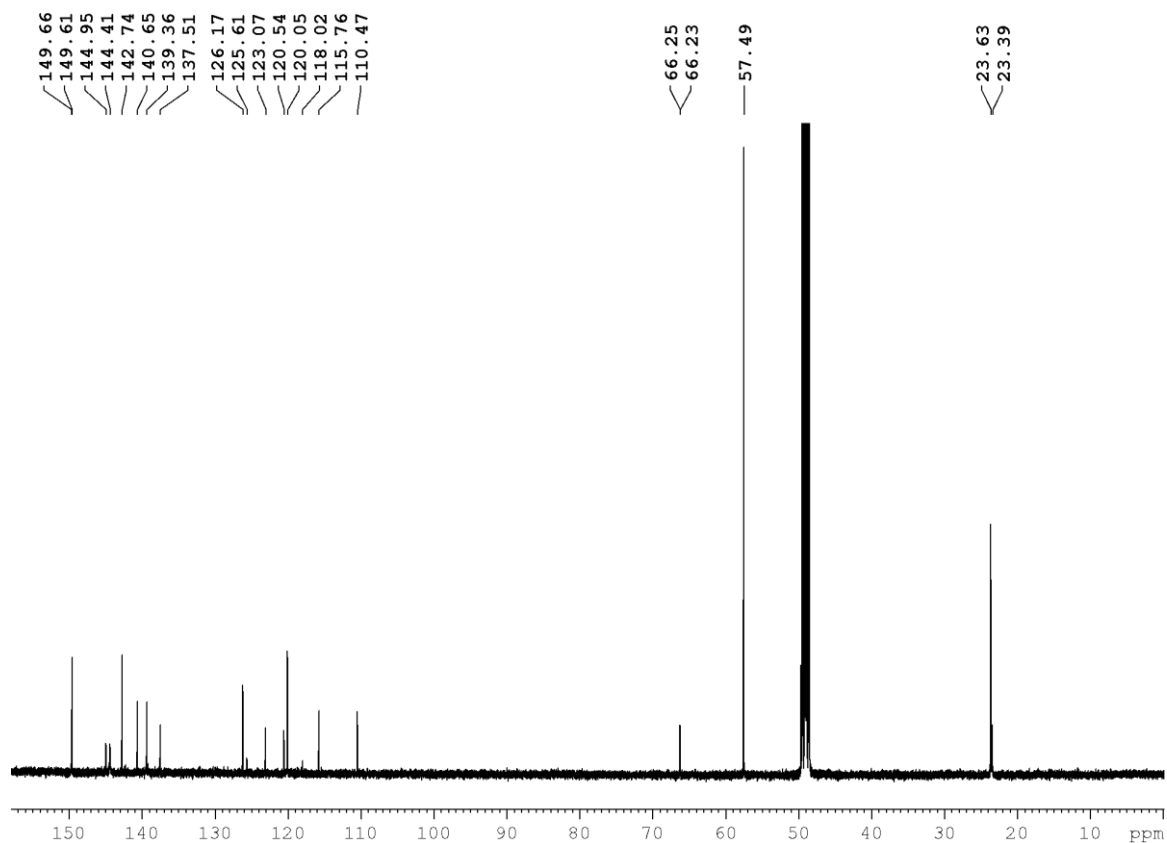
Figure S120. ^{13}C{^{1}H} NMR spectrum of **Z** in CD$_3$OD at 125 MHz.

7.3.4 Single-Crystal X-Ray Diffraction

Table S12. Single-crystal X-ray diffraction data and structure refinements of compounds **YN**.

Data	YN
Empirical formula	$C_{65.45}H_{79.89}B_2N_4O_{4.22}S_4$
Formula weight	1140.03
Temperature/K	100(2)
Crystal system	monoclinic
Space group	$P2_1/n$
a/Å	16.72280(10)
b/Å	16.11870(10)
c/Å	46.3545(4)
α/°	90
β/°	93.9260(10)
γ/°	90
Volume/Å^3	12465.52(15)
Z	8
ρ_{calc}g/cm^3	1.215
μ/mm^{-1}	1.789
F(000)	4867.0
Crystal size/mm^3	0.465 × 0.104 × 0.035
Radiation	Cu-K$_\alpha$ (λ = 1.54184)
2Θ range for data collection/°	5.506 to 149.006
Index ranges	-12 ≤ h ≤ 20, -20 ≤ k ≤ 18, -57 ≤ l ≤ 57
Reflections collected	132996
Independent reflections	25334 [R_{int} = 0.0530, R_σ = 0.0345]
Data/restraints/parameters	25334/337/1570
Goodness-of-fit on F^2	1.147
Final R indices [I>=2σ (I)]	R_1 = 0.0755, wR_2 = 0.1848
Final R indices [all data]	R_1 = 0.0837, wR_2 = 0.1898
Largest diff. peak/hole / e Å^{-3}	0.93/-0.62
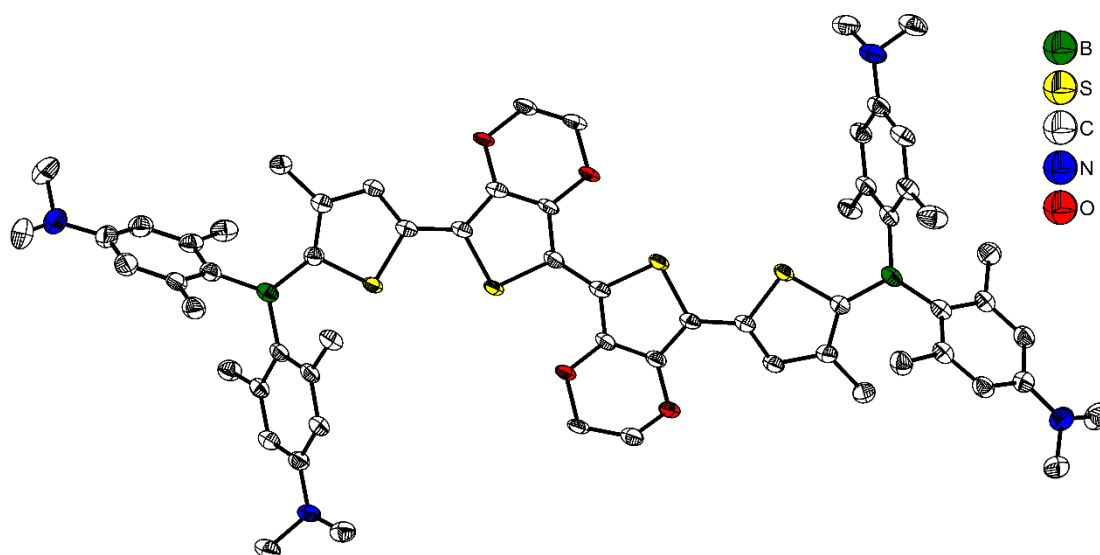
Figure S121. Molecular structure of compound **YN** in the solid state at 100 K. Atomic displacement ellipsoids are drawn at the 50% probability level, and H atoms and co-crystallized solvent molecules (hexane and ethylacetate) are omitted for clarity.

7.3.5 Linear Optical Properties

Table S13. Photophysical data for compounds **X-Z** in various solvents.

	solvent	λ_{abs} / nm	ε / M^{-1} cm^{-1}	λ_{em} / nm	Stokes shift[a] / cm^{-1}	Φ_f	τ / ns	k_r / 10^8 s^{-1}	k_{nr} / 10^8 s^{-1}
X	MeCN	462	53 000	492	1 300	0.03	0.3	1.2	38.8
	H$_2$O	458		495	1 600	-[b]	-[b]		
Y[c]	MeCN	536	-[c]	601	2 000	-[c]	-[c]		
	H$_2$O	526		614	2 700	-[c, b]	-[c, b]		
Z	MeCN	482	56 000	662	5 600	0.07	0.8	0.9	11.8
	H$_2$O[a]	465		651	6 100	0.01	< 0.2		

[a] apparent Stokes shift; [b] not measurable due to rapid decomposition; [c] for **Y** only the spectra are given and they should be interpreted with care due to an unidentified impurity. For the same reason, measurements of ε, Φ_f and τ were not performed.

7.3.5 Electrochemistry

Half-wave potentials were determined for all six compounds even though their reduction and oxidation events are not always fully chemically reversible. In particular, the redox events of the sterically less protected compounds **X**, **X'**, **Y** and **Y'** are accompanied by irreversible processes.
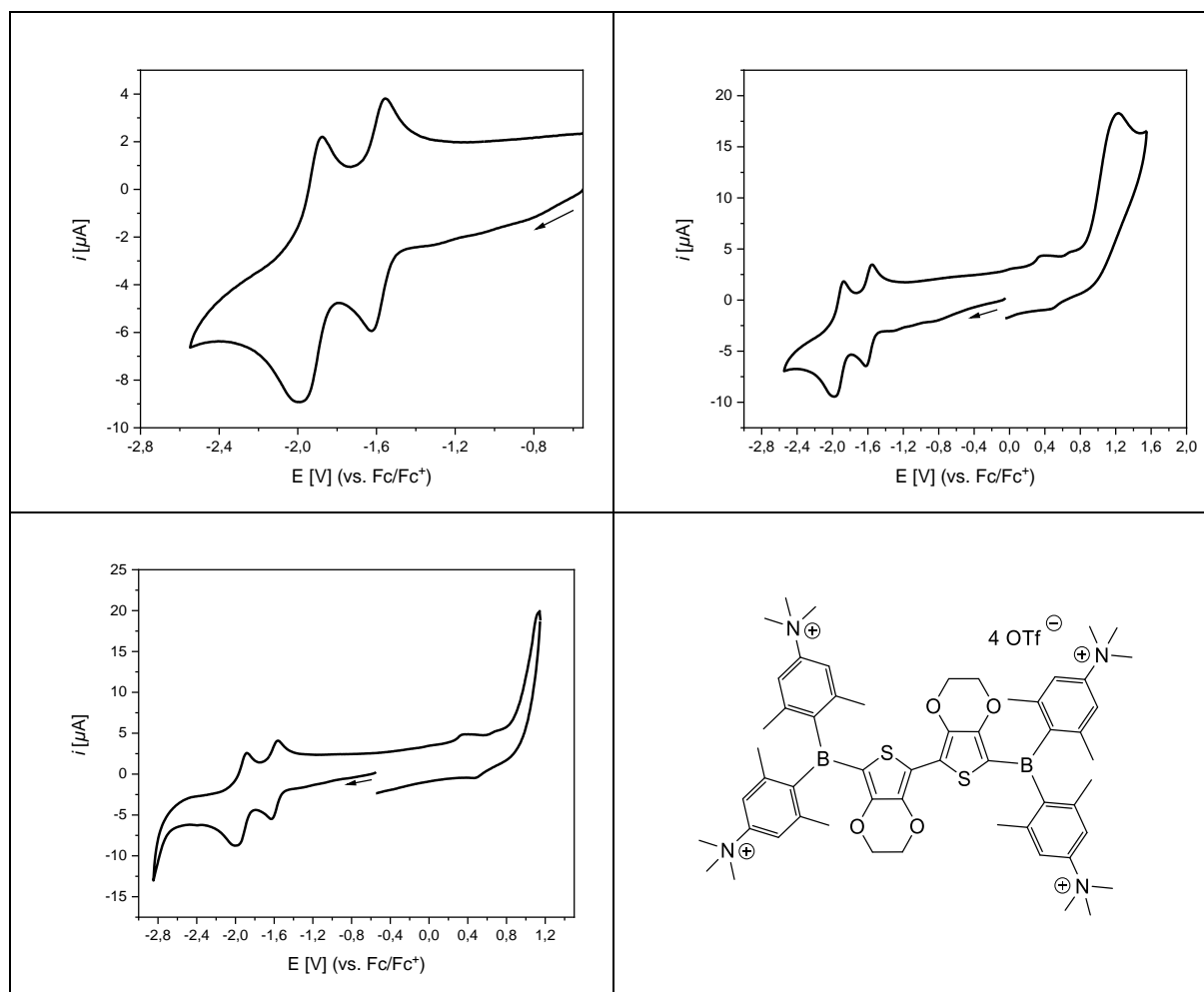
Figure S122. Cyclic voltammograms of compound **X**. All measurements were performed in acetonitrile with [*n*Bu₄N][PF₆] as the electrolyte with a scan rate of 250 mV s^{-1} and are referenced to the Fc/Fc$^+$ ion couple.

Table S14. Half-wave potentials of partially reversible reduction processes of **X**.

	1st reduction potential $E_{1/2}$ [V] vs. Fc/Fc$^+$	2nd reduction potential $E_{1/2}$ [V] vs. Fc/Fc$^+$
X	-1.59	-1.93
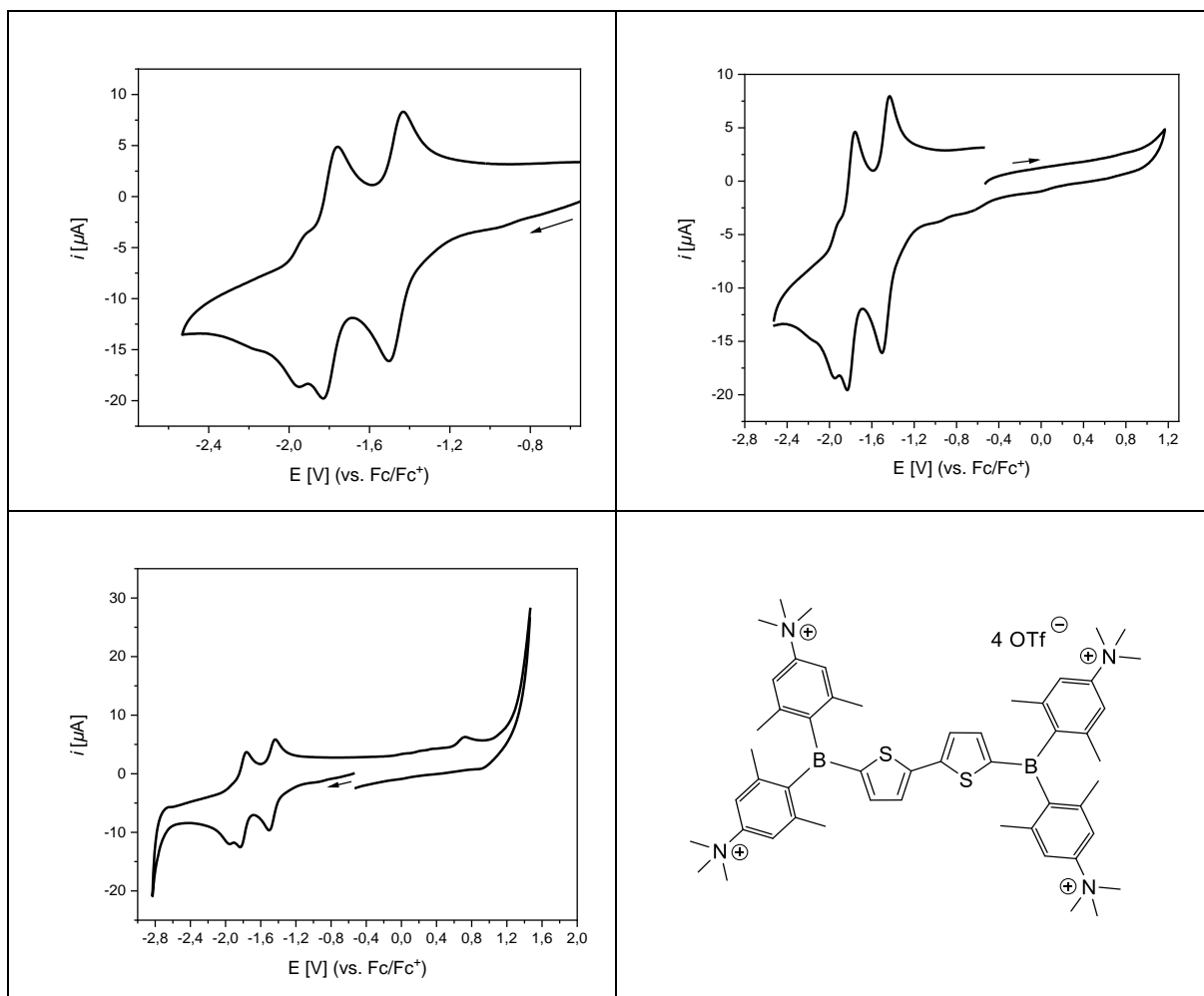
Figure S123. Cyclic voltammograms of compound **X'**. All measurements were performed in acetonitrile with [nBu$_4$N][PF$_6$] as the electrolyte with a scan rate of 250 mV s^{-1} and are referenced to the Fc/Fc$^+$ ion couple.

Table S15. Half-wave potentials of partially reversible reduction processes of **X'**.

	1st reduction potential E$_{1/2}$ [V] vs. Fc/Fc$^+$	2nd reduction potential E$_{1/2}$ [V] vs. Fc/Fc$^+$
X'	-1.46	-1.79
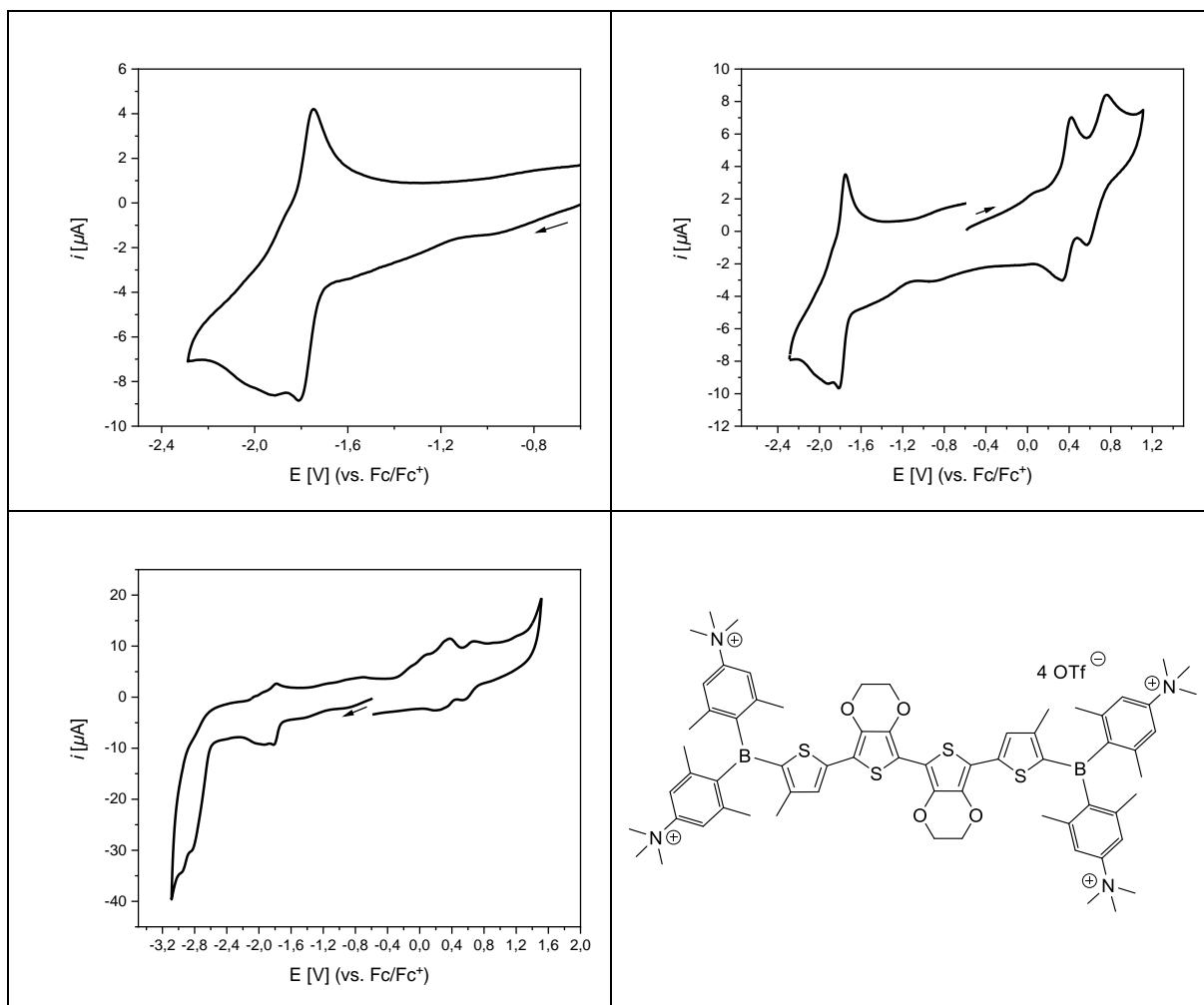
Figure S 124. Cyclic voltammograms of compound **Y**. All measurements were performed in acetonitrile with [nBu$_4$N][PF$_6$] as the electrolyte with a scan rate of 250 mV s^{-1} and are referenced to the Fc/Fc$^+$ ion couple.

Table S16. Half-wave potentials of partially reversible reduction and oxidation processes of **Y**.

	1st reduction potential E$_{1/2}$ [V] vs. Fc/Fc$^+$	1st oxidation potential E$_{1/2}$ [V] vs. Fc/Fc$^+$	2nd oxidation potential E$_{1/2}$ [V] vs. Fc/Fc$^+$
Y	-1.78	0.38	0.67
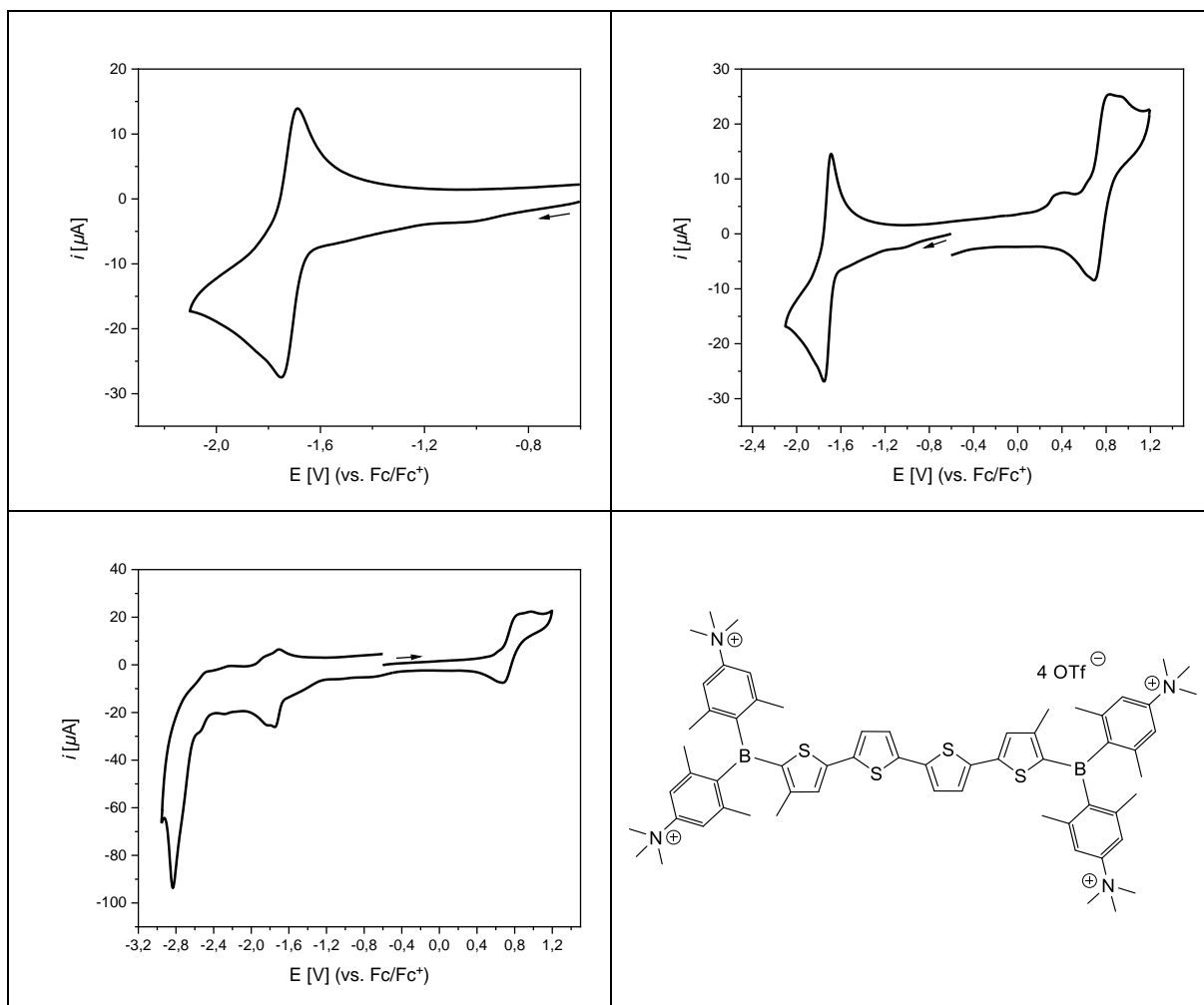
Figure S125. Cyclic voltammograms of compound **Y'**. All measurements were performed in acetonitrile with [*n*Bu$_4$N][PF$_6$] as the electrolyte with a scan rate of 250 mV s^{-1} and are referenced to the Fc/Fc$^+$ ion couple.

Table S17. Half-wave potentials of partially reversible reduction and oxidation processes of **Y'**.

	1st reduction potential $E_{1/2}$ [V] vs. Fc/Fc$^+$	1st oxidation potential $E_{1/2}$ [V] vs. Fc/Fc$^+$	2nd oxidation potential $E_{1/2}$ [V] vs. Fc/Fc$^+$
Y'	-1.71	0.76	-

- 214 -

Figure S126. Cyclic voltammograms of compound **Z**. All measurements were performed in acetonitrile with [*n*Bu₄N][PF₆] as the electrolyte with a scan rate of 250 mV s^{-1} and are referenced to the Fc/Fc$^+$ ion couple.

Table S18. Half-wave potentials of partially reversible reduction and oxidation processes of **Z**.

	1st reduction potential $E_{1/2}$ [V] vs. Fc/Fc$^+$	1st oxidation potential $E_{1/2}$ [V] vs. Fc/Fc$^+$	2nd oxidation potential $E_{1/2}$ [V] vs. Fc/Fc$^+$
Z	-1.97	0.34	0.80
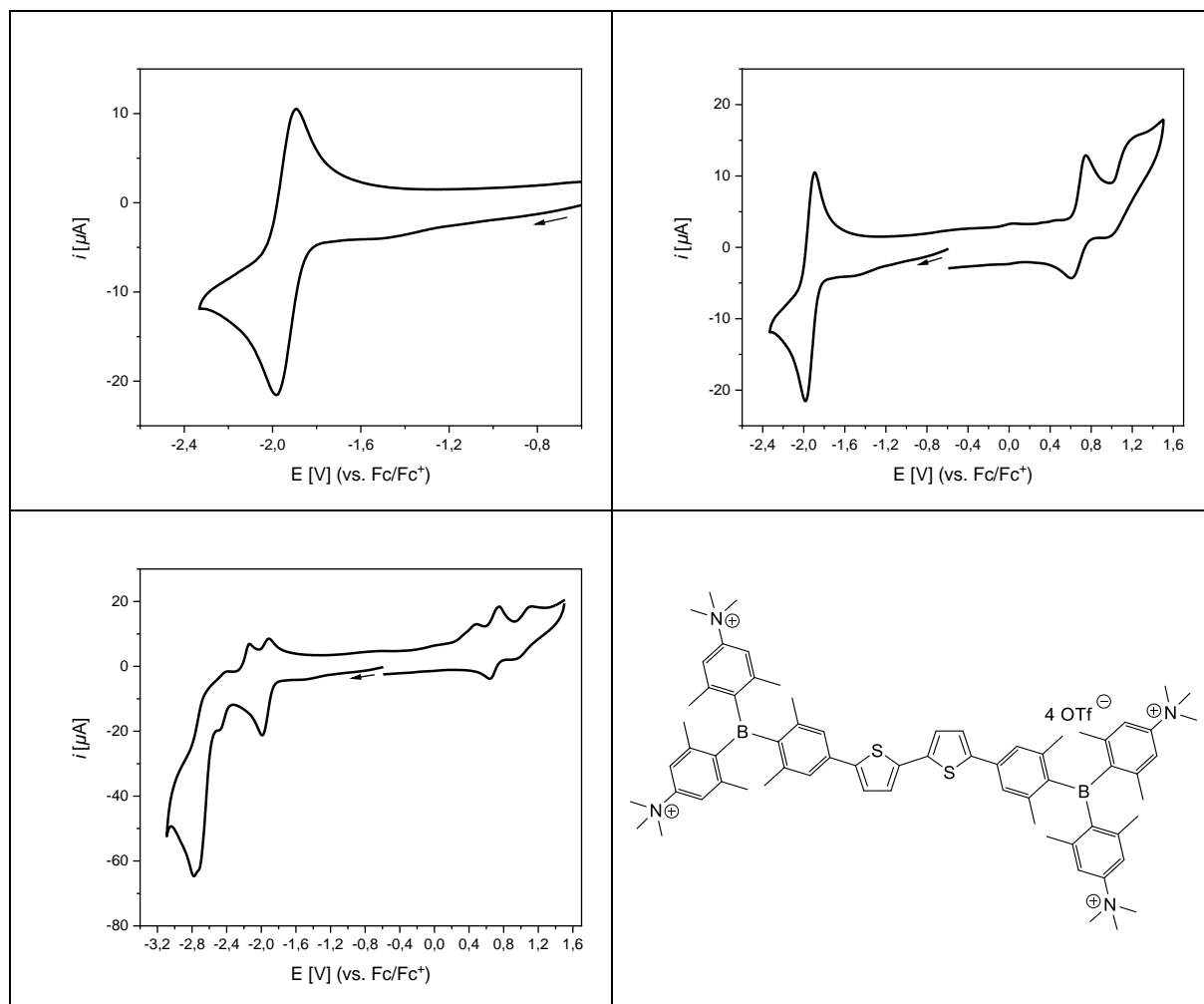
Figure S127. Cyclic voltammograms of compound **Z'**. All measurements were performed in acetonitrile with [nBu$_4$N][PF$_6$] as the electrolyte with a scan rate of 250 mV s^{-1} and are referenced to the Fc/Fc$^+$ ion couple.

Table S19. Half-wave potentials of partially reversible reduction and oxidation processes of **Z'**.

	1st reduction potential E$_{1/2}$ [V] vs. Fc/Fc$^+$	1st oxidation potential E$_{1/2}$ [V] vs. Fc/Fc$^+$	2nd oxidation potential E$_{1/2}$ [V] vs. Fc/Fc$^+$
Z'	-1.92	0.68	-

7.3.6 Transient Absorption
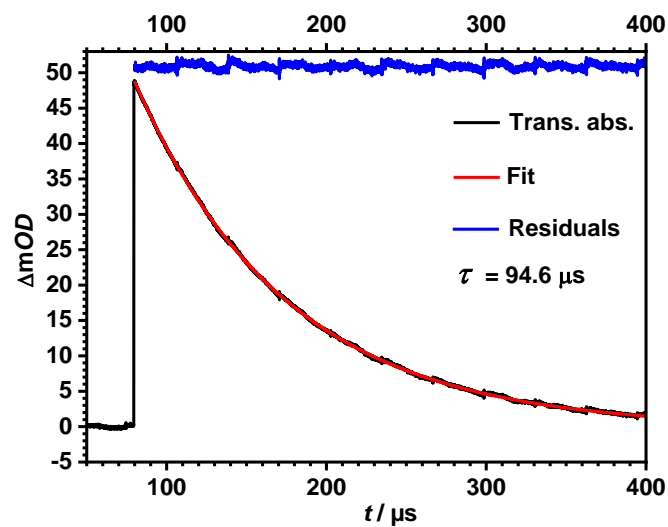
Figure S128. Transient absorption decay curve at 565 nm (black) and fit (red).
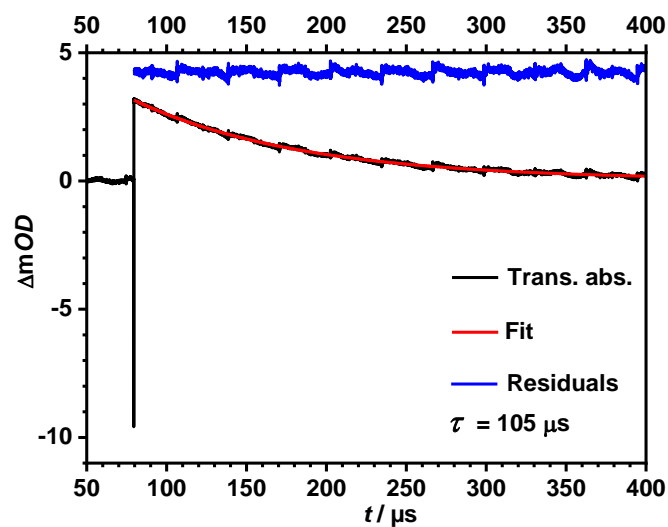
Figure S129. Transient absorption decay curve at 575 nm (black) and fit (red).

7.3.7 Theoretical Studies

Compound XN
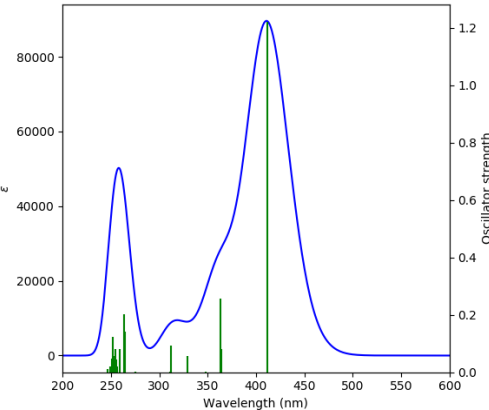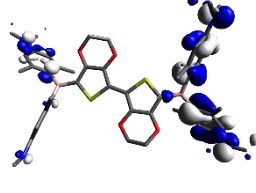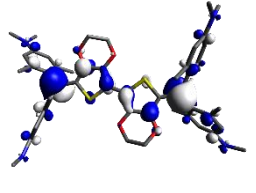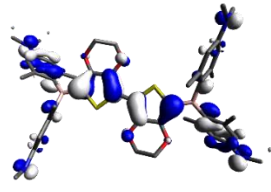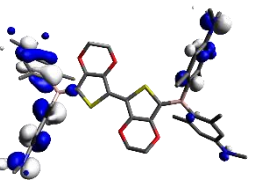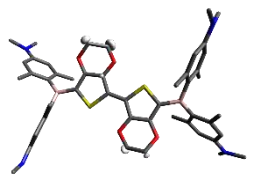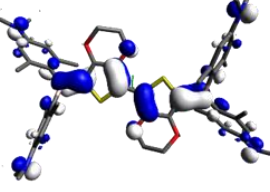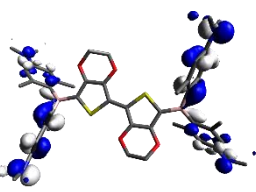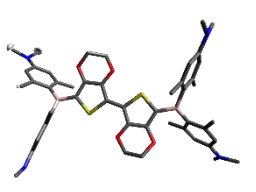
Calculated absorption spectrum	Orbital	Energy [eV]		Sym.
		gas phase	toluene	
TD-DFT CAM-B3LYP/6-31G+(d,p), gas phase	L+4	0.80	0.80	A
	L+3	0.77	0.72	A
	L+2	0.64	0.59	A
	L+1	0.04	-0.12	A
	LUMO	-0.94	-1.11	A
	HOMO	-6.13	-6.28	A
	H-1	-6.27	-6.40	A
	H-2	-6.27	-6.40	A
	H-3	-6.34	-6.47	A
	H-4	-6.61	-6.75	A

Orbitals relevant to the $S_1 \leftarrow S_o$ transition	other relevant orbitals	
LUMO	**HOMO-1**	**LUMO+1**
HOMO	**HOMO-2**	**LUMO+2**
HOMO-4	**HOMO-3**	**LUMO+3**

- 218 -

Table S20. Lowest energy singlet electronic transition of **XN** (TD-DFT CAM-B3LYP/6-31G+(d,p), gas phase).

State	E [eV]	λ [nm]	f	Sym.	Major contributions	Λ
1	3.01	411.52	1.2219	A	H-4->LUMO (12%), HOMO->LUMO (77%)	0.63
2	3.41	363.78	0.0811	A	H-2->L+1 (12%), H-1->LUMO (69%)	0.36
3	3.41	363.54	0.2564	A	H-2->LUMO (70%), H-1->L+1 (13%)	0.36
4	3.56	347.98	0.0007	A	H-3->LUMO (68%), HOMO->L+1 (19%)	0.45
5	3.77	328.91	0.0553	A	H-4->LUMO (68%), H-3->L+1 (11%)	0.67
6	3.97	312.52	0.0934	A	H-5->LUMO (77%)	0.66
7	3.98	311.60	0.0037	A	H-6->LUMO (78%)	0.65
8	4.21	294.76	0.0001	A	H-4->L+1 (28%), H-3->LUMO (12%), HOMO->L+1 (43%)	0.60
9	4.44	279.09	0.0005	A	H-7->LUMO (45%), H-7->L+1 (18%)	0.29
10	4.45	278.89	0.0006	A	H-8->LUMO (44%), H-8->L+1 (17%)	0.32
11	4.51	274.96	0.0024	A	H-10->LUMO (26%), H-10->L+1 (11%), H-9->LUMO (14%)	0.28
12	4.51	274.92	0.0023	A	H-10->LUMO (14%), H-9->LUMO (26%), H-9->L+1 (11%)	0.28
13	4.69	264.15	0.1424	A	H-2->L+1 (11%), H-1->LUMO (16%), H-1->L+1 (24%)	0.38
14	4.70	263.54	0.2024	A	H-2->LUMO (16%), H-2->L+1 (25%), H-1->L+1 (10%)	0.39
15	4.79	259.01	0.0801	A	H-3->L+1 (17%), HOMO->L+3 (12%)	0.38
16	4.81	257.66	0.0002	A	H-3->L+3 (14%), H-2->L+5 (11%)	0.33
17	4.83	256.45	0.0198	A		0.29
18	4.83	256.45	0.0068	A	H-3->L+4 (10%)	0.30
19	4.86	255.33	0.0457	A		0.40
20	4.87	254.68	0.0795	A	H-8->LUMO (15%)	0.36
21	4.88	253.89	0.0554	A	H-3->L+1 (12%)	0.37
22	4.93	251.63	0.1243	A	H-10->LUMO (18%)	0.37
23	4.93	251.47	0.0481	A	H-9->LUMO (16%)	0.34
24	4.97	249.44	0.0211	A	H-11->LUMO (13%), H-4->L+1 (25%), HOMO->L+1 (11%)	0.60
25	5.03	246.72	0.0127	A	H-4->L+2 (18%), HOMO->L+2 (25%)	0.35

Table S21. Lowest energy singlet electronic transition of **XN** (TD-DFT CAM-B3LYP/6-31G+(d,p), toluene).

State	E [eV]	λ [nm]	*f*	Sym.	Major contributions	Λ
1	2.94	421.56	1.3486	A	H-4->LUMO (15%), HOMO->LUMO (74%)	0.62
2	3.37	368.38	0.0917	A	H-2->L+1 (15%), H-1->LUMO (68%)	0.35
3	3.37	368.10	0.36	A	H-2->LUMO (68%), H-1->L+1 (16%)	0.36
4	3.51	352.82	0.0006	A	H-3->LUMO (67%), HOMO->L+1 (20%)	0.44
5	3.72	333.04	0.072	A	H-5->LUMO (11%), H-4->LUMO (65%), H-3->L+1 (11%)	0.68
6	3.93	315.36	0.1354	A	H-5->LUMO (77%)	0.66
7	3.95	313.62	0.0011	A	H-6->LUMO (80%)	0.66
8	4.18	296.95	0.0001	A	H-4->L+1 (31%), H-3->LUMO (13%), HOMO->L+1 (40%)	0.60
9	4.45	278.84	0.0007	A	H-7->LUMO (42%), H-7->L+1 (17%)	0.31
10	4.45	278.70	0.0011	A	H-8->LUMO (41%), H-8->L+1 (16%)	0.32
11	4.51	275.08	0.0065	A	H-9->LUMO (34%), H-9->L+1 (12%)	0.28
12	4.51	275.03	0.0057	A	H-10->LUMO (34%), H-10->L+1 (13%)	0.29
13	4.66	266.04	0.2128	A	H-2->L+1 (11%), H-1->LUMO (18%), H-1->L+1 (26%)	0.38
14	4.67	265.47	0.2696	A	H-2->LUMO (18%), H-2->L+1 (27%), H-1->L+1 (11%)	0.40
15	4.77	259.80	0.1312	A	H-3->L+1 (31%), HOMO->L+3 (10%)	0.50
16	4.81	257.84	0.0232	A	H-7->LUMO (13%)	0.37
17	4.82	257.45	0.0559	A	H-8->LUMO (15%)	0.34
18	4.85	255.60	0.0546	A	H-3->L+3 (12%)	0.40
19	4.88	254.25	0.0912	A	H-9->LUMO (18%)	0.31
20	4.88	253.83	0.1542	A	H-10->LUMO (13%)	0.33
21	4.90	252.86	0.035	A	H-10->LUMO (10%)	0.33
22	4.91	252.67	0.0076	A	H-1->L+6 (11%)	0.36
23	4.91	252.42	0.1066	A		0.34
24	4.96	250.22	0.0159	A	H-11->LUMO (10%), H-4->L+1 (20%), HOMO->L+1 (11%)	0.55
25	5.03	246.51	0.0053	A	H-11->LUMO (38%), H-5->L+1 (27%), H-4->L+1 (11%)	0.64

Compound YN
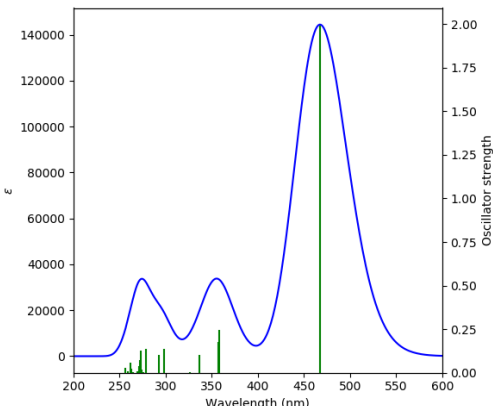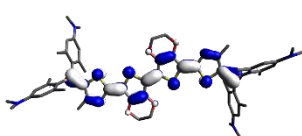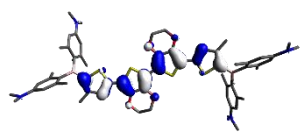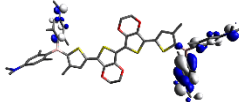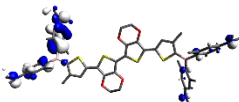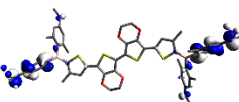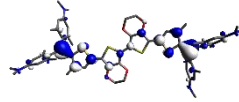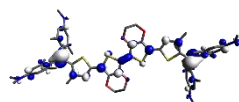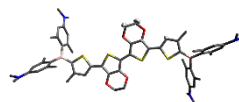
Calculated absorption spectrum	Orbital	Energy [eV]		Sym.
		gas phase	toluene	
	L+4	0.71	0.64	A
	L+3	0.67	0.59	A
	L+2	0.21	0.06	A
	L+1	-0.43	-0.59	A
	LUMO	-1.08	-1.25	A
	HOMO	-5.76	-5.92	A
	H-1	-6.31	-6.43	A
	H-2	-6.32	-6.43	A
	H-3	-6.37	-6.48	A
TD-DFT CAM-B3LYP/6-31G+(d,p), gas phase	H-4	-6.44	-6.54	A
Orbitals relevant to the S$_1$←S$_o$ transition	**other relevant orbitals**			

LUMO

HOMO

HOMO-1

HOMO-2

HOMO-3

LUMO+1

LUMO+2

LUMO+3

Table S22. Lowest energy singlet electronic transition of **YN** (TD-DFT CAM-B3LYP/6-31G+(d,p), gas phase).

State	E [eV]	λ [nm]	f	Sym.	Major contributions	Λ
1	2.65	467.41	1.9931	A	HOMO->LUMO (88%)	0.76
2	3.35	369.96	0.0001	A	H-5->LUMO (11%), H-3->LUMO (15%), HOMO->L+1 (49%)	0.56
3	3.46	357.87	0.244	A	H-2->LUMO (14%), H-1->LUMO (29%), H-1->L+1 (29%)	0.33
4	3.47	357.14	0.1788	A	H-2->LUMO (30%), H-2->L+1 (30%)	0.32
5	3.69	336.24	0.1037	A	H-4->LUMO (45%), H-3->L+1 (27%)	0.45
6	3.80	326.15	0.0021	A	H-4->L+1 (26%), H-3->LUMO (29%), HOMO->L+1 (23%)	0.49
7	4.11	302.02	0	A	H-5->LUMO (66%), HOMO->L+1 (10%)	0.73
8	4.16	298.28	0.1386	A	H-5->L+1 (15%), H-4->LUMO (10%), HOMO->L+2 (55%)	0.64
9	4.24	292.54	0.1004	A	H-6->LUMO (76%)	0.63
10	4.28	289.89	0.0002	A	H-11->LUMO (25%), H-9->LUMO (38%)	0.59
11	4.46	278.26	0.1364	A	H-13->L+1 (13%), H-12->LUMO (39%), H-10->LUMO (11%)	0.56
12	4.50	275.78	0.0004	A	H-7->LUMO (20%), H-7->L+1 (16%)	0.23
13	4.50	275.39	0.0019	A	H-8->LUMO (20%), H-8->L+1 (16%)	0.24
14	4.53	273.72	0.0019	A	H-10->L+1 (17%)	0.49
15	4.53	273.58	0.0173	A	H-13->LUMO (10%), H-1->LUMO (14%)	0.49
16	4.54	272.86	0.1287	A	H-12->LUMO (11%)	0.44
17	4.56	271.76	0.0738	A	H-2->LUMO (20%), H-2->L+2 (10%), H-1->LUMO (10%), H-1->L+1 (11%)	0.34
18	4.57	271.31	0.0373	A	H-13->LUMO (15%), H-2->LUMO (12%), H-2->L+1 (10%), H-1->LUMO (15%)	0.43
19	4.58	270.48	0.0105	A	HOMO->L+3 (20%), HOMO->L+20 (15%)	0.28
20	4.61	269.02	0.0077	A	H-13->LUMO (30%), H-12->L+1 (14%)	0.56
21	4.69	264.52	0.002	A	HOMO->L+19 (17%), HOMO->L+25 (14%)	0.35
22	4.71	262.97	0.0234	A	H-4->LUMO (10%), HOMO->L+16 (13%)	0.33
23	4.74	261.32	0.057	A	H-4->LUMO (22%), H-4->L+2 (15%), H-3->L+1 (13%)	0.44
24	4.79	258.75	0.0072	A	H-4->L+1 (14%), H-3->LUMO (18%)	0.46
25	4.85	255.79	0.0265	A	H-1->L+8 (16%)	0.27

Table S23. Lowest energy singlet electronic transition of **YN** (TD-DFT CAM-B3LYP/6-31G+(d,p), toluene).

State	E [eV]	λ [nm]	f	Sym.	Major contributions
1	2.57	482.11	2.0819	A	HOMO->LUMO (88%)
2	3.27	379.31	0.0004	A	H-5->LUMO (13%), H-3->LUMO (19%), HOMO->L+1 (50%)
3	3.41	363.90	0.2784	A	H-1->LUMO (42%), H-1->L+1 (32%), H-1->L+2 (10%)
4	3.41	363.19	0.262	A	H-2->LUMO (42%), H-2->L+1 (32%), H-2->L+2 (10%)
5	3.62	342.63	0.1836	A	H-4->LUMO (45%), H-3->L+1 (29%)
6	3.76	330.10	0.0017	A	H-4->L+1 (28%), H-3->LUMO (32%), HOMO->L+1 (20%)
7	4.07	304.42	0.0001	A	H-5->LUMO (61%), HOMO->L+1 (13%)
8	4.12	300.62	0.2835	A	H-5->L+1 (17%), H-4->LUMO (12%), HOMO->L+2 (47%)
9	4.19	296.24	0.0962	A	H-6->LUMO (72%)
10	4.26	290.85	0.0003	A	H-11->LUMO (39%), H-9->LUMO (24%)
11	4.44	279.43	0.1342	A	H-13->L+1 (14%), H-12->LUMO (42%)
12	4.49	276.36	0.0098	A	H-7->LUMO (10%)
13	4.49	276.07	0.0508	A	H-1->LUMO (25%), H-1->L+2 (14%)
14	4.50	275.77	0.0218	A	H-8->LUMO (13%), H-8->L+1 (10%)
15	4.50	275.29	0.2838	A	H-2->LUMO (22%), H-2->L+2 (12%)
16	4.51	274.79	0.003	A	H-9->LUMO (10%), HOMO->L+3 (15%)
17	4.54	273.24	0.0009	A	H-10->LUMO (13%)
18	4.54	273.10	0.0296	A	H-13->LUMO (16%), H-11->LUMO (11%)
19	4.58	270.46	0.0087	A	H-13->LUMO (36%), H-12->L+1 (16%)
20	4.60	269.79	0.0099	A	HOMO->L+4 (17%), HOMO->L+21 (21%)
21	4.66	266.33	0.002	A	HOMO->L+17 (21%), HOMO->L+22 (11%)
22	4.68	264.97	0.0717	A	H-4->LUMO (30%), H-4->L+2 (20%), H-3->L+1 (19%)
23	4.73	262.25	0.0069	A	HOMO->L+4 (14%), HOMO->L+16 (14%)
24	4.76	260.45	0.0031	A	H-4->L+1 (16%), H-3->LUMO (18%), HOMO->L+3 (11%)
25	4.85	255.87	0.0322	A	H-14->LUMO (11%), H-7->LUMO (11%)

Compound ZN
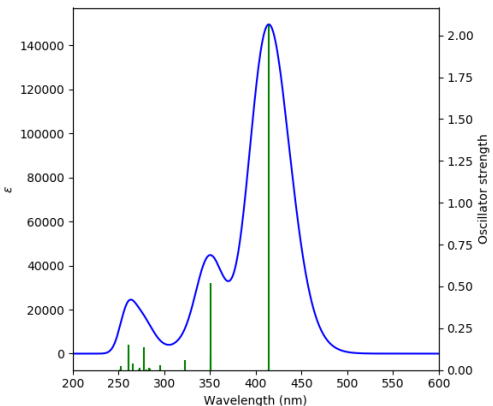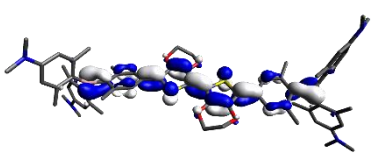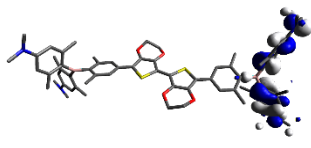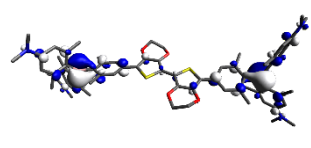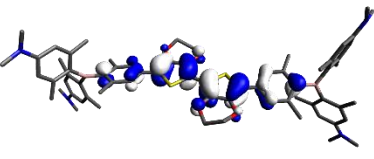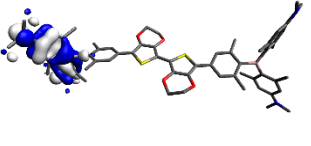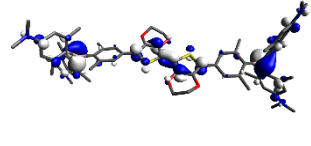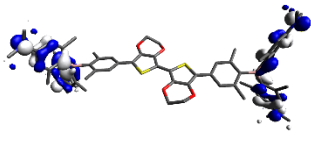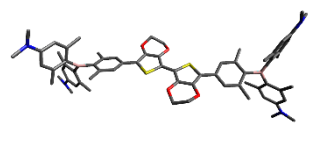
Calculated absorption spectrum	Orbital	Energy [eV]		Sym.
		gas phase	toluene	
TD-DFT CAM-B3LYP/6-31G+(d,p), gas phase	L+4	0.67	0.62	A
	L+3	0.66	0.61	A
	L+2	0.10	-0.05	A
	L+1	-0.28	-0.42	A
	LUMO	-0.70	-0.88	A
	HOMO	-5.77	-5.96	A
	H-1	-6.31	-6.40	A
	H-2	-6.31	-6.40	A
	H-3	-6.49	-6.58	A
	H-4	-6.51	-6.59	A

Orbitals relevant to the $S_1 \leftarrow S_o$ transition	other relevant orbitals	
LUMO **HOMO**	**HOMO-1** **HOMO-2** **HOMO-3**	**LUMO+1** **LUMO+2** **LUMO+3**

Table S24. Lowest energy singlet electronic transition of **ZN** (TD-DFT CAM-B3LYP/6-31G+(d,p), gas phase).

State	E [eV]	λ [nm]	f	Sym.	Major contributions	Λ
1	2.99	414.27	2.0619	A	HOMO->LUMO (84%)	0.71
2	3.54	350.41	0.08	A	H-2->LUMO (19%), H-2->L+1 (15%), H-2->L+2 (11%), H-1->LUMO (12%), H-1->L+1 (26%)	0.34
3	3.54	350.27	0.5229	A	H-2->LUMO (12%), H-2->L+1 (26%), H-1->LUMO (19%), H-1->L+1 (15%), H-1->L+2 (11%)	0.33
4	3.63	341.77	0	A	H-5->LUMO (11%), H-4->L+1 (11%), H-3->LUMO (14%), HOMO->L+1 (43%)	0.49
5	3.84	322.70	0.0614	A	H-4->LUMO (24%), H-4->L+2 (10%), H-3->L+1 (32%), HOMO->L+2 (18%)	0.51
6	4.04	306.64	0	A	H-4->L+1 (29%), H-3->LUMO (22%), HOMO->L+1 (24%)	0.48
7	4.20	295.20	0.0302	A	H-5->L+1 (16%), H-4->LUMO (12%), HOMO->L+2 (43%)	0.54
8	4.37	283.91	0.0063	A	H-7->LUMO (25%), H-5->LUMO (24%)	0.64
9	4.38	283.34	0.0118	A	H-11->L+1 (11%), H-10->LUMO (17%), H-8->LUMO (10%), H-6->LUMO (28%)	0.52
10	4.42	280.34	0.003	A	H-11->LUMO (21%), H-5->LUMO (26%)	0.59
11	4.46	278.02	0.137	A	H-10->LUMO (10%), H-6->LUMO (47%)	0.55
12	4.54	273.35	0.0027	A	H-9->LUMO (10%), H-9->L+2 (10%), H-8->L+1 (14%)	0.48
13	4.54	273.34	0.0128	A	H-9->L+1 (17%)	0.47
14	4.55	272.30	0.0001	A	H-12->L+1 (17%)	0.45
15	4.56	271.69	0.0016	A	H-13->L+1 (20%), H-12->LUMO (11%), H-12->L+2 (11%)	0.43
16	4.59	270.19	0.0004	A	H-5->L+2 (11%), HOMO->L+5 (20%)	0.52
17	4.66	266.11	0.0004	A	H-7->LUMO (39%)	0.62
18	4.67	265.67	0.0379	A	HOMO->L+3 (14%), HOMO->L+7 (31%)	0.21
19	4.76	260.62	0.0968	A	H-2->LUMO (23%), H-2->L+2 (12%), H-1->LUMO (16%)	0.28
20	4.76	260.61	0.1544	A	H-2->LUMO (16%), H-1->LUMO (22%), H-1->L+2 (12%)	0.28
21	4.84	255.97	0.0001	A	H-4->L+6 (13%), H-2->L+3 (13%), H-1->L+4 (15%)	0.27
22	4.85	255.86	0	A	H-3->L+6 (13%), H-2->L+4 (15%), H-1->L+3 (13%)	0.27
23	4.91	252.41	0	A	H-4->L+4 (15%), H-3->L+3 (14%), H-1->L+6 (10%)	0.24
24	4.91	252.34	0.0217	A	H-4->L+3 (14%), H-3->L+4 (16%), H-2->L+6 (10%)	0.24
25	4.93	251.33	0.0012	A	HOMO->L+9 (33%)	0.32

Table S25. Lowest energy singlet electronic transition of **ZN** (TD-DFT CAM-B3LYP/6-31G+(d,p), toluene).

State	E [eV]	λ [nm]	f	Sym.	Major contributions
1	2.93	423.86	2.1235	A	HOMO->LUMO (86%)
2	3.47	357.47	0.103	A	H-2->LUMO (19%), H-2->L+1 (14%), H-2->L+2 (12%), H-1->LUMO (11%), H-1->L+1 (27%)
3	3.47	357.36	0.6769	A	H-2->LUMO (11%), H-2->L+1 (27%), H-1->LUMO (19%), H-1->L+1 (14%), H-1->L+2 (12%)
4	3.58	345.85	0.0001	A	H-5->LUMO (12%), H-4->L+1 (12%), H-3->LUMO (15%), HOMO->L+1 (39%)
5	3.79	327.49	0.1189	A	H-4->LUMO (25%), H-4->L+2 (11%), H-3->L+1 (34%), HOMO->L+2 (14%)
6	4.00	309.61	0	A	H-4->L+1 (28%), H-3->LUMO (20%), HOMO->L+1 (24%)
7	4.21	294.65	0.0263	A	H-5->L+1 (17%), H-4->LUMO (11%), HOMO->L+2 (44%)
8	4.35	285.17	0.0042	A	H-7->LUMO (27%), H-5->LUMO (37%)
9	4.36	284.49	0.0891	A	H-12->LUMO (10%), H-6->LUMO (57%)
10	4.42	280.44	0.0082	A	H-13->LUMO (33%), H-12->L+1 (18%), H-5->LUMO (11%)
11	4.44	279.45	0.157	A	H-13->L+1 (13%), H-12->LUMO (31%), H-6->LUMO (19%)
12	4.52	274.33	0.0061	A	H-9->LUMO (10%), H-9->L+2 (12%), H-8->L+1 (18%)
13	4.52	274.33	0.0281	A	H-9->L+1 (19%), H-8->LUMO (10%), H-8->L+2 (12%)
14	4.54	273.24	0.0002	A	H-10->L+1 (16%), HOMO->L+3 (11%)
15	4.55	272.59	0.0056	A	H-11->L+1 (17%), H-10->LUMO (10%), H-10->L+2 (11%)
16	4.58	270.93	0.0007	A	H-5->L+2 (11%), HOMO->L+3 (25%)
17	4.65	266.56	0.0029	A	H-7->LUMO (35%), H-5->LUMO (11%), HOMO->L+3 (10%)
18	4.68	265.16	0.1231	A	H-2->LUMO (20%), H-1->LUMO (11%), HOMO->L+6 (12%)
19	4.68	265.06	0.2055	A	H-2->LUMO (16%), H-1->LUMO (30%), H-1->L+2 (13%)
20	4.68	264.95	0.0036	A	H-2->LUMO (10%), HOMO->L+4 (11%), HOMO->L+6 (25%), HOMO->L+26 (10%)
21	4.85	255.59	0.0177	A	H-4->LUMO (15%), H-4->L+2 (10%)
22	4.86	255.31	0	A	H-3->LUMO (13%)
23	4.94	250.92	0.0119	A	H-4->L+5 (15%), H-3->L+4 (15%), H-2->L+8 (11%), H-1->L+7 (11%)
24	4.94	250.87	0.0634	A	H-4->L+4 (14%), H-3->L+5 (16%), H-2->L+7 (11%), H-1->L+8 (11%)
25	4.97	249.40	0.0652	A	H-14->LUMO (13%), H-10->LUMO (10%), H-5->L+1 (11%), HOMO->L+2 (18%)

Compound X
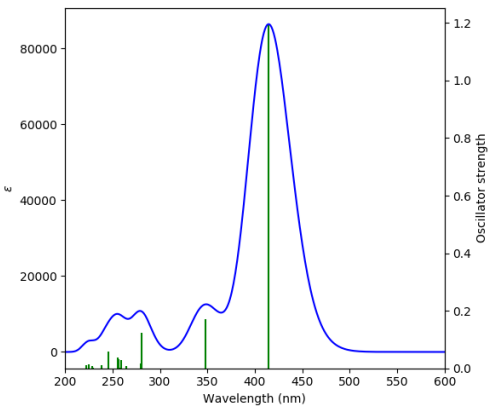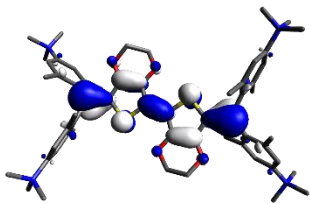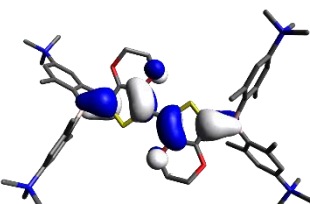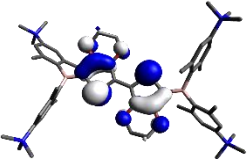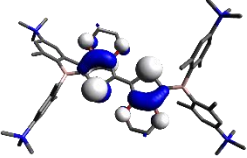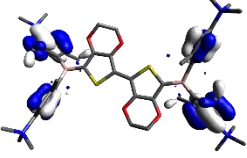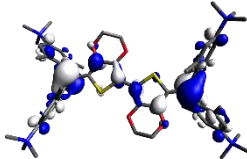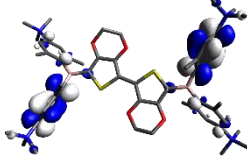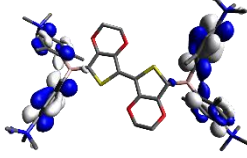
Calculated absorption spectrum	Orbital	Energy [eV]		Sym.
		gas phase	toluene	
TD-DFT CAM-B3LYP/6-31G+(d,p), gas phase	L+4	-6.65	-0.15	A
	L+3	-6.74	-0.15	A
	L+2	-6.75	-0.17	A
	L+1	-7.50	-1.02	A
	LUMO	-8.45	-2.04	A
	HOMO	-13.65	-7.30	A
	H-1	-14.29	-7.96	A
	H-2	-14.39	-8.07	A
	H-3	-15.17	-8.60	A
	H-4	-15.17	-8.61	A
Orbitals relevant to the $S_1 \leftarrow S_o$ transition	**other relevant orbitals**			

Orbitals relevant to the $S_1 \leftarrow S_o$ transition	other relevant orbitals	
LUMO	HOMO-1	LUMO+1
HOMO	HOMO-2	LUMO+2
	HOMO-3	LUMO+3

Table S26. Lowest energy singlet electronic transition of **X** (TD-DFT CAM-B3LYP/6-31G+(d,p), gas phase).

State	E [eV]	λ [nm]	*f*	Sym.	Major contributions	Λ
1	2.99	414.59	1.193	A	HOMO->LUMO (94%)	0.71
2	3.56	348.11	0.1715	A	H-1->LUMO (89%)	0.66
3	3.60	344.00	0.0001	A	H-2->LUMO (87%), H-1->L+1 (10%)	0.64
4	4.04	306.88	0.0002	A	HOMO->L+1 (79%)	0.56
5	4.42	280.47	0.1247	A	H-6->LUMO (63%), H-5->L+1 (21%)	0.46
6	4.43	280.18	0.0158	A	H-9->LUMO (11%), H-6->L+1 (24%), H-5->LUMO (55%)	0.50
7	4.64	267.00	0.0001	A	H-9->LUMO (30%), H-1->L+1 (25%), HOMO->L+1 (10%)	0.51
8	4.68	264.92	0.0093	A	H-4->LUMO (53%), H-3->L+1 (21%)	0.35
9	4.68	264.65	0.0039	A	H-4->L+1 (23%), H-3->LUMO (55%)	0.36
10	4.78	259.22	0.0292	A	H-10->LUMO (62%), H-9->L+1 (14%)	0.46
11	4.80	258.53	0.0028	A	H-10->L+1 (13%), H-9->LUMO (23%), H-1->L+1 (33%)	0.53
12	4.83	256.46	0.0021	A	H-8->LUMO (42%), H-7->L+1 (17%)	0.43
13	4.84	256.30	0.033	A	H-8->L+1 (20%), H-7->LUMO (44%)	0.47
14	4.85	255.60	0.0362	A	H-2->L+1 (69%)	0.46
15	5.02	246.81	0.0004	A	H-11->LUMO (69%), H-1->L+1 (13%)	0.69
16	5.06	245.27	0.0588	A	HOMO->L+2 (29%), HOMO->L+4 (47%)	0.44
17	5.19	238.90	0.0104	A	HOMO->L+2 (53%), HOMO->L+4 (24%)	0.35
18	5.19	238.85	0.0032	A	HOMO->L+3 (80%)	0.24
19	5.39	229.94	0.0005	A	H-8->L+3 (11%), H-7->LUMO (11%), H-3->LUMO (13%)	0.53
20	5.39	229.92	0.0029	A	H-8->LUMO (15%), H-8->L+2 (11%), H-4->LUMO (12%)	0.50
21	5.43	228.24	0.0073	A	H-8->LUMO (16%), H-4->LUMO (12%)	0.46
22	5.43	228.21	0.0002	A	H-7->LUMO (15%), H-3->LUMO (11%)	0.49
23	5.51	224.99	0.0143	A	H-2->L+3 (11%), H-1->L+2 (19%), HOMO->L+6 (16%), HOMO->L+14 (17%)	0.22
24	5.51	224.88	0.004	A	H-2->L+2 (13%), H-1->L+3 (16%), HOMO->L+5 (16%), HOMO->L+7 (15%), HOMO->L+11 (14%)	0.28
25	5.58	222.39	0.0115	A	H-2->L+3 (16%), H-1->L+2 (22%), HOMO->L+6 (19%)	0.23

Table S27. Lowest energy singlet electronic transition of **X** (TD-DFT CAM-B3LYP/6-31G+(d,p), MeCN).

State	E [eV]	λ [nm]	*f*	Symmetry	Major contributions
1	2.97	417.84	1.2718	A	HOMO->LUMO (95%)
2	3.61	343.63	0.2186	A	H-1->LUMO (90%)
3	3.66	338.67	0.0002	A	H-2->LUMO (88%)
4	4.07	304.91	0.0004	A	HOMO->L+1 (76%)
5	4.33	286.15	0.1483	A	H-8->LUMO (10%), H-6->LUMO (56%), H-5->L+1 (20%)
6	4.34	285.76	0.0188	A	H-6->L+1 (21%), H-5->LUMO (53%)
7	4.58	270.79	0.01	A	H-4->LUMO (58%), H-3->L+1 (20%)
8	4.58	270.77	0.002	A	H-4->L+1 (20%), H-3->LUMO (54%)
9	4.62	268.10	0.0001	A	H-10->L+1 (13%), H-9->LUMO (48%), HOMO->L+1 (11%)
10	4.67	265.70	0.0236	A	H-10->LUMO (64%), H-9->L+1 (16%)
11	4.73	262.33	0.0003	A	H-8->LUMO (47%), H-7->L+1 (18%)
12	4.73	262.31	0.0503	A	H-8->L+1 (17%), H-7->LUMO (46%)
13	4.83	256.87	0.0001	A	H-11->LUMO (26%), H-1->L+1 (46%)
14	4.96	250.03	0.039	A	H-2->L+1 (74%)
15	5.06	245.15	0.0003	A	H-11->LUMO (58%), H-1->L+1 (27%)
16	5.15	240.91	0.0852	A	HOMO->L+2 (53%), HOMO->L+4 (18%)
17	5.33	232.83	0.0009	A	H-4->LUMO (11%)
18	5.33	232.81	0.0008	A	H-3->LUMO (11%)
19	5.34	232.31	0.0191	A	HOMO->L+2 (19%), HOMO->L+4 (34%)
20	5.37	230.84	0.0021	A	HOMO->L+3 (60%)
21	5.38	230.28	0.0071	A	H-8->LUMO (13%), H-4->LUMO (10%), H-4->L+4 (12%)
22	5.39	230.13	0.004	A	H-7->LUMO (12%), H-3->L+4 (10%), HOMO->L+3 (11%)
23	5.43	228.34	0.0318	A	HOMO->L+4 (14%), HOMO->L+7 (32%), HOMO->L+13 (18%)
24	5.59	221.89	0.0026	A	H-13->L+1 (11%), H-12->LUMO (59%)
25	5.61	221.10	0.0024	A	HOMO->L+8 (20%), HOMO->L+11 (13%), HOMO->L+14 (12%)

Compound Y
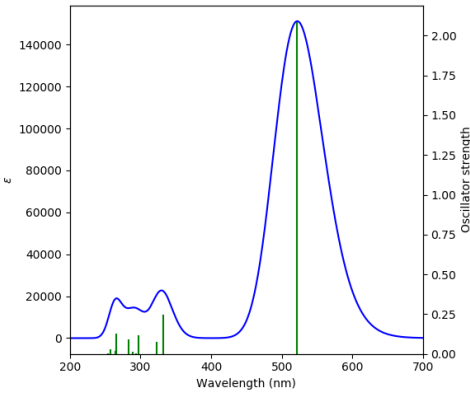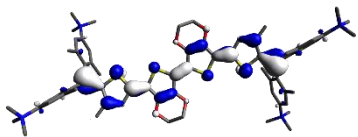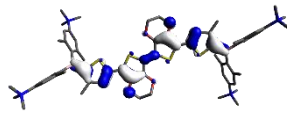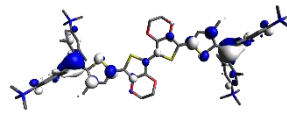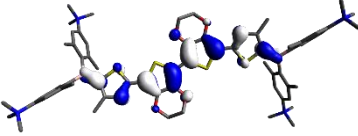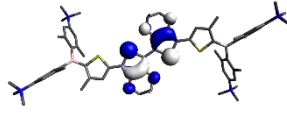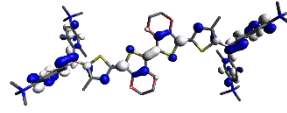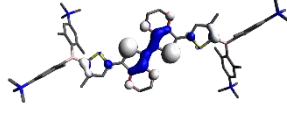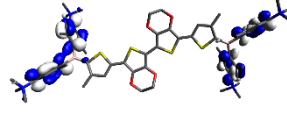
Calculated absorption spectrum	Orbital	Energy [eV]		Sym.
		gas phase	toluene	
	L+4	-6.07	-0.16	A
	L+3	-6.07	-0.16	A
	L+2	-6.22	-0.65	A
	L+1	-7.00	-1.44	A
	LUMO	-7.45	-2.04	A
	HOMO	-11.69	-6.48	A
	H-1	-12.91	-7.65	A
	H-2	-13.07	-7.95	A
TD-DFT CAM-B3LYP/6-31G+(d,p), gas phase	H-3	-13.37	-8.25	A
	H-4	-13.95	-8.58	A

Orbitals relevant to the $S_1 \leftarrow S_o$ transition	other relevant orbitals	
LUMO **HOMO**	**HOMO-1** **HOMO-2** **HOMO-3**	**LUMO+1** **LUMO+2** **LUMO+3**

Table S28. Lowest energy singlet electronic transition of **Y** (TD-DFT CAM-B3LYP/6-31G+(d,p), gas phase).

State	E [eV]	λ [nm]	f	Sym.	Major contributions	Λ
1	2.38	521.97	2.0866	A	HOMO->LUMO (88%)	0.67
2	3.05	406.49	0	A	H-1->LUMO (13%), HOMO->L+1 (77%)	0.56
3	3.70	334.74	0	A	H-1->LUMO (64%)	0.67
4	3.73	332.17	0.2476	A	H-2->LUMO (71%)	0.53
5	3.84	322.89	0.0743	A	H-2->LUMO (10%), HOMO->L+2 (63%)	0.60
6	3.97	312.13	0.0004	A	H-3->LUMO (63%)	0.62
7	4.17	297.57	0.1195	A	H-5->L+1 (30%), H-4->LUMO (57%)	0.54
8	4.22	293.82	0.0028	A	H-5->LUMO (53%), H-4->L+1 (22%)	0.54
9	4.28	289.45	0.0151	A	HOMO->L+4 (72%)	0.18
10	4.29	289.24	0.0035	A	HOMO->L+3 (74%)	0.17
11	4.31	287.93	0.0002	A	H-1->L+2 (11%), HOMO->L+5 (57%)	0.45
12	4.38	283.37	0.0897	A	H-6->LUMO (21%), H-1->L+1 (33%), HOMO->L+2 (12%)	0.61
13	4.63	267.72	0.0009	A	H-2->L+1 (74%)	0.37
14	4.66	266.04	0.0026	A	H-9->LUMO (10%), HOMO->L+7 (54%)	0.26
15	4.66	265.90	0.0297	A	H-10->LUMO (14%), H-9->L+1 (12%), HOMO->L+6 (47%)	0.26
16	4.67	265.57	0.0421	A	H-10->L+1 (29%), H-9->LUMO (33%), HOMO->L+7 (16%)	0.43
17	4.67	265.50	0.127	A	H-10->LUMO (29%), H-9->L+1 (26%), HOMO->L+6 (24%)	0.37
18	4.69	264.40	0.0208	A	H-6->LUMO (12%), H-3->L+1 (38%), H-1->L+1 (26%)	0.55
19	4.77	259.66	0.0001	A	HOMO->L+7 (11%), HOMO->L+32 (36%)	0.33
20	4.79	258.93	0.0002	A	HOMO->L+34 (52%)	0.36
21	4.83	256.78	0.0304	A	HOMO->L+8 (48%), HOMO->L+14 (10%)	0.34
22	4.86	254.91	0.0003	A	H-8->L+1 (19%), H-7->LUMO (19%)	0.40
23	4.89	253.48	0.0048	A	H-8->LUMO (18%), H-7->L+1 (17%), HOMO->L+8 (10%)	0.40
24	4.89	253.29	0.001	A	H-13->LUMO (16%), HOMO->L+5 (17%), HOMO->L+9 (15%)	0.49
25	4.96	249.73	0.0008	A	H-12->LUMO (20%), H-11->L+1 (17%)	0.50

Table S29. Lowest energy singlet electronic transition of **Y** (TD-DFT CAM-B3LYP/6-31G+(d,p), MeCN).

State	E [eV]	λ [nm]	f	Sym.	Major contributions
1	2.43	509.91	2.1271	A	HOMO->LUMO (90%)
2	3.18	389.69	0	A	H-1->LUMO (21%), HOMO->L+1 (69%)
3	3.84	323.20	0	A	H-1->LUMO (61%), HOMO->L+1 (16%)
4	3.89	319.13	0.4363	A	H-2->LUMO (66%), H-1->L+1 (11%), HOMO->L+2 (12%)
5	4.01	309.06	0.0493	A	H-2->LUMO (18%), HOMO->L+2 (48%)
6	4.12	301.22	0.0007	A	H-3->LUMO (65%)
7	4.27	290.10	0.1778	A	H-7->L+1 (14%), H-6->LUMO (11%), H-4->LUMO (42%)
8	4.35	284.94	0.0025	A	H-7->LUMO (32%), H-3->LUMO (10%)
9	4.42	280.35	0.0411	A	H-9->LUMO (36%), H-8->L+1 (29%)
10	4.42	280.22	0.1754	A	H-9->L+1 (28%), H-8->LUMO (33%)
11	4.50	275.47	0.0045	A	H-1->L+2 (12%), HOMO->L+3 (11%), HOMO->L+5 (30%)
12	4.57	271.44	0.0444	A	H-12->LUMO (28%), H-1->L+1 (13%), HOMO->L+2 (22%)
13	4.61	269.16	0.0043	A	HOMO->L+4 (20%), HOMO->L+20 (39%)
14	4.61	269.09	0.0006	A	HOMO->L+3 (11%), HOMO->L+5 (12%), HOMO->L+19 (21%)
15	4.66	265.91	0.0284	A	H-6->LUMO (30%), H-5->L+1 (27%)
16	4.66	265.90	0.0004	A	H-6->L+1 (21%), H-5->LUMO (29%)
17	4.74	261.32	0.0037	A	H-13->LUMO (39%), H-12->L+1 (15%)
18	4.78	259.64	0.0008	A	H-11->L+1 (18%), H-10->LUMO (25%)
19	4.78	259.29	0.0538	A	H-11->LUMO (28%), H-10->L+1 (20%)
20	4.80	258.33	0.0026	A	H-14->LUMO (12%), H-13->L+1 (18%), H-12->LUMO (13%), H-1->L+1 (20%)
21	4.85	255.80	0.0019	A	HOMO->L+9 (27%), HOMO->L+12 (31%)
22	4.95	250.30	0.0001	A	H-2->L+1 (75%)
23	4.98	248.82	0.0121	A	H-14->LUMO (24%), H-3->L+1 (32%), H-1->L+1 (18%)
24	5.05	245.56	0.0095	A	HOMO->L+3 (44%), HOMO->L+17 (12%)
25	5.07	244.68	0.0148	A	HOMO->L+4 (56%), HOMO->L+20 (14%)

Compound Z
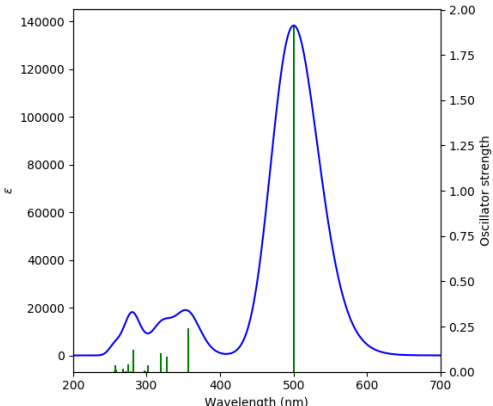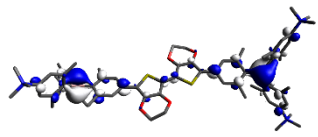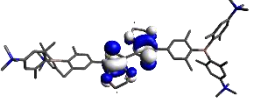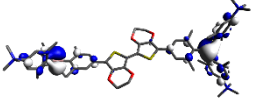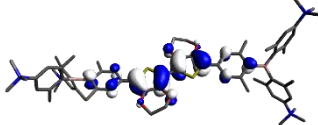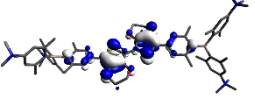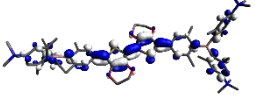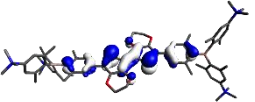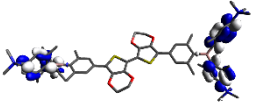
Calculated absorption spectrum	Orbital	Energy [eV]		Sym.
		gas phase	toluene	
	L+4	-6.01	-0.16	A
	L+3	-6.01	-0.16	A
	L+2	-6.09	-0.83	A
	L+1	-7.01	-1.44	A
	LUMO	-7.16	-1.77	A
	HOMO	-11.29	-6.45	A
	H-1	-12.57	-7.70	A
	H-2	-12.59	-7.84	A
	H-3	-12.93	-8.13	A
TD-DFT CAM-B3LYP/6-31G+(d,p), gas phase	H-4	-13.47	-8.35	A
Orbitals relevant to the S₁←S₀ transition	**other relevant orbitals**			

$S_1 \leftarrow S_0$

Orbitals relevant to the S₁←S₀ transition	other relevant orbitals
LUMO	**HOMO-1** / **LUMO+1**
HOMO	**HOMO-2** / **LUMO+2**
	HOMO-3 / **LUMO+3**

Table S30. Lowest energy singlet electronic transition of **Z** (TD-DFT CAM-B3LYP/6-31G+(d,p), gas phase).

State	E [eV]	λ [nm]	f	Symmetry	Major contributions	Λ
1	2.48	500.20	1.9083	A	HOMO->LUMO (77%), HOMO->L+2 (11%)	0.47
2	2.88	430.74	0	A	HOMO->L+1 (80%)	0.38
3	3.48	356.25	0.2418	A	HOMO->L+2 (70%)	0.60
4	3.77	328.91	0.0002	A	H-2->LUMO (51%), H-1->L+1 (12%)	0.44
5	3.79	327.37	0.0833	A	H-5->L+1 (10%), H-4->LUMO (12%), H-1->LUMO (46%), H-1->L+2 (11%)	0.37
6	3.85	321.76	0.0002	A	H-5->LUMO (42%), H-4->L+1 (34%)	0.36
7	3.88	319.80	0.1048	A	H-5->L+1 (27%), H-4->LUMO (37%), H-1->LUMO (13%)	0.36
8	4.05	305.94	0.0001	A	H-6->L+1 (10%), H-3->LUMO (49%)	0.51
9	4.11	301.77	0.0351	A	H-6->LUMO (22%), H-3->L+1 (22%), H-2->L+1 (12%), HOMO->LUMO (11%)	0.47
10	4.15	298.65	0.0014	A	HOMO->L+3 (14%), HOMO->L+5 (23%), HOMO->L+7 (17%), HOMO->L+11 (18%)	0.31
11	4.17	297.53	0.0015	A	HOMO->L+4 (87%)	0.15
12	4.17	297.39	0.0063	A	HOMO->L+3 (73%)	0.15
13	4.40	281.64	0.0724	A	H-9->L+1 (40%), H-8->LUMO (44%)	0.61
14	4.40	281.62	0.124	A	H-9->LUMO (42%), H-8->L+1 (42%)	0.62
15	4.45	278.75	0.0015	A	H-2->L+2 (10%), H-1->L+1 (74%)	0.28
16	4.52	274.51	0.0418	A	H-3->L+1 (21%), H-2->L+1 (51%), H-1->L+2 (11%)	0.39
17	4.56	271.97	0.0012	A	HOMO->L+6 (88%)	0.07
18	4.56	271.94	0.0011	A	HOMO->L+5 (38%), HOMO->L+7 (50%)	0.24
19	4.63	267.76	0.0171	A	HOMO->L+8 (73%)	0.31
20	4.68	264.69	0.0001	A	H-7->LUMO (13%), H-3->L+2 (11%), HOMO->L+5 (14%), HOMO->L+7 (11%)	0.46
21	4.73	261.98	0	A	H-10->L+1 (10%), HOMO->L+11 (36%)	0.45
22	4.79	258.60	0.0147	A	H-11->L+1 (25%), H-10->LUMO (30%)	0.51
23	4.82	257.12	0.0356	A	HOMO->L+30 (19%)	0.37
24	4.82	257.11	0.0099	A	HOMO->L+29 (14%)	0.43
25	4.83	256.63	0.0013	A	H-11->LUMO (18%), H-10->L+1 (15%)	0.49

Table S31. Lowest energy singlet electronic transition of **Z** (TD-DFT CAM-B3LYP/6-31G+(d,p), MeCN).

State	E [eV]	λ [nm]	f	Sym.	Major contributions
1	2.70	458.95	2.1617	A	HOMO->LUMO (82%)
2	3.33	372.73	0	A	H-1->LUMO (16%), HOMO->L+1 (67%)
3	3.80	326.10	0.0652	A	H-1->L+1 (15%), HOMO->L+2 (56%)
4	4.06	305.32	0.0017	A	H-5->LUMO (19%), H-4->L+1 (15%), H-3->LUMO (11%), H-1->LUMO (26%)
5	4.06	305.08	0.0259	A	H-5->L+1 (21%), H-4->LUMO (33%), H-2->LUMO (22%)
6	4.11	301.85	0.0058	A	H-5->LUMO (23%), H-4->L+1 (17%), H-1->LUMO (28%)
7	4.16	297.97	0.1628	A	H-4->LUMO (14%), H-2->LUMO (45%), H-2->L+2 (12%)
8	4.26	291.18	0.1437	A	H-8->LUMO (12%), H-8->L+1 (21%), H-7->LUMO (20%), H-7->L+1 (14%)
9	4.26	290.97	0.1639	A	H-8->LUMO (18%), H-8->L+1 (13%), H-7->LUMO (11%), H-7->L+1 (20%)
10	4.34	285.66	0.0007	A	H-6->L+1 (12%), H-3->LUMO (37%)
11	4.44	279.22	0	A	H-3->LUMO (13%), H-1->L+2 (11%), HOMO->L+5 (37%)
12	4.46	278.25	0.0348	A	H-13->L+1 (14%), H-6->LUMO (20%), HOMO->L+2 (18%)
13	4.62	268.54	0	A	H-10->L+1 (18%), H-9->LUMO (31%), H-9->L+2 (11%), H-6->L+1 (16%)
14	4.62	268.31	0.0688	A	H-10->LUMO (23%), H-9->L+1 (34%)
15	4.67	265.68	0.0224	A	H-12->L+1 (10%), H-11->LUMO (26%), H-11->L+1 (21%)
16	4.67	265.66	0.0598	A	H-12->LUMO (26%), H-12->L+1 (21%), H-11->L+1 (10%)
17	4.71	263.11	0	A	H-14->L+1 (16%), H-13->LUMO (32%), H-10->L+1 (10%), HOMO->L+5 (13%)
18	4.77	259.93	0.0153	A	HOMO->L+9 (16%), HOMO->L+12 (48%), HOMO->L+22 (11%)
19	4.85	255.65	0.0007	A	H-14->LUMO (26%), H-13->L+1 (22%), H-1->L+1 (24%)
20	4.95	250.68	0.0028	A	HOMO->L+3 (27%), HOMO->L+17 (14%), HOMO->L+18 (13%)
21	4.96	249.93	0.0446	A	HOMO->L+4 (33%), HOMO->L+15 (11%)
22	5.06	245.05	0.0005	A	H-2->L+1 (56%), H-1->L+2 (14%)
23	5.11	242.43	0.0093	A	HOMO->L+10 (14%), HOMO->L+16 (29%)
24	5.13	241.82	0.0044	A	H-3->L+1 (26%), H-1->L+1 (17%)
25	5.15	240.53	0	A	H-15->LUMO (13%), H-14->L+1 (16%), H-3->L+2 (11%), H-2->L+1 (14%)

Theoretical Studies: Cartesian Coordinates

Compound XN

DFT B3LYP/6-31G+(d,p), gas phase, S_0
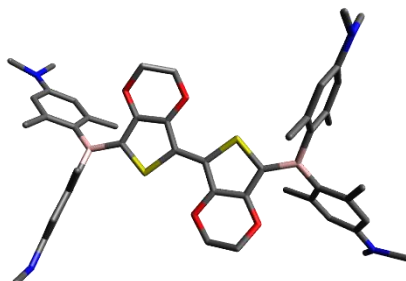
Point group: C_1

Total energy: -2,124,876.35

kcal mol^{-1}

Dipole moment: 0.62 D

Immaginary frequencies: 0

C	3.24722200	0.31432500	-0.04771500
B	4.74683100	-0.06772800	0.00386200
C	5.80737800	0.94329600	0.59545600
C	5.15935600	-1.50611500	-0.52428800
C	6.98341700	1.29213600	-0.12512100
C	7.92349600	2.17925900	0.40457100
C	7.78148400	2.73569600	1.69207200
C	6.61988700	2.38693300	2.40970100
C	5.65102200	1.53032700	1.88082900
C	5.84063200	-2.43331400	0.31292700
C	6.19398600	-3.70210100	-0.14963400
C	5.91629700	-4.12079900	-1.46826200
C	5.27660200	-3.18964000	-2.30883400
C	4.88624700	-1.92630000	-1.85275700
C	4.44867100	1.25104700	2.76500500
C	7.25715800	0.75854500	-1.51883100
C	6.18438600	-2.10068000	1.75263400
C	4.19825500	-1.02952800	-2.86819000
N	8.75351200	3.57231800	2.23799500
N	6.25138200	-5.40011900	-1.91230100
C	7.17258500	-6.20284300	-1.12217100
C	9.80398700	4.09295000	1.37733100
C	8.43784600	4.33628800	3.43477800
C	2.60715900	1.54736300	-0.09471000
C	1.19027800	1.48063600	-0.15083400
C	0.68551200	0.18666700	-0.14037300
S	2.01986000	-0.94923400	-0.08534200
O	3.26320700	2.74725800	-0.09222000
C	2.44663200	3.84611300	-0.51892900
C	1.08143200	3.79588600	0.14713600
O	0.39240500	2.59172200	-0.21874400
C	-0.69796500	-0.21343500	-0.14544200
S	-2.03371000	0.92172100	-0.10679900
C	-3.26030200	-0.34287700	-0.07366400
C	-2.61888900	-1.57558700	-0.10992800
C	-1.20156500	-1.50781200	-0.15462700
O	-3.27352900	-2.77587400	-0.10751100
C	-2.45281600	-3.87596300	-0.52352800
C	-1.09303900	-3.82219200	0.15311300
O	-0.40231900	-2.61815800	-0.21106200
B	-4.76094000	0.03703800	-0.03620300
C	-5.82227600	-0.97541600	0.55114200
C	-5.17370300	1.47114100	-0.57578800
C	-6.99817900	-1.32252000	-0.17146600
C	-7.93464700	-2.21651600	0.35261100
C	-7.78040500	-2.79775700	1.62770300
C	-6.63672300	-2.42386300	2.36107500
C	-5.67049900	-1.56064600	1.83777700
C	-5.85099900	2.40565200	0.25560600
C	-6.20808200	3.66990600	-0.21709000
C	-5.95531800	4.06810600	-1.54699100
C	-5.28900200	3.14163200	-2.37216900
C	-4.89636900	1.88289000	-1.90609700
C	-4.48054600	-1.26629500	2.73376600
C	-7.28138600	-0.77268900	-1.55704300
C	-6.17746800	2.08853800	1.70274200
C	-4.19246400	0.98419200	-2.90888800
N	-8.70971100	-3.70570000	2.13344700
N	-6.36653200	5.31127200	-2.02706800
C	-6.82064200	6.31951500	-1.08228400
C	-5.84102400	5.78482000	-3.29798100
C	-8.64431200	-4.07487300	3.53881800
C	6.18028600	-5.69259500	-3.33524300
C	-10.00284100	-3.83199300	1.47856600
H	8.78383300	2.42979300	-0.20430000
H	6.45814900	2.78165400	3.40591500
H	6.69659000	-4.37097900	0.53868300
H	5.07406500	-3.43854400	-3.34408100
H	3.60216100	1.88887400	2.48847700
H	4.10361700	0.21678200	2.69726800
H	4.68696700	1.45602100	3.81359800
H	6.44859800	1.00669200	-2.21488600
H	8.17980700	1.18640200	-1.92244000
H	7.35833600	-0.33028900	-1.52247800
H	5.28887800	-1.85884600	2.33625800
H	6.67394000	-2.94861800	2.24099500
H	6.85190200	-1.23699800	1.82005200
H	4.59735400	-1.20921000	-3.87223200
H	3.12052000	-1.22762800	-2.90078100
H	4.31906100	0.03205400	-2.64412800
H	7.29410900	-7.17697500	-1.59970500
H	8.16782700	-5.73908500	-1.02048500
H	6.77562300	-6.37874600	-0.11733300
H	10.49487300	4.68675600	1.97873200
H	10.37912000	3.27787900	0.92641500
H	9.41700100	4.72906600	0.56379200
H	9.31817300	4.90784500	3.73456400
H	8.17965600	3.67271400	4.26653500
H	7.60121200	5.03916300	3.28648600
H	2.98841800	4.75171400	-0.23607600
H	2.33676100	3.81724200	-1.61150100
H	0.44798800	4.62075900	-0.18671400
H	1.18617400	3.83749100	1.23950400
H	-2.99637700	-4.78069300	-0.24143400
H	-2.33451600	-3.85116400	-1.61528900
H	-0.45588100	-4.64722200	-0.17307300
H	-1.20621700	-3.86029900	1.24472600
H	-8.80104800	-2.45558000	-0.25227700
H	-6.48479400	-2.80625200	3.36354300
H	-6.69683200	4.34933700	0.47086500
H	-5.07125900	3.38979500	-3.40459400
H	-3.62949300	-1.90642500	2.47691000
H	-4.13634400	-0.23249400	2.65732100
H	-4.73228800	-1.45864700	3.78170000
H	-7.39217800	0.31507800	-1.54682900
H	-6.47335000	-1.00476800	-2.25907800
H	-8.20150600	-1.20382500	-1.96288400
H	-5.27385400	1.86470900	2.28124000
H	-6.67296100	2.93669400	2.18472800
H	-6.83416700	1.21793700	1.78676700
H	-4.57486000	1.16188600	-3.91964400

- 236 -

H	-3.11402900	1.18058300	-2.92395900
H	-4.31816300	-0.07686500	-2.68449000
H	-7.14044900	7.20539300	-1.63420900
H	-7.68324000	5.96019800	-0.51200700
H	-6.03838700	6.62083200	-0.36554300
H	-6.28571500	6.75491700	-3.52763400
H	-6.10802100	5.10186500	-4.11109800
H	-4.74405600	5.89741900	-3.29331300
H	-9.41019300	-4.82483800	3.74544200
H	-8.80470500	-3.21928200	4.21599600
H	-7.67445000	-4.52150100	3.78005100
H	6.87278100	-5.07900300	-3.93576900
H	6.42620800	-6.74418300	-3.49488300
H	5.16669600	-5.53139900	-3.71580900
H	-9.88426900	-4.14045200	0.43493200
H	-10.58294700	-4.60642500	1.98393100
H	-10.58489200	-2.89569700	1.49434800

Compound X

DFT B3LYP/6-31G+(d,p), gas phase, S_0
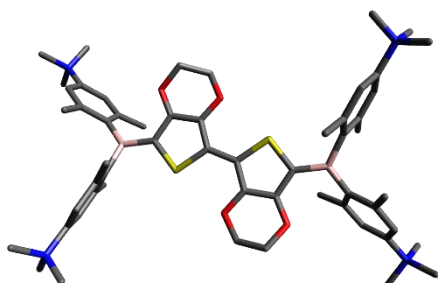
Point group: C_1

Total energy: -2,224,338.35

kcal mol^{-1}

Dipole moment: 0.31 D

Immaginary frequencies: 0

C	-3.25662900	0.31927900	0.01926600
B	-4.74732800	-0.02275500	0.01014200
C	-5.83375800	1.05127300	-0.47978200
C	-5.23674400	-1.47851900	0.48514700
C	-6.87627500	1.49509900	0.37229300
C	-7.85920900	2.38516200	-0.09381800
C	-7.82983700	2.83697700	-1.40725300
C	-6.80613200	2.42850400	-2.25820500
C	-5.80248600	1.56007100	-1.80699500
C	-5.90794900	-2.36081200	-0.40223200
C	-6.40387300	-3.59514000	0.04706900
C	-6.24851100	-3.97111900	1.37726900
C	-5.57233300	-3.13561000	2.25965200
C	-5.05430000	-1.90423500	1.82821700
C	-4.70290100	1.22379300	-2.79361100
C	-6.96725500	1.07143800	1.82256700
C	-6.09133500	-2.03553500	-1.86855000
C	-4.32438000	-1.08400800	2.87436800
N	-8.89612300	3.76725600	-1.94893600
N	-6.81456500	-5.27555400	1.90171800
C	-7.51416700	-6.08647500	0.83406400
C	-5.69815100	-6.13492400	2.46611700
C	-9.94027100	4.13162600	-0.91750800

C	-8.25997100	5.06017100	-2.42691500
C	-2.61214700	1.56064100	-0.00325900
C	-1.19584300	1.49394300	0.04843000
C	-0.69364900	0.19638400	0.09461600
S	-2.02460300	-0.94621800	0.10602900
O	-3.26507100	2.74837600	-0.05812300
C	-2.44418500	3.88510600	0.29399300
C	-1.08514000	3.79328300	-0.37483200
O	-0.39885600	2.59726500	0.05046200
C	0.69369000	-0.19641500	0.09461800
S	2.02466700	0.94618500	0.10592900
C	3.25666300	-0.31931300	0.01910300
C	2.61218500	-1.56067700	-0.00336400
C	1.19587400	-1.49397200	0.04840000
O	3.26509300	-2.74841900	-0.05822700
C	2.44421300	-3.88513800	0.29392400
C	1.08514700	-3.79331000	-0.37485600
O	0.39888400	-2.59728800	0.05046900
B	4.74736800	0.02275000	0.01000100
C	5.83383800	-1.05123000	-0.47992200
C	5.23671100	1.47850100	0.48508700
C	6.87645300	-1.49482700	0.37216300
C	7.85938500	-2.38494300	-0.09384900
C	7.82994600	-2.83699900	-1.40720000
C	6.80618400	-2.42870500	-2.25816700
C	5.80253800	-1.56022100	-1.80705300
C	5.90776300	2.36089600	-0.40231900
C	6.40360700	3.59525300	0.04698300
C	6.24834300	3.97116100	1.37721900
C	5.57233500	3.13554900	2.25962600
C	5.05438100	1.90413400	1.82819100
C	4.70292800	-1.22407600	-2.79368400
C	6.96766600	-1.07073100	1.82230100
C	6.09108400	2.03567400	-1.86865700
C	4.32482200	1.08376800	2.87449000
N	8.89619500	-3.76739800	-1.94874600
N	6.81426800	5.27565200	1.90167200
C	7.51370900	6.08671300	0.83401700
C	5.69777800	6.13484800	2.46617300
C	9.94042800	-4.13149200	-0.91730800
C	8.26001300	-5.06044100	-2.42634400
C	-7.83084900	-4.99027600	2.99449600
C	9.61634200	-3.10289000	-3.10945700
C	7.83065000	4.99046400	2.99438300
C	-9.61636500	3.10246100	-3.10942200
H	-8.62987900	2.69277800	0.60012200
H	-6.75693400	2.77140700	-3.28640800
H	-6.90910100	-4.22684700	-0.67109400
H	-5.43343200	-3.40654400	3.30141300
H	-3.85469200	1.90385300	-2.65842100
H	-4.32066300	0.20926000	-2.67687000
H	-5.05122900	1.33340000	-3.82423300
H	-6.07094000	1.36305300	2.37903500
H	-7.82177700	1.53707500	2.31903300
H	-7.07792400	-0.01206100	1.91878600
H	-5.12550200	-1.95711900	-2.37918700
H	-6.66494400	-2.81195100	-2.38009600
H	-6.61695900	-1.08725600	-2.00788500
H	-4.87781800	-1.07312500	3.81874700
H	-3.33778500	-1.51567500	3.07759700
H	-4.16268100	-0.05178500	2.56629500
H	-7.88468000	-6.99930500	1.29962000
H	-8.35061600	-5.51550800	0.43401600
H	-6.80545000	-6.33858600	0.04660100
H	-6.12851600	-7.07070600	2.82466700
H	-5.21745600	-5.61017900	3.28861900
H	-4.97739000	-6.32625300	1.67161200
H	-10.65940000	4.79750800	-1.39368500
H	-10.44680000	3.22905400	-0.57907200
H	-9.46363000	4.64442100	-0.08337500
H	-9.04700800	5.71702100	-2.79915200
H	-7.55234800	4.84247100	-3.22367500
H	-7.74546200	5.52141400	-1.58439400
H	-2.99044500	4.76611700	-0.04693800
H	-2.34061800	3.92222700	1.38474000
H	-0.44760600	4.62859600	-0.08093400
H	-1.18417400	3.77812100	-1.46685400

H	2.99046000	-4.76615600	-0.04701300
H	2.34067900	-3.92224900	1.38467500
H	0.44761300	-4.62861900	-0.08094700
H	1.18414700	-3.77813700	-1.46688100
H	8.63011700	-2.69240600	0.60009200
H	6.75692200	-2.77180500	-3.28630100
H	6.90869900	4.22703700	-0.67120800
H	5.43350500	3.40642000	3.30141500
H	3.85462900	-1.90397800	-2.65827400
H	4.32084500	-0.20945600	-2.67718300
H	5.05118200	-1.33399500	-3.82429700
H	7.07995200	0.01265300	1.91807200
H	6.07080600	-1.36074000	2.37870300
H	7.82138300	-1.53743100	2.31915500
H	5.12522900	1.95694900	-2.37920100
H	6.66439400	2.81226900	-2.38026500
H	6.61698800	1.08755200	-2.00803900
H	4.87960100	1.07113700	3.81807100
H	3.33911800	1.51657100	3.07960700
H	4.16128600	0.05210100	2.56554700
H	7.88415600	6.99955500	1.29960400
H	8.35019600	5.51586500	0.43387800
H	6.80491300	6.33879600	0.04661800
H	6.12803900	7.07066400	2.82475900
H	5.21718800	5.60999100	3.28866700
H	4.97695400	6.32613500	1.67171600
H	10.65953400	-4.79747800	-1.39337500
H	10.44696300	-3.22882500	-0.57913400
H	9.46386000	-4.64409000	-0.08301300
H	9.04702400	-5.71738200	-2.79847400
H	7.55232600	-4.84294600	-3.22310300
H	7.74557300	-5.52147000	-1.58366500
H	-8.62187200	-4.36976900	2.57436500
H	-8.23721800	-5.93916900	3.34659900
H	-7.34291200	-4.46837000	3.81461600
H	10.06435500	-2.17663100	-2.75083000
H	10.38700900	-3.78284500	-3.47446100
H	8.90365700	-2.88989600	-3.90300800
H	8.62173100	4.37007900	2.57418300
H	8.23691100	5.93939700	3.34650200
H	7.34282500	4.46846200	3.81450900
H	-10.06436100	2.17629900	-2.75052300
H	-10.38705000	3.78233100	-3.47454500
H	-8.90373600	2.88925300	-3.90296800

Compound YN

DFT B3LYP/6-31G+(d,p), gas phase, S$_0$

Point group: C$_1$

Total energy: -2,866,771.33

kcal mol^{-1}

Dipole moment: 0.51 D

Immaginary frequencies: 0

C	-6.96847200	0.91629700	0.03604600
B	-8.33289100	0.17553500	-0.00591200
C	-8.43770200	-1.24576500	0.68784400
C	-9.56040900	0.83118200	-0.75785400
C	-8.88138900	-2.39473200	-0.02473600
C	-8.96642100	-3.64332300	0.59440800
C	-8.64253000	-3.82586500	1.95522500
C	-8.24181700	-2.68107300	2.67220100
C	-8.11799600	-1.43008500	2.06098200
C	-10.82840100	0.98102300	-0.12995500
C	-11.90367200	1.57142900	-0.79842300
C	-11.79868500	2.02016900	-2.13128000
C	-10.55565000	1.83025800	-2.76970800
C	-9.45887800	1.27524300	-2.10568800
C	-7.66738500	-0.28592500	2.95321000
C	-9.24865900	-2.32891100	-1.49535200
C	-11.06964300	0.54031200	1.30191400
C	-8.17982300	1.13569600	-2.91377400
N	-8.70728200	-5.08092600	2.55755800
N	-12.86856200	2.62823700	-2.78221500
C	-14.19525000	2.55287500	-2.18982000
C	-9.39994500	-6.16057400	1.87107700
C	-6.61919700	2.26900100	0.01438200
C	-5.21949000	2.49771500	0.06218500
C	-4.45509100	1.33808200	0.10379200
S	-5.49914400	-0.05971100	0.12552300
C	-3.01753100	1.22596000	0.12138700
S	-2.20430900	-0.33474700	0.14035600
C	-0.60151600	0.39944300	0.15610800
C	-0.73237500	1.77762800	0.14729900
C	-2.07466800	2.24026800	0.13391700
C	0.60648600	-0.37574500	0.15860700
C	0.73730300	-1.75395300	0.16316000
C	2.07954000	-2.21676000	0.15141400
C	3.02240800	-1.20268100	0.12676300
S	2.20925500	0.35817800	0.13207400
C	4.45991700	-1.31511900	0.10713400
S	5.50423400	0.08265500	0.11246600
C	6.97318500	-0.89436800	0.02967900
C	6.62363400	-2.24712300	0.02215700
C	5.22405800	-2.47524800	0.07546400
O	0.33999300	2.62889100	0.16795000
C	-0.00449800	3.96568900	-0.22553700
C	-1.27396500	4.41327000	0.48070700
O	-2.38279700	3.57467000	0.11644000
O	-0.33505400	-2.60494100	0.19461200
C	0.00853600	-3.94552100	-0.18646100
C	1.27951200	-4.38619200	0.52141700
O	2.38759000	-3.55131900	0.14647200
B	8.33796200	-0.15484200	-0.02170300
C	8.44632600	1.27237600	0.65914200
C	9.56458600	-0.81610600	-0.77056900
C	8.89386200	2.41353700	-0.06386800
C	8.98196400	3.66751900	0.54369100
C	8.65800600	3.86370200	1.90260900
C	8.25369700	2.72682700	2.63000500
C	8.12639900	1.47055000	2.03038600
C	10.82953500	-0.97124800	-0.13870700
C	11.90563400	-1.56369900	-0.80436100
C	11.80949300	-1.99102500	-2.14483300
C	10.55960200	-1.82592400	-2.77682800
C	9.46240400	-1.26879300	-2.11558800
C	7.67165300	0.33668200	2.93366800
C	9.26229600	2.33351500	-1.53350100
C	11.06282200	-0.54267400	1.29809400
C	8.17970500	-1.14429900	-2.92037000
N	8.72618500	5.12410300	2.49315700
N	12.90139900	-2.53024500	-2.81922500
C	14.09237900	-2.89242600	-2.06679900
C	12.68904800	-3.19688500	-4.09477000
C	9.42245100	6.19527900	1.79704100
C	-12.79260600	2.85119500	-4.21762100

- 238 -
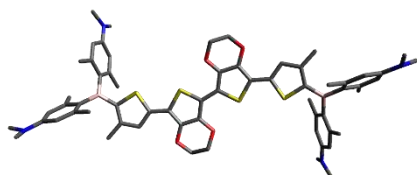
C	-8.60466700	-5.17661300	4.00525200
C	8.62254400	5.23377800	3.93977500
C	7.59234700	-3.40417800	-0.00455900
C	-7.58791200	3.42581900	-0.02119400
H	-9.29324700	-4.48518400	-0.00411500
H	-8.02012100	-2.75162800	3.73052900
H	-12.83934300	1.67529600	-0.26230300
H	-10.42952600	2.11434800	-3.80768000
H	-7.91249100	-0.49553400	3.99941600
H	-6.58353200	-0.13768800	2.89039500
H	-8.13166100	0.66587100	2.68491200
H	-8.40996700	-1.97625700	-2.10595300
H	-9.53163900	-3.31754800	-1.86897600
H	-10.08367300	-1.64585500	-1.67448300
H	-10.37936700	1.02609900	2.00021400
H	-12.08632400	0.79207100	1.61820000
H	-10.93333900	-0.53820100	1.42073800
H	-8.39474100	1.20277700	-3.98491500
H	-7.45967100	1.92395600	-2.67089800
H	-7.67191700	0.18478500	-2.73424400
H	-14.89561400	3.11031200	-2.81435400
H	-14.56314200	1.51814500	-2.09399100
H	-14.20660800	3.01098900	-1.19540900
H	-9.32339100	-7.06962100	2.47051200
H	-10.46791300	-5.94534900	1.70140300
H	-8.93713500	-6.36834500	0.90091100
H	-4.77498900	3.48502200	0.06356100
H	4.77940700	-3.46241500	0.08759400
H	0.84392800	4.59265000	0.05692600
H	-0.13796200	4.00190500	-1.31475900
H	-1.55191600	5.42661200	0.18220500
H	-1.13612700	4.37945500	1.56932600
H	-0.83929000	-4.56965000	0.10397400
H	0.13967700	-3.99246800	-1.27556200
H	1.55676200	-5.40246200	0.23235500
H	1.14401700	-4.34159700	1.60994400
H	9.31138500	4.50284600	-0.06249700
H	8.03171000	2.80785900	3.68752900
H	12.83506200	-1.68360900	-0.26080200
H	10.42964400	-2.12920000	-3.80894100
H	7.92320600	0.55284700	3.97702700
H	6.58640100	0.19616600	2.87715000
H	8.12749600	-0.62059200	2.67084700
H	8.42650400	1.96857200	-2.14072400
H	9.53917600	3.31971900	-1.91792900
H	10.10199100	1.65413600	-1.70445200
H	10.36539300	-1.03002600	1.98825500
H	12.07621700	-0.80083800	1.61973000
H	10.93065900	0.53572200	1.42309000
H	7.45933400	-1.92628900	-2.65898400
H	7.67411600	-0.18920400	-2.75650700
H	8.38940800	-1.23156300	-3.99101400
H	14.85392400	-3.25547500	-2.75926300
H	14.50782000	-2.02152200	-1.54936800
H	13.90293200	-3.67788200	-1.31660500
H	13.65156900	-3.53091600	-4.48612100
H	12.25745700	-2.50936300	-4.82974300
H	12.02420000	-4.07246100	-4.01418900
H	9.34823000	7.11008400	2.38794600
H	10.48985200	5.97530900	1.63004800
H	8.96082800	6.39536500	0.82470300
H	-12.71203300	1.91445700	-4.79357100
H	-13.69102200	3.37839900	-4.54359700
H	-11.93301300	3.48046800	-4.47006200
H	-9.42504200	-4.65839200	4.52938100
H	-8.62314600	-6.22911600	4.29426800
H	-7.65731600	-4.75613300	4.35738000
H	9.44090400	4.71810000	4.46953100
H	8.64390800	6.28890200	4.21886300
H	7.67363000	4.81945200	4.29498600
H	7.33366300	-4.13616400	0.76935600
H	7.55024700	-3.92750800	-0.96832900
H	8.62218600	-3.08343600	0.15013700
H	-8.61649600	3.10795900	0.14704100
H	-7.32231100	4.16899500	0.73955100
H	-7.55430400	3.93490200	-0.99287100

Compound Y

DFT B3LYP/6-31G+(d,p), gas phase, S_0
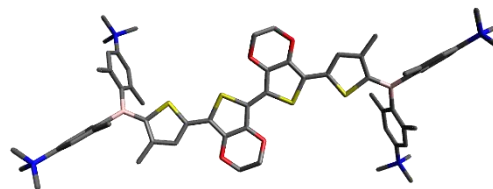
Point group: C_1

Total energy: -2966258.88

kcal mol^{-1}

Dipole moment: 0.16 D

Immaginary frequencies: 0

C	7.01040300	-0.83208000	-0.06783000
B	8.37768700	-0.16665900	-0.03514900
C	8.57097700	1.25789200	0.68797700
C	9.63951800	-0.88231800	-0.72687700
C	9.02339100	2.40691900	-0.01121100
C	9.24632700	3.62080400	0.65972000
C	9.03182100	3.71144800	2.03012700
C	8.57399000	2.60467600	2.73712900
C	8.32874400	1.38750800	2.08399600
C	10.78750400	-1.26411900	0.01164200
C	11.87909600	-1.88557800	-0.61967500
C	11.85320100	-2.12255600	-1.98849200
C	10.74032000	-1.74941700	-2.73782400
C	9.63287300	-1.14708000	-2.12481900
C	7.80529500	0.25817100	2.94949600
C	9.24989800	2.39792900	-1.50708500
C	10.87928300	-1.06709500	1.50954500
C	8.45446700	-0.81925900	-3.02077600
N	9.29545100	4.99652100	2.78958900
N	13.01716000	-2.78138900	-2.70073000
C	14.15230500	-3.13807100	-1.76858600
C	12.55333700	-4.06628000	-3.36358400
C	9.78528200	6.11580600	1.90042500
C	8.01800900	5.47096100	3.45666900
C	6.62708700	-2.17900600	-0.24668300
C	5.23662200	-2.38375100	-0.19873800
C	4.48362300	-1.22142000	-0.00851700
S	5.54760100	0.14803200	0.16970400
C	3.05104500	-1.12173800	0.02592800
S	2.19707400	0.41792500	0.07914000
C	0.61668300	-0.36613300	0.08815900
C	0.78227400	-1.74346700	0.05425300
C	2.13430900	-2.16876700	0.02070600
C	-0.61665800	0.36642100	0.08796900
C	-0.78225200	1.74372500	0.05296400
C	-2.13429200	2.16900800	0.01937500
C	-3.05103800	1.12198700	0.02562500
S	-2.19704600	-0.41763800	0.07996200
C	-4.48362400	1.22161100	-0.00861700
S	-5.54749600	-0.14795800	0.16934700
C	-7.01040600	0.83216900	-0.06763000
C	-6.62718700	2.17915300	-0.24614300

C	-5.23672000	2.38396000	-0.19838400
O	-0.26317000	-2.61753900	0.05542700
C	0.11202400	-3.94127300	-0.37826900
C	1.39288700	-4.37690300	0.31040600
O	2.47816800	-3.48264100	-0.02189700
O	0.26319600	2.61779800	0.05315900
C	-0.11208900	3.94111000	-0.38173900
C	-1.39276200	4.37742500	0.30685300
O	-2.47814900	3.48284300	-0.02425800
B	-8.37762800	0.16662900	-0.03507900
C	-8.57081500	-1.25820700	0.68748800
C	-9.63953300	0.88251500	-0.72644000
C	-9.02330200	-2.40694300	-0.01212100
C	-9.24622800	-3.62109300	0.65833800
C	-9.03160800	-3.71229300	2.02868800
C	-8.57366300	-2.60582100	2.73609200
C	-8.32843600	-1.38839700	2.08343300
C	-10.78746400	1.26396700	0.01236000
C	-11.87915100	1.88562000	-0.61859500
C	-11.85341700	2.12312800	-1.98732700
C	-10.74060000	1.75034300	-2.73692300
C	-9.63305600	1.14782200	-2.12426800
C	-7.80484500	-0.25946100	2.94937300
C	-9.24989700	-2.39734400	-1.50798000
C	-10.87908000	1.06629300	1.51018600
C	-8.45475100	0.82041200	-3.02051100
N	-9.29526400	-4.99764400	2.78767000
N	-13.01749900	2.78215900	-2.69918300
C	-14.15257500	3.13838300	-1.76678100
C	-12.55383900	4.06734900	-3.36157200
C	-9.78516000	-6.11657400	1.89809300
C	-8.01782900	-5.47239600	3.45454000
C	13.57303700	-1.84250300	-3.75629000
C	10.35789000	4.75858200	3.84777000
C	-13.57341600	1.84365200	-3.75505900
C	-10.35766600	-4.76005700	3.84596700
C	-7.56364800	3.34868800	-0.43068400
C	7.56344300	-3.34855000	-0.43171100
H	9.59059500	4.46399600	0.07601500
H	8.39757400	2.65015500	3.80695100
H	12.72465400	-2.16525700	-0.00560100
H	10.69845800	-1.91920300	-3.80868300
H	8.23890000	0.30151900	3.95311000
H	6.71709900	0.33188000	3.05569500
H	8.01179100	-0.72647200	2.53165400
H	8.30783000	2.24971100	-2.04584100
H	9.67412000	3.34426500	-1.85137300
H	9.93166700	1.59822000	-1.80692400
H	10.11664700	-1.65164500	2.03520100
H	11.85158800	-1.38445400	1.89391700
H	10.73616900	-0.01923100	1.78593100
H	8.77461400	-0.70009300	-4.05962500
H	7.70927700	-1.62176400	-2.99721300
H	7.93745200	0.09252900	-2.72144200
H	14.93682900	-3.60473800	-2.36360800
H	14.53693200	-2.23253200	-1.30184400
H	13.79699800	-3.84035100	-1.01596900
H	13.40837100	-4.53057800	-3.85643300
H	11.78248200	-3.83764600	-4.09598200
H	12.15277400	-4.72470800	-2.59330400
H	9.94604100	6.99258500	2.52716400
H	10.72418400	5.82323500	1.43293200
H	9.03122200	6.33680700	1.14651600
H	8.22706800	6.40214200	3.98476400
H	7.67472600	4.71510200	4.15929000
H	7.26649200	5.62954700	2.68376200
H	4.77482800	-3.35612800	-0.30353900
H	-4.77501000	3.35640300	-0.30290400
H	-0.71875600	-4.59451700	-0.10649100
H	0.23474500	-3.94005100	-1.46802900
H	1.70607700	-5.36525100	-0.03022200
H	1.26538600	-4.38870500	1.39919400
H	0.71876800	4.59461100	-0.11082000
H	-0.23509700	3.93882300	-1.47146400
H	-1.70604200	5.36543600	-0.03466800
H	-1.26496200	4.39030200	1.39559300
H	-9.59055700	-4.46403800	0.07431300

H	-8.39714000	-2.65174600	3.80587900
H	-12.72465100	2.16503500	-0.00432000
H	-10.69886400	1.92053300	-3.80772400
H	-8.23889900	-0.30281000	3.95279500
H	-6.71673000	-0.33372000	3.05603200
H	-8.01068100	0.72535800	2.53163200
H	-8.30788300	-2.24876800	-2.04673000
H	-9.67402300	-3.34358600	-1.85264800
H	-9.93178000	-1.59759500	-1.80743400
H	-10.11605600	1.65018700	2.03600000
H	-11.85116200	1.38395500	1.89487200
H	-10.73645100	0.01821800	1.78604600
H	-7.71002600	1.62336900	-2.99741000
H	-7.93710200	-0.09098300	-2.72109700
H	-8.77515500	0.70079800	-4.05923200
H	-14.93718300	3.60525500	-2.36153300
H	-14.53710200	2.23262500	-1.30038200
H	-13.79724000	3.84036900	-1.01390400
H	-13.40896000	4.53178900	-3.85413400
H	-11.78305300	3.83906000	-4.09415000
H	-12.15322800	4.72549000	-2.59107300
H	-9.94587200	-6.99360400	2.52449100
H	-10.72409700	-5.82381700	1.43078800
H	-9.03115500	-6.33726700	1.14403800
H	-8.22691700	-6.40377500	3.98227400
H	-7.67450100	-4.71683100	4.15745500
H	-7.26633300	-5.63071100	2.68155800
H	13.89656300	-0.92569500	-3.26424200
H	14.41624300	-2.33102000	-4.24612700
H	12.79823100	-1.61994000	-4.48639400
H	11.26488500	4.41418200	3.35177600
H	10.54229700	5.69691700	4.37238300
H	10.00757400	4.00389700	4.54820700
H	-13.89683800	0.92663100	-3.26334000
H	-14.41669900	2.33230700	-4.24462600
H	-12.79866700	1.62142400	-4.48532500
H	-11.26466300	-4.41544600	3.35012400
H	-10.54209100	-5.69857700	4.37024300
H	-10.00730200	-4.00563700	4.54666600
H	-7.07334300	4.27537800	-0.12156400
H	-7.85043900	3.46935400	-1.48173400
H	-8.48234400	3.24165700	0.14853600
H	8.48199700	-3.24195500	0.14782200
H	7.07294600	-4.27535800	-0.12325200
H	7.85050300	-3.46862400	-1.48274800

Compound ZN

DFT B3LYP/6-31G+(d,p), gas phase, S_0

Point group: C_1

Total energy: -2513546.50

kcal mol^{-1}

Dipole moment: 0.05 D

Immaginary frequencies: 0

C	-4.63710100	-0.04056500	0.55481000
C	-5.49390400	0.33113100	1.60619900
C	-6.88260100	0.36420100	1.44878600
C	-7.48728100	-0.00889800	0.21672700
C	-6.62157000	-0.40155700	-0.84255900
C	-5.23672700	-0.39844600	-0.66593000
B	-9.06688700	0.01184600	0.02958000
C	-9.80871500	-1.26955800	-0.52300000
C	-9.88177700	1.31489300	0.39790800
C	-10.76461900	-1.17782200	-1.57497200
C	-11.39753600	-2.31532500	-2.08161000
C	-11.16397000	-3.60065200	-1.55007400
C	-10.21969200	-3.69405500	-0.50667600
C	-9.54741900	-2.57360600	-0.01376100
C	-11.05831400	1.25266100	1.19833600
C	-11.76071200	2.40859000	1.54709100
C	-11.37516100	3.68527200	1.08821000
C	-10.21180400	3.74952200	0.29351600
C	-9.47408400	2.60957400	-0.03302200
C	-8.55689900	-2.82226200	1.11003300
C	-11.12275200	0.14172800	-2.23703900
C	-11.59603100	-0.05446100	1.75513300
C	-8.24367900	2.82720600	-0.89592800
C	-7.14431800	-0.81856700	-2.20541700
C	-7.69957900	0.79424400	2.65437000
C	-3.18369100	-0.04550500	0.71442300
N	-11.84068700	-4.71979300	-2.02234500
N	-12.11274600	4.82391200	1.39309000
C	-13.16859900	4.74330600	2.39039400
C	-11.54083700	6.13509800	1.12690900
C	-12.63211200	-4.61354500	-3.23824100
C	-11.38162400	-6.04519300	-1.63531500
C	-2.41568100	-0.05223200	1.86342800
C	-1.01206100	-0.06191800	1.62363800
C	-0.65971200	-0.06587700	0.28685800
S	-2.12393100	-0.04527200	-0.69123200
C	4.63711400	-0.04055600	-0.55482900
C	5.49391300	0.33115500	-1.60621600
C	6.88261100	0.36422700	-1.44880700
C	7.48729400	-0.00888500	-0.21675400
C	6.62158700	-0.40155900	0.84252900
C	5.23674400	-0.39844900	0.66590500
B	9.06690500	0.01184200	-0.02961200
C	9.80870300	-1.26957100	0.52298100
C	9.88179900	1.31489000	-0.39791900
C	10.76456600	-1.17785900	1.57499300
C	11.39744600	-2.31537500	2.08164500
C	11.16388600	-3.60069300	1.55008600
C	10.21964600	-3.69407300	0.50665000
C	9.54740700	-2.57361200	0.01372000
C	11.05836700	1.25265600	-1.19830100
C	11.76077100	2.40858400	-1.54704800
C	11.37519000	3.68527000	-1.08820100
C	10.21181800	3.74952000	-0.29352800
C	9.47409400	2.60957200	0.03299900
C	8.55692200	-2.82224400	-1.11011400
C	11.12267200	0.14167800	2.23710000
C	11.59612500	-0.05447400	-1.75504100
C	8.24368600	2.82720900	0.89589900
C	7.14434000	-0.81858800	2.20537800
C	7.69957800	0.79430100	-2.65438800
C	3.18370500	-0.04550000	-0.71444000
N	11.84056500	-4.71984600	2.02237300
N	12.11277200	4.82390800	-1.39307300
C	13.16871400	4.74328600	-2.39028000
C	11.54087800	6.13509400	-1.12686800
C	12.63198700	-4.61360700	3.23827200
C	11.38149200	-6.04523800	1.63532600
C	2.41569500	-0.05222800	-1.86344600
C	1.01207500	-0.06191900	-1.62365700
C	0.65972600	-0.06587700	-0.28687600
S	2.12394400	-0.04526900	0.69121400

O	-2.92479000	-0.04980800	3.13916200
C	-1.96700800	-0.45609300	4.12713800
C	-0.64258800	0.25737600	3.91230700
O	-0.08906800	-0.09428000	2.63668300
O	2.92480600	-0.04980100	-3.13917900
C	1.96702500	-0.45608900	-4.12715500
C	0.64260200	0.25737400	-3.91232500
O	0.08908200	-0.09428200	-2.63670100
H	-5.06718700	0.60990400	2.56204600
H	-4.60915800	-0.70331100	-1.49942600
H	-12.08636300	-2.18718300	-2.90790300
H	-9.99588900	-4.65656800	-0.06257000
H	-12.62621500	2.30196500	2.18989700
H	-9.86490400	4.70405000	-0.08368200
H	-7.52427700	-2.67316400	0.78085500
H	-8.71629300	-2.15106000	1.95952400
H	-8.64654900	-3.84792800	1.48046400
H	-10.23785100	0.72187300	-2.51551100
H	-11.70310600	-0.03300800	-3.14821300
H	-11.71821100	0.77844300	-1.57583700
H	-10.81660400	-0.65575000	2.23284600
H	-12.36960700	0.13883900	2.50465400
H	-12.03545200	-0.67851200	0.97119000
H	-7.31998100	2.64797800	-0.33788700
H	-8.22214800	2.15984100	-1.76304400
H	-8.21521700	3.85442700	-1.27169300
H	-7.85471900	-0.09415900	-2.61692900
H	-6.31996400	-0.91202400	-2.91883900
H	-7.66574200	-1.77958300	-2.16308700
H	-7.06341800	0.85826900	3.54218100
H	-8.16559100	1.77235800	2.50059300
H	-8.50968800	0.09300400	2.87960000
H	-13.66739200	5.71159900	2.45942700
H	-13.92345400	4.00464400	2.10155300
H	-12.79248200	4.47501800	3.39128600
H	-12.26782100	6.90214700	1.39926000
H	-11.31849100	6.25719200	0.06161000
H	-10.61344100	6.31919200	1.69310800
H	-13.12644900	-5.56838300	-3.42547000
H	-13.41374100	-3.85435000	-3.13081400
H	-12.02573400	-4.35787100	-4.12262300
H	-12.04572300	-6.79313100	-2.07189400
H	-11.41632300	-6.17032100	-0.54796800
H	-10.35332000	-6.25570100	-1.97118700
H	5.06719200	0.60993900	-2.56205800
H	4.60917800	-0.70332100	1.49940200
H	12.08623900	-2.18725200	2.90797100
H	9.99584700	-4.65658000	0.06252900
H	12.62630300	2.30195700	-2.18981400
H	9.86491500	4.70405100	0.08366500
H	7.52429300	-2.67312500	-0.78097600
H	8.71636500	-2.15104400	-1.95959800
H	8.64656800	-3.84791100	-1.48054200
H	10.23775500	0.72178300	2.51560700
H	11.70304300	-0.03307300	3.14825900
H	11.71809900	0.77843700	1.57591300
H	10.81673400	-0.65575700	-2.23282300
H	12.36977000	0.13881300	-2.50449200
H	12.03546500	-0.67852800	-0.97105600
H	7.31998800	2.64802400	0.33784200
H	8.22212700	2.15981600	1.76299300
H	8.21524800	3.85441900	1.27169700
H	7.85486300	-0.09426900	2.61683200
H	6.32000700	-0.91190800	2.91884100
H	7.66562700	-1.77968100	2.16305600
H	7.06343500	0.85820900	-3.54222100
H	8.16546500	1.77248200	-2.50064500
H	8.50978000	0.09315400	-2.87956100
H	13.66749400	5.71158500	-2.45930800
H	13.92355800	4.00464500	-2.10134900
H	12.79268800	4.47495500	-3.39119400
H	12.26786200	6.90214200	-1.39922200
H	11.31854200	6.25718000	-0.06156500
H	10.61347800	6.31919900	-1.69305500
H	13.12629800	-5.56845700	3.42551300
H	13.41363700	-3.85443400	3.13084100
H	12.02561300	-4.35790800	4.12264800

H	12.04556000	-6.79318800	2.07192900
H	11.41622500	-6.17036600	0.54797900
H	10.35317200	-6.25572700	1.97116100
H	-2.40166800	-0.19391500	5.09457000
H	-1.82626300	-1.54406600	4.07529900
H	0.09556100	-0.04811400	4.65740100
H	-0.78223000	1.34550300	3.96311500
H	2.40168500	-0.19391100	-5.09458700
H	1.82628400	-1.54406300	-4.07531500
H	-0.09554600	-0.04811800	-4.65741900
H	0.78224100	1.34550200	-3.96313400

Compound Z

DFT B3LYP/6-31G+(d,p), gas phase, S₀
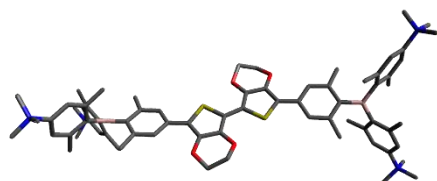
Point group: C₁

Total energy: -2613033.08

kcal mol⁻¹

Dipole moment: 0.27 D

Immaginary frequencies: 0

C	-4.63002100	-0.01484400	0.53283500
C	-5.49646400	0.24034700	1.61625500
C	-6.88224300	0.27305300	1.46823600
C	-7.49605900	-0.00070900	0.20302600
C	-6.61533200	-0.28316900	-0.89260300
C	-5.23435200	-0.26277300	-0.71741900
B	-9.04723100	0.00584300	0.02789600
C	-9.79152200	-1.12270700	-0.83957700
C	-9.95400400	1.14046000	0.71433500
C	-10.68193700	-0.80443800	-1.89514600
C	-11.32938800	-1.81801800	-2.62334600
C	-11.12147000	-3.15296500	-2.29983000
C	-10.25940000	-3.49113300	-1.25926700
C	-9.58394700	-2.49824200	-0.53746700
C	-11.05568500	0.82901100	1.54967900
C	-11.82977300	1.84783600	2.13245000
C	-11.53840100	3.18150600	1.87519700
C	-10.47032800	3.51311400	1.04472000
C	-9.66977200	2.51453200	0.47465300
C	-8.64131300	-2.96632900	0.55327200
C	-10.96196700	0.62389200	-2.31578900
C	-11.44121300	-0.59712300	1.88592700
C	-8.51006100	2.97468900	-0.38596100
C	-7.11107200	-0.56843000	-2.29930100
C	-7.67857500	0.56202800	2.72907300
C	-3.18394600	-0.01709200	0.69060300
N	-11.81174700	-4.26909200	-3.05726500
N	-12.35640100	4.30292700	2.48266400
C	-13.47997000	3.80332600	3.36146100
C	-11.46411100	5.18169600	3.34124800
C	-12.71512900	-3.76300100	-4.15808500
C	-10.77378200	-5.17181100	-3.69984500
C	-2.42071300	-0.01677900	1.85131400
C	-1.01884600	-0.03029000	1.61867400
C	-0.66206700	-0.04578700	0.27906800
S	-2.11595700	-0.03735900	-0.71193500

C	4.62990500	-0.01485100	-0.53287700
C	5.49638300	0.23979000	-1.61640500
C	6.88215200	0.27258500	-1.46836000
C	7.49591600	-0.00051500	-0.20298500
C	6.61517000	-0.28236600	0.89276600
C	5.23418600	-0.26207600	0.71753200
B	9.04709200	0.00595000	-0.02780200
C	9.79128000	-1.12239500	0.83997300
C	9.95398600	1.14027500	-0.71454100
C	10.68180700	-0.80383700	1.89535600
C	11.32932300	-1.81721300	2.62378200
C	11.12133100	-3.15225000	2.30067600
C	10.25910000	-3.49070400	1.26034100
C	9.58358000	-2.49801000	0.53832700
C	11.05584900	0.82835400	-1.54944800
C	11.83013500	1.84685500	-2.13255400
C	11.53878200	3.18065800	-1.87601400
C	10.47051500	3.51273400	-1.04595600
C	9.66976300	2.51448600	-0.47560900
C	8.64070200	-2.96642200	-0.55206400
C	10.96197000	0.62461700	2.31550100
C	11.44154600	-0.59796300	-1.88476900
C	8.50983500	2.97513500	0.38445100
C	7.11090600	-0.56674000	2.29964600
C	7.67855500	0.56093000	-2.72929400
C	3.18382500	-0.01719500	-0.69069000
N	11.81168600	-4.26817700	3.05833900
N	12.35698200	4.30174200	-2.48383600
C	13.48075400	3.80165900	-3.36209500
C	11.46494800	5.18011900	-3.34309000
C	12.71519400	-3.76179100	4.15891800
C	10.77379500	-5.17071900	3.70129200
C	2.42060500	-0.01743600	-1.85140600
C	1.01873100	-0.03092500	-1.61877200
C	0.66194300	-0.04586800	-0.27916400
S	2.11582200	-0.03694300	0.71184600
O	-2.93483600	-0.00678300	3.11480300
C	-1.97869900	-0.37932800	4.12971900
C	-0.65741100	0.33240900	3.90344200
O	-0.10218600	-0.04286400	2.62815500
O	2.93473000	-0.00792800	-3.11490200
C	1.97862000	-0.38094900	-4.12966500
C	0.65729200	0.33081100	-3.90369000
O	0.10208000	-0.04397500	-2.62825600
C	-12.97903700	5.14143800	1.38073800
C	-12.66793500	-5.08454000	-2.10475300
C	12.97936600	5.14077900	-1.38216700
C	12.66775200	-5.08388100	2.10594300
H	-5.07210900	0.42222900	2.59494700
H	-4.60617800	-0.46034200	-1.58120600
H	-11.98569400	-1.51970800	-3.42998400
H	-10.08248300	-4.52627600	-0.98735200
H	-12.64735200	1.55447500	2.77732500
H	-10.22519100	4.54716200	0.82691700
H	-7.59675300	-2.83017000	0.25721900
H	-8.77492300	-2.41447600	1.48685600
H	-8.79354800	-4.02642900	0.77204800
H	-10.03961800	1.18294700	-2.49880300
H	-11.54750100	0.65650200	-3.23784100
H	-11.52148600	1.16408300	-1.54647200
H	-10.58681100	-1.17620700	2.24789800
H	-12.20480200	-0.62579800	2.66706600
H	-11.83989700	-1.11916800	1.01108400
H	-7.55508900	2.82811400	0.12774500
H	-8.44520300	2.42500300	-1.32808800
H	-8.60183200	4.03646200	-0.62907900
H	-7.85945400	0.15429700	-2.63739600
H	-6.28139700	-0.52892100	-3.00937300
H	-7.56207800	-1.56264500	-2.37980100
H	-7.02939900	0.50664000	3.60610000
H	-8.12057200	1.56346200	2.71314600
H	-8.49494200	-0.14899200	2.88609200
H	-14.00903000	4.67266100	3.75087600
H	-14.16166400	3.19544400	2.76850600
H	-13.06596000	3.22663400	4.18719900
H	-12.07438600	5.97221400	3.77969700
H	-10.68199900	5.61623200	2.72288900

```
H     -11.02182600    4.56310000    4.12166600
H     -13.16466000   -4.62876300   -4.64355100
H     -13.49624900   -3.13800700   -3.72792000
H     -12.12593400   -3.20220200   -4.88209400
H     -11.29138000   -5.95839700   -4.25028800
H     -10.14761100   -5.61047100   -2.92630300
H     -10.16594900   -4.56967700   -4.37460600
H       5.07205800    0.42120700   -2.59519600
H       4.60599300   -0.45913000    1.58142200
H      11.98569400   -1.51868000    3.43028600
H      10.08210200   -4.52592600    0.98877600
H      12.64785300    1.55313500   -2.77708900
H      10.22538800    4.54690300   -0.82871900
H       7.59621200   -2.83036000   -0.25570800
H       8.77391100   -2.41470900   -1.48578600
H       8.79302300   -4.02654000   -0.77068600
H      10.03969800    1.18428500    2.49692400
H      11.54631100    0.65749200    3.23830300
H      11.52282200    1.16403200    1.54658800
H      10.58690700   -1.17798400   -2.24461100
H      12.20385200   -0.62707400   -2.66714800
H      11.84203400   -1.11876800   -1.00998800
H       7.55501800    2.82851300   -0.12953500
H       8.44455800    2.42581900    1.32676300
H       8.60167900    4.03698900    0.62719100
H       7.85905700    0.15640600    2.63738200
H       6.28118600   -0.52707700    3.00965600
H       7.56221000   -1.56076900    2.38073100
H       7.02938900    0.50531400   -3.60631500
H       8.12072700    1.56229000   -2.71374200
H       8.49481200   -0.15029000   -2.88601600
H      14.00996800    4.67078000   -3.75178300
H      14.16226100    3.19402400   -2.76867100
H      13.06693300    3.22459600   -4.18766800
H      12.07536800    5.97039300   -3.78177600
H      10.68269600    5.61499400   -2.72515000
H      11.02284200    4.56115000   -4.12331400
H      13.16480100   -4.62742200    4.64454800
H      13.49625500   -3.13689600    3.72850100
H      12.12607900   -3.20081600    4.88285400
H      11.29146200   -5.95715200    4.25188800
H      10.14753500   -5.60960100    2.92794900
H      10.16604400   -4.56839900    4.37595900
H      -2.42459300   -0.08711800    5.08212600
H      -1.84194400   -1.46722000    4.10927400
H       0.07987500    0.03797500    4.65240000
H      -0.79168300    1.42074800    3.93123600
H       2.42450200   -0.08911200   -5.08219300
H       1.84192000   -1.46884000   -4.10876800
H      -0.07997200    0.03603500   -4.65253600
H       0.79151000    1.41914500   -3.93192500
H     -13.61213900    4.49516900    0.77342100
H     -13.57143100    5.93363000    1.84014800
H     -12.19239100    5.57482700    0.76736300
H     -13.40305400   -4.42105400   -1.65011600
H     -13.16432700   -5.87257600   -2.67234100
H     -12.03633400   -5.52305400   -1.33554800
H      13.61226600    4.49478400   -0.77434800
H      13.57192900    5.93270400   -1.84182000
H      12.19257500    5.57452300   -0.76922800
H      13.40282000   -4.42052300    1.65103800
H      13.16421200   -5.87177000    2.67367700
H      12.03605100   -5.52259000    1.33692900
```

8 References

[1] Z. M. Hudson, S. Wang, *Dalton Trans.* **2011**, *40*, 7805-7816.

[2] G. Turkoglu, M. E. Cinar, T. Ozturk, *Molecules* **2017**, *22*, 1522-1545.

[3] Y. Yu, C. Dong, A. F. Alahmadi, B. Meng, J. Liu, F. Jäkle, L. Wang, *J. Mater. Chem. C* **2019**, *7*, 7427-7432.

[4] K. C. Song, K. M. Lee, N. V. Nghia, W. Y. Sung, Y. Do, M. H. Lee, *Organometallics* **2013**, *32*, 817-823.

[5] G. Turkoglu, M. E. Cinar, T. Ozturk, *Eur. J. Org. Chem.* **2017**, *2017*, 4552-4561.

[6] H. R. Bhat, P. S. S. Gupta, S. Biswal, M. K. Rana, *ACS Omega* **2019**, *4*, 4505-4518.

[7] J. Liu, C. Zhang, J. Dong, J. Zhu, C. Shen, G. Yang, X. Zhang, *New. J. Chem.* **2017**, *41*, 4733-4737.

[8] H. J. Li, S. K. Mellerup, X. Wang, S. Wang, *Org. Lett.* **2019**, *21*, 2838-2842.

[9] S. Griesbeck, Z. Zhang, M. Gutmann, T. Lühmann, R. M. Edkins, G. Clermont, A. N. Lazar, M. Haehnel, K. Edkins, A. Eichhorn, M. Blanchard-Desce, L. Meinel, T. B. Marder, *Chem. Eur. J.* **2016**, *22*, 14701-14706.

[10] S. Griesbeck, M. Ferger, C. Czernetzi, C. Wang, R. Bertermann, A. Friedrich, M. Haehnel, D. Sieh, M. Taki, S. Yamaguchi, T. B. Marder, *Chem. Eur. J.* **2019**, *25*, 7679-7688.

[11] S. Griesbeck, E. Michail, F. Rauch, H. Ogasawara, C. Wang, Y. Sato, R. Edkins, Z. Zhang, M. Taki, C. Lambert, S. Yamaguchi, T. B. Marder, *Chem. Eur. J.* **2019**, *25*, 13164-13175.

[12] S. Griesbeck, E. Michail, C. Wang, H. Ogasawara, S. Lorenzen, L. Gerstner, T. Zang, J. Nitsch, Y. Sato, R. Bertermann, M. Taki, C. Lambert, S. Yamaguchi, T. B. Marder, *Chem. Sci.* **2019**, *10*, 5405-5422.

[13] Z. Ban, S. Griesbeck, S. Tomic, J. Nitsch, T. B. Marder, I. Piantanida, *Chem. Eur. J.* **2020**, *26*, 2195-2203.

[14] J. Liu, S. Zhang, J. Zhu, X. Liu, G. Yang, X. Zhang, *Anal. Bioanal. Chem.* **2019**, *411*, 5223-5231.

[15] K. C. Yan, A. C. Sedgwick, Y. Zang, G. R. Chen, X. P. He, J. Li, J. Yoon, T. D. James, *Small Methods* **2019**, 1900013.

[16] C. D. Entwistle, T. B. Marder, *Angew. Chem. Int. Ed.*, **2002***, 41*, 2927-2931.

[17] C. D. Entwistle, T. B. Marder, *Chem. Mater.* **2004**, *16*, 4574-4585.

[18] Z. M. Hudson, S. Wang, *Acc. Chem. Res.* **2009**, *42*, 1584-1596.

[19] L. Ji, S. Griesbeck, T. B. Marder, *Chem. Sci.* **2017**, *8*, 846-863.

[20] C. Jiménez, A. Enríquez-Cabrera, O. González-Antonio, J. Ordóñez-Hernández, P. Lacroix, P. Labra-Vázquez, N. Farfán, R. Santillan, *Inorganics* **2018**, *6*, 131-169.

[21] J.-B. Li, H.-W. Liu, T. Fu, R. Wang, X.-B. Zhang, W. Tan, *Trends Chem.* **2019**, *1*, 224-234.

[22] S. K. Mellerup, S. Wang, *Chem. Soc. Rev.* **2019**, *48*, 3537-3549.

[23] S. K. Mellerup, S. Wang, *Trends Chem.* **2019**, *1*, 77-89.

[24] M. F. Lappert, *Chem. Rev.* **1956**, *56*, 959-1064.

[25] J. L. Carden, A. Dasgupta, R. L. Melen, *Chem. Soc. Rev.* **2020**, *49*, 1706-1725.

[26] A. Michaelis, *Liebigs Ann. Chem.* **1885**, *229*, 295-334.

[27] W. E. Piers, D. J. Morrison, M. Parvez, *Synlett* **2004**, 2429-2433.

[28] Á. Gyömöre, M. Bakos, T. Földes, I. Pápai, A. Domján, T. Soós, *ACS Catal.* **2015**, *5*, 5366-5372.

[29] K. Schickedanz, T. Trageser, M. Bolte, H. W. Lerner, M. Wagner, *Chem. Commun.* **2015**, *51*, 15808-15810.

[30] J. Merz, J. Fink, A. Friedrich, I. Krummenacher, H. H. Al Mamari, S. Lorenzen, M. Haehnel, A. Eichhorn, M. Moos, M. Holzapfel, H. Braunschweig, C. Lambert, A. Steffen, L. Ji, T. B. Marder, *Chem. Eur. J.* **2017**, *23*, 13164-13180.

[31] J. Merz, A. Steffen, J. Nitsch, J. Fink, C. B. Schurger, A. Friedrich, I. Krummenacher, H. Braunschweig, M. Moos, D. Mims, C. Lambert, T. B. Marder, *Chem. Sci.* **2019**, *10*, 7516-7534.

[32] M. Ito, E. Ito, M. Hirai, S. Yamaguchi, *J Org Chem* **2018**, *83*, 8449-8456.

[33] J. He, F. Rauch, M. Finze, T. B. Marder, *Chem. Sci.* **2021**.

[34] E. von Grotthuss, A. John, T. Kaese, M. Wagner, *Asian J. Org. Chem.* **2018**, *7*, 37-53.

[35] H. Budy, J. Gilmer, T. Trageser, M. Wagner, *Eur. J. Inorg. Chem.* **2020**, *2020*, 4148-4162.

[36] A. Escande, M. J. Ingleson, *Chem. Commun.* **2015**, *51*, 6257-6274.

[37] A. Michaelis, P. Becker, *Ber. Dtsch. Chem. Ges.* **1880**, *13*, 58-61.

[38] A. Michaelis, P. Becker, *Ber. Dtsch. Chem. Ges.* **1882**, *15*, 180-185.

[39] M. M. Hansen, R. A. Jolly, R. J. Linder, *Org. Process Res. Dev.* **2015**, *19*, 1507-1516.

[40] B. Ames, N., F. D. Lee, W. E. Durston, *Proc. Natl. Acad. Sci. U. S. A.* **1973**, *70*, 782-786.

[41] K. Mortelmans, E. Zeigerb, *Mutat. Res.* **2000**, *455*, 29-60.

[42] A. Michaelis, A. Reese, *Ber. Dtsch. Chem. Ges.* **1882**, *15*, 1610-1610.

[43] A. Michaelis, A. Reese, *Ber. Dtsch. Chem. Ges.* **1882**, *15*, 2876-2877.

[44] A. Michaelis, *Ber. Dtsch. Chem. Ges.* **1889**, *22*, 241-243.

[45] A. Dequasie, *The Green Flame: Surviving Government Secrecy, Vol. 1*, American Chemical Society, Washington, DC (USA), **1991**.

[46] L. Gattermann, *Ber. Dtsch. Chem. Ges.* **1889**, *22*, 186-197.

[47] A. Michaelis, *Ber. Dtsch. Chem. Ges.* **1894**, *27*, 244-262.

[48] A. Michaelis, *Liebigs Ann. Chem.* **1901**, *315*, 19-43.

[49] V. Grignard, *C.R. Hebd. Seances Acad. Sci.* **1900**, *130*, 1322-1324.

[50] E. Khotinsky, M. Melamed, *Ber. Dtsch. Chem. Ges.* **1909**, *42*, 3090-3096.

[51] W. Strecker, *Ber. Dtsch. Chem. Ges.* **1910**, *43*, 1131-1136.

[52] W. König, W. Scharrnbeck, *J. Prakt. Chem.* **1930**, *128*, 153-170.

[53] K. Albrecht, V. Kaiser, R. Boese, J. Adams, D. E. Kaufmann, *J. Chem. Soc., Perkin Trans. 2* **2000**, 2153-2157.
[54] Y. Gu, H. Pritzkow, W. Siebert, *Eur. J. Inorg. Chem.* **2001**, *2*, 373-379.
[55] A. Pron, G. Zhou, H. Norouzi-Arasi, M. Baumgarten, K. Müllen, *Org. Lett.* **2009**, *11*, 3550-3553.
[56] A. Tsurusaki, T. Sasamori, A. Wakamiya, S. Yamaguchi, K. Nagura, S. Irle, N. Tokitoh, *Angew. Chem. Int. Ed.*, **2011**, *50*, 10940-10943.
[57] A. Sengupta, A. Doshi, F. Jäkle, R. M. Peetz, *J. Polym. Sci. Pol. Chem.* **2015**, *53*, 1707-1718.
[58] X. Guo, X. Zhang, S. Wang, S. Li, R. Hu, Y. Li, G. Yang, *Anal. Chim. Acta* **2015**, *869*, 81-88.
[59] H. Schiff, *Ann. Chem. Supl.* **1867**, *5*, 154-218.
[60] E. Krause, R. Nitsche, *Ber. Dtsch. Chem. Ges.* **1921**, *54*, 2784-2791.
[61] E. Krause, R. Nitsche, *Ber. Dtsch. Chem. Ges.* **1922**, *55*, 1261-1265.
[62] E. Krause, *Ber. Dtsch. Chem. Ges.* **1924**, *57*, 216-217.
[63] E. Krause, H. Polack, *Ber. Dtsch. Chem. Ges.* **1926**, *59*, 777-785.
[64] E. Krause, H. Polack, *Ber. Dtsch. Chem. Ges.* **1928**, *61*, 271-276.
[65] E. Krause, P. Nobbe, *Ber. Dtsch. Chem. Ges.* **1930**, *63*, 934-942.
[66] E. Krause, P. Nobbe, *Ber. Dtsch. Chem. Ges.* **1931**, *64*, 2112-2116.
[67] H. C. Brown, S. Sujish, *J. Am. Chem. Soc.* **1945**, *70*, 2793-2802.
[68] G. Wittig, G. Keicher, *Naturwissenschaften* **1947**, *34*, 216.
[69] G. Wittig, G. Keicher, A. Rückert, P. Raff, *Liebigs Ann. Chem.* **1949**, *563*, 110-126.
[70] G. Wittig, W. Herwig, *Chem. Ber.* **1955**, *88*, 962-976.
[71] Z. Wu, J. Nitsch, J. Schuster, A. Friedrich, K. Edkins, M. Loebnitz, F. Dinkelbach, V. Stepanenko, F. Würthner, C. M. Marian, L. Ji, T. B. Marder, *Angew. Chem. Int. Ed.*, **2020**, *59*, 17137-17144.
[72] H. C. Brown, V. H. Dodson, *J. Am. Chem. Soc.* **1957**, *79*, 2302-2306.
[73] R. T. Hawkins, W. J. Lennarz, H. R. Snyder, *J. Am. Chem. Soc.* **1960**, *82*, 3053-3059.
[74] H. E. Ramsden, A. E. Balint, W. R. Whitford, J. J. Walburn, R. Cserr, *J. Org. Chem.* **1957**, *22*, 1202-1206.
[75] J. L. R. Williams, J. C. Doty, P. J. Grisdale, R. Searle, T. H. Regan, G. P. Happ, D. P. Maier, *J. Am. Chem. Soc.* **1967**, *89*, 5153-5157.
[76] J. C. Doty, B. Babb, P. J. Grisdale, M. Glogowski, J. L. R. Williams, *J. Organomet. Chem.* **1972**, *38*, 229-236.
[77] H. Gilman, L. O. Moore, *J. Am. Chem. Soc.* **1958**, *80*, 3609-3611.
[78] W. Gerrard, M. Howarth, E. F. Mooney, D. E. Pratt, *J. Chem. Soc.* **1963**, 1582-1584.
[79] B. E. Carpenter, W. E. Piers, R. McDonald, *Can. J. Chem.* **2001**, *79*, 291-295.
[80] V. C. Williams, W. E. Piers, W. Clegg, M. R. J. Elsegood, S. Collins, T. B. Marder, *J. Am. Chem. Soc.* **1999**, *121*, 3244-3245.
[81] Y. Sun, W. E. Piers, M. Parvez, *Can. J. Chem.* **1998**, *76*, 513-517.
[82] A. Sundararaman, F. Jäkle, *J. Organomet. Chem.* **2003**, *681*, 134-142.
[83] A. E. Ashley, T. J. Herrington, G. G. Wildgoose, H. Zaher, A. L. Thompson, N. H. Rees, T. Krämer, D. O'Hare, *J. Am. Chem. Soc.* **2011**, *133*, 14727-14740.
[84] P. Chen, A. S. Marshall, S.-H. Chi, X. Yin, J. W. Perry, F. Jäkle, *Chem. Eur. J.* **2015**, *21*, 18237-18247.
[85] P. Chen, X. Yin, N. Baser-Kirazli, F. Jäkle, *Angew. Chem. Int. Ed.*, **2015**, *54*, 10768-10772.
[86] J. E. Burch, W. Gerrard, M. Howarth, E. F. Mooney, *J. Chem. Soc.* **1960**, 4916-4918.
[87] T. Chivers, *Can. J. Chem.* **1970**, *48*, 3856-3859.
[88] A. Sundararaman, M. Victor, R. Varughese, F. Jäkle, *J. Am. Chem. Soc.* **2005**, *127*, 13748-13749.
[89] P. Chen, F. Jäkle, *J. Am. Chem. Soc.* **2011**, *133*, 20142-20145.
[90] X. Yin, F. Guo, R. A. Lalancette, F. Jäkle, *Macromolecules* **2016**, *49*, 537-546.
[91] W. Haubold, J. Herdtle, W. Gollinger, W. Einholz, *J. Organomet. Chem.* **1986**, *35*, 1-8.
[92] D. Kaufmann, *Chem. Ber.* **1987**, *120*, 853-854.
[93] D. Kaufmann, *Chem. Ber.* **1987**, *120*, 901-905.
[94] M. J. Sharp, W. Cheng, V. Snieckus, *Tetrahedron Lett.* **1987**, *28*, 5093-5096.
[95] Y. Qin, G. Cheng, A. Sundararaman, F. Jäkle, *J. Am. Chem. Soc.* **2002**, *124*, 12672-12673.
[96] Y. Qin, G. Cheng, O. Achara, K. Parab, F. Jäkle, *Macromolecules* **2004**, *37*, 7123-7131.
[97] A. Lik, L. Fritze, L. Müller, H. Helten, *J. Am. Chem. Soc.* **2017**, *139*, 5692-5695.
[98] A. Lik, S. Jenthra, L. Fritze, L. Müller, K. N. Truong, H. Helten, *Chem. Eur. J.* **2018**, *24*, 11961-11972.
[99] H. Helten, L. Fritze, N. Riensch, *Synthesis* **2018**, *51*, 399-406.
[100] R. D. Chambers, H. C. Clark, C. J. Willis, *J. Am. Chem. Soc.* **1960**, *82*, 5298-5301.
[101] S. L. Stafford, *Can. J. Chem.* **1963**, *41*, 807-808.
[102] R. D. Chambers, T. Chivers, D. A. Pyk, *J. Chem. Soc.* **1965**, 5144-5145.
[103] D. Thierig, F. Umland, *Naturwissenschaften* **1967**, *54*, 563-563.
[104] G. Bir, W. Schacht, D. Kaufmann, *J. Organomet. Chem.* **1988**, *340*, 267-271.
[105] E. Vedejs, R. W. Chapman, S. C. Fields, S. Lin, M. R. Schrimpf, *J. Org. Chem.* **1995**, *60*, 3020-3027.
[106] G. A. Molander, N. Ellis, *Acc. Chem. Res.* **2007**, *40*, 275-286.
[107] É. Dorkó, B. Kótai, T. Földes, Á. Gyömöre, I. Pápai, T. Soós, *J. Organomet. Chem.* **2017**, *847*, 258-262.
[108] É. Dorkó, M. Szabó, B. Kótai, I. Pápai, A. Domján, T. Soós, *Angew. Chem. Int. Ed.*, **2017**, *56*, 9512-9516.
[109] Y. Hoshimoto, T. Kinoshita, S. Hazra, M. Ohashi, S. Ogoshi, *J. Am. Chem. Soc.* **2018**, *140*, 7292-7300.
[110] K. Schickedanz, J. Radtke, M. Bolte, H. W. Lerner, M. Wagner, *J. Am. Chem. Soc.* **2017**, *139*, 2842-2851.
[111] E. Yamamoto, K. Izumi, R. Shishido, T. Seki, N. Tokodai, H. Ito, *Chem. Eur. J.* **2016**, *22*, 17547-17551.
[112] R. Shishido, I. Sasaki, T. Seki, T. Ishiyama, H. Ito, *Chem. Eur. J.* **2019**, *25*, 12924-12928.
[113] P. J. Grisdale, J. L. R. Williams, M. E. Glogowski, B. E. Babb, *J. Org. Chem.* **1971**, *36*, 544-549.
[114] R. L. Letsinger, N. Remes, *J. Am. Chem. Soc.* **1955**, *77*, 2489-2491.

[115]   B. M. Mikhailov, T. V. Kostroma, N. S. Fedotov, *Chem. Zentralblatt* **1958**, *129*, 10916-10917.
[116]   J. Liu, C. Zhang, J. Dong, J. Zhu, C. Shen, G. Yang, X. Zhang, *RSC Adv.* **2017**, *7*, 14511-14515.
[117]   A. Pelter, K. Smith, D. Buss, Z. Jin, *Heteroat. Chem.* **1992**, *3*, 275-277.
[118]   R. J. Blagg, G. G. Wildgoose, *RSC Adv.* **2016**, *6*, 42421-42427.
[119]   J. Liu, S. Zhang, C. Zhang, J. Dong, C. Shen, J. Zhu, H. Xu, M. Fu, G. Yang, X. Zhang, *Chem. Commun.* **2017**, *53*, 11476-11479.
[120]   K. Parab, K. Venkatasubbaiah, F. Jäkle, *J. Am. Chem. Soc.* **2006**, *128*, 12879-12885.
[121]   A. Sundararaman, K. Venkatasubbaiah, M. Victor, L. N. Zakharov, A. L. Rheingold, F. Jäkle, *J. Am. Chem. Soc.* **2006**, *128*, 16554-16565.
[122]   H. Li, A. Sundararaman, T. Pakkirisamy, K. Venkatasubbaiah, F. Schödel, F. Jäkle, *Macromolecules* **2011**, *44*, 95-103.
[123]   K. Parab, A. Doshi, F. Cheng, F. Jäkle, *Macromolecules* **2011**, *44*, 5961-5967.
[124]   X. Yin, K. Liu, Y. Ren, R. A. Lalancette, Y. L. Loo, F. Jäkle, *Chem. Sci.* **2017**, *8*, 5497-5505.
[125]   X. Yin, J. Chen, R. A. Lalancette, T. B. Marder, F. Jäkle, *Angew. Chem. Int. Ed.*, **2014***, 53*, 9761-9765.
[126]   M. J. Kelly, R. Tirfoin, J. Gilbert, S. Aldridge, *J. Organomet. Chem.* **2014**, *769*, 11-16.
[127]   R. Stahl, C. Lambert, C. Kaiser, R. Wortmann, R. Jakober, *Chem. Eur. J.* **2006**, *12*, 2358-2370.
[128]   D. Reitzenstein, C. Lambert, *Macromolecules* **2009**, *42*, 773-782.
[129]   A. Ito, K. Kawanishi, E. Sakuda, N. Kitamura, *Chem. Eur. J.* **2014**, *20*, 3940-3953.
[130]   Z. Zhang, R. M. Edkins, J. Nitsch, K. Fucke, A. Eichhorn, A. Steffen, Y. Wang, T. B. Marder, *Chem. Eur. J.* **2015**, *21*, 177-190.
[131]   Z. Zhang, R. M. Edkins, J. Nitsch, K. Fucke, A. Steffen, L. E. Longobardi, D. W. Stephan, C. Lambert, T. B. Marder, *Chem. Sci.* **2015**, *6*, 308-321.
[132]   Y.-g. Shi, J.-w. Wang, H. Li, G.-f. Hu, X. Li, S. K. Mellerup, N. Wang, T. Peng, S. Wang, *Chem. Sci.* **2018**, *9*, 1902-1911.
[133]   Z. Yuan, N. J. Taylor, T. B. Marder, I. D. Williams, S. K. Kurtz, L.-T. Cheng, *J. Chem. Soc. Chem. Comm.* **1990**, 1489-1492.
[134]   M. Lequan, R. M. Lequan, K. C. Ching, *J. Mater. Chem.* **1991**, *1*, 997-999.
[135]   M. Lequan, R. M. Lequan, K. C. Ching, M. Barzoukas, A. Fort, H. Lahoucine, G. Bravic, D. Chasseau, J. Gaultier, *J. Mater. Chem.* **1992**, *2*, 719-725.
[136]   Z. Yuan, C. D. Entwistle, J. C. Collings, D. Albesa-Jové, A. S. Batsanov, J. A. K. Howard, N. J. Taylor, H. M. Kaiser, D. E. Kaufmann, S.-Y. Poon, W.-Y. Wong, C. Jardin, S. Fathallah, A. Boucekkine, J.-F. Halet, T. B. Marder, *Chem. Eur. J.* **2006**, *12*, 2758-2771.
[137]   Z. Yuan, N. J. Taylor, R. Ramachandran, T. B. Marder, *Appl. Organomet. Chem.* **1996**, *10*, 305-316.
[138]   Z. Yuan, N. J. Taylor, Y. Sun, T. B. Marder, I. D. Williams, L.-T. Cheng, *J. Organomet. Chem.* **1993**, *449*, 27-37.
[139]   Z. Yuan, J. C. Collings, N. J. Taylor, T. B. Marder, C. Jardin, J.-F. Halet, *J. Solid State Chem.* **2000**, *154*, 5-12.
[140]   C.-W. Chiu, Y. Kim, F. P. Gabbaï, *J. Am. Chem. Soc.* **2009**, *131*, 60-61.
[141]   T. W. Hudnall, F. P. Gabbaï, *J. Am. Chem. Soc.* **2007**, *129*, 11978-11986.
[142]   M. H. Lee, T. Agou, J. Kobayashi, T. Kawashima, F. P. Gabbaï, *Chem. Commun.* **2007**, 1133-1135.
[143]   J. Liu, K. Cheng, C. Yang, J. Zhu, C. Shen, X. Zhang, X. Liu, G. Yang, *Anal. Chem.* **2019**, *91*, 6340–6344.
[144]   J. Liu, X. Guo, R. Hu, X. Liu, S. Wang, S. Li, Y. Li, G. Yang, *Anal. Chem.* **2016**, *88*, 1052-1057.
[145]   X. Li, X. Guo, L. Cao, Z. Xun, S. Wang, S. Li, Y. Li, G. Yang, *Angew. Chem. Int. Ed.* **2014**, *53*, 7809-7813.
[146]   M. Varlan, B. A. Blight, S. Wang, *Chem. Commun.* **2012**, *48*, 12059-12061.
[147]   Y. Liu, K. Mo, Y. Cui, *Inorg. Chem.* **2013**, *52*, 10286-10291.
[148]   X. Wang, J. Yang, L. Zhang, F. Liu, F. Dai, D. Sun, *Inorg. Chem.* **2014**, *53*, 11206-11212.
[149]   S. Helten, B. Sahoo, V. Bon, I. Senkovska, S. Kaskel, F. Glorius, *CrystEngComm* **2015**, *17*, 307-312.
[150]   T. J. Crevier, B. K. Bennett, J. D. Soper, J. A. Bowman, A. Dehestani, D. A. Hrovat, S. Lovell, W. Kaminsky, J. M. Mayer, *J. Am. Chem. Soc.* **2001**, *123*, 1059-1071.
[151]   E. L. Bennett, E. J. Lawrence, R. J. Blagg, A. S. Mullen, F. MacMillan, A. W. Ehlers, D. J. Scott, J. S. Sapsford, A. E. Ashley, G. G. Wildgoose, J. C. Slootweg, *Angew. Chem. Int. Ed.* **2019**, *58*, 8362-8366.
[152]   S. M. Berger, M. Ferger, T. B. Marder, **2020**, *submitted*.
[153]   N. Suzuki, K. Suda, D. Yokogawa, H. Kitoh-Nishioka, S. Irle, A. Ando, L. M. G. Abegão, K. Kamada, A. Fukazawa, S. Yamaguchi, *Chem. Sci.* **2018**, *9*, 2666-2673.
[154]   F. Rauch, P. Endres, A. Friedrich, D. Sieh, M. Hähnel, I. Krummenacher, H. Braunschweig, M. Finze, L. Ji, T. B. Marder, *Chem. Eur. J.* **2020**, *26*, 12951-12963.
[155]   F. Rauch, J. Krebs, J. Günther, A. Friedrich, M. Hähnel, I. Krummenacher, H. Braunschweig, M. Finze, T. B. Marder, *Chem. Eur. J.* **2020**, *26*, 10626-10633.
[156]   M. Matsura, T. Yamada, H. Kita, **2003***, US 20030137239*.
[157]   S. Sasaki, F. Murakami, M. Murakami, M. Watanabe, K. Kato, K. Sutoh, M. Yoshifuji, *J. Organomet. Chem.* **2005**, *690*, 2664-2672.
[158]   Y. Liu, X. Xu, F. Zheng, Y. Cui, *Angew. Chem. Int. Ed.* **2008**, *47*, 4538-4541.
[159]   M. Mao, M.-G. Ren, Q.-H. Song, *Chem. Eur. J.* **2012**, *18*, 15512-15522.
[160]   M.-G. Ren, M. Mao, Q.-H. Song, *Chem. Commun.* **2012**, *48*, 2970-2972.
[161]   B. A. Blight, R. Guillet-Nicolas, F. Kleitz, R.-Y. Wang, S. Wang, *Inorg. Chem.* **2013**, *52*, 1673-1675.
[162]   J. Yoshino, Y. Nakamura, S. Kunitomo, N. Hayashi, H. Higuchi, *Tetrahedron Lett.* **2013**, *54*, 2817-2820.
[163]   G. R. Kumar, P. Thilagar, *Dalton Trans.* **2014**, *43*, 3871-3879.
[164]   Z. Li, H. Li, H. Xia, X. Ding, X. Luo, X. Liu, Y. Mu, *Chem. Eur. J.* **2015**, *21*, 17355-17362.

[165] F. M. Ebrahim, T. N. Nguyen, S. Shyshkanov, A. Gładysiak, P. Favre, A. Zacharia, G. Itskos, P. J. Dyson, K. C. Stylianou, *J. Am. Chem. Soc.* **2019**, *141*, 3052-3058.
[166] N. Mihara, T. K. Ronson, J. R. Nitschke, *Angew. Chem. Int. Ed.* **2019**, *58*, 12497-12501.
[167] S. Shyshkanov, T. N. Nguyen, F. M. Ebrahim, K. C. Stylianou, P. J. Dyson, *Angew. Chem. Int. Ed.* **2019**, *58*, 5371-5375.
[168] Y. Kim, F. P. Gabbaï, *J. Am. Chem. Soc.* **2009**, *131*, 3363-3369.
[169] Y. Kim, H.-S. Huh, M. H. Lee, I. L. Lenov, H. Zhao, F. P. Gabbaï, *Chem. Eur. J.* **2011**, *17*, 2057-2062.
[170] J. Kwak, N. Van Nghia, J. Lee, H. Kim, M. H. Park, M. H. Lee, *Dalton Trans.* **2015**, *44*, 4765-4772.
[171] M. E. Glogowski, N. Zumbulyadis, J. L. R. Williams, *J. Organomet. Chem.* **1982**, *231*, 97-107.
[172] P. Sudhakar, S. Mukherjee, P. Thilagar, *Organometallics* **2013**, *32*, 3129-3133.
[173] S. Pagidi, N. K. Kalluvettukuzhy, P. Thilagar, *Organometallics* **2018**, *37*, 1900-1909.
[174] S. Pagidi, N. K. Kalluvettukuzhy, P. Thilagar, *Langmuir* **2018**, *34*, 8170-8177.
[175] J. Yoshino, S. Konishi, R. Kanno, N. Hayashi, H. Higuchi, *Eur. J. Org. Chem.* **2019**, *2019*, 6117-6121.
[176] A. Pelter, R. Drake, *Tetrahedron* **1994**, *50*, 13801-13828.
[177] A. Pelter, R. Drake, *Tetrahedron* **1994**, *50*, 13775-13800.
[178] A. Pelter, R. Drake, M. Stewart, *Tetrahedron* **1994**, *50*, 13829-13846.
[179] S. H. Kim, K. M. Lee, J. An, M. S. Shin, H. Kim, J. H. Lee, H. Hwang, J. Lee, M. Kim, M. H. Park, Y. Kim, *ChemistrySelect* **2016**, *1*, 1239-1242.
[180] S. W. Kwak, B. H. Choi, J. H. Lee, H. Hwang, J. Lee, H. Kwon, Y. Chung, K. M. Lee, M. H. Park, *Inorg. Chem.* **2017**, *56*, 6039-6043.
[181] S. Yamaguchi, T. Shirasaka, K. Tamao, *Org. Lett.* **2000**, *2*, 4129-4132.
[182] X. Liu, Y. Zhang, H. Li, S. A, H. Xia, Y. Mu, *RSC Adv.* **2013**, *3*, 21267-21270.
[183] H.-J. Park, S.-B. Ko, I. W. Wyman, S. Wang, *Inorg. Chem.* **2014**, *53*, 9751-9760.
[184] A. Nakagawa, E. Sakuda, A. Ito, N. Kitamura, *Inorg. Chem.* **2015**, *54*, 10287-10295.
[185] A. Nakagawa, A. Ito, E. Sakuda, S. Fujii, N. Kitamura, *Eur. J. Inorg. Chem.* **2017**, *2017*, 3794-3798.
[186] A. Nakagawa, A. Ito, E. Sakuda, S. Fujii, N. Kitamura, *Inorg. Chem.* **2018**, *57*, 9055-9066.
[187] H. Hao, K. A. Thompson, Z. M. Hudson, L. L. Schafer, *Chem. Eur. J.* **2018**, *24*, 5562-5568.
[188] J. Y. Ryu, J. M. Lee, N. Van Nghia, K. M. Lee, S. Lee, M. H. Lee, P. J. Stang, J. Lee, *Inorg. Chem.* **2018**, *57*, 11696-11703.
[189] H. Amini, Ž. Ban, M. Ferger, S. Lorenzen, F. Rauch, A. Friedrich, I. Crnolatac, A. Kenđel, S. Miljanić, I. Piantanida, T. B. Marder, *Chem. Eur. J.* **2020**, *26*, 6017-6028.
[190] M. Ferger, Ž. Ban, I. Krošl, S. Tomić, L. Dietrich, S. Lorenzen, F. Rauch, D. Sieh, A. Friedrich, S. Griesbeck, A. Kenđel, S. Miljanić, I. Piantanida, T. B. Marder, **2020**, *submitted*.
[191] T. Ishiyama, J. Takagi, K. Ishida, N. Miyaura, N. R. Anastasi, J. F. Hartwig, *J. Am. Chem. Soc.* **2002**, *124*, 390-391.
[192] I. A. I. Mkhalid, J. H. Barnard, T. B. Marder, J. M. Murphy, J. F. Hartwig, *Chem. Rev,* **2010**, *110*, 890-931.
[193] Z. Zhang, R. M. Edkins, M. Haehnel, M. Wehner, A. Eichhorn, L. Mailänder, M. Meier, J. Brand, F. Brede, K. Müller-Buschbaum, H. Braunschweig, T. B. Marder, *Chem. Sci.* **2015**, *6*, 5922-5927.
[194] A. J. J. Lennox, G. C. Lloyd-Jones, *Chem. Soc. Rev.* **2014**, *43*, 412-443.
[195] G. A. Molander, *J. Org. Chem.* **2015**, *80*, 7837-7848.
[196] H. H. Jaffé, *Chem. Rev,* **1953**, *53*, 191-261.
[197] R. Ting, C. W. Harwig, J. Lo, Y. Li, M. J. Adam, T. J. Ruth, D. M. Perrin, *J. Org. Chem.* **2008**, *73*, 4662-4670.
[198] A. J. J. Lennox, G. C. Lloyd-Jones, *J. Am. Chem. Soc.* **2012**, *134*, 7431-7441.
[199] J. D. Roberts, R. L. Webb, E. A. McElhill, *J. Am. Chem. Soc.* **1950**, *72*, 408-411.
[200] U. M. Reinscheid, J. Vervoort, H. Zuilhof, *Chemosphere* **2006**, *65*, 318-323.
[201] L. A. Jacob, B.-L. Chen, D. Stec, *Synthesis* **1993**, *1993*, 611-614.
[202] Y. Nakao, T. Hiyama, *Chem. Soc. Rev.* **2011**, *40*, 4893-4901.
[203] A. P. Lothian, C. A. Ramsden, M. M. Shaw, R. G. Smith, *Tetrahedron* **2011**, *67*, 2788-2793.
[204] F. Effenberger, W. Spiegler, *Chem. Ber.* **1985**, *118*, 3872-3899.
[205] G. Félix, J. Dunoguès, F. Pisciotti, R. Calas, *Angew. Chem. Int. Ed.* **1977**, *16*, 488-489.
[206] D. N. Coventry, A. S. Batsanov, A. E. Goeta, J. A. K. Howard, T. B. Marder, R. N. Perutz, *Chem. Commun.* **2005**, 2172-2174.
[207] A. G. Crawford, Z. Liu, I. A. I. Mkhalid, M.-H. Thibault, N. Schwarz, G. Alcaraz, A. Steffen, J. C. Collings, A. S. Batsanov, J. A. K. Howard, T. B. Marder, *Chem. Eur. J.* **2012**, *18*, 5022-5035.
[208] L. Ji, K. Fucke, S. K. Bose, T. B. Marder, *J. Org. Chem.* **2015**, *80*, 661-665.
[209] J. Merz, M. Dietz, Y. Vonhausen, F. Wöber, A. Friedrich, D. Sieh, I. Krummenacher, H. Braunschweig, M. Moos, M. Holzapfel, C. Lambert, T. B. Marder, *Chem. Eur. J.* **2020**, *26*, 438-453.
[210] D. P. Clark, N. J. Pazdernik, in *Biotechnology (Second Edition)* (Eds.: D. P. Clark, N. J. Pazdernik), Academic Cell, Boston, **2016**, pp. 33-61.
[211] F. H. Crick, *Symp. Soc. Exp. Biol*, **1958***, 12*, 138-163.
[212] F. Crick, *Nature* **1970**, *227*, 561-563.
[213] M. Morange, *Resonance* **2009**, *14*, 236-247.
[214] M. P. Camacho, *Philos. Theor. Pract. Biol.* **2019**, *11*, 1-15.
[215] S. Banerjee, E. B. Veale, C. M. Phelan, S. A. Murphy, G. M. Tocci, L. J. Gillespie, D. O. Frimannsson, J. M. Kelly, T. Gunnlaugsson, *Chem. Soc. Rev.* **2013**, *42*, 1601-1618.
[216] M. Wang, Y. Yu, C. Liang, A. Lu, G. Zhang, *Int. J. Mol. Sci.* **2016**, *17*, 779-802.
[217] K. Starčević, G. Karminski-Zamola, I. Piantanida, M. Žinić, L. Šuman, M. Kralj, *J. Am. Chem. Soc.* **2005**, *127*, 1074-1075.

[218]   J. Wu, Y. Zou, C. Li, W. Sicking, I. Piantanida, T. Yi, C. Schmuck, *J. Am. Chem. Soc.* **2012**, *134*, 1958-1961.
[219]   R. Bortolozzi, H. Ihmels, L. Thomas, M. Tian, G. Viola, *Chem. Eur. J.* **2013**, *19*, 8736-8741.
[220]   J. Gershberg, M. Radić Stojković, M. Škugor, S. Tomić, T. H. Rehm, S. Rehm, C. R. Saha-Möller, I. Piantanida, F. Würthner, *Chem. Eur. J.* **2015**, *21*, 7886-7895.
[221]   D. Maity, M. Matković, S. Li, M. Ehlers, J. Wu, I. Piantanida, C. Schmuck, *Chem. Eur. J.* **2017**, *23*, 17356-17362.
[222]   K. Schäfer, H. Ihmels, E. Porcù, G. Viola, *Chem. Eur. J.* **2017**, *23*, 370-379.
[223]   H. Ihmels, M. Karbasiyoun, K. Löhl, C. Stremmel, *Org. Biomol. Chem.* **2019**, *17*, 6404-6413.
[224]   P. M. Pithan, C. Kuhlmann, C. Engelhard, H. Ihmels, *Chem. Eur. J.* **2019**, *25*, 16088-16098.
[225]   D. V. Berdnikova, J. Heider, H. Ihmels, N. Sewald, P. M. Pithan, *ChemPhotoChem* **2020**, *4*, 1-7.
[226]   Ž. Ban, J. Matić, B. Žinić, A. F. Füchtbauer, L. M. Wilhelmsson, I. Piantanida, *Molecules* **2020**, *25*, 2188-2205.
[227]   A. A. Zinchenko, N. Chen, S. Murata, *J. Synth. Org. Chem. Jpn.* **2006**, *64*, 1122-1131.
[228]   S. E. Patterson, J. M. Coxon, L. Strekowski, *Bioorg. Med. Chem.* **1997**, *5*, 277-281.
[229]   D. W. Boykin, *J. Braz. Chem. Soc.* **2002**, *13*, 763-771.
[230]   P. E. Pjura, K. Grzeskowiak, R. E. Dickerson, *J. Mol. Biol.* **1987**, *197*, 257-271.
[231]   M. Demeunynck, C. Bailly, W. D. Wilson, *Small Molecule DNA and RNA Binders: From Synthesis to Nucleic Acid Complexes, Vol. 2*, John Wiley & Sons, Weinheim, **2006**.
[232]   G. M. Blackburn, in *Nucleic Acids in Chemistry and Biology (3)*, The Royal Society of Chemistry, Cambridge, **2006**, pp. 341-382.
[233]   H. Ihmels, D. Otto, in *Supermolecular Dye Chemistry* (Ed.: F. Würthner), Springer Berlin Heidelberg, Heidelberg, **2005**, pp. 161-204.
[234]   M. J. Hannon, *Chem. Soc. Rev.* **2007**, *36*, 280-295.
[235]   G. S. Khan, A. Shah, Z. ur-Rehman, D. Barker, *J. Photochem. Photobiol. B* **2012**, *115*, 105-118.
[236]   S. Neidle, *Biopolymers* **1997**, *44*, 105-121.
[237]   S. K. Pal, A. H. Zewail, *Chem. Rev,* **2004**, *104*, 2099-2124.
[238]   G. S. Manning, *Q. Rev. Biophys* **1978**, *11*, 179-246.
[239]   M. T. Record Jr, C. F. Anderson, T. M. Lohman, *Q. Rev. Biophys* **1978**, *11*, 103-178.
[240]   J. Lipfert, S. Doniach, R. Das, D. Herschlag, *Annu. Rev. Biochem.* **2014**, *83*, 813-841.
[241]   M.-J. Lee, B. Jin, H. M. Lee, M. J. Jung, S. K. Kim, J.-M. Kim, *Bull. Korean Chem. Soc.* **2008**, *29*, 1533-1538.
[242]   D. V. Berdnikova, N. I. Sosnin, O. A. Fedorova, H. Ihmels, *Org. Biomol. Chem.* **2018**, *16*, 545-554.
[243]   C. Bustamante, S. B. Smith, J. Liphardt, D. Smith, *Curr. Opin. Struct. Biol.* **2000**, *10*, 279-285.
[244]   L. H. Hurley, *Nat. Rev. Cancer* **2002**, *2*, 188-200.
[245]   M. F. Brana, M. Cacho, A. Gradillas, B. d. Pascual-Teresa, A. Ramos, *Curr. Pharm. Des.* **2001**, *7*, 1745-1780.
[246]   R. Martinez, L. Chacon-Garcia, *Curr. Med. Chem.* **2005**, *12*, 127-151.
[247]   X. Cai, P. J. Gray, D. D. Von Hoff, *Cancer Treat. Rev.* **2009**, *35*, 437-450.
[248]   M. P. Barrett, C. G. Gemmell, C. J. Suckling, *Pharmacol. Ther.* **2013**, *139*, 12-23.
[249]   T. Hermann, *Angew. Chem. Int. Ed.* **2000**, *39*, 1890-1904.
[250]   J. R. Thomas, P. J. Hergenrother, *Chem. Rev,* **2008**, *108*, 1171-1224.
[251]   T. Hermann, *WIREs RNA* **2016**, *7*, 726-743.
[252]   C. M. Connelly, M. H. Moon, J. S. Schneekloth, *Cell Chem. Biol.* **2016**, *23*, 1077-1090.
[253]   A. Donlic, A. E. Hargrove, *WIREs RNA* **2018**, *9*, e1477.
[254]   Z. Darzynkiewicz, in *Methods in Cell Biology, Vol. 33* (Eds.: Z. Darzynkiewicz, H. A. Crissman), Academic Press, **1990**, pp. 285-298.
[255]   T. Suzuki, K. Fujikura, T. Higashiyama, K. Takata, *J. Histochem. Cytochem.* **1997**, *45*, 49-53.
[256]   P. Prentø, *Biotech. Histochem.* **2001**, *76*, 137-161.
[257]   Z. Darzynkiewicz, G. Juan, E. F. Srour, *Cur. Protoc. Cytom.* **2004**, *30*, 7.3.1-7.3.16.
[258]   J. Liu, X. Guo, R. Hu, J. Xu, S. Wang, S. Li, Y. Li, G. Yang, *Anal. Chem.* **2015**, *87*, 3694-3698.
[259]   B. Chen, G. Feng, B. He, C. Goh, S. Xu, G. Ramos-Ortiz, L. Aparicio-Ixta, J. Zhou, L. Ng, Z. Zhao, B. Liu, B. Z. Tang, *Small* **2016**, *12*, 782-792.
[260]   J. Liu, S. Li, S. Zhang, C. Shen, J. Zhu, G. Yang, X. Zhang, *Sensors Actuat. B: Chem.* **2018**, *261*, 531-536.
[261]   J. Liu, S. Zhang, B. Zhao, C. Shen, X. Zhang, G. Yang, *Biosens. Bioelectron.* **2019**, *142*, 111497.
[262]   J. Dong, C. Zhang, B. Zhao, X. Zhang, Z. Leng, J. Liu, *Dyes Pigm.* **2020**, *174*, 108077.
[263]   T. Noda, Y. Shirota, *J. Am. Chem. Soc.* **1998**, *120*, 9714-9715.
[264]   W.-L. Jia, D.-R. Bai, T. McCormick, Q.-D. Liu, M. Motala, R.-Y. Wang, C. Seward, Y. Tao, S. Wang, *Chem. Eur. J.* **2004**, *10*, 994-1006.
[265]   H. Li, A. Sundararaman, K. Venkatasubbaiah, F. Jäkle, *J. Am. Chem. Soc.* **2007**, *129*, 5792-5793.
[266]   J. C. Collings, S.-Y. Poon, C. Le Droumaguet, M. Charlot, C. Katan, L.-O. Pålsson, A. Beeby, J. A. Mosely, H. M. Kaiser, D. Kaufmann, W.-Y. Wong, M. Blanchard-Desce, T. B. Marder, *Chem. Eur. J.* **2009**, *15*, 198-208.
[267]   Y. Kim, H. Zhao, F. P. Gabbaï, *Angew. Chem. Int. Ed.* **2009**, *48*, 4957-4960.
[268]   N. Uzunbajakava, C. Otto, *Opt. Lett.* **2003**, *28*, 2073-2075.
[269]   H.-J. van Manen, Y. M. Kraan, D. Roos, C. Otto, *Proc. Natl. Acad. Sci. U. S. A.* **2005**, *102*, 10159-10164.
[270]   N. K. Das, Y. Dai, P. Liu, C. Hu, L. Tong, X. Chen, Z. J. Smith, *Sensors* **2017**, *17*, 1592-1611.
[271]   H.-J. van Manen, C. Otto, *Nano Lett.* **2007**, *7*, 1631-1636.

[272] R. P. Carney, S. Hazari, M. Colquhoun, D. Tran, B. Hwang, M. S. Mulligan, J. D. Bryers, E. Girda, G. S. Leiserowitz, Z. J. Smith, K. S. Lam, *Anal. Chem.* **2017**, *89*, 5357-5363.
[273] Z. Huang, H. Lui, D. I. McLean, M. Korbelik, H. Zeng, *Photochem. Photobiol.* **2005**, *81*, 1219-1226.
[274] O. R. Šćepanović, Z. Volynskaya, C.-R. Kong, L. H. Galindo, R. R. Dasari, M. S. Feld, *Rev. Sci. Instrum.* **2009**, *80*, 043103.
[275] O. R. Šćepanović, M. Fitzmaurice, A. Miller, C.-R. Kong, Z. I. Volynskaya, R. R. Dasari, J. R. Kramer Jr., M. S. Feld, *J. Biomed. Opt.* **2011**, *16*, 1-10.
[276] S. Jeong, Y.-i. Kim, H. Kang, G. Kim, M. G. Cha, H. Chang, K. O. Jung, Y.-H. Kim, B.-H. Jun, D. W. Hwang, Y.-S. Lee, H. Youn, Y.-S. Lee, K. W. Kang, D. S. Lee, D. H. Jeong, *Sci. Rep.* **2015**, *5*, 9455.
[277] E.-O. Ganbold, J. Yoon, D. Kim, S.-W. Joo, *Phys. Chem. Chem. Phys.* **2015**, *17*, 3019-3023.
[278] B. Kang, M. M. Afifi, L. A. Austin, M. A. El-Sayed, *ACS Nano* **2013**, *7*, 7420-7427.
[279] T. Hirschfeld, *Appl. Spectrosc.* **1977**, *31*, 328-329.
[280] X. Li, M. Jiang, J. W. Y. Lam, B. Z. Tang, J. Y. Qu, *J. Am. Chem. Soc.* **2017**, *139*, 17022-17030.
[281] J. Gala de Pablo, D. R. Chisholm, A. Steffen, A. K. Nelson, C. Mahler, T. B. Marder, S. A. Peyman, J. M. Girkin, C. A. Ambler, A. Whiting, S. D. Evans, *Analyst* **2018**, *143*, 6113-6120.
[282] F. Hu, C. Zeng, R. Long, Y. Miao, L. Wei, Q. Xu, W. Min, *Nat. Methods* **2018**, *15*, 194-200.
[283] F. Hu, L. Shi, W. Min, *Nat. Methods* **2019**, *16*, 830-842.
[284] L. Gong, W. Zheng, Y. Ma, Z. Huang, *Nat. Photonics* **2020**, *14*, 115-122.
[285] J. S. Siddle, R. M. Ward, J. C. Collings, S. R. Rutter, L. Porres, L. Applegarth, A. Beeby, A. S. Batsanov, A. L. Thompson, J. A. K. Howard, A. Boucekkine, K. Costuas, J.-F. Halet, T. B. Marder, *New. J. Chem.* **2007**, *31*, 841-851.
[286] B. A. Coombs, S. R. Rutter, A. E. Goeta, H. A. Sparkes, A. S. Batsanov, A. Beeby, *RSC Adv.* **2012**, *2*, 1870-1876.
[287] S. i. Nakatsuji, K. Matsuda, Y. Uesugi, K. Nakashima, S. Akiyama, W. Fabian, *J. Chem. Soc. Perkin Trans. I* **1992**, 755-758.
[288] M. Levitus, K. Schmieder, H. Ricks, K. D. Shimizu, U. H. F. Bunz, M. A. Garcia-Garibay, *J. Am. Chem. Soc.* **2001**, *123*, 4259-4265.
[289] A. Beeby, K. Findlay, P. J. Low, T. B. Marder, *J. Am. Chem. Soc.* **2002**, *124*, 8280-8284.
[290] A. Beeby, K. S. Findlay, P. J. Low, T. B. Marder, P. Matousek, A. W. Parker, S. R. Rutter, M. Towrie, *Chem. Commun.* **2003**, 2406-2407.
[291] T. M. Fasina, J. C. Collings, J. M. Burke, A. S. Batsanov, R. M. Ward, D. Albesa-Jové, L. Porrès, A. Beeby, J. A. K. Howard, A. J. Scott, W. Clegg, S. W. Watt, C. Viney, T. B. Marder, *J. Mater. Chem.* **2005**, *15*, 690-697.
[292] S. Amthor, C. Lambert, S. Dümmler, I. Fischer, J. Schelter, *J. Phys. Chem. A* **2006**, *110*, 5204-5214.
[293] D. D. Nguyen, N. C. Jones, S. V. Hoffmann, S. H. Andersen, P. W. Thulstrup, J. Spanget-Larsen, *Chem. Phys.* **2012**, *392*, 130-135.
[294] P. Nguyen, S. Todd, D. Van den Biggelaar, N. J. Taylor, T. B. Marder, F. Wittmann, R. H. Friend, *Synlett* **1994**, *1994*, 299-301.
[295] M. Levitus, M. A. Garcia-Garibay, *J. Phys. Chem. A* **2000**, *104*, 8632-8637.
[296] A. D. Malakhov, M. V. Skorobogatyi, I. A. Prokhorenko, S. V. Gontarev, D. T. Kozhich, D. A. Stetsenko, I. A. Stepanova, Z. O. Shenkarev, Y. A. Berlin, V. A. Korshun, *Eur. J. Org. Chem.* **2004**, *2004*, 1298-1307.
[297] B. Strehmel, S. Amthor, J. Schelter, C. Lambert, *ChemPhysChem* **2005**, *6*, 893-896.
[298] A. Beeby, K. S. Findlay, A. E. Goeta, L. Porrès, S. R. Rutter, A. L. Thompson, *Photochem. Photobiol. Sci.* **2007**, *6*, 982-986.
[299] C. V. Suneesh, K. R. Gopidas, *J. Phys. Chem. C* **2009**, *113*, 1606-1614.
[300] M. Mitsui, Y. Kawano, R. Takahashi, H. Fukui, *RSC Adv.* **2012**, *2*, 9921-9931.
[301] P. W. Thulstrup, N. C. Jones, S. V. Hoffmann, J. Spanget-Larsen, *Chem. Phys. Lett.* **2013**, *559*, 35-40.
[302] R. Iwaura, H. Yui, Y. Someya, M. Ohnishi-Kameyama, *J. Photochem. Photobiol. B* **2014**, *130*, 199-204.
[303] Y. Shiraishi, Y. Tokitoh, G. Nishimura, T. Hirai, *Org. Lett.* **2005**, *7*, 2611-2614.
[304] X. Zhang, K. Sasaki, Y. Kuroda, *J. Org. Chem.* **2006**, *71*, 4872-4877.
[305] T. H. Rehm, M. R. Stojković, S. Rehm, M. Škugor, I. Piantanida, F. Würthner, *Chem. Sci.* **2012**, *3*, 3393-3397.
[306] W. M. Hewitt, D. R. Calabrese, J. S. Schneekloth, *Bioorg. Med. Chem.* **2019**, *27*, 2253-2260.
[307] J.-L. Mergny, L. Lacroix, *Oligonucleotides* **2003**, *13*, 515-537.
[308] G. Scatchard, *Ann. N. Y. Acad. Sci.* **1949**, *51*, 660-672.
[309] J. D. McGhee, P. H. von Hippel, *J. Mol. Biol.* **1974**, *86*, 469-489.
[310] C. A. M. Seidel, A. Schulz, M. H. M. Sauer, *J. Phys. Chem.* **1996**, *100*, 5541-5553.
[311] A. Rodger, B. Nordén, *Circular dichroism and linear dichroism, Vol. 1*, Oxford University Press, New York, **1997**.
[312] M. Eriksson, B. Nordén, in *Methods in Enzymology, Vol. 340*, Academic Press, San Diego, **2001**, pp. 68-98.
[313] T. Šmidlehner, I. Piantanida, G. Pescitelli, *Beilstein J. Org. Chem.* **2018**, *14*, 84-105.
[314] R. F. Pasternack, J. I. Goldsmith, S. Szép, E. J. Gibbs, *Biophys. J.* **1998**, *75*, 1024-1031.
[315] V. Casagrande, A. Alvino, A. Bianco, G. Ortaggi, M. Franceschin, *J. Mass Spectrom.* **2009**, *44*, 530-540.
[316] W. Hu, C. Blecking, M. Kralj, L. Šuman, I. Piantanida, T. Schrader, *Chem. Eur. J.* **2012**, *18*, 3589-3597.
[317] A. Lucotti, M. Tommasini, D. Fazzi, M. Del Zoppo, W. A. Chalifoux, R. R. Tykwinski, G. Zerbi, *J. Raman Spectrosc.* **2012**, *43*, 1293-1298.
[318] B. Meng, Y. Ren, J. Liu, F. Jäkle, L. Wang, *Angew. Chem. Int. Ed.* **2018**, *57*, 2183-2187.

[319] M. Charlot, L. Porres, C. D. Entwistle, A. Beeby, T. B. Marder, M. Blanchard-Desce, *Phys. Chem. Chem. Phys.* **2005**, *7*, 600-606.
[320] C. D. Entwistle, J. C. Collings, A. Steffen, L.-O. Palsson, A. Beeby, D. Albesa-Jove, J. M. Burke, A. S. Batsanov, J. A. K. Howard, J. A. Mosely, S.-Y. Poon, W.-Y. Wong, F. Ibersiene, S. Fathallah, A. Boucekkine, J.-F. Halet, T. B. Marder, *J. Mater. Chem.* **2009**, *19*, 7532-7544.
[321] L. Ji, R. M. Edkins, L. J. Sewell, A. Beeby, A. S. Batsanov, K. Fucke, M. Drafz, J. A. K. Howard, O. Moutounet, F. Ibersiene, A. Boucekkine, E. Furet, Z. Liu, J.-F. Halet, C. Katan, T. B. Marder, *Chem. Eur. J.* **2014**, *20*, 13618-13635.
[322] H. Shi, C. Liu, Q. Jiang, J. Xu, *Adv. Electron. Mater.* **2015**, *1*, 1500017.
[323] Y. Wen, J. Xu, *J. Polym. Sci. Pol. Chem.* **2017**, *55*, 1121-1150.
[324] Y. Xia, S. Dai, *J. Mater. Sci.: Mater. Electron* **2020**, DOI: 10.1007/s10854-10020-03473-w.
[325] G. A. Sotzing, J. R. Reynolds, P. J. Steel, *Adv. Mater.* **1997**, *9*, 795-798.
[326] O. Stéphan, P. Schottland, P.-Y. Le Gall, C. Chevrot, C. Mariet, M. Carrier, *J. Electroanal. Chem.* **1998**, *443*, 217-226.
[327] A. Donat-Bouillud, I. Lévesque, Y. Tao, M. D'Iorio, S. Beaupré, P. Blondin, M. Ranger, J. Bouchard, M. Leclerc, *Chem. Mater.* **2000**, *12*, 1931-1936.
[328] J. J. Apperloo, L. B. Groenendaal, H. Verheyen, M. Jayakannan, R. A. J. Janssen, A. Dkhissi, D. Beljonne, R. Lazzaroni, J. L. Brédas, *Chem. Eur. J.* **2002**, *8*, 2384-2396.
[329] J. Cao, J. W. Kampf, M. D. Curtis, *Chem. Mater.* **2003**, *15*, 404-411.
[330] M. Turbiez, P. Frère, J. Roncali, *J. Org. Chem.* **2003**, *68*, 5357-5360.
[331] J. Roncali, P. Blanchard, P. Frère, *J. Mater. Chem.* **2005**, *15*, 1589-1610.
[332] J. Pina, H. D. Burrows, R. S. Becker, F. B. Dias, A. L. Maçanita, J. Seixas de Melo, *J. Phys. Chem. B* **2006**, *110*, 6499-6505.
[333] D. Wasserberg, S. C. J. Meskers, R. A. J. Janssen, E. Mena-Osteritz, P. Bäuerle, *J. Am. Chem. Soc.* **2006**, *128*, 17007-17017.
[334] B. Milián Medina, D. Wasserberg, S. C. J. Meskers, E. Mena-Osteritz, P. Bäuerle, J. Gierschner, *J. Phys. Chem. A* **2008**, *112*, 13282-13286.
[335] Q. Dai, Y. Li, L. Zhai, W. Sun, *J. Photochem. Photobiol. A* **2009**, *206*, 164-168.
[336] G. Trippé-Allard, J.-C. Lacroix, *Tetrahedron* **2013**, *69*, 861-866.
[337] T. Nishinaga, Y. Sotome, *J. Org. Chem.* **2017**, *82*, 7245-7253.
[338] K. König, *J. Microsc.* **2000**, *200*, 83-104.
[339] C. Chen, C. Fang, *Chem. Asian J.* **2020**, *15*, 1514-1523.
[340] S. Zhang, H.-w. Ai, *Nat. Chem. Biol.* **2020**, *16*, 1434-1439.
[341] P. Bäuerle, F. Würthner, G. Götz, F. Effenberger, *Synthesis* **1993**, *1993*, 1099-1103.
[342] M. J. G. Peach, P. Benfield, T. Helgaker, D. J. Tozer, *J. Chem. Phys.* **2008**, *128*, 044118.
[343] R. Englman, J. Jortner, *Mol. Phys.* **1970**, *18*, 145-164.
[344] A. Schulz, W. Kaim, *Chem. Ber.* **1989**, *122*, 1863-1868.
[345] S. A. Cummings, M. Iimura, C. J. Harlan, R. J. Kwaan, I. V. Trieu, J. R. Norton, B. M. Bridgewater, F. Jäkle, A. Sundararaman, M. Tilset, *Organometallics* **2006**, *25*, 1565-1568.
[346] J. H. Uhlenbroek, J. D. Bijloo, *Recl. Trav. Chim. Pays-Bas* **1958**, *77*, 1004-1009.
[347] F. J. Gommers, *Nematologica* **1972**, *18*, 458-462.
[348] J. Bakker, F. J. Gommers, I. Nieuwenhuis, H. Wynberg, *J. Biol. Chem.* **1979**, *254*, 1841-1844.
[349] F. J. Gommers, J. Barker, H. Wynberg, *Photochem. Photobiol.* **1982**, *35*, 615-619.
[350] R. S. Becker, J. Seixas de Melo, A. L. Maçanita, F. Elisei, *J. Phys. Chem.* **1996**, *100*, 18683-18695.
[351] R. Boch, B. Mehta, T. Connolly, T. Durst, J. T. Arnason, R. W. Redmond, J. C. Scaiano, *J. Photochem. Photobiol. A* **1996**, *93*, 39-47.
[352] D. Wasserberg, P. Marsal, S. C. J. Meskers, R. A. J. Janssen, D. Beljonne, *J. Phys. Chem. B* **2005**, *109*, 4410-4415.
[353] C. S. Foote, R. W. Denny, *J. Am. Chem. Soc.* **1968**, *90*, 6233-6235.
[354] C. S. Foote, R. W. Denny, *J. Am. Chem. Soc.* **1971**, *93*, 5168-5171.
[355] R. H. Young, K. Wehrly, R. L. Martin, *J. Am. Chem. Soc.* **1971**, *93*, 5774-5779.
[356] C. A. Long, D. R. Kearns, *J. Am. Chem. Soc.* **1975**, *97*, 2018-2020.
[357] P. R. Ogilby, C. S. Foote, *J. Am. Chem. Soc.* **1983**, *105*, 3423-3430.
[358] E. Oliveros, P. Suardi-Murasecco, T. Aminian-Saghafi, A. M. Braun, H.-J. Hansen, *Helv. Chim. Acta* **1991**, *74*, 79-90.
[359] F. Wilkinson, W. P. Helman, A. B. Ross, *J. Phys. Chem. Ref. Data* **1993**, *22*, 113-262.
[360] R. Schmidt, C. Tanielian, R. Dunsbach, C. Wolff, *J. Photochem. Photobiol. A* **1994**, *79*, 11-17.
[361] C. Martí, O. Jürgens, O. Cuenca, M. Casals, S. Nonell, *J. Photochem. Photobiol. A* **1996**, *97*, 11-18.
[362] S. P. McIlroy, E. Cló, L. Nikolajsen, P. K. Frederiksen, C. B. Nielsen, K. V. Mikkelsen, K. V. Gothelf, P. R. Ogilby, *J. Org. Chem.* **2005**, *70*, 1134-1146.
[363] C. B. Nielsen, J. Arnbjerg, M. Johnsen, M. Jørgensen, P. R. Ogilby, *J. Org. Chem.* **2009**, *74*, 9094-9104.
[364] P. R. Ogilby, *Chem. Soc. Rev.* **2010**, *39*, 3181-3209.
[365] J. Merz, L. Dietrich, J. Nitsch, I. Krummenacher, H. Braunschweig, M. Moos, D. Mims, C. Lambert, T. B. Marder, *Chem. Eur. J.* **2020**, *26*, 12050-12059.
[366] M. C. DeRosa, R. J. Crutchley, *Coord. Chem. Rev.* **2002**, *233-234*, 351-371.
[367] E. L. Clennan, A. Pace, *Tetrahedron* **2005**, *61*, 6665-6691.
[368] T. Ben Amor, G. Jori, *Insect Biochem. Mol. Biol.* **2000**, *30*, 915-925.
[369] M. R. Detty, S. L. Gibson, S. J. Wagner, *J. Med. Chem.* **2004**, *47*, 3897-3915.

[370] L. Sobotta, P. Skupin-Mrugalska, J. Mielcarek, T. Goslinski, J. Balzarini, *Mini Rev. Med. Chem.* **2015**, *15*, 503-521.

[371] W. Fan, P. Huang, X. Chen, *Chem. Soc. Rev.* **2016**, *45*, 6488-6519.

[372] P. K. Frederiksen, S. P. McIlroy, C. B. Nielsen, L. Nikolajsen, E. Skovsen, M. Jørgensen, K. V. Mikkelsen, P. R. Ogilby, *J. Am. Chem. Soc.* **2005**, *127*, 255-269.

[373] C. B. Nielsen, M. Johnsen, J. Arnbjerg, M. Pittelkow, S. P. McIlroy, P. R. Ogilby, M. Jørgensen, *J. Org. Chem.* **2005**, *70*, 7065-7079.

[374] L. Beverina, M. Crippa, M. Landenna, R. Ruffo, P. Salice, F. Silvestri, S. Versari, A. Villa, L. Ciaffoni, E. Collini, C. Ferrante, S. Bradamante, C. M. Mari, R. Bozio, G. A. Pagani, *J. Am. Chem. Soc.* **2008**, *130*, 1894-1902.

[375] G. Liu, X. Xu, Y. Chen, X. Wu, H. Wu, Y. Liu, *Chem. Commun.* **2016**, *52*, 7966-7969.

[376] A. N. Macpherson, T. G. Truscott, P. H. Turner, *J. Chem. Soc. Faraday Trans.* **1994**, *90*, 1065-1072.

[377] M. Bregnhøj, M. Westberg, B. F. Minaev, P. R. Ogilby, *Acc. Chem. Res.* **2017**, *50*, 1920-1927.

[378] R. Uson, L. A. Oro, J. A. Cabeza, H. E. B. Bryndza, M. P. Stepro, *Inorg. Synth.* **1985**, *23*, 126-130.

[379] S. S. Zalesskiy, V. P. Ananikov, *Organometallics* **2012**, *31*, 2302-2309.

[380] A. P. Liesen, A. T. Silva, j. C. Sousa, P. H. Menezes, R. A. Oliveira, *Tetrahedron Lett.* **2012**, *53*, 4240-4242.

[381] S. Darses, G. Michaud, J.-P. Genêt, *Eur. J. Org. Chem.* **1999**, *1999*, 1875-1883.

[382] G. Sheldrick, *Acta Crystalogr.* **2015**, *A71*, 3-8.

[383] G. Sheldrick, *Acta Crystalogr.* **2008**, *A64*, 112-122.

[384] M. Lübtow, I. Helmers, V. Stepanenko, R. Q. Albuquerque, T. B. Marder, G. Fernández, *Chem. Eur. J.* **2017**, *23*, 6198-6205.

[385] N. Miyaura, A. Suzuki, *Org. Synth.* **1990**, *68*, 130.

[386] S.-F. Liu, Q. Wu, H. L. Schmider, H. Aziz, N.-X. Hu, Z. Popović, S. Wang, *J. Am. Chem. Soc.* **2000**, *122*, 3671-3678.

[387] C. B. Hübschle, G. M. Sheldrick, B. Dittrich, *J. Appl. Crystallogr.* **2011**, *44*, 1281-1284.

[388] K. Brandenburg, Diamond (version 4.4.0) - Crystal and Molecular Structure Visualization, Crystal Impact H. Putz & K. Brandenburg GbR, Bonn (Germany), **2017**.

[389] J. B. Chaires, N. Dattagupta, D. M. Crothers, *Biochemistry* **1982**, *21*, 3933-3940.

[390] L.-M. Tumir, I. Piantanida, I. J. Cindrić, T. Hrenar, Z. Meić, M. Žinić, *J. Phys. Org. Chem.* **2003**, *16*, 891-899.

[391] D. A. Case, R. M. Betz, D. S. Cerutti, T. E. Cheatham, T. Darden, R. E. Duke, T. J. Giese, H. Gohlke, A. W. Goetz, N. Homeyer, S. Izadi, P. Janowski, J. Kaus, A. Kovalenko, T. S. Lee, S. LeGrand, P. Li, C. Lin, T. Luchko, R. Luo, B. Madej, D. Mermelstein, K. M. Merz, G. Monard, H. Nguyen, H. T. Nguyen, I. Omelyan, A. Onufriev, D. R. Roe, A. Roitberg, C. Sagui, C. Simmerling, W. M. Botello-Smith, J. Swails, R. C. Walker, J. Wang, R. M. Wolf, X. Wu, L. Xiao, P. A. Kollman, AMBER16, University of California, San Francisco, **2016**.

[392] J. Wang, R. M. Wolf, J. W. Caldwell, P. Kollman, *J. Comput. Chem.* **2004**, *25*, 1157-1174.

[393] M. Zgarbová, M. Otyepka, J. Šponer, A. Mládek, P. Banáš, T. E. Cheatham, P. Jurečka, *J. Chem. Theory Comput.* **2011**, *7*, 2886-2902.

[394] W. L. Jorgensen, J. Chandrasekhar, J. D. Madura, R. W. Impey, M. L. Klein, *J. Chem. Phys.* **1983**, *79*, 926-935.

[395] I. S. Joung, T. E. Cheatham, *J. Phys. Chem. B* **2008**, *112*, 9020-9041.

[396] R. J. Loncharich, B. R. Brooks, R. W. Pastor, *Biopolymers* **1992**, *32*, 523-535.

[397] H. J. C. Berendsen, J. P. M. Postma, W. F. v. Gunsteren, A. DiNola, J. R. Haak, *J. Chem. Phys.* **1984**, *81*, 3684-3690.

[398] M. J. Frisch, G. W. Trucks, H. B. Schlegel, G. E. Scuseria, M. A. Robb, J. R. Cheeseman, G. Scalmani, V. Barone, B. Mennucci, G. A. Petersson, H. Nakatsuji, M. Caricato, X. Li, H. P. Hratchian, A. F. Izmaylov, J. Bloino, G. Zheng, J. L. Sonnenberg, M. Hada, M. Ehara, K. Toyota, R. Fukuda, J. Hasegawa, M. Ishida, T. Nakajima, Y. Honda, O. Kitao, H. Nakai, T. Vreven, J. A. Montgomery, J. E. Peralta, F. Ogliaro, M. Bearpark, J. J. Heyd, E. Brothers, K. N. Kudin, V. N. Staroverov, R. Kobayashi, J. Normand, K. Raghavachari, A. Rendell, J. C. Burant, S. S. Iyengar, J. Tomasi, M. Cossi, N. Rega, J. M. Millam, M. Klene, J. E. Knox, J. B. Cross, V. Bakken, C. Adamo, J. Jaramillo, R. Gomperts, R. E. Stratmann, O. Yazyev, A. J. Austin, R. Cammi, C. Pomelli, J. W. Ochterski, R. L. Martin, K. Morokuma, V. G. Zakrzewski, G. A. Voth, P. Salvador, J. J. Dannenberg, S. Dapprich, A. D. Daniels, Farkas, J. B. Foresman, J. V. Ortiz, J. Cioslowski, D. J. Fox, **2016**.

[399] M. D. Hanwell, D. E. Curtis, D. C. Lonie, T. Vandermeersch, E. Zurek, G. R. Hutchison, *J. Cheminformatics* **2012**, *4*, 17.

[400] T. Lu, F. Chen, *J. Comput. Chem.* **2012**, *33*, 580-592.

[401] C. Lee, W. Yang, R. G. Parr, *Phys. Rev. B* **1988**, *37*, 785-789.

[402] G. A. Petersson, A. Bennett, T. G. Tensfeldt, M. A. Al-Laham, W. A. Shirley, J. Mantzaris, *J. Chem. Phys.* **1988**, *89*, 2193-2218.

[403] G. A. Petersson, M. A. Al-Laham, *J. Chem. Phys.* **1991**, *94*, 6081-6090.

[404] W. Saenger, *Principles of nucleic acid structure*, Springer Science & Business Media, New York, **2013**.

[405] C. Cantor, P. Schimmel, in *Biophysical Chemistry Part III: The Behaviour of Biological Macromolecules*, Freeman and Company, Oxford, **1980**, pp. 1109-1181.

[406] C.-W. Chiu, F. P. Gabbaï, *Organometallics* **2008**, *27*, 1657-1659.